Binuclear complexes as quantitative imaging agents

Leila Hill

The Queen's College

University of Oxford



A thesis submitted for the degree of

Doctor of Philosophy

Trinity Term 2018

Contents

Abstract v
Publications vi
Acknowledgements vii
Abbreviations ix
Chapter 1 Introduction 1
1.1 Lanthanide chemistry 1
1.2 Lanthanide photophysics 3
1.2.1 Selection rules 4
1.2.2 Antenna effect 5
1.3 Mechanisms of energy transfer 8
1.4 Quenching 8
1.5 NMR 13
1.6 Isomerism 15
1.7 Hypoxia 17
1.8 MRI 18
1.9 Optical imaging 21
1.10 Self-assembly 24
1.11 Aims and objectives 29
1.12 References 30
Results and discussion 33
Chapter 2 Establishing the fundamentals of isophthalate binding 33
2.1 Self-assembly between dicarboxylate ions and binuclear lanthanide complexes – "a surprisingly complicated problem"[1] 33
2.1.1 Self-assembly 34
2.1.2 Photophysics 34
2.1.3 Binding constants 38
2.2 Exploring the effect of remote substituents and solution structure on the luminescence of three lanthanide complexes[11] 42
2.3 Thermodynamics of self-assembly of dicarboxylate ions with binuclear lanthanide complexes[12] 46
2.3.1 Data 48
2.3.2 Competitive binding 49
2.3.3 Binding in other solvent systems 50
2.3.4 Temperature-dependence 50
2.3.5 Aqueous conditions 51
2.3.6 Biological relevance 51
2.3.7 Luminescence spectra 51
2.3.8 Luminescence lifetimes 52

2.3.9 Conclusions 52
2.4 References 53
Part A: Synthesis and characterisation 54
Chapter 3 *m*-Xylyl complexes 55
3.1 Introduction 55
3.2 Synthesis and characterisation 55
3.2.1 NMR 63
3.2.2 UV-vis spectroscopy 66
3.2.3 Luminescence excitation 68
3.2.4 Luminescence emission 70
3.2.5 Luminescence lifetimes and *q* values 72
3.3 Choice of complexes 75
3.3.1 Europium 75
3.3.2 Terbium 75
3.3.3 Ytterbium 76
3.4 Gadolinium 76
3.5 Yttrium 76
3.6 References 77
Chapter 4 Mononuclear complexes 78
4.1 Introduction 78
4.2 3-Nitrobenzyl complex 78
4.3 Coumarin complex 82
4.3.1 Synthesis 82
4.3.2 Structural chemistry 83
4.3.3 pH-dependence 85
4.4 Propargyl complex 91
4.5 References 91
Chapter 5 Naphthyl-bridged bicyclic systems 92
5.1 Introduction 92
5.2 Synthesis of the 2,6-naphthyl complex 93
5.3 Synthesis of the 2,7-naphthyl complex 95
5.4 Characterisation of the naphthyl complexes 96
5.5 References 99
Chapter 6 Acridone-appended complexes 100
6.1 Introduction 100
6.2 Synthesis of acridone-appended complexes 101
6.3 Photophysical characterisation of acridone-appended complexes 102
6.3.1 Absorption and excitation spectra 103
6.3.2 Emission spectra 105

6.3.3 Luminescence lifetimes 107
6.4 References 107
Part B: Binding studies 108
Chapter 7 Binding of anions to lanthanide complexes 109
7.1 Introduction 109
7.2 Techniques for studying binding 110
7.2.1 Luminescence 110
7.2.2 NMR 111
7.3 Luminescence binding studies 112
7.3.1 *m*-Xylyl complexes 115
7.3.2 3-NitrobenzylDO3A complex 118
7.3.3 Coumarin-appended complex 119
7.3.4 Propargyl complex 119
7.3.5 Naphthyl complexes 120
7.3.6 Acridone-appended complexes 122
7.4 Luminescence lifetimes 124
7.5 NMR binding studies 127
7.5.1 Preliminary NMR studies 127
7.5.1.1 NMR spectra 127
7.5.1.2 Relaxation measurements 129
7.5.2 NMR titrations 132
7.6 References 134
Chapter 8 Binding of glycolysis products 135
8.1 Introduction 135
8.2 Luminescence binding titrations 136
8.3 Binding modes 139
8.4 Binding constants from luminescence titrations 140
8.5 NMR binding studies and titrations 146
8.6 References 149
Chapter 9 Binding of anionic phosphate species 150
9.1 Introduction 150
9.2 Luminescence binding titrations 150
9.3 NMR binding studies and titrations 156
9.4 References 162
Chapter 10 Binding of catechols 163
10.1 Introduction 163
10.2 Luminescence binding titrations 163
10.3 Binding mode 169
10.4 Binding constants from luminescence titrations 171

10.5 References 174
Chapter 11 Conclusions and future work 175
11.1 References 177
Chapter 12 Experimental 178
12.1 General methods 178
12.2 Synthetic procedures 180
12.3 Isothermal titration calorimetry 209
12.4 Luminescence titrations 210
12.5 Data processing and fitting 213
12.5.1 Luminescence titrations 213
12.5.2 NMR titrations 221
12.6 Degassed measurements 222
12.7 References 222
Appendix A Molecular structures of hosts and guests 223
Appendix B NMR spectra from catechol binding studies 225
Appendix C X-ray crystallographic data 226
C.1 3,5-bis(bromomethyl)nitrobenzene (2) 226
C.2 *α*,*α*'-bis(DO3A *tert*-butyl triester)-3,5-dimethylnitrobenzene (3) 228
C.3 (*E*)-1,2-bis(*α*,*α*'-bis(DO3A *tert*-butyl triester)-3,5-dimethylphenyl)diazene (4a) 230
C.4 *α*-(Eu.DO3A)-4-methyl-7-methoxycoumarin (Eu.10) 233
C.4.1 Monoclinic 235
C.4.2 Orthorhombic 237
C.5 *α*,*α*'-bis(DO3A *tert*-butyl triester)-2,6-dimethylnaphthalene (13) 239
C.6 ethyl-2-(9-oxo-9,10-dihydro-10-acridinyl)acetate (17) 242
Appendix D Publications 244

Abstract

"Binuclear complexes as quantitative imaging agents"

Leila Hill, The Queen's College, University of Oxford

DPhil Thesis, Trinity Term 2018

This thesis explores the synthesis of and subsequent use of mono- and binuclear lanthanide complexes in their binding to biologically endogenous dianions.

Chapter 1 outlines the properties of the lanthanides with a focus on their chemical and photophysical behaviour and self-assembly involving lanthanide-containing complexes. Medical applications are also discussed.

Chapter 2 sets the scene for anion binding with lanthanide complexes by establishing the fundamentals and thermodynamics of their interactions with dicarboxylate species. In this chapter, the focus is on the use of luminescence spectroscopy to explore the nature of self-assemblies and establish the role of local and remote structural variations (in concert with solvation effects) in tuning binding affinity for dicarboxylate guests.

Chapter 3 covers the synthesis and characterisation of a set of binuclear lanthanide complexes of ligands in which *m*-xylyl derivatives bridge two DO3A-derived domains.

Chapter 4 describes the synthesis and characterisation of mononuclear complexes. These exhibit greater structural variation than the *m*-xylyl systems, containing the DO3A core with pendent benzyl, propargyl and coumarin groups.

Chapter 5 discusses the synthesis and characterisation of two binuclear naphthyl complexes, in which 2,6- and 2,7- substituents are used to form the bridge between the two DO3Ayl domains.

Chapter 6 extends the synthesis of the style of binuclear complex described in Chapter 3 by coupling the amino derivative to the longer wavelength sensitiser acridone.

Chapter 7 provides an overview of the binding studies performed in this thesis with mono- and binuclear host complexes to an array of anionic guests, outlining and comparing methods for using luminescence and NMR to explore guest binding events.

Chapter 8 considers specifically binding to species from the glycolytic pathway and to the similar chain-length carboxylate species tartrate and lactate. These studies reveal that the dianionic species in the pathway can act as bridging ligands, and that differences in structure and photophysics can give rise to selective responses from different guests.

Chapter 9 evaluates binding to endogenous and non-biological phosphate species, both by luminescence measurements and phosphorus NMR.

Chapter 10 focuses on binding to and interactions with catechol species including dopamine. In these systems, the relative instability of catechols in solution combines with inner filter effects to present challenges to method development.

Chapter 11 lays out the conclusions reached over the course of this work and suggests possible opportunities for further work.

Chapter 12 contains experimental procedures and techniques for processing data.

A series of appendices provide supplementary information to the core thesis, including a reference to the molecular structures of host complexes and guest anions in this thesis, X-ray crystallography data, and published papers.

Publications

1. T. J. Sørensen, L. R. Hill, J. A. Tilney, O. A. Blackburn, M. W. Jones, M. Tropiano, and S. Faulkner, *Eur. J. Inorg. Chem.*, 2014, **15**, 2520-8 (2014)
   "Self-Assembly between Dicarboxylate Ions and Dinuclear Lanthanide Complexes: A Surprisingly Complicated Problem" 10.1002/ejic.201402169

2. T. J. Sørensen, L. R. Hill, and S. Faulkner, *ChemistryOpen*, 2015, **4**, 509-15 (2015)
   "Thermodynamics of Self-Assembly of Dicarboxylate Ions with Binuclear Lanthanide Complexes" 10.1002/open.201500060

3. M. Tropiano, O. A. Blackburn, J. A. Tilney, L. R. Hill, T. J. Sørensen, and S. Faulkner, *J. Lumin.*, 2015, **167**, 296-304 (2015)
   "Exploring the effect of remote substituents and solution structure on the luminescence of three lanthanide complexes" 10.1016/j.jlumin.2015.06.035

4. A. K. R. Junker, L. R. Hill, A. L. Thompson, S. Faulkner, and T. J. Sørensen, *Dalton Trans.*, 2018, **47**, 4794-4803 (2018)
   "Shining light on the antenna chromophore in lanthanide based dyes" 10.1039/c7dt04788f

Acknowledgements

Wow. It's been a long one. When I first waved goodbye to my parents on 3rd October 2007 at the Florey Building (11 years ago this week), I never could've predicted quite what an innings I'd be serving.

First, the sensible part.

It's been a pleasure to work for Steve since 2011. I'm very grateful Steve took me on and let me stay for a DPhil. I left every single meeting with Steve more reassured than when I went in, whether it was about chemistry or anything else. There is no-one else I'd rather have worked for.

Thanks to Cancer Research UK and the Cancer Imaging Centre in Oxford for the funding that made this project possible.

Thanks to other members of the Faulkner group, including Mike who has long since left but kept offering thesis advice, Doc Oc, Manuel, Wendy, Louise, Becky, especially to Laura and Gearoid for supplying me with compounds when I'd lost or used up or dropped mine, and to everyone else who has taught me everything I know and also everything I've since forgotten. The rest of you can acknowledge me in your theses.

I don't want to pick favourite Part II students, but they were Alice, Matthew, and Izzy. (Don't tell the others.)
And the Beer group have been decent with the advice too – special thanks to Andrew for keeping me company during the writeup.

Thanks to Prof Thomas Sørensen for the help and advice right from the beginning to the collaborations on the papers and for the tasty quiche in Copenhagen.

Thanks to Dr Louise Natrajan for the advice and answers and help with the LS55.

Thanks to Dr Asha Brown for the pyridyl ligand that's still going strong in this thesis and the synthetic advice.

Thanks to Dr Nick Rees who always knew the NMR answers and delivered the solutions at breakneck speed and had the world's most annoying CDs playing in the NMR lab.

Thanks to the mass spec department, particularly Dr Colin Sparrow, Dr Victor Mikhailov, and Dr James Wickens.

Thanks to Dr Amber Thompson and Dr Kirsten Christensen for solving my crystals (and thanks to Mother Nature's eternal patience for crystallising them for me).

I am grateful for the CHN analysis by Stephen Boyer in London, and Birgitta Kegel and Niels Vissing Holst in Copenhagen.

Thanks to all of my proofreaders who checked over my ~~Engilsh~~English for me.
2×MJ, AH, DS, SRV, RB, EH, AM, RM, VG, CG: I cherish every, additional, comma.

To Mr Reynolds and others for catalysing an interest in chemistry back at school, and to all my tutors at Oxford who picked up the baton and dragged me through every painstaking curly arrow.

Outside of academia, I'd also like to thank Oxford Uni Lacrosse Club for the years of huffing

and puffing and muscle strain, and Oxford Uni Women's Lightweight Rowing Club for the 5am starts, bleeding blisters that meant I was unable to wash my own hair, for the solid friendships, solid abs, and the rapid immersion in the unstoppable force that is "rowing chat" (and one or two not-so-rapid immersions in the Thames), and to every Queen's College and Wolfson College sports team that allowed me to crash/thrash around on a field/river with them for an hour or so.

To everyone who gave me a sports injury, those were a blessing in disguise pushing me to do more chemistry, and to the surgeons and physios who got me up and running again.

I'd like to thank Wales Lacrosse for the swift snap that made my left knee one ACL lighter, and Mr Bottomley who screwed it back together (he was a surgeon, but I'm not convinced that there's anything that Ron and Jude and co. in the workshop can't fix) – see page 20 Figure 1.11.

Special thanks to Joyce Millar (who has been indescribably excellent) and the College Office at Queen's for looking after me when I've needed it, to Dawn and the college kitchen staff who have done their best to feed up a scrawny northerner for the past decade, to Sue and Tracey and the scouts and crew, to all of the friendly college librarians, to the college porters who were always up for a chat/gossip, and to David in the IT office with his patience every time I took a screwdriver to the innards of my computer. As well as all of the help, being here this long means a high turnover of friends, so consistent friendly faces were always a welcome sight.

That's not to say that I haven't had some great times with some great mates: Rose, Rob, Anna, Jenny, 2×Dani, Gen, Tom, Rahil, Jo, Violet, Adam, James, Stevie, it would've been very different without you. Some of you were a good influence, some of you were a terrible influence, and some of you let me stay over at your houses.

In the template I'm copying, normally I think people thank a partner here, but if I could hold onto anyone for more than a year that would be a miracle.

Thanks to my family. Mum and Dad and Josh, I reckon you've got absolutely no idea what I've been doing down here but I'll explain it one day.

And Nanny. I remember this academic journey starting with you teaching me how to write 26 years ago and even though you couldn't hold on for the final 7 months, here's me keeping my promise of becoming a doctor.

I've made a lot of friends and had a lot of fun.

Time to leave before I outstay my welcome.

Abbreviations

ADP	adenosine diphosphate
AMP	adenosine monophosphate
ATP	adenosine triphosphate
ATR	attenuated total reflectance
a.u.	arbitrary units
BBS	borate buffered saline
BOP	(benzotriazol-1-yloxy)tris(dimethylamino)phosphonium hexafluorophosphate
br.	broad
ca.	circa
CHN	carbon, hydrogen, nitrogen elemental analysis
COSY	correlated spectroscopy
cyclen	1,4,7,10-tetraazacyclododecane
d	doublet
Da	Daltons
dinicotinic acid	pyridine-3,5-dicarboxylic acid
DIPEA	*N*,*N*-diisopropylethylamine
DMF	dimethylformamide
DMSO	dimethyl sulfoxide
DO3A	1,4,7,10-tetraazacyclododecane-1,4,7-triacetic acid
DO3AM	2,2',2"-(1,4,7,10-tetraazacyclododecane-1,4,7-triyl)triacetamide
DOSY	diffusion-ordered NMR spectroscopy
DOTA	1,4,7,10-tetraazacyclododecane-1,4,7,10-tetraacetic acid
δ	chemical shift
δ^+	partial positive charge
δ^-	partial negative charge
EPA	ethylphosphonic acid
ES	electrospray
ESI	electrospray ionisation
FBP	fructose bisphosphate
FI	field ionisation
FWHM	full width at half-maximum peak height
HBS	HEPES buffered saline

HEPES (buffer)	4-(2-hydroxyethyl)piperazine-1-ethanesulfonic acid
HRMS	high resolution mass spectrometry
I	intensity
IR	infrared
isophthalic acid	benzene-1,3-dicarboxylic acid
K	equilibrium constant, typically a binding constant
K_a	association constant
L	ligand
LMCT	ligand-to-metal charge transfer
Ln	lanthanide
λ	wavelength
λ_{em}	wavelength of emission
λ_{ex}	wavelength of excitation
λ_{max}	wavelength of maximum intensity
OTf	trifluoromethanesulfonate (triflate)
m	multiplet
M	mol dm^{-3}
M	parent molecule
M±	parent ion
MALDI	matrix assisted laser desorption and ionisation
MLCT	metal-to-ligand charge transfer
MPA	methylphosphonic acid
MRI	magnetic resonance imaging
MS	mass spectrometry
nicotinic acid	pyridine-3-carboxylic acid (niacin/vitamin B_3)
NMR	nuclear magnetic resonance
PA	pyruvic acid
PBS	phosphate buffered saline
PEP	phospho(enol)pyruvate
PET	positron emission tomography
2PG	2-phosphoglycerate
P_i	inorganic phosphate
ppm	parts per million
protocatechualdehyde	3,4-dihydroxybenzaldehyde
protocatechuic acid	3,4-dihydroxybenzoic acid

q	quartet
q	number of bound solvent molecules
r	distance/bond length
R_f	retardation factor
s	singlet
SAP	square antiprism
s.w.	slit width
$s.w._{em}$	emission slit width
$s.w._{ex}$	excitation slit width
S_0	lowest singlet state
S_1	first excited singlet state
t	triplet
τ	luminescence lifetime
t_e	echo time
TFA	trifluoroacetic acid
TfOH	trifluoromethanesulfonic acid (triflic acid)
THF	tetrahydrofuran
t_i	inversion time
TLC	thin layer chromatography
TOF	time of flight
t_R	repetition time
triflate	trifluoromethanesulfonate
TRIS (buffer)	2-amino-2-hydroxymethyl-propane-1,3-diol
TSAP	twisted square antiprism
TsOH	toluenesulfonic acid
T_1	lowest triplet state
T_1	spin-lattice relaxation time (NMR)
	longitudinal relaxation time (MRI)
T_2	spin-spin relaxation time (NMR)
	transverse relaxation time (MRI)
UV	ultraviolet
vis	visible
v/v	volume per volume

Chapter 1 Introduction

The properties of lanthanide complexes have long been of benefit in bioassay and imaging. This thesis explores the binding of binuclear lanthanide complexes with biologically relevant molecules, exploiting their luminescence properties in considering their application as cancer imaging agents.

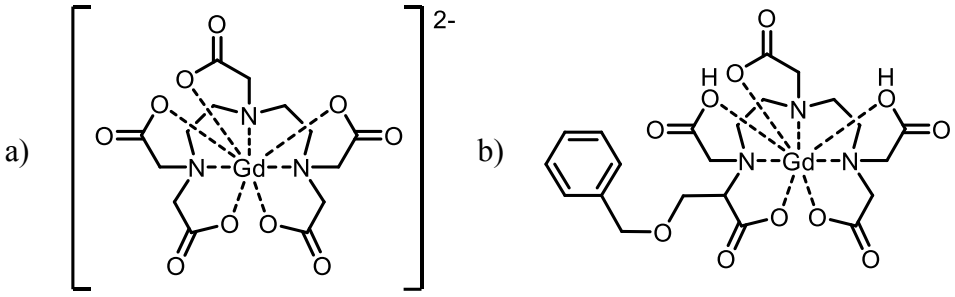
1.1 Lanthanide chemistry

The characteristic chemistry of the lanthanides is a result of their partially-filled 4*f* orbital. The trivalent oxidation state dominates due to the enthalpic balance between the cost of the sum of the ionisation energies and the gain from electrostatic bonding or from solvation. *f*-Orbitals are not sufficiently radially extended to allow significant orbital overlap with other atoms and therefore limited covalent character is found in their bonding. Instead, bonding in lanthanide complexes is predominantly electrostatic, including in dative bonding, and non-directional, with ligands arranging around the lanthanide in a fashion which minimises mutual repulsions. Lanthanides have large ionic radii allowing higher coordination numbers than those found in complexes of *d*-metals, where ligand position is also dictated by the orientation of the *d*-orbitals. Early lanthanides tend to adopt 9-coordinate geometries, and later, smaller lanthanides typically accommodate 8 donors.

Lanthanides form stable complexes with polydentate ligands, exploiting the additional stability afforded by the chelate effect. Ligands with hard donors such as N or O are often chosen in order to exploit the strong electrostatic interactions with hard lanthanide ions.

Examples of polydentate lanthanide complexes are shown in Figure 1.1. Compounds **I** and **II** benefit from the kinetic and thermodynamic stability afforded by an octadentate ligand

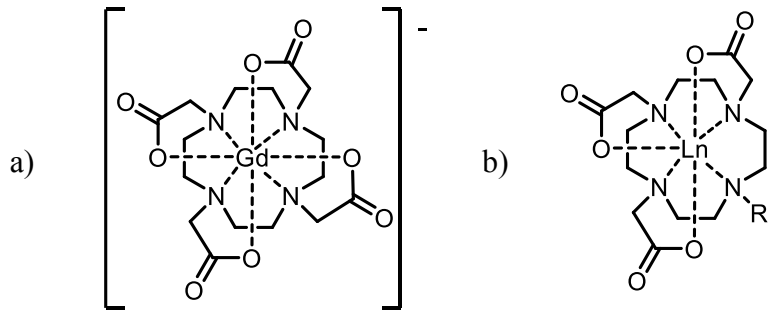
possessing hard O and N donors.



I **II**

Figure 1.1 a) Gadopentetic acid ([Gd.DTPA]$^{2-}$, brand name Magnevist®), b) gadobenic acid (brand name MultiHance®)

Macrocyclic complexes are also commonly synthesised and are generally more stable than complexes with open-chain chelating ligands owing to the macrocyclic effect. For lanthanides, cyclen derivatives such as DOTA are frequently used due to the stability provided by a combination of structural rigidity and five-membered chelate rings. These macrocycles often have carboxylate arms appended at three or four of the cyclen nitrogen atoms which are able to wrap around and encapsulate the lanthanide ion, as with compounds **III** and **IV** in Figure 1.2. Structures based on DO3A are widely exploited, with functionalisation at the fourth nitrogen atom. As with the polydentate complexes, the vacant coordination sites are occupied by solvent molecules. Complexes of this type and of the open-chain type shown in Figure 1.1 will be discussed in further detail later in view of their application in magnetic resonance imaging.



III **IV**

Figure 1.2 a) Gadoteric acid ([Gd.DOTA]$^{-}$, brand name Dotarem®), b) Ln.DO3A (R = H)

1.2 Lanthanide photophysics

Each lanthanide has characteristic absorption and emission spectra arising from electronic transitions within the manifold of $^{2S+1}L_J$ states. Lanthanides may emit light *via* fluorescence ($\Delta S = 0$, for example, the $^2F_{5/2} \rightarrow {}^2F_{7/2}$ transition in ytterbium(III), lifetime typically 10^{-7} seconds in water) or phosphorescence ($\Delta S \neq 0$, long-lived or delayed luminescence, between 10^{-6} and 1 second) which may be grouped together under the term "luminescence". The vast majority of transitions involve a change in spin.[1–4]

Absorption and emission spectra tend to have a relatively large number of peaks compared to *d*-metals as a result of the large number of terms arising from the multitude of microstates available for each electronic configuration (Figure 1.3).[5] The wavelength of transitions is related to the energy spacing between the electronic microstates, which is specific to each lanthanide.

For example, the transitions for the f^6 Eu^{3+} ion are from its excited $^5D_0$ state to its ^7F_J levels, giving peaks in emission spectra where ΔJ is 0, 1, 2, 3, 4, 5, or 6. For europium(III), emission from higher-lying excited states ($^5D_1$, $^5D_2$, $^5D_3$) is less common, particularly for molecular compounds and especially at room temperature, where quenching of these states would occur by non-radiative processes.[6] The peaks in these spectra are sharp on account of the negligible vibronic coupling experienced by lanthanides as their contracted valence orbitals have little overlap with ligand-centred orbitals.[7] The internuclear distance differs little between ground and excited states, giving rise to good Franck-Condon overlap and small Stokes shifts upon direct excitation. This poor overlap also leads to little crystal field splitting of spectral peaks. The small ligand field that is present dictates the electronic energy levels of the lanthanide ion and the $(2J + 1)$ degeneracy is lifted.[8] This Stark splitting is a manifestation of the Stark

effect and gives rise to the m_j levels.[9]

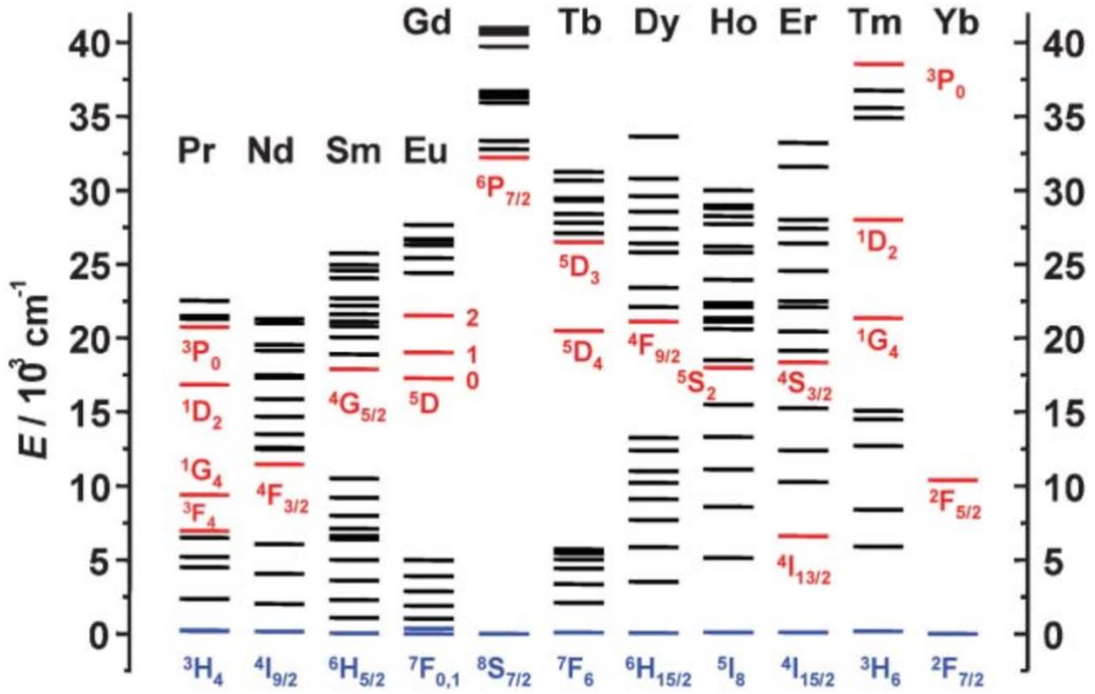


Figure 1.3 Partial energy diagrams for the lanthanide aquo ions,[10–12] *with main luminescent levels (red) and fundamental levels (blue), taken from reference*[13]

Some transitions, particularly hypersensitive transitions, such as the $\Delta J = 2$ transition for Eu^{3+}, are affected by the local coordination environment at the lanthanide, therefore changes in these spectral peaks can be interpreted to provide useful information about changes at the lanthanide, and may be pH-sensitive.[14–16] These transitions obey the selection rules for *electric quadrupoles*: $\Delta S = 0$; $|\Delta L| \leq 2$; and $|\Delta J| \leq 2$; but are denoted *pseudoquadrupolar* as their oscillator strength exceeds the predicted values for *quadrupolar transitions* by a factor of 10^5. Hypersensitive transitions are usually more intense for complexed lanthanides than for the lanthanide aquo ion.

1.2.1 Selection rules

The Laporte selection rule formally forbidding *f-f* transitions explains the low probability of these transitions and therefore low absorption coefficients and low intensity spectra in the

visible region of the electromagnetic spectrum. Due to the low probability of absorption with *f-f* transitions, UV-vis absorption spectra of lanthanide complexes are often dominated by formally allowed ligand-centred transitions, and on occasion by charge transfer bands (LMCT in europium and ytterbium complexes and MLCT in cerium and terbium complexes).

The long luminescence lifetimes of lanthanides may also be attributed to the forbidden nature of these transitions and therefore low transition probabilities and long-lived excited states. Lanthanide emission may therefore be separated from the short-lived fluorescence of organic molecules, or when applied in medical imaging, from the background fluorescence of biological tissue, with time-gating techniques, which employ a delay time after the initial excitation pulse.[8]

Judd-Ofelt theory predicts the probabilities of these *induced electric dipole f-f* transitions and therefore the intensities of transitions in absorption and emission spectra of lanthanide species.[17,18]

1.2.2 Antenna effect

The low probability of direct excitation of lanthanide transitions may be circumvented by use of an antenna chromophore,[19] typically an aromatic group or moiety incorporating a *d*-metal. This chromophore must have good overlap with and a close energy match to the lanthanide *f*-orbitals.[19–22] The usual mechanism for sensitised emission is for the chromophore to absorb a photon to form an excited singlet state, which then forms a triplet state *via* intersystem crossing, which subsequently transfers energy to the lanthanide *via* Förster or Dexter exchange.[23,24] Alternatively, examples of the chromophore excited singlet

state transferring energy to the lanthanide have been observed. These pathways are illustrated in the Jablonski diagram in Figure 1.4.

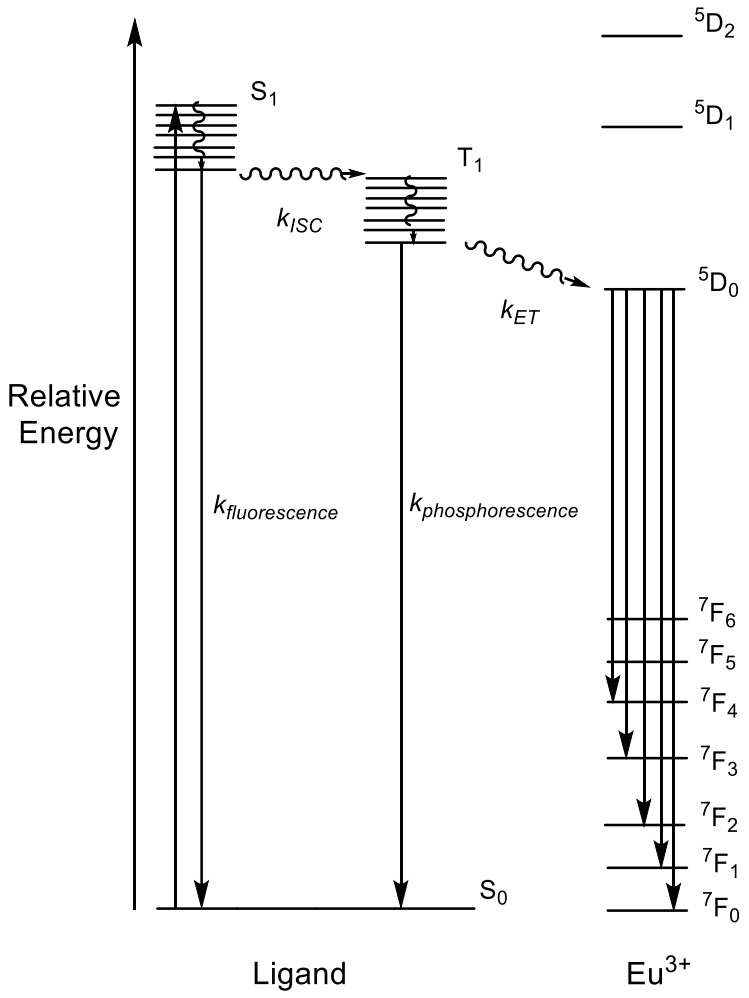


Figure 1.4 Simplified Jablonski diagram for the transitions within Eu^{3+} where ISC is intersystem crossing, and ET is energy transfer

Once populated, lanthanide excited states may decay in a number of ways. One pathway is luminescence: emission of a photon. Non-radiative energy loss is also possible, especially *via* vibrational quenching by small molecule oscillators in the coordination sphere, such as the O-H or N-H bonds in solvent molecules. It is therefore beneficial to encapsulate the lanthanide ion in a polydentate ligand with hydrophobic character in order to hinder the approach of water.[25]

The ligand may also return to its ground state *via* fluorescence ($\Delta S = 0$) or phosphorescence

($\Delta S \neq 0$) without transferring energy to the lanthanide. The probability of these energy transfer processes is governed by Fermi's golden rule, given in Equation 1.1.

$$w_{D,A} = \frac{2\pi}{\hbar} |\langle DA^* | H | D^* A \rangle|^2 \Omega_{D,A}$$

Equation 1.1 Fermi's golden rule, where $w_{D,A}$ is the probability that a resonant energy transfer process occurs from a donor D to an acceptor A, ħ is the reduced Planck constant, H is the interaction Hamiltonian that mediates energy transfer from the excited donor D to the ground state acceptor A, $\Omega_{D,A}$ is the spectral overlap integral between the emission spectrum of the donor D and the absorption spectrum of the acceptor A*

The relative rates of these processes can govern the oxygen-dependence of the emission. In some cases, ground state triplet molecular oxygen can quench the triplet state of the ligand and become excited to a singlet state. Therefore less energy is transferred to the lanthanide, resulting in a difference in quantum yield between aerated and degassed solutions of the same complex. This dependence is related to the rate of intersystem crossing as this governs the abundance of the ligand triplet state. The two cases where triplet quenching by molecular oxygen occurs are: rapid reversible energy transfer between the T_1 state and the emissive state; and slow energy transfer between the T_1 state and the emissive state.

Europium(III) and the more emissive terbium(III) are good candidates for luminescence studies due to their high quantum yields and emissions in the visible range which are easy to detect with readily available photomultiplier tubes or photodiodes.

Ytterbium(III) exhibits only one luminescence emission peak – which is found in the near-IR – as it possesses only one *f*-centred state. This peak is not a single sharp band but an envelope of bands arising from the ligand-field splitting of the emitting and/or fundamental state.[26]

Charge transfer processes are possible in ytterbium(III) complexes as the ytterbium(II) state is readily accessible.[27] LMCT states also occur in europium(III) and terbium(III) complexes, but when present, lanthanide emission is prevented as these states are of lower energy than the lanthanide emissive states.

1.3 Mechanisms of energy transfer

Dexter energy transfer involves double electron exchange through bonds and has an e^{-r} dependence, and typically occurs at short distances (~0.5 Å) where there is the required overlap of donor and acceptor wavefunctions, although larger distances may be accessed by superexchange (~20 Å).[24,28]

Förster energy transfer is a through-space dipole-dipole coupling mechanism and has an r^{-6} dependence. It relies on spectral overlap of the donor and acceptor and is possible over larger distances than Dexter energy transfer (~10 Å).[23]

1.4 Quenching

Static and dynamic (also known as collisional) quenching are possible. Static quenching is the inhibition of formation of the excited state by an external influence (quencher), whereas dynamic quenching involves non-radiative deactivation of an already-formed excited state by a quencher.[29]

One mechanism by which non-radiative deactivation of the excited state proceeds is transfer of energy to the vibrational excited states of small molecule oscillators in the coordination sphere, such as the O-H or N-H bonds in solvent molecules. Quenching by ligand oscillators is also possible.

The quantum yield of a substance is the ratio of photons emitted to photons absorbed, and is between 0 and 1 except in exceptional circumstances, for example those where the absorption of one photon leads to a cascade of emitted photons. The quantum yield for different lanthanides is affected by bound oscillators to different degrees. Quenching reduces the luminescence output and therefore quantum yield of a lanthanide complex in solution.

The q value of a complex is the number of water molecules bound to the lanthanide in the first coordination sphere. This is calculated with the modified Horrocks[30] equation (Equation 1.2) by comparison of the luminescence lifetimes of a complex in D_2O or deuterated solvent and when dissolved in H_2O or the equivalent protic solvent.[30–33]

$$q = A\left(k_{H_2O} - k_{D_2O} - B\right)$$

Equation 1.2 Modified Horrocks equation,[30] where q is the number of water molecules coordinated to the lanthanide centre, A is a proportionality constant signifying the sensitivity of the lanthanide ion to vibronic quenching by O-H oscillators, k is the rate constant for depopulation of the lanthanide excited state, and B is an empirical correlation factor accounting for outer sphere and other quenching

Equation 1.3 for europium and Equation 1.4 for terbium follow from this general equation.

$$q_{Eu} = 1.2\left(\frac{1}{\tau_{H_2O}} - \frac{1}{\tau_{D_2O}} - 0.25\right)$$

Equation 1.3 Modified Horrocks equation for europium, where q is the number of bound solvent molecules and τ is the luminescence lifetime

$$q_{Tb} = 5\left(\frac{1}{\tau_{H_2O}} - \frac{1}{\tau_{D_2O}} - 0.06\right)$$

Equation 1.4 Modified Horrocks equation for terbium, where q is the number of bound solvent molecules and τ is the luminescence lifetime

The lifetime of the excited state in the presence of a quencher may be expressed as follows

in Equation 1.5:[34]

$$\tau = \frac{1}{k_{obs}} = \frac{1}{k_f + k_{nr} + k_q[Q]}$$

Equation 1.5 Relating the observed luminescence lifetime, τ, and decay constant, k_{obs}, to the rate of fluorescence, k_f, the rate of nonradiative decay, k_{nr}, the rate of quenching by a quencher Q, k_q, and the concentration of a quencher Q, [Q]

From this, the Stern-Volmer relationship (Equation 1.6) may be derived:[34]

$$\frac{\tau_0}{\tau} = 1 + k_q \tau_0 [Q]$$

Equation 1.6 Where τ_0 is the excited state lifetime in the absence of a quencher, τ is the excited state lifetime, k_q is the rate of quenching by a quencher Q, and [Q] is the concentration of a quencher Q

In the simple case of collisional, or dynamic, quenching, the fluorophore excited state is deactivated by coming into contact with a species which may facilitate non-radiative transitions to the ground state, for example O_2, and Equation 1.7 below holds:[4,34]

$$\frac{I_0}{I} = 1 + K_{SV}[Q]$$

Equation 1.7 Stern-Volmer relation for collisional quenching, where I_0 is the luminescence emission intensity in the absence of a quencher, I is the intensity in the presence of a quencher, K_{SV} is the Stern-Volmer quenching constant and [Q] is the concentration of the quencher

Here, when $\frac{I_0}{I}$ is plotted against [Q], known as a Stern-Volmer plot, a straight line of gradient K_{SV} (which is the product of k_q and τ_0) is observed, as shown in Figure 1.5.

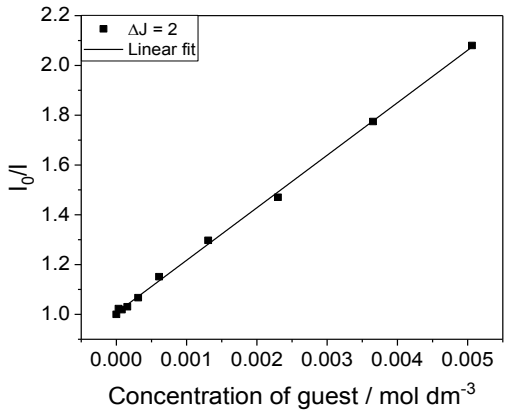


Figure 1.5 Example straight line Stern-Volmer plot indicating collisional quenching (taken from data discussed in Chapter 10)

If the fluorophore instead binds with another molecule to form an adduct, and this adduct is not luminescent (static quenching), the following equation (Equation 1.8) applies:

$$\frac{I_0}{I} = 1 + K_a[Q]$$

Equation 1.8 Stern-Volmer relation for static quenching, where I_0 is the luminescence emission intensity in the absence of a quencher, I is the intensity in the presence of a quencher, K_a is the association constant and [Q] is the concentration of the quencher

The luminescence lifetime is independent of static quenching as only the emissive species are observed, however the luminescence intensity will decrease as there are fewer fluorophores in solution. This case also gives a straight line Stern-Volmer plot, however increasing the temperature decreases the gradient of the line, whereas for collisional quenching, increasing the temperature would increase the gradient of the line due to more collisions in solution.

If both static and dynamic quenching occur in the same solution, the relationship is described by Equation 1.9:

$$\frac{I_0}{I} = (1 + k_q \tau_0 [Q])(1 + K_a [Q])$$

Equation 1.9 Stern-Volmer relation for combined quenching, where I_0 is the luminescence emission intensity in the absence of a quencher, I is the intensity in the presence of a quencher, k_q is the rate constant for quenching, τ_0 is the excited state lifetime in the absence of a quencher, K_a is the association constant and [Q] is the concentration of the quencher

This gives a Stern-Volmer plot with an upwards curve due to the $[Q]^2$ term, as seen in Figure 1.6.

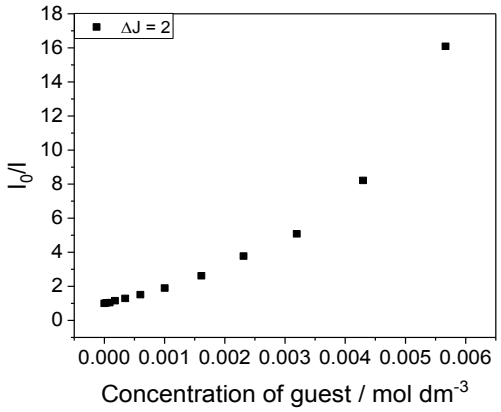


Figure 1.6 Stern-Volmer plot with upwards curve due to combined static and dynamic quenching (example taken from data discussed in Chapter 10)

As the lifetime is unaffected by the presence of a quencher, a Stern-Volmer plot with $\frac{\tau_0}{\tau}$ on the *y*-axis rather than $\frac{I_0}{I}$ would give a straight line.

More complicated cases are possible, such as the presence of both accessible and inaccessible fluorophore populations, where a Stern-Volmer plot gives a curve approaching a plateau as seen in Figure 1.7.

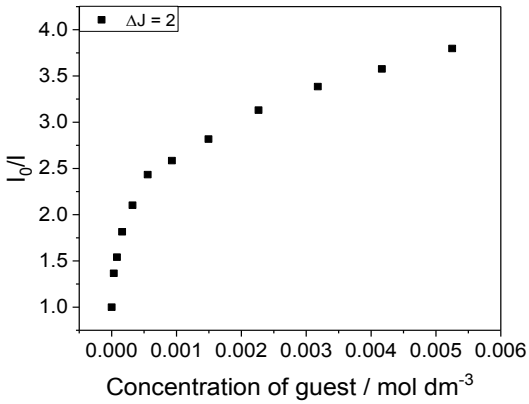


Figure 1.7 Stern-Volmer plot with a curve approaching a plateau due to two fluorophore populations (example taken from data discussed in Chapter 10)

For the systems investigated in this thesis, though the complex:guest adducts formed are not typically non-luminescent, they do typically have different luminescence properties to the original unbound complex.

1.5 NMR

The lanthanide induced shift (LIS) is the shift induced in the chemical shift of nuclei in the presence of paramagnetic lanthanides by interaction with the unpaired electrons, and has contact and pseudocontact contributions. The contact shift originates from a through-bond transmission of unpaired electron-spin density of the lanthanide ion to the nucleus in question, and the pseudocontact shift arises from through-space dipolar interaction between the magnetic moments of the unpaired electrons on the lanthanide ion and the affected nucleus.[25,35,36]

The total shift is made up of the LIS, and a contribution from diamagnetic shift which is usually small except for the donor atoms of a ligand bound to a lanthanide ion. Diamagnetic shift is a result of the redistribution of electron density within a ligand upon binding to a lanthanide ion, due to conformational changes, inductive effects, and direct field effects.[35]

The observed shift is therefore expressed as shown in Equation 1.10:

$$\Delta_{obs} = \Delta_c + \Delta_p + \Delta_d$$

Equation 1.10 Where Δ_{obs} is the observed shift, Δ_c is the contact contribution, Δ_p is the pseudocontact shift, and Δ_d is the diamagnetic shift

The contact shift is given in Equation 1.11:

$$\Delta_c = \langle S_Z \rangle \frac{\mu_B}{3kT\gamma_I} \frac{A}{\hbar} 10^6$$

Equation 1.11 Where Δ_c is the contact shift in ppm, $\langle S_z \rangle$ is the reduced value of the average spin polarisation, μ_B is the Bohr magneton, k is the Boltzmann constant, T is the absolute temperature, γ_I is the gyromagnetic ratio of the nucleus in question, and $A/\hbar$ is the hyperfine coupling constant in rad s^{-1}

The pseudocontact shift, assuming that the ligand field splitting of the lowest J state in the lanthanide complex is small compared to kT, is given by Equation 1.12, calculated by Bleaney:[37,38]

$$\Delta_p = D_1 \frac{(3\cos^2\theta - 1)}{r^3} + D_2 \frac{(\sin^2\theta \cos 2\phi)}{r^3}$$

Equation 1.12 Where Δ_p is the pseudocontact shift, D_1 and D_2 are constants taking into account ligand field coefficients and geometry-independent constants, and r, θ, and ϕ are the spherical coordinates of the observed nucleus with respect to a lanthanide ion at the origin

For axially symmetric systems, the second term vanishes so this may be simplified to Equation 1.13:

$$\Delta_p = C\left(\frac{(3\cos^2\theta - 1)}{r^3}\right)$$

Equation 1.13 Where Δ_p is the pseudocontact shift, C is a proportionality constant related to D_1 and D_2 and the Euler angles that define the position of the effective axis with respect to the principal magnetic susceptibility axis, and r and θ are spherical coordinates of the observed nucleus with respect to a lanthanide ion at the origin

The physical manifestation of this is that ^{1}H NMR spectra of lanthanide complexes have

large ranges of chemical shift and often broad resonances. Typical ^{1}H chemical shift ranges are −50 to +50 ppm for europium complexes, −150 to +150 ppm for ytterbium, and −500 to +500 ppm for terbium.

There are limitations to Bleaney theory,[37,38] such as its breakdown for systems with ligand field splitting greater than kT, and it does not take into account the contribution of higher order ligand field terms, anisotropic electron distribution,[39] the variation in position of the principal magnetic axis,[40] and systems with J-mixing instead of Russell-Saunders coupling. For more complicated systems, many more parameters may be added to Equation 1.13.

In cases of complexes related to Ln.DOTA it has been shown that the paramagnetic effects on ^{1}H NMR of complexes may be attributed entirely to pseudocontact shift.[41]

1.6 Isomerism

DOTA^{-} and DO3A-derived complexes of lanthanides are found to adopt different geometries, namely the square antiprism (SAP) and twisted square antiprism (TSAP) conformers. SAP is identified by its twist angle of 40°, whereas 30° is seen for TSAP. In DOTA, the four nitrogen atoms form one square face of the prism below the lanthanide ion, and the four carboxylate oxygen atoms the other face, above the lanthanide ion.[42] The ninth, apical, coordination site is occupied by a water molecule, which undergoes 50 times faster exchange when bound to TSAP species than to SAP.[43]

It is possible to interconvert between these isomers, as shown in Figure 1.8; the energy barrier for arm rotation is far smaller for DO3A than for DOTA, meaning that DO3A interconversion is fast on an NMR timescale and gives broad resonances, whereas slow

interconversion of DOTA on an NMR timescale gives sharp peaks.[44,45] Larger, earlier lanthanide ions – Ln^{3+} to Pm^{3+} – tend to adopt the more spacious TSAP geometry, and complexes of Sm^{3+} to Lu^{3+} tend to be found in SAP conformations.[46]

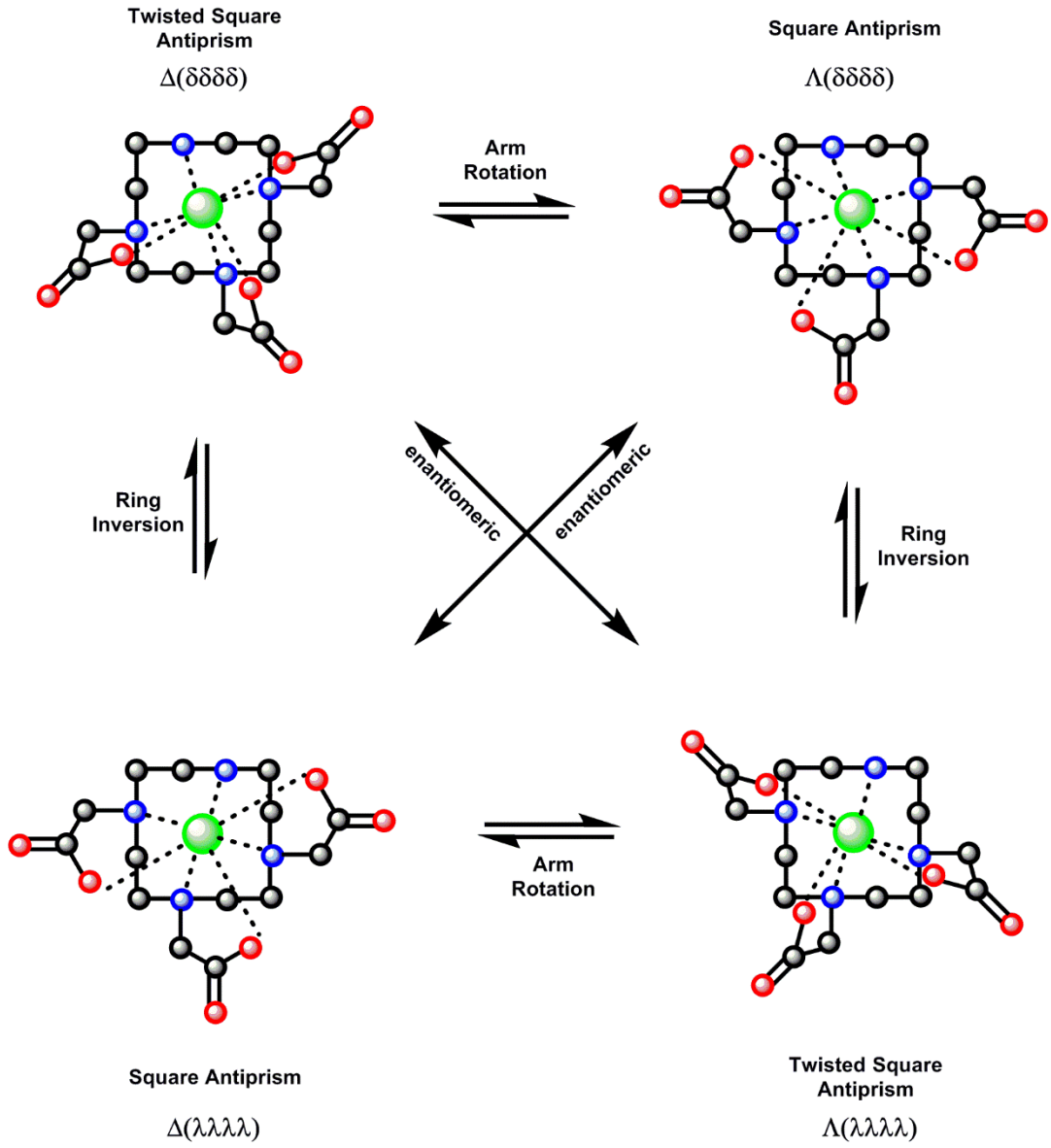


Figure 1.8 Interconversion between SAP and TSAP isomers of DO3A-based complexes[41]

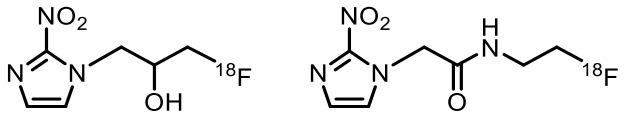
The ratio of the NMR resonances of the axial and equatorial ^1H nuclei indicates which of the SAP and TSAP species dominates in solution. For europium complexes, ^1H NMR resonances shifted to higher chemical shift values correspond to protons lying within the McConnell cone and relatively close to the magnetic axis, whereas those shifted to lower chemical shifts are closer to equatorial positions.[37] Typically, a chemical shift of 15 to

20 ppm for a europium-containing complex signals the presence of the TSAP conformer, and 30 to 40 ppm suggests that the SAP conformer dominates.

1.7 Hypoxia

Early detection of cancer improves chances of successful treatment.[47] Low oxygen concentration, hypoxia, is a marker of many human cancers and increases the likelihood of a poor prognosis and metastasis.[48] This is particularly relevant for dense and fast-growing tumours which outgrow their blood supply and therefore contain regions with low oxygen concentration. Hypoxic tumours are often chemotherapy- and radiotherapy-resistant.[49]

Nitroaromatic species such as 2-nitroimidazole compounds accumulate within hypoxic tissue,[50] due to reduction to hydroxylamine or amine compounds, followed by subsequent reaction to form molecular species which may bind to molecules endogenous to the cell, such as glutathione.[51] Different functionalisation of these types of compounds allows their use as imaging agents or hypoxia-selective targeted drugs.[52] Two example nitroaromatic radiotracer PET agents, FMISO and FETA, are shown in Figure 1.9.[52,53]



^{18}F-FMISO ^{18}F-FETA

V **VI**

Figure 1.9 PET imaging probes FMISO and FETA

The Warburg effect observes that cancer cells respire differently to those in healthy tissue,[54] leading to a different balance of concentrations of species from the glycolytic pathway (Figure 1.10). Cancerous cells experience high rates of glycolysis and subsequent lactic acid fermentation rather than the low-rate glycolysis followed by pyruvate oxidation seen in the aerobic respiration of healthy cells. For cancer cells this process occurs in the cytosol rather

than in the mitochondria.[55–60] However this increased rate of glycolysis – up to 200 times greater – occurs even in the presence of abundant oxygen.

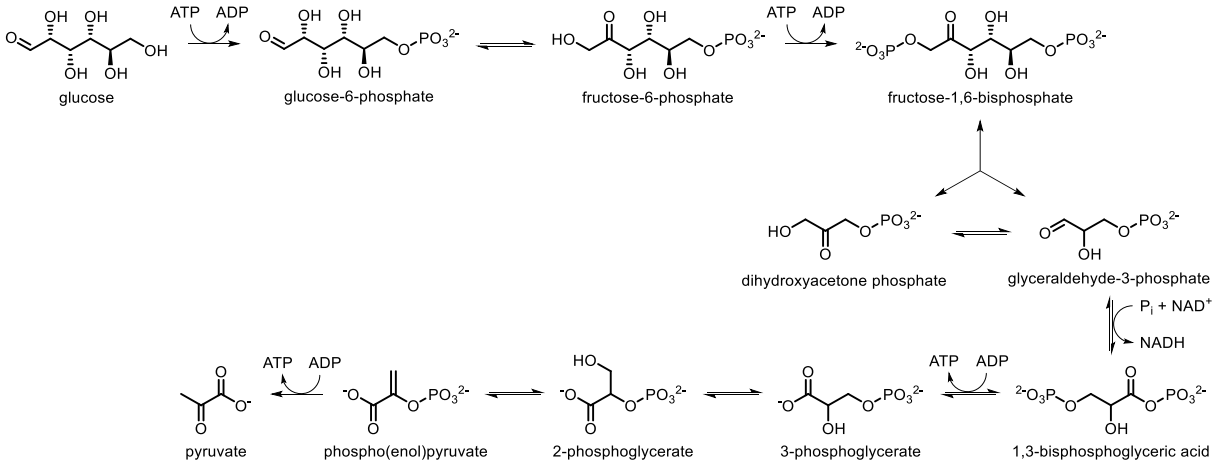


Figure 1.10 Overview of the glycolytic pathway[61]

Thus, complexes which bind selectively to biomarkers of hypoxia but whose luminescence is not perturbed by the local oxygen concentration would be desirable.

1.8 MRI

Magnetic resonance imaging is a non-invasive diagnostic technique widely utilised in medicine, which has the benefit of providing imaging with high spatial resolution and without ionising radiation. Commonly this is used to image the brain, joints, soft tissues, lesions, and tumours.[62,63]

The MRI signal is proportional to the abundance of MRI-active nuclei. A gradient field is used to provide spatial resolution, whereas a uniform field is used in NMR. The T_1 and T_2 relaxation rates are dependent on the environment. These two processes are summarised in Table 1.1. T_1 depends on mobility of molecules and therefore on the viscosity of the solvent. MRI usually relies on the relaxation of the ^1H nuclei in water molecules in the different environments in the body, although ^{31}P MRI of phosphorus-containing metabolites has also

been explored. The contrast between different types of tissues such as fluids, muscles, organs, and fat or bone marrow is easy to observe.

T_1 weighted images		**T_2 weighted images**
Inversion recovery	Saturation recovery	Spin-echo pulse
• 180° pulse • 90° pulse after t_i • $t_i > T_1$ Normal population before 90° pulse Large signal, bright image • $t_i \sim T_1$ Magnetisation does not recover between pulses Weak/non-existent signal	• Series of 90° pulses separated by t_R • $t_R \sim T_1$ Large signal, bright image • $t_R \sim T_2$ Magnetisation does not recover between pulses Weak signal	• 90° pulse • 180° pulse after t_e

Table 1.1 Differences between T_1 and T_2 weighted MRI

Figure 1.11 shows a proton density weighted image and a T_1 weighted image both of the same location within a knee. The brighter intensities in the proton density weighted image a) show areas with a greater abundance of protons – particularly water or lipid molecules, as the signal is directly proportional to the number of protons in a voxel. Shorter T_1 lifetimes correspond to a rapid recovery of longitudinal magnetisation. Therefore, in the T_1 weighted image b), tissues with shorter T_1 lifetimes (fat and bone marrow) appear brighter as more scans are possible in a given time, and tissues with longer T_1 lifetimes (fluid) appear dark. In T_2 weighted imaging, brighter areas correspond to longer T_2 lifetimes (fat and fluid) as these are associated with a slower decay of transverse magnetisation and therefore a stronger signal.

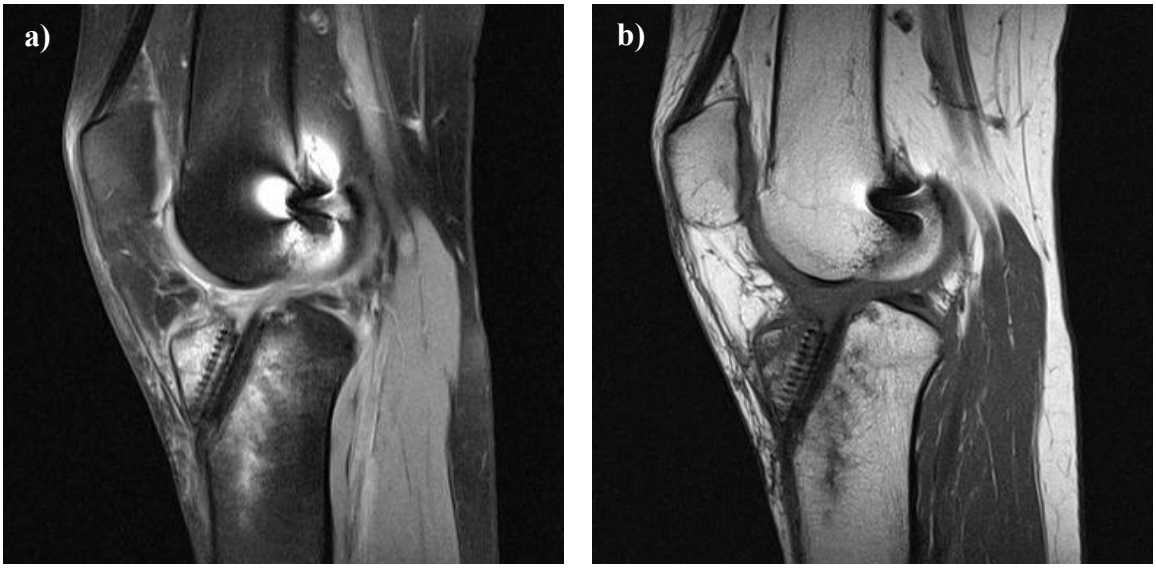
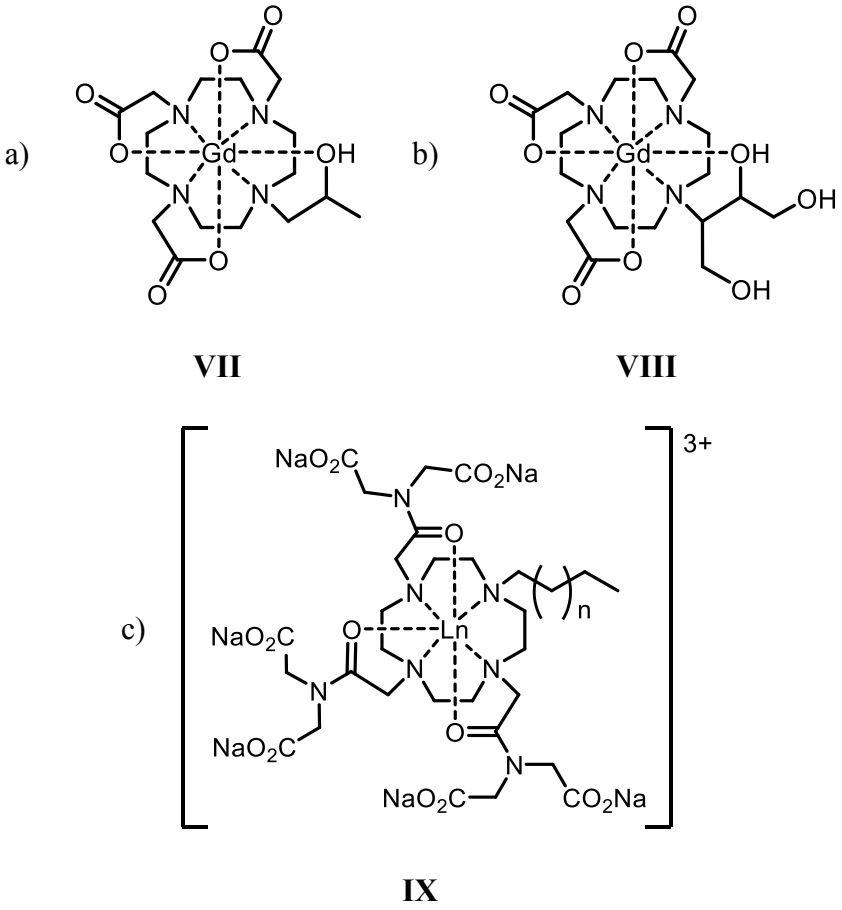


Figure 1.11 a) proton density (PD) with fat saturation (fat appears dark) weighted image of a knee, b) T_1 weighted MRI image of the same knee at approximately the same location (both images show a streak artefact from a titanium screw in the femur)

For tissues that are more similar to each other, for example cancerous tissue and surrounding tissue, protons in healthy tissue have different relaxation rates to those in diseased tissue.[64–66] Contrast agents may be administered to a patient to enhance the rate of relaxation of the protons and thus improve the contrast in the scan, as more scans can be run in a given time. These include T_1 agents containing gadolinium(III) or manganese(II), as unpaired electrons have a greater magnetic moment than protons. The paramagnetic metal ions have vacant coordination sites to accommodate inner-sphere water molecules which are in exchange with the bulk water. Good contrast agents have large relaxivities per mmol of gadolinium, and therefore require a lower dose of contrast agent. Gadolinium ions must be bound securely in the ligand as free lanthanides are toxic – the Ln^{3+} ion is a similar size to Ca^{2+} but binds more strongly due to its higher charge – and gadolinium contrast agents are associated with nephrogenic systemic fibrosis.[62,63,67–72] Typically, the Gd^{3+} ion is bound in DOTA (Figure 1.2) or a DO3A-derivatised ligand to give compounds such as **VII**, **VIII**, and **IX** shown in Figure 1.12.



VII **VIII**

IX

Figure 1.12 a) Gadoteridol (brand name ProHance®), b) Gadobutrol (brand name Gadovist®), c) micellar complex with application as a luminescent (Ln = Eu) or MRI (Ln = Gd) contrast agent (n = 1, 9) reported by Gunnlaugsson et al.[73]

1.9 Optical imaging

Optical imaging agents are again non-invasive and are used both *in vivo* and in cell imaging, though their utility is restricted by the limited penetration depth of light as it is absorbed by tissue.[13,74–76] Their use extends to intra-operative fluorescence-guided surgery – an example is given in Figure 1.13.[77–79] Longer wavelength sensitisation is preferable in order to allow deeper tissue penetration whilst reducing tissue damage and tissue autofluorescence.

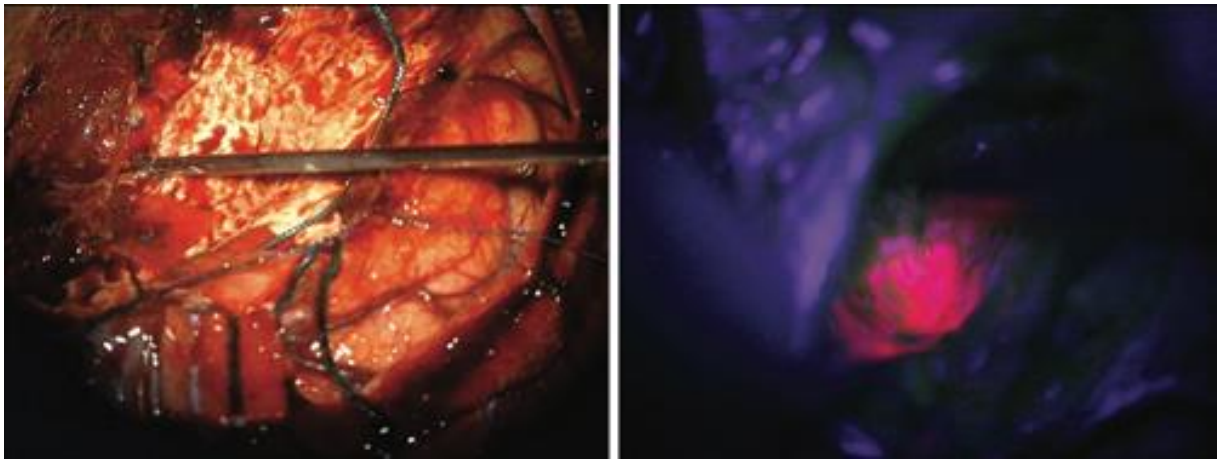
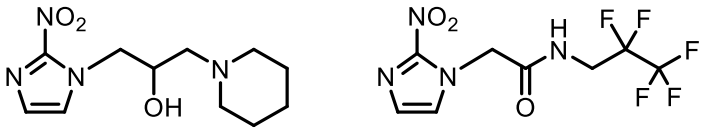


Figure 1.13 Intraoperative photographs under normal light (left) and blue light (right) showing localisation of administered 5-aminolevulinicacid in a patient's glioblastoma[79]

In 1976, Varghese *et al.* reported that ^{14}C-labelled misonidazole formed adducts in hypoxic cells *in vitro* and *in vivo*.[80] It was subsequently found that these types of compounds formed adducts with thiol groups in proteins, peptides and amino acids.[81–84] Chapman *et al.* then used this moiety as a marker for hypoxic cells.[85]

X and **XI** are two examples of structures of commercial nitroaromatic imaging agents for hypoxia, given in Figure 1.14.[86,87] Antibodies containing a fluorescent tag have been synthesised which bind to adducts of EF5, giving quantitative staining of affected tissue.

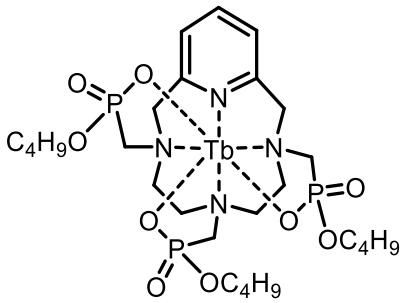


Pimonidazole (Hypoxyprobe™-1) — **X**

EF5 — **XI**

Figure 1.14 Pimonidazole and EF5 hypoxia markers

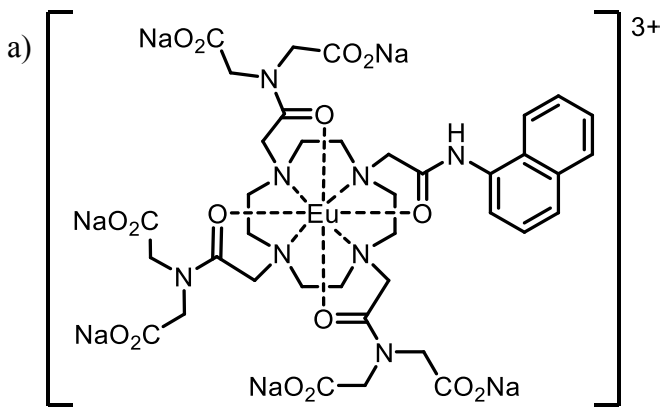
The most prevalent lanthanide ions in optical imaging are Sm^{3+}, Eu^{3+}, Tb^{3+}, Dy^{3+}, and Yb^{3+}.[25] One of the earliest examples of a luminescent lanthanide-containing cyclen-based complex for *in vivo* and *in vitro* imaging was the terbium complex **XII** able to signpost abnormal tissue such as adenocarcinoma cells, shown in Figure 1.15.[88]

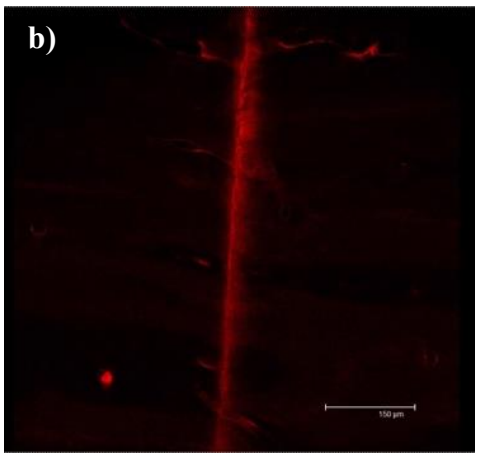


XII

Figure 1.15 Terbium complex for imaging abnormal tissue published by Bornhop et al.[88]

More recently, Gunnlaugsson *et al.* reported a functionalised Eu.DO3A complex (**XIII** in Figure 1.16) able to target mechanically damaged areas of bone such as scratches or microcracks.[89] Confocal fluorescence microscopy showed changes in luminescence emission upon binding to the exposed Ca^{2+} sites on the bone surface.

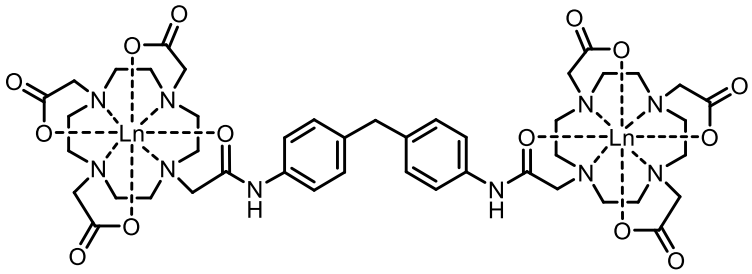




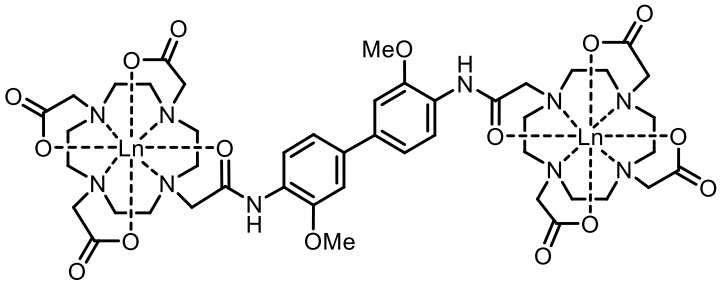
XIII

Figure 1.16 a) Functionalised europium complex for imaging the damaged hydroxyapatite lattice of bone, b) confocal laser-scanning microscopy image after bone sample was immersed in a 10^{-3} M solution of the complex for 24 hours[89]

Binuclear lanthanide complexes have been used in cellular imaging. **XIV** in Figure 1.17 exhibited binding to human serum albumin.[90] When the bridging unit was changed from a biphenyl-methylene moiety to a dimethoxy-biphenyl spacer to give **XV**, binding was inhibited.



XIV



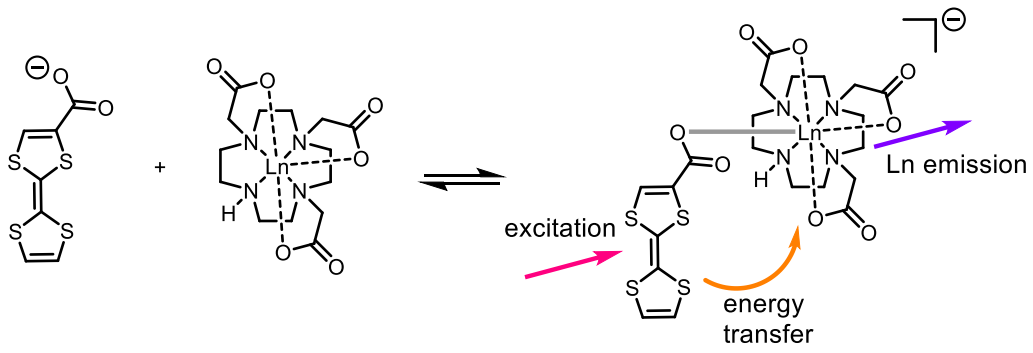
XV

Figure 1.17 Binuclear complexes reported by Wong et al. that bind human serum albumin (Ln = Eu, Gd, Tb)[90]

1.10 Self-assembly

Self-assembly has been used to build macromolecular functional structures, and electrostatic interactions with the highly charge-dense lanthanide elements have been utilised in this field.[91,92]

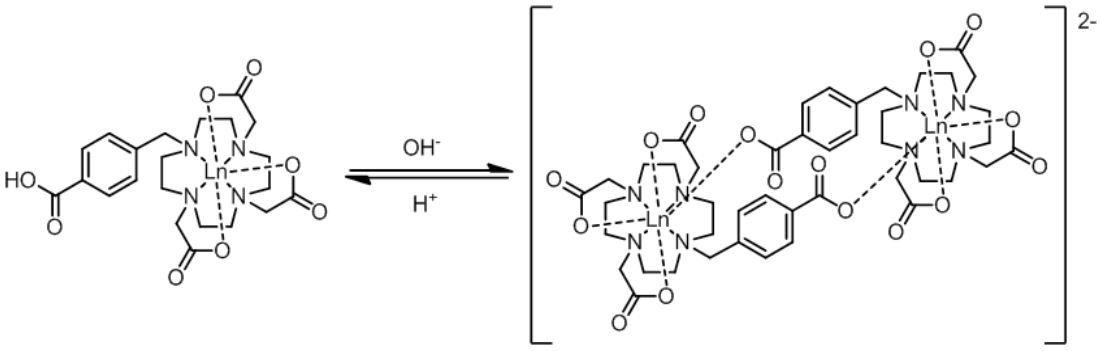
Work in the Faulkner group in this area began by exploiting the antenna effect to screen chromophores as sensitisers for simple mononuclear complexes with DO3A.[93]



XVI XVII XVIII

Figure 1.18 Lanthanide luminescence switched on by binding of Ln.DO3A to an anionic chromophore[93]

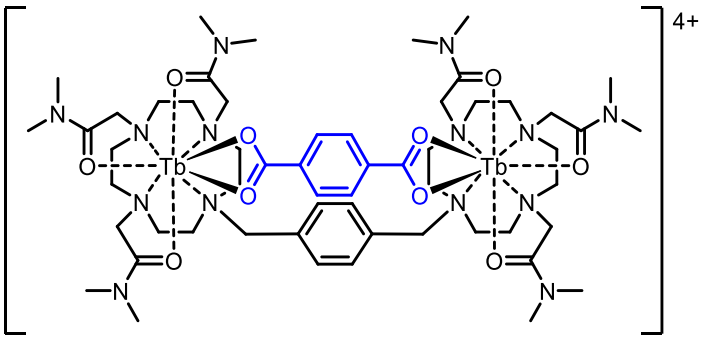
In the example shown in Figure 1.18, the lanthanide luminescence was switched on by binding of **XVII** to a suitable chromophore (**XVI**) to give the luminescent adduct **XVIII**. Later came work involving pH-dependent luminescence, shown in Figure 1.19, where electrostatic binding to the deprotonated carboxylate in basic conditions gave rise to increased luminescence intensity due to displacement of quenchers in the lanthanide solvation sphere.[94]



XIX **XX**

Figure 1.19 Lanthanide luminescence intensity increased by reducing the degree of quenching[94]

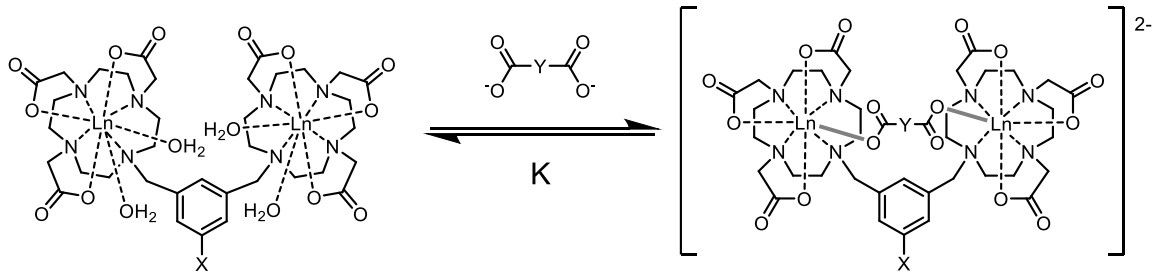
In 2003, Faulkner *et al.* reported synthesis of a series of binuclear *p*-xylyl lanthanide-DO3A complexes.[95] Subsequently, Gunnlaugsson *et al.* investigated the interaction of the similar binuclear *p*-xylyl terbium-DO3AM complex **XXI** (Figure 1.20) with mono- and dicarboxylate species in solution.[96] The terbium luminescence intensity and lifetime was perturbed by the presence of an array of carboxylates of differing sizes.



XXI

Figure 1.20 Binding of a terbium binuclear complex with terephthalic acid[96]

Similar behaviour was later studied by the Faulkner group. Substituted *m*-xylyl moieties have formed the basis for binuclear lanthanide complexes that exhibit high binding affinities to an array of dianionic guests, in what could be considered to be a reverse analogy of the chelate effect, where instead a single dianion is bound by two metal centres. The amino-substituted *m*-xylyl complex **XXII** was reported by Tilney *et al.* in 2011 to selectively bind to isophthalate over other aryldicarboxylates.[97] The proposed binding mechanism is given in Figure 1.21. It was possible to monitor the change in luminescence lifetime or the change in luminescence intensity over the course of a titration, and fitting the resulting binding isotherms with the iterative fitting software DynaFit®[98] allowed the calculation of binding constants. More data points for fitting may also be extracted by dividing the intensity of the hypersensitive peak by the intensity of each of the other peaks. In these systems, Stern-Volmer plots offer an effective way to ascertain whether the change in luminescence intensity is due to a binding event or simply due to collisional quenching.

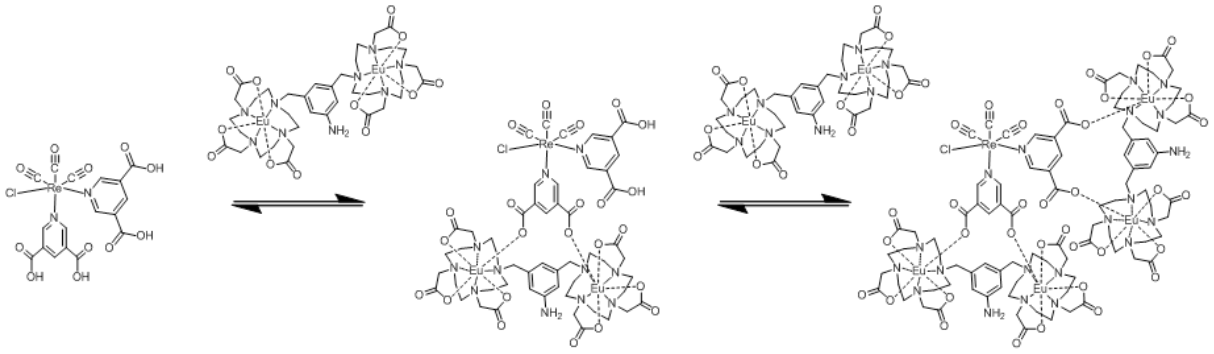


XXII **XXIII**

Figure 1.21 Proposed binding method of the dicarboxylate guest to the host lanthanide complex where X = NO_2, NH_2; Y = aromatic ring[97]

In 2013 this work was expanded by Hill *et al.* by moving into aqueous conditions, studying dinicotinate and lanthanide-appended isophthalate derivatives in their interactions with binuclear complexes in a range of different buffers at a range of different pH values, and subsequently the effect of varying the binuclear complex was investigated. This proved that changing the remote substituents on the aromatic ring had significant implications for binding.[99,100]

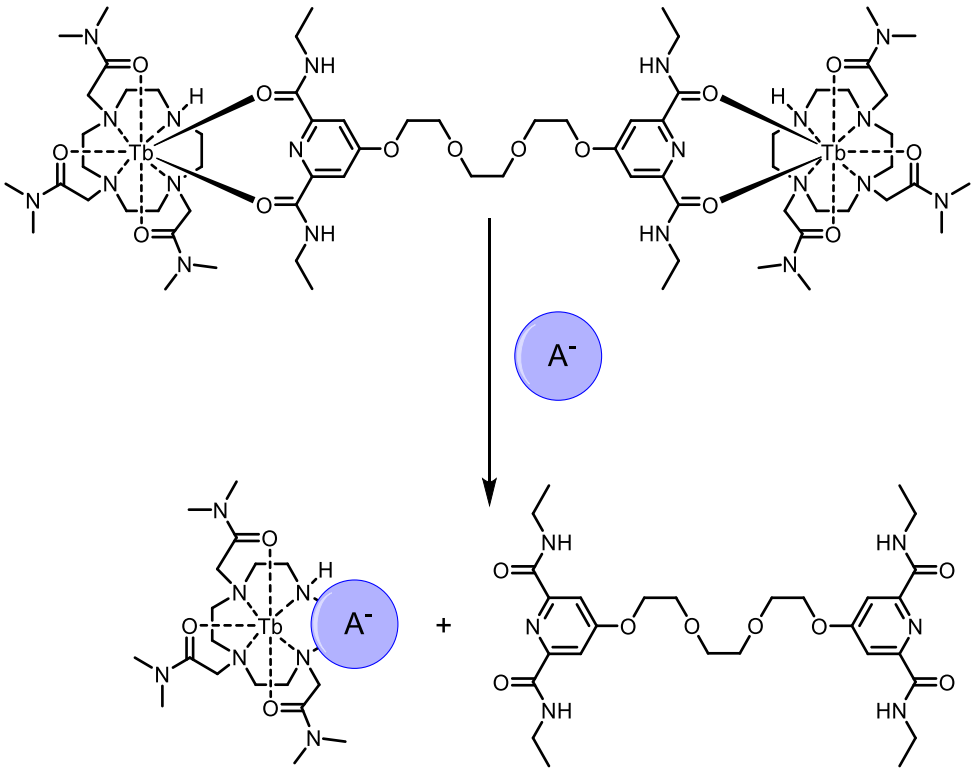
The group's previous *d-f* hybrid work was also extended by self-assembly of the aforementioned binuclear lanthanide complex **XXII** with the rhenium complex **XXIV** to give the first example of a higher order supramolecular structure defined by lanthanide-carboxylate interactions (**XXVI** in Figure 1.22).[101]



XXIV **XXV** **XXVI**

Figure 1.22 The first example of a higher order supramolecular structure defined by lanthanide-carboxylate interactions[101]

Self-assembly has been utilised in sensing. The ternary terbium complex **XXVII**, able to bind phosphate and nitrate, was reported by Gunnlaugsson *et al.* in 2014.[102] In this displacement assay technique, shown in Figure 1.23, an incoming anion displaced a labile ligand from the ternary complex, changing the photophysical properties of the assembly. Upon titration of phosphate, luminescence was quenched as the chelidamic acid-derived ligand **XXIX** was displaced.

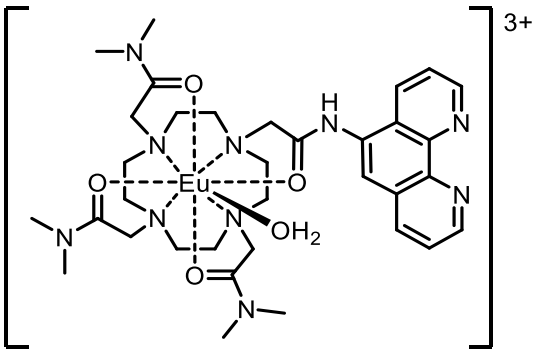


XXVII

XXVIII **XXIX**

Figure 1.23 Displacement assay with a terbium ternary complex reported by Gunnlaugsson et al., where A^- is an added anion[102]

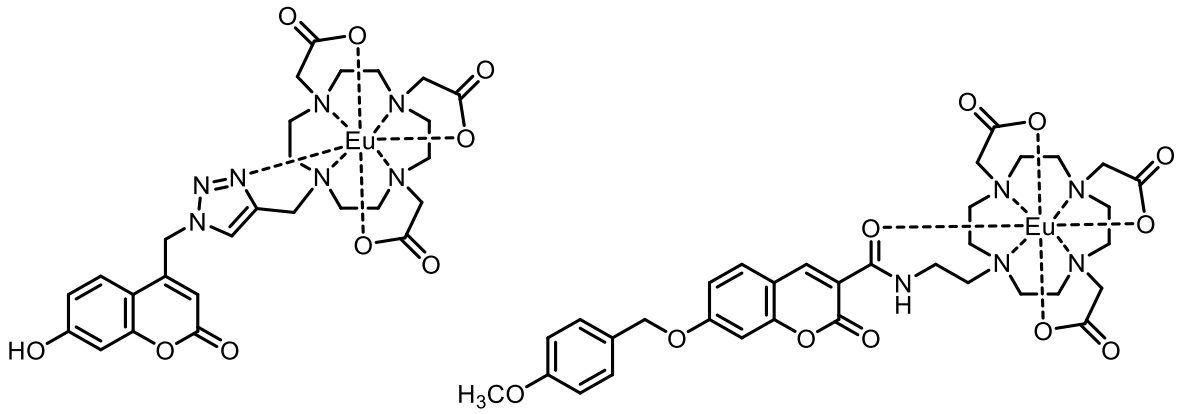
More recently, the pH-sensitive europium-based probe **XXX** in Figure 1.24 was presented, with the ability to detect the urease-mediated hydrolysis of urea, a marker of the onset of catheter-associated urinary tract infections. The luminescence of this probe was quenched upon the increase of pH associated with the enzymatic conversion of urea to ammonia and carbon dioxide.[103]



XXX

Figure 1.24 Europium probe able to detect the urease-mediated hydrolysis of urea[103]

Borbas[104–109] and Chauvin[110,111] have extensively studied energy transfer in coumarin-appended lanthanide complexes and exploited a selection of these complexes as sensors and probes. Borbas *et al.* have synthesised a diverse library of coumarin- and carbostyril-derived lanthanide-DO3A complexes to this end, examples of which are shown in Figure 1.25.



XXXI **XXXII**

*Figure 1.25 Coumarin-appended lanthanide complex **XXXI** reported by Borbas et al. (left) and coumarin-appended $ONOO^-$ sensor **XXXII** (right)*[107]

1.11 Aims and objectives

The aim of this project was to establish the potential to tune binding in binuclear lanthanide systems. The objectives of this project were to explore in detail substrate binding with binuclear complexes and to investigate the affinity of a range of guests of biological significance and to understand their binding behaviour, and to synthesise complexes with more effective sensitising chromophores.

The next chapter extends the introduction with specific literature examples of binding of carboxylates to the types of complexes studied in this thesis.

The remainder of this thesis is split into two parts: Part A explains the synthesis of the lanthanide complexes studied in this work and Part B investigates their binding to an array

of anions, with Chapter 7 providing a general overview of anion binding, before subsequent chapters consider specific groups of anions.

1.12 References

(1) *IUPAC Compendium of Chemical Terminology*; Nič, M.; Jirát, J.; Košata, B.; Jenkins, A.; McNaught, A., Eds.; IUPAC: Research Triangle Park, NC, 2009.
(2) van Grieken, R.; de Bruin, M. *Pure Appl. Chem.* **1994**, *66*.
(3) Melhuish, W. H. *Pure Appl. Chem.* **1984**, *56*.
(4) Verhoeven, J. W. *Pure Appl. Chem.* **1996**, *68*.
(5) Shriver, D. F.; Atkins, P. W.; Overton, T. L.; Rourke, J. P.; Weller, M. T.; Armstrong, F. *Inorganic Chemistry*; 4th ed.; Oxford University Press, 2006.
(6) Binnemans, K. *Coord. Chem. Rev.* **2015**, *295*, 1–45.
(7) *Lanthanide and Actinide Chemistry and Spectroscopy*; Edelstein, N. M., Ed.; ACS Symposium Series; American Chemical Society: Washington, D. C., 1980; Vol. 131.
(8) *Lanthanide Luminescence: Photophysical, Analytical and Biological Aspects*; Hänninen, P.; Härmä, H., Eds.; Springer Series on Fluorescence; Springer-Verlag: Berlin, Heidelberg, 2011; Vol. 7.
(9) Liu, G.; Jacquier, B. *Spectroscopic Properties of Rare Earths in Optical Materials*; Hull, R.; Parisi, J.; Osgood, R. M.; Warlimont, H.; Liu, G.; Jacquier, B., Eds.; Springer Series in Materials Science; Springer-Verlag: Berlin/Heidelberg, 2005; Vol. 83.
(10) Carnall, W. T.; Fields, P. R.; Rajnak, K. *J. Chem. Phys.* **1968**, *49*, 4450–4455.
(11) Carnall, W. T.; Fields, P. R.; Rajnak, K. *J. Chem. Phys.* **1968**, *49*, 4424–4442.
(12) Carnall, W. T.; Fields, P. R.; Rajnak, K. *J. Chem. Phys.* **1968**, *49*, 4443–4446.
(13) Bünzli, J.-C. G.; Piguet, C. *Chem. Soc. Rev.* **2005**, *34*, 1048–1077.
(14) Jørgensen, C. K.; Judd, B. R. *Mol. Phys.* **1964**, *8*, 281–290.
(15) Judd, B. R. *J. Chem. Phys.* **1966**, *44*, 839.
(16) Mason, S. F.; Peacock, R. D.; Stewart, B. *Chem. Phys. Lett.* **1974**, *29*, 149–153.
(17) Judd, B. R. *Phys. Rev.* **1962**, *127*, 750–761.
(18) Ofelt, G. S. *J. Chem. Phys.* **1962**, *37*, 511.
(19) Weissman, S. I. *J. Chem. Phys.* **1942**, *10*, 214–217.
(20) Yuster, P.; Weissman, S. I. *J. Chem. Phys.* **1949**, *17*, 1182–1188.
(21) Weissman, S. I. *J. Chem. Phys.* **1950**, *18*, 1258–1262.
(22) Heller, A.; Wasserman, E. *J. Chem. Phys.* **1965**, *42*, 949–955.
(23) Förster, T. 10th Spiers Memorial Lecture. Transfer mechanisms of electronic excitation. *Discussions of the Faraday Society*, 1959, *27*, 7.
(24) Dexter, D. L. *J. Chem. Phys.* **1953**, *21*, 836.
(25) Long, N. J.; Wong, W.-T. *The Chemistry of Molecular Imaging*; Long, N.; Wong, W.-T., Eds.; 1st ed.; John Wiley & Sons, Inc., 2015.
(26) Gonçalves e Silva, F. R.; Malta, O. L.; Reinhard, C.; Güdel, H.-U.; Piguet, C.; Moser, J. E.; Bünzli, J.-C. G. *J. Phys. Chem. A* **2002**, *106*, 1670–1677.
(27) Beeby, A.; Faulkner, S.; Williams, J. A. G. *J. Chem. Soc., Dalt. Trans.* **2002**, 1918–1922.
(28) Lazarides, T.; Sykes, D.; Faulkner, S.; Barbieri, A.; Ward, M. D. *Chem. Eur. J.* **2008**, *14*, 9389–9399.
(29) Braslavsky, S. E. *Pure Appl. Chem.* **2007**, *79*.
(30) Beeby, A.; Clarkson, I. M.; Dickins, R. S.; Faulkner, S.; Parker, D.; Royle, L.; de Sousa, A. S.; Williams, J. A. G.; Woods, M. *J. Chem. Soc., Perkin Trans. 2* **1999**, *2*, 493–504.
(31) Horrocks, W. D.; Sudnick, D. R. *J. Am. Chem. Soc.* **1979**, *101*, 334–340.
(32) Sudnick, D. R.; Horrocks, W. D. *Acc. Chem. Res.* **1981**, *14*, 384–392.
(33) Supkowski, R. M.; Horrocks, W. D. *Inorganica Chim. Acta* **2002**, *340*, 44–48.
(34) Valeur, B. *Molecular Fluorescence: Principles and Applications*; Wiley-VCH Verlag GmbH: Weinheim, FRG, 2001.
(35) Peters, J. A.; Huskens, J.; Raber, D. J. *Prog. Nucl. Magn. Reson. Spectrosc.* **1996**, *28*, 283–350.
(36) Desreux, J. F.; Reilley, C. N. *J. Am. Chem. Soc.* **1976**, *98*, 2105–2109.
(37) Bleaney, B. *J. Magn. Reson.* **1972**, *8*, 91–100.
(38) Bleaney, B.; Dobson, C. M.; Levine, B. A.; Martin, R. B.; Williams, R. J. P.; Xavier, A. V. *J. Chem. Soc. Chem. Commun.* **1972**, 791b.
(39) Rinehart, J. D.; Long, J. R. *Chem. Sci.* **2011**, *2*, 2078.

(40) Boulon, M.-E.; Cucinotta, G.; Luzon, J.; Degl'Innocenti, C.; Perfetti, M.; Bernot, K.; Calvez, G.; Caneschi, A.; Sessoli, R. *Angew. Chem. Int. Ed.* **2013**, *52*, 350–354.
(41) Aime, S.; Botta, M.; Ermondi, G. *Inorg. Chem.* **1992**, *31*, 4291–4299.
(42) Parker, D. *Chem. Soc. Rev.* **2004**, *33*, 156–165.
(43) Aime, S.; Barge, A.; Botta, M.; De Sousa, A. S.; Parker, D. *Angew. Chem. Int. Ed.* **1998**, *37*, 2673–2675.
(44) Cakić, N.; Verbić, T. Ž.; Jelić, R. M.; Platas-Iglesias, C.; Angelovski, G. *Dalton Trans.* **2016**, *45*, 6555–6565.
(45) Placidi, M. P.; Natrajan, L. S.; Sykes, D.; Kenwright, A. M.; Faulkner, S. *Helv. Chim. Acta* **2009**, *92*, 2427–2438.
(46) Aime, S.; Botta, M.; Fasano, M.; Marques, M. P. M.; Geraldes, C. F. G. C.; Pubanz, D.; Merbach, A. E. *Inorg. Chem.* **1997**, *36*, 2059–2068.
(47) WHO | Early detection of cancer http://www.who.int/cancer/detection/en/.
(48) Semenza, G. L. *Cancer Metastasis Rev.* **2007**, *26*, 223–224.
(49) Ren, Y.; Hao, P.; Dutta, B.; Cheow, E. S. H.; Sim, K. H.; Gan, C. S.; Lim, S. K.; Sze, S. K. *Mol. Cell. Proteomics* **2013**, *12*, 485–498.
(50) Masaki, Y.; Shimizu, Y.; Yoshioka, T.; Feng, F.; Zhao, S.; Higashino, K.; Numata, Y.; Kuge, Y. *PLoS One* **2016**, *11*, e0161639.
(51) Masaki, Y.; Shimizu, Y.; Yoshioka, T.; Tanaka, Y.; Nishijima, K.; Zhao, S.; Higashino, K.; Sakamoto, S.; Numata, Y.; Yamaguchi, Y.; Tamaki, N.; Kuge, Y. *Sci. Rep.* **2015**, *5*, 16802.
(52) Xu, Z.; Li, X.-F.; Zou, H.; Sun, X.; Shen, B. *Oncotarget* **2017**.
(53) Rasey, J. S.; Hofstrand, P. D.; Chin, L. K.; Tewson, T. J. *J. Nucl. Med.* **1999**, *40*, 1072–1079.
(54) Warburg, O. *Science* **1956**, *123*, 309–314.
(55) Alfarouk, K. O.; Verduzco, D.; Rauch, C.; Muddathir, A. K.; Bashir, A. H. H.; Elhassan, G. O.; Ibrahim, M. E.; Orozco, J. D. P.; Cardone, R. A.; Reshkin, S. J.; Harguindey, S. *Oncoscience* **2014**, *1*, 777.
(56) Alfarouk, K. O. *J. Enzyme Inhib. Med. Chem.* **2016**, *31*, 859–866.
(57) Alfarouk, K. O.; Muddathir, A. K.; Shayoub, M. E. A. *Cancers* **2011**, *3*, 408–414.
(58) Gatenby, R. A.; Gillies, R. J. *Nat. Rev. Cancer* **2004**, *4*, 891–899.
(59) Kim, J.; Dang, C. V. *Cancer Res.* **2006**, *66*, 8927–8930.
(60) Vander Heiden, M. G.; Cantley, L. C.; Thompson, C. B. *Science* **2010**, *324*, 1029–1033.
(61) Berg, J. M.; Tymoczko, J. L.; Stryer, L. *Biochemistry*; 5th ed.; W H Freeman: New York, 2002.
(62) Brant, W. E.; de Lange, E. E. *Essentials of Body MRI*; Brant, W. E.; de Lange, E. E., Eds.; Oxford University Press, 2012.
(63) Merbach, A.; Helm, L.; Tóth, É. *The Chemistry of Contrast Agents in Medical Magnetic Resonance Imaging*; Merbach, A.; Helm, L.; Tóth, É., Eds.; 2nd ed.; John Wiley & Sons, Ltd: Chichester, UK, 2013.
(64) Damadian, R. *Science* **1971**, *171*, 1151–1153.
(65) Damadian, R.; Zaner, K.; Hor, D.; DiMaio, T. *Proc. Natl. Acad. Sci.* **1974**, *71*, 1471–1473.
(66) Damadian, R.; Goldsmith, M.; Minkoff, L. *Physiol. Chem. Phys.* **1977**, *9*, 97–100.
(67) Werner, E. J.; Avedano, S.; Botta, M.; Hay, B. P.; Moore, E. G.; Aime, S.; Raymond, K. N. *J. Am. Chem. Soc.* **2007**, *129*, 1870–1871.
(68) Bottrill, M.; Kwok, L.; Long, N. J. *Chem. Soc. Rev.* **2006**, *35*, 557–571.
(69) Terreno, E.; Castelli, D. D.; Viale, A.; Aime, S. *Chem. Rev.* **2010**, *110*, 3019–3042.
(70) Woods, M.; Woessner, D. E.; Sherry, A. D. *Chem. Soc. Rev.* **2006**, *35*, 500.
(71) Thomsen, H. S. *Radiol. Clin. North Am.* **2009**, *47*, 827–831.
(72) Molnár, E.; Camus, N.; Patinec, V.; Rolla, G. A.; Botta, M.; Tircsó, G.; Kálmán, F. K.; Fodor, T.; Tripier, R.; Platas-Iglesias, C. *Inorg. Chem.* **2014**, *53*, 5136–5149.
(73) Surender, E. M.; Comby, S.; Martyn, S.; Cavanagh, B.; Lee, T. C.; Brougham, D. F.; Gunnlaugsson, T. *Chem. Commun.* **2016**, *52*, 10858–10861.
(74) Faulkner, S.; Natrajan, L. S.; Perry, W. S.; Sykes, D. *Dalton Trans.* **2009**, 3890–3899.
(75) Montgomery, C. P.; Murray, B. S.; New, E. J.; Pal, R.; Parker, D. *Acc. Chem. Res.* **2009**, *42*, 925–937.
(76) New, E. J.; Congreve, A.; Parker, D. *Chem. Sci.* **2010**, *1*, 111–118.
(77) van Dam, G. M.; Themelis, G.; Crane, L. M. A.; Harlaar, N. J.; Pleijhuis, R. G.; Kelder, W.; Sarantopoulos, A.; de Jong, J. S.; Arts, H. J. G.; van der Zee, A. G. J.; Bart, J.; Low, P. S.; Ntziachristos, V. *Nat. Med.* **2011**, *17*, 1315–1319.
(78) Stummer, W.; Pichlmeier, U.; Meinel, T.; Wiestler, O. D.; Zanella, F.; Reulen, H.-J. *Lancet Oncol.* **2006**, *7*, 392–401.
(79) Lau, D.; Hervey-Jumper, S. L.; Chang, S.; Molinaro, A. M.; McDermott, M. W.; Phillips, J. J.; Berger, M. S. *J. Neurosurg.* **2016**, *124*, 1300–1309.

(80) Varghese, A. J.; Gulyas, S.; Mohindra, J. K. *Cancer Res.* **1976**, *36*, 3761–3765.
(81) Chacon, E.; Morrow, C. J.; Leon, A. A.; Born, J. L.; Smith, B. R. *Biochem. Pharmacol.* **1988**, *37*, 361–363.
(82) Raleigh, J. A.; Franko, A. J.; Koch, C. J.; Born, J. L. *Br. J. Cancer* **1985**, *51*, 229–235.
(83) Raleigh, J. A.; Koch, C. J. *Biochem. Pharmacol.* **1990**, *40*, 2457–2464.
(84) Varghese, A. J. *Biochem. Biophys. Res. Commun.* **1983**, *112*, 1013–1020.
(85) Chapman, J. D.; Franko, A. J.; Sharplin, J. *Br. J. Cancer* **1981**, *43*, 546–550.
(86) Bennewith, K. L.; Raleigh, J. A.; Durand, R. E. *Cancer Res.* **2002**, *62*, 6827–6830.
(87) Evans, S. M.; Judy, K. D.; Dunphy, I.; Jenkins, W. T.; Nelson, P. T.; Collins, R.; Wileyto, E. P.; Jenkins, K.; Hahn, S. M.; Stevens, C. W.; Judkins, A. R.; Phillips, P.; Geoerger, B.; Koch, C. J. *Cancer Res.* **2004**, *64*, 1886–1892.
(88) Bornhop, D. J.; Hubbard, D. S.; Houlne, M. P.; Adair, C.; Kiefer, G. E.; Pence, B. C.; Morgan, D. L. *Anal. Chem.* **1999**, *71*, 2607–2615.
(89) McMahon, B.; Mauer, P.; McCoy, C. P.; Lee, T. C.; Gunnlaugsson, T. *J. Am. Chem. Soc.* **2009**, *131*, 17542–17543.
(90) Fung, Y. O.; Wu, W.; Yeung, C.-T.; Kong, H.-K.; Wong, K.-L. K. K.-C.; Lo, W.-S.; Law, G.-L.; Wong, K.-L. K. K.-C.; Lau, C.-K.; Lee, C.-S.; Wong, W.-T. *Inorg. Chem.* **2011**, *50*, 5517–5525.
(91) Elhabiri, M.; Hamacek, J.; Humbert, N.; Bünzli, J.-C. G.; Albrecht-Gary, A.-M. *New J. Chem.* **2004**, *28*, 1096.
(92) Floquet, S.; Borkovec, M.; Bernardinelli, G.; Pinto, A.; Leuthold, L.-A.; Hopfgartner, G.; Imbert, D.; Bünzli, J.-C. G.; Piguet, C. *Chem. Eur. J.* **2004**, *10*, 1091–1105.
(93) Faulkner, S.; Burton-Pye, B. P.; Khan, T.; Martin, L. R.; Wray, S. D.; Skabara, P. J. *Chem. Commun.* **2002**, 1668–1669.
(94) Faulkner, S.; Burton-Pye, B. P. *Chem. Commun.* **2005**, 259–261.
(95) Pope, S. J. A.; Kenwright, A. M.; Boote, V. A.; Faulkner, S. *Dalton Trans.* **2003**, 3780.
(96) Harte, A. J.; Jensen, P.; Plush, S. E.; Kruger, P. E.; Gunnlaugsson, T. *Inorg. Chem.* **2006**, *45*, 9465–9474.
(97) Tilney, J. A.; Sørensen, T. J.; Burton-Pye, B. P.; Faulkner, S. *Dalton Trans.* **2011**, *40*, 12063–12066.
(98) Kuzmič, P. *Anal. Biochem.* **1996**, *237*, 260–273.
(99) Hill, L. R.; Sørensen, T. J.; Blackburn, O. A.; Brown, A.; Beer, P. D.; Faulkner, S. *Dalton Trans.* **2013**, *42*, 67–70.
(100) Tropiano, M.; Blackburn, O. A.; Tilney, J. A.; Hill, L. R.; Placidi, M. P.; Aarons, R. J.; Sykes, D.; Jones, M. W.; Kenwright, A. M.; Snaith, J. S.; Sørensen, T. J.; Faulkner, S. *Chem. Eur. J.* **2013**, *19*, 16566–16571.
(101) Hill, L. R.; Blackburn, O. A.; Jones, M. W.; Tropiano, M.; Sørensen, T. J.; Faulkner, S. *Dalton Trans.* **2013**, *42*, 16255.
(102) Caffrey, D. F.; Gunnlaugsson, T. *Dalton Trans.* **2014**, *43*, 17964–17970.
(103) Surender, E. M.; Bradberry, S. J.; Bright, S. A.; McCoy, C. P.; Williams, D. C.; Gunnlaugsson, T. *J. Am. Chem. Soc.* **2017**, *139*, 381–388.
(104) Borbas, K. E.; Bruce, J. I. *Org. Biomol. Chem.* **2007**, *5*, 2274–2282.
(105) Bodi, A.; Borbas, K. E.; Bruce, J. I. *Dalton Trans.* **2007**, 4352–4358.
(106) Pershagen, E.; Nordholm, J.; Borbas, K. E. *J. Am. Chem. Soc.* **2012**, *134*, 9832–9835.
(107) Szíjjártó, C.; Pershagen, E.; Ilchenko, N. O.; Borbas, K. E. *Chem. Eur. J.* **2013**, *19*, 3099–3109.
(108) Andres, J.; Borbas, K. E. *Inorg. Chem.* **2015**, *54*, 8174–8176.
(109) Kovacs, D.; Lu, X.; Mészáros, L. S.; Ott, M.; Andres, J.; Borbas, K. E. *J. Am. Chem. Soc.* **2017**, *139*, 5756–5767.
(110) Andres, J.; Chauvin, A.-S. *Eur. J. Inorg. Chem.* **2010**, *2010*, 2700–2713.
(111) Andres, J.; Chauvin, A.-S. *Phys. Chem. Chem. Phys.* **2013**, *15*, 15981–15994.

Results and discussion

Chapter 2 Establishing the fundamentals of isophthalate binding*

This chapter explores the behaviour of a series of structurally related lanthanide complexes that bind to aryl-1,3-dicarboxylic acid derivatives, where each of the Sections 2.1, 2.2, and 2.3 corresponds to a paper published during this degree. As will be seen, apparently trivial structural variations in host and guest can have dramatically different consequences. The synthesis of relevant complexes will be covered later in Part A.

2.1 Self-assembly between dicarboxylate ions and binuclear lanthanide complexes – "a surprisingly complicated problem"[1]

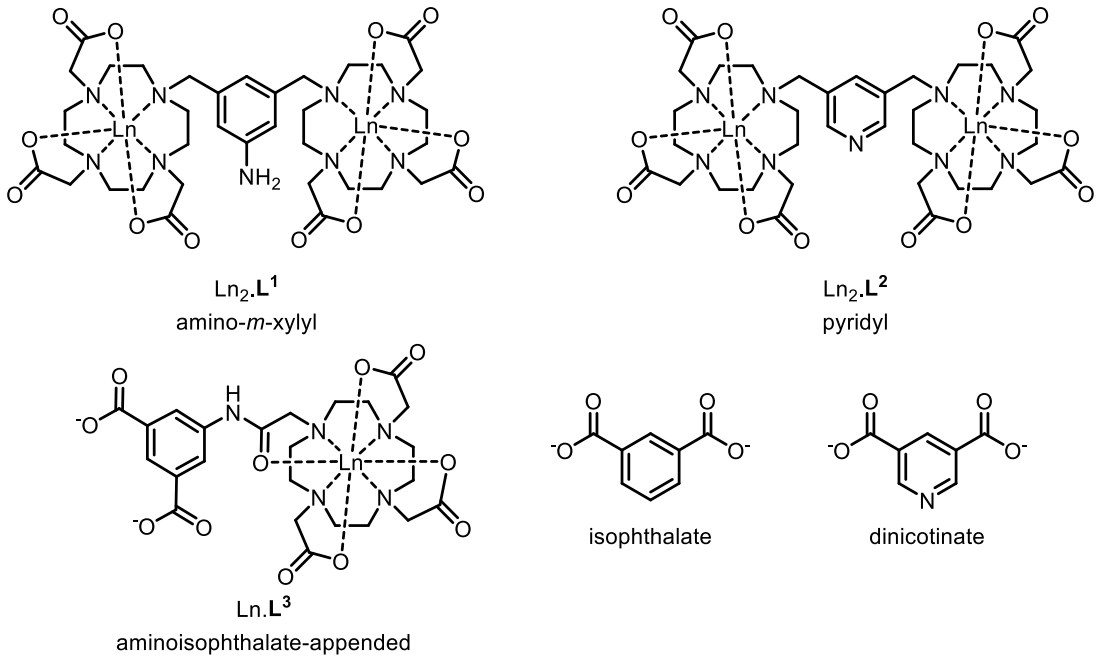


Figure 2.1 Species synthesised and studied in dicarboxylate titrations (Ln = Nd, Eu, Tb, Yb)

The complexes $Ln_2.\mathbf{L^1}$ (Ln = Nd, Eu, Tb, Yb) and $Ln_2.\mathbf{L^2}$ (Ln = Eu) in Figure 2.1 were prepared by following literature procedures[2,3] and were titrated with isophthalate, dinicotinate, and the aminoisophthalate-appended lanthanide complexes Ln.$\mathbf{L^3}$ (Ln = Nd,

* My work described in this chapter has been published in
Eur. J. Inorg. Chem., 2014, **15**, 2520-8 (2014),
J. Lumin., 2015, **167**, 296-304 (2015), and
ChemistryOpen, 2015, **4**, 509-15 (2015)

Tb)[4] in various media to compare the effects of lanthanide identity, solvent, and buffer on the strength of the binding interaction. As well as recording steady-state luminescence spectra, the luminescence lifetime was also measured before and after addition of the guest anion.

2.1.1 Self-assembly

Self-assembly of these such systems is often determined by the nature of the solvent, as binding of a guest displaces solvent molecules at the coordinatively unsaturated lanthanide. Binding was studied in methanol, 3:1 methanol:water, water, and aqueous buffers. Competitive binding must also be considered, for example in buffer systems containing phosphate ions.

Considering the Debye-Hückel model for a typical host-guest equilibrium (Equation 2.1), the activity coefficients for similarly charged species in dilute electrolytes are identical and therefore cancel out, the giving the binding constant as in Equation 2.2.

$$Ln_2.\boldsymbol{L^x} + Ln'.\boldsymbol{L^3} \rightleftharpoons Ln_2.\boldsymbol{L^x}{:}\,Ln'.\boldsymbol{L^3}$$

Equation 2.1 Host-guest equilibrium (Ln, Ln' = Nd, Eu, Tb, Yb, Ln ≠ Ln', x = 1, 2)

$$K = \frac{[Ln_2.\boldsymbol{L^x}{:}\,Ln'.\boldsymbol{L^3}]}{[Ln_2.\boldsymbol{L^x}][Ln'.\boldsymbol{L^3}]}$$

Equation 2.2 Association constant for the host-guest equilibrium in Equation 2.1

2.1.2 Photophysics

Given the binding constants described below, it was clear that the rate of dicarboxylate exchange in the ternary complexes formed during titration must be similar to the observed luminescence lifetime, which may thus reflect a quantum yield weighted average or be

dominated by a single species. Accordingly, binding titrations were conducted by monitoring luminescence intensity.[1] The changes in luminescence spectra were plotted and are shown in Figure 2.2 and Figure 2.3.

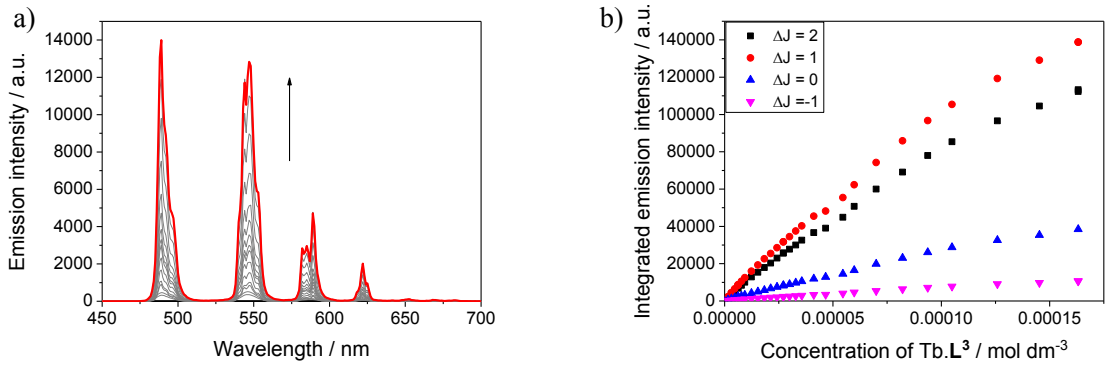


*Figure 2.2 a) Terbium luminescence spectrum and b) binding isotherm from titration of 5 × 10^{-5} M Yb_2.**L**^{1} with Tb.**L**^{3} in TRIS buffer at pH 9*

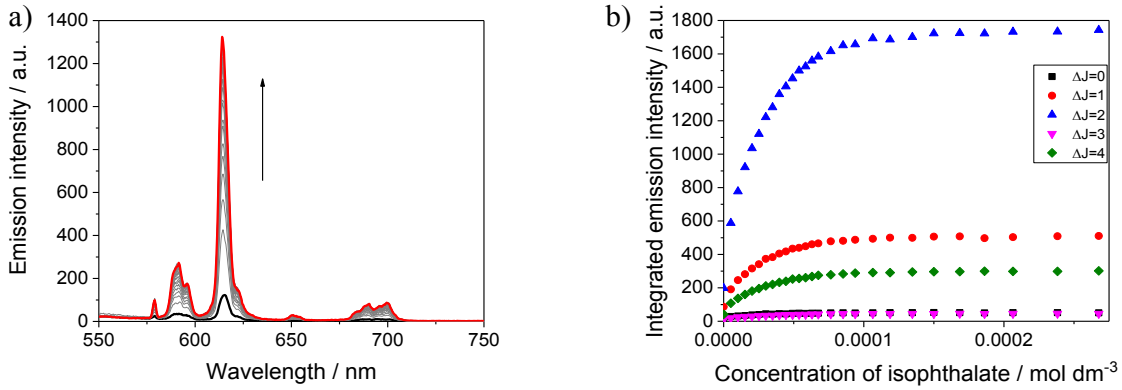


*Figure 2.3 a) Europium luminescence spectrum and b) binding isotherm from titration of 3 × 10^{-5} M Eu_2.**L**^{1} with isophthalate in methanol*

When studying the binding of the aminoisophthalate-appended complex Ln.**L**^{3} as a guest, it proved possible to study a greater selection of Ln_2.**L**^{1} lanthanide complexes, including lanthanides such as neodymium (whose luminescence occurs with low intensity outside the range of easy detection by the spectrometer used for these titrations[†]), as the luminescence intensity from the aminoisophthalate-appended complex Ln.**L**^{3} could be measured instead.

[†] While it is straightforward enough to acquire luminescence spectra from neodymium using the experimental setup described by the group in earlier publications, acquiring spectra is time-intensive, and was inappropriate for use with titration studies.

The intensity would obviously increase over the course of the titration as a result of the increasing concentration of the Ln.$\mathbf{L^3}$ complex in the cuvette, but the increase would not simply follow the Beer-Lambert law, due to the binding event. This precluded the possibility of titration combinations where the host complex and the guest complex contained the same lanthanide due to the difficulty in deconvolution of the two components.[1]

In cases with europium emission, the hypersensitivity of the $\Delta J = 2$ peak can be exploited. This transition is sensitive to changes in the ligand sphere of the europium ion,[5,6] and may provide a method to monitor binding ratiometrically.[7] This direct measure of the changing ligand sphere is probed mathematically by dividing the integrated intensity of this band by the integrated intensity of another band.

All guests in this chapter are dicarboxylates, where the guest bridges the two lanthanide-containing domains of the host complex, and each carboxylate binds to a lanthanide ion in a monodentate fashion through one of the carboxylate oxygen atoms. Conformational degrees of freedom are lost upon binding, as the adduct structure is more rigid than the host structure.[8] Because entropy decreases upon binding, this event must be driven by a significant enthalpic contribution.

Perdeuterated buffers are not readily available, therefore the number of inner sphere solvent molecules q was calculated for Eu2.$\mathbf{L^1}$ and the adduct Eu2.$\mathbf{L^1}$:Tb.$\mathbf{L^3}$ from their lifetimes in PBS in H_2O and D_2O. The lifetimes were within experimental error, and gave a q value of 0.9 for all conditions. This indicated that the binding proceeded without displacement of solvent.

The lifetime of the host complex was usually found change very little upon binding, as shown in Table 2.1. The calculated *q* values are shown in Table 2.2.

Host	**Guest**	**Solvent**	**τ_{start} / ms**	**τ_{end} / ms**
Eu_2.**L¹**	Tb.**L³**	3:1 MeOH:H_2O	0.54	1.10
Eu_2.**L¹**	Tb.**L³**	PBS pH 7.0	0.56 [a]	0.52 [a]
Eu_2.**L¹**	Tb.**L³**	TRIS pH 9.0	0.63	0.66
Eu_2.**L¹**	isophthalate	3:1 MeOH:H_2O	0.61	0.84
Eu_2.**L¹**	dinicotinate	3:1 MeOH:H_2O	0.61	0.87
Eu_2.**L¹**	dinicotinate	TRIS pH 9.0	0.69	0.70
Tb_2.**L¹**	isophthalate	3:1 MeOH:H_2O	1.96	2.10
Eu_2.**L²**	dinicotinate	TRIS pH 7.0	0.42 [b]	0.52 [b]
Eu_2.**L²**	dinicotinate	TRIS pH 8.0	0.52 [b]	0.61 [b]
Eu_2.**L²**	dinicotinate	TRIS pH 9.0	0.69 [b]	0.70 [b]
Eu_2.**L²**	dinicotinate	TRIS pH 10.5	0.85 [b]	0.80 [b]
Eu_2.**L²**	dinicotinate	HEPES pH 7.0	0.37 [b]	0.79 [b]
Eu_2.**L²**	dinicotinate	HEPES pH 8.0	0.49 [b]	0.72 [b]
Eu_2.**L²**	dinicotinate	HEPES pH 9.0	0.76 [b]	0.79 [b]
Eu_2.**L²**	dinicotinate	PBS pH 7.0	0.57 [b]	0.57 [b]
Eu_2.**L²**	dinicotinate	PBS pH 8.0	0.64 [b]	0.58 [b]
Eu_2.**L²**	dinicotinate	PBS pH 9.0	0.84 [b]	0.78 [b]

Table 2.1 Luminescence lifetimes of start and end titration solutions of lanthanide complexes with aryldicarboxylate titrants

[a] From reference,[9] [b] from reference[3]

As no solvent was displaced upon binding, and the lifetimes before and after binding were similar, the increase in emission intensity must be due to the increase in chromophore density

and the exclusion of outer sphere quenchers. The emission intensity was also found to increase in cases of direct excitation at the lanthanide rather than *via* the chromophore, therefore indicating that there must be some contribution from the exclusion of outer sphere solvent molecules.

Complex	**Buffer/pH**	τ_{H2O} / **ms**	+/−	τ_{D2O} / **ms**	+/−	q_{Eu}
$Eu_2.\mathbf{L^1}$	pH 2.0	0.41	0.05	1.39	0.13	1.8
$Eu_2.\mathbf{L^1}$ [a]	pH 6.7	0.38	0.03	0.92	0.04	1.2
$Eu_2.\mathbf{L^1}$	pH 9.0	0.68	0.07	1.24	0.10	0.5
$Eu_2.\mathbf{L^1}$	pH 12.5	0.61	0.04	1.37	0.06	0.8
$Eu_2.\mathbf{L^1}$ [b]	PBS pH 7.0	0.56	0.06	1.26	0.10	0.9
$Eu_2.\mathbf{L^1}$:Tb.$\mathbf{L^3}$ [b]	PBS pH 7.0	0.52	0.05	1.10	0.10	0.9

Table 2.2 Europium luminescence lifetimes and q values for $Eu_2.\boldsymbol{L^1}$ in various aqueous media

[a] From reference,[3] [b] D_2O with protonated PBS

Titration of $Ln_2.\mathbf{L^1}$ with isophthalate in methanol displayed an increase in emission intensity up to approximately 5 equivalents of guest, however the intensity ratio of the $\Delta J = 2$ to $\Delta J \neq 2$ bands exhibited different behaviour. These showed a sharper rise in intensity up until approximately a third of an equivalent of guest followed by a slower increase, where the maximum value was again reached at approximately 5 equivalents of guest. This may be attributed to a structural response of $Ln_2.\mathbf{L^1}$ to the altered medium. The total ion concentration and proton activity changes drastically for the first few data points, which was not the case in aqueous buffers at constant ionic strength.

2.1.3 Binding constants

As isophthalate is not water-soluble, the pyridine analogue dinicotinic acid was recruited. This species acted as a quencher of the $Ln_2.\mathbf{L^1}$ lanthanide excited state, and the quenching

efficiency was coincidentally identical to the intensity gain following binding. Since the effects cancel one another out, it was not possible to fit this straight line data meaningfully. The binding constants are given in Table 2.3, and augment data from previous studies focusing on dinicotinate binding to $Eu_2.\mathbf{L^2}$.[3]

Considering this data along with data from previous experiments it can be concluded that there is little change in binding constant when the lanthanide ion is varied. For the same host-guest pair, binding is highly solvent-dependent, and is far stronger in methanol or in a mixture of methanol and water than in buffer solution, presumably due to solvation factors. The binding constant for isophthalate with $Eu_2.\mathbf{L^1}$ is far greater in 3:1 MeOH:H_2O mixtures than in methanol alone, because isophthalate is poorly soluble in this medium and so there is an enthalpic gain upon binding, which is greater than the enthalpic gain for dinicotinate when considering the analogous titrations with $Tb_2.\mathbf{L^1}$. Dinicotinate also exhibits this behaviour in TRIS buffer, where it has a lower solubility than in 3:1 MeOH:H_2O.[1] In contrast, association of $Eu_2.\mathbf{L^1}$ with $Tb.\mathbf{L^3}$ is insensitive to the medium and gives similar binding constants in four different solvent systems.

$Tb.\mathbf{L^3}$ binds equally strongly to $Eu_2.\mathbf{L^1}$ and $Eu_2.\mathbf{L^2}$ but the binding constants for titrations of isophthalate are two orders of magnitude greater with $Eu_2.\mathbf{L^1}$ than $Eu_2.\mathbf{L^2}$. These two hosts have very similar structures, therefore the differences must lie in the specific solvation of these two complexes and/or assemblies owing to the differences between the proton acceptor-donor properties of the pyridine and the aniline group. This agrees with the significantly different binding constants for titrations of isophthalate and dinicotinate in different media.

Host	Guest	Solvent	log K [90% confidence]
Eu_2.**L**^{1}	Tb.**L**^{3}	3:1 MeOH:H_2O	4.37 [4.36 – 4.38]
Eu_2.**L**^{1}	Tb.**L**^{3}	TRIS pH 9	4.30 [4.29 – 4.32]
Eu_2.**L**^{1}	Tb.**L**^{3}	HEPES	4.41 [4.39 – 4.42]
Eu_2.**L**^{1}	Tb.**L**^{3}	PBS	4.45 [4.44 – 4.47]
Eu_2.**L**^{1}	Nd.**L**^{3}	TRIS pH 9	4.67 [4.59 – 4.75]
Eu_2.**L**^{1}	isophthalate	MeOH	5.07 [5.05 – 5.09]
Eu_2.**L**^{1}	isophthalate	3:1 MeOH:H_2O	8.08 [7.61 – 9.52]
Eu_2.**L**^{2}	Tb.**L**^{3}	3:1 MeOH:H_2O	4.39 [4.36 – 4.41]
Eu_2.**L**^{2}	Tb.**L**^{3}	TRIS pH 9	4.21 [4.19 – 4.24]
Eu_2.**L**^{2}	isophthalate	3:1 MeOH:H_2O	5.56 [5.45 – 5.69]
Eu_2.**L**^{2}	dinicotinate	3:1 MeOH:H_2O	6.20 [6.11 – 6.27]
Eu_2.**L**^{2}	dinicotinate	TRIS pH 9	4.18 [4.17(6) – 4.18(3)]
Tb_2.**L**^{1}	Nd.**L**^{3}	TRIS pH 9	4.91 [4.89 – 4.95]
Tb_2.**L**^{1}	isophthalate	MeOH	4.57 [4.51 – 4.64]
Tb_2.**L**^{1}	isophthalate	3:1 MeOH:H_2O	5.14 [5.05 – 5.23]
Tb_2.**L**^{1}	dinicotinate	3:1 MeOH:H_2O	4.89 [4.80 – 5.00]
Tb_2.**L**^{1}	dinicotinate	TRIS pH 9	3.95 [3.94 – 4.00]
Yb_2.**L**^{1}	Tb.**L**^{3}	TRIS pH 9	4.53 [4.50 – 4.55]
Nd_2.**L**^{1}	Tb.**L**^{3}	TRIS pH 9	4.39 [4.34 – 4.50]

Table 2.3 Binding constants for lanthanide-containing complexes calculated with DynaFit®[10]

Titrant solutions in 3:1 MeOH:H_2O and in MeOH contained 3 equivalents of LiOH in order to deprotonate the dicarboxylate

The binding constant in PBS, despite being the only buffer expected to exhibit competitive binding, is higher than for analogous titrations in HEPES and TRIS. Thus the contribution of competitive binding by the buffer is not as great as initially expected, and is outweighed

by other factors relating to the general composition of the medium such as ionic strength and specific solvation as PBS has the highest ionic strength of these buffer media. Previous work on the binding of dinicotinate to $Eu_2.\mathbf{L^2}$ under various conditions supports the assertion that binding is most affected by the medium in which association takes place.[3] The relative strengths of binding of isophthalate and dinicotinate to the same $Ln_2.\mathbf{L^1}$ complex are highly solvent-dependent whereas the strength of binding with the aminoisophthalate-appended $Ln.\mathbf{L^3}$ complexes is not as affected by the solvent, possibly due to the differences in solvation of the host-guest complex assembly. The solvation effects do not affect the metal centre greatly, as indicated by the unchanging luminescence lifetime and therefore unchanging (low) number of coordinated solvent molecules upon binding.[1]

There is no systematic variation in binding constant across the lanthanide series due to charge density and no correlation to SAP or TSAP conformation of the host complexes. The changes owing to different lanthanide ions are small compared to the differences in solvation.

2.2 Exploring the effect of remote substituents and solution structure on the luminescence of three lanthanide complexes[11]

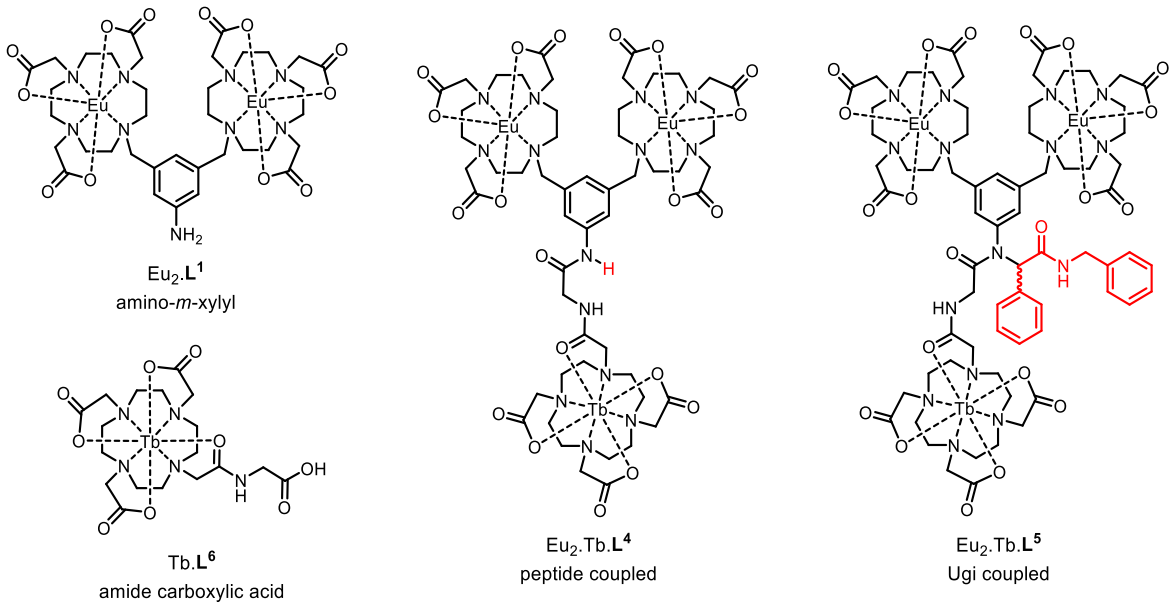


Figure 2.4 Lanthanide complexes used in photophysical studies

Work published by the group in 2013[8] showed that anionic guest activity at an apparently identical binding site could be influenced by functionalising the complex at a remote position, with binding constants differing by up to two orders of magnitude. Extending this work by studying the photophysical properties of these complexes in more detail revealed information on the role of structure and solvent on the complexes' solution structure. Specifically, it was found that an increase in chromophore density did not necessarily correlate to an increase in luminescence intensity, as not all lanthanide centres were populated efficiently by the chromophores.

In Eu_2.Tb.**L**^{4} and Eu_2.Tb.**L**^{5}, the two additional phenyl rings increase crowding significantly compared to Eu_2.**L**^{1}, and are not in a fixed position relative to the lanthanide centres and so conformations where there are sensitisers close to any of the three lanthanide centres are possible. The anilide is the same distance from the europium centres in the three complexes, but the terbium-to-chromophore distance is likely to differ. As there is no conjugation

between the chromophores and the lanthanide ions, energy transfer must proceed *via* through-space interactions. Therefore, the energy transfer and sensitisation in $Eu_2.Tb.\mathbf{L^5}$ depends on the solution structure – in particular, the conformational freedom of the two phenyl groups.

The absorption spectra suggest that the formation of a fully conjugated anilide is precluded as the usual aniline to anilide blue shift is not observed.

Comparison of the relative intensity of europium bands and terbium bands in emission spectra of $Eu_2.Tb.\mathbf{L^4}$ reveal the relative population of the excited states of the two lanthanide centres following excitation in the chromophore manifold. Changing the solvent had little effect other than a change in the relative intensities of terbium-centred emission bands, indicating a solvent dependence in the emission from the terbium $^5D_4$. Changing the concentration had no effect, therefore no excimer was formed and aggregation was unlikely.

For $Eu_2.Tb.\mathbf{L^5}$, the $\Delta J = 4$ band was twice as intense as for $Eu_2.Tb.\mathbf{L^4}$ relative to terbium-centred emission. This suggests that the anilide chromophore preferentially sensitises the terbium excited state, whereas the two phenyl chromophores increase the population of the europium excited state. The solvent-dependence of the terbium emission of $Eu_2.Tb.\mathbf{L^5}$ was similar to that of $Eu_2.Tb.\mathbf{L^4}$. For $Eu_2.Tb.\mathbf{L^5}$, the europium emission was highly solvent-dependent.

The excitation spectra of $Eu_2.Tb.\mathbf{L^4}$ and $Eu_2.Tb.\mathbf{L^5}$ are the same when analysing terbium emission, but different when monitoring europium emission. It appears that the europium excited state is preferentially populated through the anilide chromophore in both complexes,

but there is no significant population of the terbium excited state from the two phenyl chromophores in Eu_2.Tb.**L**^{5}.

Time resolved emission spectra of Eu_2.Tb.**L**^{4} and Eu_2.Tb.**L**^{5} agreed with luminescence emission spectra and lifetime measurements and showed slow decay of terbium emission and shorter-lived europium emission. This provided information on quenching. The europium centres in Eu_2.**L**^{1} and Eu_2.Tb.**L**^{4} exhibited identical lifetimes and q values on account of their similar environments. However the europium centres in Eu_2.Tb.**L**^{5} show a much longer lifetime due to their decreased q value, as the bulk of the phenyl rings disrupted the average structure. The q value of the terbium centre reduces from Tb.**L**^{6} to in Eu_2.Tb.**L**^{4} and Eu_2.Tb.**L**^{5}, while the luminescence lifetime stays the same, indicating that the face of the terbium binding pocket is more crowded in the coupled complexes than in the terbium starting material Tb.**L**^{6} but is unaffected by the additional phenyl rings introduced by the Ugi coupling.

The luminescence was highly solvent-dependent, and it was possible to separate the contributions from solvation and from changes in molecular structure. Comparison of the change in refractive index with the distance-dependence of energy transfer indicates that the change must be due to the differing solution structure. This is also supported by evidence from the relative lifetimes of europium and terbium in different solvents. Upon moving to methanol, terbium should be quenched and europium emission should be favoured, however europium emission is only slightly increased in methanol but is greatly increased in acetonitrile. Thus, the change is ascribable to increased energy transfer from the sensitising chromophore due to variations in the molecular structure and therefore in the effective chromophore density.

Binding of isophthalic acid in the binuclear europium binding pocket of Eu_2.**L**^{1} and Eu_2.Tb.**L**^{4} in methanol increases the emission as the presence of isophthalate augments the chromophore manifold. For Eu_2.Tb.**L**^{5}, an increase in europium emission is seen in comparison to terbium emission, indicating a preference for generation europium excited states. The europium lifetime in Eu_2.Tb.**L**^{4} and Eu_2.Tb.**L**^{5} was unchanged upon binding isophthalate, whereas the terbium lifetime decreased, suggesting an increase in the population of molecules that are in a configuration with increased quenching of the terbium centre.

In conclusion, increasing the chromophore density only increases emission intensity if it is possible for the molecule to adopt a conformation in which through-space energy transfer to the lanthanide centres is possible.

When isophthalate was added, the peptide-coupled complex Eu_2.Tb.**L**^{4} showed only minimal changes to the relative intensities of the bands in the emission spectra. However, the Ugi-coupled complex Eu_2.Tb.**L**^{5} showed pronounced changes in emission spectra, indicating that a small change in the structure of a lanthanide complex on paper gives rise to significantly different physical behaviour of the complex.

2.3 Thermodynamics of self-assembly of dicarboxylate ions with binuclear lanthanide complexes[12]

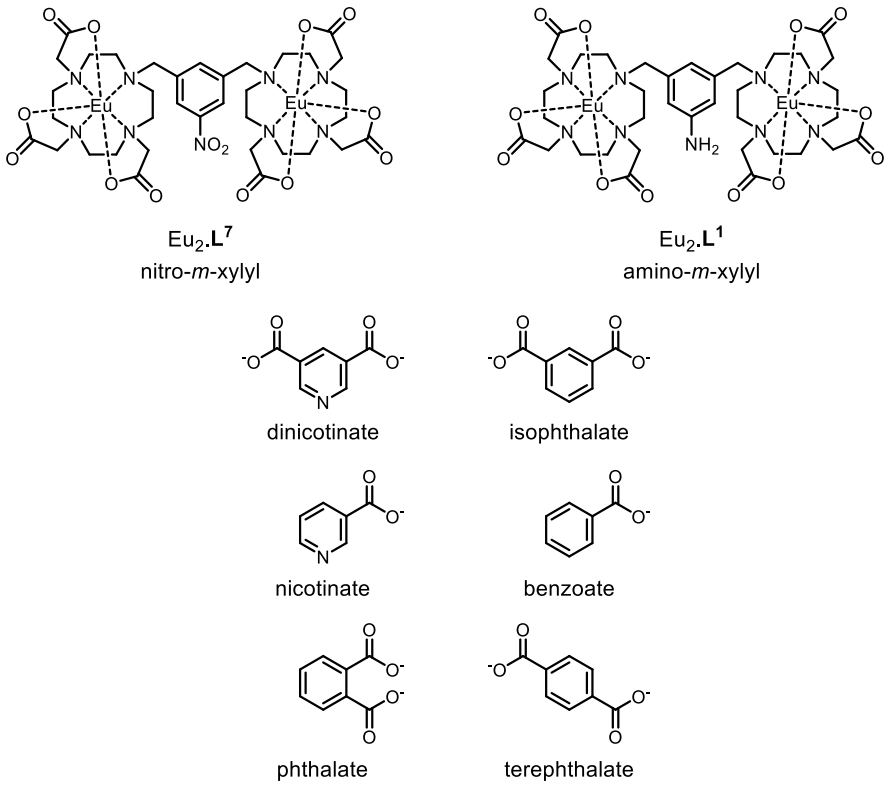


Figure 2.5 Host and guest species studied in binding experiments

After establishing a core of knowledge on the binding of aryl-1,3-dicarboxylate species to binuclear lanthanide complexes,[1,3,8,9,11,13] the thermodynamics of binding were considered in more detail. The first approach to studying this used isothermal calorimetry to attempt to establish the enthalpic and entropic contributions to anion binding. However, the data obtained from isothermal titration calorimetry titrations (see Chapter 12, Section 12.3 for details on the technique) was of poor quality and proved hard to obtain reproducibly, so alternative methods were used to attempt to explore the temperature-dependence of binding.

Instead, thermodynamic information was obtained using data from luminescence titrations at a range of temperatures in an array of solvents and buffers (at 10, 20, 30, and 40°C in methanol, ethanol, and water, and in HBS, PBS, and BBS). Values for ΔH and ΔS were extracted from a plot of $-RlnK$ against T^{-1}, related to a van't Hoff plot. These calculations

used the calculated binding constants, though these are based on only three data points and should be treated with caution. The original van't Hoff plots are shown in Figure 2.6 and Figure 2.7.

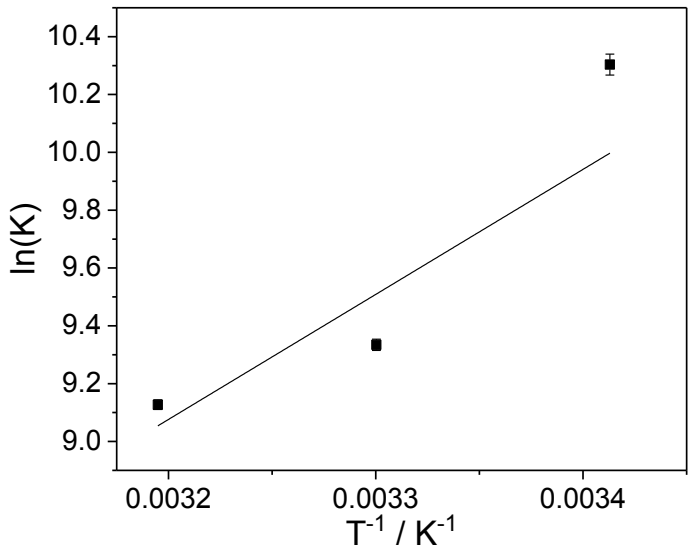


*Figure 2.6 Van't Hoff plot for binding of Eu_2.**L**^{7} to dinicotinate in BBS buffer at pH 8.1*

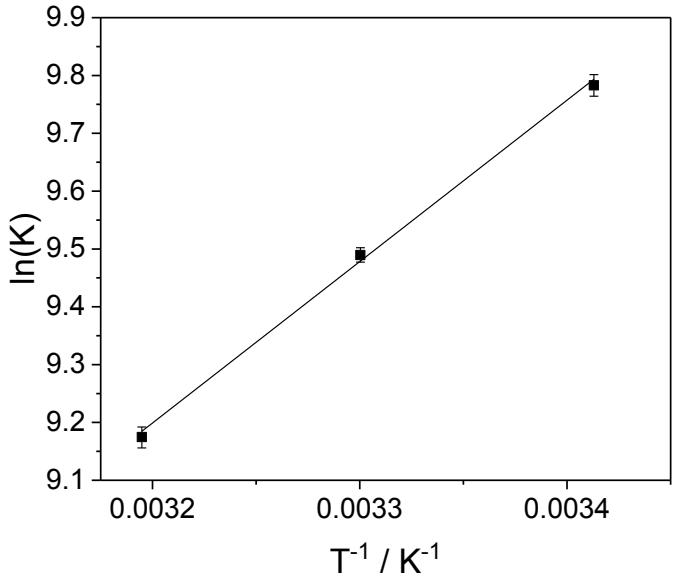


*Figure 2.7 Van't Hoff plot for binding of Eu_2.**L**^{7} to dinicotinate in HBS at pH 7.5*

Interestingly, the nitro and amino complexes, Eu_2.**L**^{7} and Eu_2.**L**^{1} respectively, were found to exhibit contrasting behaviour in terms of selectivities and buffer competition.

2.3.1 Data

The results in Table 2.4 clearly demonstrate that the interactions between the lanthanide complexes and dinicotinate were again heavily influenced by the solvent in which the binding takes place. These titrations were carried out at different pH values to previous titrations, so different protonation states of the titrant must also be considered, as well as competition by hydroxide ions. Titrations in PBS at pH 7.4 did not show binding, likely due to buffer competition, and so are not included.

The binding of the guest to the host is accompanied by a loss of entropy, not only due to the presence of one fewer molecule in solution, but also due to the loss of conformational degrees of freedom of the host complex, and likely changes to the ordering of the second (and subsequent) solvation spheres. This entropy loss is more than balanced out by the large enthalpy gain as a result of the strong electrostatic interaction between the lanthanide ion and the carboxylate.

			Buffer	
			HBS pH 7.5	**BBS pH 8.1**
Temperature / °C	**10**		16770	14860
	20		17730	29830
	30	**K / M^{-1}**	13220	11320
	40		9650	9200
		ΔH / kJ mol^{-1}	−23.2	−45
		ΔS / J K^{-1} mol^{-1}	−2.2	−69.5

Table 2.4 Thermodynamic data for the binding of $Eu_2.\boldsymbol{L^7}$ with dinicotinate

2.3.2 Competitive binding

The effect of buffer competition was also studied by performing titrations with different host concentrations (0.1 M and 0.01 M $Eu_2.\mathbf{L}^7$) and by comparing results from titrations in different buffers, and also by conducting experiments with different concentrations of HEPES buffered saline (HBS) (10 mM, 40 mM, and 80 mM). The effect of ionic strength was also considered by comparing titrations in HEPES solution made from water with titrations in HBS. The binding constants are given in Table 2.5.

	Buffer				
	HBS	**HBS**	**HBS**	**HBS**	**HEPES**
	10 mM	**20 mM**	**40 mM**	**80 mM**	**20 mM**
log K	4.37	4.32	4.14	4.41	4.19
[90% confidence]	[4.36 – 4.38]	[4.31 – 4.33]	[4.13 – 4.15]	[4.39 – 4.42]	[4.18 – 4.20]

Table 2.5 Binding constants for $Eu_2.\mathbf{L}^7$ with dinicotinate in varying concentrations of HEPES with and without sodium chloride at pH 7.4 at 20°C

The effect of buffer concentration was studied in titrations of the lanthanide complex $Eu_2.\mathbf{L}^7$ with dinicotinate. Titration solutions were made up with 0.01 mM $Eu_2.\mathbf{L}^7$ and 137 mM saline and the concentration of HEPES varied in order to judge the effect of the competitive binding of the buffer. A further titration was performed without saline in order to investigate the effect of salt on the binding of dinicotinate. The trend when considering the binding constants for the $Eu_2.\mathbf{L}^7$:dinicotinate equilibrium in 10, 20, and 40 mM HBS is that the binding becomes increasingly weaker and the initial explanation may be that despite HEPES usually being considered to be a non-competing buffer, it might actually be competing for the binding site. However, for the most concentrated HBS at 80 mM, the binding constant was greater. This result is difficult to explain, but may be a consequence of approaching saturation at high concentrations of HBS.

2.3.3 Binding in other solvent systems

Titrations of the nitro complex $Eu_2.\mathbf{L^7}$ showed no significant change in band shape over the course of a titration. In methanol, this complex exhibited selective binding for isophthalate over other dicarboxylate guests, although gave a much smaller binding constant with isophthalate than previously found for the similar amino complex $Eu_2.\mathbf{L^1}$. In basic conditions intended to deprotonate the isophthalate guest, the binding constant decreased, suggesting competitive binding by hydroxide. $Eu_2.\mathbf{L^7}$ was also found to give very different binding constants with phthalate and terephthalate than $Eu_2.\mathbf{L^1}$. Additionally, the trend differed in that larger binding constants were found for titrations with phthalate and terephthalate than with isophthalate in basic methanol, with the highest binding constants for the bidentate non-bridging guest phthalate. Terephthalate was found to bridge $Eu_2.\mathbf{L^7}$ more effectively than isophthalate: the opposite behaviour to that exhibited by $Eu_2.\mathbf{L^1}$. This reveals that a small change at the complex can dramatically change the association constant, possibly due to a change in solvation or lipophilicity.

Binding constants of $Eu_2.\mathbf{L^7}$ with isophthalate were greater than those found for binding to dinicotinate, suggesting that the electron-withdrawing group on dinicotinate reduced the negative character of the carboxylate oxygens, weakening the electrostatic attraction between the carboxylate and the lanthanide centre.

2.3.4 Temperature-dependence

The strength of dinicotinate and nicotinate binding was found to be essentially unchanged by temperature, whereas benzoate binding exhibited a small temperature dependence. Isophthalate binding was found to be very temperature-dependent, suggesting that the binding event is entropically favoured.

2.3.5 Aqueous conditions

Dinicotinate binding was studied under aqueous conditions. The binding constants in BBS and HBS were found to be larger than for in basic methanol, again suggesting competitive binding by hydroxide. There was no change in luminescence upon increasing concentration of dinicotinate, suggesting dinicotinate is unable to outcompete hydroxide in water.

For the combination of $Eu_2.\mathbf{L^7}$ and dinicotinate, there was a different temperature dependence under aqueous conditions to in basic methanol. The binding constant increased with increasing temperature in BBS and HBS, indicating the assembly was enthalpically-driven and entropically disfavoured. The lower binding constant in HBS to in BBS suggested competitive binding by HEPES.

2.3.6 Biological relevance

$Eu_2.\mathbf{L^7}$ did not exhibit detectable binding to dinicotinate in PBS and therefore would not be applicable in biological systems. $Eu_2.\mathbf{L^7}$ exhibits greater affinity for phosphate than $Eu_2.\mathbf{L^1}$, in line with the larger binding constant of $Eu_2.\mathbf{L^7}$ with the bidentate non-bridging guest phthalate.

2.3.7 Luminescence spectra

Luminescence spectra changed dramatically in both the relative intensity of bands and in the fine structure between solvents, due to the different local symmetry at the europium centres.

Excitation spectra were found to change before and after the addition of dinicotinate, and it follows that both dinicotinate and isophthalate increase the chromophore density. Therefore the luminescence is sensitised by both host and guest.

For most titrations in this paper, direct excitation showed minimal change in the shape or intensity of luminescence spectra, indicating that the overall quantum yield was unchanged. This suggests that binding occurs without the displacement of solvent.

2.3.8 Luminescence lifetimes

The luminescence lifetimes of the complexes changed only slightly upon isophthalate addition and the changes fell within experimental error, indicating that changes to the inner sphere were limited. In methanol, the lifetimes before and after addition of all guests were within error, suggesting that the guests do not displace the solvent.

For all systems, the lifetime did not change with temperature. The lower than expected q value of 1 suggests that perhaps the lipophilic *m*-xylyl group prevents approach of a second water molecule. The binding interaction is likely enhanced by hydrophobic effects and π-π stacking between the aromatic groups of the host and guest in both aqueous conditions and in methanol.

In aqueous environments, the lifetime was found to increase and the q value found to decrease with increasing pH as the bound water molecules at the europium were deprotonated. There was no evidence for aggregation.

2.3.9 Conclusions

In conclusion, the thermodynamics of these binding interactions are complicated and not explained by electrostatic interactions alone. The solvent is key, and competitive binding must be considered, as wel l as the nature of the guest. Small changes in the host or guest molecule can give very different binding affinities, and similar systems behave differently

in their interaction with phosphate, which must be borne in mind when attempting to move similar systems to *in vivo* applications.

The rest of this thesis concerns other analytes.

2.4 References

(1) Sørensen, T. J.; Hill, L. R.; Tilney, J. A.; Blackburn, O. A.; Jones, M. W.; Tropiano, M.; Faulkner, S. *Eur. J. Inorg. Chem.* **2014**, *2014*, 2520–2528.

(2) Placidi, M. P.; Natrajan, L. S.; Sykes, D.; Kenwright, A. M.; Faulkner, S. *Helv. Chim. Acta* **2009**, *92*, 2427–2438.

(3) Hill, L. R.; Sørensen, T. J.; Blackburn, O. A.; Brown, A.; Beer, P. D.; Faulkner, S. *Dalton Trans.* **2013**, *42*, 67–70.

(4) Shiells, E. J.; Natrajan, L. S.; Sykes, D.; Tropiano, M.; Cooper, P.; Kenwright, A. M.; Faulkner, S. *Dalton Trans.* **2011**, *40*, 11451.

(5) Jørgensen, C. K.; Judd, B. R. *Mol. Phys.* **1964**, *8*, 281–290.

(6) Richardson, F. S. *Chem. Rev.* **1982**, *82*, 541–552.

(7) *Lanthanide Luminescence: Photophysical, Analytical and Biological Aspects*; Hänninen, P.; Härmä, H., Eds.; Springer Series on Fluorescence; Springer-Verlag: Berlin, Heidelberg, 2011; Vol. 7.

(8) Tropiano, M.; Blackburn, O. A.; Tilney, J. A.; Hill, L. R.; Placidi, M. P.; Aarons, R. J.; Sykes, D.; Jones, M. W.; Kenwright, A. M.; Snaith, J. S.; Sørensen, T. J.; Faulkner, S. *Chem. Eur. J.* **2013**, *19*, 16566–16571.

(9) Tilney, J. A.; Sørensen, T. J.; Burton-Pye, B. P.; Faulkner, S. *Dalton Trans.* **2011**, *40*, 12063–12066.

(10) Kuzmič, P. *Anal. Biochem.* **1996**, *237*, 260–273.

(11) Tropiano, M.; Blackburn, O. A.; Tilney, J. A.; Hill, L. R.; Sørensen, T. J.; Faulkner, S. *J. Lumin.* **2015**, *167*, 296–304.

(12) Sørensen, T. J.; Hill, L. R.; Faulkner, S. *ChemistryOpen* **2015**, *4*, 509–515.

(13) Hill, L. R.; Blackburn, O. A.; Jones, M. W.; Tropiano, M.; Sørensen, T. J.; Faulkner, S. *Dalton Trans.* **2013**, *42*, 16255.

Part A: Synthesis and characterisation

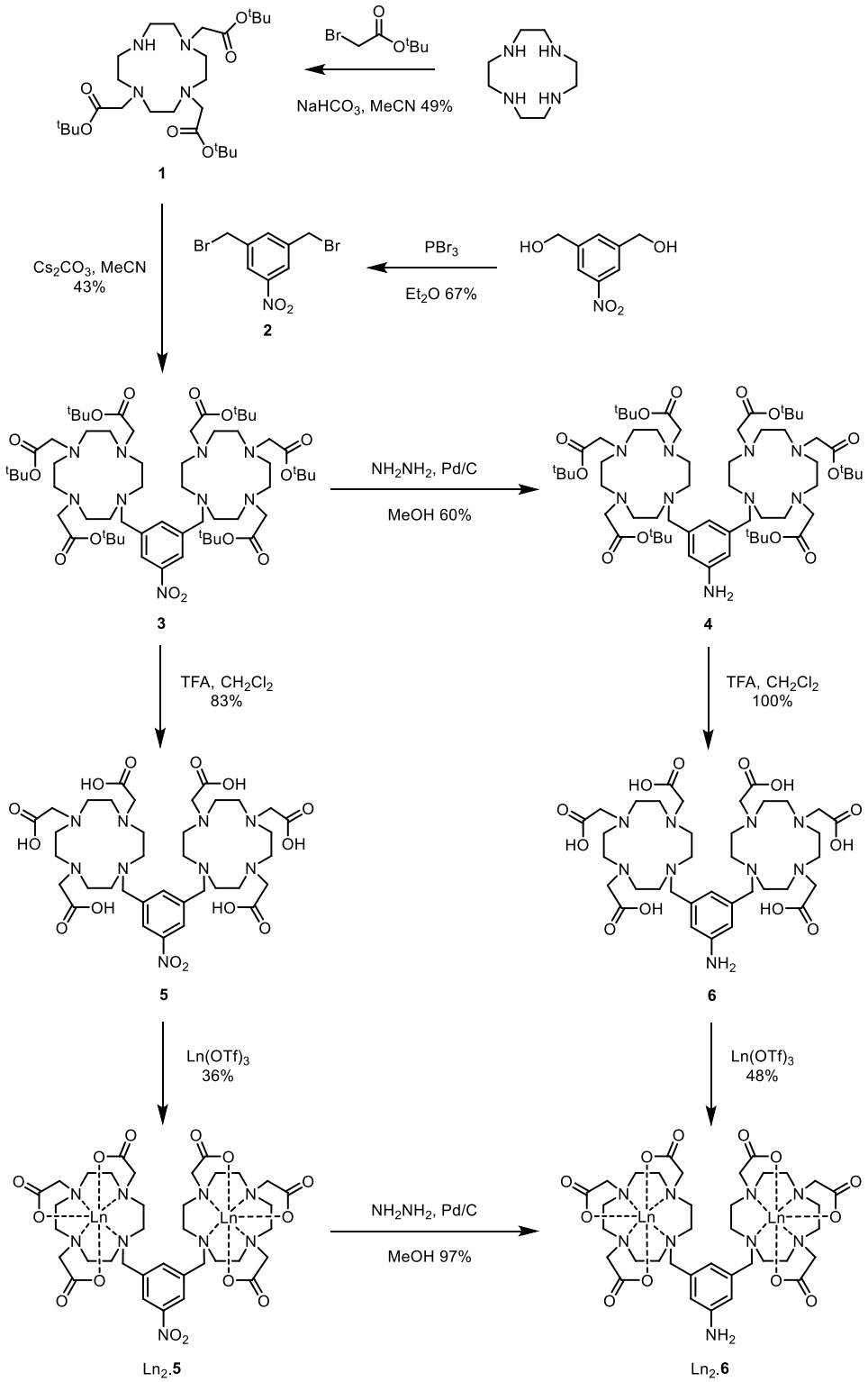
Chapter 3 *m*-Xylyl complexes

3.1 Introduction

Lanthanide complexes with bicyclic ligands containing two DO3A-like binding domains linked by a *m*-xylyl bridge have been studied by the Faulkner group for a number of years.[1,2] Originally, these were designed to offer an improvement in MRI imaging contrast, as these molecules contained multiple lanthanide centres to enhance relaxation, and larger complexes tumble more slowly in solution also leading to an increase in relaxivity. More recently, the presence of two lanthanide binding centres linked by a relatively rigid spacer group was found to accommodate particular sizes and geometries of dianionic guests derived from aryl-1,3-dicarboxylates such as isophthalate and dinicotinate,[3–7] while structural variation of groups remote from the binding domain was shown to influence conformational space and binding affinity for these species. The work described in this thesis explores how the binding to a larger array of biologically relevant dianions is influenced by structure. This chapter describes the synthesis and characterisation of a range of *m*-xylyl derivatives and their complexes with a view to exploiting the properties of individual lanthanide ions in full.

3.2 Synthesis and characterisation

The macrocyclic complexes Ln_2.**5** and Ln_2.**6** in Scheme 3.1 were prepared by functionalisation of cyclen according to literature procedures.[1,8,9] The choice of metals will be explained later. The nitro-*m*-xylyl bridging unit **2** was produced by bromination of 5-nitro-*m*-xylene-α,α'-diol by reaction with phosphorus tribromide in anhydrous ether,[9] a higher-yielding synthesis with simpler purification steps than the frequently used literature combination of hydrobromic acid and sulphuric acid. This reaction was quenched with ice and then washed with weakly basic aqueous solution to remove any unreacted or mono-brominated starting material, giving the product in up to 92% yield.



Scheme 3.1 Reaction pathway for synthesis of m-xylyl complexes (Ln = Eu, Gd, Tb, Yb, Y)

Crystals of **2** suitable for X-ray analysis were grown by slow evaporation of deuterated chloroform and analysed by Dr Amber Thompson and Dr Kirsten E. Christensen of the University of Oxford. The structure is shown in Figure 3.1, and further data is available in

Appendix C.1. The figure displays a planar molecule except for the bromine atoms which point in opposite directions out of the plane and the nitro group which is rotated out of the plane of the ring by 17.5°, as shown in Figure 3.2.

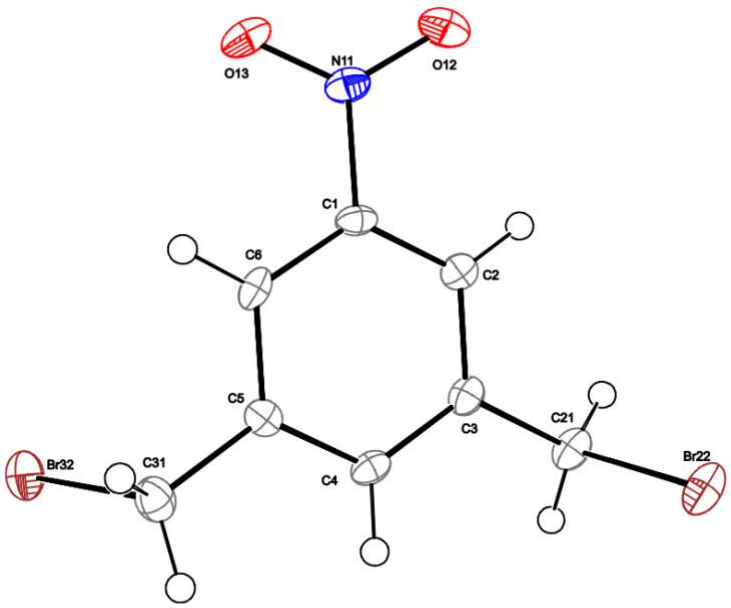


*Figure 3.1 Crystal structure of bridging unit **2***

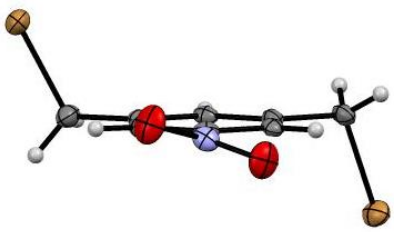


*Figure 3.2 Crystal structure of **2** viewed along N-C bond showing O and Br atoms out of plane*

The dibromo compound **2** and cyclen triester species **1** were combined in basic acetonitrile and heated under reflux for two days to encourage complete substitution. The nitro-*m*-xylyl proligand product **3** was isolated following workup as the sodium salt, which was a pale yellow solid.[1] Crystals suitable for X-ray diffraction were grown by slow evaporation of deuterated chloroform. The crystal structure of this compound is shown in Figure 3.3, and further data may be found in Appendix C.2.

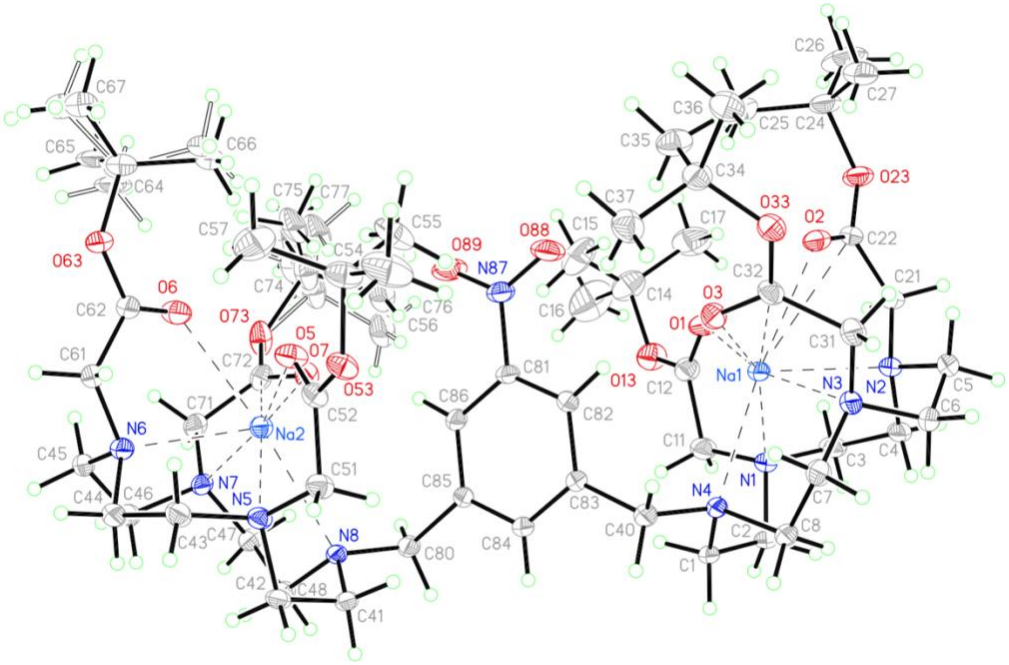


*Figure 3.3 Crystal structure of Na_2.**3**, counteranions omitted for clarity*

At this stage there were two possible routes to access the amino complexes Ln_2.**6**. In the first, the nitro group of proligand **3** could be reduced to an amino group. Reaction with hydrogen gas and a palladium on carbon catalyst gave unexpected additional peaks in the aromatic region of the NMR spectrum after three days which suggested that the reaction had not yet reached completion. After the mixture was allowed to react for a further four days, NMR appeared to show full conversion to the desired amine proligand, **4**, and agreed with the mass spectrum, as well as the disappearance of the 1532 and 1346 cm^{-1} N-O stretches in the IR spectrum.

However, crystals grown by slow evaporation of solvent showed a diazo dimer as in Figure 3.4, which was not in line with expectations. The crystal structure, shown below in Figure 3.5 (further data in Appendix C.3) was solved by Dr Amber Thompson and Dr Kirsten E. Christensen. The N=N bond length of 1.26 Å and N=N-C bond angles of 114.3° confirm that the N=N bond is a double bond and not a single bond.

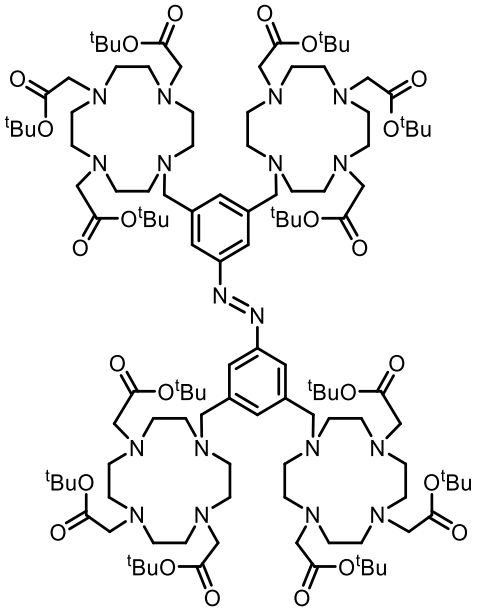


Figure 3.4 Molecular structure of the hydrogen-reduced m-xylyl diazo dimer ***4a***

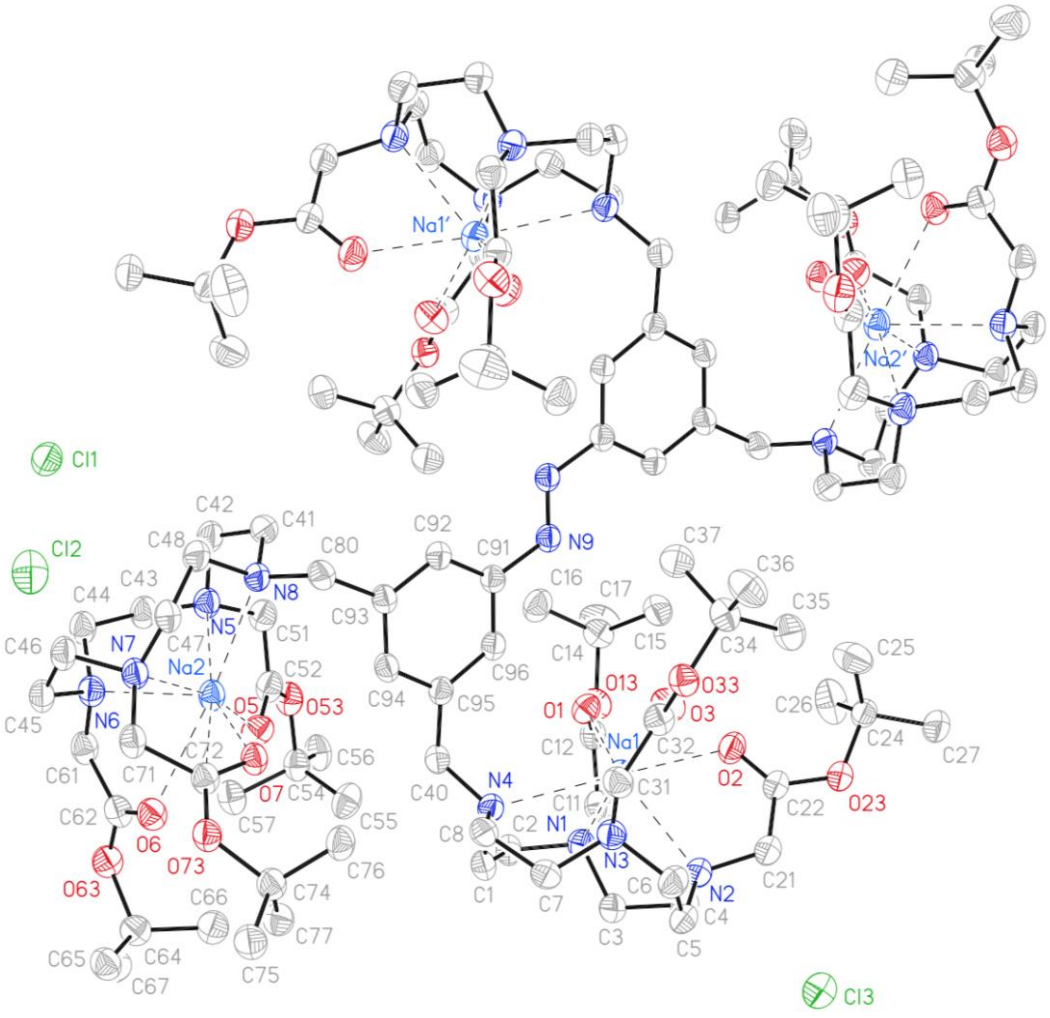


Figure 3.5 Crystal structure of the hydrogen-reduced m-xylyl diazo dimer Na_4***4a*** *with hydrogen atoms and one counteranion omitted for clarity*

Further characterisation of this hydrogen-reduced compound by ^{1}H DOSY, presented in Figure 3.6, gave large, poorly resolved bands, indicating that this sample was a mixture of different-sized molecules with overlapping ^{1}H NMR spectra, suggesting some of the amino monomer **4** and some of the diazo dimer **4a** shown in Figure 3.4.

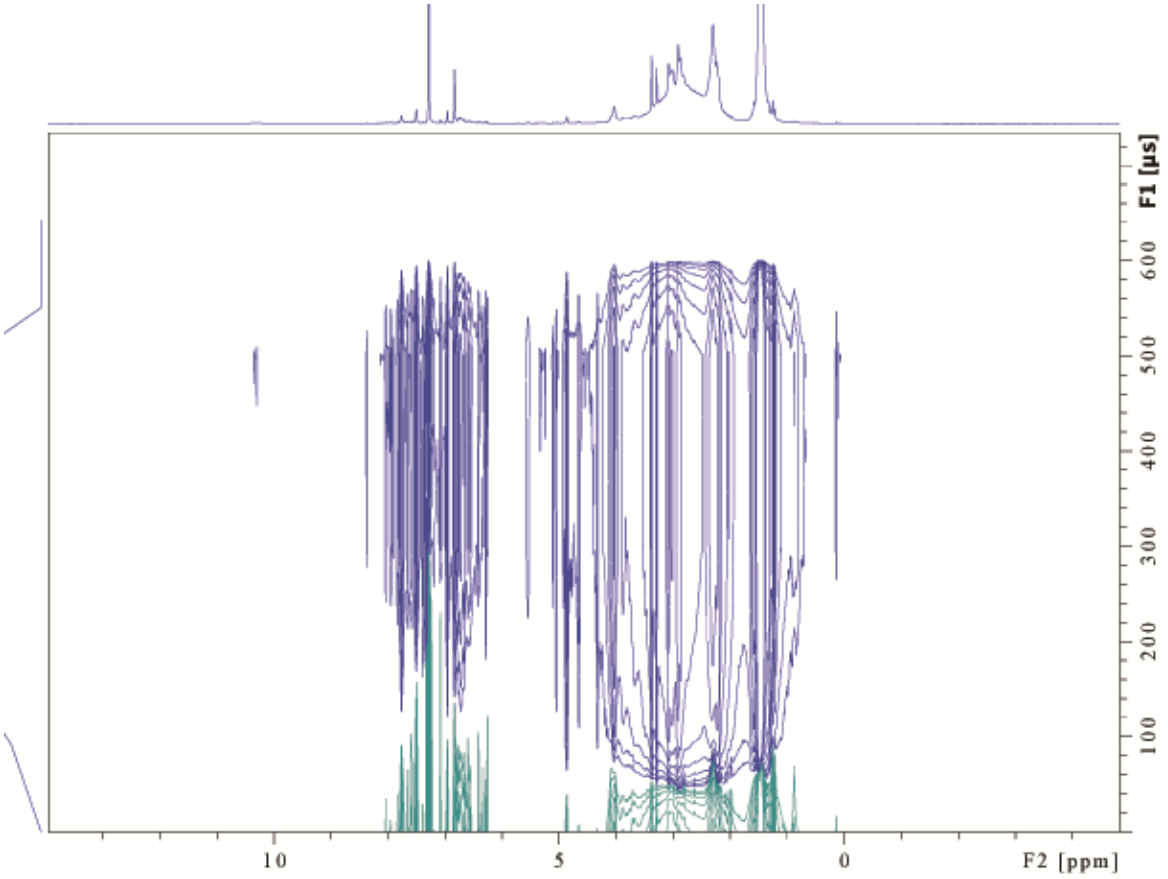


Figure 3.6 ^{1}H DOSY NMR spectrum of the hydrogen-reduced proligand suggests more than one species with different diffusion rates (blue and green)

In addition to this, despite the prediction that the UV-vis absorption spectrum of proligand **4** should be very similar to that of the amino-*m*-xylyl complexes Eu_2.**6** and Tb_2.**6** mentioned later in this chapter, the spectral form of this hydrogen-reduced proligand sample differed to those of the Eu_2.**6** and Tb_2.**6** complexes, and to a sample of hydrazine-reduced **4**.

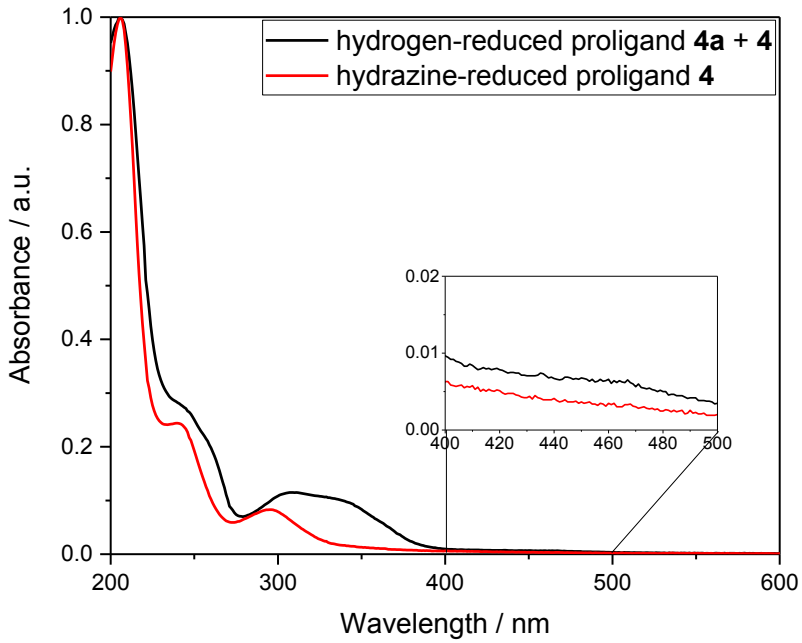


*Figure 3.7 Superimposed normalised UV-vis absorption spectra of hydrogen-reduced proligand (a mixture of **4** and **4a**) (black trace) and hydrazine-reduced proligand **4** (red trace) in water*

The absorption bands between 275 and 400 nm in the spectrum of the hydrogen-reduced proligand in Figure 3.7 (black trace) suggest that more than one species is present in this sample, supporting the evidence from the DOSY experiment. This also bears out the crystal structure obtained for the azobenzene linked tetracycle in Figure 3.5. An examination of the literature revealed that *trans*-azobenzene itself exhibits an absorption maximum around 330 nm,[10] very close to the absorption observed in the spectrum obtained following reduction with hydrogen. A smaller magnitude, broad absorption band of *trans*-azobenzene is found at 440 nm, and an expansion of the 400 to 500 nm region of the spectrum for the hydrogen-reduced sample (inset to Figure 3.7) shows weak absorption in the same long wavelength region.[10] By contrast, *cis*-azobenzene exhibits maxima in the absorption spectrum at 275 and 430 nm. Thus, while the presence of a *cis*-azobenzene system seems implausible, it is clear that the *trans*-azobenzene bridged system is present in significant quantities in the product obtained from direct hydrogenation.

Further to this, the amine N-H bend absorption peaks at 1602 cm^{-1} observed in the IR spectrum were of relative lower intensity for the hydrogen-reduced compound than for the hydrazine-reduced sample (normalised to maximum absorption at 1158 cm^{-1}), indicating that the sample did not contain only the amine.

Reaction of **3** by transfer hydrogenation with hydrazine hydrate with a palladium on carbon catalyst was therefore deemed the preferable method for reducing the nitro group to an amino group. The transfer hydrogenation approach was found to offer reliable reduction, and allowed preparation of sufficient proligand for further study.

The amino proligand **4** was then deprotected by trifluoroacetic acid in dichloromethane, cleaving the ester groups to give the carboxylic acid groups in the amino ligand **6**, and the product was then complexed with a variety of lanthanide triflate salts in methanolic or acetonitrile solution. Using basic workup to remove excess lanthanide salts by conversion to the lanthanide hydroxide, as described in the literature, was found to be associated with low yields. It encouraged precipitation from solution, possibly due to aggregation of the complexes due to the presence of excess hydroxide, as has been noted previously for mononuclear complexes.[11]

Alternative strategies in which the nitro group was reduced after complexation were also explored. Through this route, the nitro proligand **3** was deprotected by trifluoroacetic acid in dichloromethane, cleaving the ester groups to give carboxylic acid groups, and the resulting nitro ligand **5** complexed by reaction with a lanthanide triflate salt in methanol or acetonitrile.

The resulting nitro complexes Ln_2.**5** were then dialysed to reduce salt content (in a Spectrum Labs Float-A-Lyzer® G2 dialysis device with a 100 – 500 Da molecular weight cut-off) or reduced to the corresponding amino complex Ln_2.**6** with hydrazine hydrate and a palladium on carbon catalyst, followed by dialysis.

3.2.1 NMR

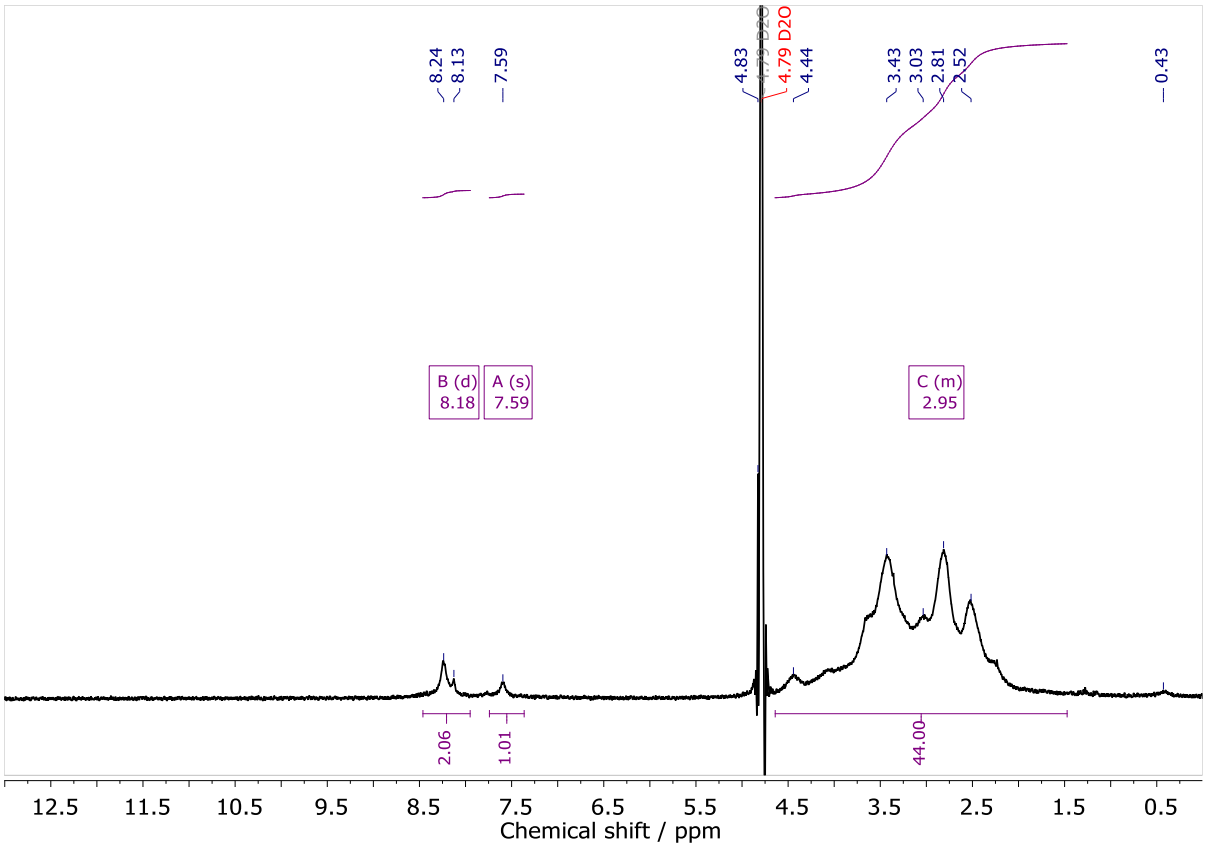


*Figure 3.8 ^1H NMR spectrum of Y_2.**5** in D_2O*

Figure 3.8 shows that the ^1H NMR spectrum of Y_2.**5** differed little to that of the **5** ligand, presumably because the free ligand is observed as a sodium salt. Splitting effects due to the ^{89}Y nucleus were difficult to discern due to the broadness of the NMR peaks as a result of the fluxional structure of the molecule. Such fluxionality is common in complexes with heptadentate DO3A derivatives, and means that a multitude of structures can average on the timescale of the NMR experiment. Each lanthanide centre can adopt four diastereomeric structures (two pairs of enantiomeric diastereoisomers) that interchange through ring

inversion and arm rotation (as outlined in Chapter 1 on page 16). The xylyl bridge complicates the picture further, since the two lanthanide centres become related, giving rise to further stereoisomerism. Further, a number of conformers can exist in equilibria and these are influenced by rotation around the single bonds in the xylyl bridge. Thus, the observed spectra reflect the interplay between numerous conformational and stereoisomers.[12]

In contrast to the diamagnetic yttrium complex, ^{1}H NMR spectra of Ln_2.**5** (Ln = Eu, Tb, Yb) and Ln_2.**6** (Ln = Eu, Tb) showed significant differences. A selection of these spectra are displayed in Figure 3.9 to Figure 3.11. It should be borne in mind that paramagnetic lanthanide complexes with anisotropic electronic distributions exhibit shifted NMR spectra as a consequence of their paramagnetism. Changes to the local ligand field can have a profound impact on the anisotropy, meaning that different stereoisomers would be expected to have different spectra. While the changes to primary ligand structure between the nitro and amino complexes do not influence the lanthanide binding site directly, changes to the electron distribution in the xylyl bridge are likely to combine with different degrees of solvation for the two complexes to change the relative abundance of all the conformational and stereoisomers at a given timepoint. This will inevitably be reflected in changes to the chemical shift observed for a given proton, since the observed chemical shift will depend upon the magnetic anisotropy at the lanthanide centre and on the geometric coordinates of the proton relative to the lanthanide and its magnetic axis. This is described by the Bleaney equation given in Chapter 1 on page 14.[13,14]

Thus, even before we have considered the binding of guests, it is clear that two apparently very similar complexes can display significant differences in their behaviour.

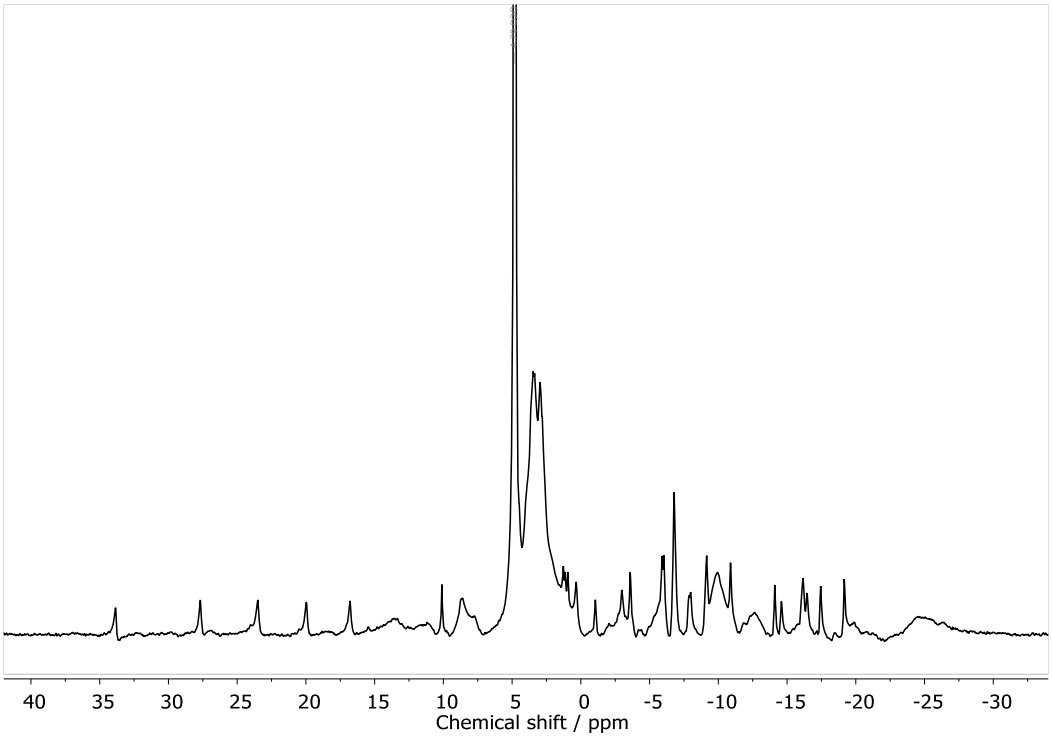


*Figure 3.9 ^{1}H NMR spectrum of Eu_2.**5** in D_2O where the peaks at 17 and 34 ppm indicate a mixture of TSAP and SAP isomers*

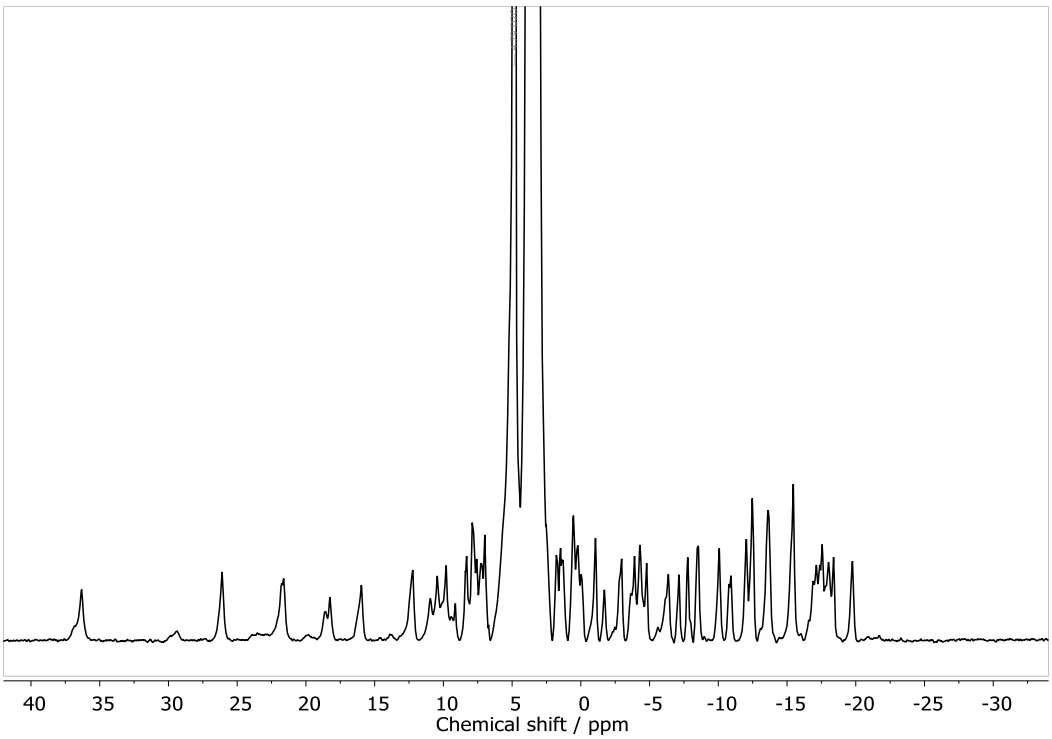


*Figure 3.10 ^{1}H NMR spectrum of Eu_2.**6** in D_2O where the peaks at 16, 18, 19, and 36 ppm indicate a mixture of TSAP and SAP isomers*

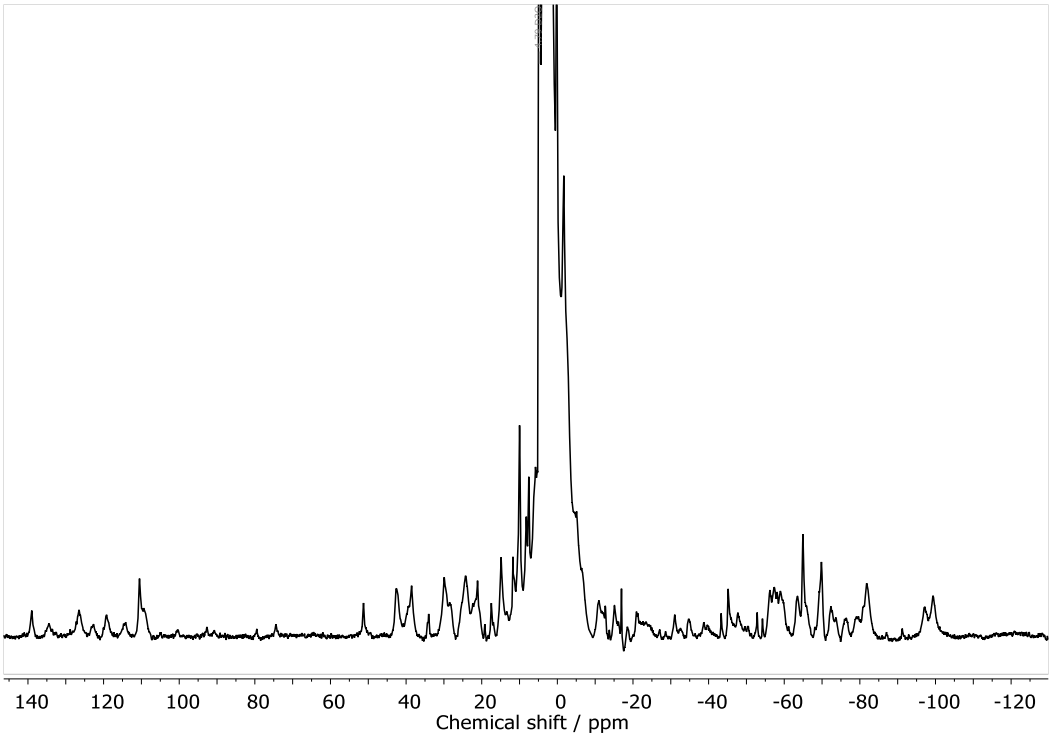


*Figure 3.11 ^{1}H NMR spectrum of Yb_2.**5** in D_2O*

3.2.2 UV-vis spectroscopy

UV-vis absorption spectra of the *m*-xylyl complexes, displayed in Figure 3.12 and Figure 3.13, showed ligand absorption dominating, as expected, because the ligand-based transitions described below are allowed by selection rules whereas *f-f* lanthanide-based transitions are Laporte forbidden. This means that changing the identity of the lanthanide in the complex had very little effect on the absorption spectrum.

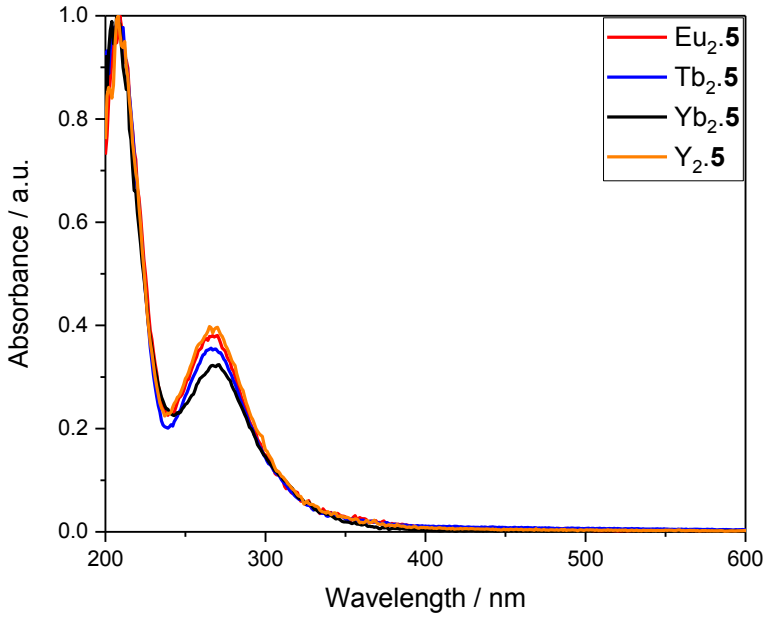


*Figure 3.12 Superimposed normalised to λ_{max} UV-vis absorption spectra of Ln_2.**5** (Ln = Eu, Tb, Yb, Y) complexes in water*

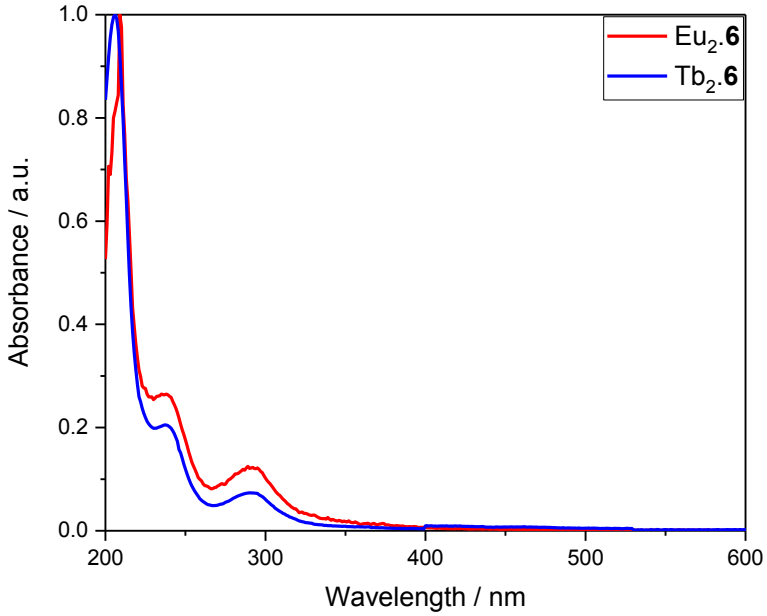


*Figure 3.13 Superimposed normalised to λ_{max} UV-vis absorption spectra of Ln_2.**6** (Ln = Eu, Tb) complexes in water*

The differences observed between the absorption spectra of the nitro-*m*-xylyl complexes shown in Figure 3.12 and the amino-*m*-xylyl complexes shown in and Figure 3.13 can be

attributed to the different electronic transitions of nitrobenzene and aniline.

The spectral peak measured for the Ln_2.**5** complexes at approximately 205 nm is attributed to a combination of the $\pi \rightarrow \pi^*$ transition on the benzene ring and a $\pi \rightarrow \pi^*$ excitation within the nitro group.[15,16] The peak at approximately 265 nm is a charge transfer band corresponding to a π(benzene ring) $\rightarrow \pi^*(NO_2)$ transition.[15–18]

For the Ln_2.**6** complexes, the absorption bands seen at around 207, 238, and 292 nm match those of aniline which may be found at approximately 200, 240, and 285 nm.[19–26] These bands correspond to $\pi \rightarrow \pi^*$ and $n(NH_2) \rightarrow \pi^*$(benzene ring) transitions.

The UV-vis absorption spectrum of aniline is sensitive to pH because when protonated to form the anilinium cation, there is no longer a nitrogen lone pair to donate into the conjugated π system. Therefore in lower pH environments the absorption band corresponding to this $n \rightarrow \pi^*$ transition is lost and only two bands remain. This provides evidence that the amino-*m*-xylyl complexes exist as the amine form and not the protonated ammonium form, which aligns with the pK_a value of 4.6 for the conjugate acid of aniline.

3.2.3 Luminescence excitation

Excitation spectra were obtained by monitoring emission at a characteristic emission wavelength of the corresponding lanthanide. The spectra in Figure 3.14 and Figure 3.15 show the absorption spectra of the europium *m*-xylyl complexes compared to their excitation spectra, where the emission intensity at 616 nm ($^5D_0 \rightarrow {}^7F_2$) was monitored. For Figure 3.16 and Figure 3.17, characteristic terbium emission at 544 nm ($^5D_4 \rightarrow {}^7F_5$) was monitored.

This provided evidence that the aromatic moiety within the ligand was able to sensitise the lanthanide emission when the complex was excited with shorter wavelengths than the direct excitation of 394 nm for europium or 366 nm for terbium, and was confirmed by emission spectra: excitation of the sample at an appropriate absorption wavelength for the ligand generated a lanthanide emission spectrum.

However, there is a mismatch between the absorption and excitation spectra. This is particularly pronounced for the europium complexes, in which a number of sharp transitions are observed in addition to the broad transitions associated with absorption by an organic chromophore. The fact that these two types of transition are of similar intensity despite the much lower probability of *f-f* transitions in absorption reflects the possibility of charge transfer quenching in europium-containing systems. The terbium complexes also show relatively inefficient energy transfer.

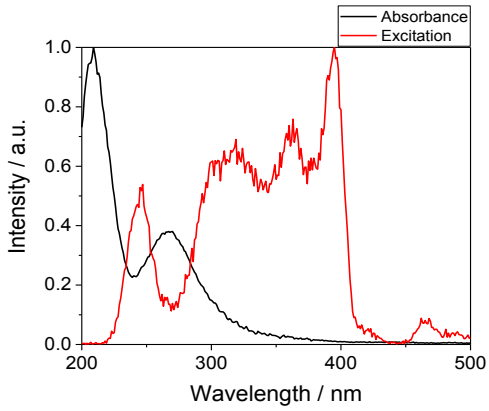


*Figure 3.14 Normalised absorption and excitation (λ_{em} = 616 nm) spectra for Eu_2.**5***

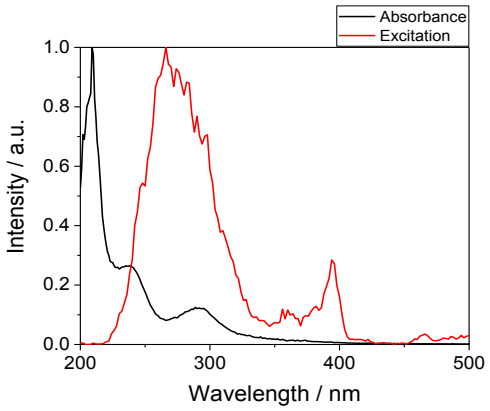


*Figure 3.15 Normalised absorption and excitation (λ_{em} = 616 nm) spectra for Eu_2.**6***

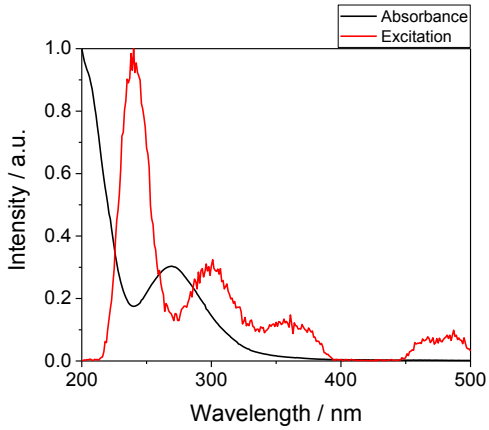


*Figure 3.16 Normalised absorption and excitation (λ_{em} = 544 nm) spectra for Tb_2.**5***

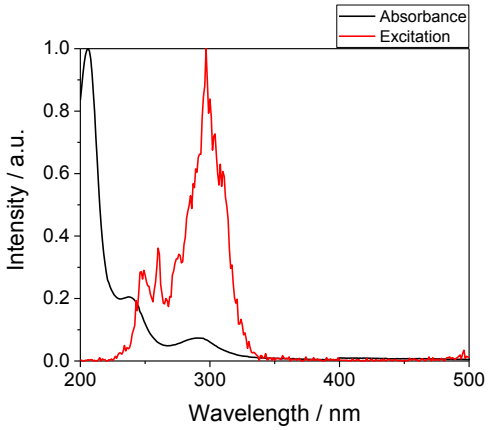


*Figure 3.17 Normalised absorption and excitation (λ_{em} = 544 nm) spectra for Tb_2.**6***

3.2.4 Luminescence emission

Excitation and emission spectra were measured for the europium and terbium *m*-xylyl complexes as their luminescence falls in the visible wavelength range and within the limits of the detector on many spectrophotometers. The emission spectra in Figure 3.18 to Figure 3.21 are generated *via* ligand excitation.

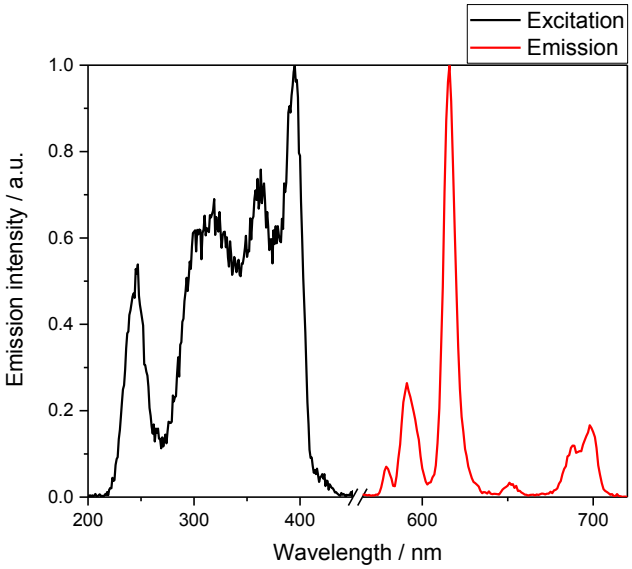


*Figure 3.18 Normalised luminescence excitation spectrum (λ_{em} = 616 nm) and emission spectrum (λ_{ex} = 240 nm) of Eu_2.**5** in HEPES at pH 7.4*

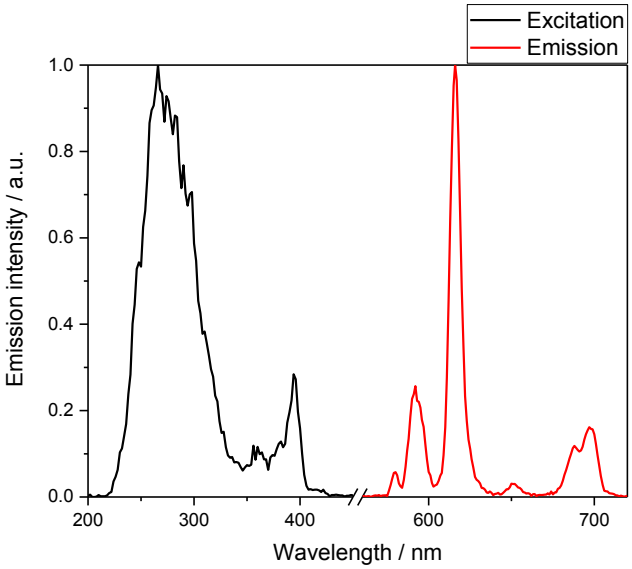


*Figure 3.19 Normalised luminescence excitation spectrum (λ_{em} = 616 nm) and emission spectrum (λ_{ex} = 270 nm) of Eu_2.**6** in HEPES at pH 7.4*

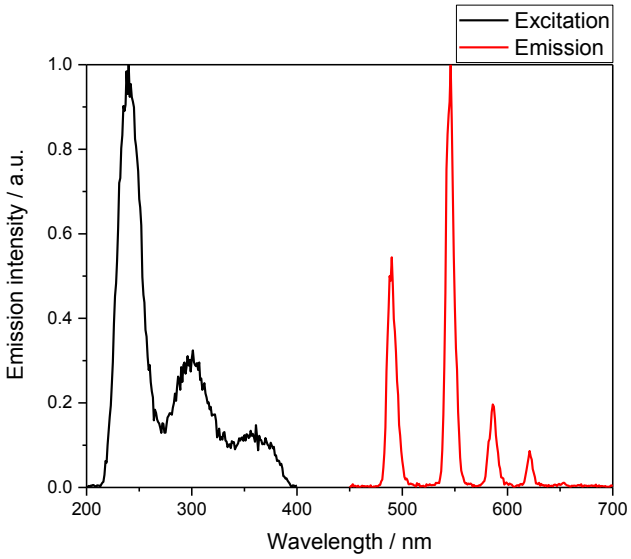


*Figure 3.20 Normalised luminescence excitation spectrum (λ_{em} = 544 nm) and emission spectrum (λ_{ex} = 240 nm) of Tb_2.**5** in HEPES at pH 7.4*

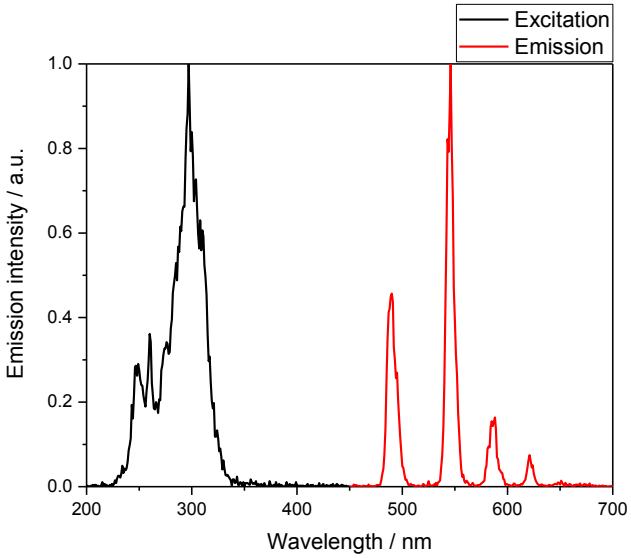


*Figure 3.21 Normalised luminescence excitation spectrum (λ_{em} = 544 nm) and emission spectrum (λ_{ex} = 290 nm) of Tb_2.**6** in HEPES at pH 7.4*

3.2.5 Luminescence lifetimes and *q* values

Luminescence lifetime measurements for the complexes whose wavelengths and timescales were within the range of the detector were recorded.

Compound	τ_{H2O} / **ms**	τ_{D2O} / **ms**	***q***
Eu_2.**5**	0.54	1.61	1.2
Eu_2.**6**	0.38	1.43	2.0
Tb_2.**5**	1.05	2.04	2.0
Tb_2.**6**	1.31	1.74	0.6

Table 3.1 Calculated q values for some m-xylyl complexes, where the mean of multiple (between 1 and 5 sets per compound) measurements which were within 10% error is given

The *q* values[27] calculated for the *m*-xylyl complexes are shown in Table 3.1. Eu_2.**5** has a *q* value close to one and Eu_2.**6** was calculated as having two bound water molecules per lanthanide centre. This held for all batches of these complexes tested. This suggests that although the structures appear similar on paper, exchanging a nitro group for an amino group apparently causes the complex to adopt a very different conformation in solution, adding weight to the evidence of the NMR spectra discussed above. In addition, it is clear that a small change in recorded lifetime can lead to a large change in *q* value so it can be noted that the output from the modified Horrocks equation[27] is very sensitive to the input values.

Perhaps even more interesting is that for the same ligand, changing the lanthanide has an apparently large effect on the number of bound solvent molecules. Tb_2.**5** gave a greater *q* value than its europium analogue. The differences in lifetime may result from differences in conformation, in which perhaps the pendent xylyl group might block or allow approach of solvent molecules. It has been shown that complexes that adopt TSAP geometry experience much faster exchange of bound water molecules than SAP isomer complexes.[28–30] The ^{1}H NMR spectrum of Eu_2.**5** suggests that this complex exists as both the SAP and TSAP conformer but the ^{1}H NMR for the terbium complex is difficult to resolve due to the fluxional nature of 7-coordinate lanthanide complexes.[31–33] This fluxional behaviour is itself

suggestive, and implies a more open structure in the terbium complex, since fast exchange between isomers suggests reduced rotational rigidity.

In contrast to this, for the amino complexes, the *q* values calculated for the europium and terbium complexes exhibited the reverse, where here the value returned for terbium was lower than that for europium. The ^{1}H NMR spectrum for Eu_2.**6** spectrum shows an obvious peak corresponding to the SAP conformation at 33 ppm but only a barely discernible spike at 20 ppm which would represent TSAP but may be an artefact in the baseline of the spectrum. Axial proton resonances in the ^{1}H NMR of Tb_2.**6** were observed at −240 and −273 ppm which are in the region usually observed for the TSAP isomer, and no peaks in the SAP region of −400 ppm were found. This is likely to be a consequence of the presence of two paramagnetic centres, and may not reflect a transition to TSAP geometry.

While both europium and terbium are paramagnetic, the paramagnetism of europium only arises from the thermal population of the $^{7}F_1$ state; since the Landé formula predicts that the magnetic moment will be given by $g_J[J(J+1)]^{½}$, the $^{7}F_0$ ground state does not give rise to a magnetic moment. Given the splitting of the $^{7}F_1$ state from the $^{7}F_0$ ground state is approximately 400 cm^{-1}, the upper state Boltzmann population would be around 14.5% at 298 K for a system containing one europium ion; in a binuclear europium complex, this would mean a 29% probability of finding **one** europium ion in the $^{7}F_1$ state at any given time point. The probability of finding **both** europium ions in this state would be around 2%. Thus, the NMR of the europium complex will reflect only small perturbations to the normal spectrum of a mononuclear europium complex. By contrast, **all** the lanthanide centres in a binuclear terbium complex will exhibit magnetic properties (ground state $^{7}F_6$), meaning that the two ions can work in concert or against one another depending on geometric (and, to a

lesser extent, through-bond) effects. This problem of multiple paramagnetic centres requires further investigation before it will be possible to make unqualified statements about structure in binuclear complexes: for now, it is probably best to rely on a europium complex when ascribing structural features to a multinuclear lanthanide complex.

The q value is an average over all lanthanide environments, so some terbium centres may have one coordinated water and others may have none, to give an average of 0.6. This again indicates the conformation in solution is not straightforward.

3.3 Choice of complexes

3.3.1 Europium

Europium complexes were found to offer favourable luminescence and NMR properties. The effect of the europium-induced shifts in ^{1}H and ^{31}P NMR spectra can be observed over a good chemical shift range with good resolution. Among many other europium complexes, the nitro-*m*-xylyl and amino-*m*-xylyl europium complexes were studied.

3.3.2 Terbium

Terbium was of interest as its slightly smaller ionic radius, and the corresponding increase in charge density, might be expected to give different binding constants to those of analogous europium complexes as a result of differing electrostatics and different conformational and isomeric equilibria, although this was shown in Chapter 2 to be a far too simplistic viewpoint. Terbium is much more luminescent than europium, however ^{1}H NMR spectra of terbium-containing species were not as well-resolved. Both the nitro-*m*-xylyl and amino-*m*-xylyl complexes of terbium were investigated.

3.3.3 Ytterbium

Only the nitro-*m*-xylyl complex of ytterbium was synthesised. Ytterbium luminescence is not as easy to observe as emission falls in the IR region, however ^{1}H NMR of ytterbium complexes and, more importantly, the effect of the presence of these complexes on the ^{1}H and ^{31}P NMR spectra of guests, gave results rich in information.

3.4 Gadolinium

It was not feasible to measure luminescence or ^{1}H NMR spectra of gadolinium complexes, however their effect on the magnetic relaxation of guest species was investigated *via* T_1 lifetime measurements.

3.5 Yttrium

While not a lanthanide, this is a useful element to consider as its chemical properties are similar to those of the lanthanides, in that is also a hard cation in the +3 oxidation state, and of similar ionic radius. The benefit of using yttrium analogues of these lanthanide complexes for NMR studies is that yttrium is not paramagnetic, giving NMR spectra which are easier to interpret. Additional information on interactions between the yttrium atoms and other atoms either nearby in the molecule or those binding to the metal centre may be gleaned, as ^{89}Y, which is the 100% naturally abundant isotope, is a spin-½ nuclide giving rise to splitting in NMR spectra. The yttrium nitro-*m*-xylyl complex Y_2.**5** was synthesised under the usual methanolic conditions.

3.6 References

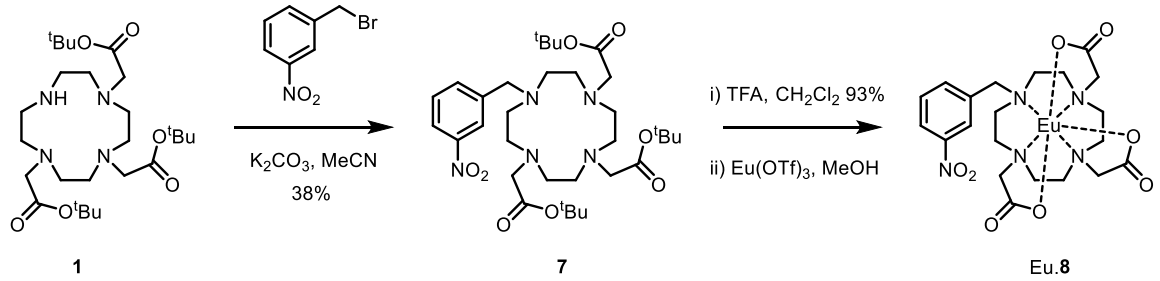
(1) Placidi, M. P.; Natrajan, L. S.; Sykes, D.; Kenwright, A. M.; Faulkner, S. *Helv. Chim. Acta* **2009**, *92*, 2427–2438.
(2) Placidi, M. P. Polymetallic Lanthanide Complexes for Application in Luminescence and Magnetic Resonance Imaging, University of Manchester, 2009.
(3) Tilney, J. A.; Sørensen, T. J.; Burton-Pye, B. P.; Faulkner, S. *Dalton Trans.* **2011**, *40*, 12063–12066.
(4) Hill, L. R.; Sørensen, T. J.; Blackburn, O. A.; Brown, A.; Beer, P. D.; Faulkner, S. *Dalton Trans.* **2013**, *42*, 67–70.
(5) Thom, J. Self-assembly and anion recognition with binuclear lanthanide complexes, University of Oxford, 2014.
(6) Sørensen, T. J.; Hill, L. R.; Faulkner, S. *ChemistryOpen* **2015**, *4*, 509–515.
(7) Sørensen, T. J.; Hill, L. R.; Tilney, J. A.; Blackburn, O. A.; Jones, M. W.; Tropiano, M.; Faulkner, S. *Eur. J. Inorg. Chem.* **2014**, *2014*, 2520–2528.
(8) Dadabhoy, A.; Faulkner, S.; Sammes, P. G. *J. Chem. Soc., Perkin Trans. 2* **2002**, 348–357.
(9) Chhikara, B. S.; Kumar, N.; Tandon, V.; Mishra, A. K. *Bioorg. Med. Chem.* **2005**, *13*, 4713–4720.
(10) Vetráková, Ľ.; Ladányi, V.; Al Anshori, J.; Dvořák, P.; Wirz, J.; Heger, D. *Photochem. Photobiol. Sci.* **2017**, *16*, 1749–1756.
(11) Hall, J.; Häner, R.; Aime, S.; Botta, M.; Faulkner, S.; Parker, D.; de Sousa, A. S. *New J. Chem.* **1998**, *22*, 627–631.
(12) Tropiano, M.; Blackburn, O. A.; Tilney, J. A.; Hill, L. R.; Placidi, M. P.; Aarons, R. J.; Sykes, D.; Jones, M. W.; Kenwright, A. M.; Snaith, J. S.; Sørensen, T. J.; Faulkner, S. *Chem. Eur. J.* **2013**, *19*, 16566–16571.
(13) Bleaney, B. *J. Magn. Reson.* **1972**, *8*, 91–100.
(14) Bleaney, B.; Dobson, C. M.; Levine, B. A.; Martin, R. B.; Williams, R. J. P.; Xavier, A. V. *J. Chem. Soc. Chem. Commun.* **1972**, 791b.
(15) Nagakura, S.; Kojima, M.; Maruyama, Y. *J. Mol. Spectrosc.* **1964**, *13*, 174–192.
(16) Galloway, D. B.; Bartz, J. A.; Huey, L. G.; Crim, F. F. *J. Chem. Phys.* **1993**, *98*, 2107–2114.
(17) Sinha, H. K.; Yates, K. *J. Chem. Phys.* **1990**, *93*, 7085.
(18) Kröhl, O.; Malsch, K.; Swiderek, P. *Phys. Chem. Chem. Phys.* **2000**, *2*, 947–953.
(19) Kimura, K.; Tsubomura, H.; Nagakura, S. *Bull. Chem. Soc. Jpn.* **1964**, *37*, 1336–1346.
(20) Kimura, K.; Nagakura, S. *Mol. Phys.* **1965**, *9*, 117–135.
(21) Honda, Y.; Hada, M.; Ehara, M.; Nakatsuji, H. *J. Chem. Phys.* **2002**, *117*, 2045–2052.
(22) Lombardi, J. R. *Chem. Phys.* **1978**, *28*, 41–45.
(23) Masaki, K. *Bull. Chem. Soc. Jpn.* **1936**, *11*, 346–348.
(24) Forbes, W. F.; Leckie, I. R. *Can. J. Chem.* **1958**, *36*, 1371–1380.
(25) Dearden, J. C.; Forbes, W. F. *Can. J. Chem.* **1960**, *38*, 896–910.
(26) Iweibo, I.; Oderinde, R. A.; Faniran, J. A. *Spectrochim. Acta Part A Mol. Spectrosc.* **1982**, *38*, 1–7.
(27) Beeby, A.; Clarkson, I. M.; Dickins, R. S.; Faulkner, S.; Parker, D.; Royle, L.; de Sousa, A. S.; Williams, J. A. G.; Woods, M. *J. Chem. Soc., Perkin Trans. 2* **1999**, *2*, 493–504.
(28) Aime, S.; Barge, A.; Botta, M.; De Sousa, A. S.; Parker, D. *Angew. Chem. Int. Ed.* **1998**, *37*, 2673–2675.
(29) Aime, S.; Barge, A.; Bruce, J. I.; Botta, M.; Howard, J. A. K.; Moloney, J. M.; Parker, D.; de Sousa, A. S.; Woods, M. *J. Am. Chem. Soc.* **1999**, *121*, 5762–5771.
(30) Dunand, F. A.; Aime, S.; Merbach, A. E. *J. Am. Chem. Soc.* **2000**, *122*, 1506–1512.
(31) Aime, S.; Botta, M.; Ermondi, G. *Inorg. Chem.* **1992**, *31*, 4291–4299.
(32) Aime, S.; Botta, M.; Fasano, M.; Marques, M. P. M.; Geraldes, C. F. G. C.; Pubanz, D.; Merbach, A. E. *Inorg. Chem.* **1997**, *36*, 2059–2068.
(33) Woods, M.; Aime, S.; Botta, M.; Howard, J. A. K.; Moloney, J. M.; Navet, M.; Parker, D.; Port, M.; Rousseaux, O. *J. Am. Chem. Soc.* **2000**, *122*, 9781–9792.

Chapter 4 Mononuclear complexes

4.1 Introduction

Although the primary concern of this thesis involves exploiting cooperative effects in binuclear lanthanide complexes, mononuclear complexes were also studied in order to better understand the behaviour of the binuclear complexes. The nitrobenzyl-appended complex Eu.**8** is as structurally similar to Eu2.**5** as possible and allows consideration of the contribution of the reverse chelate effect. The simpler Eu.**12** removes the possible contribution of π-π stacking to interactions between the complex and the guest.

4.2 3-Nitrobenzyl complex



*Scheme 4.1 Reaction pathway for synthesis of Eu.**8***

Eu.**8** was synthesised as a mononuclear analogue of the nitro-*m*-xylyl complex Eu2.**5**, in order to provide a point of comparison in which guests can coordinate to only one lanthanide ion.

The synthesis of Eu.**8** outlined in Scheme 4.1 follows a similar reaction pathway to that of the *m*-xylyl complexes described in Chapter 3 in Scheme 3.1, except here the reagents were combined in a different ratio.[1] This was because using an excess of the triester **1**, as is usual for the *m*-xylyl complexes, led to difficulty in separation during purification by column chromatography due to the similar R_f values of the product and the unreacted starting material. For the nucleophilic substitution reaction step, the temperature was lower and the

reaction time shorter than those in the *m*-xylyl scheme, as there was not the large steric bulk hindering the approach of a second triester ring. When initially attempted, using similar conditions in the first step of the pathway to those in Chapter 3 in Scheme 3.1 led to overreaction. Subsequently, the usual method of deprotection with trifluoroacetic acid gave the ligand which was then taken for complexation with europium triflate in methanol. This method was found to be suitable for complexation of the ligand **8** and did not lead to precipitation as was sometimes the case with the binuclear complexes. The salt content was reduced by dialysis in a Spectrum Labs Float-A-Lyzer® G2 dialysis device with a 100 – 500 Da molecular weight cut-off, and the product Eu.**8** used in photophysical studies and titrations.

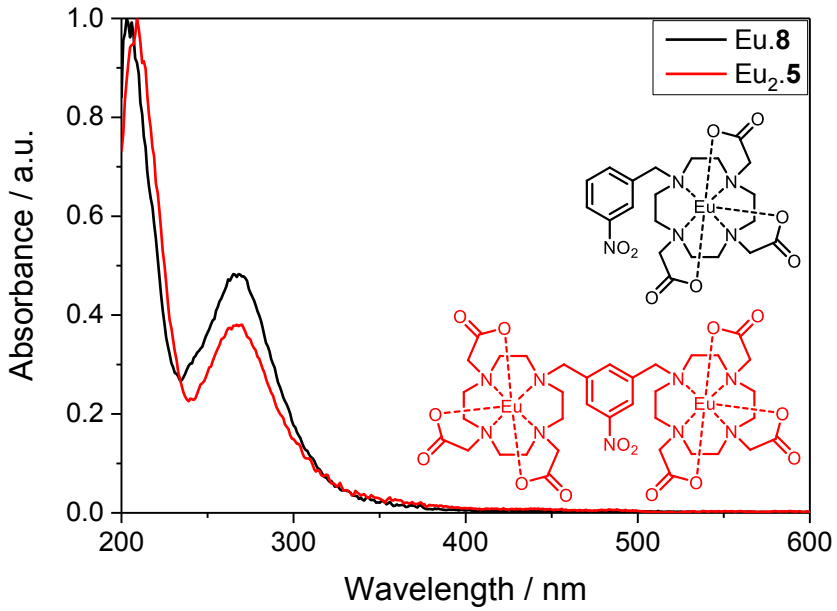


*Figure 4.1 Normalised to λ_{max} UV-vis absorption spectra of Eu.**8** (black trace) and Eu$_2$.**5** (red trace) in water*

Comparing the UV-vis absorption spectra of Eu.**8** and Eu$_2$.**5** displayed in Figure 4.1, it is obvious that the spectral forms are very similar. The europium absorption transition that would be observed at 394 nm is swamped by the red edge of the ligand absorption spectrum, and the two dominant bands which can be attributed to electronic transitions centred on the

chromophore moiety exhibit maxima at almost identical wavelengths. These are also very similar to absorption spectra recorded for nitrobenzene.

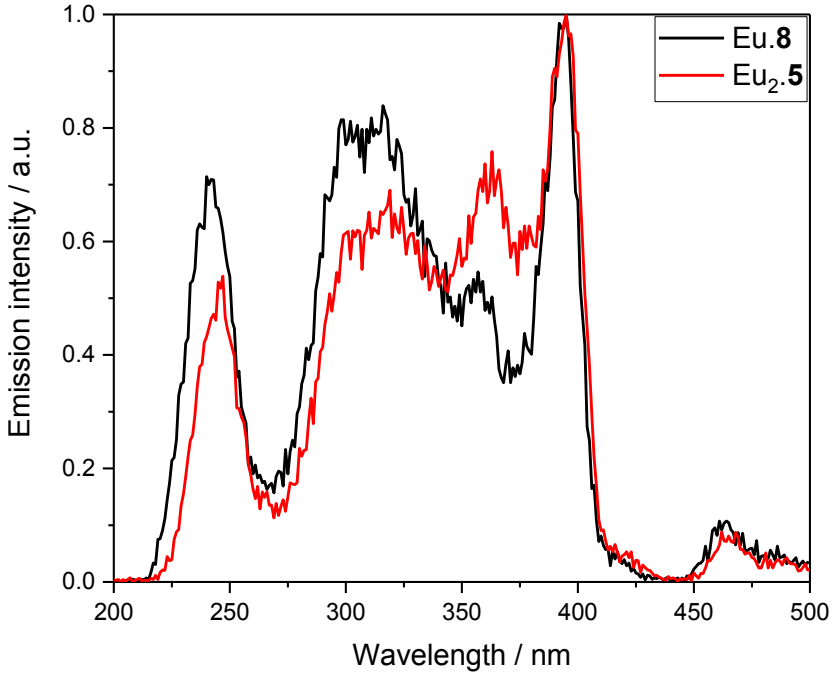


*Figure 4.2 Normalised excitation spectra of Eu.**8** (black trace) and Eu$_2$.**5** (red trace) in HEPES buffer at pH 7.4 (λ_{em} = 616 nm)*

Comparison of the excitation spectra of Eu$_2$.**5** and Eu.**8** reveals that the peaks are found at the same wavelengths but with different weightings, though both are dominated by direct excitation of the metal ion. The peak at 394 nm corresponds to direct excitation *via* the europium and it has previously been found for the europium nitro-*m*-xylyl complex that excitation *via* the n → π* transition of the ligand chromophore has a lower quantum yield than direct excitation due to inefficient sensitisation, with another process competing with population of the emissive state.[2] The different weighting of the peaks below 394 nm shows that the photophysics of energy transfer from the ligand to the lanthanide is more efficient at shorter wavelength (higher energy) for Eu.**8** but at longer wavelength (lower energy) for Eu$_2$.**5**. This could be attributed to differences in absorption probability between the two species. Alternatively, it may be that the greater conformational flexibility in the

mononuclear complex allows the ligand donor state to achieve closer proximity to the lanthanide.

Measurements of the luminescence lifetime of this nitrobenzyl complex Eu.**8** in H_2O and D_2O allowed calculation of the *q* value.[3] The data for this is shown in Table 4.1. The number of bound solvent molecules was calculated to be two, whereas for the binuclear nitro-*m*-xylyl analogue Eu_2.**5** the number was much closer to one. This difference could, as discussed during the comparison of the nitro-*m*-xylyl and amino-*m*-xylyl *q* values in Chapter 3 in Section 3.2.5, be attributed to the conformation adopted in solution by the nitro-*m*-xylyl complex.

Compound	τ_{H2O} / **ms**	τ_{D2O} / **ms**	***q***
Eu.**8**	0.41	1.70	1.9

*Table 4.1 Calculated q value for the nitrobenzyl complex Eu.**8** where the mean of two sets of measurements which were within 10% error is given*

4.3 Coumarin complex

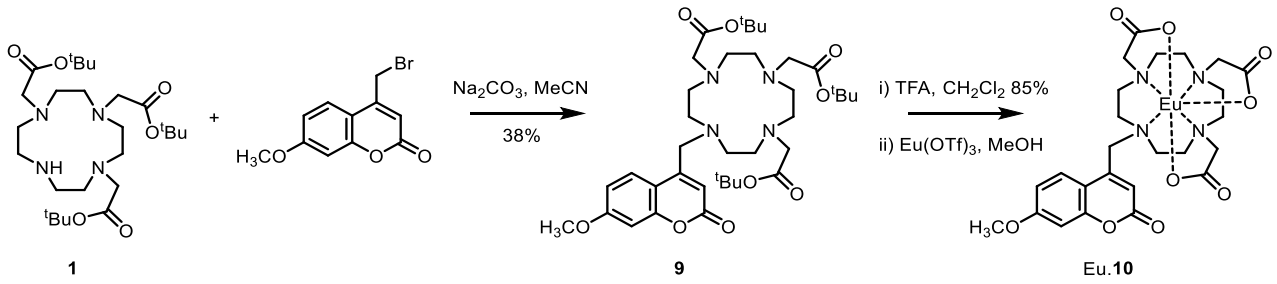
4.3.1 Synthesis

Coumarin and its derivatives have useful photophysical properties, particularly as a consequence of their high quantum yields, large spectral range, and relatively high photostability. In addition to these properties, their high solubility in common solvents allows their use in practical optical systems. Coumarin derivatives find use as laser dyes, chromophores, and fluorescent labels and probes.[4–7] Coumarin itself has a relatively low LD_{50} compared to similar molecules, and umbelliferone, or 7-hydroxycoumarin, even lower still. These compounds may thus be taken up by cells without causing cell death.[7]



Figure 4.3 Coumarin and derivatives, including herniarin

Here, a herniarin (Figure 4.3) derivative was used as the starting material and the basis for the chromophore. Herniarin absorbs strongly in the UV and is commonly used as a fluorescent label for fatty acids.[8]



*Scheme 4.2 Reaction pathway for synthesis of Eu.**10***

The coumarin complex Eu.**10** was synthesised *via* the route outlined in Scheme 4.2. Reacting triester **1** with a small excess of 4-(bromomethyl)-7-methoxycoumarin was found to give easier separation, on account of R_f values, than using excess **1** as with the syntheses of the *m*-xylyl complexes in this thesis. The reagents were heated under reflux in basic acetonitrile for 5 days. Monitoring by TLC and mass spectrometry confirmed that the bromomethyl

coumarin starting material had been consumed. The inorganic salts were removed by filtration and the solvent removed under reduced pressure. The starting material was less soluble in methanol than the product, and slow evaporation of a solution in hot methanol allowed fractional precipitation of the starting material from the product. Successive evaporations of the supernatant followed by dichloromethane-methanol gradient column chromatography on silica gel yielded the product as a yellow solid when the methanol concentration was increased to 4% v/v.

4.3.2 Structural chemistry

Crystals of Eu.**10** were grown by slow evaporation of D_2O. When removed from the mother liquor, these crystals were found to be highly sensitive to solvent loss, meaning that water was integral to the structure and therefore data collection was difficult due to crystal decomposition. The crystals were found to adopt three different morphologies. The three polymorphs – monoclinic, triclinic, and orthorhombic – were all found to be tetrameric when their structures were solved by Dr Amber Thompson (further data in Appendix C.4). Crystal structures of seven-coordinate cyclen-derived lanthanide complexes are rare, which may be attributed to their asymmetry and the consequent difficulties in packing.[16–18]

The crystal structure shown in Figure 4.4 shows a tetramer with bridging carboxylates. Other aggregated structures of cyclen derivatives have been previously investigated by the Merbach group in 2006,[9] and the Platas-Iglesias group in 2013,[10] and it is clear that coordinatively unsaturated lanthanide complexes can use carboxylates bound to one lanthanide ion as a bridging donor to another.

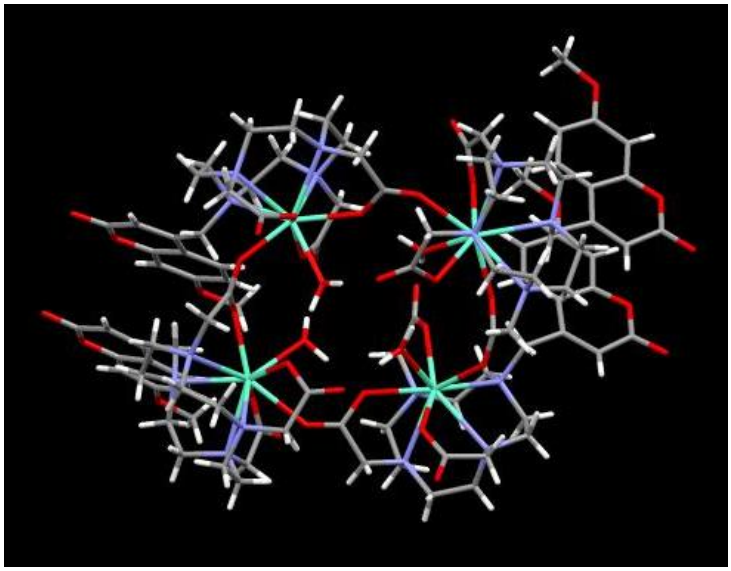


*Figure 4.4 Crystal structure of Eu.**10** (solved by Amber Thompson)*

Upon detailed inspection of the crystal structure, it can be noted that the units within the tetramer arrange in an interesting pattern. In order to maximise π-π stacking between the coumarin rings, the bridging carboxylate alternates between *cis* and *trans* in its position on the cyclen ring relative to the appended coumarin ring, in terms of which nitrogen atom it is attached to. That is, if the coumarin ring is, by definition, bound to N4, the bridging carboxylate alternates between N1 (*cis* to N4) and N2 (*trans* to N4) on each monomer, as shown in the schematic in Figure 4.5.

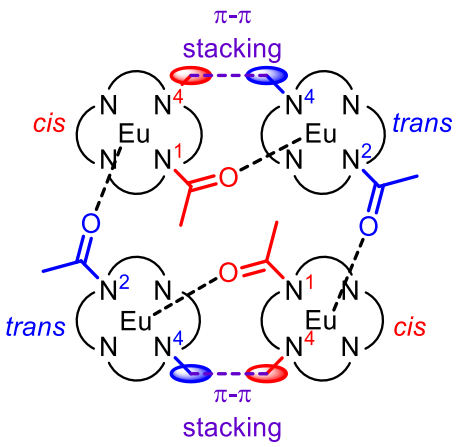


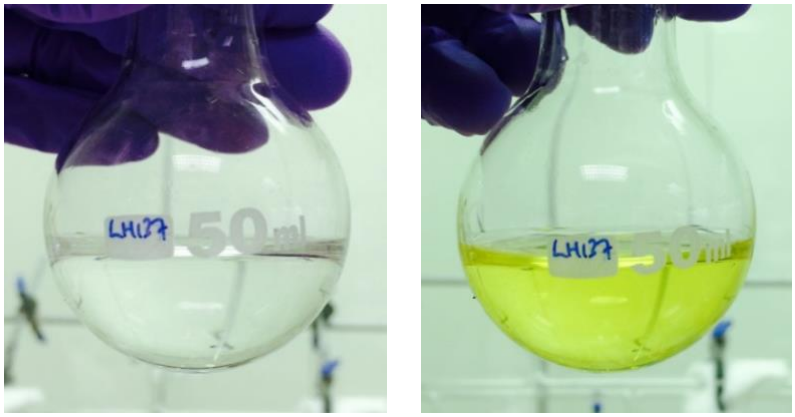
Figure 4.5 Schematic showing alternation between cis and trans of the bridging carboxylate relative to the coumarin ring, where the red and blue ellipses represent the coumarin rings

The crystal structure shows that SAP conformation is adopted, and that the coordination

sphere of the europium cation is filled with seven donor atoms from the ligand, one from a capping water molecule, and one oxygen atom from a carboxylate group from a second ligand within the tetramer.

4.3.3 pH-dependence

Interesting pH-dependent colour changes were noted with this complex. In acidic and neutral conditions, a solution of the complex was colourless, and in basic conditions the solution became bright yellow, as displayed in Figure 4.6.



neutral pH basic pH

*Figure 4.6 Solutions of Eu.**10** at neutral and basic pH*

This colour change was fully reversible, and no colour change was seen for a solution of the uncomplexed ligand. These observations, combined with evidence from luminescence emission spectra recorded at different pH values (shown later in Figure 4.9), suggested that the change must involve the presence of the europium ion rather than, for example, any enolisation affecting the electron distribution over the coumarin ring as seen by Li *et al.*,[11] or cleavage of the coumarin ring as seen by Stanchev *et al.*[12] The reversible nature of the change and its pH-dependence indicates that it is most likely that a bound water molecule was deprotonated to give a hydroxide ion. One explanation for this could be that the structure may adopt open and closed conformations where the coumarin could potentially reach around and coordinate to the europium in the manner shown in Figure 4.7.[13] Otherwise, the

change could be related to dimerisation, which correlates with the carboxylate bridging in the crystal structure.

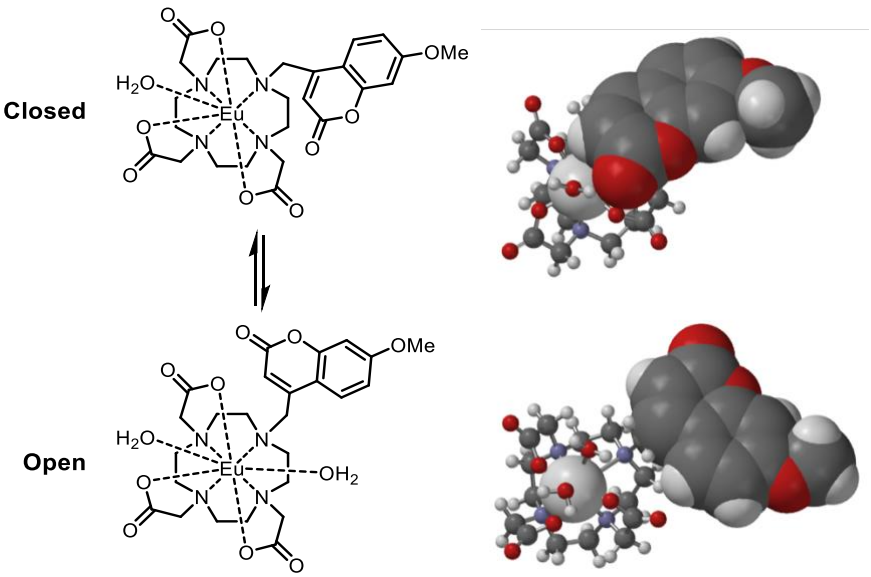


Figure 4.7 Equilibrium of the molecular solution state structure of the complex proposed by Junker et al. in 2018 (left) and a molecular model of the structure (right)

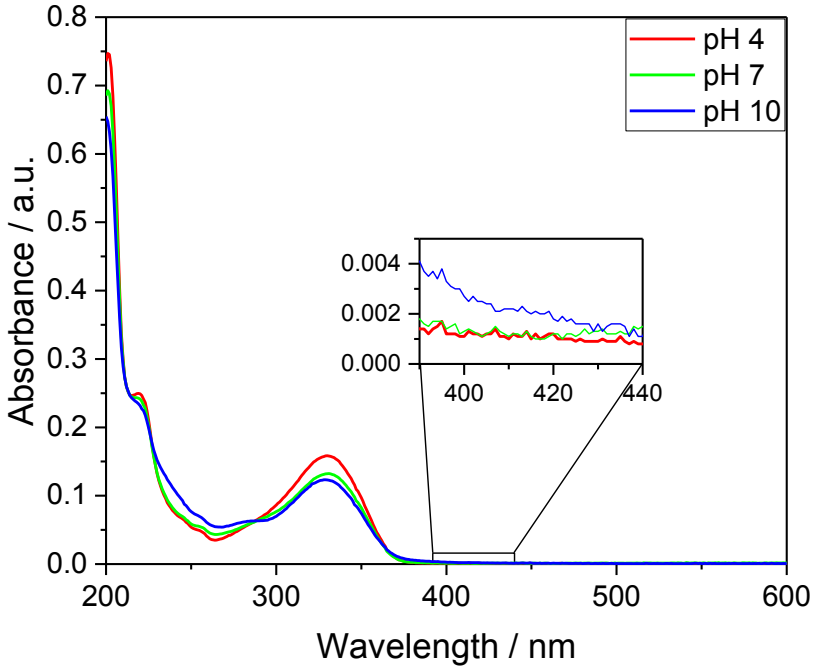


*Figure 4.8 UV-vis absorption spectra of 10^{-4} M Eu.**10** in water at pH 4 (red), 7 (green), and 10 (blue)*

The UV-vis absorption spectrum of Eu.**10** at different pH values, shown in Figure 4.8,

appeared to change very little. From these spectra, it is clear that absorption in the ultraviolet region was of far greater magnitude than that in the visible. However, close inspection of the red edge of the absorption spectra (inset to Figure 4.8) reveals that the absorption spectrum at pH 10 extends into the visible region, in agreement with the earlier visual colour change to yellow in basic conditions.

Otherwise, a decrease in intensity for the peaks at 200 and 330 nm was observed, and the shoulder at 220 nm became less pronounced. These bands lie in the region of ligand absorption and correspond to $\pi \rightarrow \pi^*$ and $n \rightarrow \pi^*$ transitions on the coumarin. This change is not ascribable to solvatochromism but to the formation of a different species in solution. If the deprotonation is postulated to be occurring for a solvent molecule at the europium centre, this could result in changes to the coordination sphere (which would also be consistent with the open and closed forms discussed above), and in turn change the absorption spectrum.

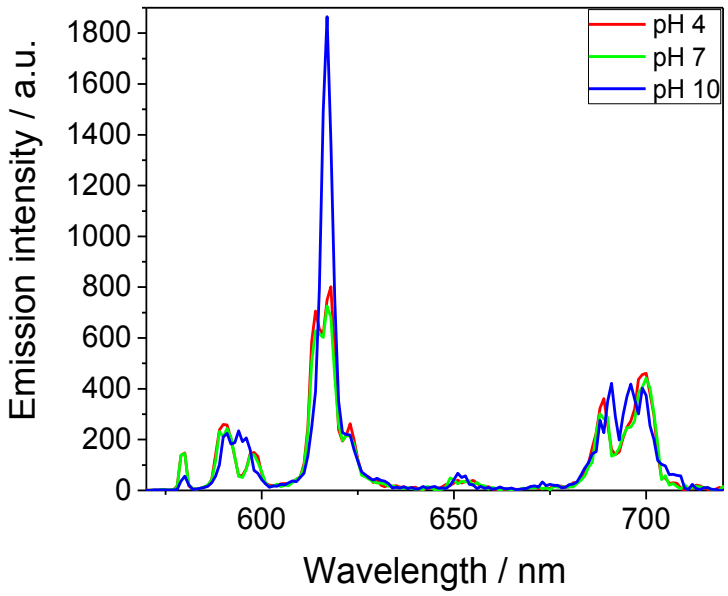


*Figure 4.9 Luminescence emission spectra of 10^{-4} M Eu.**10** at pH 4 (red), 7 (green), and 10 (blue) (λ_{ex} = 232 nm, s.w.$_{ex}$ = 14 nm, s.w.$_{em}$ = 1 nm)*

The luminescence emission spectra of Eu.**10** in Figure 4.9 showed a change in the $\Delta J = 2$ peak with pH once the pH became significantly basic. This transition is known to be hypersensitive to a change in environment at the europium atom.[14] At basic pH this peak was much larger than at neutral or acidic pH, and this increase in quantum yield is additional evidence for the deprotonation of bound water theory. Additionally, the fine structure of all the peaks in the spectrum reflected a change in the local ligand field at the lanthanide with changing pH, causing splitting of the m_j states in all peaks.

The coumarin complex also exhibited a longer luminescence lifetime in basic solution. This was observed not only for the $\Delta J = 2$ peak but also for the $\Delta J = 1$ peak whose intensity showed little change on the emission spectrum in Figure 4.9; this is consistent with deprotonation of a water molecule at the lanthanide, which would result in loss of an O-H oscillator. The results are shown in Table 4.2. The lifetimes observed around pH 4 and pH 7 are within error of one another.

pH	Emission peak	Lifetime / ms
4.0	$\Delta J = 1$	0.38
	$\Delta J = 2$	0.40
6.9	$\Delta J = 1$	0.41
	$\Delta J = 2$	0.42
10.1	$\Delta J = 1$	0.69
	$\Delta J = 2$	0.74

*Table 4.2 Luminescence lifetimes of Eu.**10** at different pH values, measured at different emission wavelengths. Excitation via the coumarin antenna or directly via the lanthanide gave numbers that agreed within a 10% error. The mean of these two values is presented*

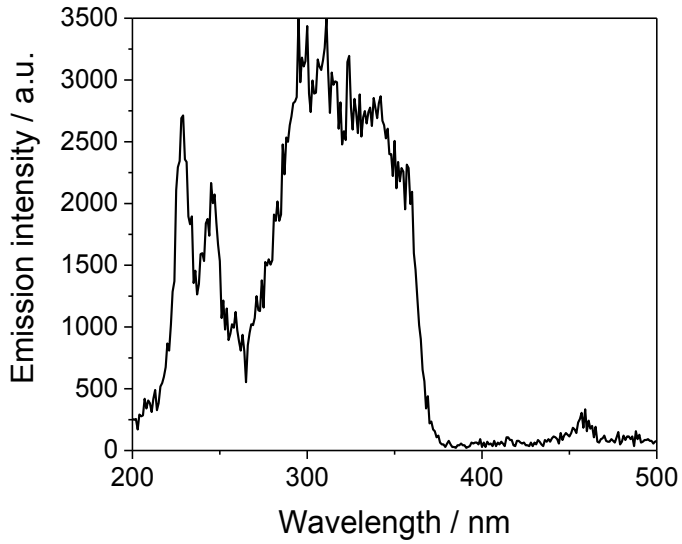


*Figure 4.10 Superimposed normalised excitation spectra of Eu.**10** in water at pH 6.9 (λ_{em} = 616 nm)*

The excitation spectrum of Eu.**10** in water in Figure 4.10 reveals that direct excitation of the lanthanide at 394 nm is of negligible effectiveness compared to the efficient energy transfer from the coumarin ligand.

The ^{1}H NMR spectra of Eu.**10** at a range of pD values in D_2O in Figure 4.11 showed sharpening with increasing pD as is observed for other cyclen-derived lanthanide complexes. Once again, this is consistent with the adoption of a more ordered (and probably closed) conformation at high pD.

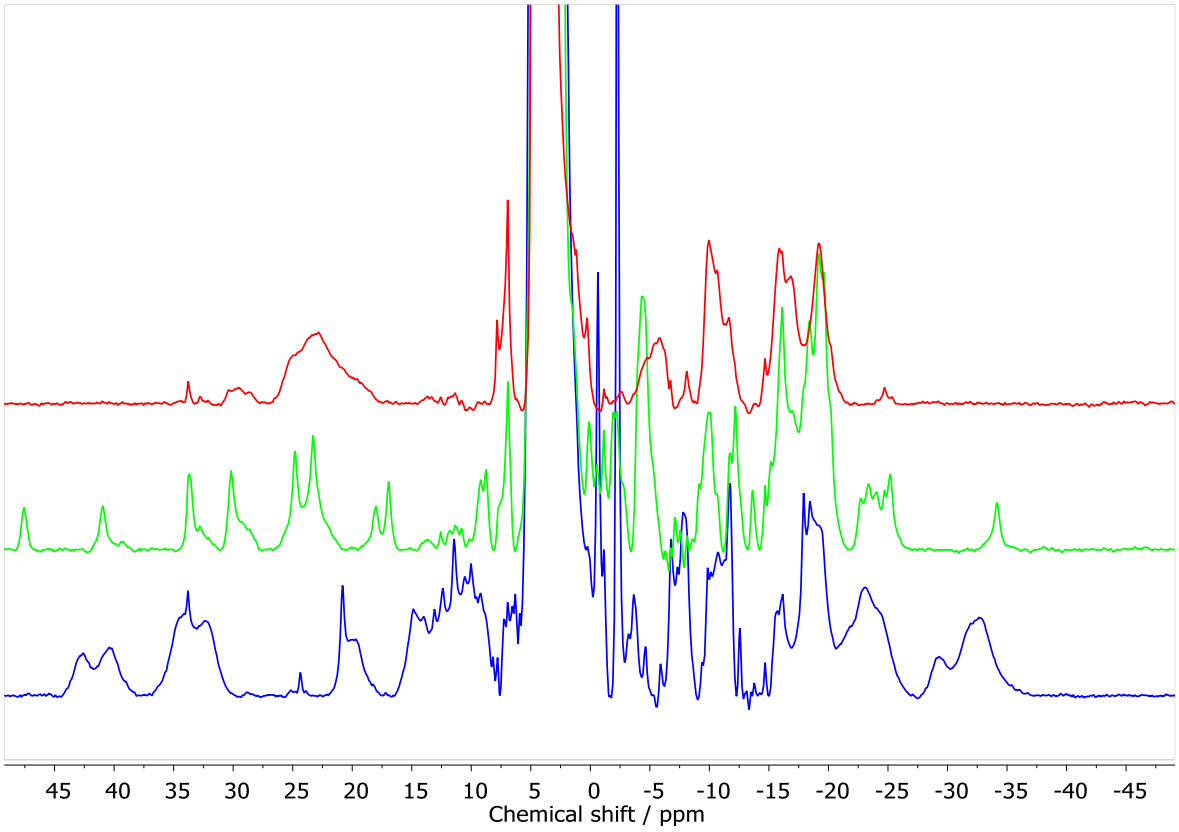


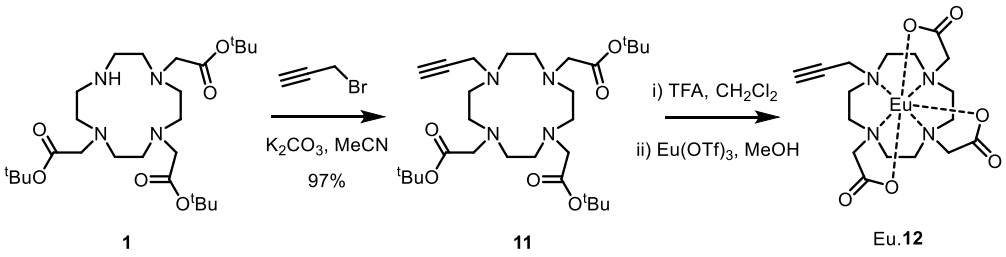
*Figure 4.11 ^{1}H NMR spectra of complex Eu.**10** in D_2O at pD = 4 (red), 6 (green), and 10 (blue)*

Compound	**τ_{H2O} / ms**	**τ_{D2O} / ms**	***q***
Eu.**10**	0.53	1.56	1.2

*Table 4.3 Calculated q value for the coumarin complex Eu.**10** where the mean of two sets of measurements which were within 10% error is given*

The calculation of the *q* value in Table 4.3 gives a result of 1.2, or one bound water molecule per europium centre. However, if the τ_{H2O} values of around 0.4 ms for the pH 6.9 solution from Table 4.2 above are instead used, this gives a *q* value closer to 1.9, again highlighting the sensitivity of the modified Horrocks equation to input values. This difference in lifetime could be affected by the salt content of the solution and is closer to the value reported by Junker *et al.*[13]

4.4 Propargyl complex



*Scheme 4.3 Reaction pathway for synthesis of Eu.**12***

The propargyl complex Eu.**12**, synthesised *via* the established pathway shown in Scheme 4.3,[15] provides an interesting point of comparison with the other lanthanide complexes investigated in this thesis, as it contains no chromophore and is again a mononuclear complex and thus binding to guests cannot benefit from an analogy to the chelate effect. In addition to the absence of a chromophore, it lacks any type of aromatic group which could participate in π-π stacking with aromatic guests such as ATP or nicotinate, but perhaps guests would experience less steric hindrance upon approach due to the smaller propargyl group.

4.5 References

(1) Karhunen, U.; Rosenberg, J.; Lamminmäki, U.; Soukka, T. *Anal. Chem.* **2011**, *83*, 9011–9016.
(2) Placidi, M. P. Polymetallic Lanthanide Complexes for Application in Luminescence and Magnetic Resonance Imaging, University of Manchester, 2009.
(3) Beeby, A.; Clarkson, I. M.; Dickins, R. S.; Faulkner, S.; Parker, D.; Royle, L.; de Sousa, A. S.; Williams, J. A. G.; Woods, M. *J. Chem. Soc., Perkin Trans. 2* **1999**, *2*, 493–504.
(4) Jones, G.; Jackson, W. R.; Choi, C. Y.; Bergmark, W. R. *J. Phys. Chem.* **1985**, *89*, 294–300.
(5) Wolfbeis, O. S.; Koller, E.; Hochmuth, P. *Bull. Chem. Soc. Jpn.* **1985**, *58*, 731–734.
(6) Yu, T.; Zhao, Y.; Ding, X.; Fan, D.; Qian, L.; Dong, W. *J. Photochem. Photobiol. A Chem.* **2007**, *188*, 245–251.
(7) Kato, M. *Curr. Pharm. Des.* **2004**, *10*, 3835–3852.
(8) Dünges, W.; Meyer, A.; Müller, K.-E.; Müller, M.; Pietschmann, R.; Plachetta, C.; Sehr, R.; Tuss, H. *Fresenius Zeitschrift für Anal. Chemie* **1977**, *288*, 361–368.
(9) Costa, J.; Balogh, E.; Turcry, V.; Tripier, R.; Le Baccon, M.; Chuburu, F.; Handel, H.; Helm, L.; Tóth, É.; Merbach, A. E. *Chem. Eur. J.* **2006**, *12*, 6841–6851.
(10) Regueiro-Figueroa, M.; Nonat, A.; Rolla, G. A.; Esteban-Gómez, D.; de Blas, A.; Rodríguez-Blas, T.; Charbonnière, L. J.; Botta, M.; Platas-Iglesias, C. *Chem. Eur. J.* **2013**, *19*, 11696–11706.
(11) Li, X.; Zhu, K.; Jiang, W.; Li, Y.; Kim, H.; Son, Y. *Phys. Status Solidi C* **2012**, *9*, 2456–2459.
(12) Stanchev, S.; Maichle-Mössmer, C.; Manolov, I. *Zeitschrift für Naturforsch. B* **2007**, *62b*, 737–741.
(13) Junker, A. K. R.; Hill, L. R.; Thompson, A. L.; Faulkner, S.; Sørensen, T. J. *Dalton Trans.* **2018**, *47*, 4794–4803.
(14) Mason, S. F.; Peacock, R. D.; Stewart, B. *Chem. Phys. Lett.* **1974**, *29*, 149–153.
(15) Jauregui, M.; Perry, W. S.; Allain, C.; Vidler, L. R.; Willis, M. C.; Kenwright, A. M.; Snaith, J. S.; Stasiuk, G. J.; Lowe, M. P.; Faulkner, S. *Dalton Trans.* **2009**, 6283–6285.
(16) Gunnlaugsson, T.; Harte, A. J.; Leonard, J. P.; Nieuwenhuyzen, M. *Chem. Commun.* **2002**, 2134–2135.
(17) Gunnlaugsson, T.; Harte, A. J.; Leonard, J. P.; Nieuwenhuyzen, M. *Supramol. Chem.* **2003**, *15*, 505.
(18) Gunnlaugsson, T.; Leonard, J. P.; Mulready, S.; Nieuwenhuyzen, M. *Tetrahedron* **2004**, *60*, 105–113.

Chapter 5 Naphthyl-bridged bicyclic systems

5.1 Introduction

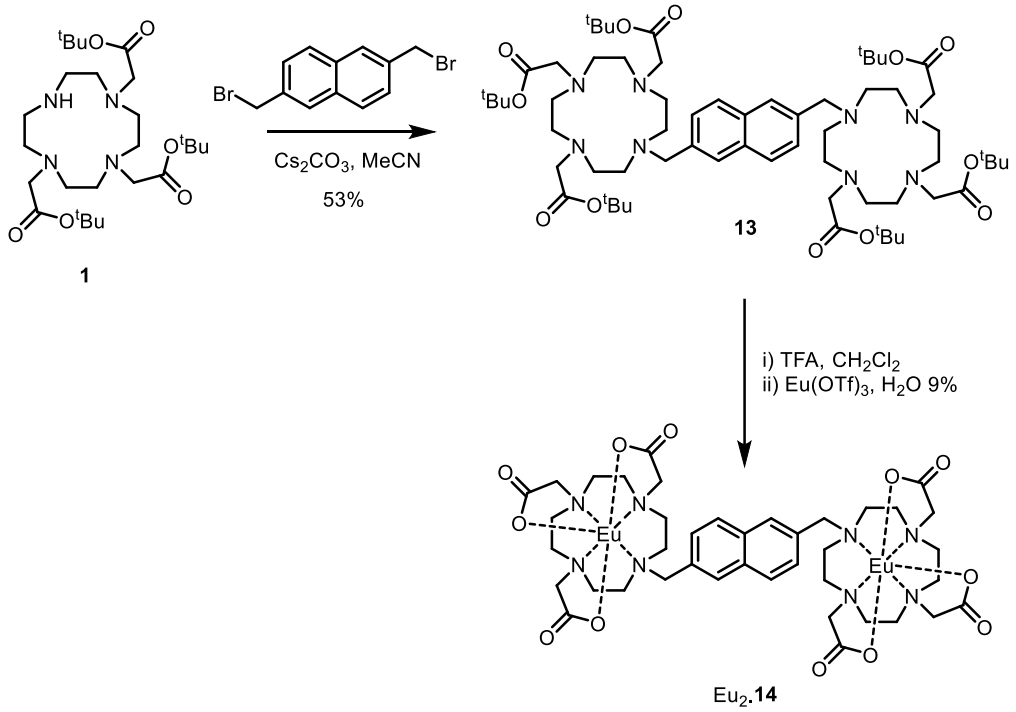
The increased conjugation in a naphthyl chromophore compared to a *m*-xylyl or similar benzene-based chromophore gives rise to a narrower HOMO-LUMO gap and therefore shifts absorption and emission to longer wavelengths. As a result of this, naphthalene emits in the blue whereas benzene emits in the UV region.

Naphthyl chromophores are also of interest because of their good energy match with certain lanthanide excited states; naphthyl moeties have previously been shown to sensitise lanthanides in a wide variety of complexes[1,2] as the triplet state is found at 21,300 cm^{-1} in polar solvents.[3,4] This enables straightforward sensitisation of the emissive $^5D_0$ state of Eu^{3+} (found at 17,300 cm^{-1}):[5–7] the energy gap approximates to 20 kT at room temperature, precluding the possibility of thermal back energy transfer. However, such back energy transfer is possible for terbium complexes bearing naphthyl chromophores, as the emissive $^5D_4$ state of Tb^{3+} is found at 20,500 cm^{-1},[8] within 4 kT of the naphthalene triplet state. As a result of this, the Faulkner group has previously found a terbium naphthalene complex to exhibit oxygen-dependence in its emission intensity.[9]

For the purposes of this thesis, a naphthyl chromophore can also act as a bridge between two lanthanide-containing domains. Naphthyl bridges offer the potential to increase the spacing between the lanthanide domains compared to the *m*-xylyl complexes, while varying the substitution pattern allows for further scope to adjust the interlanthanide separation. The selectivity of naphthyl-bridged binuclear complexes towards differently sized anionic guests may be influenced by the substitution pattern of the naphthyl bridge. Additionally, there may be differences in binding strength arising from the different electron-withdrawing

and -donating properties of the 2,6- and 2,7-substitution positions and the consequent effect of this on the partial positive charge at the lanthanide.

5.2 Synthesis of the 2,6-naphthyl complex



Scheme 5.1 Reaction pathway for synthesis of the 2,6-functionalised naphthyl complex

The 2,6-naphthyl-derived complex Eu2.**14** was prepared using the same procedures as those employed for the complexes described in earlier chapters. Crystals of the hexaester **13** were grown by slow evaporation of deuterated chloroform. The structures in Figure 5.1 solved by Dr Amber Thompson show sodium atoms bound in the cyclen rings and coordinated to the ring nitrogen atoms and the carbonyl oxygens of the ester arms, and the unit cell contains $CDCl_3$ molecules arranged around the chloride counterions (one omitted for clarity). Further crystallographic data can be found in Appendix C.5.

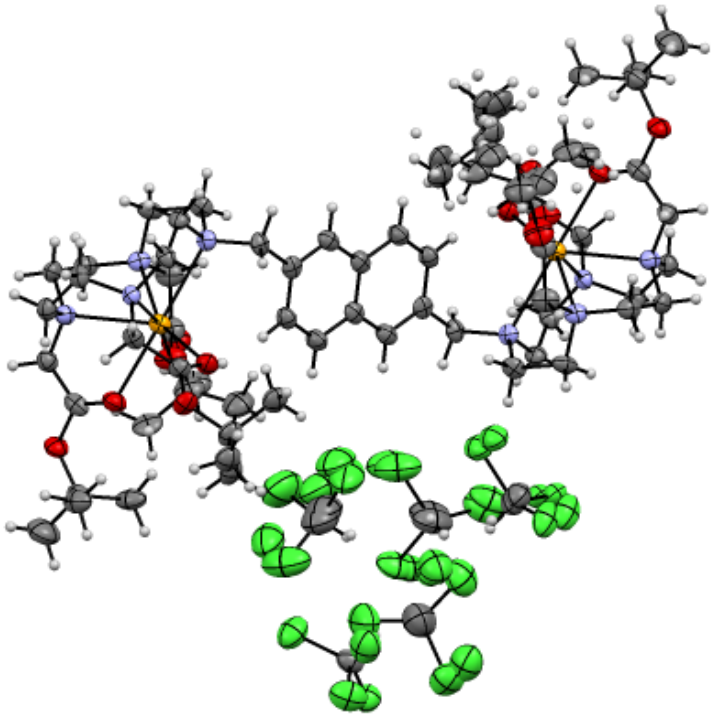
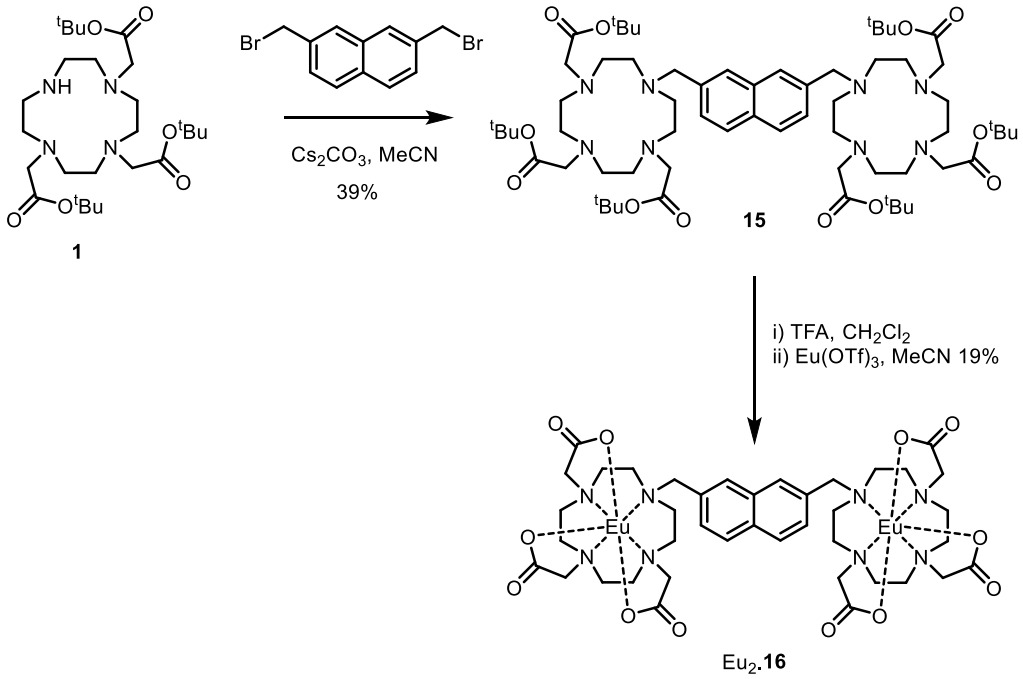
a)  b) 

*Figure 5.1 a) Molecular structure of **13** with thermal ellipsoids at 50% probability. A sodium ion (orange) in each cyclen ring means that there are two chloride counterions (only one shown) to balance charge; these are solvated by five $CDCl_3$ molecules in the manner shown in b)*

Deprotection with trifluoroacetic acid in dichloromethane followed, and subsequent complexation was achieved with europium triflate in water. Water was chosen as the complexation solvent due to its higher boiling point than methanol in order to attempt to improve upon yields from previous complexations. Dialysis was used to reduce the salt content of the product.

5.3 Synthesis of the 2,7-naphthyl complex



Scheme 5.2 Reaction pathway for synthesis of the 2,7-functionalised naphthyl complex

As previously, the dibromo bridging species was reacted with triester **1** in basic acetonitrile and purified by alumina column chromatography to give the hexaester compound **15**. The usual ester deprotection conditions were employed, followed by complexation with europium triflate in acetonitrile. Here, acetonitrile was chosen to attempt to improve upon the low yield achieved for the 2,6-analogue. The complex precipitated from solution. The precipitate was collected and redissolved in water before dialysis to reduce salt content.

5.4 Characterisation of the naphthyl complexes

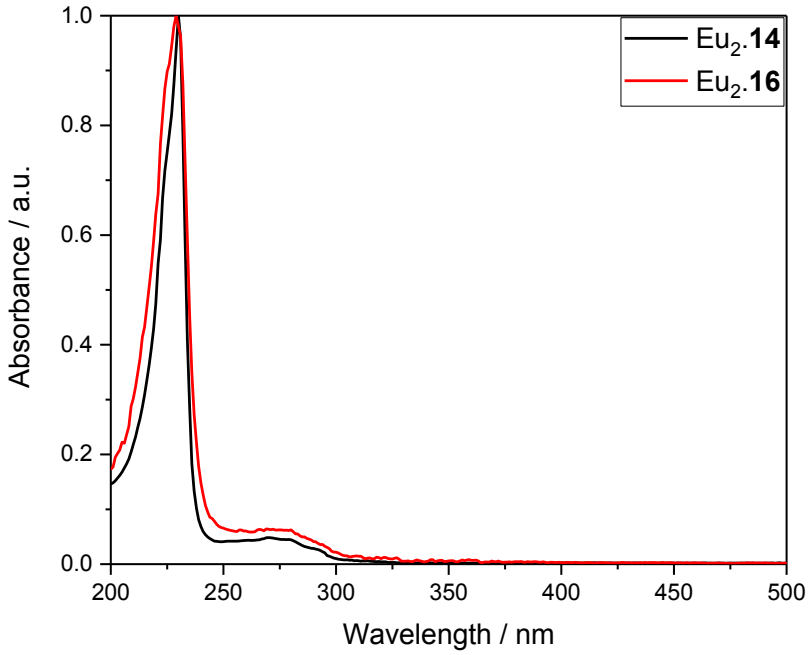


*Figure 5.2 Normalised to λ_{max} absorption spectra of Eu_2.**14** (black trace) and Eu_2.**16** (red trace) in water*

The absorption spectra of the two naphthyl complexes (Figure 5.2) were very similar, as would be expected due to the relative molar absorptivities of naphthyl and europium and, as seen in previous chapters, ligand absorption dominated over europium absorption which would be found as a sharp peak at 394 nm. These absorption bands correlate to the relatively sharp and intense *β*-band (or ^1L_a) at around 230 nm and the broad *p*-band (or ^1B_b) centred around 275 nm seen for naphthalene itself, where the *α*-band (or ^1L_b) is obscured by the larger *p*-band. These bands arise as a result of $\pi \rightarrow \pi^*$ and $\pi \rightarrow \sigma^*$ transitions.[10–12]

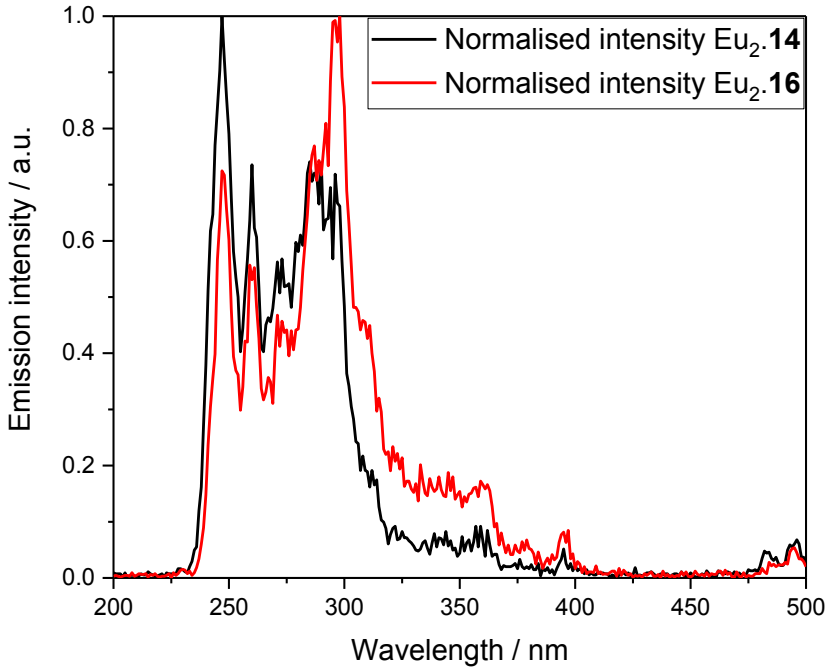


*Figure 5.3 Normalised excitation spectra of Eu$_2$.**14** (black trace) and Eu$_2$.**16** (red trace) in HEPES at pH 7.4 (λ_{em} = 616 nm)*

The overlaid luminescence excitation spectra in Figure 5.3 showed peaks at the same wavelengths, although their relative magnitudes differed. This may be attributed to the differing efficiency of the through-space energy transfer processes due to the relative position of the europium atoms to the naphthyl chromophore in solution. It is clear that sensitisation through the chromophore is possible and that it is more efficient for these complexes than direct excitation at 394 nm, which contrasts the behaviour of the binuclear nitro-*m*-xylyl complex Eu$_2$.**5** in Chapter 3 and indicates better spectral overlap of the naphthyl chromophores than the nitro-*m*-xylyl chromophore with the lanthanide.

Compound	**τ_{H2O} / ms**	**τ_{D2O} / ms**	***q***
Eu$_2$.**14**	0.37	1.33	2.0
Eu$_2$.**16**	0.42	1.50	1.7

*Table 5.1 Calculated q values for the naphthyl complexes Eu$_2$.**14** and Eu$_2$.**16** where the mean of up to four sets of measurements which were within 10% error is given*

The *q* values shown in Table 5.1 indicate that there are two bound water molecules per europium atom, which is in agreement with most of the previously mentioned DO3A-derived complexes in this thesis.

The ^{1}H NMR spectra in Figure 5.4 and Figure 5.5 show paramagnetically shifted peaks, including peaks in the TSAP region. As europium complexes do not usually adopt a TSAP conformation, this may be a weighted average of structures due to the fluxionality of the heptadentate complex.

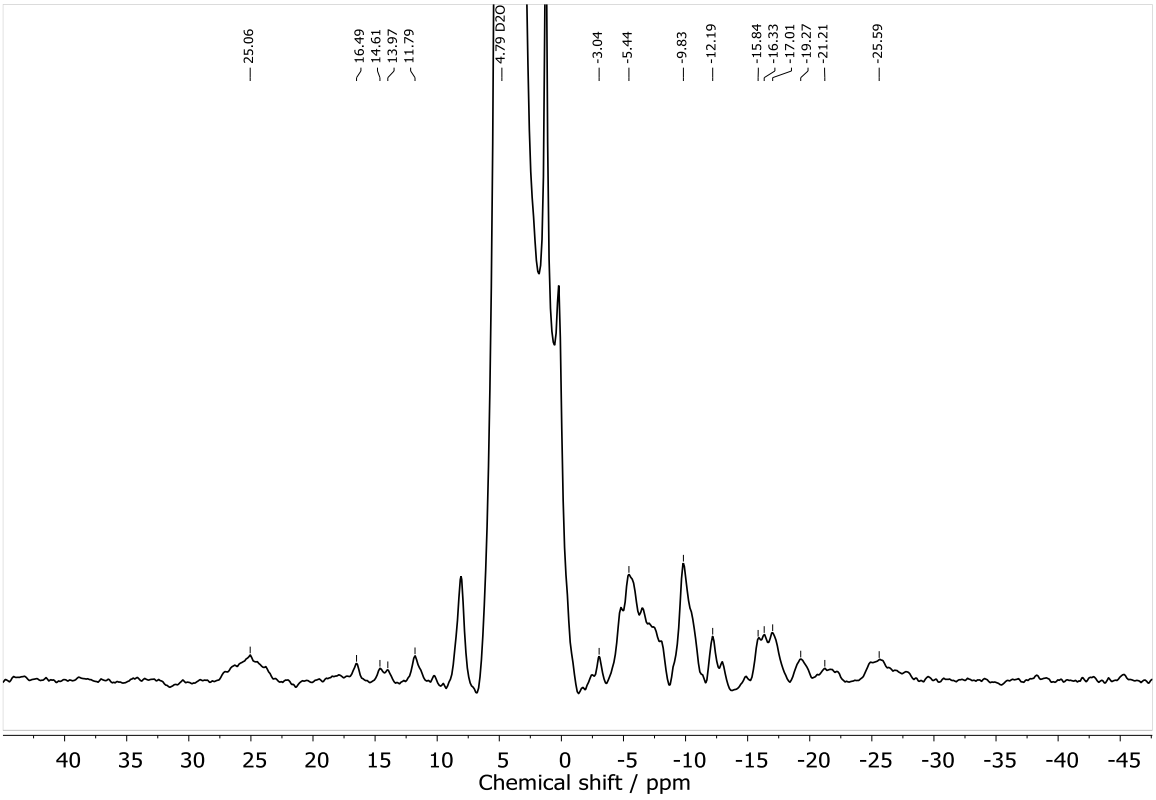


*Figure 5.4 ^{1}H NMR spectrum of Eu_2.**14** in D_2O*

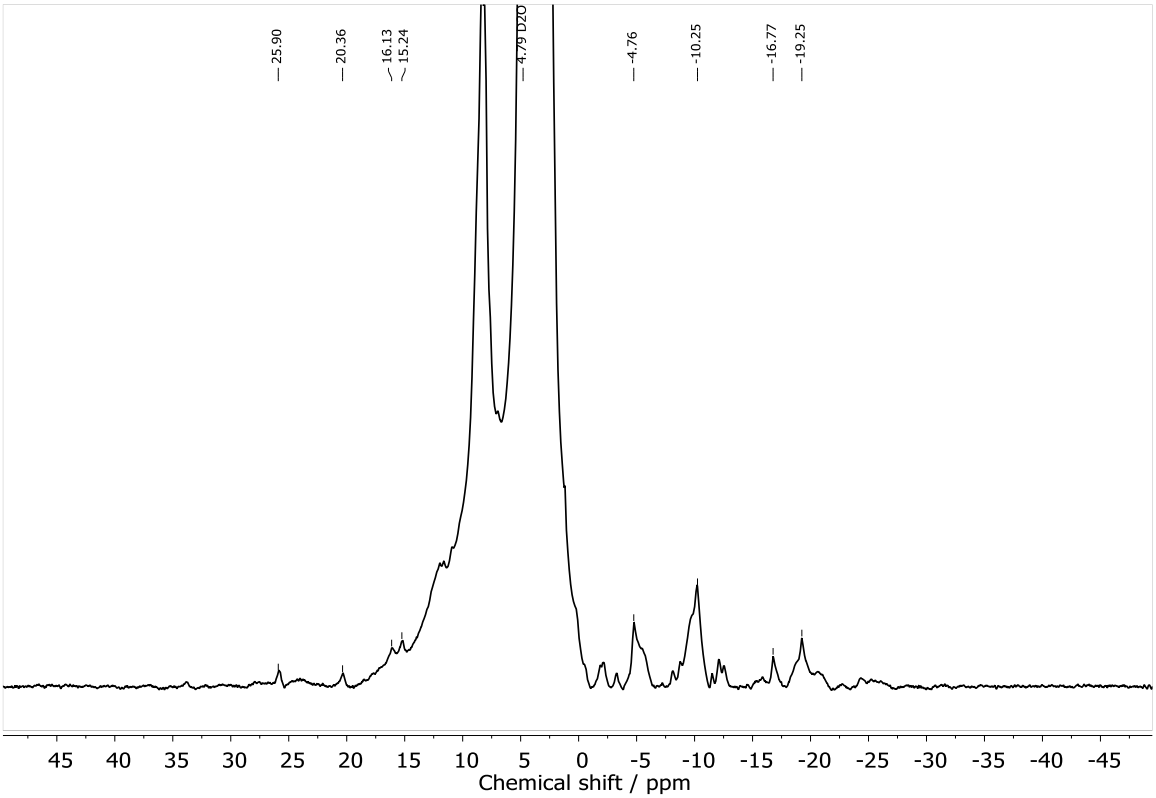


*Figure 5.5 ^{1}H NMR spectrum of Eu_2.**16** in D_2O*

5.5 References

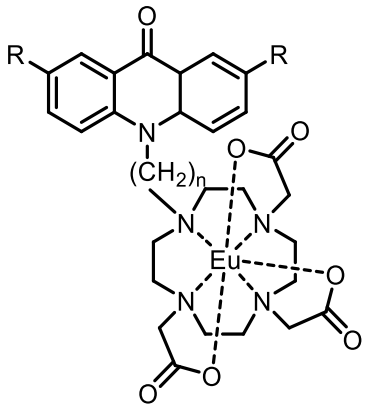
(1) Parker, D.; Williams, J. A. G. *J. Chem. Soc., Perkin Trans. 2* **1995**, 1305.
(2) Beeby, A.; Parker, D.; Williams, J. A. G. *J. Chem. Soc., Perkin Trans. 2* **1996**, 1565.
(3) Murov, S. L.; Carmichael, I.; Hug, G. L. *Handbook of Photochemistry*; 2nd ed.; Marcel Dekker, Inc.: New York, 1993.
(4) Lewis, G. N.; Kasha, M. *J. Am. Chem. Soc.* **1944**, *66*, 2100–2116.
(5) Carnall, W. T.; Fields, P. R.; Rajnak, K. *J. Chem. Phys.* **1968**, *49*, 4450–4455.
(6) Frey, S. T.; Horrocks, W. D. *Inorganica Chim. Acta* **1995**, *229*, 383–390.
(7) Choppin, G. R.; Wang, Z. M. *Inorg. Chem.* **1997**, *36*, 249–252.
(8) Carnall, W. T.; Fields, P. R.; Rajnak, K. *J. Chem. Phys.* **1968**, *49*, 4447–4449.
(9) Sørensen, T. J.; Kenwright, A. M.; Faulkner, S. *Chem. Sci.* **2015**, *6*, 2054–2059.
(10) Privalova, A. I.; Morozova, J. P.; Kashapova, E. R.; Artyukhov, V. J. *J. Appl. Spectrosc.* **2011**, *78*, 309–317.
(11) Clar, E. *Spectrochim. Acta* **1950**, *4*, 116–121.
(12) Platt, J. R. *J. Chem. Phys.* **1949**, *17*, 484–495.

Chapter 6 Acridone-appended complexes

6.1 Introduction

Acridone has one of the smallest singlet-triplet energy gaps known for simple aromatic molecules.[1] Thus the triplet energy of acridone derivatives (ca. 21,050 cm^{-1},[1,2] for N-alkyl derivatives) is higher than that of ostensibly simpler chromophores such as the naphthyl group discussed in the previous chapter, while these derivatives absorb light at dramatically longer wavelengths with absorption spectra that extend into the visible region of the spectrum. This not only allows use of all the common luminescent lanthanides, but also permits longer wavelength excitation and better biological penetration with less tissue damage.

Previous work by Dadabhoy *et al.* showed that functionalised acridone complexes of europium of the type shown in Figure 6.1 are able to sensitise europium effectively at wavelengths above 400 nm.[3]



R = H, Br
n = 2, 5

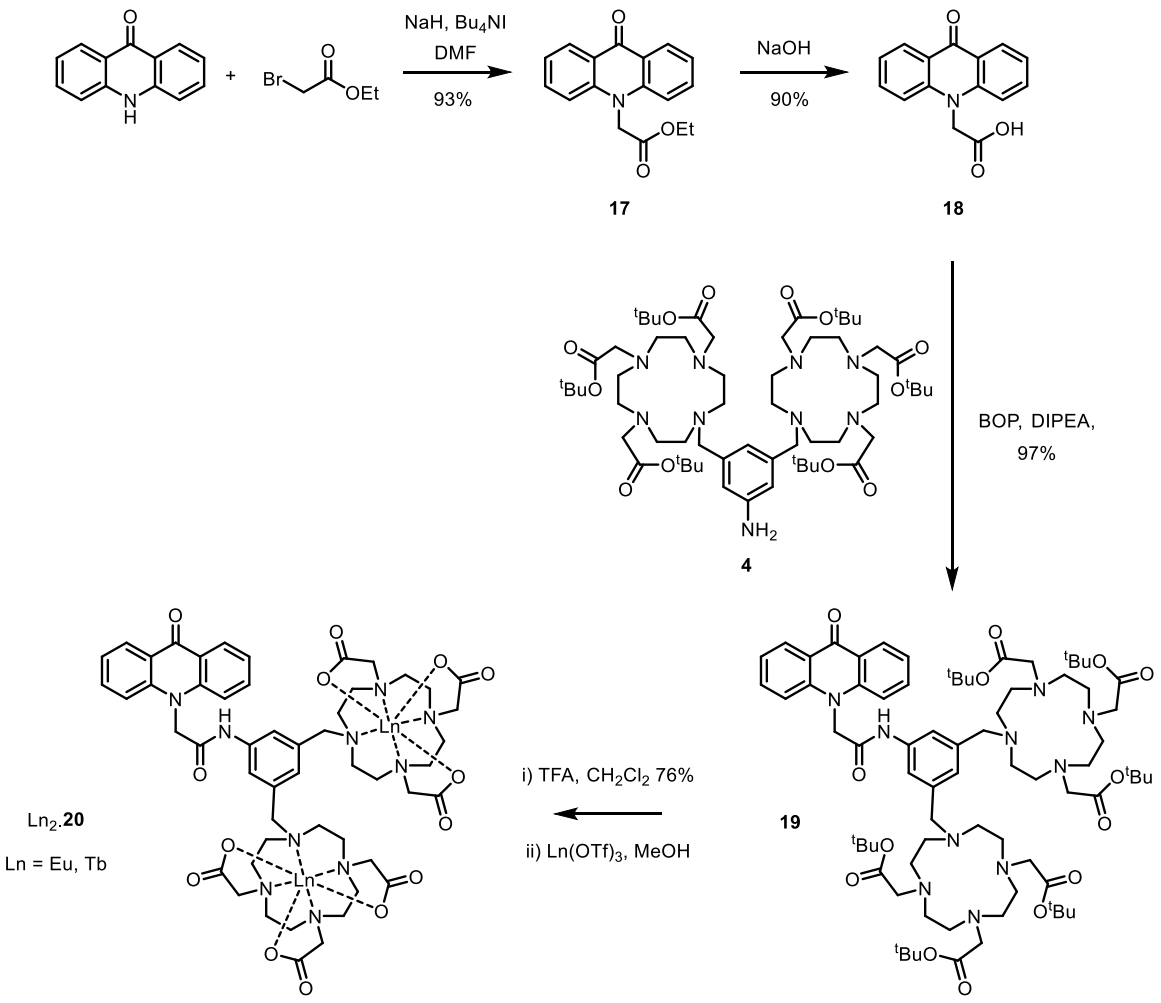
Figure 6.1 Acridone complexes previously synthesised by Dadabhoy et al.[3]

As with all antenna-appended lanthanide complexes, the energy match between the chromophore and the lanthanide must be considered, as well as the distance between the antenna and the lanthanide in solution. In the case of this work, it was resolved that acridone

should be used as a sensitising chromophore in a bimetallic system containing the *m*-xylyl bridge explored in Chapter 3.

6.2 Synthesis of acridone-appended complexes

Novel complexes of the type Ln_2.**20** (Ln = Eu, Tb, Scheme 6.1) are perhaps more complicated than those studied by Dadabhoy *et al.* in that there are two lanthanide centres to consider. Although this work restricts itself to cases in which both lanthanide ions are the same, the conformational space available to the complex is likely to mean that one centre is prone to be sensitised more effectively than the other.



*Scheme 6.1 Reaction pathway for synthesis of the acridone-appended lanthanide complexes Ln_2.**20***

The europium and terbium complexes Ln_2.**20** (Scheme 6.1) were synthesised by coupling of

the amino-*m*-xylyl hexaester **4** (from Chapter 3) with acridone acetic acid **18**, whereupon the characteristic carboxylic acid C-O stretch at 1215 cm^{-1} and O-H stretch at 2511 cm^{-1} in the IR spectrum of **18** were lost. This was followed by deprotection of the ester groups and complexation of the resulting hexaacid as described in previous chapters. The acridone acetic acid **18** was synthesised following the procedure of David-Cordonnier *et al.*[4] Crystals of **17** were grown by slow evaporation of a concentrated solution of deuterated chloroform. The structure is shown in Figure 6.2 and further information can be found in Appendix C.6.

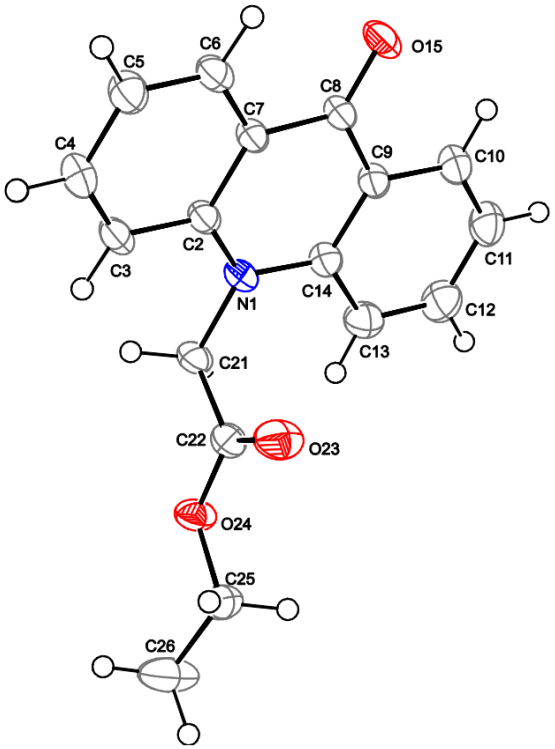


*Figure 6.2 Structure of **17** determined by X-ray diffraction showing thermal ellipsoids at 50% probability*

6.3 Photophysical characterisation of acridone-appended complexes

The photophysical properties of the complexes were investigated to confirm that the acridone chromophore was able to sensitise europium and terbium. The most obvious evidence for this was found in that for both Ln_2.**20** complexes, excitation *via* acridone at 405 nm gave an emission spectrum characteristic of the complexed lanthanide. The UV-vis

absorption observed for these complexes was primarily due to the acridone moiety, as these $\pi \rightarrow \pi^*$ transitions are formally allowed.

6.3.1 Absorption and excitation spectra

The match between the absorption spectrum and excitation spectrum of the europium complex Eu_2.**20** shown in Figure 6.3 provides evidence that absorption of the acridone chromophore at around 250 nm and 400 nm sensitises europium. It is also clear that the different acridone absorption transitions do not all lead to equally effective sensitisation of the lanthanide. For example, the band around 400 nm delivers remarkably effective sensitisation, while that around 300 nm does not. Direct excitation of europium at 394 nm is very close to the absorption of acridone at 405 nm, however ensuring that the excitation slit widths were narrower than this difference in wavelength guaranteed the precision of excitation.

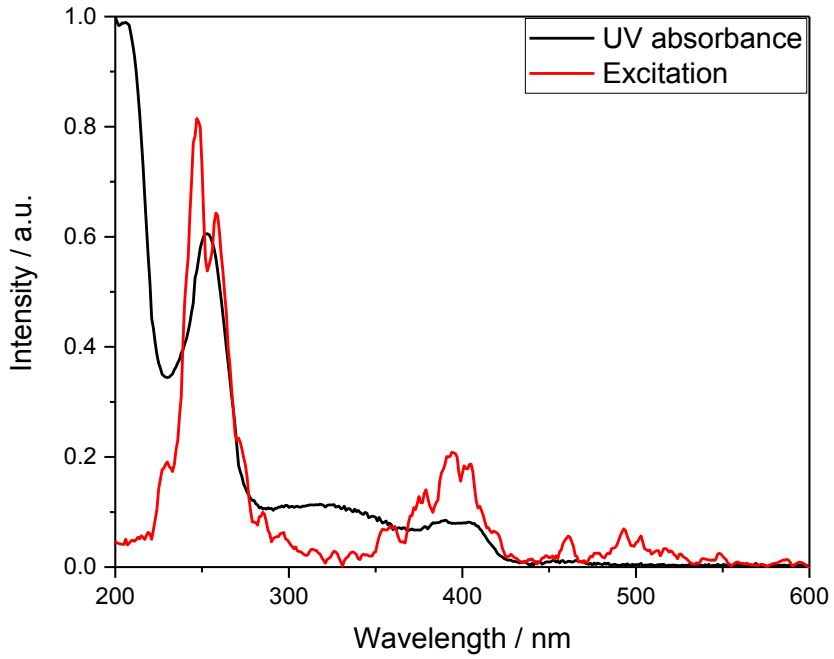


*Figure 6.3 Overlaid UV-vis absorption spectrum (black) and excitation spectrum (λ_{em} = 616 nm) (red) for Eu_2.**20**. The excitation spectrum resembles that of a simpler europium-acridone complex prepared by Dadabhoy et al.*[3]

The overlaid excitation spectra of Tb_2.**20** in degassed and aerated conditions (blue and pink) in Figure 6.4 are almost identical and therefore show negligible oxygen-dependence in the excitation profile of Tb_2.**20**; thus the emission intensity of this complex *in vivo* would be dependent on binding to biological analytes, and independent of local blood oxygen concentration.

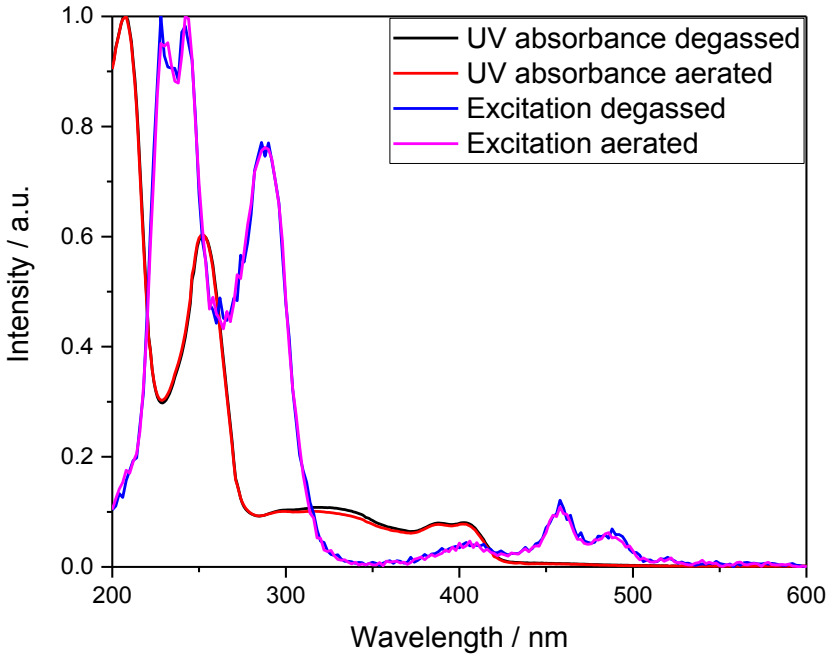


*Figure 6.4 Overlaid UV-vis absorption spectra (black, red) and excitation spectra (λ_{em} = 545 nm) (blue, pink) for Tb_2.**20** in both degassed and aerated solution*

Comparison of absorption and excitation spectra of Tb_2.**20** reveals that excitation at absorption wavelengths of the antenna ligand gives rise to terbium emission (at 545 nm) and that this excitation *via* the ligand chromophore leads to much higher emission intensity than direct excitation of terbium at 366 nm, evidencing the antenna effect.

The absorption spectrum for Tb_2.**20** (Figure 6.4) closely resembles that of Eu_2.**20** (Figure 6.3), which agrees with the assumption that ligand absorption dominates compared to the formally forbidden lanthanide electronic transitions.

Differences are observed between the excitation spectra of the two Ln_2.**20** complexes. For both Eu_2.**20** and Tb_2.**20**, excitation at 250 and 400 nm sensitises the lanthanide, however the spectral form for Tb_2.**20** displays an additional peak at 300 nm. Assuming that these two complexes adopt the same conformation in solution – which is a simplification as it has already been shown that subtle changes to structure can lead to very different physical behaviours – this additional band can be attributed to differences in charge transfer between the acridone chromophore and the lanthanide in question due to the different energy level match.

6.3.2 Emission spectra

The oxygen-dependence of spectra, as discussed in Chapter 1 on page 7, was investigated by comparing spectra of degassed solutions with those of the same solutions but with ambient concentrations of atmospheric gases. Figure 6.5 and Figure 6.6 show that no significant oxygen-dependence was found in the emission spectra. See Chapter 12, Section 12.6 for further information on the degassing method.

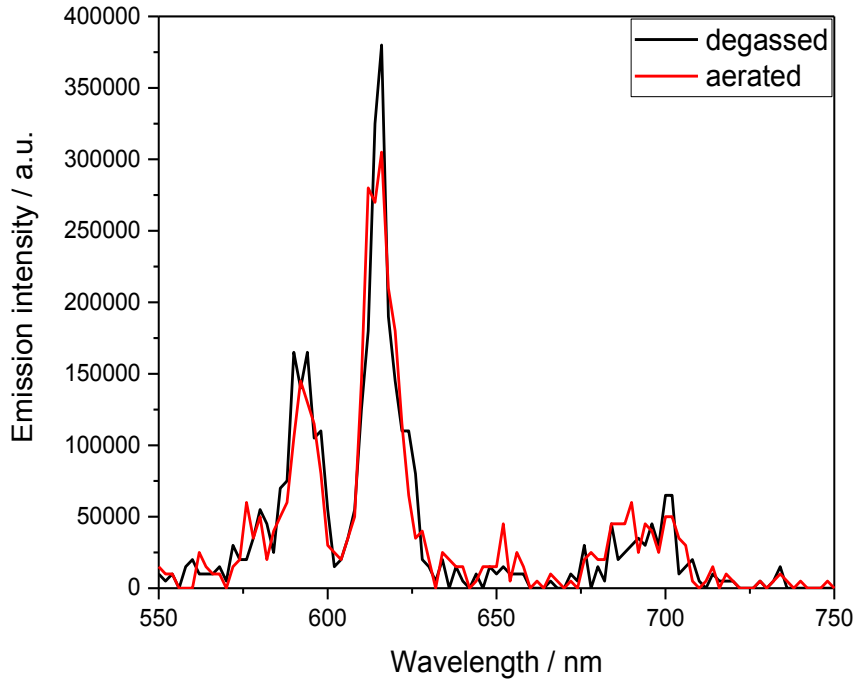


*Figure 6.5 Emission spectrum of Eu_2.**20** (λ_{ex} = 405 nm)*

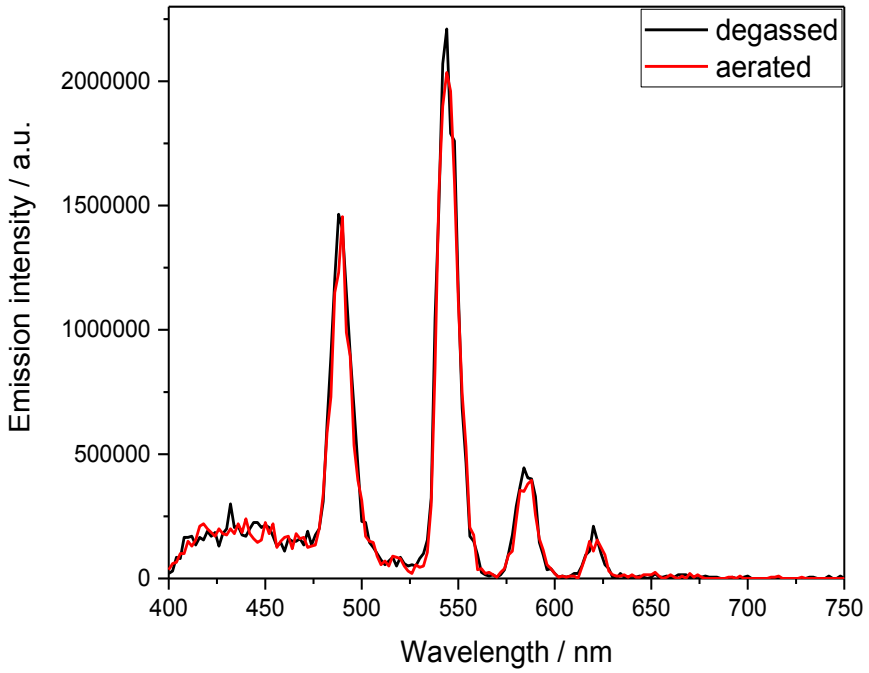


*Figure 6.6 Emission spectrum of Tb_2.**20** (λ_{ex} = 405 nm)*

6.3.3 Luminescence lifetimes

The luminescence lifetimes of the Ln_2.**20** complexes were found to be unaffected by the degree of sample aeration, which is in good agreement with the unchanged band intensities shown in Figure 6.4.

Compound	τ_{H2O} / ms	τ_{D2O} / ms	*q*
Eu_2.**20**	0.55	1.69	1.2
Tb_2.**20**	1.40	2.44	1.2

*Table 6.1 Calculated q values for the acridone-appended complexes Eu_2.**20** and Tb_2.**20**. Degassed lifetime measurements were within 10% error of these values*

The *q* values (Table 6.1) for each of the acridone complexes in both aerated and degassed conditions indicated approximately one bound water molecule per lanthanide centre, which for the terbium complex Tb_2.**20** is closer to the values found for the amino-*m*-xylyl complex Tb_2.**6** ($q = 0.6$) than for the nitro-*m*-xylyl complex Tb_2.**5** ($q = 2.0$). This indicates that the conformation adopted in solution by the acridone Tb_2.**20** complex is closest to that of the amino-*m*-xylyl terbium complex, which possesses the greatest structural similarity to the acridone complexes of any of the complexes studied in this thesis. However, for the europium analogue Eu_2.**20**, the nitro-*m*-xylyl complex had the closer *q* value (Eu_2.**5**: $q = 1.2$, whereas for Eu_2.**6**, $q = 2.0$), reinforcing that the conformation adopted and solvation in solution is not straightforward.

6.4 References

(1) Murov, S. L.; Carmichael, I.; Hug, G. L. *Handbook of Photochemistry*; 2nd ed.; Marcel Dekker, Inc.: New York, 1993.

(2) Val'kova, G. A.; Shcherbo, S. N.; Shigorin, D. N. *Dokl. Phys. Chem.* **1978**, *240*, 491–493.

(3) Dadabhoy, A.; Faulkner, S.; Sammes, P. G. *J. Chem. Soc., Perkin Trans. 2* **2000**, *2*, 2359–2360.

(4) David-Cordonnier, M.-H.; Hildebrand, M.-P.; Baldeyrou, B.; Lansiaux, A.; Keuser, C.; Benzschawel, K.; Lemster, T.; Pindur, U. *Eur. J. Med. Chem.* **2007**, *42*, 752–771.

Part B: Binding studies

Chapter 7 Binding of anions to lanthanide complexes

7.1 Introduction

Lanthanide complexes form adducts with anions in solution. The hosts, guests, and adducts exist in thermodynamic equilibrium and so data on the equilibrium position may be interpreted to give the binding strength between the complex and the anion under these conditions.

In 2002, Dickins *et al.* considered the chelating behaviour of a number of anions in binding to europium, gadolinium, or ytterbium ions in a cyclen-based complex. They observed that binding of phosphate and fluoride is monodentate, whereas binding of lactate and carbonate is bidentate about the lanthanide in the manner shown in Figure 7.1.[1]

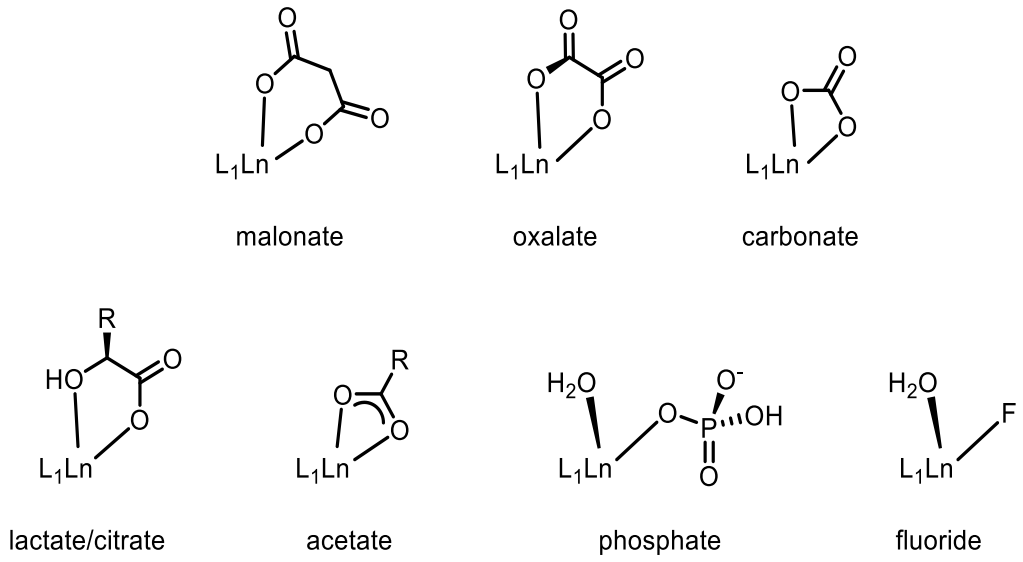


Figure 7.1 Binding modes of some chelating and non-chelating anions to lanthanides, as discussed by Dickins et al., where L_1Ln represents a lanthanide (Ln = Eu, Gd, Yb) bound in a macrocyclic ligand derived from cyclen[1]

In 2011, Tilney *et al.* published work detailing the binding of binuclear complexes with a series of isomeric aryldicarboxylate guests. It has been shown that these bind in the 1:1 fashion outlined in Chapter 1, with the guest anion bridging the lanthanide centres.[3]

7.2 Techniques for studying binding

Binding affinities between host and guest complexes may be measured using different techniques as outlined below. These methods involve titration of one species against another. Care needs to be taken when devising protocols for such titrations, and it is essential to ensure that only one parameter varies across the course of the titration.

7.2.1 Luminescence

Since two different species frequently exhibit differences in their luminescence spectra, lifetimes, or quantum yields, changes in luminescence properties can be used to quantify and indicate a change in speciation in solution. This is particularly true for lanthanide complexes where changes to the inner coordination sphere can influence the luminescence quantum yield, lifetime (where X-H oscillators are added or displaced), and spectral form (particularly for ions such as europium which exhibit symmetry-sensitive quadrupolar transitions).

Luminescence lifetime changes indicate a change in the quenching at the lanthanide centre and are thus indicative of binding at the lanthanide. Tilney *et al.*[3] also used the change in intensity of emission across a range of wavelengths in emission spectra to the same end. As the bound and unbound species have a different quantum yield in emission, the observed emission intensity reflects the position of the equilibrium and represents an average weighted by both population and quantum yield. The magnitude of the intensity change – and thus the directly related steepness of the binding isotherm curve – indicates the strength of binding. An example of changing luminescence spectra is shown in Figure 7.2 but this technique will be discussed in more detail later.

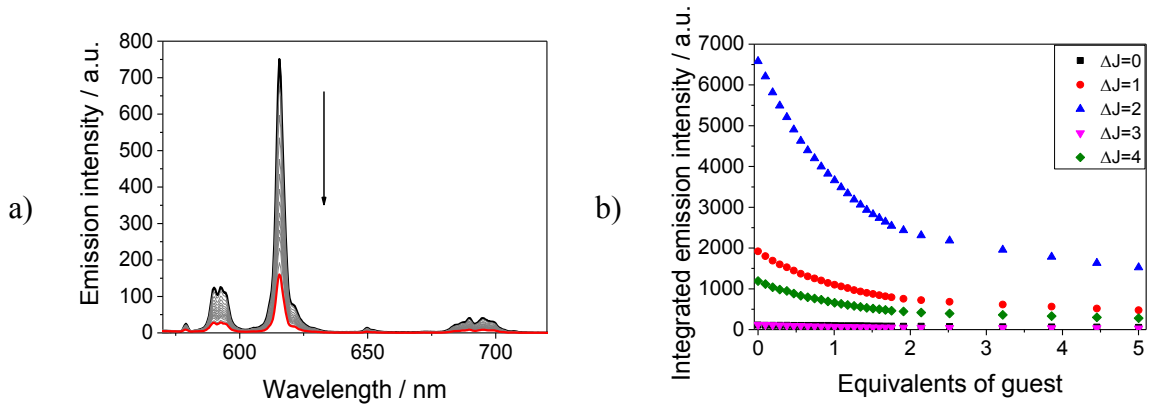


*Figure 7.2 a) Example emission spectra from a luminescence titration of a europium complex (Eu_2.**L**^{2} with dinicotinate in TRIS buffer at pH 10.5). The spectral intensity may increase or decrease over the course of a titration, in b) integration of the emission bands shows a decrease in emission intensity as the guest concentration is increased*

7.2.2 NMR

NMR is also a useful technique to investigate binding of species in solution. However, unlike in luminescence titrations, the timescale of exchange between bound and free systems becomes important. Where these species are in slow exchange on the timescale of the NMR experiment, separate sets of peaks are observed corresponding to each species, and their relative concentrations (and hence the affinity constant) can be determined directly. However, when species are in fast exchange on the NMR timescale, the observed chemical shifts reflect a population weighted average of the signals corresponding to bound and free species. For the compounds in this thesis, fast exchange was invariably observed.

NMR proved most effective when studying phosphorus-containing guests: compared to ^{1}H NMR spectra, ^{31}P NMR gave spectra that more easily lent themselves to quantitative interpretation. Figure 7.3 shows an example of the paramagnetically induced shifting of a ^{31}P resonance of a phosphate guest as the concentration of a lanthanide-containing species was increased. This chemical shift data was supplemented by T_1 relaxation measurements, as the relaxation rate of nuclei is increased in the presence of a lanthanide.

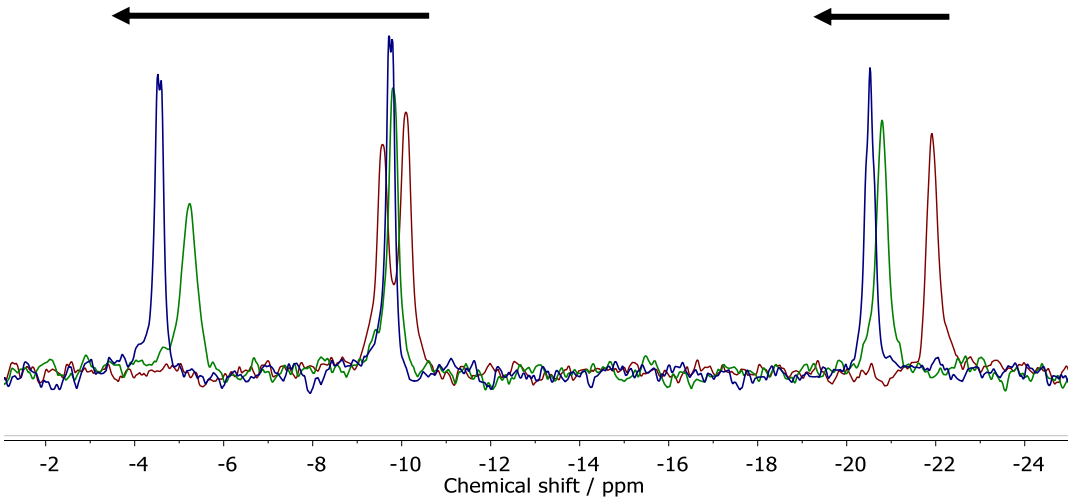


*Figure 7.3 Overlaid ^{31}P NMR spectra from an NMR binding study showing the change in chemical shift of ATP (maroon) as Yb_2.**5** was added (ATP with 0.4 equivalents of Yb_2.**5** in green, with 0.8 equivalents of Yb_2.**5** in blue) in D_2O*

7.3 Luminescence binding studies

Initial titrations with isophthalate were performed in methanol or a 3:1 methanol:water mixture due to the minimal water solubility of isophthalate. When three equivalents of lithium hydroxide were added to the titrant solution in order to deprotonate the carboxylic acids, as expected, stronger binding was observed as a result of increased electrostatic attraction to the lanthanide centre, which outweighed entropic effects. Subsequent titrations with the water-soluble analogue dinicotinate in the same media allowed comparisons to be drawn before dinicotinate was the first anionic species to be titrated with these lanthanide complexes in aqueous conditions, a move towards conditions relevant *in vivo*.[2]

In aqueous conditions, in order to maintain a constant pH throughout, titrations were performed in buffer media (see Chapter 12, Section 12.4 for procedure). Previously published work,[2–5] as well as the data presented in Chapter 2, confirmed that binding constants were affected by the identity of the solvent or buffer medium. Of the various buffers trialled, HEPES was selected as the optimum for these studies as HEPES is able to

buffer in the biologically relevant pH range around 7.4, and NMR and luminescence studies confirmed that HEPES did not bind competitively in solutions of the selected anions.

Emission spectra were recorded over the course of a titration as aliquots of the titrant solution were added. An example from a titration of Eu_2.**5** with adenosine monophosphate (AMP) is shown in Figure 7.4. Integrating each of the bands and plotting these against concentration of titrant in the cuvette, or against the number of equivalents of titrant in the cuvette, gave the binding isotherms of the form shown in Figure 7.5.

For europium complexes, the intensities of the hypersensitive $\Delta J = 2$ peaks vary significantly with coordination of a guest – meaning that peak intensity ratios can also be a powerful tool for quantifying binding, as can be seen from Figure 7.6.

Fine structure within individual transitions can also offer the means to explore binding, since the splitting of the m_j states within a $^{2S+1}L_J$ state reflects the local crystal field. Such fine structure analysis is most straightforward for the $^5D_0 \rightarrow {}^7F_1$ transition in europium complexes, since the emissive state is non-degenerate, while the m_j manifold for the acceptor state is straightforward (comprising $m_j = 0, \pm 1$ states). The most obvious consequence of the splitting of the m_j states by the ligand field is clearly visible in the changes to the form of the individual transitions in the emission spectrum. Such effects were observed in this work, particularly with guests such as AMP, where the fine structure of the $\Delta J = 1$ peak for europium showed well-defined splitting. This gave additional data that could be plotted against concentration or equivalents of the guest in order to give more parameters for the fitting software. An expanded view of the $\Delta J = 1$ peak is shown in Figure 7.7 and the change in the intensities of the maxima shown in Figure 7.8.

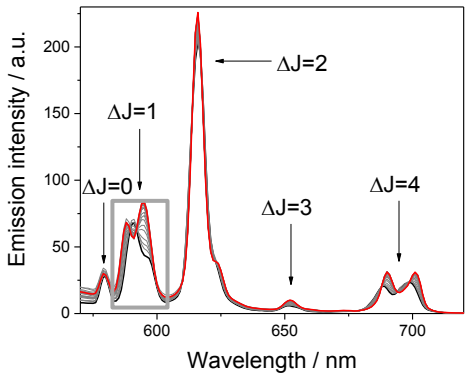


*Figure 7.4 Superimposed luminescence emission spectra from a typical titration of a europium complex, in this case Eu_2.**5** with AMP in HEPES at pH 7.5*

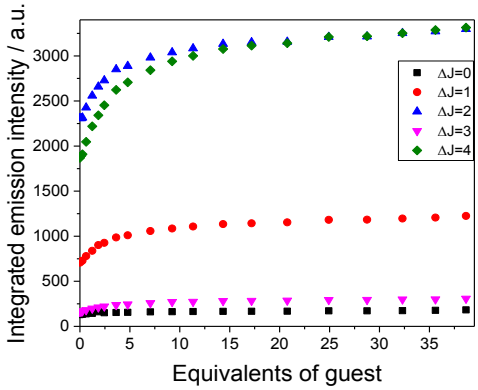


*Figure 7.5 Change in luminescence emission intensity during a typical titration (Eu_2.**5** with tartrate in HEPES at pH 7.4), quantified by integration of peaks*

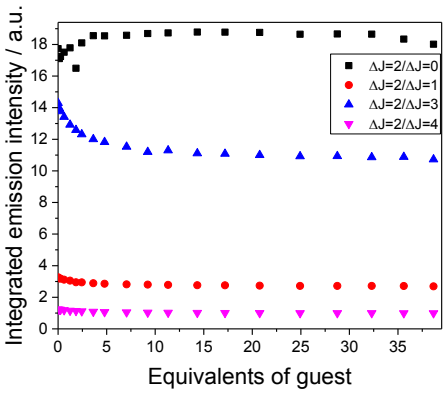


*Figure 7.6 Ratio of ΔJ = 2 peak integration to that of other peaks (Eu_2.**5**, tartrate, HEPES, pH 7.4)*

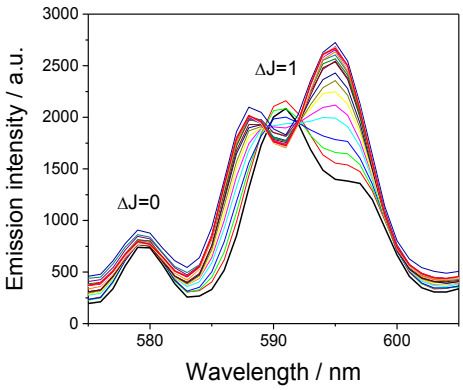


*Figure 7.7 ΔJ = 1 multiple maxima shown as the peak is symmetry-split (Eu_2.**5** with AMP in HEPES at pH 7.5)*

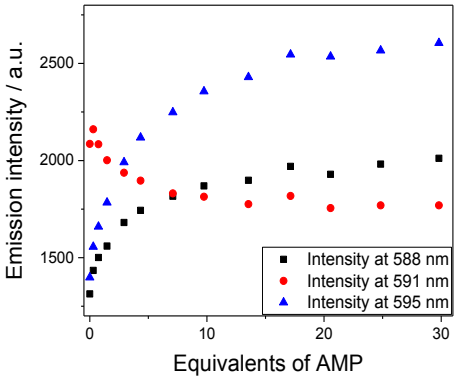


*Figure 7.8 Maxima at the split ΔJ = 1 peak plotted (Eu_2.**5** with AMP in HEPES at pH 7.5)*

Titration data was initially processed manually, then later automatically as explained in Chapter 12, Section 12.5.

An increase in emission intensity during a titration suggests displacement of bound solvent oscillators, whereas a decrease may suggest a process such as quenching through an LMCT state in the assembled adduct.

Stern-Volmer plots, as shown in Figure 7.9 and Figure 7.10, were used to remove ambiguity in the cases where it was not immediately obvious if the change in luminescence intensity was due to binding or simply due to quenching (*vide* Chapter 1).

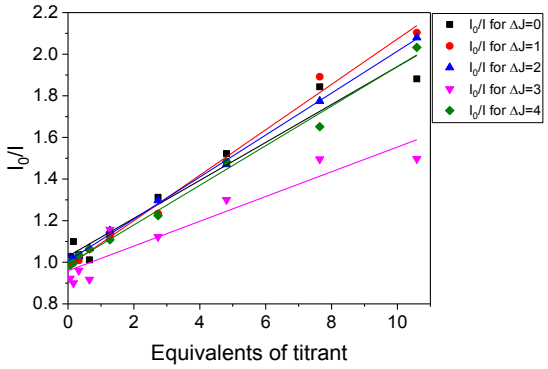


*Figure 7.9 Stern-Volmer plot of Eu.**8** with protocatechuic acid where the straight lines indicate quenching*

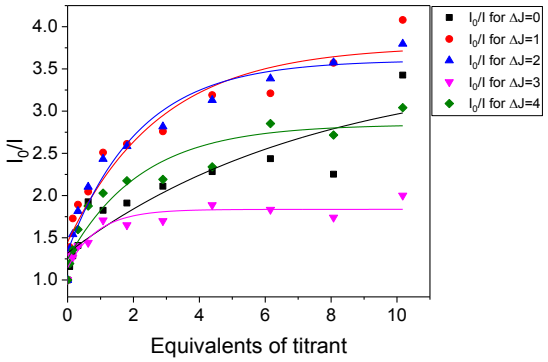


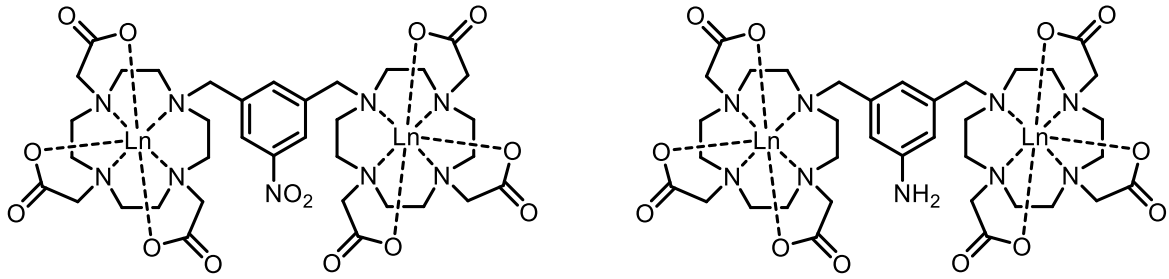
*Figure 7.10 Stern-Volmer plot of Eu_2.**5** with protocatechuic acid where the curved lines indicate binding*

Owing to the large number of titrations carried out in the course of this work, it is most straightforward to use a selection of examples to illustrate the approaches used in detail.

7.3.1 *m*-Xylyl complexes

The *m*-xylyl complexes Ln_2.**5** and Ln_2.**6** (Figure 7.11) were the first complexes studied, in order to build on the investigations published by Tilney *et al.* in 2011 and Hill *et al.* in 2013.[2,6] Titrations were carried out with an array of anionic guests, initially with arylcarboxylates as a simple model for the subsequent biologically more relevant species

such as those from the glycolytic pathway.



Ln_2.**5** Ln_2.**6**

*Figure 7.11 m-Xylyl complexes Ln_2.**5** and Ln_2.**6** where Ln = Eu, Gd, Tb, Yb, Y, with bound H_2O omitted for clarity*

At first, the complex was excited *via* the *m*-xylyl chromophore, however it was later realised that these absorption wavelengths coincided with absorption wavelengths of many of the possible anionic guests. One example of this is exhibited in the overlaid UV-vis absorption spectra in Figure 7.12. To circumvent possible inner filter problems, further titrations were therefore performed by direct excitation of the lanthanide centres although this less efficient sensitisation pathway led to lower emission intensity. Example direct excitation wavelengths were 394 nm for europium complexes and 366 nm for terbium.

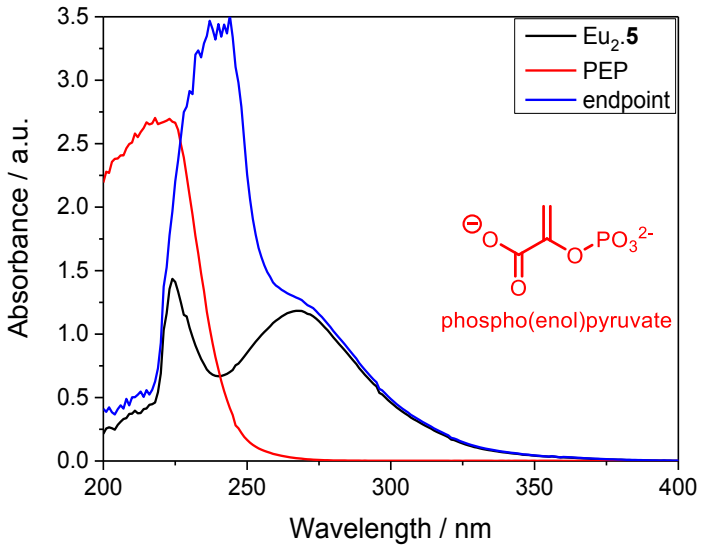


*Figure 7.12 UV-vis absorption traces of Eu_2.**5** (black), phospho(enol)pyruvate (red) and the endpoint of a titration of Eu_2.**5** with phospho(enol)pyruvate (blue)*

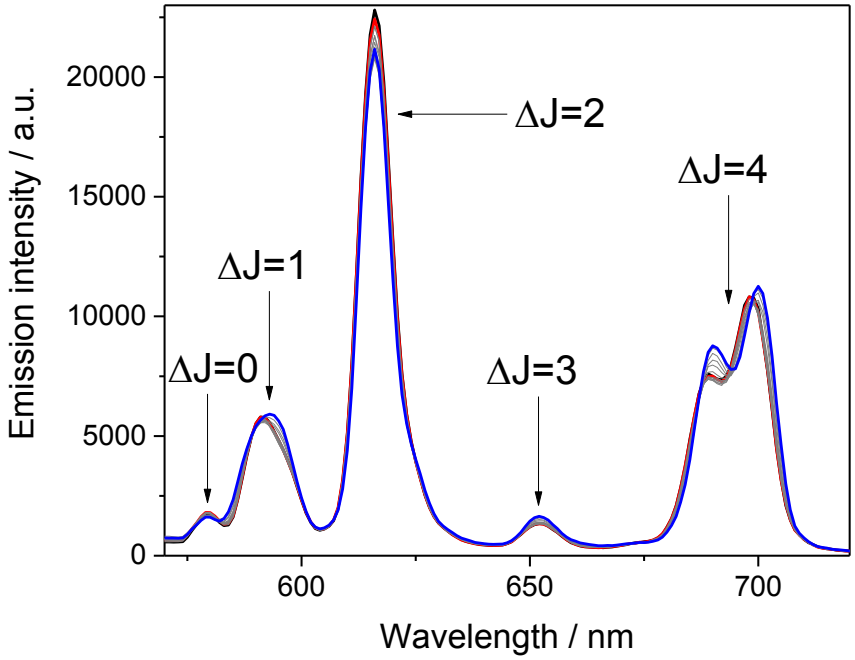


*Figure 7.13 Change in luminescence emission spectra of Eu_2.**5** as the concentration of phosphate was increased (λ_{ex} = 394 nm, s.w.$_{ex}$ = 10 nm, s.w.$_{em}$ = 5 nm)*

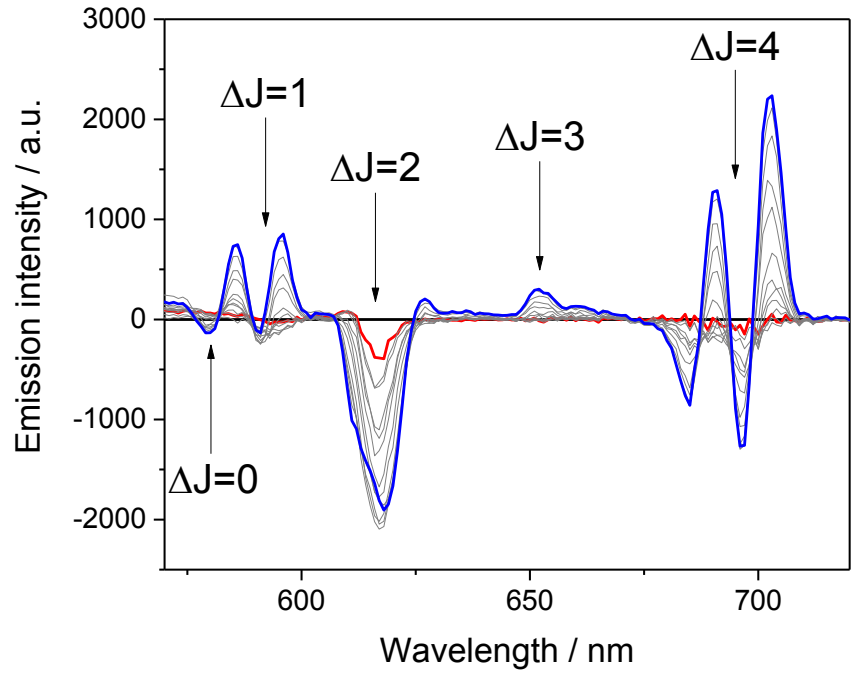
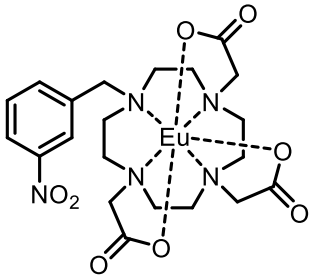


*Figure 7.14 Change in luminescence emission spectra of Eu_2.**5** as the concentration of phosphate was increased. The baseline is the emission spectrum of Eu_2.**5** alone in order to examine how some peaks increase and some peaks decrease*

Figure 7.14 was produced by subtracting the first emission spectrum of the titration of Eu_2.**5** with inorganic phosphate, measured with no titrant added, from all subsequent spectra as the concentration of phosphate is increased (original spectra shown in Figure 7.13). It is clear from this that some portions of the spectrum increase whereas others decrease, including this contrasting behaviour within a peak, most interestingly for the $\Delta J = 1$ and $\Delta J = 4$ peaks. This is as a result of the change in crystal field at the europium centre upon phosphate binding.

7.3.2 3-NitrobenzylDO3A complex

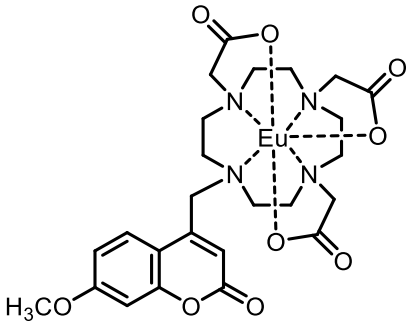


Eu.**8**

*Figure 7.15 Nitrobenzyl complex Eu.**8***

The 3-nitrobenzyl complex Eu.**8** (Figure 7.15) was chosen as it is the closest mononuclear comparison to the nitro-*m*-xylyl complex which has been studied extensively, and so provides evidence for the chelate effect in reverse. As there is only one lanthanide-containing ring, binding must be in a 1:1 fashion because there is only space for one guest. Guests which bind 2:1 to binuclear complexes, such as phosphate, were of interest as a simple point of comparison. The binding of one guest to two separate complexes – 1:2 binding – was very unlikely as the guest stock solutions were two orders of magnitude more concentrated than the host solutions.

7.3.3 Coumarin-appended complex

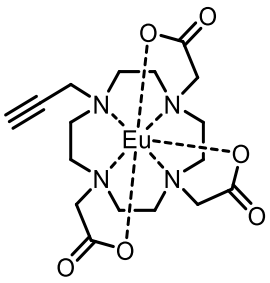


Eu.**10**

*Figure 7.16 Coumarin complex Eu.**10***

The coumarin-appended complex Eu.**10** (Figure 7.16) also offered an opportunity to study interactions based around a simpler binding model than with binuclear complexes, but here with a longer-wavelength sensitiser. Interactions with guests were predicted to be different to the benzyl complex for several reasons, including the expectation that the different ring geometry would lead to a difference in π-π stacking with guests containing an aromatic group, as well as contributions from the carbonyl group on the coumarin.

7.3.4 Propargyl complex



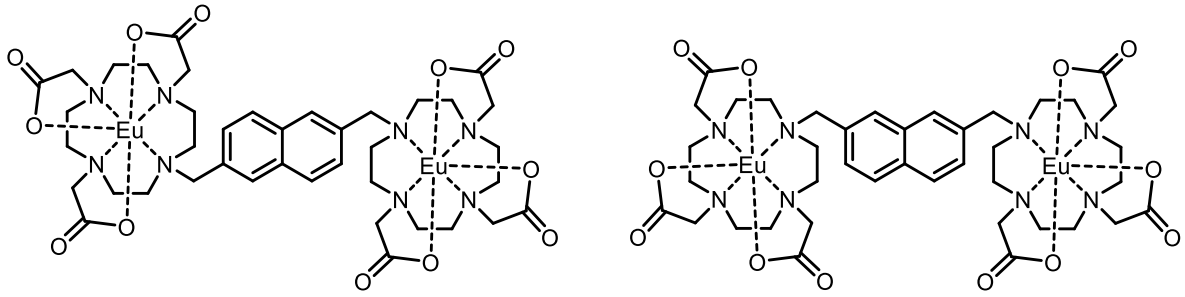
Eu.**12**

*Figure 7.17 Propargyl complex Eu.**12***

The propargyl complex Eu.**12** (Figure 7.17) is a simpler mononuclear complex with no chromophore. As it is mononuclear, again comparison of the reverse chelate effect permitted by binuclear complexes is allowed. There is no opportunity for π-π stacking with aromatic guests such as nicotinate and ATP, and therefore comparing titrations with Eu.**12** to those

with Eu.**8** provides an indication of the contribution of the appended arm to any enhancement of the interaction, though the reduced steric demand of the pendent group and the consequent change in occupation of conformational space must be taken into account.

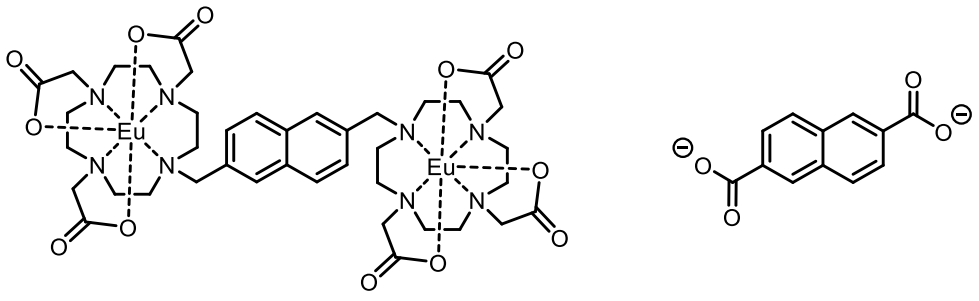
7.3.5 Naphthyl complexes



Eu_2.**14** Eu_2.**16**

*Figure 7.18 Naphthyl complexes Eu_2.**14** and Eu_2.**16***

The naphthyl complexes Eu_2.**14** and Eu_2.**16** (Figure 7.18) allowed investigation of the contribution of a spacer different in size and geometry upon binding with different sized guests by comparison with the binuclear *m*-xylyl complexes. Comparing Eu_2.**14** with Eu_2.**16** provides insight into the effect different geometry of a similar naphthyl bridge has on guest binding. For example, binding in a 1:1 fashion to Eu_2.**14** would suggest that guests were able to bind diagonally across the cavity, or if a guest were to bind 1:1 to one naphthyl complex but 2:1 to the other, this would give information on the differing conformations adopted by the complexes in solution and on the relative proximity of the europium-containing rings.



Eu_2.**14** 2,6-naphthalenedicarboxylate

*Figure 7.19 Structures of Eu_2.**14** and 2,6-naphthalenedicarboxylate*

Eu_2.**14** and 2,6-naphthalenedicarboxylate (Figure 7.19) absorb at similar wavelengths. A titration of this complex and guest combination relying on antenna excitation led to a rapid decrease in emission intensity, as the titrant absorbed the light in the antenna absorption region. This showed that sensitisation *via* the bound titrant was not occurring upon binding, unlike for another lanthanide-carboxylate binding system described in 2002.[7] Furthermore, binding between Eu_2.**14** and this titrant gave a much lower binding constant than titrations with other guests with the same host complex, with a logK value of 0.77 [0.69 – 0.84]. Therefore an analogy to the selective binding between isophthalate and *m*-xylyl complexes found by Tilney *et al.*[3] may not be drawn, despite the match between the group bridging the Eu.DO3A domains and the spacer between the two carboxylate groups in the guest. Given the nature of the guest and host, it may be that naphthyl exciplex formation or aggregation dominates in this system.

Start and endpoint excitation spectra provide further evidence for the inner filter effect in some titrations with a decrease in intensity in the chromophore absorption wavelength region. An example in Figure 7.20 shows that addition of dinicotinate to Eu_2.**14** leads to a decrease in efficiency of energy transfer for antenna excitation at 280 nm as the concentration of the titrant is increased.

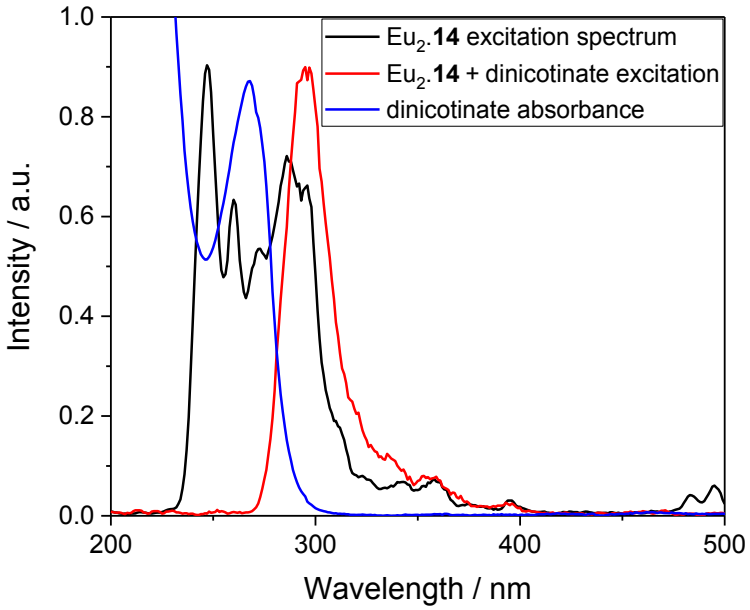
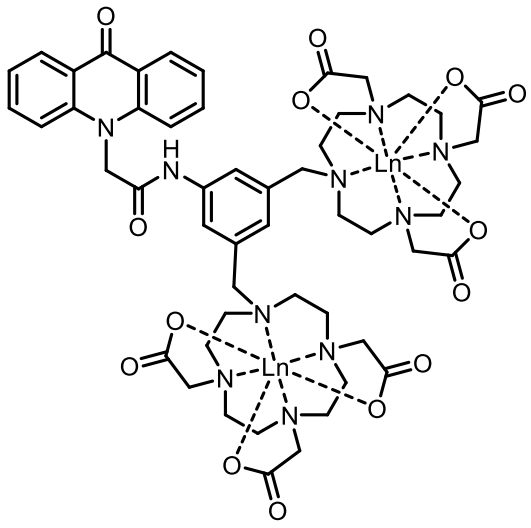


*Figure 7.20 Start and endpoint excitation spectra (black trace and red trace respectively) from a titration of Eu_2.**14** with dinicotinate, compared to the absorption spectrum of dinicotinate (blue trace)*

7.3.6 Acridone-appended complexes



Ln_2.**20**

*Figure 7.21 Acridone complex Ln_2.**20** where Ln = Eu, Tb*

The acridone complex Tb_2.**20** (Figure 7.21, Ln = Tb) was titrated with AMP, as this guest had previously been found to exhibit strong binding to other complexes in this thesis and to give rise to changes in lanthanide crystal field upon binding to a complex, as shown by the

peak splitting earlier in Figure 7.4. The changes in emission spectra for this titration are given in Figure 7.22, and the corresponding binding isotherms in Figure 7.23, and show differing responses for the transitions. Interestingly, the hypersensitive ΔJ = 2 peak appears least sensitive to the changes at the terbium upon binding.

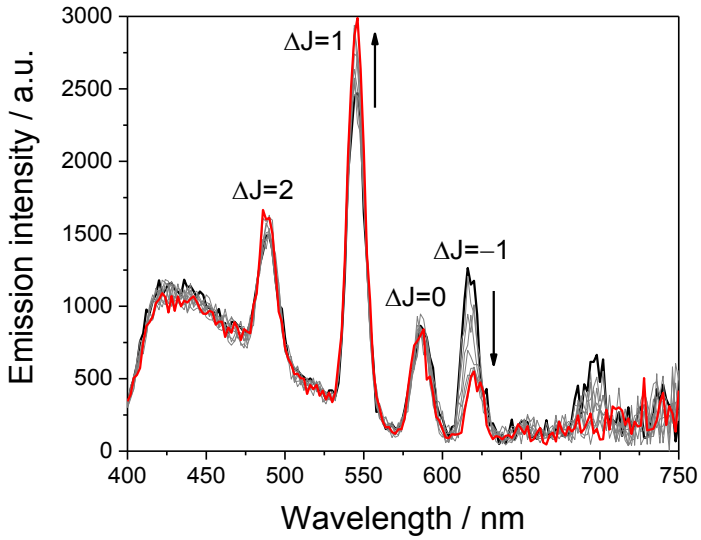


*Figure 7.22 Emission spectra for titration of Tb_2.**20** with AMP in HEPES at pH 7.4*

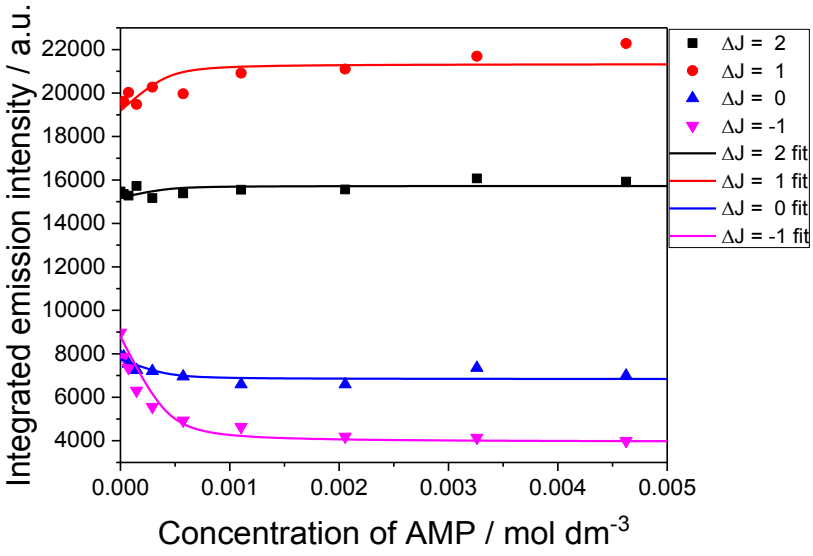


*Figure 7.23 Binding isotherm for titration of 5 × 10^{-4} M Tb_2.**20** with AMP*

7.4 Luminescence lifetimes

Lifetimes were usually found to increase by a small amount upon addition of the titrant, indicating that binding displaced solvent from the lanthanide centre, removing bound oscillators and thus extending the lifetime of the excited state. Luminescence lifetimes were calculated by fitting the decay-by-delay spectra as shown in the examples in Figure 7.24 and Figure 7.25, and the luminescence lifetime values before and after titration are presented in Table 7.1. In the cases of biexponential fits (which would indicate speciation in solution), either the weighted average of the two components was taken, or the more scientifically sensible component.

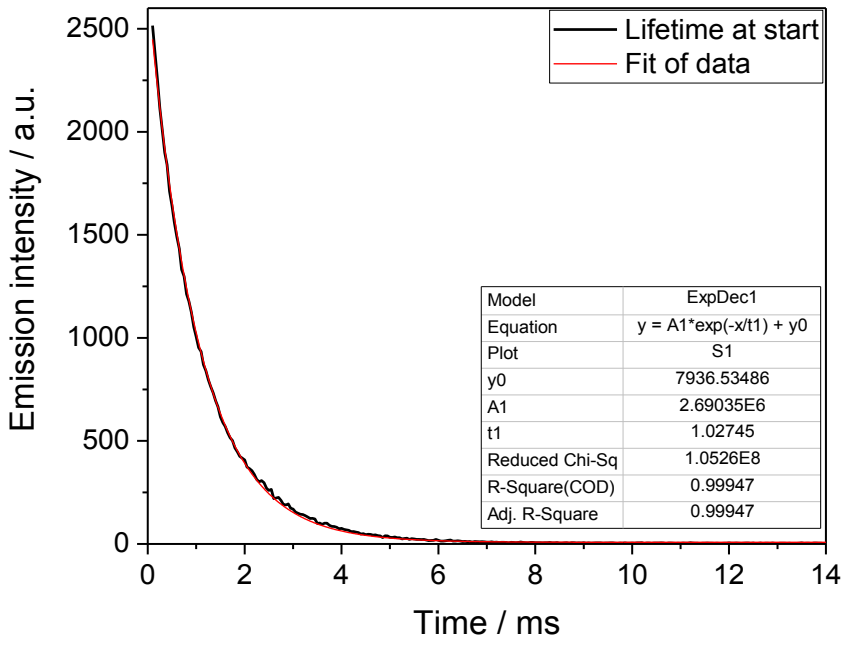


*Figure 7.24 Example decay-by-delay spectrum (black) with exponential decay lifetime fitting (red) for an initial host solution of Tb_2.**6** in HEPES at pH 7.4 (λ_{ex} = 366 nm, λ_{em} = 545 nm)*

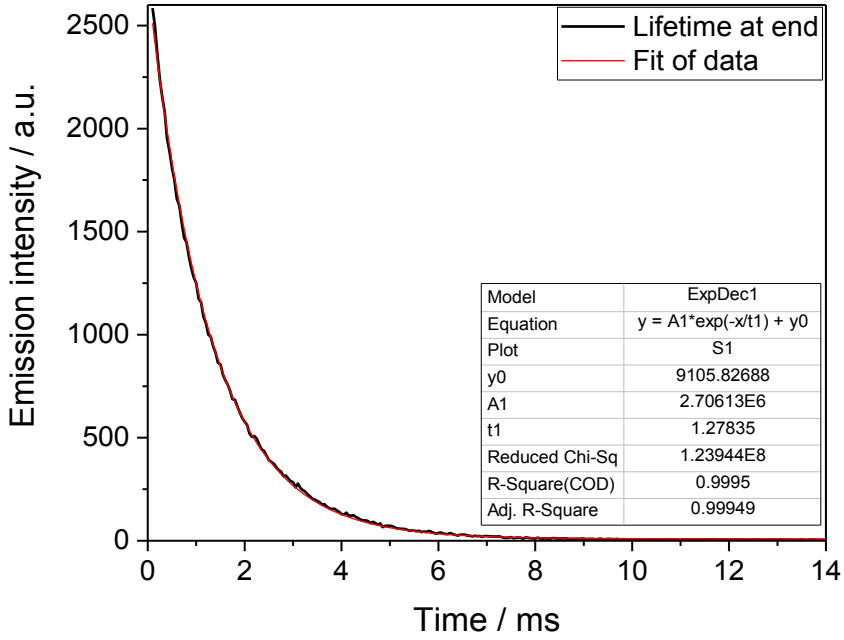


*Figure 7.25 Example decay-by-delay spectrum (black) with exponential decay lifetime fitting (red) for the final titration solution of Tb_2.**6** with fructose biphosphate (λ_{ex} = 366 nm, λ_{em} = 545 nm)*

Some cases, for example titrations with dopamine and levodopa, showed a decrease in luminescence lifetime upon binding. This was perhaps because these catechols are more effective quenchers than bound water due to a low energy LMCT state that quenches the $^5D_0$ state by charge transfer. It was not possible to calculate the luminescence lifetimes for many post-titration solutions with protocatechuic acid and protocatechualdehyde as they are very effective quenchers, and the post-titration emission intensity decreased to the extent that the signal-to-noise ratio of the measured decay-by-delay spectrum was too poor to allow effective fitting of the decay curve.

Complex	Eu_2.**5**	Eu_2.**6**	Eu.**8**	Eu.**12**	Eu.**10**	Eu_2.**14**	Eu_2.**16**	Tb_2.**5**	Tb_2.**6**
Guest	**Lifetime / ms**								
alone	0.53	0.31	0.44	0.41	0.54	0.41	0.42	1.08	1.03
FBP	0.66	0.49	-	-	-	0.50	0.52	1.49	1.28
PA	0.73	0.25	0.63	0.63	0.68	-	-	-	-
2PG	0.64	0.50	0.54	0.56	0.81	0.52	0.55	1.52	-
PEP	0.53	0.49	0.49	0.50	-	-	-	-	-
P_i	0.64	0.50	0.54	0.55	0.60	0.49	0.55	1.55	1.22
AMP	0.63	0.50	0.74	0.55	0.82	-	-	-	-
ADP	0.81	0.60	0.87	0.85	1.02	-	-	-	-
ATP	0.72	0.65	0.76	0.76	1.03	0.70	0.68	-	1.27
MPA	0.60	-	0.54	0.55	-	-	-	-	-
EPA	0.54	-	0.47	0.48	-	-	-	-	-
tartrate	0.88	0.52	-	-	-	-	0.68	1.67	1.40
lactate	-	-	0.74	-	-	-	-	-	-
dopamine	0.23	0.28	0.25	0.26	0.20	-	0.24	0.71	0.58
levodopa	-	-	-	-	-	-	-	0.84	-
nicotinate	0.36	0.33	0.48	0.45	0.60	-	-	-	-
dinicotinate	-	-	-	-	-	-	-	-	1.00

Table 7.1 Luminescence lifetimes of solutions of lanthanide complexes with and without an added guest. In cases where more than one decay component was found, a weighted average lifetime was taken for simplicity in this table.
Eu: λ_{ex} = 394 nm, s.w.$_{ex}$ = 10 – 14 nm, λ_{em} = 616 nm, s.w.$_{em}$ = 5 – 14 nm;
Tb: λ_{ex} = 366 nm s.w.$_{ex}$ = 14 nm, λ_{em} = 545 nm, s.w.$_{em}$ = 10 nm.
The guest name abbreviations may be found in the Abbreviations section or along with their molecular structures in Appendix A

7.5 NMR binding studies

Preliminary studies were carried out to establish the changes in ^{1}H and ^{31}P NMR spectra and T_1 spin-lattice relaxation times of guests upon binding to a lanthanide complex, or indeed how the spectrum of a complex changed upon addition of a guest. Recognising which peaks were most affected gave some insight into which atoms within the guest molecule were closest to the lanthanide ion (as shown previously in Figure 7.3).

From here, in some cases, more in-depth binding studies could be carried out in the form of NMR titrations. Attempting these titrations unveiled obstacles, including that the concentration required for the visibility of one species often precluded the solubility of the other. Internal referencing was usually not possible as the resonance from the inserted reference swamped the spectra as a result of the relatively low concentrations studied. Therefore referencing by substitution was employed, where an NMR spectrum of a pure reference sample (for example, phosphoric acid for ^{31}P NMR) was recorded and referenced, and this information was used to calibrate the spectrometer frequency for subsequently recorded titration spectra.

7.5.1 Preliminary NMR studies

7.5.1.1 NMR spectra

^{1}H and ^{31}P NMR spectra of an array of analytes displayed changes upon addition of varying amounts of lanthanide complexes. In the cases of europium, gadolinium, terbium, and ytterbium complexes, paramagnetic broadening was seen along with shifting of resonances. Addition of the yttrium complex Y_2.**5** was predicted to induce peak splitting upon binding to this spin-½ nuclide, and this is seen in Figure 7.26.

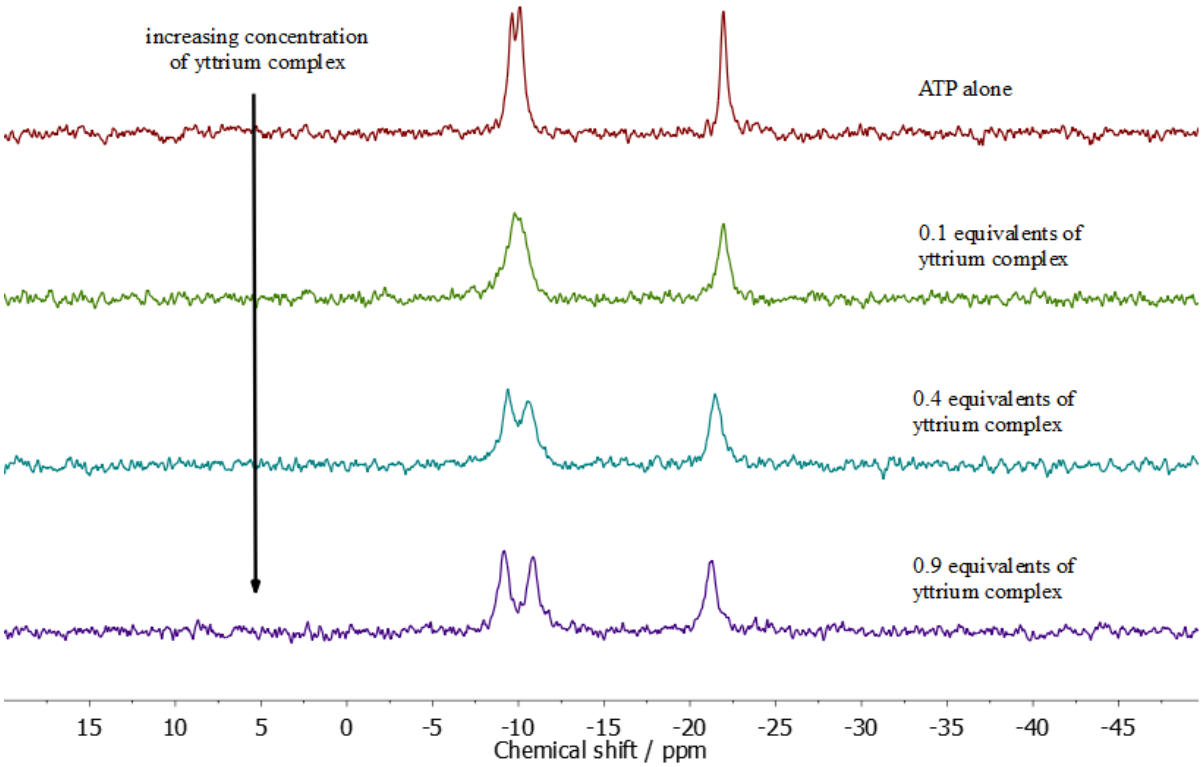


*Figure 7.26 ^{31}P NMR spectra of ATP as the concentration of Y_2.**5** was increased up to 0.9 equivalents in D_2O*

Figure 7.27 and Figure 7.28 provide evidence for binding between the lanthanide complex Eu_2.**5** and the biologically relevant species levodopa and ATP. Further NMR spectra for other host-guest combinations are given in Appendix B.

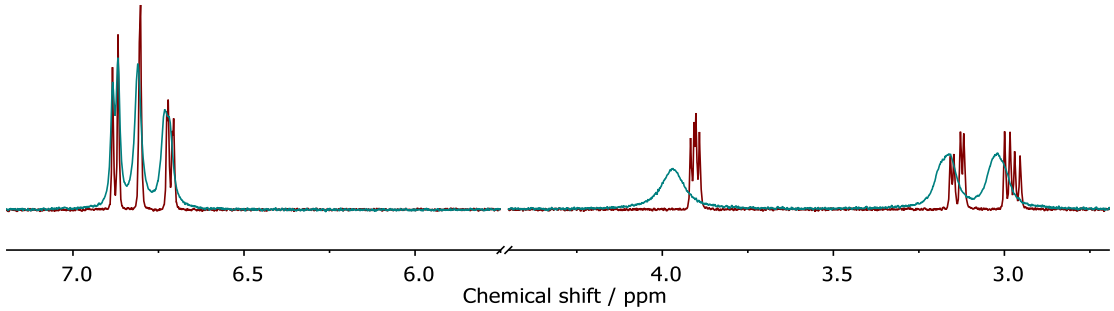


*Figure 7.27 Overlaid ^1H NMR spectra of levodopa alone (maroon trace) and with Eu_2.**5** (teal trace) in D_2O*

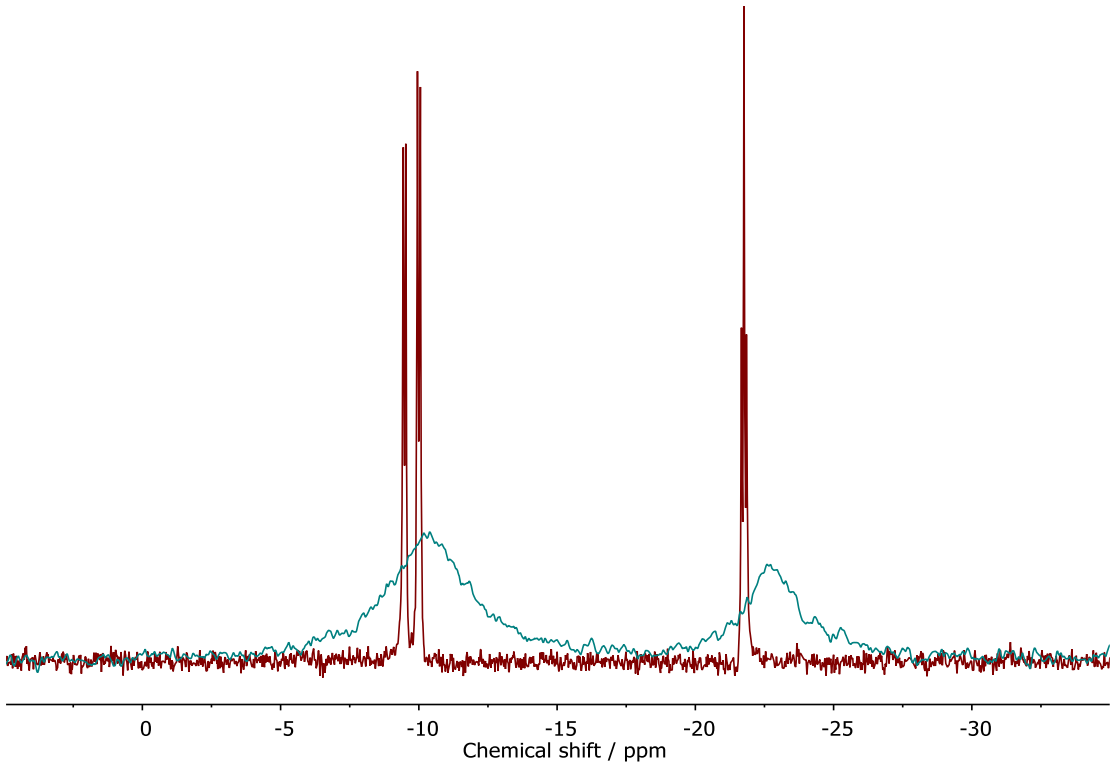


*Figure 7.28 Overlaid ^{31}P NMR spectra of ATP alone (maroon trace) and with Eu_2.**5** (teal trace) in D_2O*

7.5.1.2 Relaxation measurements

Addition of lanthanide complexes Eu_2.**5**, Eu_2.**6**, and Gd_2.**6** was found to decrease the T_1 lifetime of the ^{31}P nucleus in inorganic phosphate, fructose bisphosphate, methyl phosphonic acid, and ethyl phosphonic acid. Quantitative results from inversion recovery experiments are shown in Table 7.2. These are calculated from fitting the integrations of decaying NMR signals at set delay time intervals. An example of this signal decay is displayed in Figure 7.29, and its fitting in Figure 7.30.

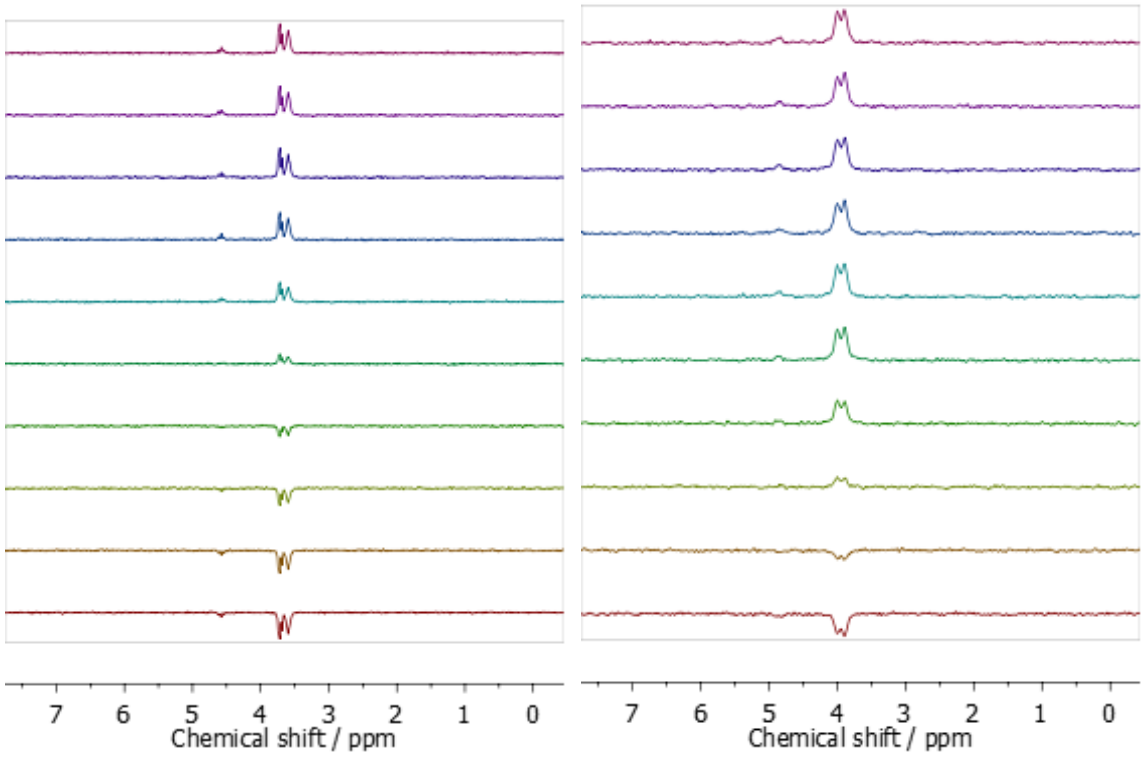


*Figure 7.29 Inversion recovery of fructose bisphosphate alone (left) and with 0.13 equivalents of Eu_2.**5** (right)*

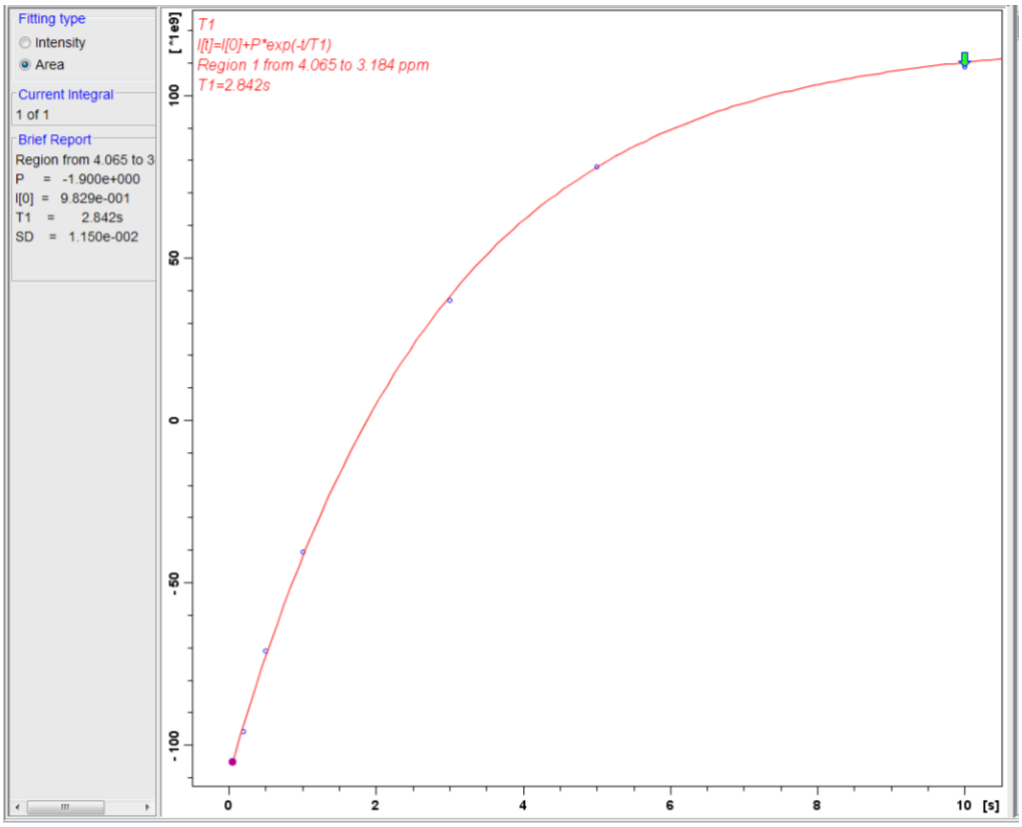


Figure 7.30 Fitting of T_1 for fructose bisphosphate from integration of the peaks around 3.7 ppm in the spectra in Figure 7.29

	^{31}P T_1 / s			
	alone in water	**0.13 equivalents** Eu_2.**5**	**0.10 equivalents** Eu_2.**6**	**<0.1 equivalents** Gd_2.**6**
FBP	2.9	0.6 [a]	0.8	1.9
P_i	9.7	-	0.8	1.8
MPA	9.5 [a]	-	2.4 [a]	-
EPA	4.5 [a]	-	3.0 [a]	-

Table 7.2 ^{31}P T_1 lifetimes of phosphate species in the absence and presence of lanthanide complexes in water

[a] *Measured in D_2O*

It is clear that a small amount of paramagnetic complex induces a significant increase in relaxivity of the sample and indicates an interaction between the paramagnetic lanthanide ions and phosphorus nuclei. This supports data from previous studies in this chapter showing paramagnetic shifting and broadening in NMR spectra upon addition of a lanthanide complex.

For each of these guests, only one set of NMR signals is observed, which indicates that the bound phosphates are in rapid exchange with the bulk.

It is interesting to note that although fructose bisphosphate and inorganic phosphate have an initially different T_1 lifetime, the measurement of the lifetime after addition of a particular amino-*m*-xylyl lanthanide complex gives the same T_1 value independent of which phosphate species is considered, suggesting that the identity of the lanthanide complex may be more important than the identity of the phosphate in these cases.

7.5.2 NMR titrations

NMR titrations were performed to support data from luminescence titrations. These were an expansion of the previous NMR studies with more data points to allow quantitative fitting of data. Binding constants were calculated from the change in chemical shift upon addition of lanthanide complex, as the signal-to-noise ratio did not allow for suitably precise measurements of the peak width at half height.

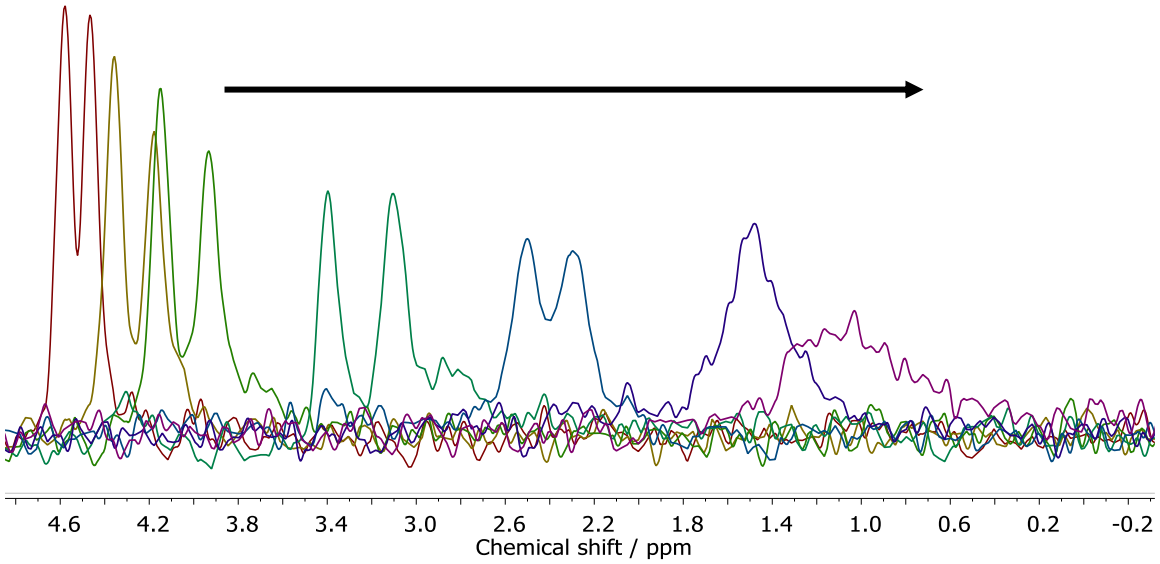


*Figure 7.31 Superimposed ^{31}P NMR spectra from a titration of 3×10^{-2} M Eu_2.**5** with 4×10^{-3} M fructose bisphosphate in D_2O*

The ^{31}P NMR spectra for the titration of fructose bisphosphate with Eu_2.**5** are shown in Figure 7.31. As the concentration of Eu_2.**5** was increased, broadening and shifting of the peaks to lower chemical shift was observed. This data is presented from the perspective of relative fructose bisphosphate concentration in Figure 7.32.

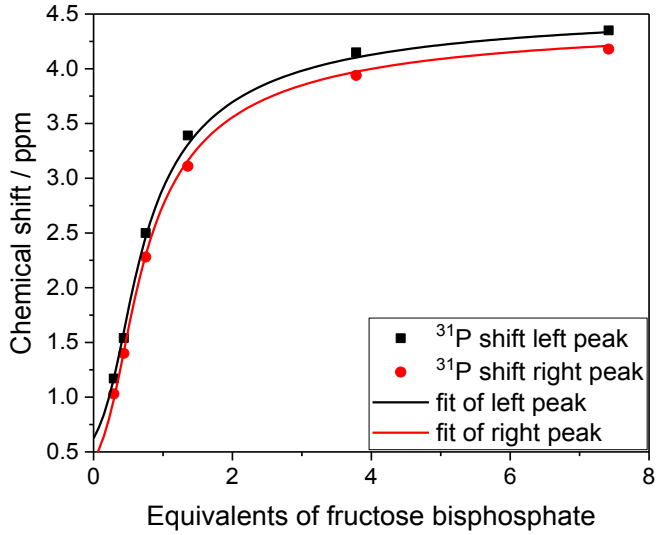


*Figure 7.32 Change in ^{31}P shift of fructose bisphosphate for varying ratios of fructose bisphosphate to Eu_2.**5***

Overlaid NMR spectra from an analogous titration with inorganic phosphate are shown in Figure 7.33 and the broadening and shifting of the single ^{31}P peak corresponding to the single phosphorus environment was noted. The binding curve is shown in Figure 7.34.

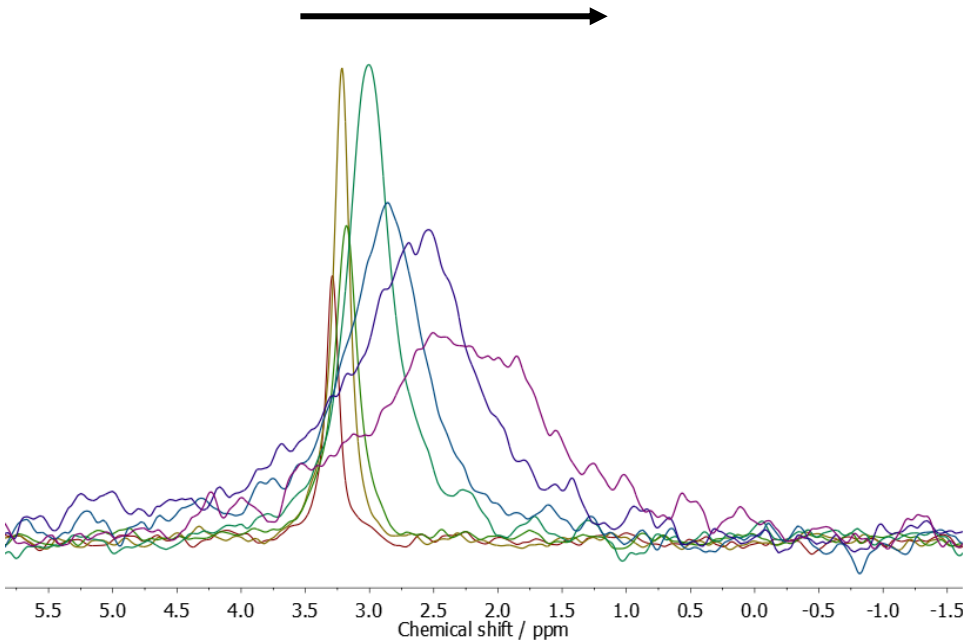


*Figure 7.33 Superimposed ^{31}P NMR spectra of inorganic phosphate showing broadening and shifting with increasing concentration of Eu_2.**5** in D_2O*

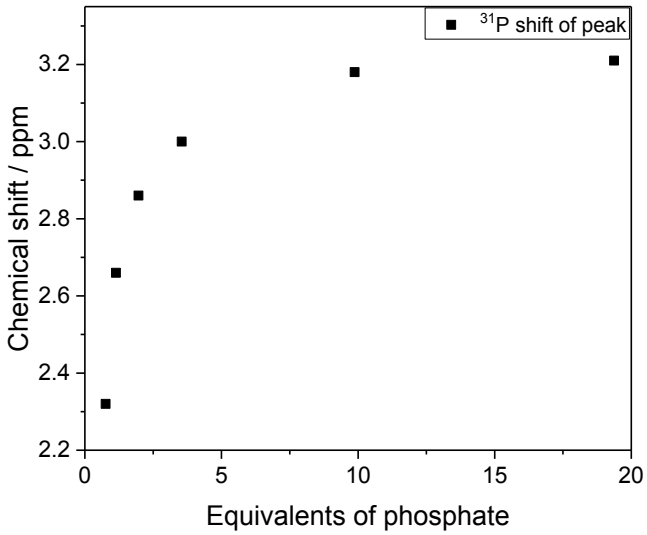


*Figure 7.34 Change in ^{31}P shift of inorganic phosphate for varying ratios of phosphate to Eu_2.**5***

The binding constants obtained from these titrations agreed approximately with those obtained from luminescence experiments. For the fructose bisphosphate titration, the logK from luminescence was 2.66 [2.63 – 2.69] and logK from the NMR titration was calculated to be 1.39 [1.35 – 1.43]. The NMR titration with inorganic phosphate gave a poor fit. These binding constants were calculated with DynaFit®, however the method differed slightly from that employed to calculate binding constants from luminescence titrations as chemical shift is related to mole fraction and is therefore an intensive property.

7.6 References

(1) Dickins, R. S.; Aime, S.; Batsanov, A. S.; Beeby, A.; Botta, M.; Bruce, J. I.; Howard, J. A. K.; Love, C. S.; Parker, D.; Peacock, R. D.; Puschmann, H. *J. Am. Chem. Soc.* **2002**, *124*, 12697–12705.
(2) Hill, L. R.; Sørensen, T. J.; Blackburn, O. A.; Brown, A.; Beer, P. D.; Faulkner, S. *Dalton Trans.* **2013**, *42*, 67–70.
(3) Tilney, J. A.; Sørensen, T. J.; Burton-Pye, B. P.; Faulkner, S. *Dalton Trans.* **2011**, *40*, 12063–12066.
(4) Sørensen, T. J.; Hill, L. R.; Tilney, J. A.; Blackburn, O. A.; Jones, M. W.; Tropiano, M.; Faulkner, S. *Eur. J. Inorg. Chem.* **2014**, *2014*, 2520–2528.
(5) Sørensen, T. J.; Hill, L. R.; Faulkner, S. *ChemistryOpen* **2015**, *4*, 509–515.
(6) Tilney, J. A.; Sørensen, T. J.; Burton-Pye, B. P.; Faulkner, S. **2011**, *1*, 5–24.
(7) Faulkner, S.; Burton-Pye, B. P.; Khan, T.; Martin, L. R.; Wray, S. D.; Skabara, P. J. *Chem. Commun.* **2002**, 1668–1669.
(8) Walker-Samuel, S.; Ramasawmy, R.; Torrealdea, F.; Rega, M.; Rajkumar, V.; Johnson, S. P.; Richardson, S.; Gonçalves, M.; Parkes, H. G.; Årstad, E.; Thomas, D. L.; Pedley, R. B.; Lythgoe, M. F.; Golay, X.; Arstad, E. *Nat. Med.* **2013**, *19*, 1067–1072.

Chapter 8 Binding of glycolysis products

8.1 Introduction

After studying aryl dicarboxylate guest species in Chapter 2, the binding of anions implicated in glycolysis and tumour hypoxia was investigated. It was reasoned that the balance between such species reflects the development of diseases such as cancer: redox stress is a hallmark of many cancerous tissues, and the balance between levels of different molecular markers may reflect disease progress.[1–4] The glycolytic pathway contains an array of carboxylate and phosphate species, many of which are dianions able to bridge the binding pocket in binuclear lanthanide complexes. Figure 8.1 shows the glycolytic pathway,[5] highlighting potential guest species in red. 3-Phosphoglycerate was not used as it was less readily available.

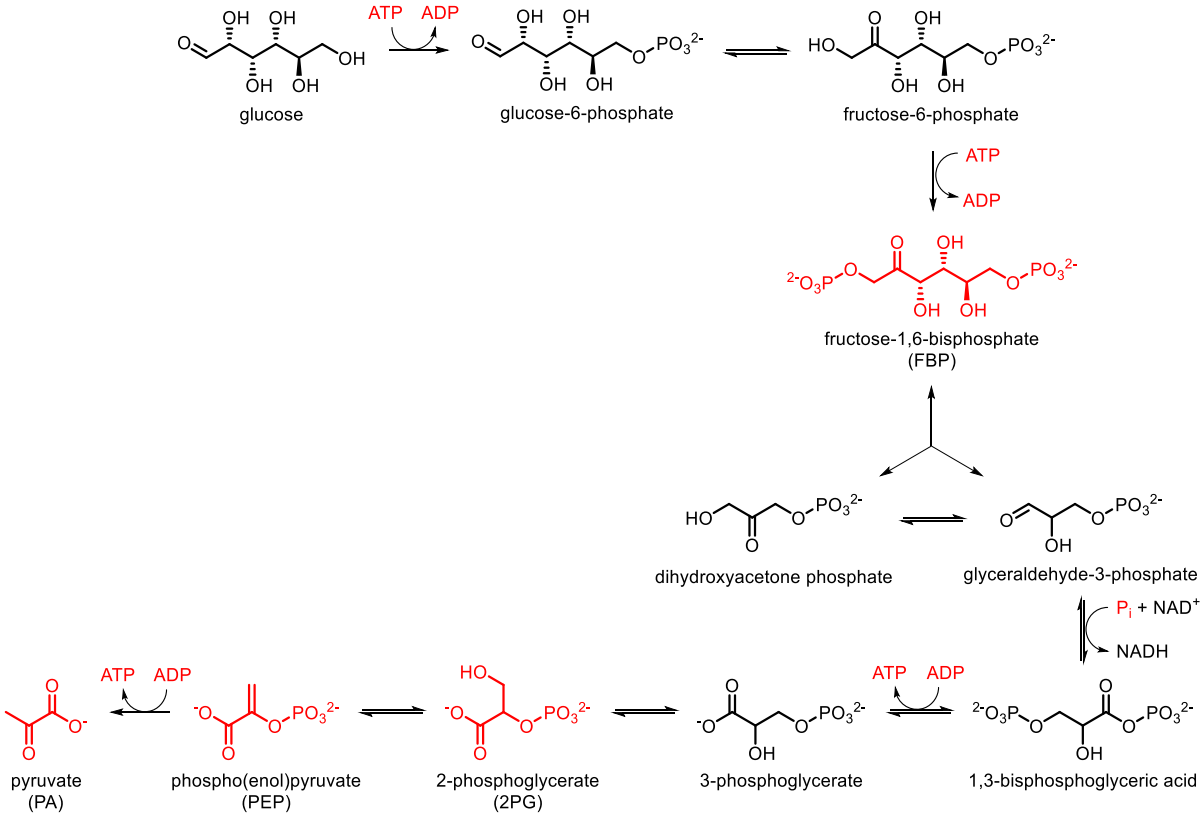


Figure 8.1 Molecules involved in the glycolytic pathway for respiration,[5] with the species studied in this work in red. ATP, ADP, and P_i are discussed in the next chapter

Fructose bisphosphate exists as both the ring form and the open chain form in solution. Thus

the implications of this with regard to binding conformation must be considered, but it can be assumed that, due to Le Chatelier's principle, the equilibrium will shift to allow binding of the more favourable structure.

8.2 Luminescence binding titrations

In contrast to previous work performed with isophthalate, some of the selected anions were found to present an obstacle as a result of the inner filter effect – manifested through absorption by the guest chromophore. In such cases, it was not possible to excite the lanthanide complex *via* the antenna as the titrant species absorbed light in this wavelength range without transferring this energy to the lanthanide. To circumvent this problem, the lanthanide was excited directly.

Some titrations with lactate and tartrate exhibited interesting behaviour at the $\Delta J = 1$ peak. Examples are shown in Figure 8.2 where there is a clear shift in wavelength of the peak maximum and in Figure 8.3 where a change in relative intensity at around 595 nm can be seen. This may be attributed to a change in symmetry at the europium centre upon binding.

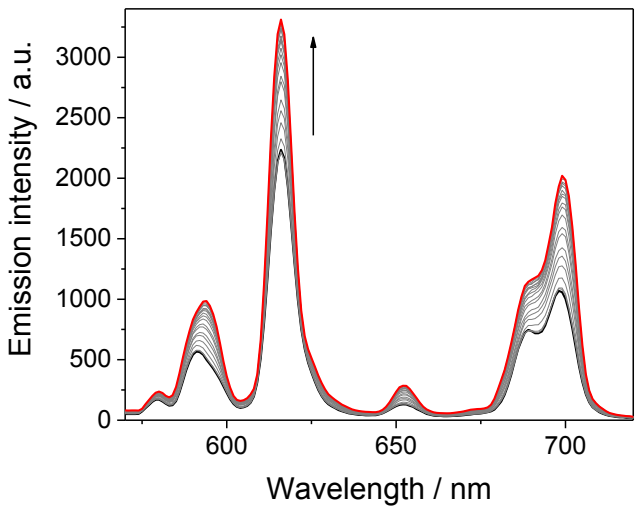


*Figure 8.2 Superimposed emission spectra from a titration of Eu_2.**5** with tartrate exhibiting interesting behaviour at the $\Delta J = 1$ peak, which is also seen for the equivalent lactate titration*

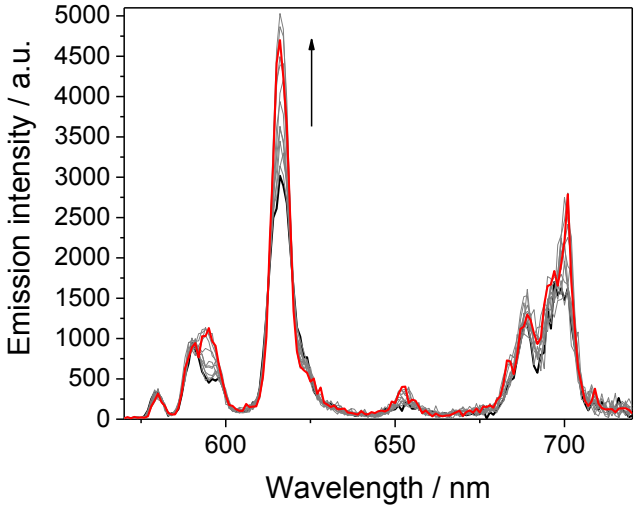


*Figure 8.3 Superimposed emission spectra from a titration of Eu.**8** with tartrate exhibiting interesting behaviour at the ΔJ = 1 peak, which is also seen for the equivalent lactate titration*

The binding isotherm in Figure 8.5 and $\Delta J = 2$ peak intensity ratios in Figure 8.6 corresponding to the emission spectra in Figure 8.4 show a rise then fall in emission intensity over the course of the titration, particularly for the $\Delta J = 2$ peak. This may be attributed to the displacement of bound solvent oscillators upon binding, followed by collisional quenching.

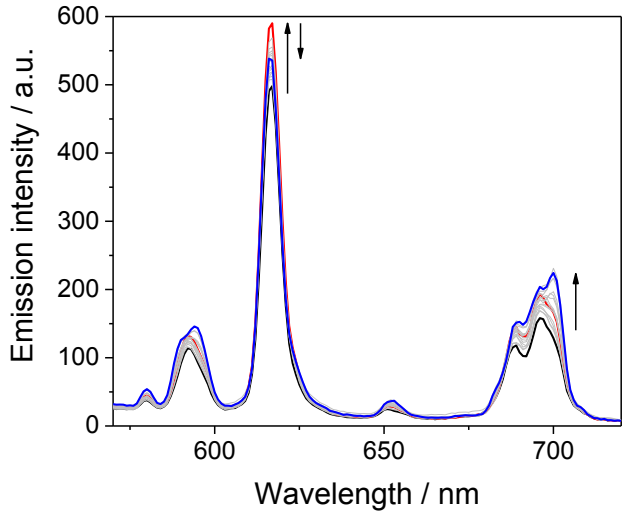


*Figure 8.4 Superimposed emission spectra from a titration of Eu_2.**6** with tartrate exhibiting a rise then fall in emission intensity*

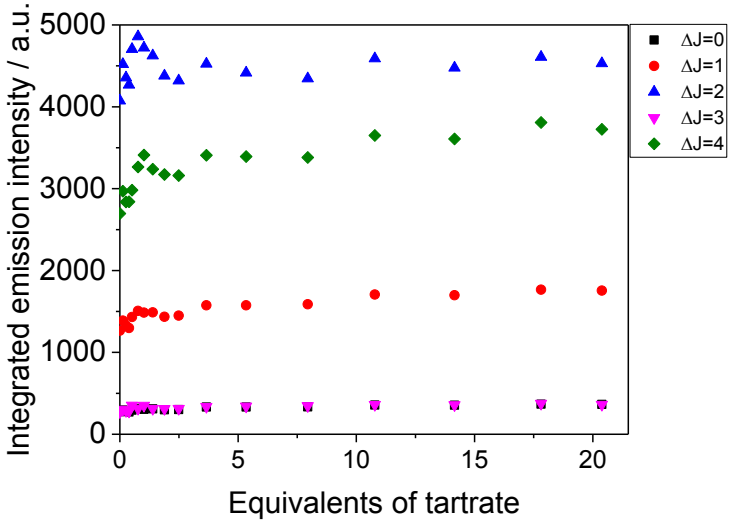


*Figure 8.5 Binding isotherm for a titration of Eu_2.**6** with tartrate exhibiting a rise then fall in emission intensity*

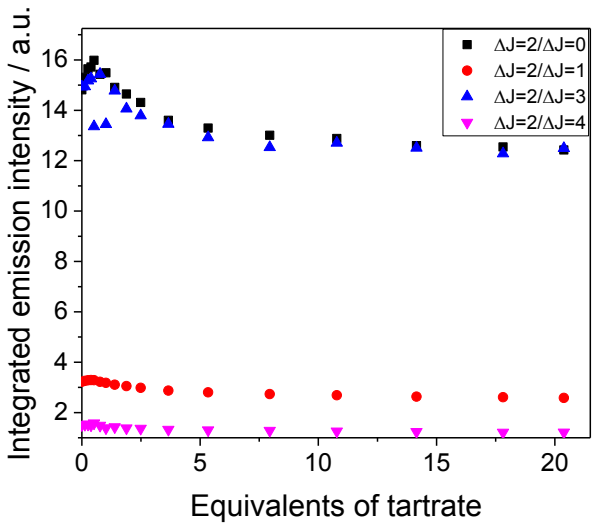


*Figure 8.6 Ratio of $\Delta J = 2$ peak integration to that of other peaks from a titration of Eu_2.**6** with tartrate exhibiting a rise then fall in emission intensity*

The data from all of these titrations was fitted with DynaFit® software.

8.3 Binding modes

When comparing the binding modes statistically found by DynaFit®, information about the conformation and geometry of the complexes in solution may be gleaned. The single lanthanide-containing domain of the mononuclear complexes Eu.**8** and Eu.**12** restricts all binding to a 1:1 mode. In a small number of cases, statistical analysis suggested 2:1 binding for these complexes. This can be rationalised by interpreting this as the software detecting more than one event, such as aggregation or some other speciation alongside the 1:1 binding event. This also suggests that the model discrimination method is not completely robust, particularly considering that these fittings gave large 95% confidence intervals.

For the binuclear complexes, 1:1 bridging of the dianion across the gap was a theoretical option but not always found. For example, both fructose bisphosphate and 2-phosphoglycerate bound to Eu_2.**14** in a 2:1 ratio, which suggests that the distance between the two europium atoms in Eu_2.**14** is too great for these dianions to span. In contrast to this, for the isomeric Eu_2.**16**, the larger fructose bisphosphate was able to bridge the smaller binding cavity than that of Eu_2.**14**, whereas the two binding anionic groups in 2-phosphoglycerate were not far enough apart to reach to bind both europium atoms.

The *m*-xylyl complexes Ln_2.**5** and Ln_2.**6** (Ln = Eu, Tb) all bound fructose bisphosphate and 2-phosphoglycerate in a bridging manner when investigated, indicating that the two lanthanide-containing rings in the *m*-xylyl complexes are closer together in solution than those of the naphthyl complexes, as expected due to the greater size of naphthalene compared to benzene.

The difference in binding mode of phospho(enol)pyruvate, pyruvate, and lactate with both

europium *m*-xylyl complexes Eu_2.**5** and Eu_2.**6** suggests that the distance between the two europium domains in solution is larger for the nitro complex than the amino complex, despite the molecular structures appearing similar on paper. This difference in conformation in solution hypothesis is in agreement with previous findings where significantly different binding constants were found for a dinicotinate guest with each of the two europium *m*-xylyl complexes.[6]

8.4 Binding constants from luminescence titrations

Previous binding studies with europium *m*-xylyl and 3,5-pyridyl complexes, including those in Chapter 2, gave log K values of around 4.2 for binding to dinicotinate under various buffer conditions.[6,7] Therefore direct and indirect comparisons of association constants reveal that binding to the glycolytic species in this chapter was weaker than to dinicotinate. The binding constants are given for binuclear complexes in Table 8.1 and mononuclear complexes in Table 8.2.

This suggested that binding to carboxylates, despite only a 1− charge which was delocalised over the whole carboxylate group, and binding *via* both oxygen atoms, was stronger than binding to the more charge-dense phosphates, which carry a 2− charge at pH 7.4 and bind through only one oxygen.[8] Therefore the reason for the weaker binding of these phosphate species did not lie in simple electrostatic attraction between the anion and the δ^+ lanthanide.

This was unexpected, and so titrations with tartrate and lactate oxyanions were performed as a more direct point of comparison. These binding constants were of a similar magnitude to those of the glycolytic phosphate species. The larger binding constants found for dinicotinate were likely to have resulted from contributions of π-π stacking of the host and guest aryl

rings, and also perhaps a better geometric fit to the binding pocket. Entropic contributions may have also played a part, with the more rigid dinicotinate molecule losing fewer degrees of freedom upon binding in comparison with the flexible chains of the other guest species. Enthalpic and entropic changes due to changes in the solvent sphere add further complications to these considerations.

The π-π stacking factor seems important, as even nicotinate with only one anionic group, and therefore the ability to bind to only lanthanide centre, generally exhibited binding with the *m*-xylyl complexes of comparable strength to that of the dianionic glycolytic species.

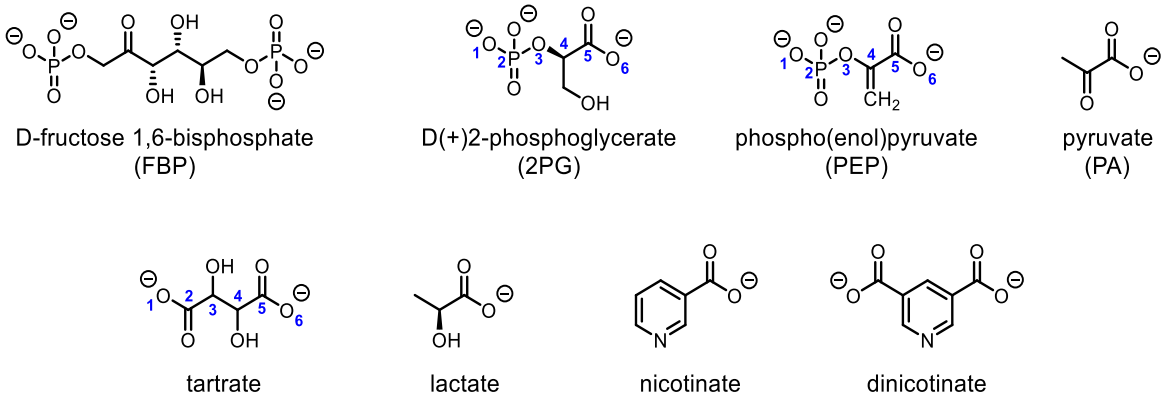


Figure 8.7 Anionic titrants studied in this chapter

Figure 8.7 shows that tartrate is likely to be very similar in size to 2-phosphoglycerate and phospho(enol)pyruvate, since there would be six atoms bridging between the two europium sites, and therefore it can be expected that these species span the binding pocket in a similar manner. This explains the generally similar binding constants of these three guests, which are given in Table 8.1 and Table 8.2.

Similarly, lactate and pyruvate are structurally related molecules, and so give binding constants of a similar order of magnitude to each other.

It was found that tartrate generally gave higher binding constants than lactate which could either be rationalised by the longer chain fitting the binding pocket better or by considering the speciation in solution. Carboxylic acid groups are more acidic than alcohols; the pK_a values of the two carboxylic acid groups in tartaric acid are 2.9 and 4.4, and for lactic acid the carboxylic acid has a pK_a of 3.9 and the alcohol is 15.1.[9,10] Therefore at pH 7.4 tartrate is dianionic whereas lactate would be a monoanion where stronger electrostatics would be expected between tartrate and the δ^+ lanthanide-containing domains. The lactate may still generally bind 1:1 with binuclear complexes because it may be bulky enough to block approach to the other lanthanide.

Complex	Eu_2.**5**	Eu_2.**6**	Eu_2.**14**	Eu_2.**16**	Tb_2.**5**	Tb_2.**6**
Guest	**log(K) [95% confidence interval]**					
FBP	2.66 [2.63 – 2.69]	3.20 [3.04 – 3.35]	2.60,[a] [2.54 – 2.67] 4.23 [b] [4.14 – 4.33]	2.74 [2.69 – 2.80]	-	3.65 [3.32 – 4.10]
2PG	2.82 [2.76 – 2.89]	4.08 [3.97 – 4.20]	2.58,[a] [2.50 – 2.67] 4.27 [b] [4.16 – 4.40]	5.74 [d] [5.63 – 5.84]	2.75 [2.60 – 2.91]	-
PEP	1.18,[a] [1.13 – 1.22] 4.04 [b] [3.95 – 4.14]	5.29 [4.86 – >10.9]	-	-	-	-
PA	1.38,[a] [1.18 – 1.54] 3.13 [b] [3.08 – 3.18]	3.24 [2.92 – 3.61]	-	-	-	-
tartrate	2.82 [2.81 – 2.83]	3.23 [3.13 – 3.32]	-	4.24 [3.86 – 4.89]	2.57 [2.51 – 2.62]	- [c]
lactate	5.64 [d] [5.53 – 5.75]	2.77 [2.71 – 2.83]	-	-	-	-
dinicotinate	-	-	-	-	-	3.36 [3.22 – 3.51]
nicotinate	3.92 [3.66 – 4.23]	3.97* [3.78 – 4.20]	-	-	-	-

Table 8.1 Binding constants for titrations of binuclear complexes in HEPES at pH 7.4

*[a] log K_1, [b] log K_2, [c] could not fit data reliably, [d] could not separate K_1 and K_2 so the log of the overall binding constant K_{tot} is given, * 1:1 binding constant given, as 2:1 gave much larger confidence intervals*

Complex	Eu.**8**	Eu.**10**	Eu.**12**
Guest	**log(K) [95% confidence interval]**		
FBP	3.33[†] [3.13 – 3.54]	-	-
2PG	3.88 [3.70 – 4.10]	0.76 [0.75 – 0.77]	0.29[†] [0.23 – 0.35]
PEP	- [c]	-	2.42 [2.30 – 2.53]
PA	2.49 [2.42 – 2.56]	3.94 [3.53 – 4.66]	2.24 [2.22 – 2.26]
tartrate	3.31 [3.26 – 3.37]	-	3.29 [3.24 – 3.34]
lactate	2.73 [2.68 – 2.79]	-	-
dinicotinate	-	-	-
nicotinate	0.57 [0.49 – 0.64]	1.92 [1.89 – 1.95]	1.60[†] [1.48 – 1.70]

Table 8.2 Binding constants for titrations of mononuclear complexes in HEPES at pH 7.4

[c] could not fit data reliably, [†] 1:1 binding constant given, as 2:1 binding was unfeasible

There was very little change in the emission intensity for the titration of Eu.**8** with phospho(enol)pyruvate and so it was not possible to fit this data. The calculated binding constant from the titration of Eu_2.**6** with phospho(enol)pyruvate gave large confidence intervals so this result should be treated with caution. For Tb_2.**6** with tartrate there was some change in intensity, however very large confidence intervals indicated a poor fit and therefore this data is not included.

Binding to Eu_2.**6** was stronger than binding to Eu_2.**5**, which is contrary to what might be expected as the electron-withdrawing nitro group would increase the partial positive charge on the lanthanide atom and therefore increase electrostatic attraction between the lanthanide and the anionic guest.

Binding to Eu.**8** was often stronger than binding to Eu_2.**5** despite the opportunity for chelation, likely as a consequence of differences in solvation and conformation, as documented earlier. However, binding to Eu.**8** was usually weaker than binding to Eu_2.**6**, since ΔG benefits from chelation, though it should always be borne in mind that the significant structural differences between these complexes may also play a role.

As the charges on the dianions were the same and guest solvation effects can be assumed to be similar, the difference in binding constants between fructose bisphosphate and the other bridging dianions can be attributed to the longer chain length of fructose bisphosphate fitting different-sized binding cavities better or worse than the shorter-chained dianions.

The greatest range of binding constant was seen for nicotinate, suggesting that the rigid structure of this guest was accommodated very well in some binding pockets but was unable

to adapt to the binding pockets in other complexes, whereas the more flexible-chained guests would be able to adopt a different conformation to fit the pocket.

Few titrations were performed for the binding of terbium complexes to these guests, however the terbium amino-*m*-xylyl complex Tb_2.**6** gave a greater binding constant with fructose bisphosphate than its europium analogue Eu_2.**6**, which may be explained by the greater electrostatic attraction of the anions to the more charge dense terbium atom. However, the europium nitro-*m*-xylyl complex Eu_2.**5** gave larger binding constants for binding to 2-phosphoglycerate and to tartrate than Tb_2.**5** exhibited, reinforcing the idea that interactions in solution are not straightforward when comparing apparently similar host complexes.

8.5 NMR binding studies and titrations

The ^{31}P NMR titration of Eu_2.**5** with fructose bisphosphate and various changes in T_1 relaxivities are discussed in the previous chapter in Section 7.5.1.2. Further examples of NMR studies are given below.

The ring form and open chain form of fructose bisphosphate can clearly be seen on the maroon trace on the ^{31}P NMR in Figure 8.8 before the addition of the lanthanide complex. It is difficult to resolve whether coalescing of the peaks upon addition of Tb_2.**5** may be attributed to the shifting of the equilibrium between the ring form and open chain form of fructose bisphosphate, or whether it is a result of paramagnetic shifting and broadening, however it can be noted that an increasing amount of the complex leads to a greater movement of the peak. The accompanying ^{1}H NMR spectra are shown in Figure 8.9 and show a similar increase in broadening but with a smaller degree of paramagnetic shifting, as binding occurs *via* the phosphate group and so the hydrogen atoms lie further away from the

lanthanide centres upon binding. Greater broadening of NMR resonances per mmol of complex is seen here than for binding to europium(III) complexes, as terbium(III) has a much larger T_2 effect.

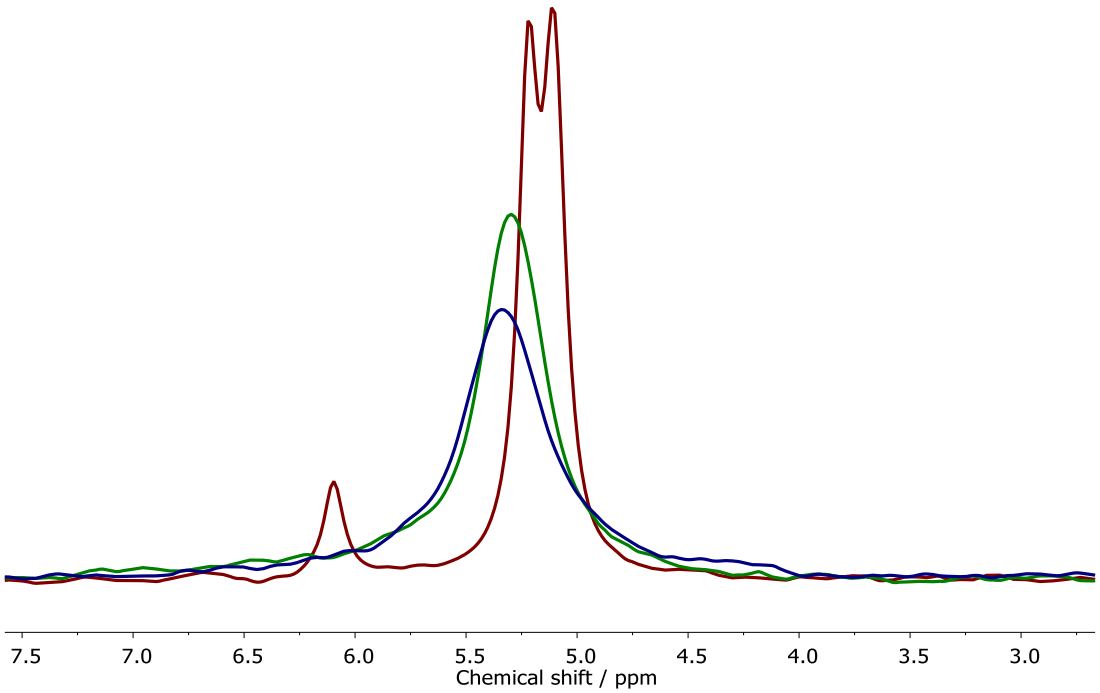


*Figure 8.8 Superimposed ^{31}P NMR spectra of fructose bisphosphate alone (maroon), with 0.03 equivalents Tb_2.**5** (green), and 0.06 equivalents Tb_2.**5** (blue) in D_2O*

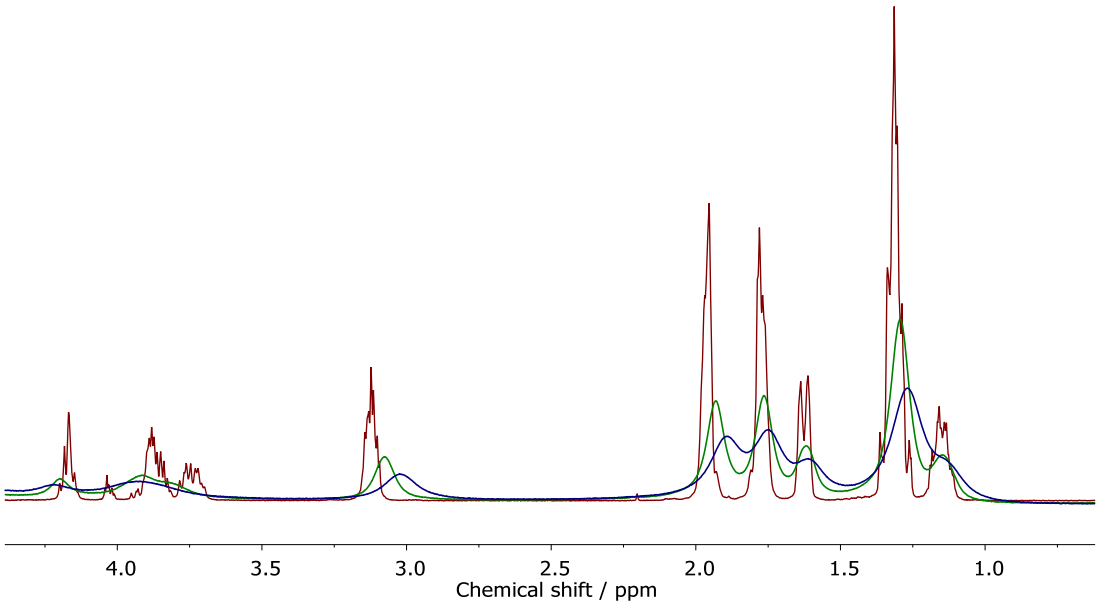


*Figure 8.9 Superimposed ^{1}H NMR spectra of fructose bisphosphate alone (maroon), with 0.03 equivalents Tb_2.**5** (green), and 0.06 equivalents Tb_2.**5** (blue) in D_2O*

The ^{31}P NMR spectra shown in Figure 8.10 present an interesting contrast to previous

experiments where a lanthanide complex is added to a guest. Upon addition of 0.1 equivalents of the paramagnetic Yb_2.**5**, the NMR resonances shift. However, upon increasing the concentration of Yb_2.**5** to 0.4 (and subsequently 0.8 equivalents), there is very little change in chemical shift or in broadening, whereas in previous experiments, a gradual further shift was seen. The ^{1}H NMR spectra in Figure 8.11 show a similar lack of shifting.

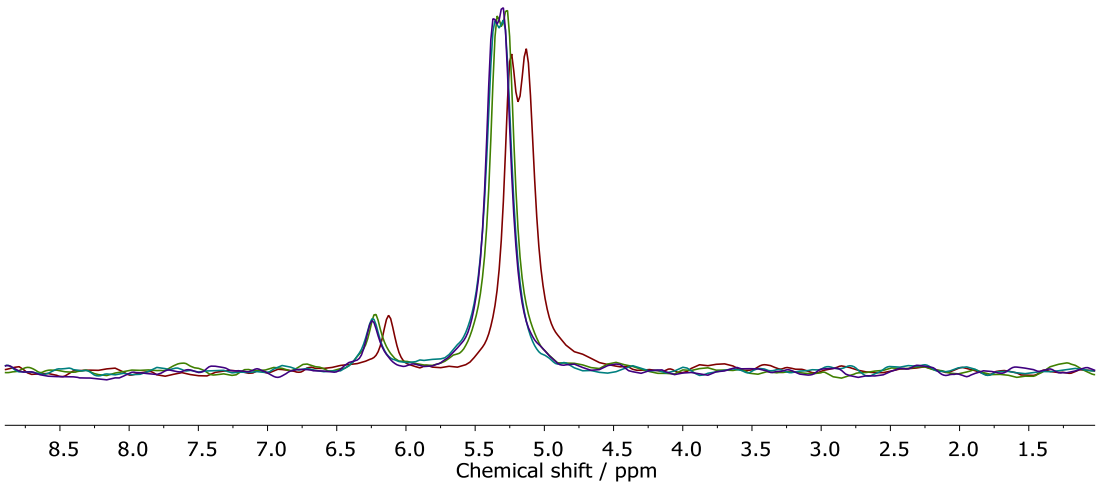


*Figure 8.10 Superimposed ^{31}P NMR spectra of fructose bisphosphate alone (maroon) and with 0.1 equivalents Yb_2.**5** (green), 0.4 equivalents (turquoise), 0.8 equivalents (purple) in D_2O*

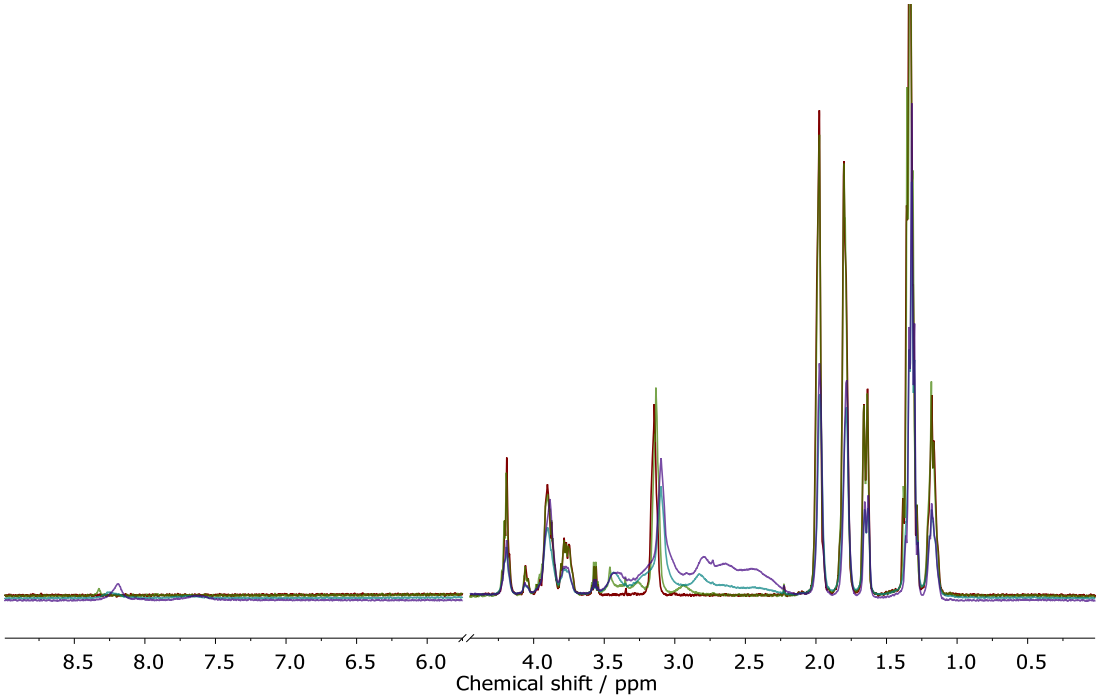


*Figure 8.11 Superimposed ^{1}H NMR spectra of fructose bisphosphate alone (maroon) and with 0.1 equivalents Yb_2.**5** (green), 0.4 equivalents (turquoise), 0.8 equivalents (purple) in D_2O*

8.6 References

(1) Warburg, O. *Science* **1956**, *123*, 309–314.
(2) Wiseman, H.; Halliwell, B. *Biochem. J.* **1996**, *313*, 17–29.
(3) Gatenby, R. A.; Gillies, R. J. *Nat. Rev. Cancer* **2004**, *4*, 891–899.
(4) Halliwell, B. *Biochem. J.* **2007**, *401*, 1–11.
(5) Berg, J. M.; Tymoczko, J. L.; Stryer, L. *Biochemistry*; 5th ed.; W H Freeman: New York, 2002.
(6) Hill, L. R.; Sørensen, T. J.; Blackburn, O. A.; Brown, A.; Beer, P. D.; Faulkner, S. *Dalton Trans.* **2013**, *42*, 67–70.
(7) Sørensen, T. J.; Hill, L. R.; Faulkner, S. *ChemistryOpen* **2015**, *4*, 509–515.
(8) Dickins, R. S.; Aime, S.; Batsanov, A. S.; Beeby, A.; Botta, M.; Bruce, J. I.; Howard, J. A. K.; Love, C. S.; Parker, D.; Peacock, R. D.; Puschmann, H. *J. Am. Chem. Soc.* **2002**, *124*, 12697–12705.
(9) Dawson, R. M. C. *Data for biochemical research*; Clarendon Press: Oxford, 1959.
(10) Silva, A. M. N.; Kong, X.; Hider, R. C. *Biometals* **2009**, *22*, 771–778.

Chapter 9 Binding of anionic phosphate species

9.1 Introduction

A variety of phosphate species (shown in Figure 9.1) were titrated with the previously investigated mononuclear and binuclear lanthanide complexes. The nucleotides AMP, ADP, and ATP are important in respiration. Nadella *et al.* have published work on the use of lanthanide complexes to sense AMP, ADP, and ATP,[1] and the Butler group[2] and Parker group[3] have used lanthanide complexes to probe the ADP/ATP ratio. Although not biologically endogenous, methylphosphonic acid and ethylphosphonic acid were also studied in order to gain a fuller picture of phosphate binding and the effect of varying the group attached to the phosphorus atom. The phosphates in Figure 9.1 are unlikely to be able to bridge the binding cavity of binuclear complexes due to their size and geometry.

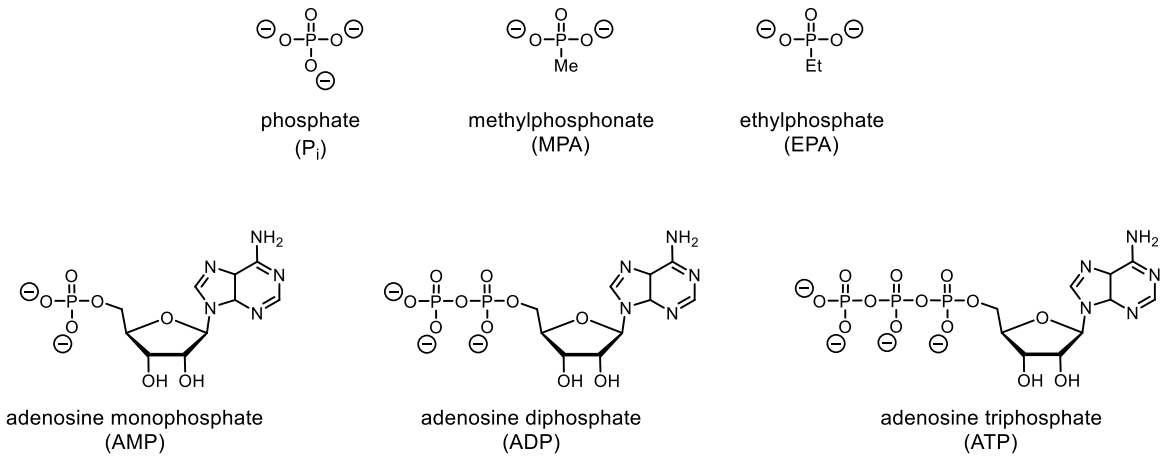


Figure 9.1 Phosphate guests studied in binding experiments

9.2 Luminescence binding titrations

Titrations were performed as previously described, and the results are given in Table 9.1 for binuclear complexes and Table 9.2 for mononuclear complexes. For some titrations, for example those with AMP, as noted in Chapter 7, additional data was collected from the crystal field splitting of peaks such as the $\Delta J = 1$ peak and incorporated into the DynaFit® script.

Complex	Eu_2.**5**	Eu_2.**6**	Eu_2.**14**	Eu_2.**16**	Tb_2.**5**	Tb_2.**6**
Guest	**log(K) [95% confidence interval]**					
P_i	1.41 [a] [1.37 – 1.44] 3.54 [b] [3.50 – 3.58]	6.81 [c] [6.55 – 7.10]	8.37 [c] [7.99 – 8.94]	2.20 [a] [2.16 – 2.25] 3.02 [b] [2.89 – 3.14]	1.35 [a] [<−1 – 1.89] 4.52 [b] [3.99 – 7.45]	7.90 [c] [6.88 – >10]
AMP	3.42 [3.36 – 3.48]	2.11 [a] [1.90 – 2.31] 4.17 [b] [4.06 – 4.30]	-	-	-	-
ADP	2.43 [a] [2.26 – 2.64] 4.81 [b] [4.61 – 5.08]*	2.56 [a] [2.41 – 2.69] 4.28 [b] [4.21 – 4.35]	-	-	-	-
ATP	3.29 [3.18 – 3.40]	2.86 [2.82 – 2.91]	7.35 [c] [7.19 – 7.52]	3.49 [a] [3.04 – 7.19] 5.99 [b] [5.46 – 9.80]	-	2.68 [2.61 – 2.76]
MPA	3.72 [3.44 – 4.06]	-	-	-	-	-
EPA	0.80 [0.74 – 0.86]	-	-	-	-	-

Table 9.1 Binding constants for titrations of binuclear complexes in HEPES at pH 7.4

*[a] log K_1, [b] log K_2, [c] could not separate K_1 and K_2 so the log of the overall binding constant K_{tot} is given, * this 2:1 binding outcome is anomalous and likely due to a poor signal-to-noise ratio in the data*

Complex	Eu.**8**	Eu.**10**	Eu.**12**
Guest	**log(K) [95% confidence interval]**		
P_i	0.94† [0.80 – 1.05]	3.15 [3.04 – 3.26]	2.81† [2.70 – 2.93]
AMP	3.53† [3.32 – 3.77]	5.23† [4.93 – 5.81]	0.63 [0.57 – 0.68]
ADP	3.38† [3.21 – 3.56]	4.17 [4.08 – 4.28]	3.09† [2.99 – 3.20]
ATP	4.34 [3.99 – 4.91]	2.93 [2.89 – 2.97]	0.64† [0.61 – 0.66]
MPA	0.60 [0.56 – 0.63]	-	3.23 [3.02 – 3.46]
EPA	0.18† [−0.07 – 0.35]	-	0.90† [0.76 – 1.00]

Table 9.2 Binding constants for titrations of mononuclear complexes in HEPES at pH 7.4

[a] log K_1, [b] log K_2, † 1:1 binding constant given as 2:1 binding was unfeasible

For the binuclear amino complex Eu_2.**6**, AMP and ADP bound in a 2:1 fashion, with a guest binding to each europium domain, whereas upon binding of the larger ATP, approach of a second guest would be blocked, giving rise to a 1:1 binding mode. In contrast to this, the larger naphthyl complexes Eu_2.**14** and Eu_2.**16**, where the lanthanide-containing macrocycles are further apart, accommodate 2:1 binding of ATP.

For binding to ATP, Eu_2.**5** bound more strongly than Eu_2.**6**, likely because the electron-withdrawing nitro group increased the δ^+ character of the lanthanide atoms, thus increasing the electrostatic attraction to the anionic guest. Eu.**8** exhibited a higher binding constant (Table 9.2) with ATP than either of the binuclear *m*-xylyl complexes, perhaps as a result of reduced steric crowding due to the presence of only one lanthanide-containing ring. The propargyl complex Eu.**12** gave much lower binding constants than the other mononuclear complexes with AMP, ADP, and ATP, as binding did not benefit from the π-π stacking with the purine ring that was possible for the nitrobenzyl and coumarin complexes.

Ethylphosphonic acid gave smaller binding constants than methylphosphonic acid, which may be explained by the greater steric hindrance and lower charge density of the longer chain phosphonic acid.

The phosphonic acids generally gave lower binding constants than inorganic phosphate, which may be attributed to the 2− charge on the conjugate bases of these acids at pH 7.4, compared to the 3− charge on inorganic phosphate, which would therefore experience greater electrostatic attraction to the lanthanide centre and perhaps also greater loss of solvent order upon binding.

The phosphonic acids bound in a 1:1 fashion with the lanthanide complexes even in cases where inorganic phosphate bound *via* a 2:1 mode, perhaps due to the steric bulk of the alkyl chain blocking the approach of a second guest into the binding cavity.

AMP was also titrated with Tb_2.**20** and gave a log K value of 4.36 [4.01 – 4.98]. This is a relatively large binding constant for a nucleotide with a binuclear complex of this type, and may be due to enhanced π-π interaction of the aromatic group in the AMP with the acridone as well as the *m*-xylyl ring. There may also be contribution from entropic factors, in that fewer degrees of conformational freedom are lost upon binding to the more restricted structure compared to that of Tb_2.**6**, analogous to results already reported in 2013.[4]

In order to highlight selectivity for particular guests, two double titrations with Eu_2.**5** were performed. These involved binding of one guest and then another. The guests chosen for this were phospho(enol)pyruvate and ATP because they gave significantly different binding constants with small confidence intervals.

In the first experiment, firstly PEP was titrated in until the endpoint, then ATP was titrated in. In the second experiment, the guests were reversed: ATP was titrated and then PEP. The binding isotherms are shown in Figure 9.2 and Figure 9.3 (and an expanded view in Figure 9.4). Attempts to fit the data yielded poor fits, likely due to the negligible changes in emission intensity.

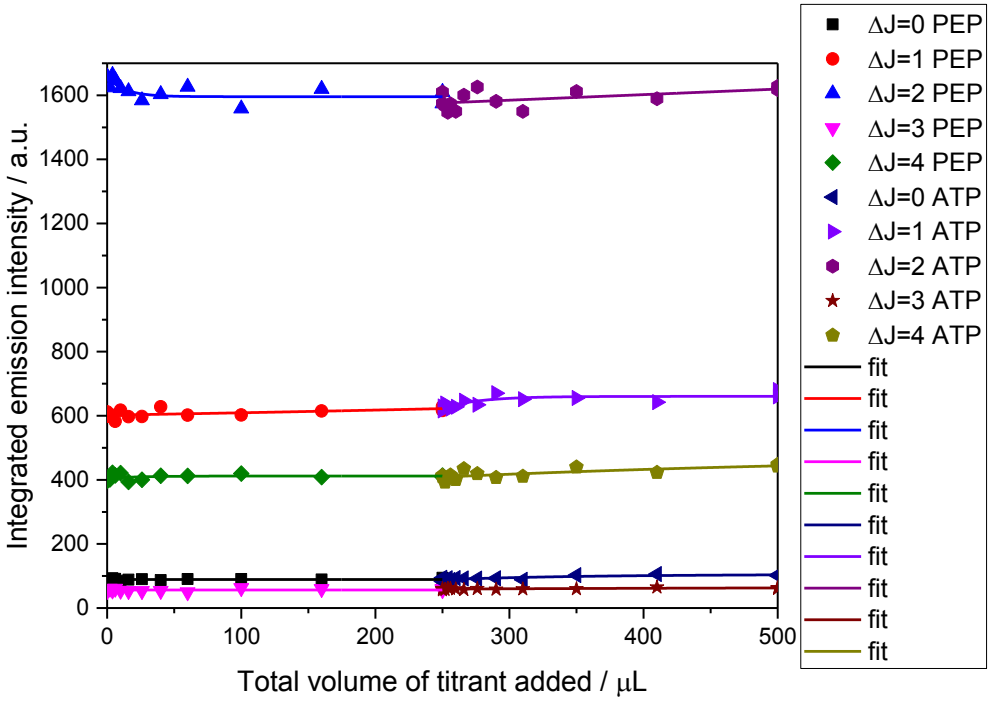


*Figure 9.2 Binding isotherms for titration of 5 × 10^{-4} M Eu_2.**5** with 3 × 10^{-2} M PEP followed by 3 × 10^{-2} M ATP*

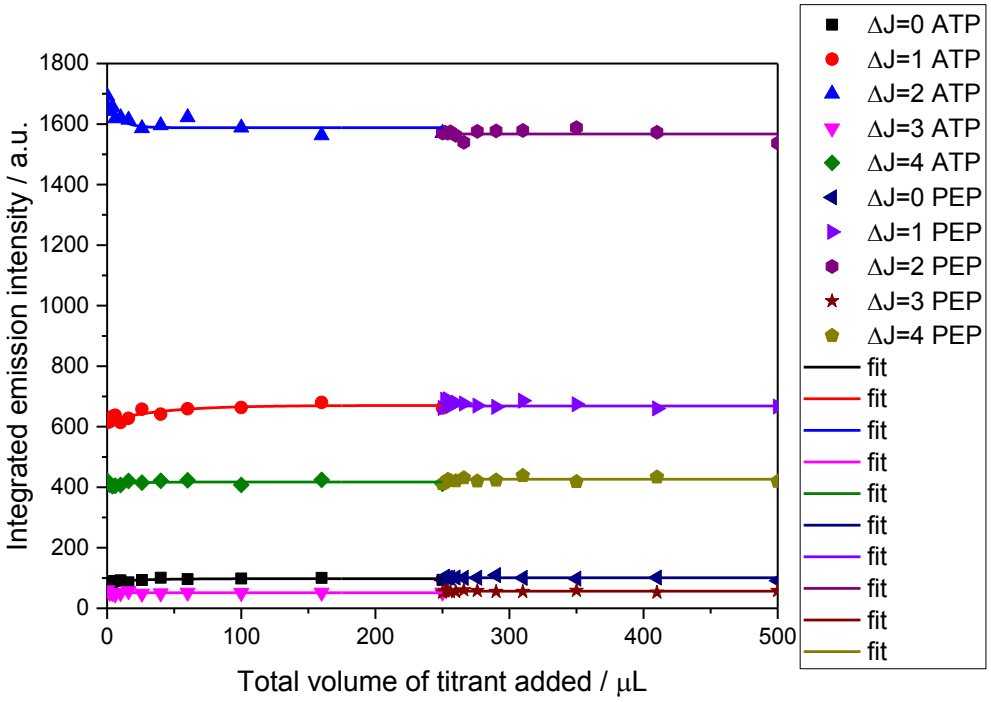


*Figure 9.3 Binding isotherms for titration of 5 × 10^{-4} M Eu_2.**5** with 3 × 10^{-2} M ATP followed by 3 × 10^{-2} M PEP*

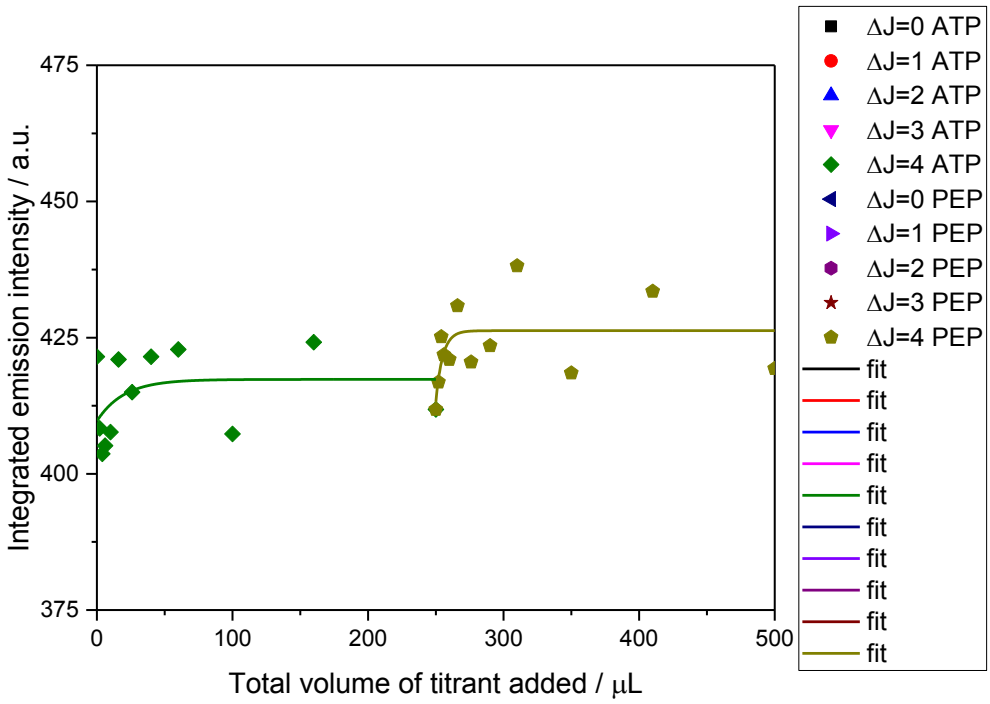


*Figure 9.4 Expanded view of integration of the ΔJ = 4 peaks for the titration of 5 × 10^{-4} M Eu2.**5** with 3 × 10^{-2} M ATP then 3 × 10^{-2} M PEP, with the ATP part of the titration shown in green and the PEP addition part shown in mustard*

9.3 NMR binding studies and titrations

An NMR titration of Eu2.**5** with inorganic phosphate was performed to support the luminescence titration. As shown in Chapter 7 and again in Figure 9.5, the ^{31}P resonance of phosphate broadened and shifted upfield as Eu2.**5** was added to the solution. The binding isotherms in their raw format are shown in Figure 9.6 and Figure 9.7, and in their inverse format with guest concentration on the *x*-axis to resemble those from luminescence in Figure 9.8 and Figure 9.9.

The inversely formatted data gave a poor fit when treated using DynaFit®, therefore the binding constant was calculated from the chemical shift values with the concentration of the europium complex as the changing variable, because adding in the data for the peak width at half height also led to poor data fitting. The binding mode was statistically determined to

be 1:1 which is physically unlikely. The logK value of 1.89 [1.85 – 1.92] agrees with the $\log K_1$ (1.41 [1.37 – 1.44]) from luminescence, suggesting that perhaps in this NMR titration only the first binding event was observed.

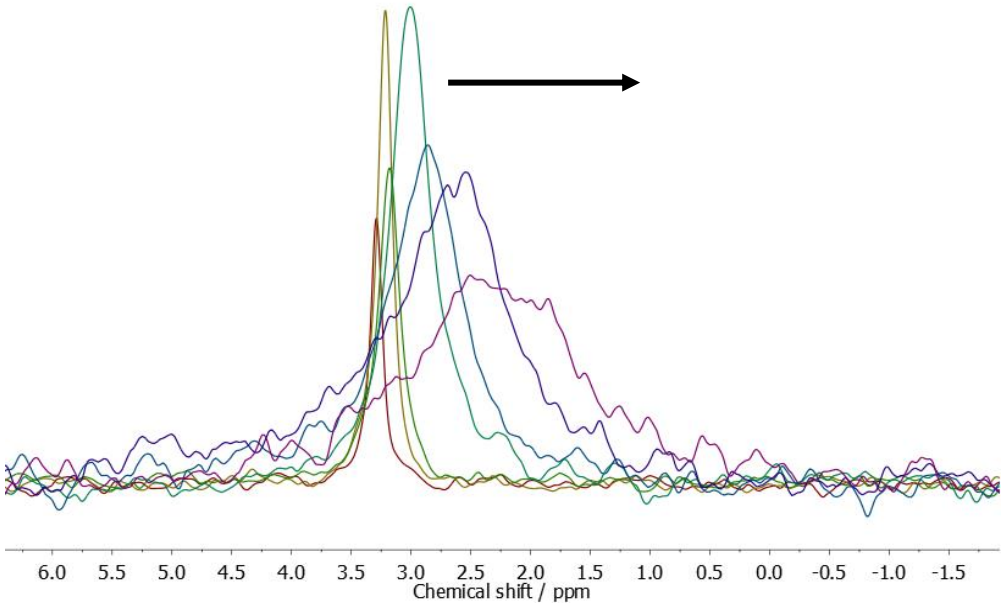


*Figure 9.5 Superimposed ^{31}P NMR spectra for titration of 10^{-2} M Eu_2.**5** with 5 × 10^{-3} M inorganic phosphate in D_2O*

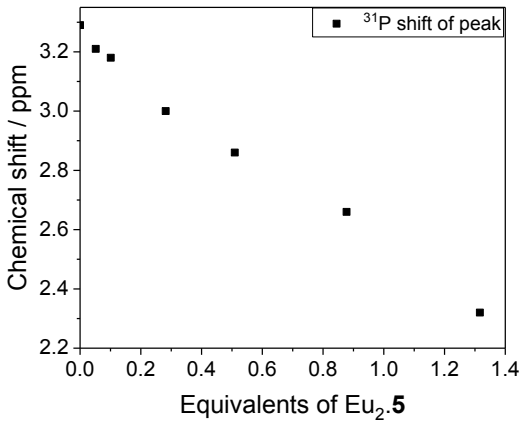


*Figure 9.6 Binding isotherm for titration of Eu_2.**5** with inorganic phosphate, with ^{31}P chemical shift plotted against equivalents of Eu_2.**5**)*

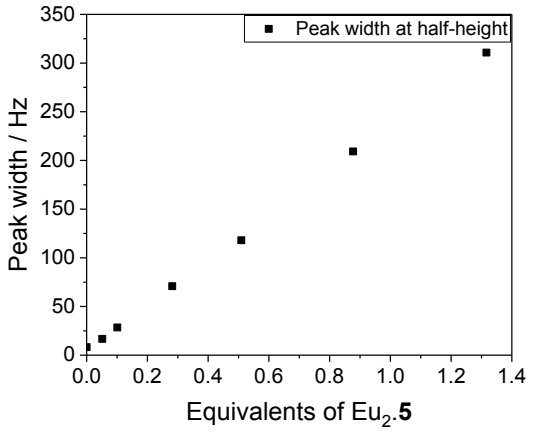


*Figure 9.7 Binding isotherm for titration of Eu_2.**5** with inorganic phosphate, with peak width at half height (FWHM) plotted against equivalents of Eu_2.**5***

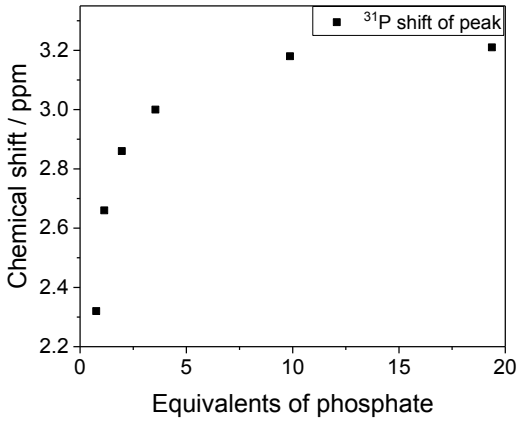


*Figure 9.8 Binding isotherm for titration of Eu_2.**5** with inorganic phosphate with the data inverted to give the equivalents of phosphate on the x-axis*

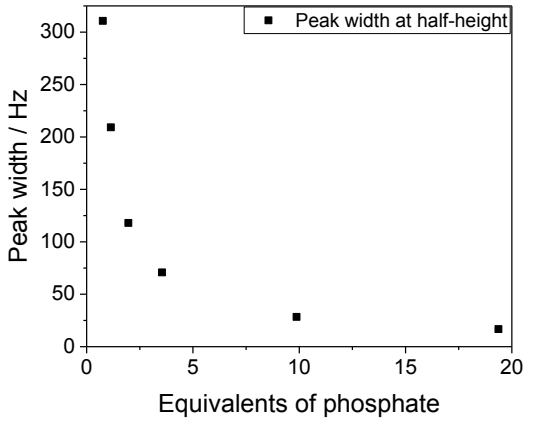


*Figure 9.9 Binding isotherm for titration of Eu_2.**5** with inorganic phosphate with the data inverted to give the equivalents of phosphate on the x-axis*

Further NMR studies were performed to investigate binding between the guest and the lanthanide complex host. The paramagnetic shifting and broadening of NMR resonances of the guests upon addition of varying amounts of lanthanide complexes confirmed the occurrence of binding. However, in the case of Y_2.**5** in Figure 9.10, the broadening of the peaks is due to incompletely resolved spin-½ splitting, and the change in chemical shift may be ascribed to a diamagnetic contribution from the highly polarising yttrium ion (as there is

no paramagnetic effect). There is clear line broadening but there were not enough points in this preliminary study to fit binding constants, as addition of a larger number of equivalents of the complex was precluded by limited solubility.

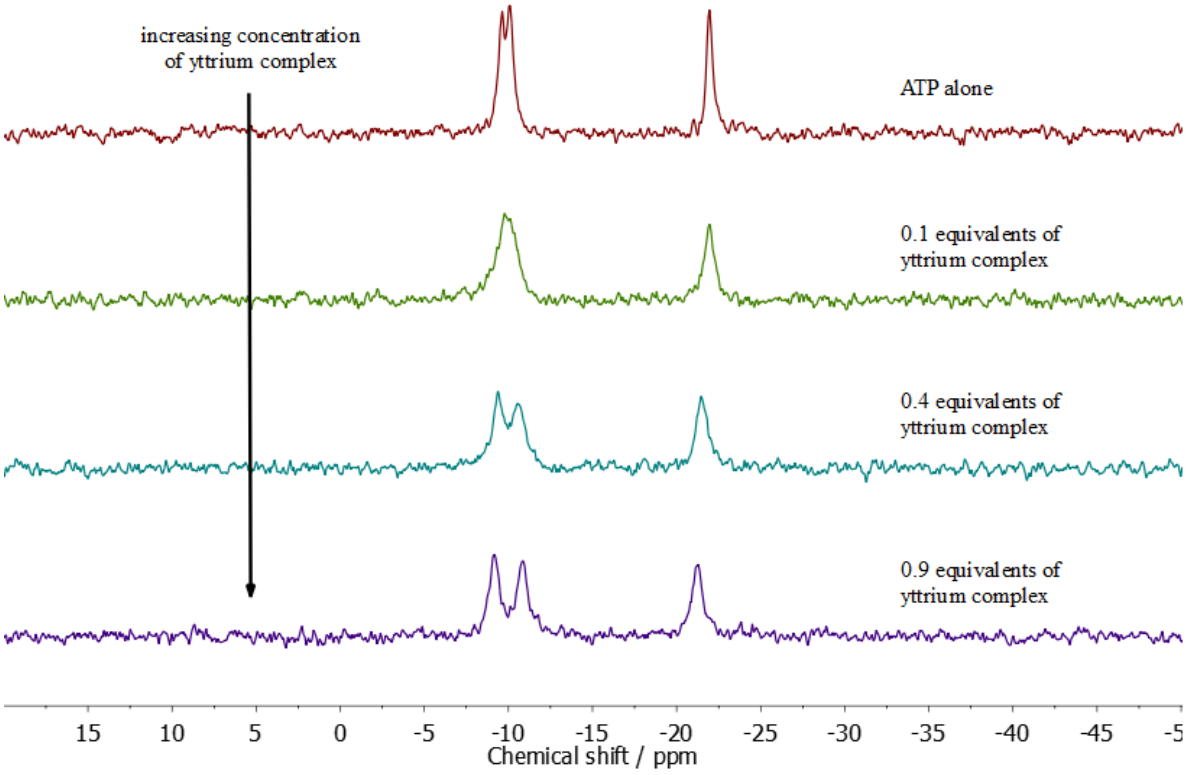


*Figure 9.10 Stacked ^{31}P NMR spectra of ATP as the concentration of Y_2.**5** was increased up to 0.9 equivalents in D_2O*

The ^{31}P peak in the NMR of inorganic phosphate was found to broaden upon addition of Eu_2.**6** or Gd_2.**6**. Additionally, as outlined in Chapter 7 in Section 7.5.1.2, inversion recovery experiments showed that the spin-lattice relaxation time of the ^{31}P in phosphate decreased in the presence of Eu_2.**6** and Gd_2.**6**.

The ^{31}P peaks of AMP, ADP, and ATP (Figure 9.11) broadened and shifted upon addition of Tb_2.**5** (Figure 9.12) and Eu_2.**5** (Figure 9.13). However, ATP with Yb_2.**5** (Figure 9.14), and the phosphonic acids with Eu_2.**6** (Figure 9.15 and Figure 9.16) showed shifting of the ^{31}P

resonances but very little broadening. The different lanthanides appear to have different broadening effects on the NMR spectra of guests. This may be explained by their differing abilities in enhancing relaxation, as outlined by Solomon,[5] Bloembergen, and Morgan.[6,7] There is no clear-cut answer at this stage, since changing geometric effects across the series will also need to be taken into account.

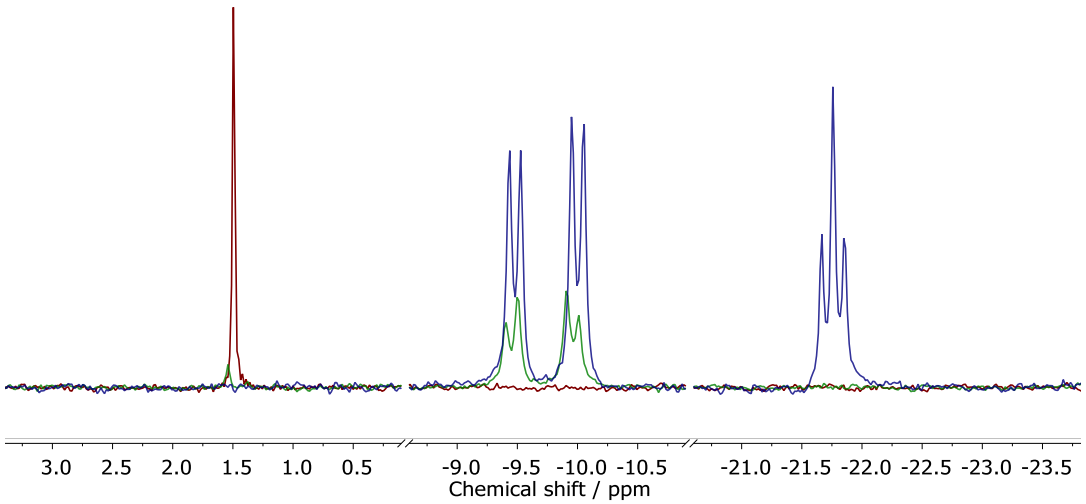


Figure 9.11 Overlaid ^{31}P NMR spectra of AMP (maroon), ADP (green), and ATP (blue) in D_2O

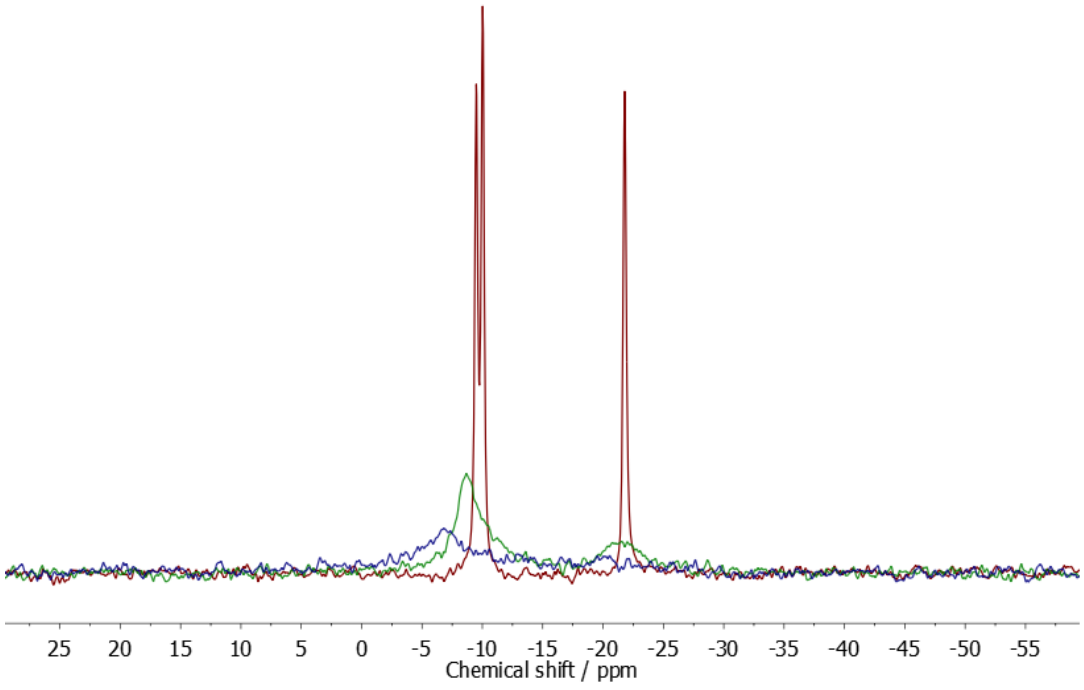


*Figure 9.12 Overlaid ^{31}P NMR spectra of ATP alone (maroon), with 0.03 equivalents Tb_2.**5** (green), and with 0.06 equivalents Tb_2.**5** (blue) in D_2O*

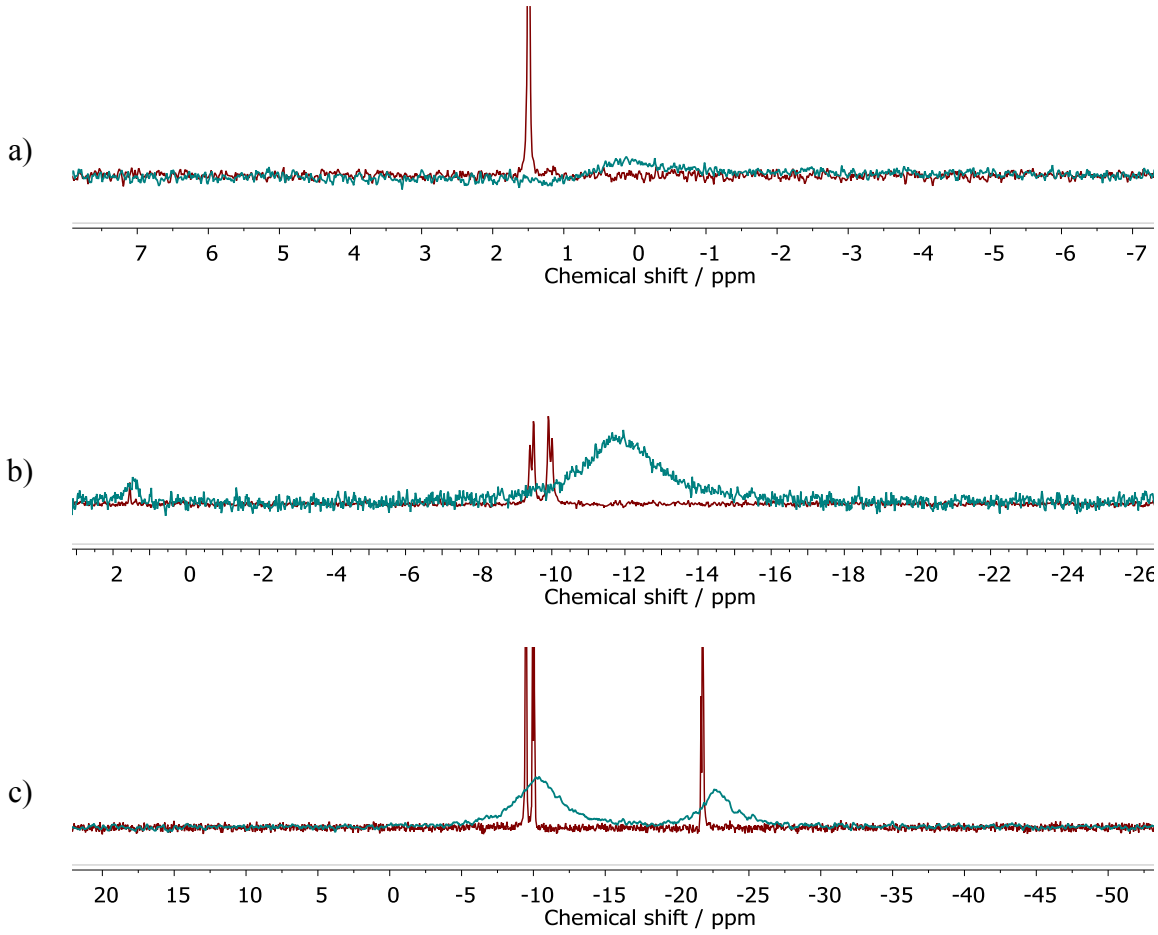


*Figure 9.13 Overlaid ^{31}P NMR spectra of a) AMP, b) ADP, c) ATP, alone (maroon) and with Eu_2.**5** (teal) in D_2O. Please note the x-axes are different scales*

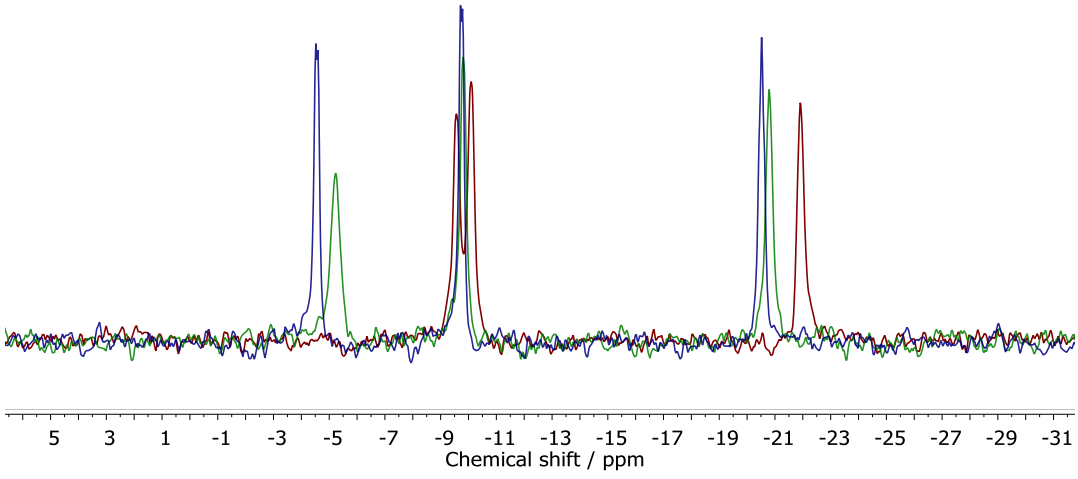


*Figure 9.14 Overlaid ^{31}P NMR spectra of ATP alone (maroon), with 0.4 equivalents Yb_2.**5** (green), and with 0.8 equivalents Yb_2.**5** (blue) in D_2O*

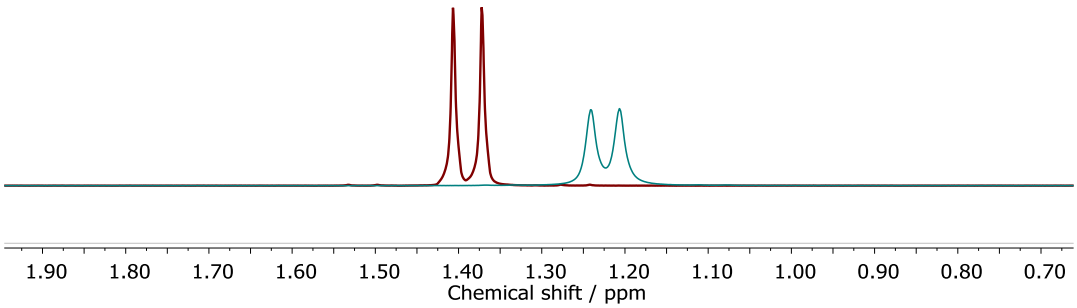


*Figure 9.15 Overlaid ^{31}P NMR spectra of methylphosphonic acid alone (maroon) and with Eu_2.**6** (teal) in D_2O*

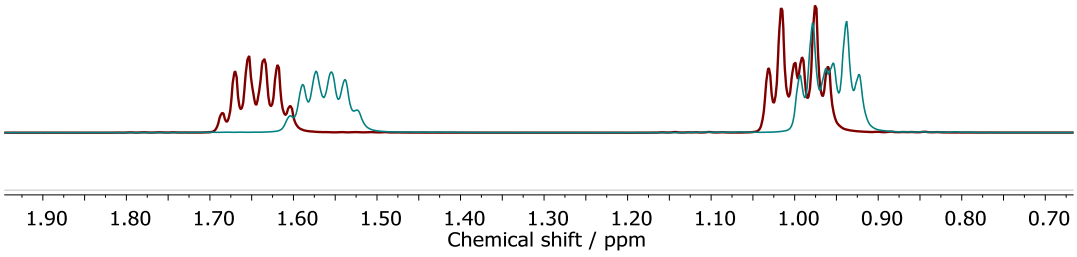


*Figure 9.16 Overlaid ^{31}P NMR spectra of ethylphosphonic acid alone (maroon) and with Eu_2.**6** (teal) in D_2O*

9.4 References

(1) Nadella, S.; Selvakumar, P. M.; Suresh, E.; Subramanian, P. S.; Albrecht, M.; Giese, M.; Fröhlich, R. *Chem. Eur. J.* **2012**, *18*, 16784–16792.
(2) Hewitt, S. H.; Parris, J.; Mailhot, R.; Butler, S. J. *Chem. Commun.* **2017**, *53* (94), 12626–12629.
(3) Shuvaev, S.; Fox, M. A.; Parker, D. *Angew. Chem. Int. Ed.* **2018**, *57* (25), 7488–7492.
(4) Tropiano, M.; Blackburn, O. A.; Tilney, J. A.; Hill, L. R.; Placidi, M. P.; Aarons, R. J.; Sykes, D.; Jones, M. W.; Kenwright, A. M.; Snaith, J. S.; Sørensen, T. J.; Faulkner, S. *Chem. Eur. J.* **2013**, *19*, 16566–16571.
(5) Solomon, I. *Phys. Rev.* **1955**, *99*, 559–565.
(6) Bloembergen, N. *J. Chem. Phys.* **1957**, *27*, 572–573.
(7) Bloembergen, N.; Morgan, L. O. *J. Chem. Phys.* **1961**, *34*, 842–850.

Chapter 10 Binding of catechols

10.1 Introduction

Dopamine is not implicated in the glycolytic pathway but is biologically relevant as a neurotransmitter. The host-guest binding interactions between dopamine and the series of lanthanide complexes synthesised in this thesis were investigated. The other catechols in Figure 10.1, including levodopa, a precursor to dopamine, were studied as a point of comparison. The catechol unit may act as a chelating ligand, however only levodopa and protocatechuic acid may easily bridge the binding pocket in binuclear complexes due to the presence of the carboxylic acid.

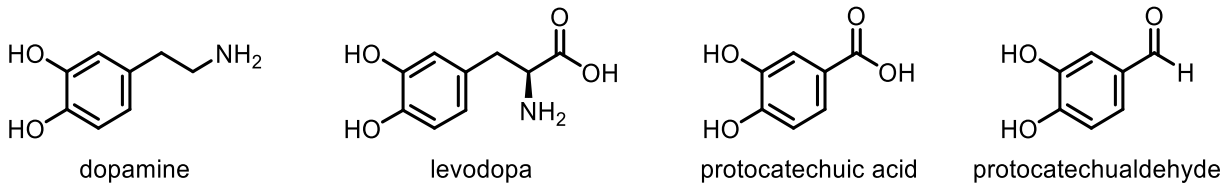


Figure 10.1 Catechols studied in this chapter

As with previously discussed guests, the lanthanide excited state was accessed by direct excitation because of the limitations of the inner filter effect, as the catechols absorb light in the same wavelength region as the ligand antennae.

10.2 Luminescence binding titrations

The chief obstacle to quantifying binding in these systems was that the catechol solution changed colour over time. Usually the solution became a purple-grey, however, as shown in Figure 10.2, the solution containing dopamine and Eu_2.**6** became yellow over time.

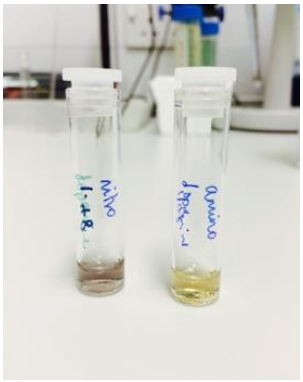


*Figure 10.2 Solutions of dopamine at pH 7.4 in HEPES buffer with Eu_2.**5** (left) and Eu_2.**6** (right) after three hours*

This colour change was a result of a redox reaction with the catechol, and is in line with behaviour observed for other systems.[1] Crude experiments which involved mixing dopamine with relevant species in water showed which of the species present in solution were reacting with the catechol. The outcome of these simple investigations (Table 10.1) showed that, over two days, the catechol reacted with HEPES and with the Eu_2.**5** complex.

Combination	**Outcome**
dopamine + Eu_2.**5**	colour change
dopamine + $Eu(OTf)_3$	minimal change
dopamine + **5** ligand	no change
dopamine + **3** proligand	colour change
dopamine + HEPES	colour change

Table 10.1 Outcome of mixing dopamine with species in water

This led to the question of whether the large decrease in emission intensity over the course of a titration – shown in Figure 10.3 – was a result of binding or quenching, or of simply the dark colour of the solution absorbing light emitted in the europium emission region through an inner filter effect.

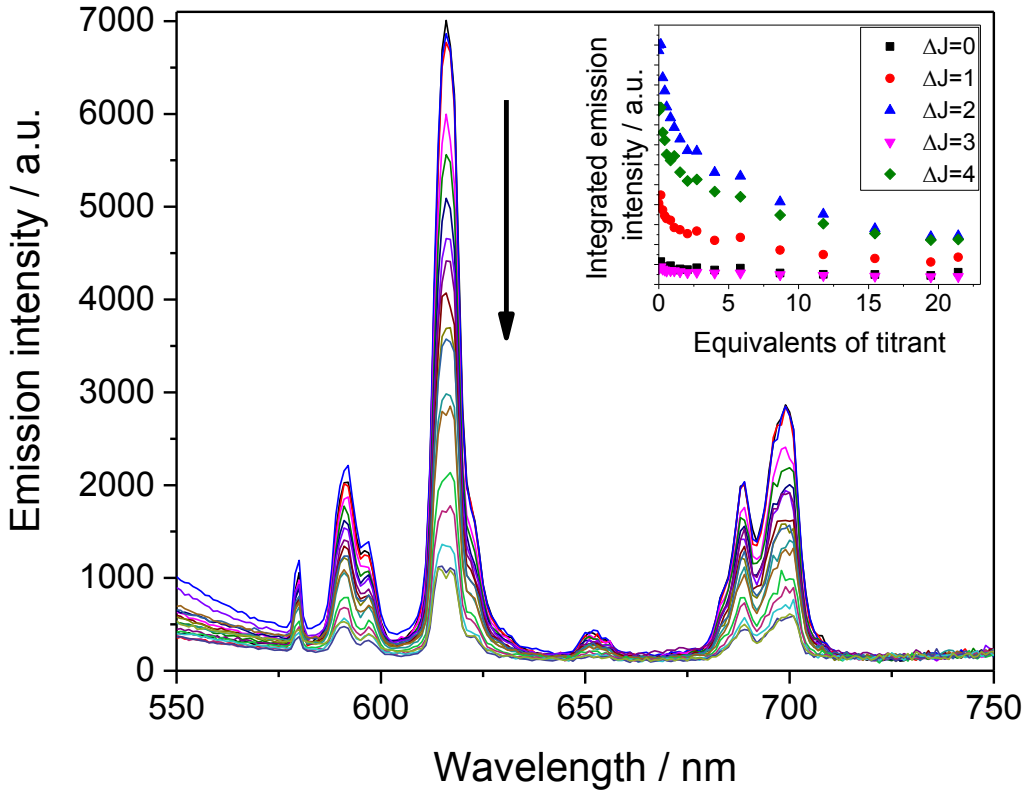


*Figure 10.3 Superimposed emission spectra for a titration of Eu_2.**5** with dopamine. Inset: decay in emission intensity over the course of the titration*

This inner filter theory was investigated by recording the UV-vis absorption spectrum of a solution of 1.5×10^{-2} M dopamine and 2.7×10^{-4} M Eu_2.**16** in 0.1 M HEPES at pH 7.4 that been allowed several days to react. Clear absorption in the europium emission region of approximately 575 to 720 nm was seen, in fact, the absorbance of this solution was so large in magnitude that the detector was saturated.

In order to avoid a decrease in luminescence intensity simply due to the increasing opacity of titration solution, titrations were performed quickly using freshly prepared stock solutions in order to minimise redox reaction time.

To determine whether the species in solution were binding or quenching, titration data was investigated by Stern-Volmer analysis (as explained in Chapter 1 in Section 1.4), where the emission intensity of the pure lanthanide host complex solution was divided by the intensity for each data point and was plotted against concentration of the titrant.

Some experiments gave a straight line indicating collisional quenching, whereas others gave curved plots indicating binding; the results are summarised in Table 10.2. The explanations for these characteristic graph shapes can be found in Chapter 1 in Section 1.4.

	Eu_2.**5**	Eu_2.**6**	Eu.**8**	Eu.**10**	Eu.**12**	Eu_2.**14**	Eu_2.**16**	Tb_2.**5**	Tb_2.**6**
dopamine	B	?	?	B	Q	?	Q	Q	?
levodopa	?	Q	?	-	-	-	-	B	-
prot' acid	B	Q	Q	-	-	-	-	-	-
prot'aldehyde	B	B	B	-	-	-	-	-	-

Table 10.2 Results of Stern-Volmer plots for titrations with catechols, where B denotes binding, Q denotes quenching, ? denotes inconclusive from Stern-Volmer plots, - denotes titrations not performed, prot' acid is protocatechuic acid, and prot'aldehyde is protocatechualdehyde

Some typical Stern-Volmer plots for these catechol titrations are displayed in Figure 10.4, showing clear difference between quenching and binding.

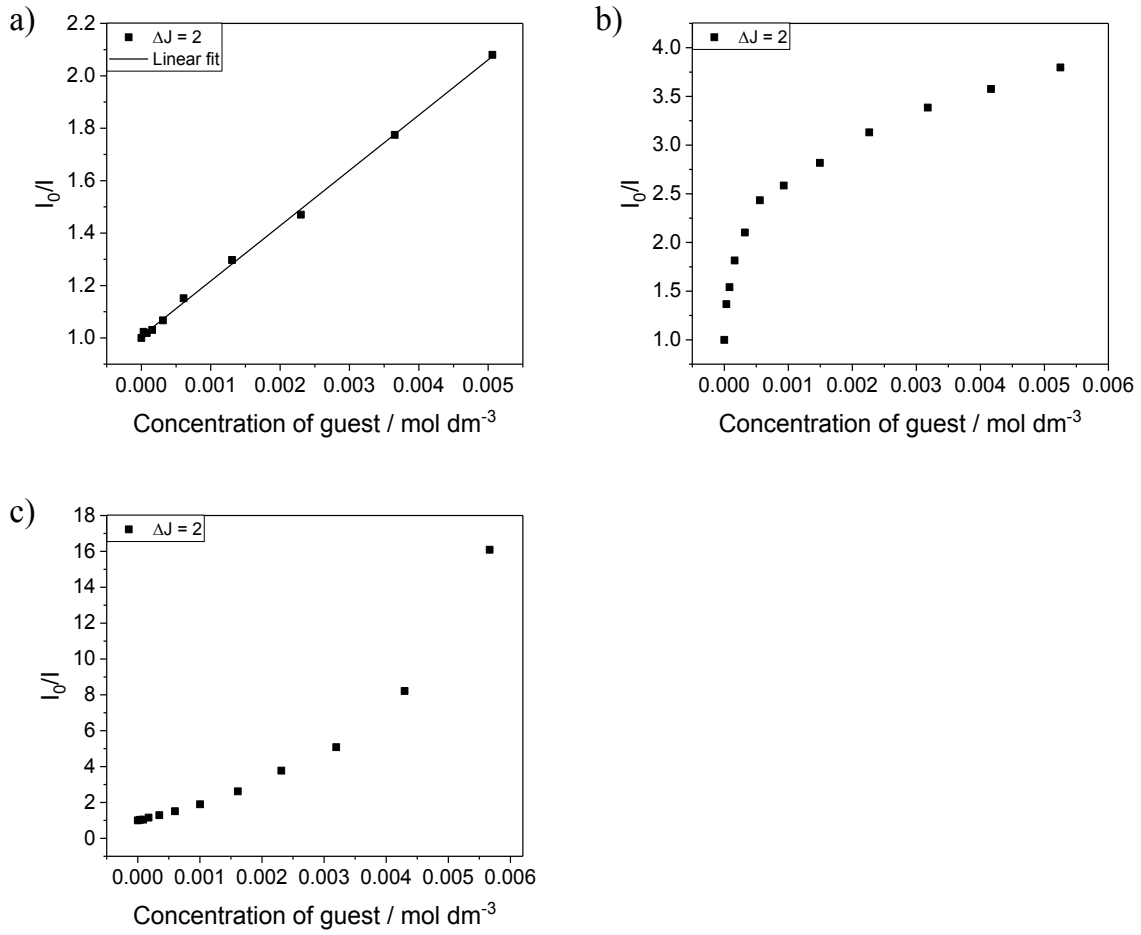


*Figure 10.4 a) Stern-Volmer plot of the ΔJ = 2 peak for 2.6 × 10^{-4} M Eu.**8** with protocatechuic acid, where the straight line indicates quenching, b) Stern-Volmer plot of the ΔJ = 2 peak for 2.3 × 10^{-4} M Eu$_2$.**5** with protocatechuic acid, where the curved line indicates binding, c) Stern-Volmer plot of the ΔJ = 2 peak for 4.9 × 10^{-4} M Eu.**10** with dopamine, where the curved line indicates binding*

The most interesting result was seen for titration of Eu.**12** with dopamine. As shown in Figure 10.5 and Figure 10.6, the emission intensity rose then fell, which can be attributed to the displacement of O-H oscillators around the lanthanide, followed by charge transfer quenching. This explains the unfeasible statistical model discrimination result of 2:1 binding to a mononuclear complex, as it in fact describes the two events: first, strong binding until one equivalent of dopamine (2.5 × 10^{-4} mol dm^{-3}, signified by the dashed line), then quenching. The Stern-Volmer plots for this are shown in Figure 10.7 and Figure 10.8 and show a straight line after one equivalent of dopamine (dashed line).

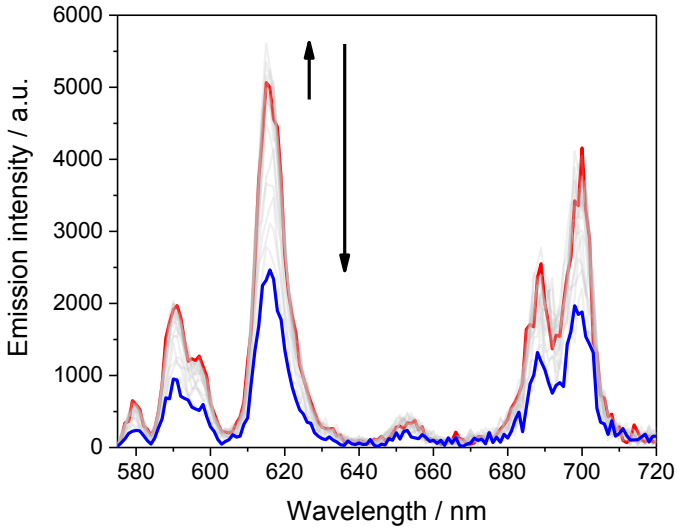


*Figure 10.5 Emission spectra for titration of Eu.**12** with dopamine*

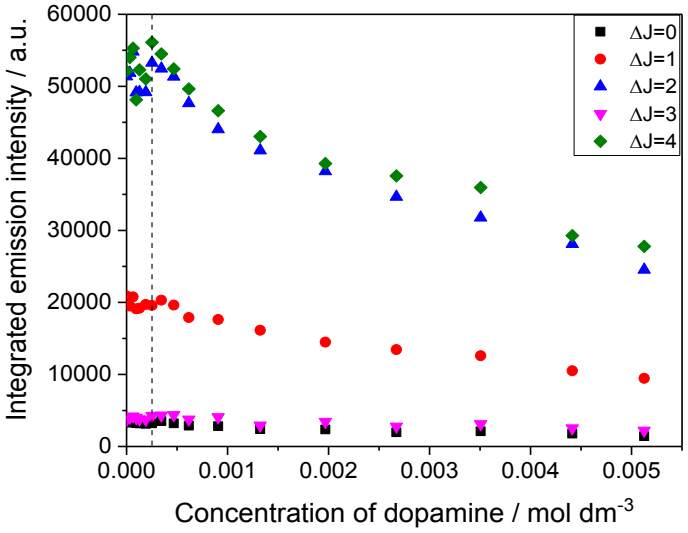


*Figure 10.6 Integrated emission intensity for titration of 2.5 × 10^{-4} M Eu.**12** with dopamine showing binding then self-quenching, with one equivalent of dopamine denoted by the dashed vertical line*

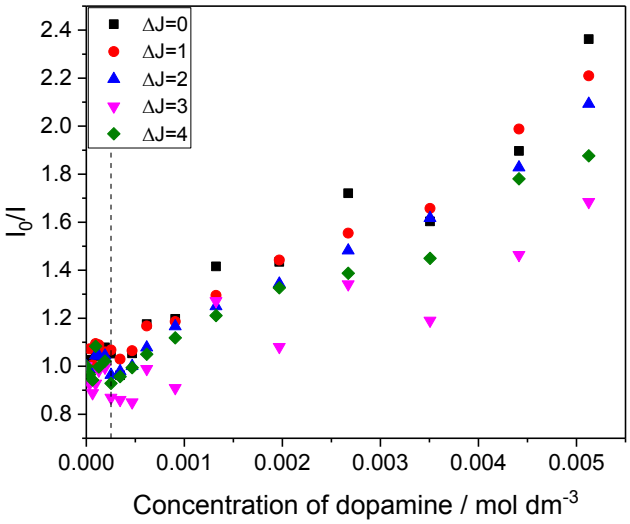


*Figure 10.7 Stern-Volmer plot for titration of 2.5 × 10^{-4} M Eu.**12** with dopamine, with one equivalent of dopamine denoted by the dashed vertical line*

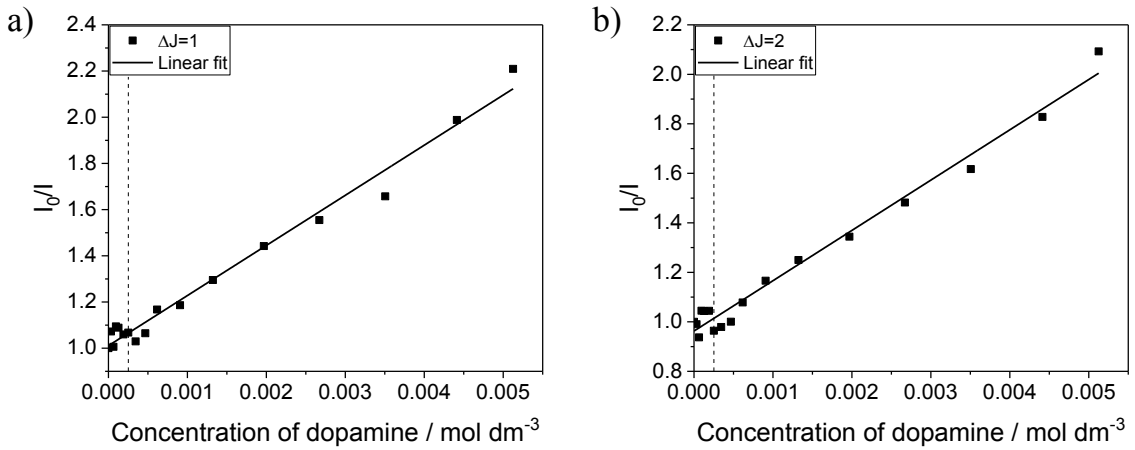


*Figure 10.8 a) Stern-Volmer plot of ΔJ = 1 for titration of 2.5 × 10^{-4} M Eu.**12** with dopamine, b) Stern-Volmer plot of ΔJ = 2 for titration of 2.5 × 10^{-4} M Eu.**12** with dopamine, with one equivalent of dopamine denoted by the dashed vertical line*

10.3 Binding mode

Statistical model discrimination with DynaFit® suggested that most binding of the catechols in this chapter occurred in a 1:1 fashion, which can be rationalised for the binuclear complexes by considering that the catechol oxygens bound at one lanthanide centre, and the steric bulk of the bound guest prevented approach of a further guest to the other lanthanide-

containing domain.

For dopamine in a protic solvent at pH 7.4, interaction with a δ^+ lanthanide centre is likely to proceed through the catechol oxygens as the amine would be protonated. Levodopa and protocatechuic acid are the only catechol guests in this chapter which may bind in a bridging fashion, through the catechol oxygens at one lanthanide and the carboxylate at the other.

This was investigated by NMR. The ^{1}H spectra are shown in Figure 10.9 and in Appendix B.

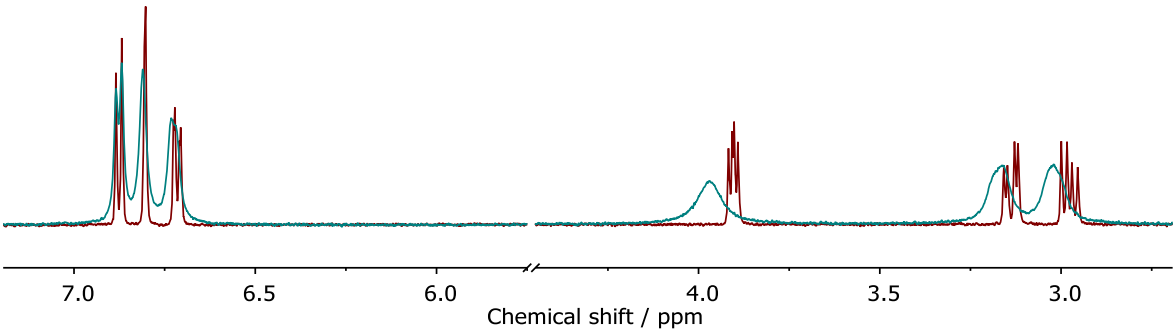


*Figure 10.9 Overlaid ^{1}H NMR spectra of levodopa alone (maroon) and with Eu$_2$.**5** (teal) in D$_2$O*

The broadening and shifting of resonances can be interpreted to give information on binding. For dopamine, upon addition of the lanthanide complex Eu$_2$.**5**, all peaks broaden (Appendix B, Figure B.1), suggesting that the contact contribution (i.e. through bonds) is significant for all the protons. The overlaid ^{1}H NMR spectra for levodopa in Figure 10.9 display a clear broadening for all resonances upon binding to Eu$_2$.**5**. Shifting of peaks is seen to a greater degree in the aliphatic region than in the aromatic region, suggesting that binding occurs preferentially *via* the carboxylate rather than the catechol. In the case of protocatechuic acid (Appendix B, Figure B.2) and protocatechualdehyde (Appendix B, Figure B.3), only their aromatic protons can be seen by NMR. Addition of the europium complex broadens these ^{1}H NMR resonances for both compounds, suggesting contribution

from binding at the catechol oxygens. The protocatechuic acid NMR spectra also exhibit peak shifting and therefore suggest stronger binding.

For these catechols it is clear that complicated speciation in solution must be considered. Examining the pKa values (Table 10.3) for these compounds indicates the likely anionic species in solution at pH 7.4 and therefore the likely donor atom: firstly the carboxylate oxygen, if present, followed by a phenol oxygen.

	pKa
dopamine	8.9 (phenol), 10.4 (amine), 13.1 (phenol)
levodopa	2.2 (carboxylic acid), 8.8 (phenol), 9.8 (amine), 13.4 (phenol)
protocatechuic acid	4.5 (carboxylic acid), 8.8 (phenol), 12.6 (phenol)
protocatechualdehyde	7.2 (phenol), 11.8 (phenol)

Table 10.3 pKa values of catechols studied in this chapter[2–5]

10.4 Binding constants from luminescence titrations

The binding constants calculated from binding studies of these catechols with an array of lanthanide complexes are shown in Table 10.4.

	Guest			
	dopamine	**levodopa**	**protocatechuic acid**	**protocatechu-aldehyde**
Complex	**log K [95% confidence interval]**			
Eu_2.**5**	3.45 [3.42 – 3.48]	2.47 [2.44 – 2.50]	4.22 [4.13 – 4.33]	5.15 [4.87 – 5.66]
Eu_2.**6**	3.01 [3.00 – 3.03]	5.63 [d] [5.51 – 5.75]	2.49 [2.46 – 2.51]	3.65 [3.63 – 3.68]
Eu.**8**	2.17* [2.16 – 2.20]	2.47* [2.44 – 2.50]	2.35 [2.34 – 2.36]	3.33* [3.32 – 3.36]
Eu.**10**	3.10* [3.09 – 3.13]	-	-	-
Eu.**12**	2.31* [2.30 – 2.34]	-	-	-
Eu_2.**14**	- [c]	-	-	-
Eu_2.**16**	2.54 [a] [2.52 – 2.56] 1.49 [b] [1.23 – 1.66]	-	-	-
Tb_2.**5**	2.37 [2.34 – 2.39]	2.96 [2.90 – 3.02]	-	-
Tb_2.**6**	2.69 [2.65 – 2.74]	-	-	-

Table 10.4 Binding constants with catechol species

*[a] log K_1, [b] log K_2, [c] could not fit data reliably, [d] could not separate K_1 and K_2 so the log of the overall binding constant K_{tot} is given, * 1:1 binding constant given as 2:1 binding was unfeasible*

Almost all binding was assessed to have occurred in a 1:1 fashion, either due to bridging or steric effects. The large Eu_2.**16** complex facilitated 2:1 binding as the two europium-containing rings are far apart. Analysis of data for the titration of Eu_2.**6** with levodopa

suggested 2:1 binding, whereas it exhibited 1:1 binding with Eu_2.**5**. This behaviour has been observed previously in Chapter 9 for AMP and again suggests that although Eu_2.**5** and Eu_2.**6** appear similar on paper, they adopt different conformations in solution.

All binding constants for the catechol species are of a similar magnitude except for the much higher binding constants observed for Eu_2.**5** with protocatechuic acid and protocatechualdehyde. This is perhaps because these smaller catechols fit the binding pocket of Eu_2.**5** very well, which agrees with the high binding constants noted in previous papers for isophthalate which is a similarly-sized bridging guest.[6]

The coumarin complex Eu.**10** showed notably strong binding to the catechol guests, suggesting that the geometry could be optimal for π-π stacking.

Tb_2.**5** bound more strongly than Eu_2.**5** to levodopa, suggesting greater electrostatic attraction to the more charge-dense lanthanide atom. However, the europium *m*-xylyl complexes (Eu_2.**5** and Eu_2.**6**) bound more strongly than their terbium analogues (Tb_2.**5** and Tb_2.**6**) to dopamine, which indicates complicated behaviour in solution.

Eu_2.**5** generally exhibited stronger binding than Eu_2.**6**, which is to be expected, as the electron-withdrawing nitro group would enhance the δ^+ nature of the lanthanide atom, thus increasing electrostatic attraction to the guest. However, the opposite was true for the terbium complexes, again highlighting the complexity of the conformation and solvation of the system.

If Table 10.4 of binding constants is compared to Table 10.2 of Stern-Volmer plot outcomes, it can be noted that those binding studies giving a confident "binding" outcome from Stern-Volmer analysis typically correspond to larger binding constants calculated by DynaFit®. These outcomes are grouped by colour in the graph in Figure 10.10.

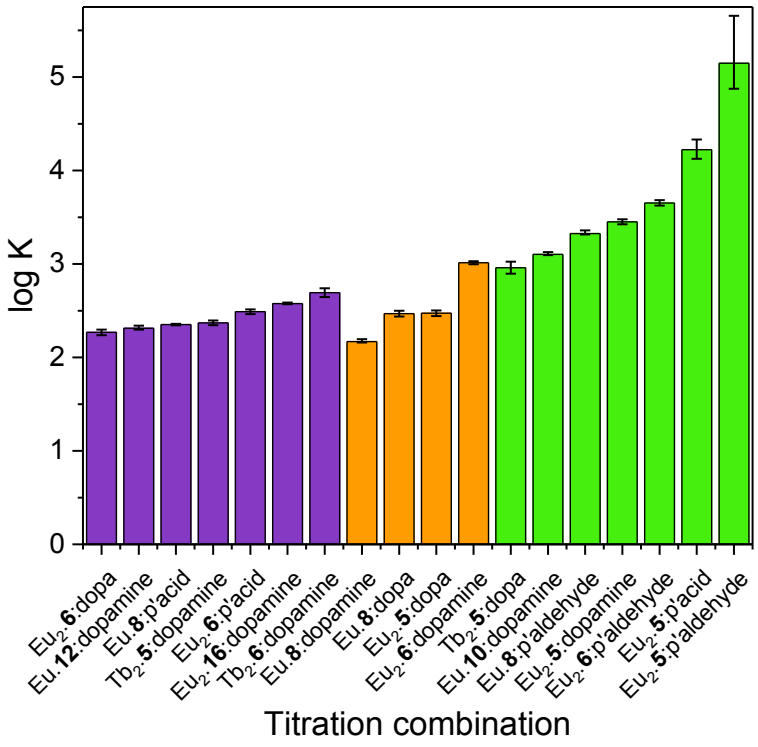


Figure 10.10 Catechol binding constants, grouped by Stern-Volmer plot outcomes: quenching (purple); inconclusive (orange); binding (green). The error bars signify the 95% confidence interval. P'acid denotes protocatechuic acid, and p'aldehyde denotes protocatechualdehyde

10.5 References

(1) Schweigert, N.; Zehnder, A. J. B.; Eggen, R. I. L. *Environ. Microbiol.* **2001**, *3*, 81–91.
(2) Kiss, T.; Gergely, A. *Inorganica Chim. Acta* **1979**, *36*, 31–36.
(3) Gergely, A.; Kiss, T.; Deák, G. *Inorganica Chim. Acta* **1979**, *36*, 113–120.
(4) Serjeant, E. P.; Dempsey, B. *Ionisation constants of organic acids in aqueous solution*; Pergamon Press: Oxford; New York, 1979.
(5) Slabbert, N. P. *Tetrahedron* **1977**, *33*, 821–824.
(6) Tilney, J. A.; Sørensen, T. J.; Burton-Pye, B. P.; Faulkner, S. *Dalton Trans.* **2011**, *40*, 12063–12066.

Chapter 11 Conclusions and future work

The key lesson from this work is that mono and binuclear lanthanide complexes can act as flexible hosts for a variety of anionic guests. It is especially notable that small changes in structure can cause dramatic variations in guest binding: this is true regardless of whether the changes are local to the binding site or in a more remote part of the molecule. In essence, electron demand and conformational space play a vital role in determining affinity and selectivity. This observation is likely to be of considerable importance as the field develops, since it ought to be possible to tune the affinity of a given host for a given guest. This has already been achieved serendipitously in the course of this work (for instance in the very high affinity of certain *m*-xylyl bridged binuclear complexes for isophthalate and dinicotinate). In addition, conformational behaviour goes a long way to explaining other apparently anomalous binding interactions (for example the high binding constant of AMP with Tb_2.**20** may be explained by the reasoning of previous work published on the effect of remote substituents in lanthanide complexes on their binding affinities).[1] Before such studies can achieve their full potential, it will be necessary to understand conformational equilibria in real solvent systems: this is a challenge for theoretical chemistry as well as experimental observation. At the moment, we are still rationalising behaviour after the event, and a predictive understanding is undoubtedly required. Even at the current level of observation and experiment, it is clear from this work that variation of host and cavity size is important in tuning binding affinity. Other areas for further exploitation include defining chirality, and controlling residual charge on the metal ion.

In the course of this work, a number of different guests and hosts have been explored.

In studying the behaviour of dinicotinate in its binding to binuclear lanthanide complexes, it

was found that even small variations (for example exchanging a nitro group for an amino group on the *m*-xylyl complexes, or changing the complexed metal) can have large effects on the binding affinities in solution.

Catechols, tartrate, and lactate are all capable of acting as chelating donor ligands. This favours more open binding sites, in which two donor atoms can bind to one lanthanide centre. From the data in this thesis, it becomes clear that restricting access to a seven-coordinate metal can mean that monodentate ligands are not invariably outcompeted by chelating analogues. The mononuclear complex Eu.**8** showed greater binding constants with the catechols and lactate, which bind through two oxygen atoms, than with simple phosphates and the carboxylate anion nicotinate, which are monodentate, as shown in Figure 11.1. Furthermore, conformational control is important with polydentate guests.

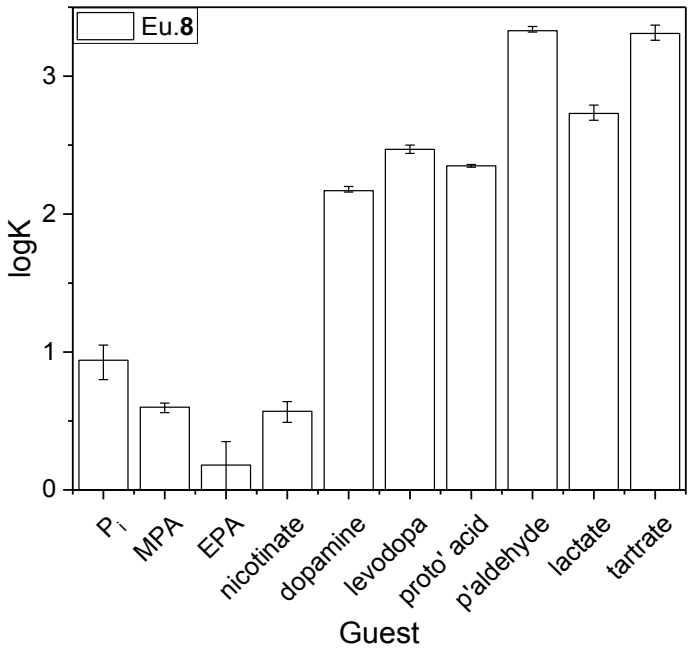


*Figure 11.1 Binding constants for Eu.**8** with simple phosphates, catechols, tartrate, and lactate*

One thing that must be considered when studying guest-host interactions is that, while such interactions may be *selective*, they are unlikely ever to be *specific*. As such, practical

application may require the use of a number of guests to allow meaningful quantification. Clearly if *n* hosts each display a different affinity for *n* guests, it will be possible to use neural network analysis to separate out the contributions of each guest (effectively by solving *n* simultaneous equations). This could easily be conceived, and has previously been proposed as a means of using responsive lanthanide complexes.[2] However, the application of such an approach to the study of glycolysis represents a project in itself.

Isothermal titration calorimetry (ITC) measurements provide direct access to the free energy change associated with binding. ITC was attempted for the titrations of dinicotinate with Eu_2.**5** and Eu_2.**6** in HEPES and PBS buffers with little success as there were problems with the baseline of the raw spectra. Therefore in the limited time available, it was resolved to use the temperature-controlled luminescence equipment to investigate the thermodynamics of binding. Improving the experimental design for these specific host-guest combinations would lead to better data.

11.1 References

(1) Tropiano, M.; Blackburn, O. A.; Tilney, J. A.; Hill, L. R.; Placidi, M. P.; Aarons, R. J.; Sykes, D.; Jones, M. W.; Kenwright, A. M.; Snaith, J. S.; Sørensen, T. J.; Faulkner, S. *Chem. Eur. J.* **2013**, *19*, 16566–16571.

(2) Faulkner, S.; Parker, D.; Williams, J. A. G. "Parallel Processing in Aqueous Solution" In *Supramolecular Science: Where It Is and Where It Is Going*; Ungaro, R.; Dalcanale, E., Eds.; Springer Netherlands: Dordrecht, 1999; pp. 53–66.

Chapter 12 Experimental

12.1 General methods

NMR spectra were recorded with a Bruker AVIIIHD 400 NanoBay, Bruker AVII 500, Bruker AVII 500 with ^{13}C detect He CryoProbe™, Bruker AVIIIHD 500, or Bruker AVIIIHD 600 with broadband Prodigy CryoProbe™.

NMR data was processed using MestreLab MestreNova, ACD Labs NMR Processor, or Bruker TopSpin™.

Mass spectrometry used a Waters LCT Premier or an Agilent 6120 mass spectrometer equipped with Agilent 1260 LC pump and CTC autosampler, and high resolution and accurate mass spectra were performed by the staff of the Chemistry Research Laboratory, University of Oxford, using a Waters MALDI Micro MX™, Bruker μTOF, or Waters Micromass® GCT.

CHN elemental analysis was performed by Stephen Boyer at London Metropolitan University, or Birgitta Kegel or Niels Vissing Holst at the University of Copenhagen, Denmark.

Solid-state IR spectra were recorded using a Bruker Tensor 27 FT-IR spectrometer with an IR Diamond Attenuated Total Reflectance module, and the data processed using Bruker OPUS software.

UV-vis absorption spectra used a PG Instruments T60U Spectrophotometer or a PerkinElmer Lambda 750S. Spectra were measured in solution using the pure solvent, usually water, as

the baseline.

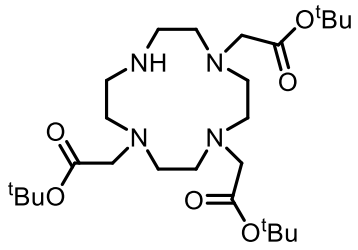
Luminescence data was measured using a Horiba FluoroLog-3, Varian Cary Eclipse, or Perkin Elmer LS55 and processed using FluorEssence™, OriginLab Origin®, a custom-written Microsoft Excel macro and DynaFit®.

Isothermal titration calorimetry was performed with a MicroCal VP-ITC and the data processed with VPViewer™ and Origin®.

Reagents were laboratory grade and obtained from standard commercial sources including Sigma-Aldrich, Fisher Scientific, Alfa Aesar, Fluorochem, CheMatech, ChemicalPoint, and Insight Biotechnology. Water was deionised and microfiltered with a Milli-Q Millipore machine.

12.2 Synthetic procedures

1,4,7,10-tetraazacyclododecane-1,4,7-triacetate *tert*-butyl triester · NaBr (1)

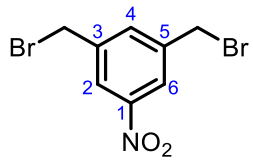


1

Prepared in accordance with the procedure described by Dadabhoy *et al.*[1]

Yield: 8.76 g, 49%. ^{1}H NMR ($CDCl_3$, 400 MHz) δ (ppm) 10.02 (1H, br. s, NH), 3.36 (4H, s, NCH_2CO), 3.28 (2H, s, NCH_2CO), 3.09 (4H, br. m, ring NCH_2), 2.89 (12H, br. m, ring NCH_2), 1.44 (27H, s, 3 × ^{t}Bu). ^{13}C NMR ($CDCl_3$, 101 MHz) δ (ppm) 170.61, 169.72, 81.96, 81.80, 58.35, 51.49, 51.37, 49.33, 48.92, 47.65, 28.36 (1 × ^{t}Bu), 28.32 (2 × ^{t}Bu). ES^+ MS (*m/z*) 515 ($[M + H]^+$), 537 ($[M + Na]^+$). ES^- MS (*m/z*) 515 (M^-).

3,5-bis(bromomethyl)nitrobenzene (2)

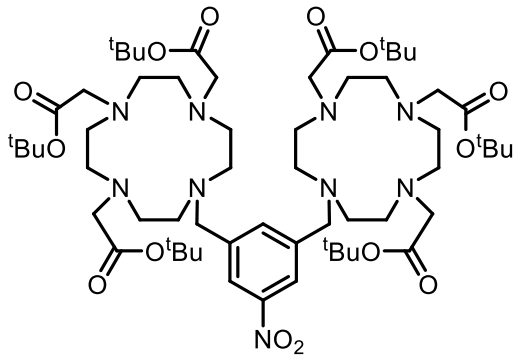


2

Prepared in accordance with the procedure described by Chhikara *et al.*[2]

Yield: 3.39 g, 67%. ^{1}H NMR ($CDCl_3$, 400 MHz) δ (ppm) 8.19 (2H, d, *J*=1.7 Hz, H2, H6), 7.75 (1H, t, *J*=1.7 Hz, H4), 4.52 (4H, s, CH_2Br). ^{13}C NMR ($CDCl_3$, 126 MHz) δ (ppm) 148.66, 140.51, 135.40, 123.82, 30.78. FI^+ HRMS (*m/z*) calculated: 306.8844, measured: 306.8850 $[C_8H_7Br_2NO_2]^+$ (M^+). Crystals suitable for single crystal X-ray diffraction were obtained by slow evaporation of a concentrated solution of the product in $CDCl_3$. Please see Appendix C.1 for X-ray diffraction data.

α,α'-bis(DO3A *tert*-butyl triester)-3,5-dimethylnitrobenzene (3)

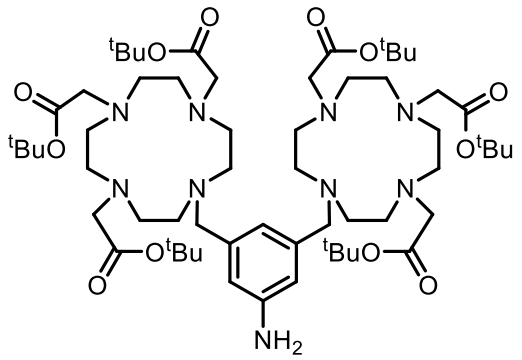


3

Prepared in accordance with the procedure described by Placidi *et al.*[3]

Yield: 3.30 g, 43%. ^{1}H NMR ($CDCl_3$, 400 MHz) δ (ppm) 8.54 (2H, s, Ar-H2, Ar-H6), 8.04 (1H, s, Ar-H4), 3.75 (4H, br., $ArCH_2$), 3.51 – 2.05 (44H, br. m, CH_2 cyclen ring, CH_2CO), 1.44 (54H, s, 6 × ^{t}Bu). ^{13}C NMR ($CDCl_3$, 126 MHz) δ (ppm) 173.63, 172.64, 148.80, 139.31, 123.83, 83.14, 82.98, 82.67, 58.12, 56.21, 55.70, 49.58, 28.31, 28.27, 28.24, 28.22, 28.19, 28.11, 27.96, 27.93. ES^+ MS (*m*/*z*) 1176.8 ($[M + H]^+$), 1198.8 ($[M + Na]^+$), 588.9 ($[M + 2Na]^{2+}$), 560.9 ($[M - {}^{t}Bu + 3H]^{2+}$), 532.8 ($[M - 2{}^{t}Bu + 4H]^{2+}$), 504.8 ($[M - 3{}^{t}Bu + 5H]^{2+}$). IR-ATR *v* ($cm^{-1}$) 3369 (cyclen C-H), 2978, 2831 (^{t}Bu C-H), 1719 (C=O), 1532, 1346 (N-O), 1456-1427 (aromatic C=C), 1158, 1227, 1099 (C-O). Crystals suitable for single crystal X-ray diffraction were obtained by slow evaporation of a concentrated solution of the product in $CDCl_3$. Please see Appendix C.2 for X-ray diffraction data.

α,α'-bis(DO3A *tert*-butyl triester)-3,5-dimethylaminobenzene (4)

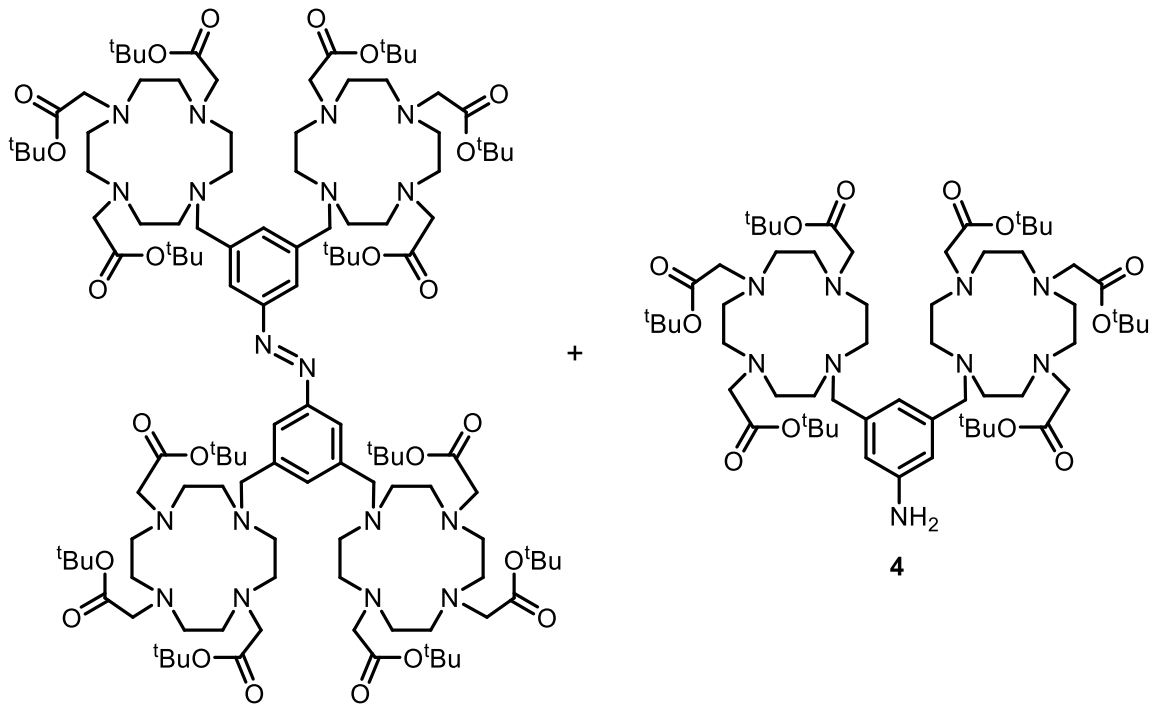


4

Prepared in accordance with the procedure described by Placidi *et al.*[3]

Yield: 164 mg, 60%. ^{1}H NMR (DMSO, 500 MHz, 353 K) δ (ppm) 6.44 (3H, br. m, ArH), 4.96 – 1.97 (48H, br. m, NCH_2), 1.47 (54H, br. s, 6 × ^{t}Bu). ES$^+$ MS (*m*/*z*) 1147 ($[M + H]^+$), 1169 ($[M + Na]^+$), 574 ($[M + 2H]^{2+}$), 546 ($[M - {}^t\text{Bu} + 3H]^{2+}$), 518 ($[M - 2{}^t\text{Bu} + 4H]^{2+}$), 585 ($[M + Na + H]^{2+}$). IR-ATR *v* (cm^{-1}) 2976, 2830 (^{t}Bu C-H), 1721 (C=O), 1602 (N-H), 1455 (aromatic C=C), 1226, 1158, 1100 (C-O).

(*E*)-1,2-bis(*α*,*α*'-bis(DO3A *tert*-butyl triester)-3,5-dimethylphenyl)diazene (4a)

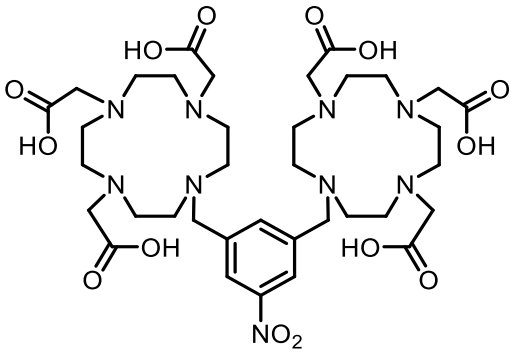


3 (1.00 g, 0.85 mmol) was dissolved in methanol (50 mL). A slurry of 10 wt. % palladium on carbon (catalytic amount, ~10 mg) in methanol (5 mL) was added to the stirring solution. The reaction mixture was flushed with 4 balloons of hydrogen gas and the reaction mixture stirred at room temperature under a hydrogen atmosphere for 3 days. The reaction mixture was filtered through a Celite® plug and the solvent removed under reduced pressure, giving a crispy/bubbly golden-yellow solid. ^{1}H NMR spectroscopy revealed that although the starting material was consumed, the presence of a species that was not fully reacted was indicated, so the crude product was redissolved in methanol and rereacted in the same way for a further 4 days and worked up in the same way. Fine needle-like crystals of **4a** suitable for single crystal X-ray diffraction were obtained by slow evaporation of a concentrated solution of the product in dichloromethane and methanol. ^{1}H DOSY and IR spectroscopy indicated a mixture of **4** and **4a**.

Yield: 0.84 g, 86%. ^{1}H NMR ($CDCl_3$, 400 MHz) δ (ppm) 7.47 (1H, s, ArH), 7.38 (1H, s,

ArH), 6.85 – 5.96 (4H, m, ArH), 4.07 – 1.67 (96H, br. m, NCH_2), 1.51 – 0.95 (108H, br. m, 12 × ^{t}Bu). ^{13}C NMR ($CDCl_3$, 126 MHz) δ (ppm) 173.54, 172.60, 172.52, 170.66, 169.82, 115.55, 82.83, 82.65, 82.53, 82.43, 81.79, 81.67, 77.37, 59.54, 58.21, 56.21, 55.81, 51.37, 49.33, 47.58, 28.30, 28.26, 28.16, 28.11, 27.96. MALDI-TOF HRMS (*m*/*z*) 1147.02 ([**4** + H]$^+$), 1168.98 ([**4** + Na]$^+$), 1090.89 ([**4** − ^{t}Bu + 2H]$^+$), 2288.89 ([**4a** + H]$^+$), 2311.81 ([**4a** + Na]$^+$), 2327.78 ([**4a** + K]$^+$). IR-ATR *v* (cm^{-1}) 3377 (cyclen C-H), 2979, 2828 (^{t}Bu C-H), 1719 (C=O), 1602 (N-H), 1456-1427 (aromatic C=C), 1226, 1158, 1100 (C-O). Please see Appendix C.3 for X-ray diffraction data.

α,α'-bis(H$_3$.DO3A)-3,5-dimethylnitrobenzene · 4TFA (5)

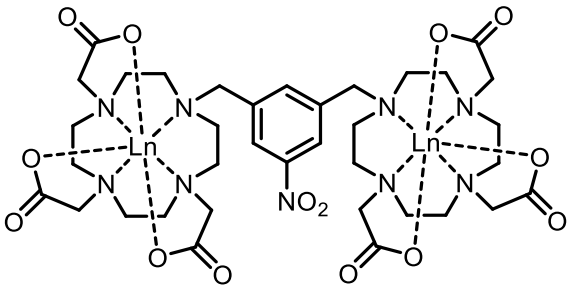


5

Prepared in accordance with the procedure described by Placidi *et al.*[3]

Yield: 2.02 g, 83%. ^{1}H NMR (MeOD, 400 MHz) δ (ppm) 8.35 (2H, s, ArH), 8.23 (1H, s, ArH), 4.17 (4H, s, $ArCH_2$), 3.78 – 2.91 (44H, br. m, CH_2 cyclen ring, CH_2CO). ^{13}C NMR (MeOD, 126 MHz) δ (ppm) 162.95, 162.68, 149.66, 126.73, 121.64, 119.31, 116.99, 114.66, 66.90, 57.63, 55.21, 54.81, 28.49, 15.44. ES$^+$ MS (*m*/*z*) 840 ([M + H]$^+$), 862 ([M + Na]$^+$). ES$^-$ MS (*m*/*z*) 838 ([M − H]$^-$), 860 ([M + Na − 2H]$^-$). Elemental calculated: C, 40.78; H, 4.74; N, 9.73; measured: C, 38.84; H, 5.02; N, 9.36; [$C_{44}H_{61}F_{12}N_9O_{22}$] (M · 4TFA).

α,α'-bis(Ln.DO3A)-3,5-dimethylnitrobenzene · *x*MOTf (M = H, Na) (Ln2.**5)**



Ln_2.**5**

Method 1

Ln = Y, Eu, Gd, Yb

5 · *x*TFA (100 to 500 mg, 1.00 mol equivalent) and the appropriate lanthanide triflate (2.2 to 3.4 mol equivalents) were combined in methanol (2 to 10 mL) with stirring. After 15 minutes the solution was adjusted to pH 5 by dropwise addition of aqueous sodium hydroxide (0.1 M). The reaction mixture was heated under reflux at 60°C with stirring for 2 days. The volatile components were removed under reduced pressure and the resulting suspension dissolved in water and adjusted to pH 10 by dropwise addition of aqueous sodium hydroxide (1.0 M). This suspension was centrifuged and the supernatant filtered through an Acrodisc® syringe filter (0.2 μm) The filtrate was neutralised by dropwise addition of aqueous hydrochloric acid (1.0 M), and the crude product dialysed in a Spectrum Labs Float-A-Lyzer® G2 (100 – 500 Da molecular weight cut-off) for 24 to 48 hours with the deionised water changed at 2, 4, 8, 12, and 24 hours in order to reduce the salt content. The water was removed under reduced pressure and the product dried in a desiccator.

Y_2.**5**: Yield: 29 mg, 11%. ^{1}H NMR (D_2O, 400 MHz) δ (ppm) 8.18 (2H, br. d, ArH), 7.59 (1H, br. s, ArH), 4.64 – 1.47 (44H, br. m, $ArCH_2$, CH_2 cyclen ring, CH_2CO). MALDI-

TOF HRMS (*m*/*z*) 1012 ($[M + H]^+$), 526 ($[M + H + K]^{2+}$). UV-vis (H_2O) λ (I/I_{max}) 208 (1.00), 267 (0.39) nm. Elemental calculated: C, 38.25; H, 4.51; N, 10.85; measured: C, 38.10; H, 5.50; N, 10.79; $[C_{37}H_{52}F_3N_9O_{17}SY_2]$ (M · TfOH).

Eu_2.**5**: Yield: 48 mg, 9%. ^{1}H NMR (D_2O, 400 MHz) δ (ppm) 33.92, 33.87, 27.72, 23.56, 23.51, 20.01, 19.97, 16.81, 10.11, −1.06, −3.00, −3.60, −5.91, −6.04, −6.82, −7.85, −8.00, −9.16, −10.02, −10.91, −12.64, −14.12, −14.61, −16.18, −16.48, −17.47, −19.18. Only major resolved peaks outside the +10 to 0 ppm range are reported. MALDI-TOF HRMS (*m*/*z*) 1137, 1139 (M^+), 1138, 1140 ($[M + H]^+$), 1160, 1162 ($[M + Na]^+$). UV-vis (H_2O) λ (I/I_{max}) 209 (1.00), 267 (0.38) nm. Elemental calculated: C, 31.74; H, 3.72; N, 8.77; measured: C, 31.62; H, 4.58; N, 9.03; $[C_{38}H_{53}Eu_2F_6N_9O_{20}S_2]$ (M · 2TfOH).

Gd_2.**5**: Yield: 27 mg, 16%. MALDI-TOF HRMS (*m*/*z*) 1150 ($[M + H]^+$), 1172 ($[M + Na]^+$), 1093 ($[M - CH_2CO_2 + 2H]^+$), 1133 ($[M - CH_2CO_2 + H + K]^+$).

Yb_2.**5**: Yield: 94 mg, 20%. ^{1}H NMR (D_2O, 400 MHz) δ (ppm) 139.15, 134.53, 126.40, 122.63, 118.99, 114.06, 110.31, 108.74, 51.40, 43.21, 40.00, 34.38, 34.09, 30.29, 24.83, −21.00, −21.39, −31.38, −33.03, −35.50, −40.89, −43.78, −46.44, −48.85, −50.96, −53.22, −54.51, −56.66, −57.86, −58.47, −60.83, −62.04, −64.37, −67.55, −71.01, −75.05, −78.17, −80.66. Only major resolved peaks outside the +20 to −20 ppm range are reported. MALDI-TOF HRMS (*m*/*z*) 1180 ($[M + H]^+$), 1204 ($[M + Na]^+$).

Method 2

Ln = Eu, Tb

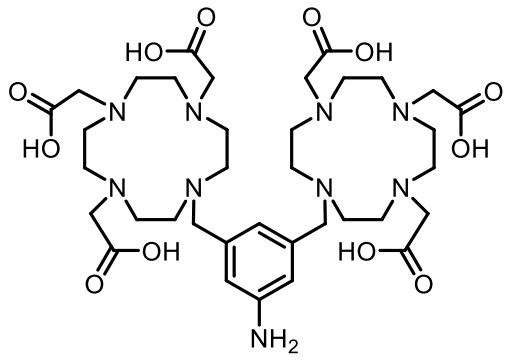
5 · *x*TFA (50 to 100 mg, 1.00 mol equivalent) and the appropriate lanthanide triflate (2.2

to 3.5 mol equivalents) were dissolved in acetonitrile (2.5 to 5 mL) and the solution was heated under reflux at 90°C with stirring for 7 days. The reaction mixture was cooled to room temperature and the solvent removed under reduced pressure, yielding small glassy flakes. The salt content of the crude product was reduced by dialysis in a Float-A-Lyzer® G2. The water was removed under reduced pressure and the product dried in a desiccator.

Eu_2.**5**: Yield: 66 mg, 36%. ^{1}H NMR as above. MALDI-TOF HRMS (*m*/*z*) 1140 ($[M + H]^+$), 1162 ($[M + Na]^+$), 1178 ($[M + K]^+$), 591 ($[M + 2Na]^{2+}$). UV-vis (H_2O) λ (I/I_{max}) 209 (1.00), 266 (0.40) nm. Elemental calculated: C, 20.56; H, 1.98; N, 4.85; measured: C, 20.71; H, 3.21; N, 4.64; $[C_{44.5}H_{51}Eu_2F_{25.5}N_9Na_{8.5}O_{39.5}S_{8.5}]$ (M · 8.5NaOTf).

Tb_2.**5**: Yield: 42 mg, 32%. ^{1}H NMR peaks too broad to observe. MALDI-TOF HRMS (*m*/*z*) 1152 ($[M + H]^+$), 1174 ($[M + Na]^+$). UV-vis (H_2O) λ (I/I_{max}) 208 (1.00), 266 (0.36) nm. Elemental calculated: C, 23.10; H, 2.35; N, 5.77; measured: C, 21.41; H, 2.98; N, 6.04; $[C_{42}H_{51}F_{18}N_9Na_6O_{32}S_6Tb_2]$ (M · 6NaOTf).

α,α'-bis(H_3.DO3A)-3,5-dimethylaminobenzene · *x*TFA (6)



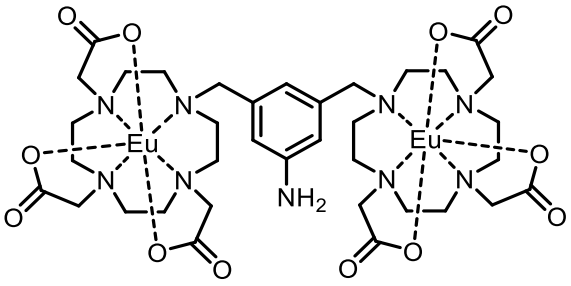
6

Prepared from **4** in accordance with the procedure described by Placidi *et al.*[3]

Yield: 65 mg, quantitative yield. ^{1}H NMR (MeOD, 400 MHz) δ (ppm) 7.39 – 6.61 (3H,

br. m, ArH), 4.36 – 2.45 (48H, br. m, NCH_2).

***α,α'*-bis(Eu.DO3A)-3,5-dimethylaminobenzene · 6NaOTf (Eu2.6)**



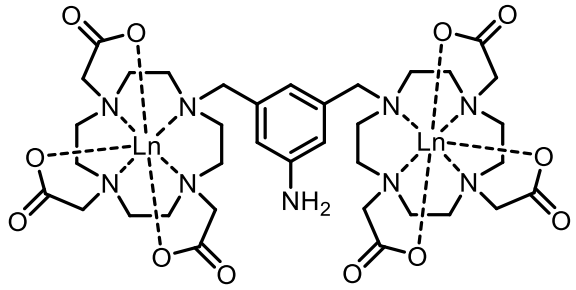
Eu_2.**6**

Method 1

6 · *x*TFA (52 mg, <0.064 mmol) and europium triflate (81 mg, 0.14 mmol) were dissolved in acetonitrile (5 mL). The reaction mixture was heated at 70°C with stirring for 4 days. The solvent was removed under reduced pressure yielding beige flakes. NMR spectroscopy indicated that the reaction had not proceeded to completion as there were still peaks in the non-paramagnetic ligand region of the spectrum. The solid was redissolved in water (15 mL) with aqueous sodium hydroxide (2 drops, 2.0 M) and this mixture was heated at 90°C with stirring for 65 hours. The water was removed under reduced pressure. The salt content of the crude product was reduced by dialysis in a Float-A-Lyzer® G2. The water was removed under reduced pressure and the product dried in a desiccator.

Yield: 66 mg, >48%. ^{1}H NMR (D_2O, 400 MHz) δ (ppm) 33.29, −7.05, −8.09, −9.87, −14.58, −15.53, −19.03. Only major resolved peaks outside the +10 to 0 ppm range are reported. MALDI-TOF HRMS (*m*/*z*) 1107, 1109 (M^+), 1108, 1110 ($[M + H]^+$), 1146 ($[M + K]^+$). UV-vis (H_2O) λ (I/I_{max}) 206 (1.00), 239 (0.24), 293 (0.08) nm. Elemental calculated: C, 23.57; H, 2.50; N, 5.89; measured: C, 21.13; H, 3.22; N, 5.89; $[C_{42}H_{53}Eu_2F_{18}N_9Na_6O_{30}S_6]$ (M · 6NaOTf).

***α,α'*-bis(Ln.DO3A)-3,5-dimethylaminobenzene · *x*NaOTf · *y*NH_2NH_2 (Ln2.6)**



Ln_2.**6**

Method 2

Ln = Eu, Gd, Tb

A slurry of 10 wt. % palladium on carbon (catalytic amount, ~10 mg) in methanol (3 to 5 mL) was added to undialysed Ln_2.**5** · *x*NaOTf (up to 300 mg) and the reaction mixture was heated to 65°C under nitrogen with stirring. Hydrazine hydrate (50-60%, 2 to 5 mL) was added and the mixture heated under reflux with stirring for 20 hours. The reaction mixture was cooled to room temperature and the catalyst removed by filtration through a Celite® slurry in methanol. The volatiles were removed under reduced pressure. The crude product was dissolved in the minimum amount of methanol and then diethyl ether added to precipitate the product. The solid was collected by filtration or the diethyl ether removed by decantation. The solid was dried under reduced pressure. The salt content of the crude white powder was reduced by dialysis in a Float-A-Lyzer® G2, the water was removed under reduced pressure, and the product dried in a desiccator to afford glassy flakes.

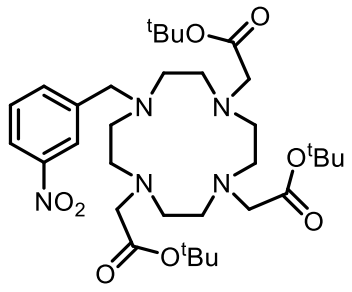
Eu_2.**6**: Yield: 290 mg, 97%. ^{1}H NMR (D_2O, 400 MHz) δ (ppm) 36.40, 29.46, 26.17, 26.13, 21.80, 18.64, 18.26, 15.98, 12.23, 10.95, 10.44, −1.08, −1.73, −2.98, −3.93, −4.33, −4.81, −6.40, −7.16, −7.81, −8.58, −10.11, −10.96, −12.07, −12.54, −13.74, −15.50, −17.60, −18.04, −18.10, −18.44, −19.82. Only major resolved peaks outside the +10 to 0 ppm

range are reported. MALDI-TOF HRMS (*m*/*z*) 1107 ($[M + H]^+$), 1130 ($[M + Na]^+$), 1146 ($[M + K]^+$). UV-vis (H_2O) λ (I/I_{max}) 209 (1.00), 238 (0.26), 292 (0.12) nm. Elemental calculated: C, 36.90; H, 5.25; N, 15.54; measured: C, 36.50; H, 5.73; N, 11.97; $[C_{36}H_{61}Eu_2N_{13}O_{12}]$ ($M \cdot 2NH_2NH_2$).

Gd_2.**6**: Yield: 59 mg, 60%. MALDI-TOF HRMS (*m*/*z*) 1120 ($[M + H]^+$), 1141 ($[M + Na]^+$), 1157 ($[M + K]^+$), 1063 ($[M - CH_2CO_2 + 2H]^+$).

Tb_2.**6**: Yield: 36 mg, 12%. ^1H NMR (D_2O, 400 MHz) δ (ppm) 259.26, 109.42, 88.60, 75.17, −0.50, −23.39, −27.78, −36.16, −62.73, −83.41, −104.22, −136.25, −159.69, −239.65, −272.56. Only major resolved peaks outside the +50 to 0 ppm range are reported. MALDI-TOF HRMS (*m*/*z*) 1122 ($[M + H]^+$), 1144 ($[M + Na]^+$). UV-vis (H_2O) λ (I/I_{max}) 206 (1.00), 239 (0.22), 291 (0.09) nm. Elemental calculated: C, 25.64; H, 3.28; N, 9.72; measured: C, 25.87; H, 3.79; N, 9.91; $[C_{40}H_{61}F_{12}N_{13}Na_4O_{24}S_4Tb_2]$ ($M \cdot 4NaOTf \cdot 2NH_2NH_2$).

α-(DO3A *tert*-butyl triester)-3-methylnitrobenzene (7)



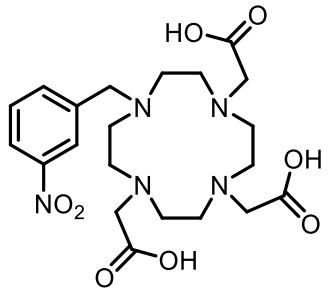
7

Prepared in accordance with the procedure described by Karhunen *et al.*[4]

3-Nitrobenzylbromide (0.42 g, 1.94 mmol), **1** (1.00 g, 1.94 mmol), and potassium carbonate (1.30 g, 4.84 mmol) were combined in acetonitrile and the mixture heated and reacted at 55°C for 3.5 hours. The white suspension was filtered to removed inorganic salts and the resulting yellow solution evaporated under reduced pressure. The bubbly, crispy, light yellow solid was dissolved in dichloromethane (30 mL) and washed with brine (3 × 30 mL). The organic layers were combined and dried over anhydrous sodium sulphate, filtered, and concentrated to dryness under reduced pressure. The crude product was purified by silica gel column chromatography in 19:1 dichloromethane:methanol (and impure fractions containing the product were subjected to another column), yielding a static white/very pale yellow candyfloss-like solid.

Yield: 482 mg, 38%. ^{1}H NMR ($CDCl_3$, 400 MHz) δ (ppm) 8.71 (1H, t, *J*=2.1 Hz, Ar-H2), 8.13 (1H, ddd, *J*=7.9, 2.1, 1.2 Hz, Ar-H4), 7.76 (1H, dt, *J*=7.9, 1.2 Hz, Ar-H6), 7.53 (1H, t, *J*=7.9 Hz, Ar-H5), 3.98 – 1.98 (24H, br. m, NCH_2), 1.42 (27H, br. s, 3 × ^{t}Bu). ^{13}C NMR ($CDCl_3$, 126 MHz) δ (ppm) 173.45, 172.51, 148.53, 139.60, 137.10, 129.54, 124.71, 122.51, 83.10, 82.55, 58.76, 55.93, 55.59, 27.79. ES^+ MS (*m*/*z*) 650 ($[M + H]^+$), 672 ($[M + Na]^+$), 594 ($[M – {}^{t}Bu + 2H]^+$), 538 ($[M – 2{}^{t}Bu + 3H]^+$), 482 ($[M – 3{}^{t}Bu + 4H]^+$).

α-(H_3.DO3A)-3-methylnitrobenzene · 2TFA (8)

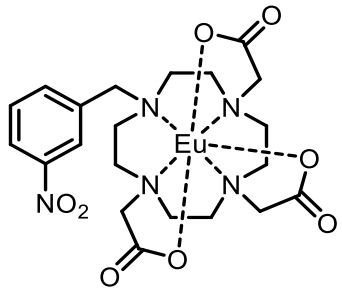


8

7 (100 mg, 0.15 mmol) was dissolved in dichloromethane (2 mL) and trifluoroacetic acid (2 mL) added dropwise to the stirring solution. The reaction mixture was stirred at room temperature for 26 hours, monitored by withdrawing small aliquots which were subjected to mass spectrometry. Once the reaction was complete, the solvent was removed under reduced pressure. The crude mixture was dissolved in methanol and then evaporated to dryness under reduced pressure in order to remove residual trifluoroacetic acid. This process was repeated three times. The crude product was dissolved in the minimum amount of methanol. Diethyl ether was added to precipitate the solid, and the diethyl ether removed by decantation. This methanol-diethyl ether process was repeated twice further. The resulting white powder was dried under reduced pressure.

Yield: 75 mg, 69%. ^{1}H NMR (MeOD, 400 MHz) δ (ppm) 8.37 (1H, s, Ar-H2), 8.23 (1H, d, *J*=8.2 Hz, Ar-H4), 8.07 (1H, d, *J*=7.8 Hz, Ar-H6), 7.60 (1H, t, *J*=7.8 Hz, Ar-H5), 4.23 (2H, br. s, $ArCH_2$), 3.55 (22H, br. m, CH_2 cyclen ring, CH_2CO). ES^+ MS (*m*/*z*) 482 ($[M + H]^+$), 504 ($[M + Na]^+$). ESI^+ HRMS (*m*/*z*) calculated: 482.22454, measured: 482.22448 $[C_{21}H_{32}N_5O_8]^+$ ($[M + H]^+$). Elemental calculated: C, 42.32; H, 4.69; N, 9.87; measured: C, 40.51; H, 4.97; N, 9.84; $[C_{25}H_{33}F_6N_5O_{12}]$ (M · 2TFA).

***α*-(Eu.DO3A)-3-methylnitrobenzene · 3NaOTf (**Eu.**8)**

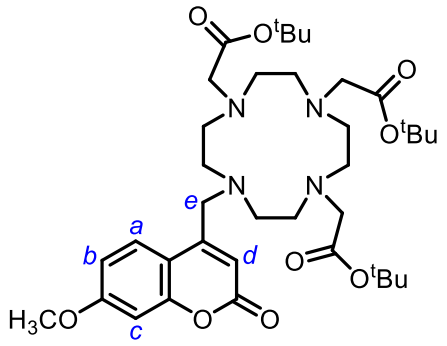


Eu.**8**

8 · 2TFA (45 mg, 0.063 mmol) and europium triflate (59 mg, 0.098 mmol) were combined in methanol (5 mL) and heated at 60°C with stirring for 21 hours, then adjusted to pH 5 by dropwise addition of aqueous sodium hydroxide (1.0 M) and further reacted at 60°C for 5 days. The methanol was removed under reduced pressure, the resulting suspension dissolved in water and adjusted to pH 10 by dropwise addition of aqueous sodium hydroxide (1.0 M). The resulting suspension was centrifuged and the supernatant filtered through an Acrodisc® syringe filter (0.2 μm), neutralised to pH 7 by dropwise addition of aqueous hydrochloric acid (1.0 M), and the water removed under reduced pressure followed by desiccation. The salt content of the crude product was reduced by dialysis in a Float-A-Lyzer® G2. The water was removed under reduced pressure and the product dried in a desiccator.

Yield: 24 mg, 33%. ^{1}H NMR (D_2O, 400 MHz) δ (ppm) 37.43, 27.82, 27.77, 17.49, 12.84, −2.31, −5.15, −10.04, −10.06, −11.94, −15.31, −16.66, −18.67, −19.32, −20.63, −24.10, −24.42, −25.33. Only major resolved peaks outside the +10 to 0 ppm range are reported. ES$^+$ MS (*m*/*z*) 632 ([M + H]$^+$), 1261 ([2M + H]$^+$). UV-vis (H_2O) λ (I/I_{max}) 204 (1.00), 268 (0.48) nm. Elemental calculated: C, 25.14; H, 2.46; N, 6.11; measured: C, 25.47; H, 3.47; N, 6.20; [$C_{24}H_{28}EuF_9N_5Na_3O_{17}S_3$] (M · 3NaOTf).

α-(DO3A *tert*-butyl triester)-4-methyl-7-methoxycoumarin (9)



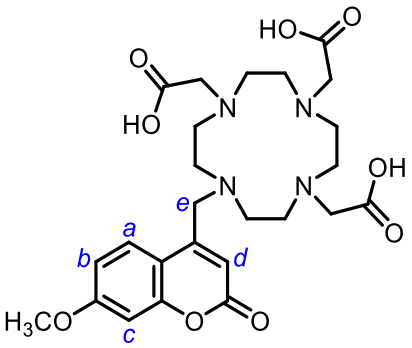
9

1 (600 mg, 1.17 mmol), 4-(bromomethyl)-7-methoxycoumarin (376 mg, 1.40 mmol), and sodium carbonate (320 mg, 2.91 mmol) were combined in acetonitrile (60 mL). The reaction mixture was heated to 85°C and heated under reflux with stirring, monitoring by TLC analysis and mass spectrometry. After 5 days, mass spectrometry indicated that the **1** starting material had been entirely consumed. The inorganic salts were removed by filtration and the solvent removed under reduced pressure. The solid was dissolved in a small amount of hot methanol and the solution was concentrated by slow evaporation at room temperature over two days, allowing unreacted starting material to precipitate from solution. The supernatant was collected by decantation and allowed to evaporate further, again resulting in solid starting material precipitating from solution and the resulting concentrated solution was again collected by decantation and the solvent removed under reduced pressure. The crude product was then purified by an elution gradient of dichloromethane-methanol on silica gel column chromatography and the product was eluted when the methanol concentration was increased to 4% v/v.

Yield: 312 mg, 38%. ^{1}H NMR ($CDCl_3$, 400 MHz) δ (ppm) 7.75 (1H, d, *J*=8.9 Hz, ArH*a*), 6.86 (1H, dd, *J*=8.9, 2.6 Hz, ArH*b*), 6.77 (1H, d, *J*=2.6 Hz, ArH*c*), 6.28 (1H, s, C=CH*d*), 4.44 (2H, br. s, 2 × H*e*), 3.83 (3H, s, OCH_3), 3.24 – 2.00 (22H, m, CH_2 cyclen ring, CH_2CO), 1.38 (27H, br. m, 3 × ^{t}Bu). ^{13}C NMR ($CDCl_3$, 126 MHz) δ (ppm) 173.53, 172.67,

162.91, 160.50, 155.48, 152.27, 125.57, 112.65, 112.50, 111.79, 101.36, 83.28, 82.60, 55.84, 55.71, 54.32, 51.09, 27.98, 27.92. ES^+ MS (*m/z*) 703 ($[M + H]^+$), 725 ($[M + Na]^+$), 1406 ($[2M + H]^+$), 647 ($[M - {}^tBu + 2H]^+$), 591 ($[M - 2{}^tBu + 3H]^+$), 535 ($[M - 3{}^tBu + 4H]^+$). ES^- MS (*m/z*) 701 ($[M - H]^-$). IR-ATR *v* (cm^{-1}) 3478, 3410 (cyclen C-H), 1718 (C=O), 1265, 1206 (C-O).

α-(H_3.DO3A)-4-methyl-7-methoxycoumarin (10)



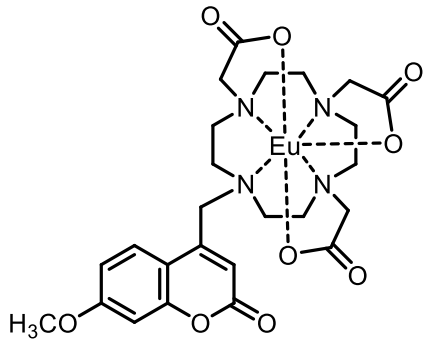
10

9 (259 mg, 0.37 mmol) was dissolved in dichloromethane (3 mL) and trifluoroacetic acid (3 mL) was added dropwise to the stirring solution. The reaction mixture was stirred at room temperature for 4 days and then the volatiles removed under reduced pressure. Methanol was repeatedly added and then removed under reduced pressure in order to co-evaporate the residual trifluoroacetic acid. The crude product was dissolved in the minimum amount of methanol, and diethyl ether added, causing the product to precipitate out. The diethyl ether was decanted off and the solid product collected by filtration and dried under reduced pressure to yield a flaky/shiny yellow powder.

Yield: 167 mg, 85%. ^1H NMR (MeOD, 400 MHz) δ (ppm) 7.86 (1H, d, *J*=8.6 Hz, ArH*a*), 6.95 (1H, d, *J*=8.6 Hz, ArH*b*), 6.86 (1H, d, *J*=11.1 Hz, ArH*c*), 6.59 (1H, d, *J*=7.3 Hz, C=CH*d*), 4.16 (2H, s, 2 × H*e*), 3.89 (3H, br. m, OCH_3), 3.83 – 2.80 (22H, br. m, NCH_2). ESI^+ HRMS (*m/z*) calculated: 535.23986, measured: 535.23991 $[C_{25}H_{35}N_4O_9]^+$ ([M +

H]$^+$). IR-ATR *v* (cm^{-1}) 3384 (cyclen C-H), 1690, 1608 (C-O), 1200, 1135 (C-O).

α-(Eu.DO3A)-4-methyl-7-methoxycoumarin (Eu.**10)**



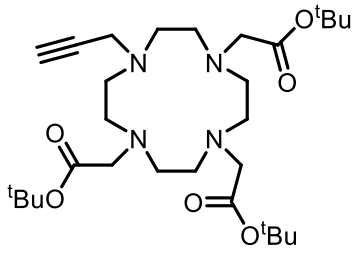
Eu.**10**

10 (100 mg 0.187 mmol) and europium triflate (118 mg, 0.196 mmol) were combined in methanol and the reaction mixture heated at 60°C under reflux with stirring for 3 days. The solvent was removed under reduced pressure to give a yellow oil which was dissolved in water to give a clear solution and adjusted to pH 11 by dropwise addition of aqueous sodium hydroxide (1.0 M) to give a bright yellow solution. *(NB: This solution was clear at acidic and neutral pH and bright yellow at basic pH, and the colour change was reversible.)* This was centrifuged and the supernatant filtered through an Acrodisc® syringe filter (0.2 μm), neutralised, and the water removed under reduced pressure. The solid was dialysed to remove salts. The water was removed under reduced pressure and the product dried in a desiccator. Crystals suitable for single crystal X-ray diffraction were obtained by slow evaporation of a concentrated solution of the product in D_2O.

Yield: 50 mg, 39%. ^{1}H NMR (D_2O, 400 MHz) δ (ppm) 47.99, 41.27, 33.93, 30.39, 25.00, 23.46, 18.21, 17.08, −1.05, −1.81, −2.16, −4.51, −10.02, −12.13, −13.58, −16.09, −18.41, −19.63, −25.23, −34.30. Only major resolved peaks outside the +10 to 0 ppm range are reported. ES$^+$ MS (*m*/*z*) 685 ([M + H]$^+$). MALDI-TOF HRMS (*m*/*z*) 684 (M$^+$), 707 ([M + Na]$^+$). UV-vis (H_2O) λ (I/I_{max}) (pH = 7) 201 (1.00), 220 (0.32), 331 (0.26) nm. IR-ATR *v*

(cm^{-1}) 3385 (cyclen C-H), 1710, 1603 (C-O), 1385-1084 (C-O). Please see Appendix C.4 for X-ray diffraction data.

propargyl(DO3A *tert*-butyl triester) (11)

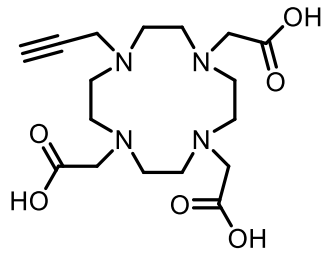


11

Prepared in accordance with the procedure described by Jauregui *et al*.[5]

Yield: 522 mg, 97%. ^{1}H NMR ($CDCl_3$, 400 MHz) δ (ppm) 3.57 – 2.90 (8H, br. m, NCH_2), 2.87 – 2.33 (12H, br. m, NCH_2), 2.14 (1H, br. q, *J*=4.4, 3.4 Hz, C≡CH), 1.93 (4H, br. d, NCH_2R), 1.65 – 1.18 (27H, br. m, 3 × ^{t}Bu). ES^+ MS (*m*/*z*) 553 ($[M + H]^+$), 575 ($[M + Na]^+$), 591 ($[M + K]^+$), 497 ($[M - {}^t\text{Bu} + 2H]^+$), 441 ($[M - 2{}^t\text{Bu} + 3H]^+$), 385 ($[M - 3{}^t\text{Bu} + 4H]^+$), 193 ($[M - 3{}^t\text{Bu} + 5H]^{2+}$), 232 ($[M - 2{}^t\text{Bu} + 3H + Na]^{2+}$).

propargyl(H_3.DO3A) (12)

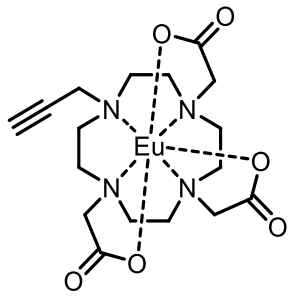


12

Prepared in accordance with the procedure described by Jauregui *et al*.[5]

Yield: quantitative yield. ^{1}H NMR (MeOD, 400 MHz) δ (ppm) 3.83 (8H, br. s, NCH_2), 3.45 (8H, br. m, NCH_2), 3.10 (8H, br. s, NCH_2), 2.87 (1H, s, C≡CH). ES^+ MS (*m*/*z*) 385 ($[M + H]^+$).

propargyl(Eu.DO3A) (Eu.**12)**

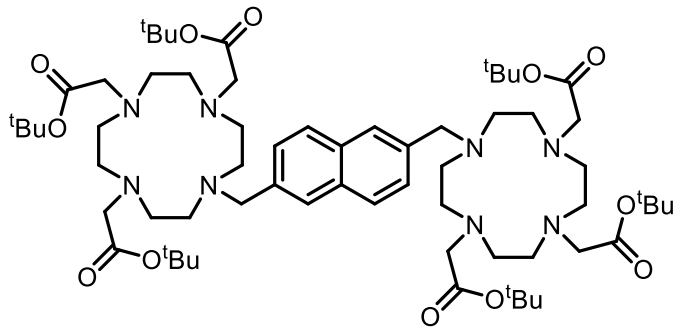


Eu.**12**

Prepared in accordance with the procedure described by Jauregui *et al*.[5]

Yield: 93 mg, 68%. ^{1}H NMR (D_2O, 400 MHz) δ (ppm) 26.91, 18.85, 17.59, 15.47, 10.48, −1.21, −5.80, −9.05, −10.13, −15.07, −16.16, −19.36. Only major resolved peaks outside the +10 to 0 ppm range are reported. MALDI-TOF HRMS (*m*/*z*) 535 ($[M + H]^+$), 557 ($[M + Na]^+$). UV-vis (H_2O) λ (I/I_{max}) 200 (1.00) nm.

***α*,*α*'-bis(DO3A *tert*-butyl triester)-2,6-dimethylnaphthalene (13)**



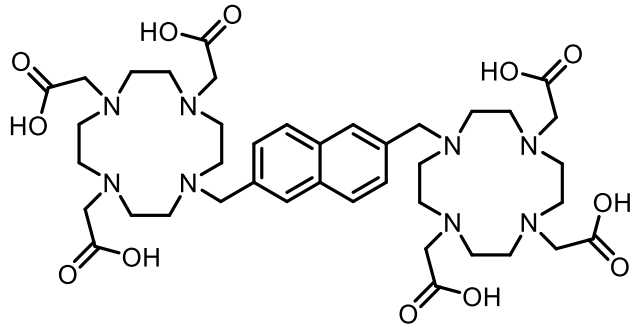
13

2,6-Bis(bromomethyl)naphthalene (250 mg, 0.80 mmol), **1** (983 mg, 1.91 mmol), and caesium carbonate (1.30 g, 3.98 mmol) were combined in acetonitrile (30 mL). The reaction mixture was heated under reflux with stirring for 52 hours. The clear solution became a pale orange-white suspension. The reaction mixture was cooled to room temperature and filtered to remove inorganic salts and the solvent removed under reduced pressure. The resulting brown oil was dissolved in dichloromethane (30 mL) and washed

with brine (3 × 30 mL). The organic layer was dried over anhydrous sodium sulphate, filtered, and the solvent removed under reduced pressure. The crude product was purified *via* alumina gradient column chromatography, in dichloromethane with an increasing concentration of methanol. The solvent was removed under reduced pressure to yield a crispy yellow solid. Crystals suitable for single crystal X-ray diffraction were obtained by slow evaporation of a concentrated solution of the product in $CDCl_3$.

Yield: 497 mg, 53%. ^{1}H NMR ($CDCl_3$, 400 MHz) δ (ppm) 7.82 – 7.53 (4H, m, Ar-H1, Ar-H5, Ar-H4, Ar-H8), 7.53 – 7.37 (2H, m, Ar-H3, Ar-H7), 3.96 – 1.84 (48H, br. m, NCH_2), 1.60 – 0.84 (54H, br. m, 6 × ^{t}Bu). ^{13}C NMR ($CDCl_3$, 126 MHz) δ (ppm) 173.64, 172.69, 135.36, 132.54, 129.50, 129.47, 128.44, 127.85, 82.98, 82.87, 82.55, 82.51, 77.36, 59.84, 56.25, 56.22, 56.12, 55.90, 28.36, 28.33, 28.29, 28.26, 28.22, 28.20, 28.11, 28.01. ES$^+$ MS (*m*/*z*) 1181.94 ($[M + H]^+$), 1203.93 ($[M + Na]^+$), 591.69 ($[M + 2H]^{2+}$), 563.65 ($[M - {}^tBu + 3H]^{2+}$), 535.60 ($[M - 2{}^tBu + 4H]^{2+}$), 507.56 ($[M - 3{}^tBu + 5H]^{2+}$). IR-ATR *ν* (cm^{-1}) 3367 (cylen C-H), 2977, 2933 (^{t}Bu C-H), 1719 (C=O), 1224, 1157, 1111 (C-O). Please see Appendix C.5 for X-ray diffraction data.

α,α'-bis(H$_3$.DO3A)-2,6-dimethylnaphthalene (14)



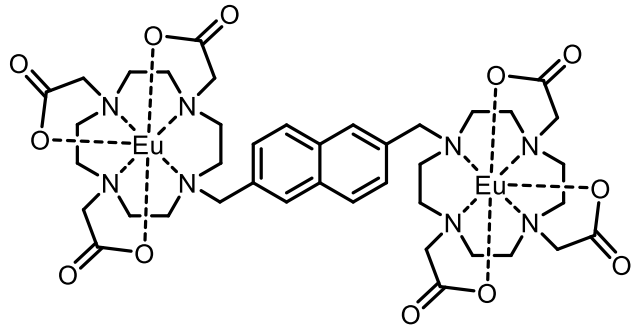
14

13 (200 mg, 0.17 mmol) was dissolved in dichloromethane (2 mL). Trifluoroacetic acid was added dropwise (2 mL) and the reaction mixture was stirred at room temperature

overnight, monitoring by withdrawing small aliquots which were subjected to mass spectrometry. The solvent was removed under reduced pressure. The crude mixture was dissolved in dichloromethane and then evaporated to dryness under reduced pressure in order to remove residual trifluoroacetic acid. This process was repeated three times with dichloromethane and subsequently three times with methanol. The crude product was dissolved in the minimum amount of methanol and diethyl ether added. The product precipitated from solution and was collected by filtration and dried under reduced pressure to give a cream solid.

Yield: 119 mg, 83%. ^{1}H NMR (MeOD, 400 MHz) δ (ppm) 8.34 – 7.84 (4H, m, Ar-H1, Ar-H5, Ar-H4, Ar-H8), 7.78 (2H, m, Ar-H3, Ar-H7), 4.28 (4H, br. s, $ArCH_2$), 3.95 – 2.14 (44H, m, CH_2 cyclen ring, CH_2CO). ^{13}C NMR (DMSO, 126 MHz) δ (ppm) 157.70, 132.40, 128.55, 118.55, 116.16, 54.23, 49.74. ES^+ MS (*m*/*z*) 845 ($[M + H]^+$), 867 ($[M + Na]^+$). MALDI-TOF HRMS (*m*/*z*) 844 (M^+), 786 ($[M - CH_2CO_2H + H]^+$). IR-ATR *v* (cm^{-1}) 3392 (cylen C-H), 1675, 1630 (C=O), 1199, 1179, 1125 (C-O).

α,α'-bis(Eu.DO3A)-2,6-dimethylnaphthalene (Eu_2**.14)**



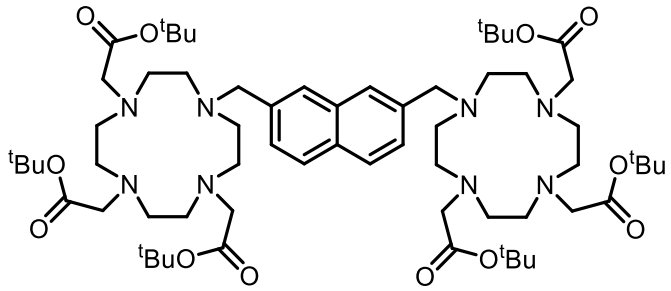
Eu_2.**14**

14 (40 mg, 0.047 mmol) and europium triflate (60 mg, 0.099 mmol) were combined in water (2 mL) and heated at 60°C with stirring for 3 days. The solution was adjusted to pH 5 by dropwise addition of aqueous sodium hydroxide (1.0 M) and the reaction mixture

heated at 60°C with stirring for a further 4 days. The suspension was centrifuged and the supernatant filtered through an Acrodisc® syringe filter (0.2 μm), the water removed under reduced pressure and remaining water removed in a desiccator. The salt content was reduced by dialysis in a Float-A-Lyzer® G2. The water was removed under reduced pressure and the product dried in a desiccator.

Yield: 5 mg, 9%. ^{1}H NMR (D_2O, 400 MHz) δ (ppm) 25.06, 16.49, 14.61, 13.97, 11.79, −3.04, −5.44, −9.83, −12.19, −15.84, −16.33, −17.01, −19.27, −21.21, −25.59. Only major resolved peaks outside the +10 to 0 ppm range are reported. MALDI-TOF HRMS (*m*/*z*) 1144 (M^+), 1145 ($[M + H]^+$). UV-vis (H_2O) λ (I/I_{max}) 231 (1.00), 274 (0.05) nm. IR-ATR *v* (cm^{-1}) 3414 (cylen C-H), 1578 (C=O).

α,α'-bis(DO3A *tert*-butyl triester)-2,7-dimethylnaphthalene (15)



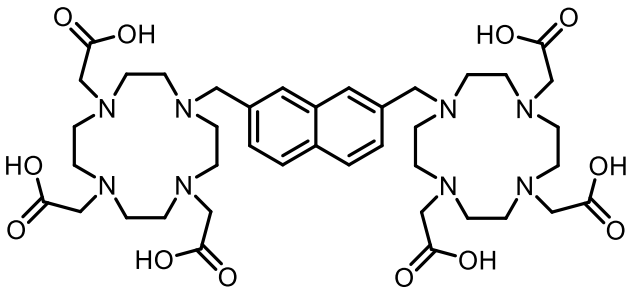
15

2,7-Bis(bromomethyl)naphthalene (250 mg, 0.80 mmol), **1** (901 mg, 1.75 mmol), and caesium carbonate (1.30 g, 3.98 mmol) were combined in acetonitrile (30 mL). The reaction mixture was heated under reflux with stirring for 2 days, monitoring by TLC analysis. Once the 2,7-bis(bromomethyl)naphthalene had been consumed, the reaction mixture was cooled to room temperature and filtered to remove inorganic salts, giving an orange solution. The solvent was removed under reduced pressure to afford a brown oil. This oil was dissolved in dichloromethane (50 mL) and washed with brine (3 × 30 mL). The organic layer was dried over anhydrous sodium sulphate, filtered and the solvent

removed under reduced pressure. The crude product was purified *via* alumina gradient column chromatography, in dichloromethane with an increasing concentration of methanol. The solvent was removed under reduced pressure to afford the desired product as a pale orange solid.

Yield: 369 mg, 39%. ^{1}H NMR ($CDCl_3$, 400 MHz) δ (ppm) 7.97 – 7.33 (6H, m, 6 × ArH), 4.14 – 1.70 (48H, br. m, NCH_2), 1.28 (54H, m, 6 × ^{t}Bu). ^{13}C NMR ($CDCl_3$, 126 MHz) δ (ppm) 173.66, 172.70, 135.39, 133.29, 131.89, 129.91, 127.98, 82.82, 82.53, 59.77, 56.31, 55.88, 53.56, 49.89, 28.25, 28.22, 28.06, 28.01. ES^{+} MS (*m/z*) 1182 ($[M + H]^{+}$), 1204 ($[M + Na]^{+}$), 591 ($[M + 2H]^{2+}$), 563 ($[M - {}^{t}Bu + 3H]^{2+}$), 535 ($[M - 2{}^{t}Bu + 4H]^{2+}$), 507 ($[M - 3{}^{t}Bu + 5H]^{2+}$). IR-ATR *ν* ($cm^{-1}$) br. 3600 (cylen C-H), 2977, 2935, 2829 (^{t}Bu C-H), 1719 (C=O), 1155, 1101 (C-O).

α,α'-bis(H_3.DO3A)-2,7-dimethylnaphthalene · 3TFA (16)

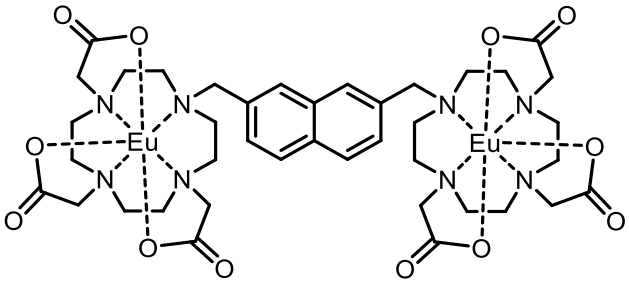


16

15 (201 mg, 0.17 mmol) was dissolved in dichloromethane (2 mL). Trifluoroacetic acid was added dropwise (2 mL) and the reaction mixture was stirred at room temperature overnight, monitoring by withdrawing small aliquots which were subjected to mass spectrometry. The solvent was removed under reduced pressure. The crude mixture was dissolved in methanol and then evaporated to dryness under reduced pressure in order to remove residual trifluoroacetic acid. This process was repeated three times to afford the product.

Yield: 180 mg, 89%. ^{1}H NMR (MeOD, 400 MHz) δ (ppm) 8.16 (2H, s, 2 × ArH), 7.93 (2H, d, *J*=8.5 Hz, 2 × ArH), 7.82 – 7.49 (2H, m, 2 × ArH), 4.50 (4H, br. s, $ArCH_2$), 3.35 (44H, br., CH_2 cyclen ring, CH_2CO). ES$^+$ MS (*m/z*) 845 ($[M + H]^+$), 867 ($[M + Na]^+$). MALDI-TOF HRMS (*m/z*) calculated: 845.4409, measured: 845.5363 $[C_{40}H_{61}N_8O_{12}]^+$ ($[M + H]^+$). IR-ATR *v* (cm^{-1}) 3081 (cylen C-H), 1673 (C=O), 1189, 1121 (C-O).

α,α'-bis(Eu.DO3A)-2,7-dimethylnaphthalene · 6NaOTf (Eu_2**.16)**

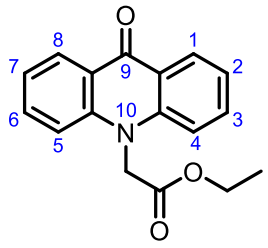


Eu_2**.16**

16 · 3TFA (170 mg, 0.14 mmol) and europium triflate (253 mg, 0.42 mmol) were combined in acetonitrile (5 mL) and heated under reflux with stirring for 12 days. The resulting suspension was centrifuged and gave a beige supernatant, a layer of white solid presumed to be excess lanthanide salt, and below this a layer of beige solid presumed to be the product. The supernatant was removed, and the residues taken forward to dialysis in a Float-A-Lyzer® G2 in order to reduce salt and lanthanide triflate content. Freeze-drying gave a flocculent cream solid.

Yield: 84 mg, 27%. ^{1}H NMR (D_2O, 400 MHz) δ (ppm) 25.90, 20.36, 16.13, 15.24, −4.76, −10.25, −16.77, −19.25. Only major resolved peaks outside the +10 to 0 ppm range are reported. MALDI-TOF HRMS (*m/z*) 1144 (M^+), 1145 ($[M + H]^+$), 1167 ($[M + Na]^+$), 1088 ($[M - CH_2CO_2 + 2H]^+$). UV-vis (H_2O) λ (I/I_{max}) 229 (1.00), 276 (0.06) nm. IR-ATR *v* (cm^{-1}) 3421 (cylen C-H), 1578 (C=O). Elemental calculated: C, 25.40; H, 2.50; N, 5.15; measured: C, 25.27; H, 3.06; N, 5.35; $[C_{46}H_{54}Eu_2F_{18}N_8Na_6O_{30}S_6]$ (M · 6NaOTf).

ethyl-9-oxo-10(9*H*)-acridineacetate (17)

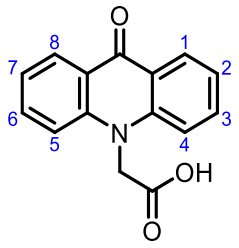


17

Prepared in accordance with the procedure described by David-Cordonnier *et al.*[6]

Yield: 1.34 g, 93%. ^{1}H NMR ($CDCl_3$, 400 MHz) δ (ppm) 8.53 (2H, dt, *J*=8.1, 1.9 Hz, acridone-H1, acridone-H8), 7.69 (2H, ddq, *J*=8.8, 6.9, 1.9 Hz, acridone-H), 7.37 – 7.26 (4H, m, acridone-H), 5.04 (2H, d, *J*=1.7 Hz, NCH_2), 4.30 (2H, qd, *J*=7.2, 1.7 Hz, OCH_2CH_3), 1.36 – 1.22 (3H, m, OCH_2CH_3). ES^+ MS (*m*/*z*) 282 ($[M + H]^+$), 304 ($[M + Na]^+$), 585 ($[2M + Na]^+$). Crystals suitable for single crystal X-ray diffraction were obtained by slow evaporation of a concentrated solution of the product in $CDCl_3$. Please see Appendix C.6 for X-ray diffraction data. Elemental calculated: C, 72.58; H, 5.37; N, 4.98; measured: C, 72.45; H, 5.44; N, 5.12; [$C_{17}H_{15}NO_3$] (M).

9-oxo-10(9*H*)-acridineacetic acid (18)



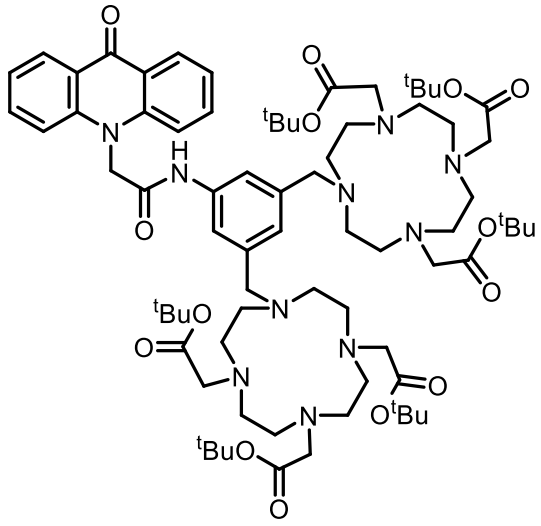
18

Prepared in accordance with the procedure described by David-Cordonnier *et al.*[6]

Yield: 573 mg, 90%. ^{1}H NMR (DMSO, 400 MHz) δ (ppm) 8.36 (2H, dd, *J*=7.9, 1.7 Hz, acridone-H1, acridone-H8), 7.81 (2H, ddd, *J*=8.7, 6.9, 1.7 Hz, acridone-H3, acridone-H6),

7.67 (2H, d, *J*=8.7 Hz, acridone-H4, acridone-H5), 7.35 (2H, ddd, *J*=7.9, 6.9, 0.9 Hz, acridone-H2, acridone-H7), 5.33 (2H, s, NCH_2). ^1H-^1H COSY NMR (DMSO, 400 MHz) supported the assignment. ES^- MS (*m*/*z*) 252 ($[M - H]^-$). FI^+ HRMS (*m*/*z*) calculated: 253.0739, measured: 253.0746 $[C_{15}H_{11}NO_3]^+$ (M^+). IR-ATR ν (cm^{-1}) 1735 (C=O). Elemental calculated: C, 71.14; H, 4.38; N, 5.53; measured: C, 71.07; H, 4.26; N, 5.48; $[C_{15}H_{11}NO_3]$ (M).

_N_-(*α*,*α*'-bis(DO3A *tert*-butyl triester)-3,5-dimethylphenyl)-9-oxo-10(9*H*)-acridineacetamide (19)



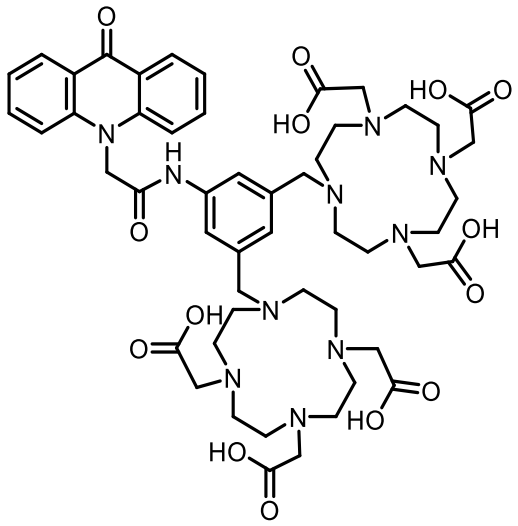
19

18 (100 mg, 0.395 mmol), **4** (500 mg, 0.434 mmol), and BOP (192 mg, 0.434 mmol) were combined in DMF (2 mL). DIPEA (160 µL, 0.919 mmol) was added and the reaction mixture stirred at room temperature overnight. After 23 hours, analysis of a small aliquot of the reaction mixture using mass spectrometry suggested that unreacted starting materials remained. More BOP (96 mg, 0.217 mmol) and DIPEA (160 µL, 0.919 mmol) were added and the reaction mixture stirred for a further 6 days at room temperature, periodically monitoring by withdrawing small aliquots which were subjected to mass

spectrometry, and by TLC analysis. After this time, water (6 mL) was added to the reaction mixture. The mixture was sonicated, filtered, washed with water, dried under a stream of nitrogen, washed with diethyl ether, and dried under reduced pressure to afford the product as a beige solid.

Yield: 531 mg, 97%. ^{1}H NMR (DMSO, 400 MHz) δ (ppm) 8.95 – 6.09 (11H, br. m, ArH), 4.33 – 1.87 (50H, br. m, NCH_2), 1.68 – 1.18 (54H, br. m, 6 × ^{t}Bu). ES$^+$ MS (*m*/*z*) 1382 ($[M + H]^+$), 1292 ($[M - 2^tBu + 2H + Na]^+$), 691 ($[M + 2H]^{2+}$). IR-ATR *v* (cm^{-1}) 1719 (C=O).

_N_-(*α*,*α*'-bis(H$_3$.DO3A)-3,5-dimethylphenyl)-9-oxo-10(9*H*)-acridineacetamide (20)



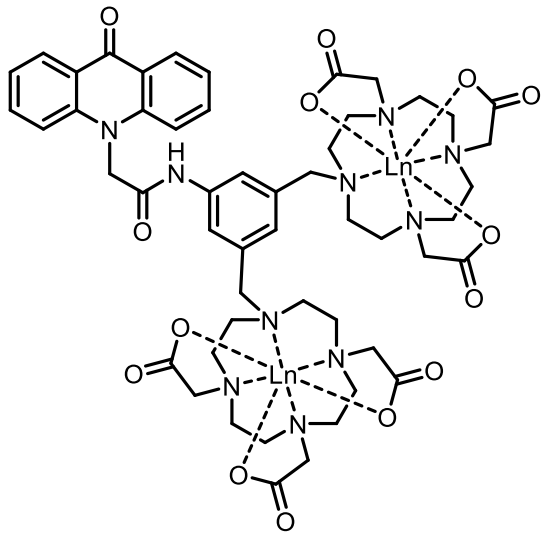
20

Trifluoroacetic acid (5 mL) was added dropwise to a stirred solution of **19** (258 mg, 0.187 mmol) in dichloromethane (5 mL) at room temperature. The reaction mixture was stirred at room temperature for 48 hours. The volatile components were removed under reduced pressure. The crude mixture was dissolved in methanol and then evaporated to dryness under reduced pressure in order to remove residual trifluoroacetic acid. This process was repeated three times. The crude product was dissolved in the minimum

amount of methanol, and diethyl ether added, causing the product to precipitate out. The diethyl ether was decanted off, and further diethyl ether added and the process repeated. The product was dried under reduced pressure to yield a cream solid.

Yield: 148 mg, 76%. ^{1}H NMR (MeOD, 400 MHz) δ (ppm) 8.65 – 6.85 (11H, br. m, ArH), 4.65 – 2.24 (50H, br. m, NCH_2). ES^+ MS (*m*/*z*) 1045.58 ($[M + H]^+$), 523.28 ($[M + 2H]^{2+}$). IR-ATR *v* (cm^{-1}) 1609-1721 (C=O).

_N_-(*α*,*α*'-bis(Ln.DO3A)-3,5-dimethylphenyl)-9-oxo-10(9*H*)-acridineacetamide (Ln_2.**20)**



Ln_2.**20**

Ln = Eu, Tb

20 (20 mg, 0.019 mmol) and the appropriate lanthanide triflate (0.39 mmol) were dissolved in methanol (2 mL) and adjusted to pH 5 by dropwise addition of aqueous sodium hydroxide (1.0 M). The reaction mixture was heated under reflux at 60°C with stirring for 3 days, then cooled to room temperature and the methanol removed under reduced pressure. The resulting suspension was dissolved in the minimum amount of water and adjusted to pH 10 by dropwise addition of aqueous sodium hydroxide (1.0 M).

The resulting suspension was centrifuged and the supernatant filtered through an Acrodisc® syringe filter (0.2 μm). The filtrate was neutralised to pH 7 by dropwise addition of aqueous hydrochloric acid (1.0 M) and the water removed under reduced pressure. Remaining water was removed in a desiccator. These compounds were used without dialysis.

Eu_2.**20**: MALDI-TOF HRMS (*m*/*z*) 1343 ($[M + H]^+$). UV-vis (H_2O) λ (I/I_{max}) 206 (1.00), 253 (0.61), 320 (0.11), 400 (0.08) nm. Excitation at 405 nm sensitises europium. q = 1.2.

Tb_2.**20**: ^1H NMR peaks too broad to observe. MALDI-TOF HRMS (*m*/*z*) 1357 ($[M + H]^+$). UV-vis (H_2O) λ (I/I_{max}) 207 (1.00), 252 (0.60), 318 (0.10), 400 (0.08) nm. Excitation at 405 nm sensitises terbium. q = 1.2.

12.3 Isothermal titration calorimetry

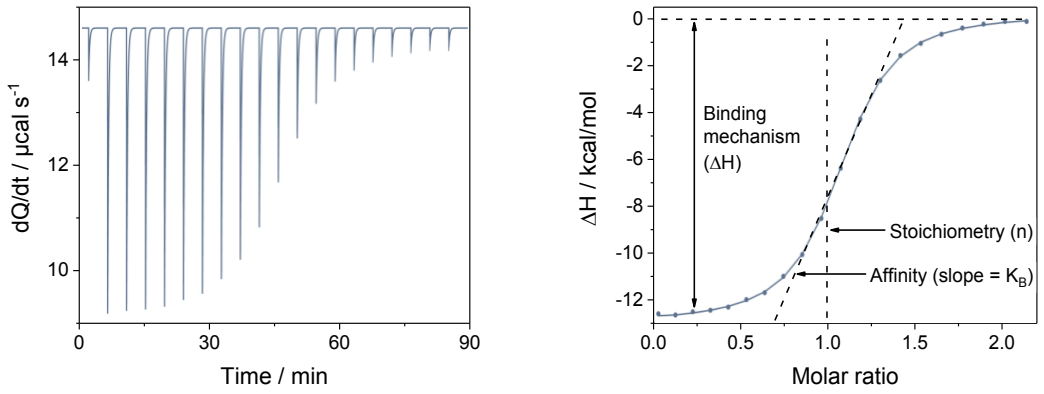


Figure 12.1 Theoretical example of ITC output (left) and interpretation of ITC data (right)

In isothermal titration calorimetry (ITC) the energy change associated with the binding event is obtained directly by monitoring the energy input required to maintain a constant solution temperature upon addition of one species to another, and comparing this to the energy input required by a reference cell containing a solution with the same heat capacity – for example, when performing titrations in an aqueous buffer, the reference cell should contain water. This is also compared to the data obtained from the heat of dilution when pure solvent or buffer is added to the host solution, and, more importantly, when the guest solution is added to buffer, as this is a greater proportional change in concentration. Additionally, the heat generated by the rotation of the stirrer should be accounted for, and so the data may be supplemented with information from the addition of buffer to buffer, however this is often already accounted for by the guest into buffer addition. When all these factors are considered, ITC measurements provide direct access to the free energy change associated with binding. This enables determination of binding constants, stoichiometry (and therefore provides an indication of the binding mode), enthalpy, and entropy. The value for the enthalpy is obtained from the height of the curve as shown in Figure 12.1, and once the binding constant has been calculated from the slope of this curve, the entropy data may then be extracted using Equation 12.1 overleaf.

$$\Delta H - T\Delta S = -RTln(K)$$

Equation 12.1 Combination of equations related to the Gibbs free energy, where ΔH is the change in enthalpy, T is the temperature in Kelvin, ΔS is the change in entropy, R is the gas constant 8.314 J K^{-1} mol^{-1}, and K is the binding constant

12.4 Luminescence titrations

Luminescence titrations and luminescence lifetimes of europium and terbium complexes were studied using a HORIBA FluoroLog-3 and the data processed with FluorEssence™, OriginLab Origin®, Microsoft Excel, and DynaFit® software.

Analyte stock solutions (~3×10^{-4} M) of the host complex were made up with methanol or 3:1 MeOH:H_2O or aqueous buffer solutions and the pH adjusted with a Hanna benchtop pH meter (±0.01 pH units) with microlitres of concentrated $HCl_{(aq)}$ or $NaOH_{(aq)}$. Titrant stock solutions (~1.5×10^{-2} M) of the guest anion were made using the analyte stock solution as the solvent, ensuring that the analyte concentration was kept constant so that the luminescence intensity was not altered by dilution. All solids for the solutions were weighed out on a balance (±0.01 mg). Titrations were repeated up to five times and different batches of host complex were used.

Typically, 1.00 mL of the analyte stock solution was added to the cuvette with a volume-displacement micropipette.

During the titration, successive emission spectra were recorded as 2 to 100 μL aliquots of the titrant stock solution were added using a volume-displacement micropipette.

Typical settings were:

Excitation wavelength:	direct excitation:	394 nm (europium complexes)
		366 nm (terbium complexes)
	antenna excitation:	single wavelength chosen between 245 nm and 405 nm, dependent on the identity of the ligand
Excitation slit width:	14 nm	
Emission wavelengths:	550 nm to 750 nm (europium complexes)	
	400 nm to 750 nm (terbium complexes)	
Emission slit width:	1 nm to 4 nm	

Titrations were mainly performed in phosphorescence (delayed luminescence) mode in order to reduce background signal interference from the decay of the organic chromophore excited state.

These settings were typically:

Flash delay:	0.1 ms
Sample window:	0.2 ms
Time per flash:	41 ms
Flash count:	10
	averaged over 3 to 5 scans

Fluorescence (luminescence with no additional delay time) titrations with europium complexes as the analyte used an emission filter to remove wavelengths of 495 nm and below, those with terbium complexes used a 400 nm filter.

An excitation spectrum was recorded for the initial analyte stock solution before commencing the titration, and another for the final post-titration solution in the cuvette after completing the titration. Typical slit widths and delay times would be the same as for the emission spectra, and:

Excitation wavelengths:	200 nm to 500 nm
Emission wavelength:	616 nm (europium complexes)
	544 nm (terbium complexes)

A decay-by-delay luminescence spectrum was also taken for the same solutions in order to calculate the luminescence lifetimes. In decay-by-delay experiments the sample was excited at a particular wavelength and the emission intensity at a particular wavelength observed over time. The emission intensity was plotted against time and the decay curve fitted to an exponential function, in order to give a τ_1 lifetime, and in some cases also a τ_2 lifetime.

Typical settings here would be:

Excitation slit:	14 nm
Emission slit:	5 nm
Excitation wavelength:	optimum for the lanthanide or the chromophore
Emission wavelength:	that of the most intense peak on the lanthanide emission spectrum:
	616 nm (europium complexes)
	544 nm (terbium complexes)

Titrations were carried out at room temperature, other than those in the thermodynamic studies in Chapter 2 which were conducted on a temperature-controlled stage at a constant temperature of 10, 20, 30, or 40°C. All solutions were allowed to equilibrate to room

temperature before use, and the additions of small volume aliquots (2 to 100 μL) to the bulk solution in the cuvette (at least 1.0 mL) would give a negligible, if any, change in temperature.

12.5 Data processing and fitting

12.5.1 Luminescence titrations

The luminescence titration data was fitted to give a binding constant with the iterative least-squares fitting software DynaFit®,[7] which is able to derive the mathematical models for the binding mechanism. The major benefit of using DynaFit® is that the mechanism may be inputted symbolically, avoiding the necessity for the user to solve long complicated equations such as Wang's equation[8] or combinations of differential equations.

DynaFit® uses the relationship between emission intensity and concentration of chemical species in the titration solution in order to generate a binding constant from the change in emission intensity over the course of a titration.

The raw data from the fluorimeter had to be converted to a suitable format for DynaFit®.

Initially, data was processed manually, until later an Excel file was created to automate this. Processing involved integrating the intensity of peaks (by summing over the wavelength range of each peak) in the emission spectra and calculating responses, which are the numerical relationship between emission intensity and concentration of species. The response of the host complex was calculated from the emission intensity at the start of the titration, and the response of the fully bound assembled adduct was estimated from the intensity at the plateau of the binding isotherm or at the titration endpoint. These, along with necessary concentration and binding model information, were then inserted into a script

written in a format suitable for DynaFit®. The concentrations may be floated for analyte/host but not for titrant/guest. The responses may be floated.

The fluorimeter recorded data in a format suitable for Origin. This intensity vs. wavelength data was copied into the custom Excel file, and information on the identity and concentrations of the species in the titration was added. The Excel file integrated peaks and calculated responses for europium or terbium complexes, and then from this generated the script for DynaFit®. This Excel file also generated Stern-Volmer plots. This was subsequently automated further by writing a macro to output the script as a text file in an appropriate directory at the click of a button, which could be opened directly by DynaFit®. This saved time (10 minutes of data processing per titration – from raw data to script file – was reduced to less than 30 seconds per titration) as well as removed the opportunity for human error in data processing. The form of parts of the Excel file is shown in Figure 12.2, Figure 12.3, and Figure 12.4, and the macro shown in Figure 12.5. An excerpt from an example DynaFit® input script is shown in Figure 12.6. An example of the binding constant data output is shown in Figure 12.7, and the associated fitted output isotherms in Figure 12.8.

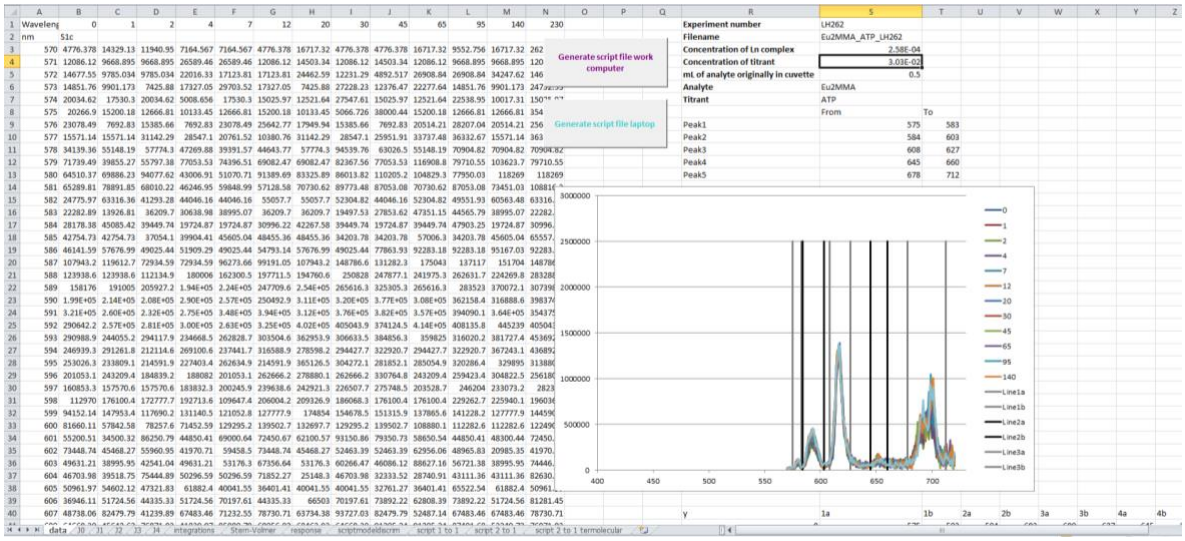


Figure 12.2 Excel file for processing data, including a tab for automatic generation of a Stern-Volmer plot

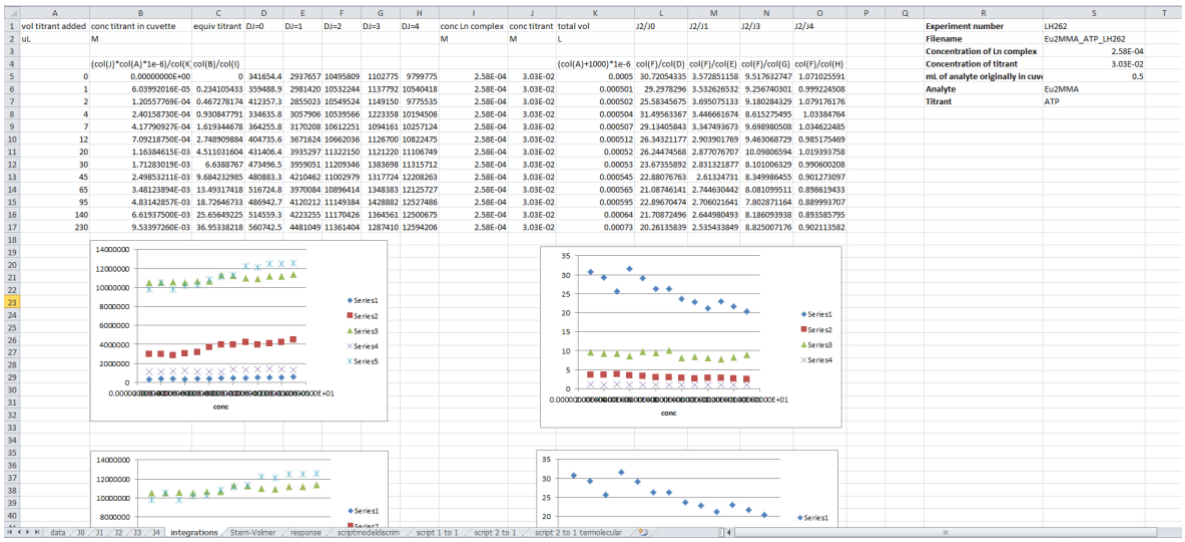


Figure 12.3 Excel file for processing data, showing integrated peak emission intensity

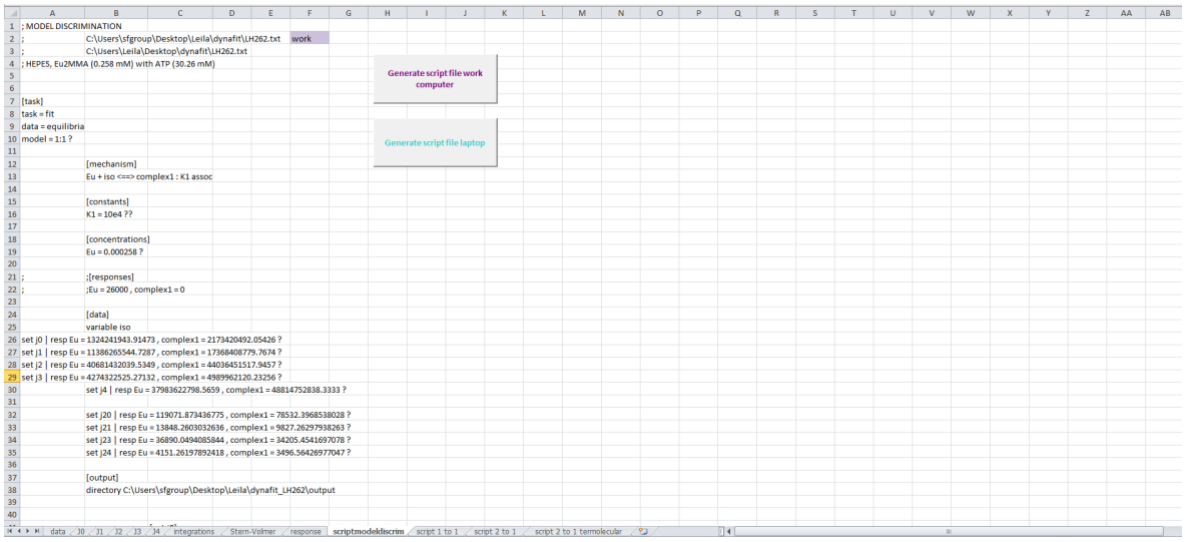


Figure 12.4 Excel file for processing data

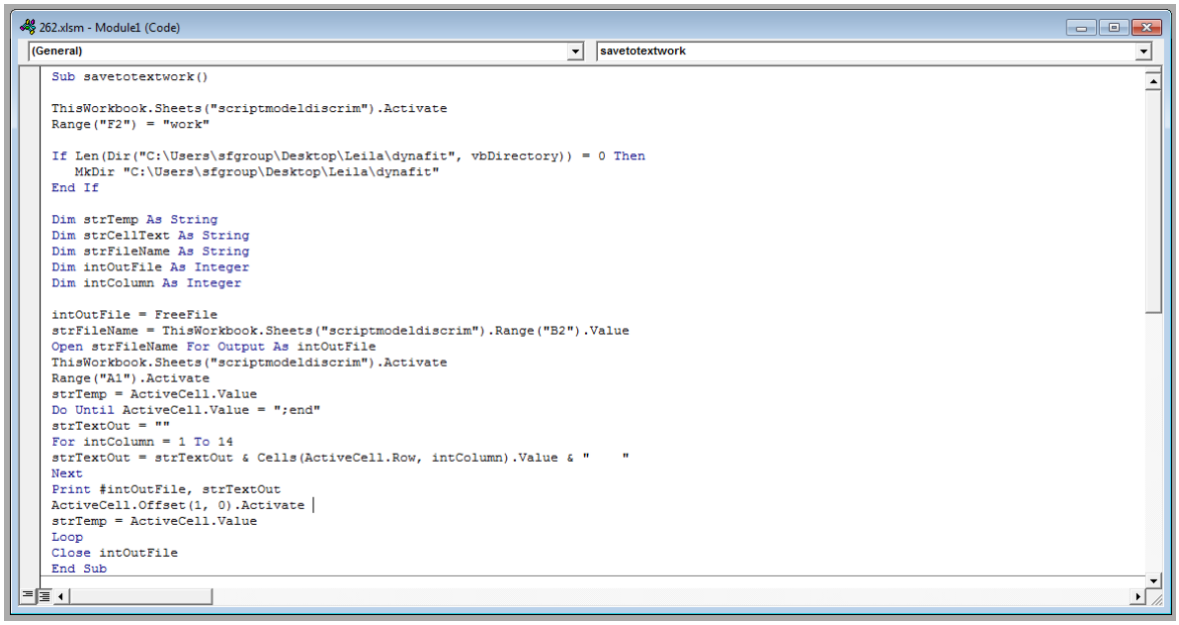


Figure 12.5 Macro for creating script file

Script

Input Script

```
; MODEL DISCRIMINATION
;    C:\Users\sfgroup\Desktop\Leila\dynafit\LH262.txt
;    C:\Users\Leila\Desktop\dynafit\LH262.txt
; HEPES, Eu2MMA (0.258 mM) with ATP (30.26 mM)


[task]
task = fit
data = equilibria
model = 1:1 ?

    [mechanism]
    Eu + iso <==> complex1 : K1 assoc

    [constants]
    K1 = 10e4 ??

    [concentrations]
    Eu = 0.000258

;    ;[responses]
;    ;Eu = 26000 , complex1 = 0

    [data]
    variable iso
set j0 | resp Eu = 1324241943.91473 , complex1 = 2173420492.05426 ?
set j1 | resp Eu = 11386265544.7287 , complex1 = 17368408779.7674 ?
set j2 | resp Eu = 40681432039.5349 , complex1 = 44036451517.9457 ?
set j3 | resp Eu = 4274322525.27132 , complex1 = 4989962120.23256 ?
     set j4 | resp Eu = 37983622798.5659 , complex1 = 48814752838.333

     set j20 | resp Eu = 119071.873436775 , complex1 = 78532.39685380
     set j21 | resp Eu = 13848.2603032636 , complex1 = 9827.262979382
     set j23 | resp Eu = 36890.0494085844 , complex1 = 34205.45416970
     set j24 | resp Eu = 4151.26197892418 , complex1 = 3496.564269770

    [output]
    directory C:\Users\sfgroup\Desktop\Leila\dynafit_LH262\output


        [set:j0]
         0    341654.42153
         6.03992015968064E-05    359488.86728
         1.20557768924303E-04    412357.25766
         2.40158730158730E-04    334635.78645
         4.17790927021696E-04    364255.83143
         0.00070921875    404735.63194
         1.16384615384615E-03    431406.36922
         1.71283018867925E-03    473496.46415
         2.49853211009174E-03    480883.28152
         3.48123893805310E-03    516724.80345
         4.83142857142857E-03    486942.71726
         0.006619375    514559.28097
         9.53397260273972E-03    560742.48695




        [set:j1]
         0    2837656.51054
```

Figure 12.6 Excerpt from a DynaFit® input script

Parameters

Marquardt Minimization Algorithm

Optimized Parameters

No.	Par#Set	Initial	Final	Std. Error	CV (%)	Low	Low P (%)	High	High P (%)	Note
#1	K1	100000	**729.866**	79.937	10.95	662.872	95	804.114	95	
#2	r(complex1)#1	2.17342e+009	**2.18782e+009**	2.38484e+008	10.90					
#3	r(complex1)#2	1.73684e+010	**1.80277e+010**	3.09627e+008	1.72					
#4	r(complex1)#3	4.40365e+010	**4.42036e+010**	2.59538e+008	0.59					
#5	r(complex1)#4	4.98996e+009	**5.49153e+009**	2.39868e+008	4.37					
#6	r(complex1)#5	4.88148e+010	**5.07901e+010**	4.51319e+008	0.89					
#7	r(complex1)#6	78532.4	**73428.4**	2.37074e+008	322864.30					
#8	r(complex1)#7	9827.26	**8971.5**	2.37074e+008	2642523.06					
#9	r(complex1)#8	34205.5	**31017.8**	2.37074e+008	764315.54					
#10	r(complex1)#9	3496.56	**3316.79**	2.37074e+008	7147687.20					

All Model Parameters

Optimized *and* fixed model parameters: [TAB-DELIMITED TEXT]

100 × Correlation Matrix

No.	Par#Set	#1	#2	#3	#4	#5	#6	#7	#8	#9	#10
#1	K1	*	-11	-64	-41	-15	-85	0	0	0	0
#2	r(complex1)#1	-11	*	7	4	2	9	-0	-0	-0	-0
#3	r(complex1)#2	-64	7	*	26	10	55	-0	-0	-0	-0
#4	r(complex1)#3	-41	4	26	*	6	35	-0	-0	-0	-0
#5	r(complex1)#4	-15	2	10	6	*	13	-0	-0	-0	-0
#6	r(complex1)#5	-85	9	55	35	13	*	-0	-0	-0	-0
#7	r(complex1)#6	0	-0	-0	-0	-0	-0	*	0	0	0
#8	r(complex1)#7	0	-0	-0	-0	-0	-0	0	*	0	0
#9	r(complex1)#8	0	-0	-0	-0	-0	-0	0	0	*	0
#10	r(complex1)#9	0	-0	-0	-0	-0	-0	0	0	0	*

Condition Indices and Redundancy Matrix

No.	Par#Set	1.2	0.3	0.3	0.3	0.3	0.3	0.3	0.3	0.3	0.0
#1	K1	50	0	0	0	0	0	0	0	0	50
#2	r(complex1)#1	0	99	0	0	0	0	0	0	0	0

Figure 12.7 Example DynaFit® data output of binding constant and other parameters

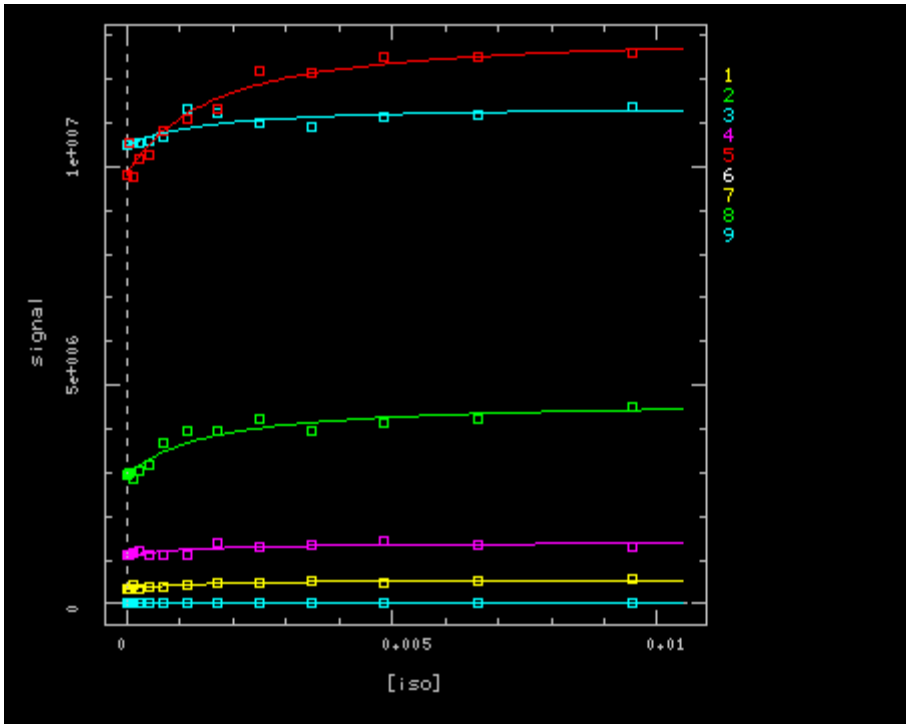


Figure 12.8 Example fitted binding isotherm output from DynaFit®

DynaFit® was able to test which model statistically fitted the data best.[9] The models considered were 1:1 binding (guest bridging the two lanthanide centres, or binding to one centre and blocking approach to the other centre), 2:1 binding (each lanthanide centre binds to a guest, as shown schematically in Figure 12.9), and termolecular 2:1 binding (simultaneous binding of each lanthanide centre to a guest – this is physically unlikely in solution but if DynaFit® was unable to separate the two binding constants for each binding event, this gave an overall binding constant $K_{tot} = K_1.K_2$ for 2:1 binding).

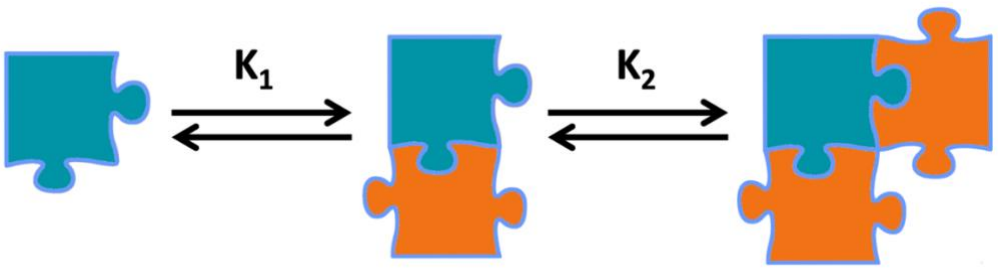


Figure 12.9 Stepwise 2:1 binding

This stepwise 2:1 binding would be represented as follows in Figure 12.10.

```
[mechanism]
host + guest <==> complex1 : K1 assoc
complex1 + guest <==> complex2 : K2 assoc
```

Figure 12.10 Scripting for stepwise 2:1 binding

An example output from model discrimination analysis is given in Figure 12.11.

Model discrimination analysis

Number of data points = 117

Minimum sum of squares = 1.42961e+012

	model	n_p	SS_{rel}	AIC	$w^{(AIC)}$	BIC	$w^{(BIC)}$
[1]	1:1	10	1.000	2742.0	0.999	2772.4	0.999
[2]	2:1	11	1.131	2758.9	0.000	2792.0	0.000
[3]	termolecular 2:1	10	1.131	2756.4	0.001	2786.8	0.001

Figure 12.11 Typical output for model discrimination with DynaFit®. In the example shown, it is clear that 1:1 binding is statistically favoured[9]

12.5.2 NMR titrations

Fitting for NMR titrations required a somewhat different process. Chemical shift is an intensive property, related to mole fraction, rather than an extensive property as with emission counts per second which are related to the number of molecules in solution. Therefore the scripting commands required were different, as shown in Figure 12.12. The chemical shift, in ppm, was determined for each titration point and this used to generate the concentration vs observed variable (chemical shift) file. The titrations were carried out with increasing concentration of host complex affecting the ^{31}P shift of the phosphate guest. If this gave a poor fit, the data was inverted to give the change in equivalents of anionic guest species as the independent variable and responses adjusted accordingly. This gave a more familiar curve form to the binding isotherm.

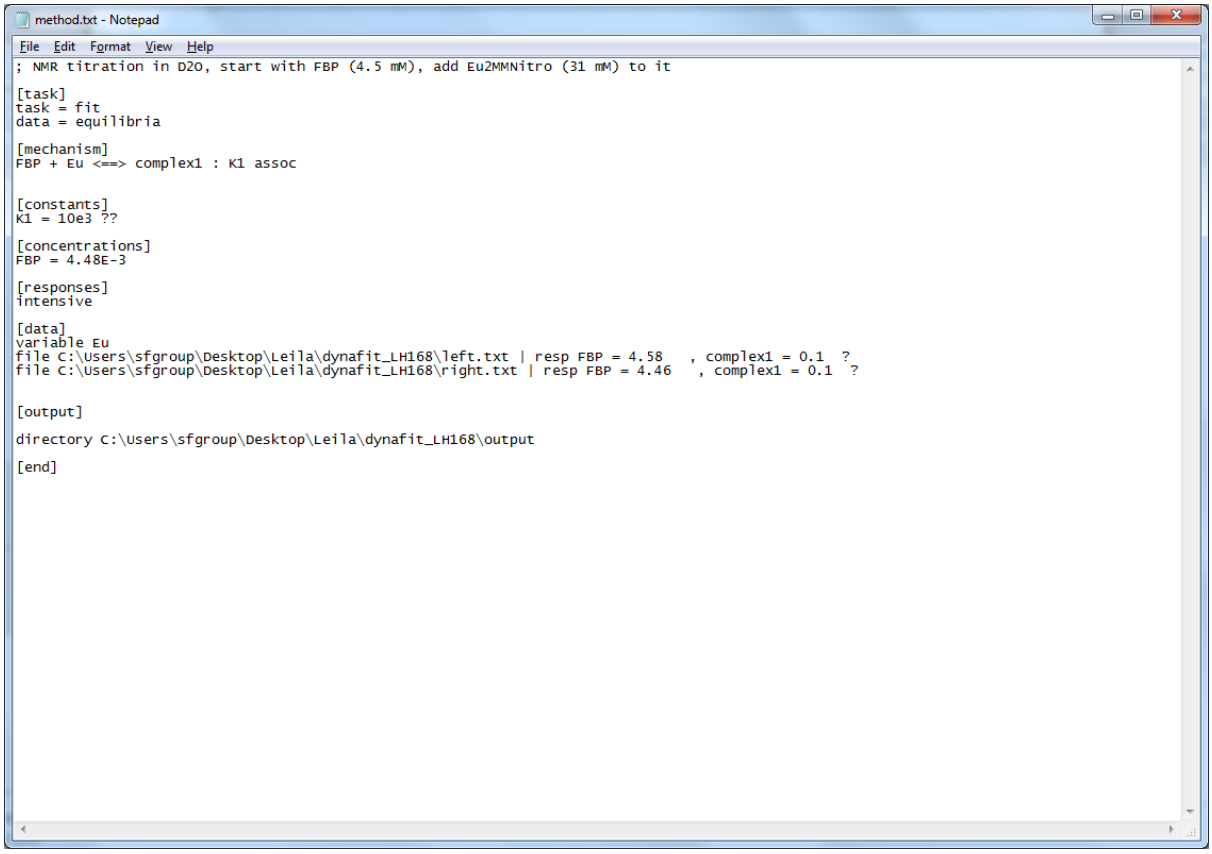


Figure 12.12 Example input script for DynaFit® fitting of NMR data

12.6 Degassed measurements

The oxygen-dependence of spectra, as discussed in Chapter 1 and Chapter 6 was investigated by comparing spectra of degassed solutions with those of the same solutions but with ambient concentrations of atmospheric gases. In this case degassing refers to removal of oxygen. Solutions were degassed with between three and five freeze-pump-thaw cycles in a custom-made airtight cuvette with a Young's tap and a reservoir.

Subsequent aeration of these samples for later measurements was achieved by opening the Young's tap and shaking the sample to allow ambient air to access and dissolve in the solution.

12.7 References

(1) Dadabhoy, A.; Faulkner, S.; Sammes, P. G. *J. Chem. Soc., Perkin Trans. 2* **2002**, 348–357.
(2) Chhikara, B. S.; Kumar, N.; Tandon, V.; Mishra, A. K. *Bioorg. Med. Chem.* **2005**, *13*, 4713–4720.
(3) Placidi, M. P.; Natrajan, L. S.; Sykes, D.; Kenwright, A. M.; Faulkner, S. *Helv. Chim. Acta* **2009**, *92*, 2427–2438.
(4) Karhunen, U.; Rosenberg, J.; Lamminmäki, U.; Soukka, T. *Anal. Chem.* **2011**, *83*, 9011–9016.
(5) Jauregui, M.; Perry, W. S.; Allain, C.; Vidler, L. R.; Willis, M. C.; Kenwright, A. M.; Snaith, J. S.; Stasiuk, G. J.; Lowe, M. P.; Faulkner, S. *Dalton Trans.* **2009**, 6283–6285.
(6) David-Cordonnier, M.-H.; Hildebrand, M.-P.; Baldeyrou, B.; Lansiaux, A.; Keuser, C.; Benzschawel, K.; Lemster, T.; Pindur, U. *Eur. J. Med. Chem.* **2007**, *42*, 752–771.
(7) Kuzmič, P. *Anal. Biochem.* **1996**, *237*, 260–273.
(8) Wang, Z.-X. *FEBS Lett.* **1995**, *360*, 111–114.
(9) Gasa, T. B.; Spruell, J. M.; Dichtel, W. R.; Sørensen, T. J.; Philp, D.; Stoddart, J. F.; Kuzmic, P. *Chem. Eur. J.* **2009**, *15*, 106–116.

Appendix A Molecular structures of hosts and guests

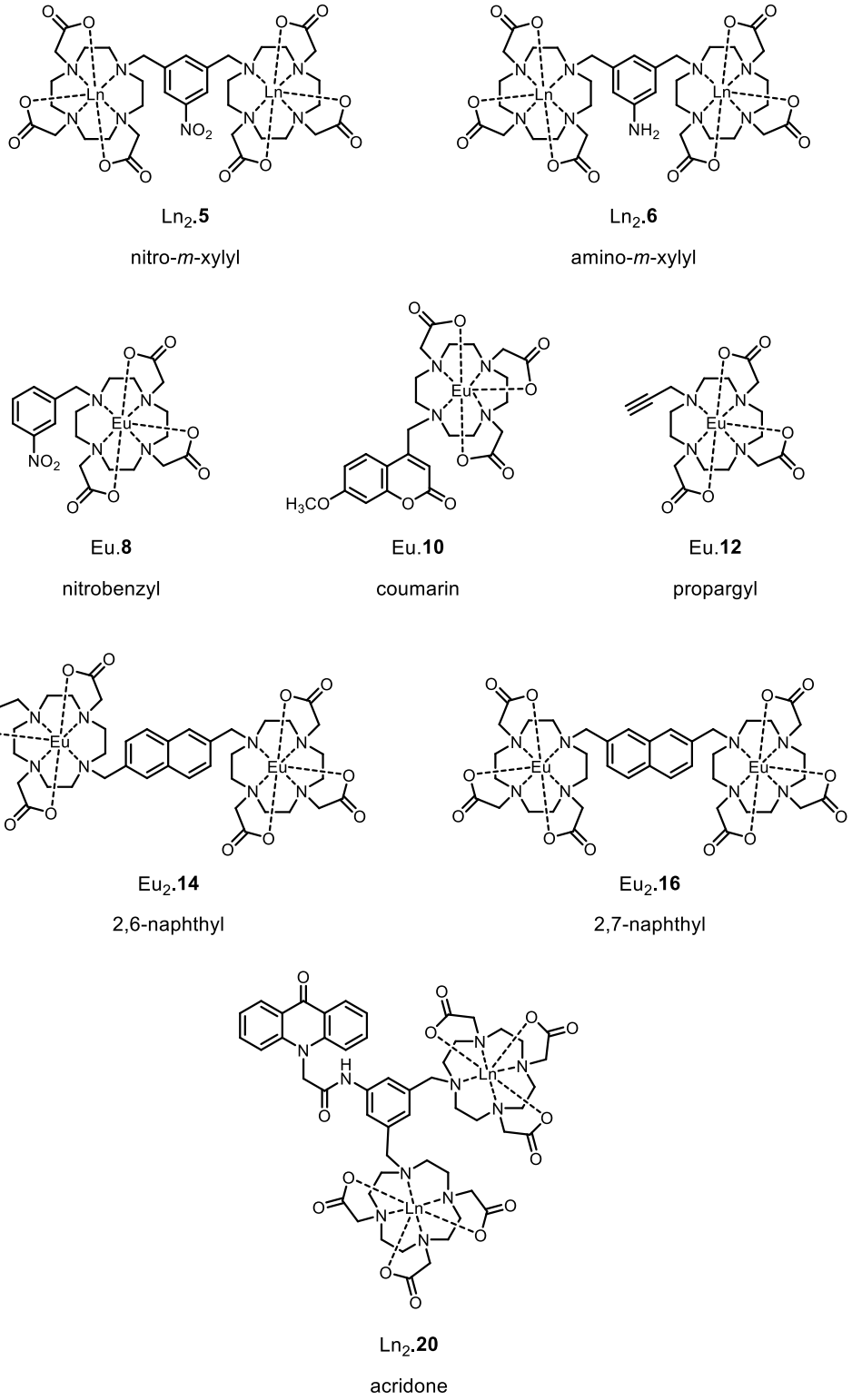


Figure A.1 Host lanthanide complexes

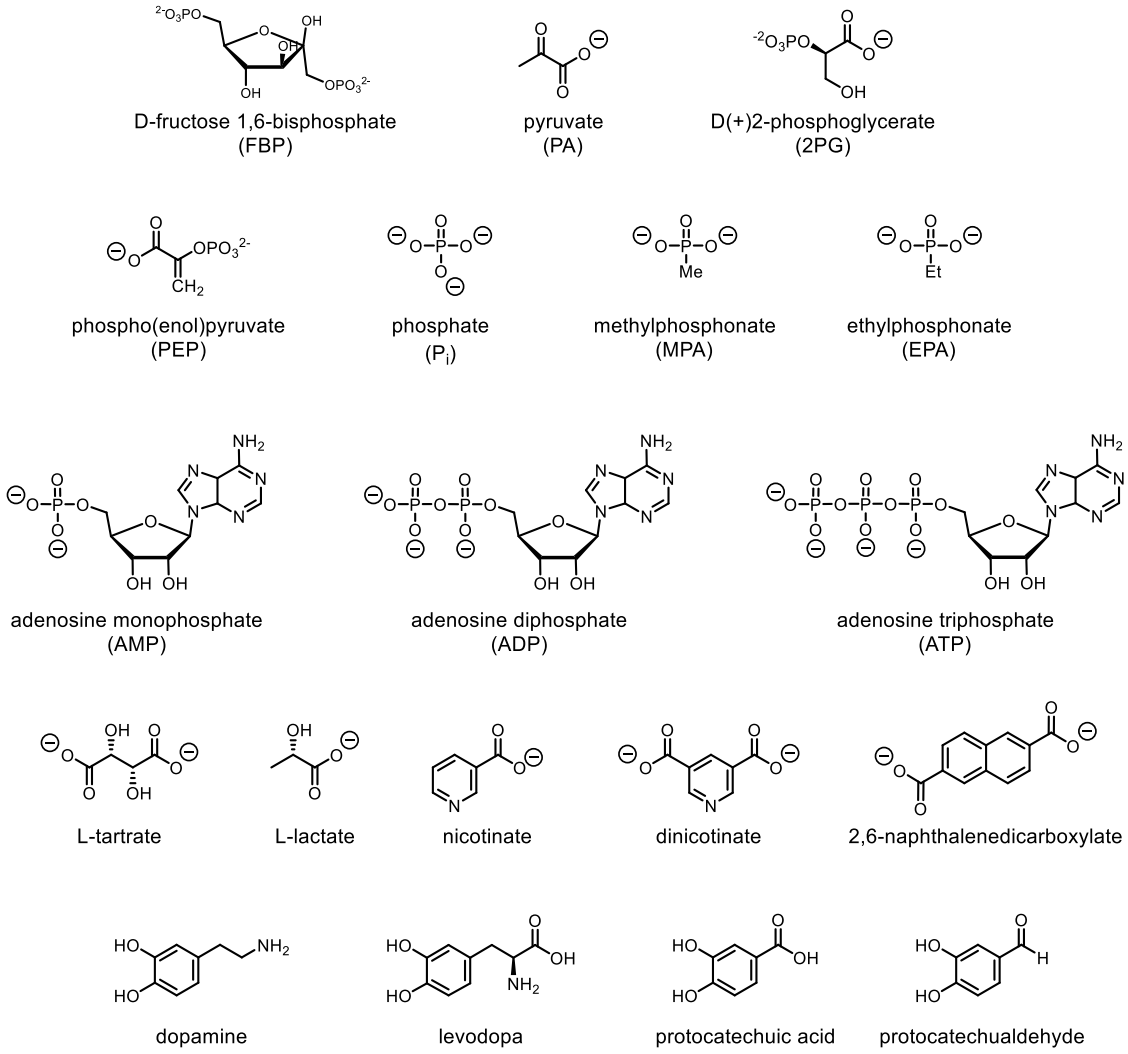


Figure A.2 Guest species used in titrations

Appendix B NMR spectra from catechol binding studies

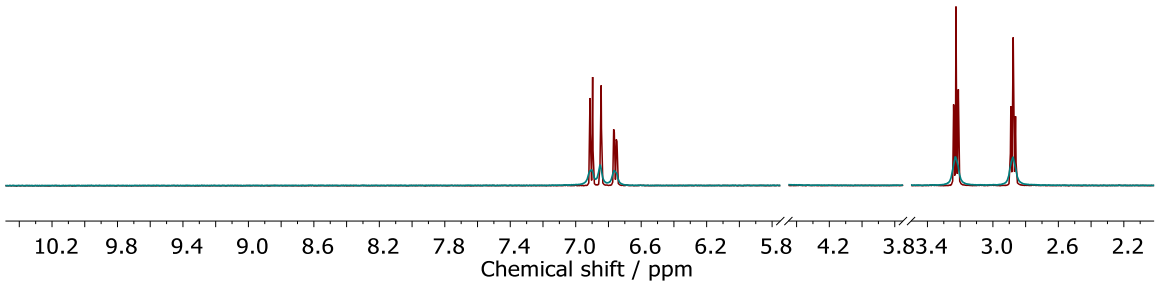


*Figure B.1 ^{1}H NMR spectra of dopamine alone (maroon) and with Eu_2.**5** (teal) in D_2O*

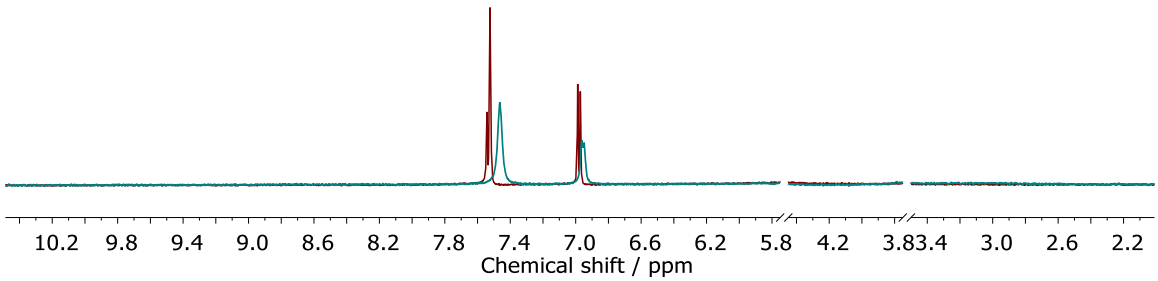


*Figure B.2 ^{1}H NMR spectra of protocatechuic acid alone (maroon) and with Eu_2.**5** (teal) in D_2O*

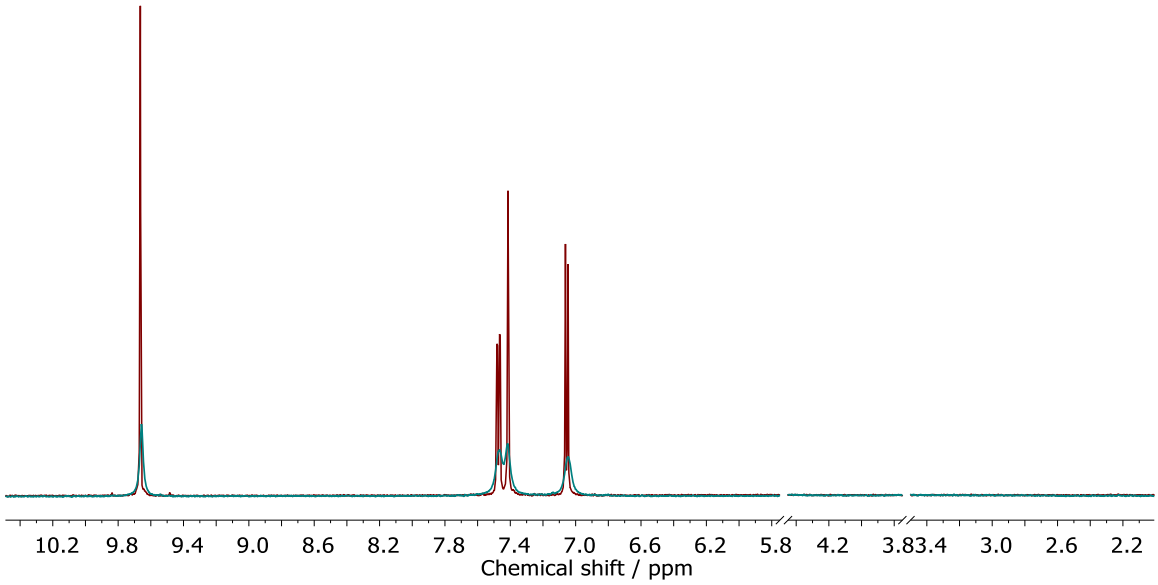


*Figure B.3 ^{1}H NMR spectra of protocatechualdehyde alone (maroon) and with Eu_2.**5** (teal) in D_2O*

Appendix C X-ray crystallographic data

X-ray crystallographic data was measured and processed by Dr Amber L. Thompson and Dr Kirsten E. Christensen of the University of Oxford Chemical Crystallography Service. The cif files are also supplied as an electronic appendix.

C.1 3,5-bis(bromomethyl)nitrobenzene (2)

Crystals suitable for X-ray diffraction were obtained by slow evaporation of a concentrated solution of the product in $CDCl_3$.

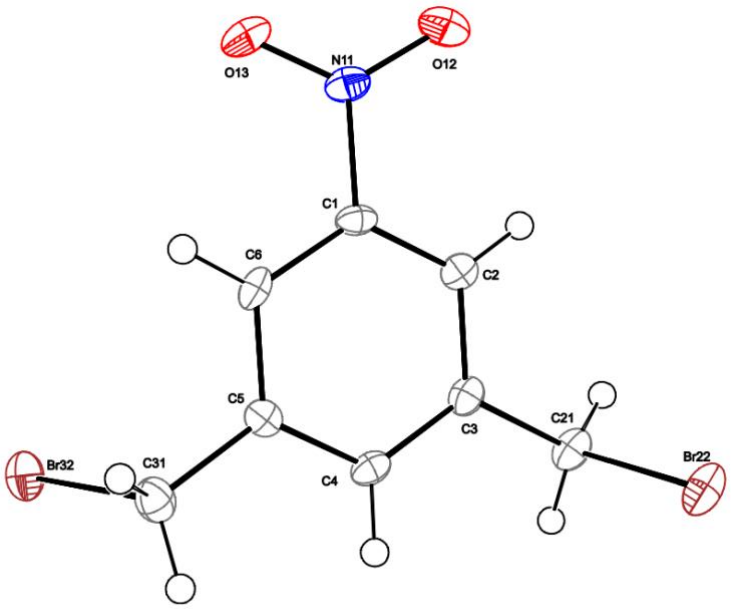


*Figure C.1.1 Structure of **2** determined by X-ray diffraction showing thermal ellipsoids at 50% probability*

*Table C.1.1 Crystal data and structure refinement for **2***

Identification code	**2**
Empirical formula	C8 H7 Br2 N1 O2
Formula weight	308.96 g mol^{-1}
Temperature	150 K

Wavelength	1.54184 Å	
Crystal system	Triclinic	
Space group	P -1	
Unit cell dimensions	a = 7.3523(6) Å	α = 61.910(12)°
	b = 8.649(1) Å	β = 72.110(9)°
	c = 9.0200(11) Å	γ = 78.298(9)°
Volume	480.39(11) $Å^3$	
Z	2	
Density (calculated)	2.136 Mg/m^3	
Absorption coefficient	10.452 mm^{-1}	
F(000)	296	
Crystal size	0.25 x 0.21 x 0.08 mm^3	
Theta range for data collection	5.735 to 75.919°	
Index ranges	$-8 \leq h \leq 9$, $-10 \leq k \leq 10$, $-8 \leq l \leq 11$	
Reflections collected	3783	
Independent reflections	1945 [R(int) = 0.025]	
Completeness to theta = 69.545°	98.5%	
Absorption correction	Semi-empirical from equivalents	
Max. and min. transmission	0.43 and 0.18	
Refinement method	Full-matrix least-squares on F^2	
Data / restraints / parameters	1635 / 0 / 118	
Goodness-of-fit on F^2	1.0268	
Final R indices [I>2sigma(I)]	R1 = 0.0323, wR2 = 0.0870	
R indices (all data)	R1 = 0.0337, wR2 = 0.0876	
Largest diff. peak and hole	0.97 and -0.78 $e.Å^{-3}$	

C.2 *α,α'*-bis(DO3A *tert*-butyl triester)-3,5-dimethylnitrobenzene (3)

Crystals suitable for X-ray diffraction were obtained by slow evaporation of a concentrated solution of the product in $CDCl_3$.

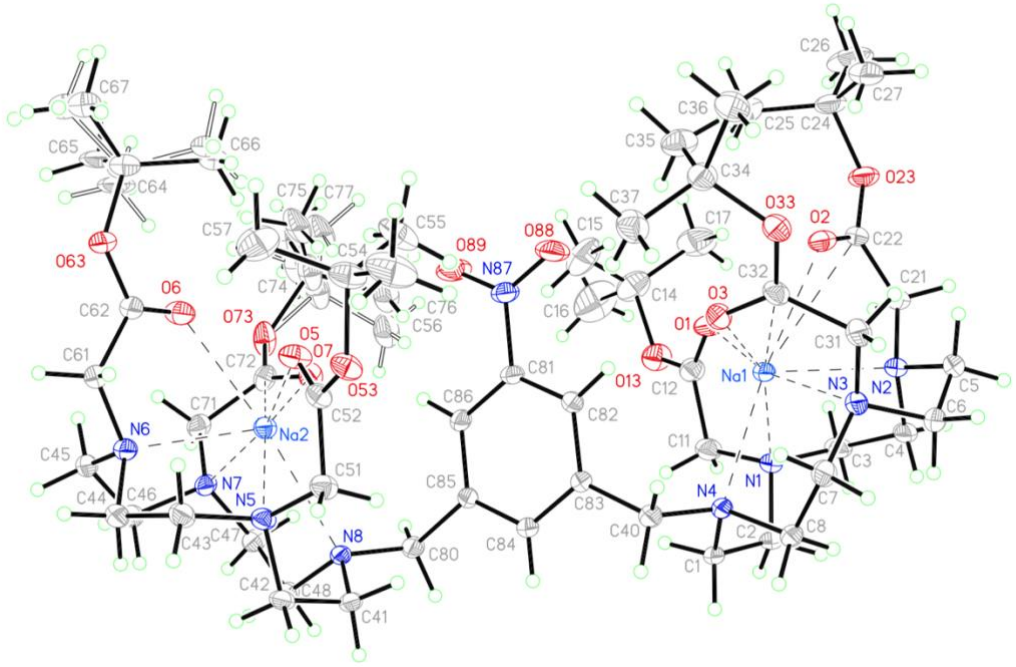


*Figure C.2.1 Structure of Na_2.**3** determined by X-ray diffraction showing thermal ellipsoids at 50% probability. Counteranions omitted for clarity*

*Table C.2.1 Crystal data and structure refinement for **3***

Identification code	**3**	
Empirical formula	C65.023 H110.023 Cl17.069 N9 Na2 O14	
Formula weight	1893.09 g mol^{-1}	
Temperature	150 K	
Wavelength	1.54180 Å	
Crystal system	Triclinic	
Space group	P -1	
Unit cell dimensions	a = 16.4090(8) Å	α = 72.850(3)°
	b = 17.2408(6) Å	β = 69.036(4)°

	c = 19.2281(7) Å γ = 81.112(3)°
Volume	4846.4(4) $Å^3$
Z	2
Density (calculated)	1.297 Mg/m^3
Absorption coefficient	4.974 mm^{-1}
F(000)	1974.689
Crystal size	0.52 x 0.50 x 0.32 mm^3
Theta range for data collection	2.548 to 76.328°
Index ranges	$-20 \leq h \leq 16$, $-21 \leq k \leq 21$, $-24 \leq l \leq 23$
Reflections collected	69583
Independent reflections	20035 [R(int) = 0.066]
Completeness to theta = 74.038°	99.6%
Absorption correction	Semi-empirical from equivalents
Max. and min. transmission	0.20 and 0.11
Refinement method	Full-matrix least-squares on F^2
Data / restraints / parameters	20034 / 1215 / 1123
Goodness-of-fit on F^2	0.9678
Final R indices [I>2sigma(I)]	R1 = 0.0726, wR2 = 0.1861
R indices (all data)	R1 = 0.0912, wR2 = 0.2075
Largest diff. peak and hole	1.46 and -1.08 $e.Å^{-3}$

C.3 (*E*)-1,2-bis(*α*,*α*'-bis(DO3A *tert*-butyl triester)-3,5-dimethylphenyl)diazene (4a)

Crystals suitable for X-ray diffraction were obtained by slow evaporation of a concentrated solution of the product in dichloromethane and methanol mixture.

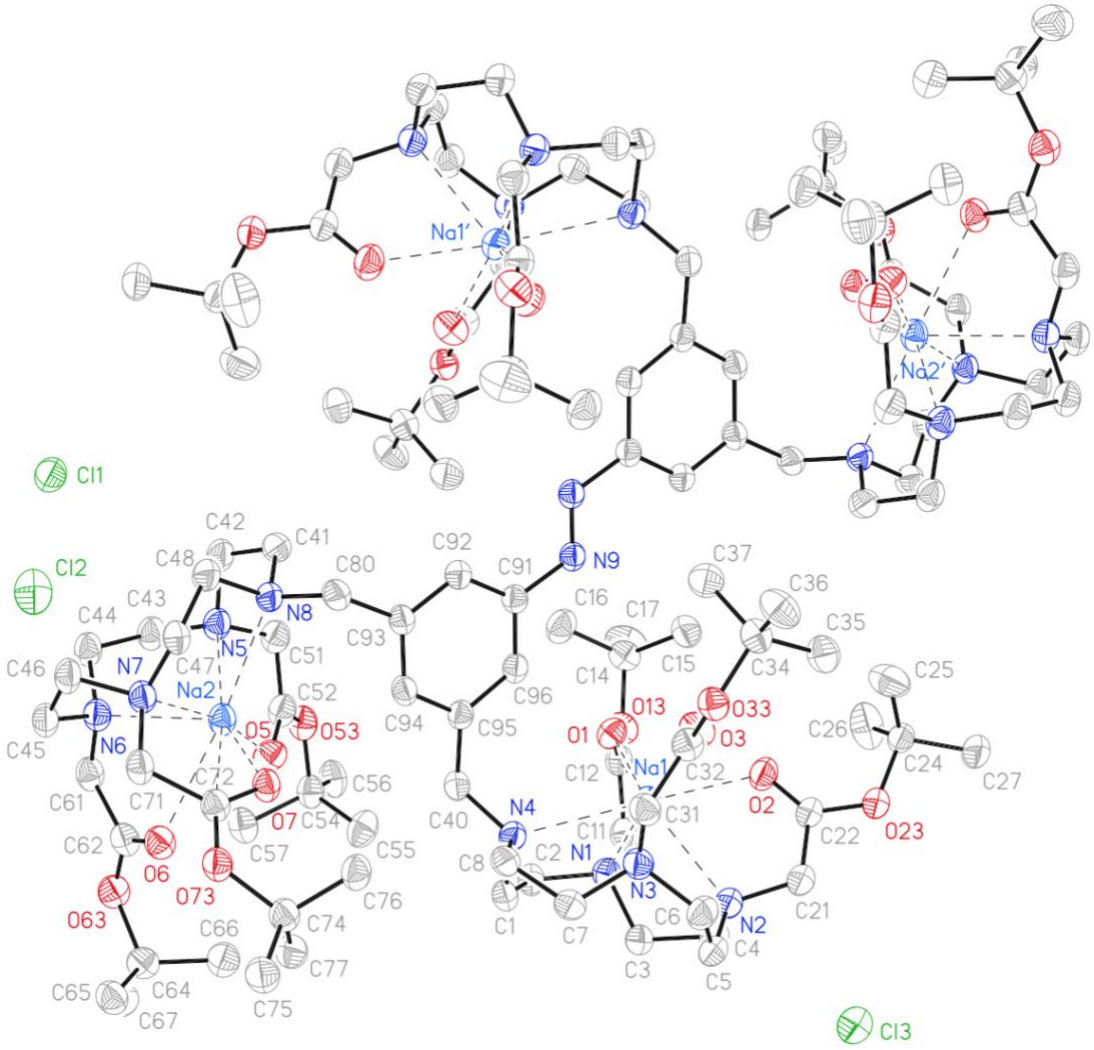


*Figure C.3.1 Structure of the diazo dimer Na_4.**4a** determined by X-ray diffraction showing thermal ellipsoids at 20% probability with hydrogen atoms and one counteranion omitted for clarity*

*Table C.3.1 Crystal data and structure refinement for **4a***

Identification code	**4a**	
Empirical formula	C120 H210 Cl4 N18 Na4 O24	
Formula weight	2522.86 g mol^{-1}	
Temperature	100 K	
Wavelength	0.68890 Å	
Crystal system	Monoclinic	
Space group	C 1 2/c 1	
Unit cell dimensions	a = 28.519(3) Å	α = 90°
	b = 34.363(4) Å	β = 123.965(7)°
	c = 21.107(2) Å	γ = 90°
Volume	17155(3) $Å^3$	
Z	4	
Density (calculated)	0.977 Mg/m^3	
Absorption coefficient	0.136 mm^{-1}	
F(000)	5440	
Crystal size	0.07 x 0.02 x 0.01 mm^3	
Theta range for data collection	1.013 to 36.214°	
Index ranges	$-46 \leq h \leq 39$, $-55 \leq k \leq 39$, $-33 \leq l \leq 34$	
Reflections collected	96911	
Independent reflections	39660 [R(int) = 0.210]	
Completeness to theta = 25.350°	98.1%	
Absorption correction	Empirical	
Max. and min. transmission	1.00 and 0.99	
Refinement method	Full-matrix least-squares on F^2	

Data / restraints / parameters	11698 / 0 / 775
Goodness-of-fit on F^2	0.9732
Final R indices [I>2sigma(I)]	R1 = 0.0816, wR2 = 0.2200
R indices (all data)	R1 = 0.1068, wR2 = 0.2701
Largest diff. peak and hole	0.45 and -0.54 e.$Å^{-3}$

C.4 *α*-(Eu.DO3A)-4-methyl-7-methoxycoumarin (Eu.10)

Crystals suitable for X-ray diffraction were obtained by slow evaporation of a concentrated solution of the product in D_2O.

Data collection revealed three different polymorphs: monoclinic, triclinic, and orthorhombic. All three polymorphs were tetrameric. In addition to the tetramer, developing the structure showed the presence of NaOTf and additional water molecules. For further details please see the supplementary information of *Dalton Trans.*, 2018, **47**, 4794-4803 (2018).

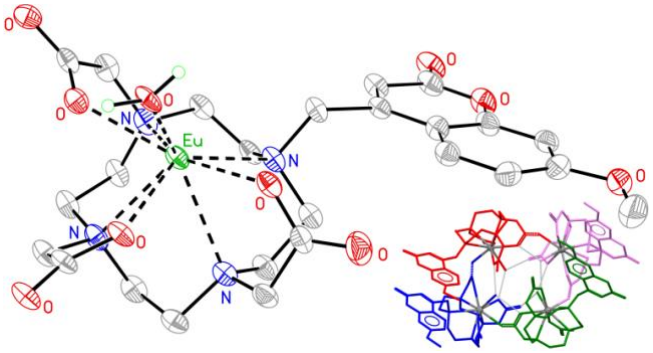


*Figure C.4.1 Displacement ellipsoid plot for the orthorhombic polymorph of Eu.**10** drawn at 20% probability. The main picture shows one formula unit with selected hydrogen atoms and sodium triflate omitted for clarity. In the solid state, Eu.**10** forms tetramers held together by hydrogen bonding between the apical water and ligand acetate moieties (shown inset), a feature seen in all three structures determined*

	Eu.10 Monoclinic	**Eu.10 Triclinic**	**Eu.10 Orthorhombic**
Data source	SuperNova	I19-1 at Diamond	XtaLAB Synergy
Crystal system	Monoclinic	Triclinic	Orthorhombic
Formula (excluding void)	$C_{100}H_{132}Eu_4N_{16}O_{40}$	$C_{100}H_{132}Eu_4N_{16}O_{40}$	$C_{100}H_{132}Eu_4N_{16}O_{40}$ ·NaOTf·H_2O
Cell a / Å	52.668(3)	17.4223(9)	17.9227(7)
Cell b / Å	18.1007(6)	25.1438(15)	32.9420(9)
Cell c / Å	32.7146(17)	33.2547(15)	47.9786(16)
Cell α / °	90	106.177(5)	90
Cell β / °	106.632(6)	90.802(5)	90
Cell γ / °	90	102.807(5)	90
Cell Volume / $Å^3$	29883(3)	13598.1(13)	28326.9(16)
Space group	P2/c	P1	Pcan
Collection temperature / K	150	100	90
Crystal size / mm	0.10 × 0.22 × 0.40	0.05 × 0.10 × 0.15	0.040 × 0.085 × 0.085
Crystal colour	colourless	colourless	colourless
Z	8	4	8
Z’	2	2	1
λ / Å	1.54184	0.6889	1.54184
Data / restraints / parameters	15564/8786/2881	14186/8786/2881	27811/4401/1525
Void as a % of unit cell	32.0	24.5	24.2
Δρ(min, max) / $e.Å^{-3}$	-1.14, 2.75	-1.87, 4.21	-5.30, 8.30
R_1 [I > 2σ(I)]	0.1773	0.1613	0.1745
wR_2 [I > 2σ(I)]	0.2135	0.1774	0.4583
Goodness of fit	1.1332	1.1658	0.9996

Table C.4.1 Selected statistics for the data collections and final refinements

C.4.1 Monoclinic

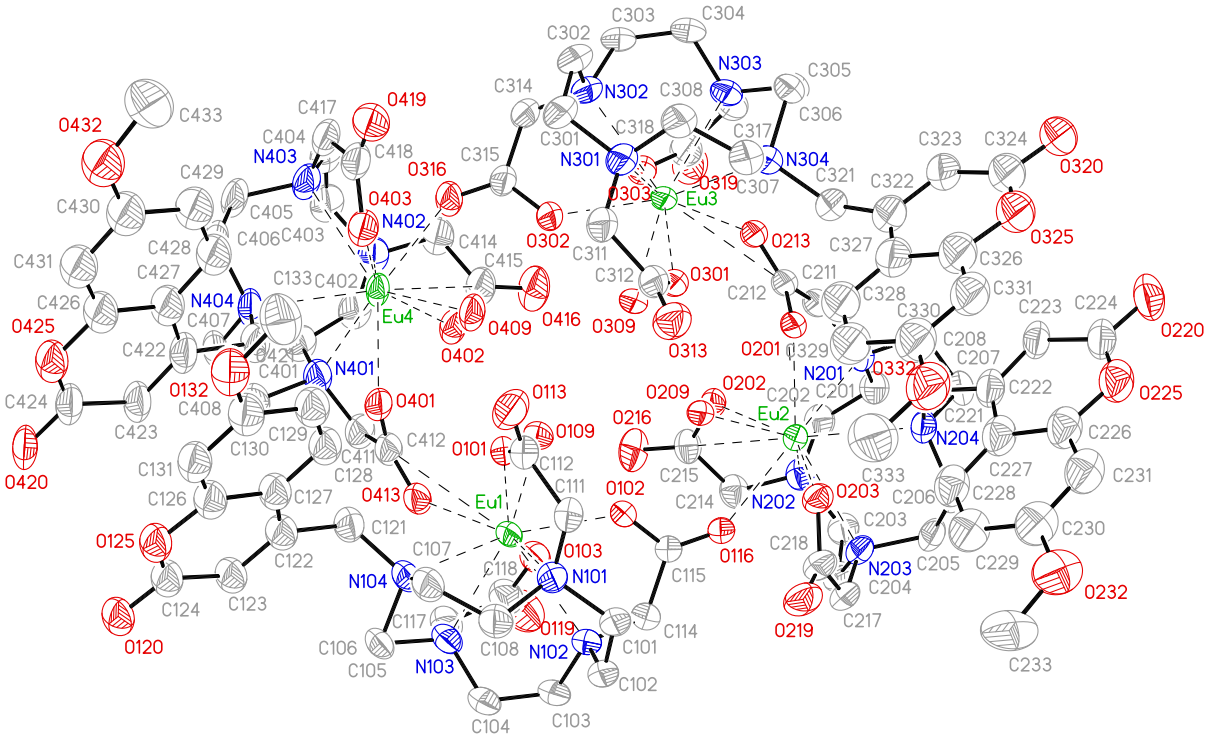


*Figure C.4.1.1 Monoclinic structure of Eu.**10** determined by X-ray diffraction. The second molecule is numbered as above with an offset. Ellipsoids drawn at 20% probability and hydrogen atoms omitted for clarity*

*Table C.4.1.1 Crystal data and structure refinement for monoclinic Eu.**10***

Identification code	Monoclinic Eu.**10**	
Empirical formula	C100 H132 Eu4 N16 O40	
Formula weight	2806.06 g mol^{-1}	
Temperature	150 K	
Wavelength	1.54184 Å	
Crystal system	Monoclinic	
Space group	P 1 2/c 1	
Unit cell dimensions	a = 52.668(3) Å	α = 90°
	b = 18.1007(6) Å	β = 106.632(6)°
	c = 32.7146(17) Å	γ = 90°

Volume	29883(3) $Å^3$
Z	8
Density (calculated)	1.247 Mg/m^3
Absorption coefficient	12.422 mm^{-1}
F(000)	11328
Crystal size	0.40 x 0.22 x 0.10 mm^3
Theta range for data collection	2.441 to 77.123°
Index ranges	$-63 \leq h \leq 66$, $-10 \leq k \leq 22$, $-41 \leq l \leq 40$
Reflections collected	176702
Independent reflections	61303 [R(int) = 0.128]
Completeness to theta = 69.411°	99.5%
Absorption correction	Semi-empirical from equivalents
Max. and min. transmission	0.29 and 0.02
Refinement method	Full-matrix least-squares on F^2
Data / restraints / parameters	15564 / 8786 / 2881
Goodness-of-fit on F^2	1.1332
Final R indices [I>2sigma(I)]	R1 = 0.1773, wR2 = 0.2135
R indices (all data)	R1 = 0.2314, wR2 = 0.2790
Largest diff. peak and hole	2.75 and -1.14 $e.Å^{-3}$

C.4.2 Orthorhombic

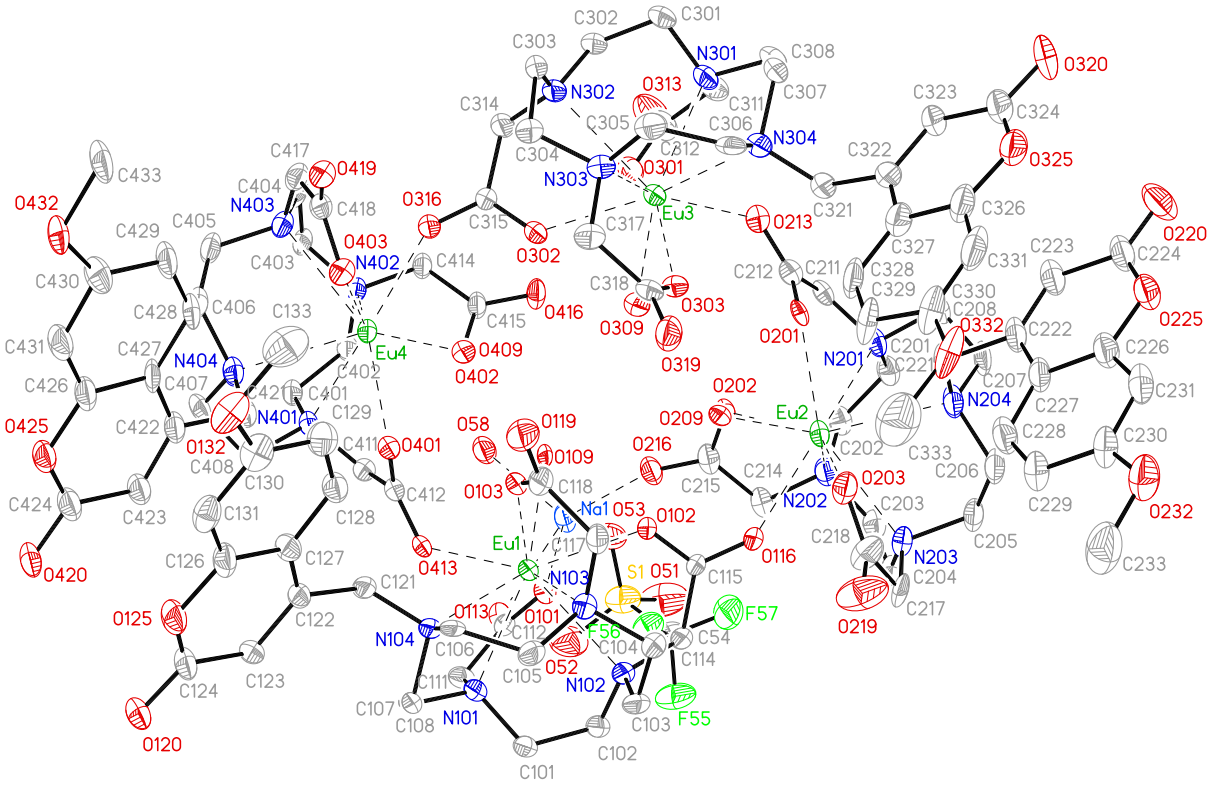


*Figure C.4.2.1 Orthorhombic structure of Eu.**10** determined by X-ray diffraction. Ellipsoids drawn at 20% probability and hydrogen atoms omitted for clarity*

*Table C.4.2.1 Crystal data and structure refinement for orthorhombic Eu.**10***

Identification code	Orthorhombic Eu.**10**	
Empirical formula	C101 H134 Eu4 F3 N16 Na1 O44 S1	
Formula weight	2996.16 g mol^{-1}	
Temperature	90 K	
Wavelength	1.54180 Å	
Crystal system	Orthorhombic	
Space group	P c a n	
Unit cell dimensions	a = 17.9227(7) Å	α = 90°
	b = 32.9420(9) Å	β = 90°
	c = 47.9786(16) Å	γ = 90°

Volume	28326.9(16) $Å^3$
Z	8
Density (calculated)	1.405 Mg/m^3
Absorption coefficient	13.356 mm^{-1}
F(000)	12080
Crystal size	0.085 x 0.085 x 0.040 mm^3
Theta range for data collection	3.685 to 58.931°
Index ranges	$-19 \leq h \leq 18$, $-36 \leq k \leq 28$, $-53 \leq l \leq 44$
Reflections collected	103297
Independent reflections	19887 [R(int) = 0.121]
Completeness to theta = 58.931°	99.8%
Absorption correction	Semi-empirical from equivalents
Max. and min. transmission	0.59 and 0.38
Refinement method	Full-matrix least-squares on F^2
Data / restraints / parameters	27811 / 4401 / 1525
Goodness-of-fit on F^2	0.9996
Final R indices [I>2sigma(I)]	R1 = 0.1745, wR2 = 0.4583
R indices (all data)	R1 = 0.1953, wR2 = 0.4690
Largest diff. peak and hole	8.30 and -5.30 $e.Å^{-3}$

C.5 *α,α'*-bis(DO3A *tert*-butyl triester)-2,6-dimethylnaphthalene (13)

Crystals suitable for X-ray diffraction were obtained by slow evaporation of a concentrated solution of the product in $CDCl_3$. The counterion to the cyclen-bound sodium ion was concluded to be chloride.

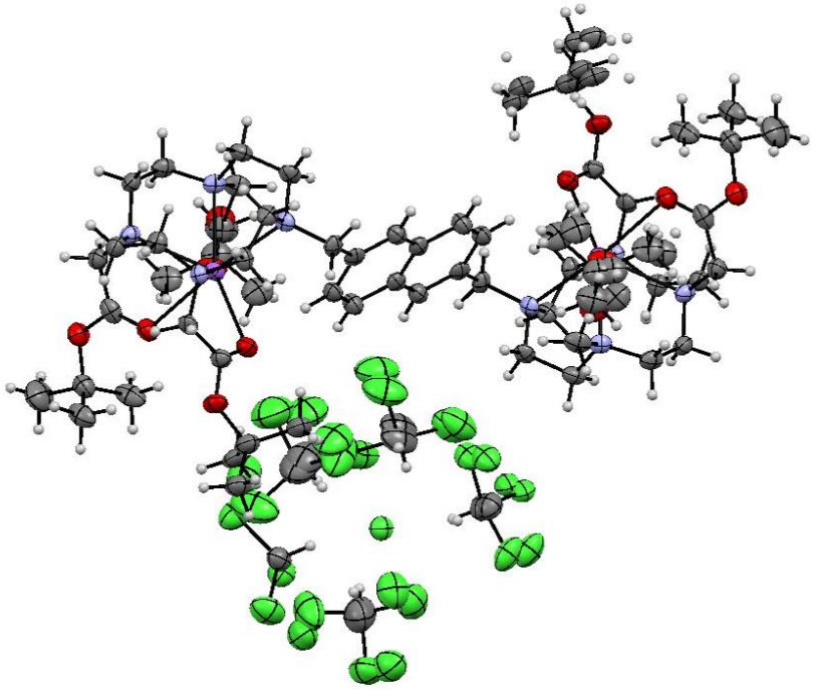


*Figure C.5.1 Structure of Na_2.**13** determined by X-ray diffraction showing thermal ellipsoids at 50% probability. One counteranion omitted for clarity*

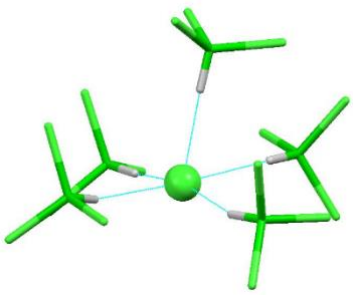


Figure C.5.2 Arrangement of $CDCl_3$ molecules about the chloride counteranion

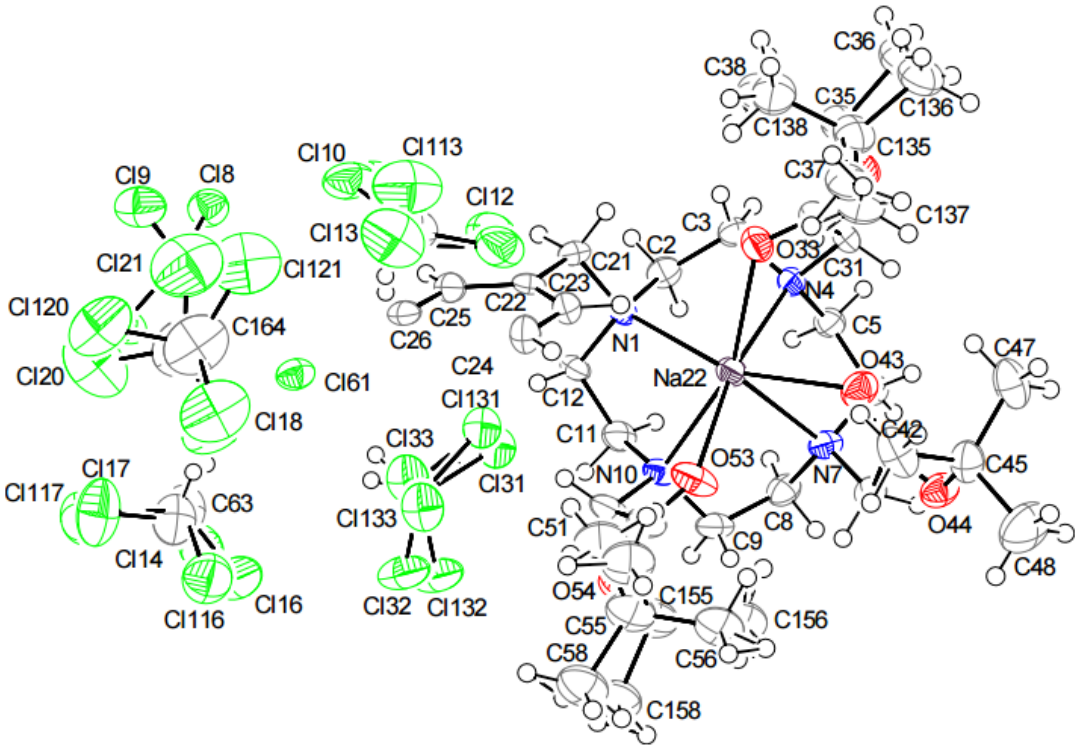


*Figure C.5.3 Structure of Na_2.**13** determined by X-ray diffraction showing thermal ellipsoids at 50% probability. Please note that only the asymmetric unit is shown*

*Table C.5.1 Crystal data and structure refinement for **13***

Identification code	**13**	
Empirical formula	C74 H118 Cl32 N8 Na2 O12	
Formula weight	2492.26 g mol^{-1}	
Temperature	150 K	
Wavelength	0.71073 Å	
Crystal system	Monoclinic	
Space group	C 2/c	
Unit cell dimensions	a = 38.6105(18) Å	α = 90°
	b = 16.4133(8) Å	β = 98.360(5)°
	c = 19.0427(10) Å	γ = 90°
Volume	11939.6(10) $Å^3$	

Z	4
Density (calculated)	1.386 Mg/m^3
Absorption coefficient	0.784 mm^{-1}
F(000)	5119.971
Crystal size	0.35 x 0.11 x 0.10 mm^3
Theta range for data collection	2.941 to 30.380°
Index ranges	$-54 \leq h \leq 40$, $-16 \leq k \leq 22$, $-27 \leq l \leq 25$
Reflections collected	41576
Independent reflections	15818 [R(int) = 0.086]
Completeness to theta = 30.380°	87.8%
Absorption correction	Semi-empirical from equivalents
Max. and min. transmission	0.92 and 0.80
Refinement method	Full-matrix least-squares on F^2
Data / restraints / parameters	9453 / 1212 / 739
Goodness-of-fit on F^2	1.0075
Final R indices [I>2sigma(I)]	R1 = 0.0843, wR2 = 0.2407
R indices (all data)	R1 = 0.1446, wR2 = 0.3181
Largest diff. peak and hole	1.78 and -1.21 $e.Å^{-3}$

C.6 ethyl-2-(9-oxo-9,10-dihydro-10-acridinyl)acetate (17)

Crystals suitable for X-ray diffraction were obtained by slow evaporation of a concentrated solution of the product in $CDCl_3$.

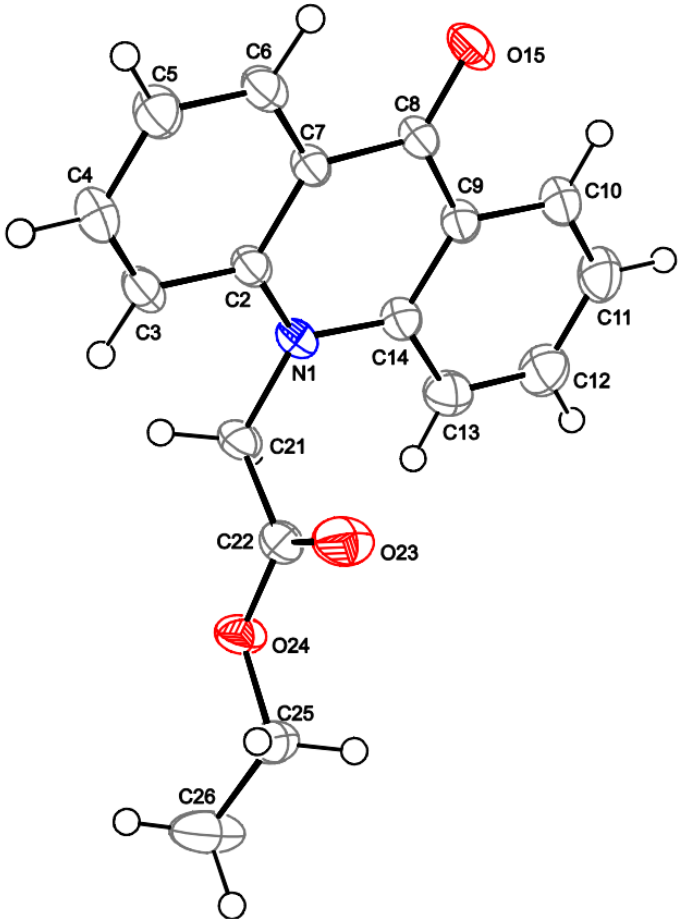


*Figure C.6.1 Structure of **17** determined by X-ray diffraction showing thermal ellipsoids at 50% probability*

*Table C.6.1 Crystal data and structure refinement for **17***

Identification code	**17**
Empirical formula	C17 H15 N1 O3
Formula weight	281.31 g mol^{-1}
Temperature	150 K
Wavelength	1.54184 Å

Crystal system	Monoclinic
Space group	P 21/n
Unit cell dimensions	a = 11.3020(4) Å α = 90°
	b = 10.4391(4) Å β = 95.906(3)°
	c = 11.8771(4) Å γ = 90°
Volume	1393.85(9) $Å^3$
Z	4
Density (calculated)	1.340 Mg/m^3
Absorption coefficient	0.753 mm^{-1}
F(000)	592
Crystal size	0.45 x 0.32 x 0.08 mm^3
Theta range for data collection	5.144 to 76.365°
Index ranges	$-14 \leq h \leq 13$, $-13 \leq k \leq 13$, $-14 \leq l \leq 12$
Reflections collected	14762
Independent reflections	2900 [R(int) = 0.026]
Completeness to theta = 74.838°	99.7%
Absorption correction	Semi-empirical from equivalents
Max. and min. transmission	0.94 and 0.77
Refinement method	Full-matrix least-squares on F^2
Data / restraints / parameters	2891 / 0 / 190
Goodness-of-fit on F^2	0.9952
Final R indices [I>2sigma(I)]	R1 = 0.0382, wR2 = 0.1004
R indices (all data)	R1 = 0.0421, wR2 = 0.1050
Largest diff. peak and hole	0.26 and -0.18 $e.Å^{-3}$

Appendix D Publications

1. Junker, A. K. R., Hill, L. R. *et al.*, *Dalton Trans.*, 2018, **47**, 4794-4803 (2018) 10.1039/c7dt04788f

2. Tropiano, M. *et al.*, *J. Lumin.*, 2015, **167**, 296-304 (2015) 10.1016/j.jlumin.2015.06.035

3. Sørensen, T. J., Hill, L. R. *et al.*, *ChemistryOpen*, 2015, **4**, 509-15 (2015) 10.1002/open.201500060

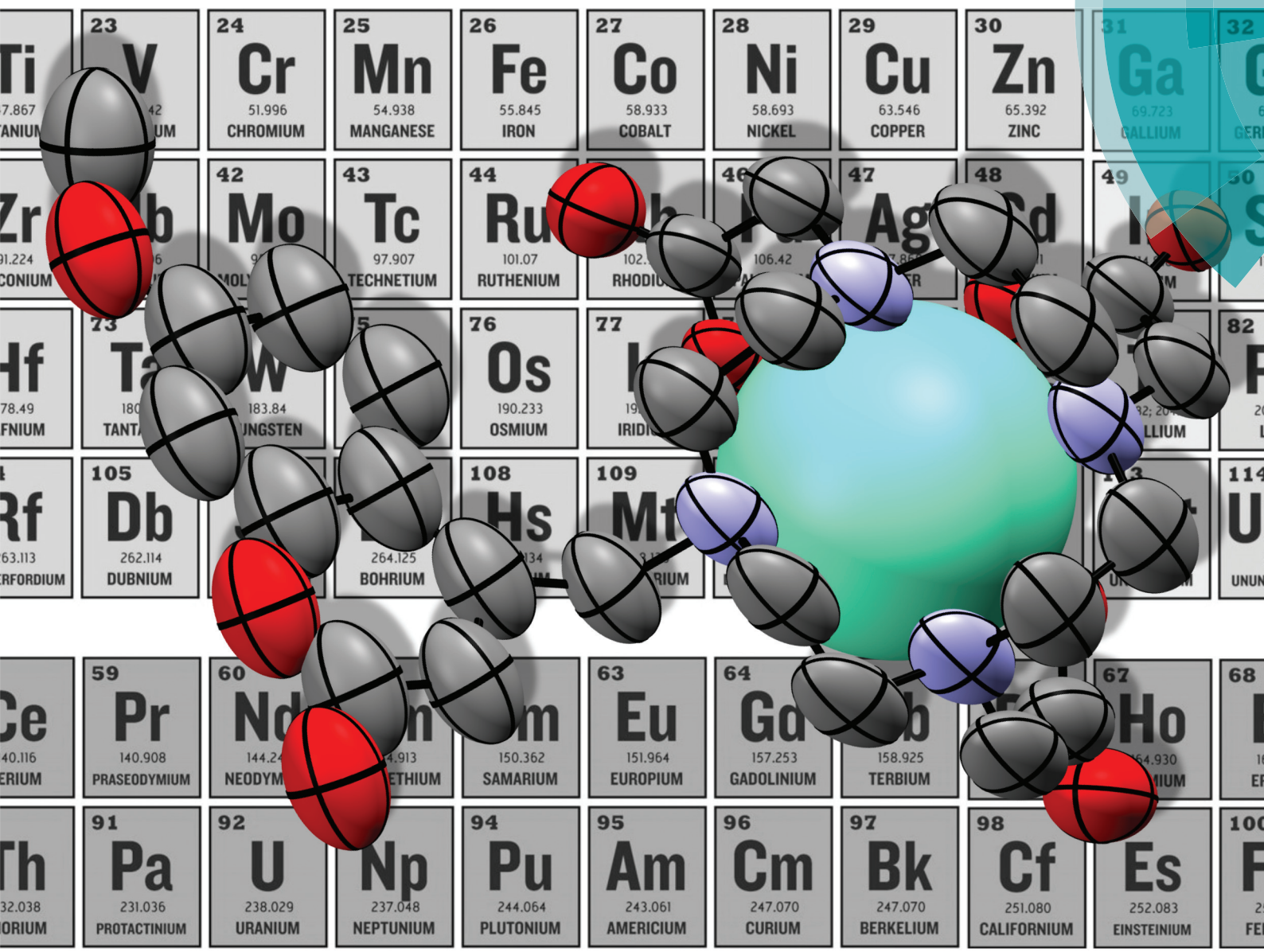
4. Sørensen, T. J., Hill, L. R. *et al.*, *Eur. J. Inorg. Chem.*, 2014, **15**, 2520-8 (2014) 10.1002/ejic.201402169

Volume 47 | Number 14 | 14 April 2018 | Pages 4741–5104

Dalton Transactions

An international journal of inorganic chemistry

rsc.li/dalton



ISSN 1477-9226

ROYAL SOCIETY OF CHEMISTRY

PAPER

Stephen Faulkner, Thomas Just Sørensen *et al.*

Shining light on the antenna chromophore in lanthanide based dyes

Dalton Transactions

PAPER

View Article Online
View Journal | View Issue

Check for updates

Cite this: *Dalton Trans.*, 2018, **47**, 4794

Shining light on the antenna chromophore in lanthanide based dyes†

Anne Kathrine R. Junker,[a] Leila R. Hill,[b] Amber L. Thompson,[b] Stephen Faulkner *[b] and Thomas Just Sørensen *[a]

Received 19th December 2017,
Accepted 9th March 2018

DOI: 10.1039/c7dt04788f

rsc.li/dalton

Lanthanide based dyes and assays exploit the antenna effect, where a sensitiser-chromophore is used as a light harvesting antenna and subsequent excited state energy transfer populates the emitting lanthanide centred excited state. A rudimentary understanding of the design criteria for designing efficient dyes and assays based on the antenna effect is in place. By preparing kinetically inert lanthanide complexes based on the DO3A scaffold, we are able to study the excited state energy transfer from a 7-methoxy-coumarin antenna chromophore to europium(III) and terbium(III) centred excited states. By contrasting the photophysical properties of complexes of metal centres with and without accessible excited states, we are able to separate the contributions from the heavy atom effect, photoinduced electron transfer quenching, excited state energy transfer and molecular conformations. Furthermore, by studying the photophysical properties of the antenna chromophore, we can directly monitor the solution structure and are able to conclude that excited state energy transfer from the chromophore singlet state to the lanthanide centre does occur.

Published on 09 March 2018. Downloaded by University of Oxford on 9/16/2018 6:57:18 PM.

Introduction

Lanthanide luminescence is characterised by uniquely narrow emission bands, long excited state lifetimes and relatively environmentally invariant emission spectra.[1–3] These unique features arise due to the forbidden nature of f–f transitions, but come with a cost of very low molar absorption coefficients.[4] Therefore, direct excitation into the lanthanide centred excited state is in the best case around a million times less efficient than that for standard organic fluorescent dyes.[5,6] Despite this apparent downside, lanthanide luminescence gives rise to background-free images, highly sensitive binding and high-content screening assays.[7–22]

These applications exploit the antenna effect, where an organic chromophore is used as a sensitiser for lanthanide centred luminescence.[23–42] The antenna chromophore absorbs light with a high molar absorptivity, and transfers the excited state energy to the lanthanide centre that subsequently emits; see Fig. 1. The chromophore typically has a molar absorptivity in the range from 5000 to 50 000 M^{-1} cm^{-1}, which despite the introduction of an energy transfer step of limited efficiency, gives rise to an improved brightness of the lanthanide based dye. As the antenna chromophore can absorb, where the lanthanide ion does not, close to perfect signal-to-background can be achieved in time-gated assays based on sensitised lanthanide luminescence.[8,15,17] For imaging, the use of lanthanide based dyes has been limited by excitation in the UV region.[3,7,12,19] This limitation has been circumvented using two-photon excitation and by using dyes with more than one antenna chromophore.[43–45]

Efficient dyes have been developed for commercial assays,[8,47] and for use in luminescence microscopy.[18,19] These

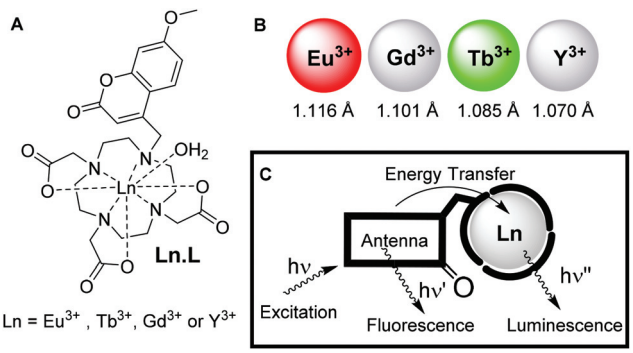


Fig. 1 (A) Molecular structure of the investigated complexes Ln·L, (B) a scaled representation of the ionic radius of the europium(III), gadolinium(III), terbium(III), and yttrium(III) ions[46] and (C) a schematic representation of the antenna effect.

[a]*Nano-Science Center & Department of Chemistry, University of Copenhagen, Universitetsparken 5, 2100 København Ø, Denmark. E-mail: TJS@chem.ku.dk*
[b]*Chemistry Research Laboratory, University of Oxford, 12 Mansfield Road, Oxford OX1 3TA, UK. E-mail: stephen.faulkner@chem.ox.ac.uk*

†Electronic supplementary information (ESI) available: Synthetic procedures, data from compound characterisation, NMR spectra, absorption spectra, time-resolved emission decay profiles, time gated emission spectra, steady-state emission and excitation spectra, and structural information in CIF format. CCDC 1589835–1589837. For ESI and crystallographic data in CIF or other electronic format see DOI: 10.1039/c7dt04788f

This journal is © The Royal Society of Chemistry 2018

Published on 09 March 2018. Downloaded by University of Oxford on 9/16/2018 6:57:18 PM.

follow established guidelines that are based on the assumption that the excited state energy transfer occurs from the lowest excited triplet state of an antenna chromophore and *via* the Dexter mechanism.[3,27,38,48] Therefore, the chromophore must be in contact with the lanthanide ion, ideally coordinating to the metal centre, for the energy transfer to occur. Bearing in mind that lanthanide based dyes are used in solutions with competitive ligands, evaluating the solution structure around the lanthanide ion is a prerequisite for unravelling the physicochemical properties of the complex.[49–51]

With the antenna chromophore guidelines,[3,27,38] we can start designing efficient lanthanide based dyes, but there is still vital information missing. Thus, the current solution is to build large libraries of antenna chromophores and test the resulting library of lanthanide based dyes.[38,52–54] This requires a large effort as each antenna chromophore must be tested with several lanthanide(III) ions. Rather than performing a screening, we aim to rationalise the physicochemical properties thereby enabling designing lanthanide based dyes.

Fig. 1 shows the complexes we used to investigate the antenna principle in detail. A 1,4,7,10-tetraazadodecane-1,4,7-triacetic acid (DO3A) ligand with a 4-methyl-7-methoxy-coumarin as the fourth pendant arm was synthesised, and complexes of yttrium(III) **Y·L**, europium(III) **Eu·L**, gadolinium(III) **Gd·L**, and terbium(III) **Tb·L** were made in significant quantities. We recently showed that the curium(III) complex **Cm·L** of this ligand gave rise to direct perturbation of the ligand chromophore by the 5f orbitals.[55] **Cm·L** was contrasted to the complexes of europium(III) and terbium(III), and all three were shown to be kinetically inert with stability constants in HEPES buffer around 10^{28}. **Eu·L** was shown to have a lower stability constant and higher hydration number q than **Cm·L** and **Tb·L**; a surprising fact that we will treat in detail here.[55]

We have started to explore the perturbation caused by lanthanide(III) ions to the excited state properties of organic chromophores by studying them in collision quenching conditions, where the freely diffusing lanthanide(III) ions deactivate the chromophore exited states upon following excitation of the chromophore if the two species are brought together by free diffusion within the excited state lifetime of the chromophore.[56–58] The one conclusion reached so far is that studying model systems will not reveal the detailed photophysics of lanthanide based dyes. Therefore, we now scrutinize the antenna and lanthanide centred photophysics when the lanthanide(III) ion and chromophore are in the same complex. While two forms of the **Ln·L** complexes are expected to be present in solution, the complexity of the investigated system is greatly reduced when compared to two freely diffusing units.[56] Fig. 2 shows the two forms—designated open and closed—and the expected effect the solution structure will have on the excited energy transfer processes. Note that the induced inter-system crossing and phosphorescence is treated as a medium effect and is not dependent on solution structure.

By contrasting the solution structure and photophysics of six compounds: **Y·L**, **Eu·L**, **Gd·L**, **Tb·L**, $\mathbf{H_3}$**·L**, and $\mathbf{H_5}$**·**$\mathbf{L^{2+}}$ using

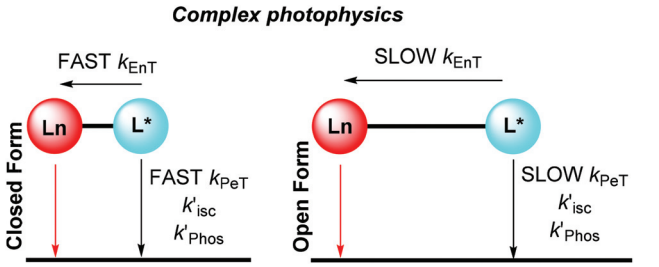


Fig. 2 The two complex modes in solution; left: The closed form where the Ln centre and antenna are in close proximity, enabling fast energy transfer and fast deactivation of the excited antenna state. Right: The open form where the Ln centre and antenna are far from each other, resulting in slow energy transfer and slow deactivation of the antenna excited state.

^{1}H NMR and optical spectroscopy, we can confirm that two forms (open and closed, Fig. 2) describe the solution structure of these complexes. We can confirm that the europium(III) complex differs in both solution structure and photophysics from the other metal complexes. In addition, we can separate the four distinct excited state processes introduced in the antenna chromophore by the metal ions. Here, we focus on the ligand-centred singlet excited state and the first step of the excited state energy transfer cascade that leads to the lanthanide(III) centred excited state.

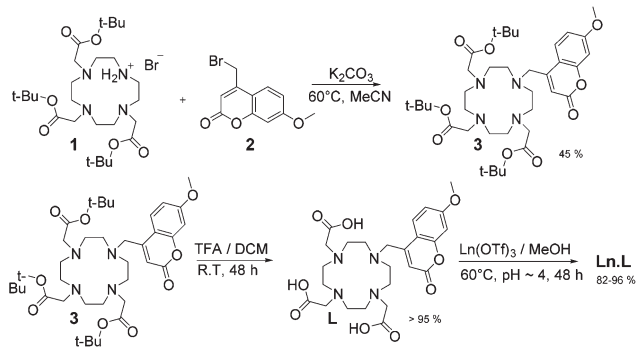
Results and discussion

Synthesis and characterisation

The complexes were synthesised in three steps from 1,4,7,10-tetraazacyclododecane or cyclen. The first step is a chemoselective alkylation of three of the four amines using *t*-butyl bromoacetate. Steric congestion and the very different solubility in toluene of the tetraalkylated byproduct and the bromide salt of the tri-alkylated cyclen **1** allowed it to be isolated in a good yield on a multigram scale.[59] In our hands, the reaction runs well using up to 0.1 mol of cyclen. On a larger scale reaction, the yield is reduced to <50%. The trialkylated cyclen, also known as DO3A-triester **1**, is the readily available starting material for functionalised DO3A (1,4,7,10-tetraazacyclododecane-1,4,7-triacetic acid) ligands. The synthetic route to the studied lanthanide complexes is shown in Scheme 1. The fourth cyclen amine in triester **1** was alkylated with 4-bromomethyl-7-methoxy-coumarin **2** in acetonitrile at 60 °C. The resulting product **3** was isolated using column chromatography in an acceptable yield. The ester of the proligand **3** was cleaved using trifluoroacetic acid in dichloromethane, and upon trituration with diethyl ether from methanol, the ligand $\mathbf{H_3}$**·L** was isolated as a pale yellow powder.

The complexes of yttrium(III), europium(III), gadolinium(III) and terbium(III) were formed from the corresponding triflate salts in methanol at pH 4. The complexes were isolated upon removal of excess lanthanide ions as a mixed hydroxide precipitate formed at pH 10. All compounds were characterized using ^{1}H NMR and high-resolution mass spectrometry.

Published on 09 March 2018. Downloaded by University of Oxford on 9/16/2018 6:57:18 PM.



Scheme 1 Synthetic pathway to ligand L and lanthanide complexes Ln·L. Ln = Y^{3+}, Eu^{3+}, Gd^{3+}, and Tb^{3+}.

Fig. 3 shows the ^{1}H NMR spectra of the free ligand **H_3·L** and the **Y·L**, **Eu·L**, and **Tb·L** complexes. Note that it is not possible to obtain a ^{1}H NMR spectrum of the **Gd·L** complex, a consequence of the rapid relaxation of protons held in close proximity to Gd^{3+}, an f^7-ion.[60] While the ^{1}H NMR spectra of the ligands are pH dependent, the ^{1}H NMR spectra of the complexes do not change with pH, although the complexes precipitate at low pH.

For **Eu·L**, we were able to confirm the constitution of the complexes using single crystal X-ray diffraction; see the ESI† for details. The crystal structure consists of tetramers of **Eu·L**, where each europium(III) cation is encapsulated by the ligand and bridged by the carboxylate pendant arms from a neighbouring complex. The coordination sphere of europium(III) is thus filled with seven donor atoms from the ligand, one from a capping water molecule, and one oxygen atom from a carboxylate group on a second ligand in the tetramer, see Fig. 4. The tetramers enclose the hydrophilic surface of the complexes, and expose the hydrophobic surface of the cyclen ring, creating hydrophobic pores in the structure. In the crystal structure, the coumarin units exhibit π–π stacking. The overall structure of the complex is the square antiprismatic form **SAP** expected for a DO3A complex, and in the crystal, the **Eu·L** is in the open form (contrasts Fig. 2 and 4).

Solution structure part I

The solution structure alluded to in Fig. 2 must be considered when inspecting the ^{1}H NMR spectra in Fig. 3. The diamagnetic species **Y·L** and **H_3·L** show sharp resonances from protons on the coumarin and carboxylate arms. The ring protons can be identified in the free ligand, while those in the

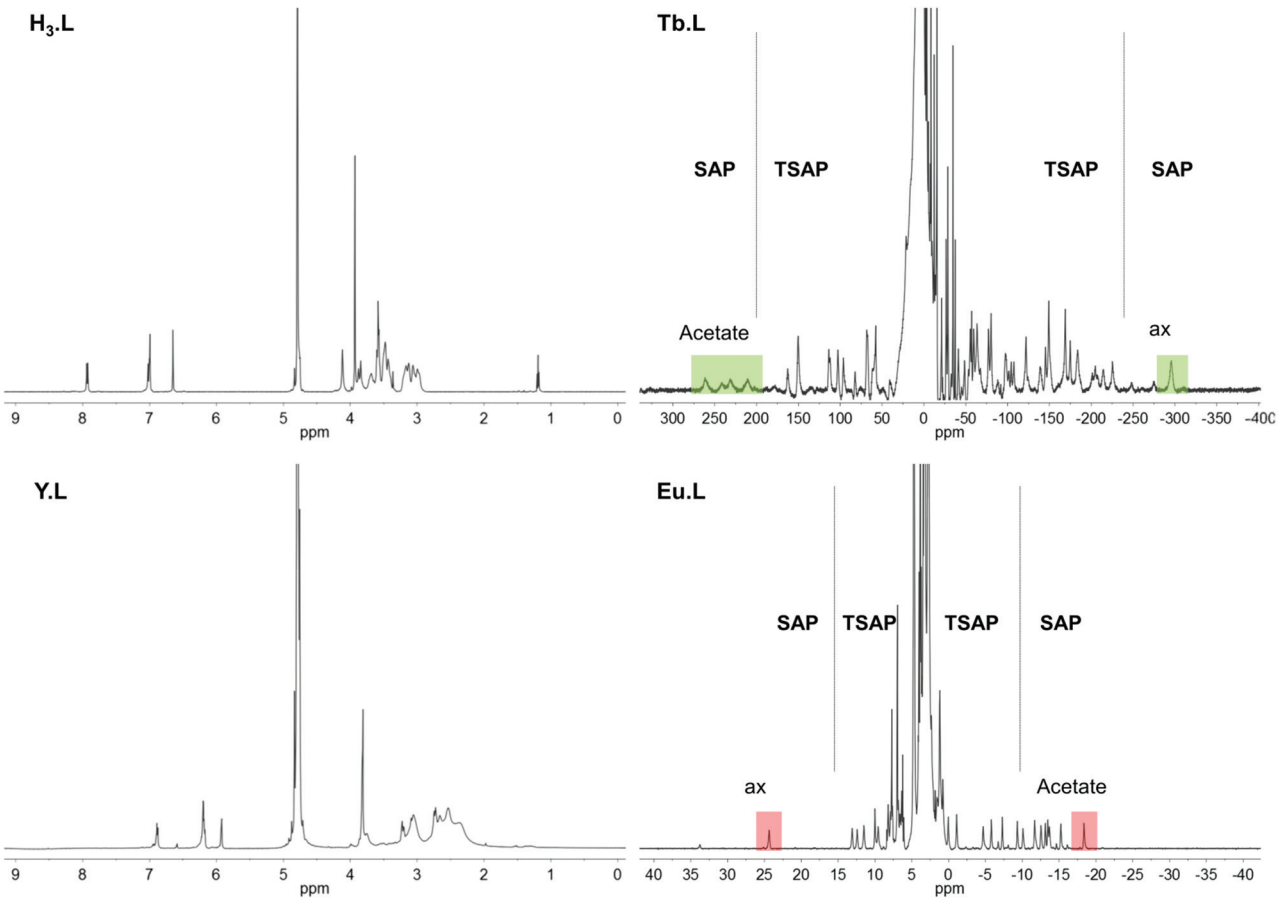


Fig. 3 ^{1}H NMR spectra of the free ligand **H_3·L** and the lanthanide complexes **Ln·L** in D_2O. The spectrum of the free ligand was obtained at pH ~ 4, and at pH 7 for the complexes. On the spectra lanthanide complexes, the regions corresponding to the SAP and TSAP conformers are indicated based on the corresponding Ln.DOTA complexes, and the resonances corresponding to the axial and acetate arm protons are highlighted.

 This journal is © The Royal Society of Chemistry 2018

Published on 09 March 2018. Downloaded by University of Oxford on 9/16/2018 6:57:18 PM.

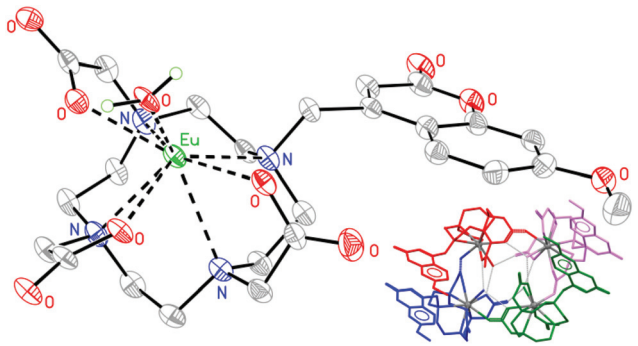


Fig. 4 Displacement ellipsoid plot for the orthorhombic polymorph of **Eu·L** drawn at 20% probability. The main picture shows one formula unit with selected hydrogen atoms and NaOTf omitted for clarity. In the solid state, **Eu·L** forms tetramers held together by hydrogen bonding between the apical water and ligand acetate moieties (shown inset), a feature seen in all three structures studied.

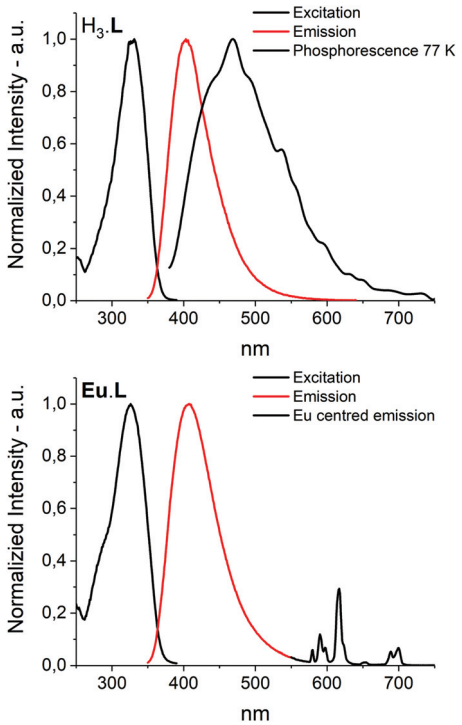


Fig. 5 Excitation and emission spectra of H_3**L** (top) and **Eu·L** (bottom). Both excitation spectra followed emission at 402 nm. Emission spectra followed excitation at 325 nm measured at room temperature in HEPES buffer at pH 7.4. The phosphorescence spectrum of H_3**L** was recorded at 77 K. Data for all complexes can be seen in the ESI.†

yttrium complex give rise to overlapping and broad signals implying exchange between multiple closely related species. The paramagnetic ^{1}H NMR spectrum of the **Eu·L** and **Tb·L** complexes gives rise to resonances in a wide ppm region. The paramagnetic ^{1}H NMR spectra of Ln.DO3A and Ln.DOTA complexes are well understood.[61–66] Tb^{3+} complexes with functionalised DO3A ligands usually give rise to four resonances arising from the axial protons of the cyclen ring between −350 and −400 ppm for the square anti-prismatic **SAP** conformation of the complex. Similarly, the axial protons of Eu^{3+} complexes derived from DO3A give rise to four resonances around 40 ppm. For the europium(III) complex, both the **SAP** and the twisted square anti-prismatic **TSAP** conformation must be considered. The latter gives rise to resonances from the axial protons around 20 ppm. Fig. 3 shows that the spectra of **Eu·L** and **Tb·L** do not show four distinct resonances of the axial cyclen protons. Rather a single resonance is observed at a significantly lower ppm than was expected for an axial proton in the **SAP** conformation of DO3A. This indicates that the structure of the complexes is in rapid exchange between several diastereoisomers on the NMR timescale. Exchange between **SAP** and **TSAP** should not make the resonances from different axial protons coalesce. At this point, we speculate that the equilibrium between an open and closed form as proposed in Fig. 2 is the cause of this observation. Note that the signal from the **SAP** form is observed as a single resonance for both **Eu·L** and **Tb·L**. We have previously attributed this form of spectrum to complexes of flexible DO3A ligands, that is ligands without a fourth coordinating pendant arm.[67] The acetate resonances between 280 and 200 ppm are clearly resolved in the **Tb·L** spectrum. This indicates that an open form does not contribute significantly to the solution structure of this complex.

Lanthanide centred luminescence

The **Eu·L** and **Tb·L** complexes luminesce following excitation of the lanthanide centre or the coumarin chromophore. In the excitation spectra of the complexes (Fig. 5 and ESI†), the absorption bands corresponding to direct excitation of the lanthanide ions cannot be distinguished, indicating that the lanthanide excited state is predominantly populated through excitation of the coumarin chromophore. As we reported recently,[55] the coumarin chromophore is an efficient sensitiser for europium(III), while only very weak terbium(III) centred luminescence could be observed. This is unexpected as the energy level of the coumarin-centred excited state should be able to populate the lanthanide centred excited states.[38] We must conclude that all terbium(III) centred emission arises from energy transfer from the antenna singlet state, *vide infra*. By inspection of Fig. 6 it can be seen that direct energy transfer to the europium(III) excited state manifold is possible, to *e.g.* the $^5G_4$ and $^5L_6$ states; however, in the terbium(III) excited state manifold, the $^5D_3$ state lies below the S_1 state but is above the T_1 state of the antenna chromophore. This suggests that excited state energy transfer *via* a Dexter exchange mechanism favours energy transfer through the intermediate states in the excited state manifold.[57]

If efficient energy transfer was possible from T_1 to the terbium(III) centre, a quantum yield of luminescence ϕ_{HEPES} for terbium(III) should be higher than that for europium(III). We can speculate that the energy difference between the antenna centred triplet state and the lanthanide centred excited state is too large to allow for efficient energy transfer to occur,[57,58] see Fig. 6. This is in direct conflict with previously published results.[38]

Published on 09 March 2018. Downloaded by University of Oxford on 9/16/2018 6:57:18 PM.

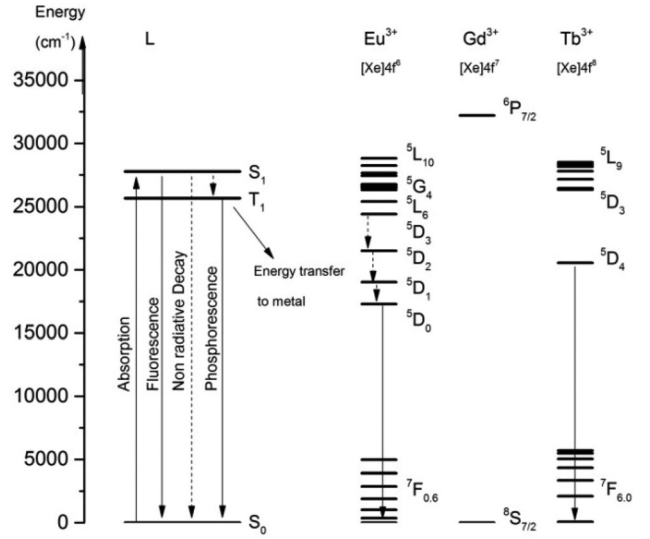


Fig. 6 Energy levels of the coumarin antenna chromophore (L) and the Eu^{3+}, Gd^{3+}, and Tb^{3+}, free ions.

Table 1 shows the luminescent properties of the **Eu·L** and **Tb·L** complexes. By determining the luminescence lifetimes and using the modified Horrocks' equation, the number of solvent molecules coordinated to the lanthanide centre q was determined.[68,69] For **Eu·L**, $q = 2$ and for **Tb·L**, $q = 1$ confirming the difference observed in the ^{1}H NMR spectra; see Fig. 3. The difference was further confirmed by the stability constants of the two complexes.[55] Despite the similarities of the two ions, see Fig. 1, the europium(III) complex is 2 orders of magnitude less stable than the terbium(III) complex. Clearly, the solution structure of the two complexes differs, which in turn must influence the photophysical properties of the complexes as indicated in Fig. 2.

Antenna centred fluorescence

The paramagnetic ^{1}H NMR and the lanthanide centred luminescence show that at least two conformers are present in solution and that the speciation in **Eu·L** and **Tb·L** differs. Fig. 5 shows the excitation and emission spectra of **Eu·L**, and **H_3·L**. Apart from the additional europium(III) centred bands in the emission spectrum, Fig. 5 shows that under steady-state conditions, the ligand centred optical transition is unchanged by protonation state and the complexation of a trivalent metal ion. Fig. 5 includes the phosphorescence spectrum recorded at 77 K, which enables the determination of the energy of the coumarin-centred triplet excited state T_1. Fig. 6 shows the energy levels of the first singlet S_1 and triplet T_1 excited state in the coumarin chromophore along the lowest energy levels of Eu^{3+}, Gd^{3+}, and Tb^{3+} ions. Cursory inspection of Fig. 6 shows that the excited state energy transfer from S_1 can occur to the $^5D_3$ state of Tb^{3+} and to several states in the excited state manifold of Eu^{3+}. Excited state energy transfer from T_1 to the Tb^{3+} excited state manifold does not seem feasible as there are no states of similar energy. For Eu^{3+}, the $^5L_6$ and $^5D_3$ states are of similar energy to the T_1 state, which allow excited state energy transfer to be possible. The *f–f* transitions of Gd^{3+} are not accessible in energy, and neither are the excited states of the Y^{3+} ion; the latter is not included in Fig. 6.

All lanthanide centred emission in this system originates from the first singlet excited state of the coumarin. Therefore, a detailed understanding of the excited state processes depopulating the S_1 state in the **Y·L**, **Eu·L**, **Gd·L**, **Tb·L**, **H_3·L**, and **H_5·L^{2+}** is required.

Fig. 6 includes arrows corresponding to the processes that depopulate S_1 in the absence of a lanthanide ion: fluorescence k_f, non-radiative deactivation *via* internal conversion to S_0 k_{ic}, and intersystem crossing to T_1 k_{isc}. In Table 2, each process is listed with the first order rate constant of the process. The total non-radiative decay from S_1 is $k_{nr} = k_{ic} + k_{isc}$. In the presence of a lanthanide ion, or other quenchers, additional pathways of deactivation become possible. These processes are listed in Fig. 2. All paramagnetic lanthanide ions add induced intersystem crossing, $k_{isc'}$, as a deactivation pathway for S_1. This is a medium effect and comes into effect above a critical concentration of lanthanide ions in solution.[56] Two other

Table 1 Luminescence properties of **Eu·L** and **Tb·L** complexes in 0.1 M HEPES buffer at pH 7.4; all data can be seen in the ESI

	Eu·L	**Tb·L** [a]
τ_{H_2O} (ms)	0.41 ± 0.02	1.12 ± 0.06
τ_{D_2O} (ms)	1.68 ± 0.01	1.41 ± 0.07
q [b]	1.90 ± 0.1	0.62 ± 0.2
Ln ϕ_{HEPES} (%)	5.26	—
Log β [c]	26.92 ± 0.2	28.71 ± 0.1

[a] Lifetimes were determined in aerated and degassed samples and were unchanged. [b] Equations $q = A(\tau_{H_2O}^{-1} - \tau_{D_2O}^{-1} - B)$, for europium(III) $A = 1.2$ ms and $B = 0.25$ ms, for terbium(III) $A = 5.0$ ms and $B = 0.06$ ms.[68,70] [c] From ref. 55.

Table 2 Photophysical properties of **H_3·L**, **Eu·L**, **Gd·L**, and **Tb·L**. The data, fits and errors for all experimental numbers behind the reported values can be found as the ESI

	H_3·L	**Eu·L**	**Gd·L**	**Tb·L**	**Y·L**
λ_{abs} (nm)	328	326	327	328	329
ε (M^{-1} cm^{-1})	7450	3290	3400	3600	3860
Log ε (M^{-1} cm^{-1})	3.87	3.52	3.53	3.56	3.59
E_T (cm^{-1})	26 040	25 000	25 000	25 000	25 000
E_{Ln} (cm^{-1})					
$\phi_{F(H_2O)}$ (%)	20	7.3	21	18	24
$\langle\tau_{F(H_2O)}\rangle$(ns)	0.81	0.53	1.7	1.3	1.7
$\langle\tau_{F(D_2O)}\rangle$(ns)	0.86	0.96	1.6	1.7	1.8
τ_0 (ns)[a]	4.0	7.3	8.2	7.5	7.2
k_f (10^8 s^{-1})[b]	2.5	1.4	1.2	1.3	1.4
k_{obs} (10^8 s^{-1})[c]	12	19	5.9	7.5	5.9
k_{nr} (10^8 s^{-1})[d]	9.8	18	4.6	6.1	4.5
k_{PeT} (10^8 s^{-1})[e]	5.3	13	—	—	—
k_{EnT} (10^8 s^{-1})[f]	—		—	1.6	—

[a] $\tau_0 = \tau_{F(H_2O)}/\phi_{F(H_2O)}$. [b] $k_f = 1/\tau_0$. [c] $k_{obs} = 1/\tau_{F(H_2O)}$. [d] $k_{nr} = k_{obs} - k_f$. [e] For **H_3·L**: $k_{PeT} = k_{nr} - k_{nr}$(Y/Gd). [f] For **Tb·L**: $k_{EnT} = k_{nr} - k_{nr}$(Y/Gd).

This journal is © The Royal Society of Chemistry 2018

Published on 09 March 2018. Downloaded by University of Oxford on 9/16/2018 6:57:18 PM.

deactivation pathways are possible: photoinduced electron transfer, k_{PeT}, if a lanthanide ion with suitable redox chemistry is complexed, and excited state energy transfer, k_{EnT}, if a lanthanide ion with a close lying excited state is coordinated. Both these processes are distance dependent.[57,58] PeT and energy transfer *via* the Dexter mechanism requires that the chromophore and lanthanide ion collide, resulting in orbital overlap. Therefore, the magnitude of k_{PeT} and k_{EnT} will be directly linked to the solution structure of the complex, see Fig. 2.

The photophysical properties of **Y·L**, **Eu·L**, **Gd·L**, **Tb·L**, and **H_3·L** are compiled in Table 2. The energies of states in the coumarin excited state manifold are not changed by the trivalent lanthanide ions, but the fluorescence quantum yield $\phi_{F(H_2O)}$ is significantly reduced in the europium(III) complex. This is to be expected as Eu^{3+} is an efficient PeT quencher.[71–73] More surprising is the fact that Tb^{3+} also reduces the fluorescence quantum yield, as this can only occur by energy transfer to the terbium(III) centre. This is confirmed by the data from the Gd^{3+} and Y^{3+} complexes. For **Y·L**, the fluorescence quantum yield is increased. This is due to the coordination of the cyclen nitrogen atoms that in **H_3·L** gives rise to PeT quenching.

By determining the amplitude averaged excited state lifetime of $S_1\langle\tau\rangle$, the rate constant for depopulation S_1 k_{obs} can be determined. From $\langle\tau\rangle$ and ϕ_F, the k_{obs} can be separated into radiative k_f and a non-radiative k_{nr} contribution. Table 2 includes these numbers for all complexes.

By comparing the five compounds, we can go a step further. **Y·L** does not allow for induced intersystem crossing, excited state energy transfer, and photoinduced electron transfer quenching. **Gd·L** contributes only to induced intersystem crossing, while for **Tb·L** excited state energy transfer may be possible. **Eu·L** may have induced intersystem crossing, excited state energy transfer, and photoinduced electron transfer quenching. Finally, **H_3·L** will only show photoinduced electron transfer quenching by the aza bridged cyclen. These stipulations allow the rate constants for the individual processes to be separated as done in Table 2. The most noteworthy entry in Table 2, is that excited state energy transfer from S_1 to the terbium(III) excited state manifold occurs with a rate constant equal to k_f. It follows directly that the quantum yield of energy transfer ϕ_{EnT} must be equal to the quantum yield of fluorescence: $\phi_F = \phi_{EnT} = 18\%$, which should, but does not, give rise to a significant amount of terbium(III) centred luminescence. Thus back energy transfer from the terbium(III) centre to the antenna chromophore T_1 state must be possible. The numbers in Table 2 also show that induced intersystem crossing does not influence the depopulation of S_1 to an appreciable degree. Note that k_{EnT} and k_{PeT} cannot be separated for the europium(III) complex.

Solution structure part II

The values reported in Table 2 are averages. The quantum yield of fluorescence $\phi_{F(H_2O)}$ is a weighted average of contributions from all possible emitting species in solution. And in Table 2, the amplitude averaged fluorescence lifetime $\langle\tau_{F(H_2O)}\rangle$ is used. While the number of emitting species cannot be resolved in the steady-state experiments, the time-resolved data provide this information and show the contribution from two different emitting species. Thus the antenna chromophore photophysics shows that two conformations are present in solution. With support from ^{1}H NMR spectroscopy, the stability constants $\log\beta$, and the number of solvent molecules bound at the lanthanide centre q, we can draw up the equilibrium shown in Fig. 7. Fig. 7 also includes a molecular model that shows the two isomers, where the coumarin is either in contact with the metal centre or as far as possible from the metal centre. The latter is similar to the crystal structure found for **Eu·L**.

The difference in the distance between the antenna chromophore and the metal centre should influence the photophysics of the antenna chromophore as outlined in Fig. 2. Indeed, the time resolved data showed two emitting species, one with a *ca.* 2 ns S_1 lifetime and one where the S_1 lifetime is *ca.* 0.6 ns. To elucidate which species corresponds to the open and closed confirmations (Fig. 2 and 7), time-resolved emission spectra were recorded. Two forms of the free ligand were included, as the amino groups of the cyclen ring are efficient PeT quenchers. Quenchers can be removed by protonation, which allows us to determine the photophysical properties of the antenna chromophore with and without additional pathways for the deactivation of S_1. The results are compiled in Table 3.

In the time-resolved emission spectra, three emission bands with distinct excited state lifetimes (τ_1, τ_2, and τ_3) were resolved, two bands (τ_2, and τ_3) with identical shape and emission maxima corresponding to the antenna chromophore fluorescence. The third band τ_1, a minor contribution, is a red-shifted band that coincides with coumarin phosphorescence. The phosphorescence lifetime is reduced to nanoseconds due to quenching by oxygen, but is clearly resolved on the red side of the fluorescence; see the ESI.† τ_1 is not seen in **Gd·L**, which may be due to rapid induced intersystem crossing from T_1 to S_1.[56]

Two conformations (τ_2, and τ_3) are differentiated in the time-resolved emission spectra. The distribution between τ_2

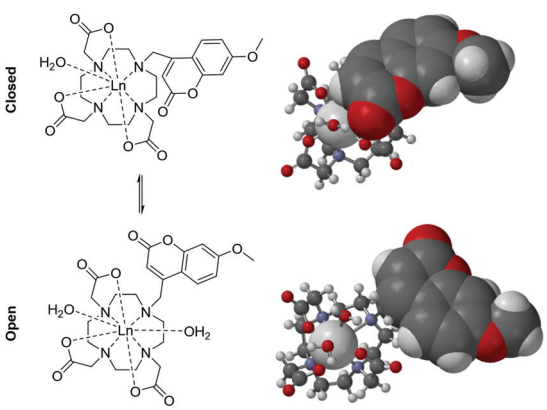


Fig. 7 Equilibrium of the molecular solution state structure of the complexes. Ln = Y(III), Eu(III), Gd(III) and Tb(III), and a molecular model of the structure (right).

Published on 09 March 2018. Downloaded by University of Oxford on 9/16/2018 6:57:18 PM.

Table 3 Fluorescence lifetime τ and fractional amplitude A determined from a global fit of the time-resolved emission spectra of **Y·L**, **Eu·L**, **Gd·L**, **Tb·L**, H_3·**L**, and H_5·L^{2+} in the HEPES buffer at pH 7.4; data and fits can be found in the ESI

H_2O	H_5·L^{2+}	H_3·L	Eu·L	Gd·L	Tb·L	Y.L
τ_1[a] (ns)	—	3.5	2.9	—	2.9	3.6
A_1 (%)	0	1	4	0	2	2
τ_2[a] (ns)	2.1	1.3	1.3	2.0	1.5	1.9
A_2 (%)	35	28	15	80	81	82
τ_3[a] (ns)	0.6	0.5	0.3	0.8	0.4	0.4
A_3 (%)	65	71	81	20	17	16

[a] Error <0.1 ns; see the ESI for details.

and τ_3 vary within the series of compounds **Y·L**, **Eu·L**, **Gd·L**, **Tb·L**, H_3·**L**, and H_5·L^{2+} but fall in two groups. **Y·L**, **Gd·L**, and **Tb·L** are primarily (≥80%) in the conformation with the long fluorescence lifetime τ_2. In contrast, **Eu·L**, H_3·**L**, and H_5·L^{2+} are primarily found in the other (>60%) conformation characterised by the shorter τ_3 lifetime. Clearly, **Eu·L** has a different solution structure than **Y·L**, **Gd·L**, and **Tb·L**. Note that the time-resolved emission spectrum following the antenna chromophore fluorescence can reveal the solution structure as the nanosecond timescale is faster than the conformational fluctuations. The lanthanide luminescence does not reveal conformational fluctuations, as the millisecond luminescence lifetime will only report the weighted average. In this case, the difference between the two conformers and the ratio 20 : 80 *vs.* 80 : 20 is large enough to be seen in q.

In Fig. 2, two conformations were labelled open and closed, and Table 3 includes two conformations τ_2 and τ_3. In the free ligand, photoinduced electron transfer quenching requires direct contact between the coumarin chromophore and the cyclen nitrogen atoms. PeT is only possible in H_3·**L** as the amino groups are protonated in H_5·L^{2+} and cannot act as PeT quenchers. Table 3 shows that τ_3 is very similar in the two compounds, indicating that a lifetime of 0.5–0.6 ns corresponds to the lifetime of the antenna chromophore in the open form. Water must be an efficient quencher for the coumarin S_1 state. In H_3·**L**, PeT quenching reduces the τ_2 lifetime by 0.8 ns compared to H_5·L^{2+}, confirming that τ_2 corresponds to the closed conformation. Thus, the solution structure of **Eu·L** is the open conformation in complete agreement with the results presented above. Both the open (τ_3 = 0.3 ns) and the closed (τ_2 = 1.3 ns) conformers of **Eu·L** have a shorter lifetime than the free ligand, which matches the lower fluorescence quantum yield determined for **Eu·L**.

Y·L, **Gd·L**, and H_5·L^{2+} have a lifetime of τ_2 = 2 ns and τ_3 = 0.4–0.8 ns in the closed and open conformers, respectively. The reduced lifetime of the closed conformation of **Tb·L** (τ_2 = 1.5 ns) confirms that the chromophore S_1 state must be depopulated by the excited state energy transfer to terbium(III). The inefficient population of the emitting $^5D_4$ state of Tb^{3+} must be due to the back energy transfer to the chromophore T_1 state.

Conclusion

Rationalising the photophysical and physicochemical properties of lanthanide dyes exploiting the antenna effect is still a work in progress. By synthesising lanthanide complexes of a 4-methyl-7-methoxy-coumarin appended 1,4,7,10-tetraazadodecane-1,4,7-triacetic acid (DO3A) ligand, we are able to conclude that detailed studies of solution structure and residual sensitiser fluorescence are essential if we are to complete the work.

Our detailed investigation exploiting ^{1}H NMR, europium(III) and terbium(III) centred luminescence, model systems, and detailed fluorescence spectroscopy allows us to conclude that: (i) the **Ln·L** system exists in two conformations in solution; (ii) the europium(III) and terbium(III) complexes are significantly different, much more than the small difference in ionic radius dictates; (iii) excited state energy transfer from short lived ($\langle\tau_F\rangle \approx 2$ ns) excited states to lanthanide centred states can occur with high efficiencies and (iv) back energy transfer from the lanthanide centre to the lower lying ligand centred excited state can occur with high efficiency.

Experimental

Materials and methods

All chemicals for synthesis were used as received. All solvents for spectroscopic experiments were of HPLC grade and used as received. Water was deionized and microfiltered using a Milli-Q Millipore machine. Chromatographic purification was performed on silica gel (SiO_2) with a pore size of 60 Å and a particle size of 60–200 μm. Mass spectra were recorded on a high resolution Micro-TOF-QII-system using ESP (calibrated using formic acid). ^{1}H NMR spectra were recorded on a Bruker 500 MHz instrument. ^{13}C NMR spectra were recorded on a Bruker 126 MHz instrument equipped with a (noninverse) cryoprobe. All chemical shifts (δ) are given in parts per million.

Synthetic procedures

1-(7-Methoxy-4-methyl-coumarin)-4-7-10-tris(*tert*-butoxycarbonylmethyl)-1,4,7,10-tetraazacyclododacane (1). 4-Bromomethyl-7-methoxy-coumarin (546.7 mg, 2.03 mmol) was dissolved in acetonitrile (30 ml) together with 1,4,7-tris(*tert*-butylcarbonylmethyl)-1,4,7,10-tetracyclododecane (1.10 g, 1.85 mmol) and potassium carbonate (1.15 g, 8.31 mmol); the mixture was heated to 60 °C and stirred overnight. After the reaction was complete, the mixture was filtered and washed with dichloromethane. The filtrate was then evaporated to dryness under reduced vacuum. The crude product was purified by column chromatography (10% MeOH/DCM). Yield 586 mg, 45%. ESI-MS: m/z calculated for $C_{37}H_{58}N_4O_9$ $[M + H]^+$ 703.4276, found 703.4287. ^{1}H NMR (500 MHz, chloroform-d) δ 7.67 (d, J = 8.9 Hz, 1H), 6.85 (dd, J = 8.8, 2.6 Hz, 1H), 6.82 (d, J = 2.5 Hz, 1H), 6.45 (s, 1H), 4.12 (s, 2H), 3.87 (s, 5H), 3.57 (s, 3H), 3.31 (s, 3H), 3.19 (s, 7H), 3.00 (d, J = 5.3 Hz, 4H), 1.49 (s, 9H), 1.40 (s, 18H). ^{13}C NMR (126 MHz, $CDCl_3$) δ 173.69, 172.79, 163.03, 160.59, 155.62, 152.54, 125.59, 112.81, 112.59,

 This journal is © The Royal Society of Chemistry 2018

Published on 09 March 2018. Downloaded by University of Oxford on 9/16/2018 6:57:18 PM.

111.79, 101.49, 101.21, 83.33, 82.62, 56.74, 55.92, 55.85, 55.33, 54.46, 51.76, 51.40, 28.38, 28.34, 28.22, 28.19, 28.10, 28.03.

1-(7-Methoxy-4-methyl-coumarin)-4-7-10-tris(carboxylmethyl)-1,4,7,10-tetraazacyclododacane (L). Proligand **1** (586 mg, 0.83 mmol) was dissolved in dichloromethane (10 ml); trifluoroacetic acid (10 ml) was then added to the mixture. The reaction mixture was left to stir for 48 hours at room temperature. The solvent was removed under reduced pressure and the residue dissolved in a minimum amount of methanol and precipitated with diethyl ether. Trituration with diethyl ether yielded the product as a slightly yellow solid in quantitative yield. ESI-MS: *m*/*z* calculated for $C_{25}H_{34}N_4O_9$ $[M + H]^+$ 535.2398, found 535.2398. ^{1}H NMR (500 MHz, deuterium oxide) δ 7.93 (d, J = 8.8 Hz, 1H), 7.05–6.98 (m, 2H), 6.65 (s, 1H), 4.12 (s, 2H), 3.94–3.91 (m, 3H), 3.86 (d, J = 16.8 Hz, 2H), 3.64–3.36 (m, 13H), 3.09 (dd, J = 58.6, 28.0 Hz, 10H).

General method for the complexes Ln·L

To a solution of the ligand (**H_3·L**) in methanol, the appropriate lanthanide triflate salt was added (1.1 eq.) and the reaction mixture was stirred at 60 °C for 30 min, at which point the pH of the solution was adjusted to ~4 by dropwise addition of hydrochloric acid (2 M). The reaction was left stirring at 60 °C for 48 h. The methanol was removed under reduced pressure leaving an oil that was dissolved in water. The pH was adjusted to ~10 by the addition of sodium hydroxide (1 M) to remove excess lanthanide as its insoluble hydroxide. The resulting precipitate was centrifuged and the supernatant was filtered through a syringe filter. The solvent was removed under reduced pressure to obtain the product as an off-white solid.

Eu·L. Yield 85%. ESI-MS: *m*/*z* calculated for $C_{25}H_{31}EuN_4O_9$ $[M + Na]^+$ 707.1198, found 707.1201. ^{1}H NMR (500 MHz, D_2O) δ 33.86, 24.40, 13.10, 12.40, 11.47, 10.00, 9.52, 8.19, 7.72, 6.97, 6.94, 6.22, 3.84, 3.27, 2.75, 1.24, 1.18, 0.78, 0.04, −1.11, −4.67, −5.81, −7.29, −9.31, −10.13, −11.68, −12.54, −13.15, −13.49, −13.70, −15.25, −18.38.

Tb·L. Yield 93%. ESI-MS: *m*/*z* calculated for $C_{25}H_{31}N_4O_9Tb$ $[M + H]^+$ 691.1417, found 691.1440. ^{1}H NMR (500 MHz, D_2O) δ 261.53, 241.73, 231.34, 210.21, 162.77, 150.61, 113.56, 103.02, 95.94, 81.98, 68.59, 57.62, −21.15, −26.60, −28.65, −34.72, −37.37, −41.41, −48.78, −55.54, −57.04, −59.69, −63.83, −77.43, −80.43, −98.17, −104.35, −107.63, −122.12, −139.75, −145.22, −149.28, −169.10, −184.57, −205.02, −215.04, −225.90, −296.13. Only resolved peaks outside the −40–40 ppm region are reported.

Gd·L. Yield 82%. ESI-MS: *m*/*z* calculated for $C_{25}H_{31}GdN_4O_9$ $[M + H]^+$ 690.1411, found 690.1491.

Y·L. Yield 86%. ESI-MS: *m*/*z* calculated for $C_{25}H_{31}YN_4O_9$ $[M + H_3O^+]^+$ 639.1327, found 639.1348. ^{1}H NMR (500 MHz, deuterium oxide) δ 6.89 (m, 1H), 6.19 (m, 3H), 5.93 (dd, J = 5.8, 2.8 Hz, 1H), 3.85–3.78 (m, 4H), 3.29–2.90 (m, 10H), 2.79–2.24 (m, 30H).

Optical spectroscopy

Absorption spectra were measured with a Cary 300 UV-Vis double beam spectrometer from Agilent Technologies against air using a pure solvent as the baseline. The fluorescence and time-gated emission spectra were recorded on a Cary Eclipse fluorescence spectrometer with a photomultiplier tube from Agilent Technologies. The fluorescence and metal centred lifetimes were determined using a FluoTime 300 instrument from PicoQuant. The excitation source was the 355 nm line from a VisUV laser or a Xenon Cw lamp from PicoQuant. The data were fitted as monoexponential or triexponential decay using the deconvolution as implemented in the FluoFit software (version 4.6.6) from PicoQuant. The phosphorescence measurements were done on a Cary Eclipse fluorescence spectrometer with a photomultiplier tube from Agilent Technologies.

For all spectroscopic measurements, the absorbance at the excitation wavelength was kept below 0.1 to avoid inner filter effects and intermolecular interactions. Absorption and fluorescence experiments at ambient temperatures were performed in 10.00 mm Hellma quartz fluorescence cuvettes. The phosphorescence experiments at 77 K were performed in Dewar fitted with a quartz cold finger accessory; the sample solution was placed in a quartz tube, positioned in the Dewar and flash frozen using liquid nitrogen.

Quantum yields were determined against quinine sulphate in 0.1 N sulphoric acid; see the ESI† for details.

Crystallography

Multiple attempts were made to determine the structure of **Eu·L** using low temperature single crystal X-ray diffraction. Data were variously collected using a (Rigaku) Oxford Diffraction Supernova, an XtaLAB Synergy with a HyPix detector and synchrotron radiation using I19-1 at the Diamond Light Source.[74] Data were reduced using CrysAlisPro or Xia2[75] as appropriate and solved using ShelXT[76] or Superflip[77] prior to refinement with CRYSTALS.[78–80] In each case, the voids were treated using PLATON/SQUEEZE.[81,82] All three polymorphs/solvates were found exhibiting the same tetrameric packing. Further details can be found in the ESI.†

Conflicts of interest

There are no conflicts to declare.

Acknowledgements

The authors thank Oticon Fonden, Diamond Light Source for an award of beamtime (MT13639), Carlsbergfondet, Knud Højgaards Fond, Villum Fonden (grant#14922), Kirsten E. Christensen for support, Cancer Research UK, Cancer Imaging Centre Oxford, the University of Copenhagen, and Dyanne Cruickshank and Rigaku Oxford Diffraction for help with collection of diffraction data using the XtaLAB Synergy.

Published on 09 March 2018. Downloaded by University of Oxford on 9/16/2018 6:57:18 PM.

Notes and references

1 P. Hänninen and H. Härmä, *Lanthanide Luminescence*, Springer, Heidelberg, 2011.
2 A. de Bettencourt-Dias, *Luminescence of Lanthanide Ions in Coordination Compounds and Nanomaterials*, John Wiley & Sons Ltd, 2014.
3 J. C. G. Bunzli, *Coord. Chem. Rev.*, 2015, **293**, 19–47.
4 W. T. Carnall, in *Handbook on the Physics and Chemistry of Rare Earths*, ed. K. A. Gschneidner Jr. and E. LeRoy, Elsevier, 1979, vol. 3, pp. 171–208.
5 R. P. Haugland, *Handbook of Fluorescent Probes and Research Chemicals*, Molecular Probes, Eugene, Oregon, 11th edn, 2010.
6 L. D. Lavis and R. T. Raines, *ACS Chem. Biol.*, 2008, **3**, 142–155.
7 A. T. Frawley, R. Pal and D. Parker, *Chem. Commun.*, 2016, **52**, 13349–13352.
8 J. M. Zwier and N. Hildebrandt, in *Reviews in Fluorescence 2016*, ed. C. D. Geddes, Springer, 2017, pp. 17–43, DOI: 10.1007/978-3-319-48260-6_3.
9 D. Geißler, S. Stufler, H.-G. Löhmannsröben and N. Hildebrandt, *J. Am. Chem. Soc.*, 2012, **135**, 1102–1109.
10 M. Delbianco, V. Sadovnikova, E. Bourrier, G. Mathis, L. Lamarque, J. M. Zwier and D. Parker, *Angew. Chem.*, 2014, **53**, 10718–10722.
11 A. T. Bui, A. Grichine, A. Duperray, P. Lidon, F. Riobe, C. Andraud and O. Maury, *J. Am. Chem. Soc.*, 2017, **139**, 7693–7696.
12 Z. Liao, M. Tropiano, K. Mantulnikovs, S. Faulkner, T. Vosch and T. Just Sørensen, *Chem. Commun.*, 2015, **51**, 2372–2375.
13 Z. Liao, M. Tropiano, S. Faulkner, T. Vosch and T. J. Sørensen, *RSC Adv.*, 2015, 70282–70286, DOI: 10.1039/c5ra15759e.
14 H. Siitari, I. Hemmilä, E. Soini, T. Lövgren and V. Koistinen, *Nature*, 1983, **301**, 258–260.
15 I. Hemmilä, S. Dakubu, V.-M. Mukkala, H. Siitari and T. Lövgren, *Anal. Biochem.*, 1984, **137**, 335–343.
16 G. Marriott, R. M. Clegg, D. J. Arndt-Jovin and T. M. Jovin, *Biophys. J.*, 1991, **60**, 1374–1387.
17 P. R. Selvin, *Annu. Rev. Biophys. Biomol. Struct.*, 2002, **31**, 275–302.
18 G. Vereb, E. Jares-Erijman, P. R. Selvin and T. M. Jovin, *Biophys. J.*, 1998, **74**, 2210–2222.
19 J.-C. G. Bünzli, in *Luminescence of Lanthanide Ions in Coordination Compounds and Nanomaterials*, John Wiley & Sons Ltd, 2014, pp. 125–196, DOI: 10.1002/9781118682760.ch04.
20 F. S. Richardson, *Chem. Rev.*, 1982, **82**, 541–552.
21 M. C. Heffern, L. M. Matosziuk and T. J. Meade, *Chem. Rev.*, 2014, **114**, 4496–4539.
22 A. Grichine, A. Haefele, S. Pascal, A. Duperray, R. Michel, C. Andraudd and O. Maury, *Chem. Sci.*, 2014, **5**, 3475.
23 E. G. Moore, A. P. Samuel and K. N. Raymond, *Acc. Chem. Res.*, 2009, **42**, 542–552.
24 W. S. Perry, S. J. Pope, C. Allain, B. J. Coe, A. M. Kenwright and S. Faulkner, *Dalton Trans.*, 2010, **39**, 10974–10983.
25 H. Uh and S. Petoud, *C. R. Chim.*, 2010, **13**, 668–680.
26 E. Pershagen, J. Nordholm and K. E. Borbas, *J. Am. Chem. Soc.*, 2012, **134**, 9832–9835.
27 L. Armelao, S. Quici, F. Barigelletti, G. Accorsi, G. Bottaro, M. Cavazzini and E. Tondello, *Coord. Chem. Rev.*, 2010, **254**, 487–505.
28 S. Faulkner, L. S. Natrajan, W. S. Perry and D. Sykes, *Dalton Trans.*, 2009, 3890–3899, DOI: 10.1039/b902006c.
29 A. D'Aleo, E. G. Moore, J. Xu, L. J. Daumann and K. N. Raymond, *Inorg. Chem.*, 2015, **54**, 6807–6820.
30 P. Kadjane, L. Charbonniere, F. Camerel, P. P. Laine and R. Ziessel, *J. Fluoresc.*, 2008, **18**, 119–129.
31 F. Kielar, G. L. Law, E. J. New and D. Parker, *Org. Biomol. Chem.*, 2008, **6**, 2256–2258.
32 J. F. Lemonnier, L. Guenee, C. Beuchat, T. A. Wesolowski, P. Mukherjee, D. H. Waldeck, K. A. Gogick, S. Petoud and C. Piguet, *J. Am. Chem. Soc.*, 2011, **133**, 16219–16234.
33 M. Soulie, F. Latzko, E. Bourrier, V. Placide, S. J. Butler, R. Pal, J. W. Walton, P. L. Baldeck, B. Le Guennic, C. Andraud, J. M. Zwier, L. Lamarque, D. Parker and O. Maury, *Chem.– Eur. J.*, 2014, **20**, 8636–8646.
34 E. Kasprzycka, V. A. Trush, V. M. Amirkhanov, L. Jerzykiewicz, O. L. Malta, J. Legendziewicz and P. Gawryszewska, *Chemistry*, 2017, **23**, 1318–1330.
35 T. Lazarides, M. A. Alamiry, H. Adams, S. J. Pope, S. Faulkner, J. A. Weinstein and M. D. Ward, *Dalton Trans.*, 2007, 1484–1491, DOI: 10.1039/b700714k.
36 A. Beeby, S. Faulkner, D. Parker and J. A. G. Williams, *J. Chem. Soc., Perkin Trans. 2*, 2001, 1268–1273, DOI: 10.1039/b009624p.
37 A. Dadabhoy, S. Faulkner and P. G. Sammes, *J. Chem. Soc., Perkin Trans. 2*, 2000, 2359–2360, DOI: 10.1039/b008179p.
38 M. Latva, H. Takalo, V.-M. Mukkala, C. Matachescu, J. C. Rodriguez-Ubis and J. Kankare, *J. Lumin.*, 1997, **75**, 149–169.
39 J. D. Routledge, M. W. Jones, S. Faulkner and M. Tropiano, *Inorg. Chem.*, 2015, **54**, 3337–3345.
40 B. Alpha, R. Ballardini, V. Balzani, J. M. Lehn, S. Perathoner and N. Sabbatini, *Photochem. Photobiol.*, 1990, **52**, 299–306.
41 C. Szijjarto, E. Pershagen, N. O. Ilchenko and K. E. Borbas, *Chem. – Eur. J.*, 2013, **19**, 3099–3109.
42 H. Sund, K. Blomberg, N. Meltola and H. Takalo, *Molecules*, 2017, **22**, 1807.
43 A. D'Aleo, G. Pompidor, B. Elena, J. Vicat, P. L. Baldeck, L. Toupet, R. Kahn, C. Andraud and O. Maury, *ChemPhysChem*, 2007, **8**, 2125–2132.
44 A. Picot, A. D'Aléo, P. L. Baldeck, A. Grichine, A. Duperray, C. Andraud and O. Maury, *J. Am. Chem. Soc.*, 2008, **130**, 1532–1533.
45 A. D'Aléo, C. Andraud and O. Maury, in *Luminescence of Lanthanide Ions in Coordination Compounds and Nanomaterials*, John Wiley & Sons Ltd, 2014, pp. 197–230, DOI: 10.1002/9781118682760.ch05.

This journal is © The Royal Society of Chemistry 2018

Published on 09 March 2018. Downloaded by University of Oxford on 9/16/2018 6:57:18 PM.

46 D. Lundberg and I. Persson, *Coord. Chem. Rev.*, 2016, **318**, 131–134.
47 I. Hemmilá and V.-M. Mukkala, *Crit. Rev. Clin. Lab. Sci.*, 2008, **38**, 441–519.
48 T. Lazarides, D. Sykes, S. Faulkner, A. Barbieri and M. D. Ward, *Chemistry*, 2008, **14**, 9389–9399.
49 M. Tropiano, O. A. Blackburn, J. A. Tilney, L. R. Hill, M. P. Placidi, R. J. Aarons, D. Sykes, M. W. Jones, A. M. Kenwright, J. S. Snaith, T. J. Sørensen and S. Faulkner, *Chem.– Eur. J.*, 2013, **19**, 16566–16571.
50 T. J. Sørensen, M. Tropiano, A. M. Kenwright and S. Faulkner, *Eur. J. Inorg. Chem.*, 2017, **2017**, 2165–2172.
51 T. J. Sørensen, A. M. Kenwright and S. Faulkner, *Chem. Sci.*, 2015, **6**, 2054–2059.
52 D. Kovacs, X. Lu, L. S. Meszaros, M. Ott, J. Andres and K. E. Borbas, *J. Am. Chem. Soc.*, 2017, **139**, 5756–5767.
53 J. Andres and K. E. Borbas, *Inorg. Chem.*, 2015, **54**, 8174–8176.
54 C. Szijjarto, E. Pershagen and K. E. Borbas, *Dalton Trans.*, 2012, **41**, 7660–7669.
55 A. K. R. Junker, G. J. Deblonde, R. J. Abergel and T. J. Sørensen, manuscript submitted.
56 R. Arppe, N. Kofod, A. K. R. Junker, L. G. Nielsen, E. Dallerba and T. Just Sørensen, *Eur. J. Inorg. Chem.*, 2017, 5246–5253.
57 B. Valeur, *Molecular Fluorescence: Principles and Applications*, Wiley-VCH, Weinheim, 2002.
58 N. J. Turro, *Modern Molecular Photochemistry*, University Science Books, Sausalito, 1991.
59 A. Dadabhoy, S. Faulkner and P. G. Sammes, *J. Chem. Soc., Perkin Trans. 2*, 2002, 348–357, DOI: 10.1039/b104541p.
60 P. Caravan, J. J. Ellison, T. J. McMurry and R. B. Lauffer, *Chem. Rev.*, 1999, **99**, 2293–2352.
61 S. Aime, M. Botta, Z. Garda, B. E. Kucera, G. Tircso, V. G. Young and M. Woods, *Inorg. Chem.*, 2011, **50**, 7955–7965.
62 K. J. Miller, A. A. Saherwala, B. C. Webber, Y. Wu, A. D. Sherry and M. Woods, *Inorg. Chem.*, 2010, **49**, 8662–8664.
63 M. Woods, Z. Kovacs, R. Király, E. Brucher, S. Zhang and A. D. Sherry, *Inorg. Chem.*, 2004, **43**, 2845–2851.
64 S. Aime, M. Botta and G. Ermondi, *Inorg. Chem.*, 1992, **31**, 4291–4299.
65 S. Aime, M. Botta, M. Fasano, M. P. M. Marques, C. F. G. C. Geraldes, D. Pubanz and A. E. Merbach, *Inorg. Chem.*, 1997, **36**, 2059–2068.
66 A. Takacs, R. Napolitano, M. Purgel, A. C. Benyei, L. Zekany, E. Brucher, I. Toth, Z. Baranyai and S. Aime, *Inorg. Chem.*, 2014, **53**(6), 2858–2872.
67 A. K. R. Junker, M. Tropiano, S. Faulkner and T. J. Sørensen, *Inorg. Chem.*, 2016, **55**, 12299–12308.
68 A. Beeby, I. M. Clarkson, R. S. Dickins, S. Faulkner, D. Parker, L. Royle, A. S. de Sousa, J. A. G. Williams and M. Woods, *J. Chem. Soc., Perkin Trans. 2*, 1999, 493–504, DOI: 10.1039/a808692c.
69 M. Tropiano, O. A. Blackburn, J. A. Tilney, L. R. Hill, T. Just Sørensen and S. Faulkner, *J. Lumin.*, 2015, **167**, 296–304.
70 W. D. Horrocks and D. R. Sudnick, *J. Am. Chem. Soc.*, 1979, **101**, 334–340.
71 G. E. BUONO-CORE, H. Li and B. MARCINIAK, *Coord. Chem. Rev.*, 1990, **99**, 55–87.
72 N. Sabbatini, M. T. Indelli, M. T. Gandolfi and V. Balzani, *J. Phys. Chem.*, 1982, **86**, 3585–3591.
73 T. A. Shakhverdov, *Opt. Spectrosc.*, 1970, **29**, 166–169.
74 D. R. Allan, H. Nowell, S. A. Barnet, M. R. Warren, A. Wilcox, J. Christensen, L. K. Saunders, A. Peach, M. T. Hooper, L. Zaja, S. Patel, L. Cahill, R. Mashall, S. Trimnell, A. J. Foster, T. Bates, S. Lay, M. A. Williams, P. V. Hathaway, G. Winter, M. Gerstel and R. W. Wooley, *Crystals*, 2017, **7**(11), 336.
75 G. Winter, *J. Appl. Crystallogr.*, 2010, **43**, 186–190.
76 G. M. Sheldrick, *Acta Crystallogr., Sect. A: Found. Adv.*, 2015, **71**, 3–8.
77 L. Palatinus and G. Chapuis, *J. Appl. Crystallogr.*, 2007, **40**, 786–790.
78 P. W. Betteridge, J. R. Carruthers, R. I. Cooper, K. Prout and D. J. Watkin, *J. Appl. Crystallogr.*, 2003, **36**, 1487.
79 P. Parois, R. I. Cooper and A. L. Thompson, *Chem. Cent. J.*, 2015, **9**, 30.
80 R. I. Cooper, A. L. Thompson and D. J. Watkin, *J. Appl. Crystallogr.*, 2010, **43**, 1100–1107.
81 A. Spek, *J. Appl. Crystallogr.*, 2003, **36**, 7–13.
82 P. van der Sluis and A. L. Spek, *Acta Crystallogr., Sect. A: Found. Crystallogr.*, 1990, **A46**, 194–201.

Journal of Luminescence 167 (2015) 296–304

Contents lists available at ScienceDirect

Journal of Luminescence

journal homepage: www.elsevier.com/locate/jlumin

Exploring the effect of remote substituents and solution structure on the luminescence of three lanthanide complexes

Manuel Tropiano [a], Octavia A. Blackburn [a], James A. Tilney [a], Leila R. Hill [a], Thomas Just Sørensen [a,b,*], Stephen Faulkner [a,**]

[a] Chemistry Research Laboratory, University of Oxford, 12 Mansfield Road, Oxford OX1 3TA, UK
[b] Nano-Science Center and Department of Chemistry, University of Copenhagen, Universitetsparken 5, 2100 København Ø, Denmark

ARTICLE INFO

Article history:
Received 5 March 2015
Received in revised form
8 June 2015
Accepted 23 June 2015
Available online 2 July 2015

Keywords:
Kinetically inert lanthanide complexes
Lanthanide emission
Sensitized emission
Lanthanide solvation
Solution structure

ABSTRACT

Sensitized luminescence from trivalent lanthanide ions relies on an appropriate energy match between the sensitizer's excited state (triplet or singlet) and the lanthanide excited state manifold, and also an efficient mechanism of energy transfer between the two. Here, the effect of remote substituents on the luminescence properties of a series of related lanthanide complexes has been investigated. The sensitized lanthanide centered emission is not invariably found to occur following excitation of all chromophores in all systems, and it is shown that only the most structurally congested of the systems investigated exhibited pronounced solvatochromism.

© 2015 Elsevier B.V. All rights reserved.

1. Introduction

While the electronic transitions between the electronic states of lanthanide ions are characterized in the solid state, and in well-defined geometries [1–8], our understanding of the photophysical properties of lanthanide ions and lanthanide complexes in solution is limited to describing the simplest and most symmetric complexes [9–15]. This is a direct consequence of the long luminescence lifetime of the trivalent lanthanide ions, which in combination with the fast exchange of simple ligands by these ions [16], makes the emission detected from any solution-based experiment a weighted average. Constitutional isomers aside, even conformational isomers may have different properties, which make it a big challenge to produce data that can be correlated to a single lanthanide species. Three approaches to meet this challenge can be adopted: (1) synthesis of lanthanide complexes that are locked i.e. displaying only a single species and a single conformation in solution; (2) synthesis of large quantities of ultrapure complexes that can be used to perform absorption based experiments; (3) synthesis of elaborate molecular structures that can be used to probe the structure-property relationships in lanthanide complexes indirectly.

We recently demonstrated that the synthesis of a range of multinuclear lanthanide complexes can be achieved using the Ugi reaction, 'click' chemistry, and peptide coupling reactions to link kinetically stable building blocks together [17–22], and observed for the first time that changes to substituents remote from the binding site could have a profound effect on the affinity of such complexes for anionic guests [23]. Here, we continue the investigation into these systems, establishing the photophysical properties of these multinuclear lanthanide complexes in detail, and elucidating key information about the role of structure and solvent in determining their solution structure.

Due to the very low molar absorptivity of the f–f transitions, direct excitation of lanthanide centered transitions is inefficient [24,25]. Therefore, sensitizing chromophores are used to generate lanthanide centered excited states. This process is called the antenna effect, see Fig. 1. Instead of direct excitation of the lanthanide, light is absorbed by a chromophore with a high molar absorptivity, generating an excited state that is able to populate the lanthanide centered excited state via an appropriate energy transfer process. While the efficiency of the energy transfer is not unity, the lanthanide excited state population generated following irradiation is still multiple times what would be obtained following excitation directly into the f-manifold using irradiation of similar intensity. Here, we show how important the spatial

* Corresponding author at: Nano-Science Center and Department of Chemistry, University of Copenhagen, Universitetsparken 5, 2100 København Ø, Denmark. Tel.: +45 35 32 02 13; fax: +45 35 32 02 14.
** Corresponding author. Tel.: +44 1865 285 148.
E-mail addresses: TJS@chem.ku.dk (T. Just Sørensen), stephen.faulkner@chem.ox.ac.uk (S. Faulkner).

http://dx.doi.org/10.1016/j.jlumin.2015.06.035
0022-2313/© 2015 Elsevier B.V. All rights reserved.

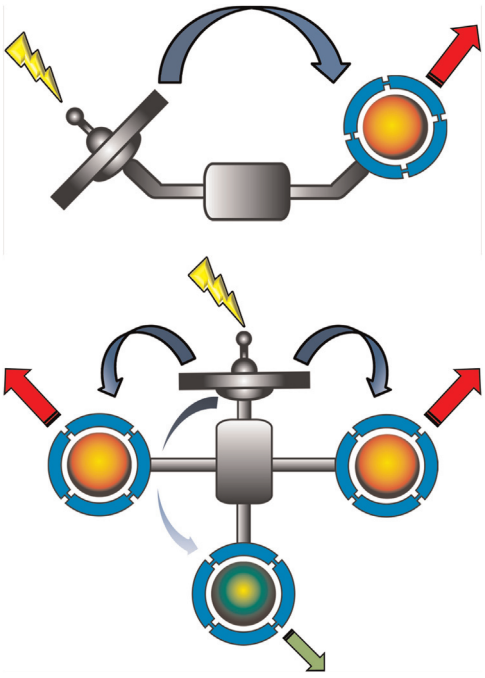


Fig. 1. Cartoon showing sensitized population of lanthanide centered excited states in simple mononuclear complexes (top) and in multinuclear heterometallic complexes (bottom).

relationship between lanthanide center and the sensitizing chromophore can be in determining the observed emission intensity, by comparing two similar trinuclear (and bimetallic) lanthanide complexes. From these results, it will be seen that an increased chromophore density alone does not make for highly luminescent lanthanide complexes, as not all lanthanide centers in the investigated molecules are populated efficiently by the chromophores in the structure.

2. Methods and materials

2.1. Materials

All materials were used as received; solvents were of HPLC grade and were used without further purification. The molecules investigated were prepared as described in ref. [23].

2.2. Spectroscopy

Spectroscopy was performed using conventional absorption (Agilent Cary 300/PerkinElmer Lambda1050) and emission spectrometers (Agilent Cary Eclipse/Horiba Fluorolog) and 1 cm quartz cuvettes (Helma). Time-gating and phosphorescence spectra were recorded by applying a delay time and subsequently recording over a suitable time-window. The time-resolved emission spectra (TRES) were produced by increasing the delay time and keeping the time-window constant. Luminescence lifetimes were determined using the same method and at a single wavelength in the spectrum.

2.3. Calculations of q – the number of inner sphere solvent molecules

It has been recognized that lanthanide excited states can be quenched by transferring energy to overtones of molecular vibrations [25,26], and it was found that the OH stretching vibration is an effective energy acceptor for energy transfer from a lanthanide excited state [27]. As the rate of energy transfer is strongly distance dependent ($k_{ET} \propto r^{-6}$) [28,29], the degree of quenching of a lanthanide centered excited state can be used to calculate the number of molecules containing OH oscillators that are bound to the lanthanide center. This was realized by Horrocks, who developed a method to determine q – the number of water molecules bound at a lanthanide center [27]. The Horrocks equation in its native and modified form is described below. Another approach to use the quenching of lanthanide excited states by OH oscillators was developed by Kimura [30]. The foundation for the Kimura approach, discussed below, is significantly different from that of the Horrocks equation.

Each approach uses the observed luminescence lifetime τ_{LM} to determine q. The luminescence lifetime can be related to the rate constant for depopulating the excited state k_{obs}, with $\tau_{LM}{}^{-1} = k_{obs}$. The observed rate constant is the sum of processes depopulating the lanthanide excited state (Eq. (1)), where the most important contributions are:

- k_r radiative decay from the lanthanide excited state.
- k_{nr} non-radiative decay from the lanthanide excited state, a sum of a series of quenching processes:
  - k_{OH} quenching by OH oscillators of inner-sphere solvent molecules, note that a single water molecule has two OH oscillators whereas e.g. alcohols have one OH oscillator; the degree of quenching is proportional to the number of oscillators and not the number of solvent molecules.
  - k_{NH} quenching by NH oscillators in close proximity to the lanthanide center that can undergo deuterium exchange, not necessarily coordinated.
  - k_{ligand} quenching by specific ligand structures, not OH or NH oscillators.
  - k_{other} quenching from other contributions such as solvated ions, outer sphere solvent (k_{outer}) etc.

The radiative decay constant k_r is the sum of all the radiative processes depopulating the excited state of a given lanthanide i.e. a sum over seven independent processes for terbium and europium, while the non-radiative decay constant k_{nr} is dominated by the listed contributions in the absence of specific quenching pathways such as electron transfer in europium and ytterbium and energy back-transfer to low lying chromophore states.

2.4. Horrocks equation

In order to evaluate the effect of solvent induced quenching of lanthanide excited states, the observed luminescence lifetime can be used by considering the following relationships:

$$\tau_{LM}{}^{-1} = k_{obs} = k_r + k_{nr} = k_r + k_{ligand} + k_{OH} + k_{NH} + k_{other} \quad (1)$$

$$\tau_{LM}(H_2O)^{-1} = k^{H}_{obs} = k_r + k_{ligand} + k_{OH} + k_{NH} + k_{other} \quad (2)$$

$$\tau_{LM}(D_2O)^{-1} = k^{D}_{obs} = k_r + k_{ligand} + k_{NH} + k_{other} \quad (3)$$

$$\tau_{LM}(H_2O)^{-1} - \tau_{LM}(D_2O)^{-1} = + k_{OH} = k^{H}_{oH} - k^{D}_{obs} = \Delta k_{obs} = k_{OH} \quad (4)$$

$$k_{OH} = k^{1}_{OH} + k^{2}_{OH} + k^{3}_{OH} \ldots + k^{n}_{OH} \text{ if } k^{1}_{OH} = k^{n}_{OH} \text{ then } k_{OH} = nk^{`}_{OH} \quad (5)$$

$$nk^{`}_{OH} = \Delta k_{obs} = \tau_{LM}(H_2O)^{-1} - \tau_{LM}(D_2O)^{-1} \quad (6)$$

$$n = (k_{OH}^{`})^{-1}(\tau_{LM}(H_2O)^{-1} - \tau_{LM}(D_2O)^{-1}) \quad (7)$$

Assuming that only inner-sphere (k_{OH}) solvent is responsible for reduced quenching between H and D, if $A=(k_{OH}^{`})^{-1}$ and $n=q$ then the Horrocks equation is obtained [27]:

$$q = A(\tau_{LM}(H_2O)^{-1} - \tau_{LM}(D_2O)^{-1}) \quad (8)$$

If more contributions are present, then:

$$\begin{aligned}&\tau_{LM}(H_2O)^{-1} - \tau_{LM}(D_2O)^{-1}\\ &= k_{obs}^{H} - k_{obs}^{D}\\ &= \Delta k_{obs}\\ &= k_{OH} + k_{NH} + k_{outer}\\ &= nk_{OH}^{`} + k_{NH} + k_{outer}\end{aligned} \quad (9)$$

$$nk_{OH}^{`} = \tau_{LM}(H_2O)^{-1} - \tau_{LM}(D_2O)^{-1} - k_{NH} - k_{outer} \quad (10)$$

$$n = (k_{OH}^{`})^{-1}(\tau_{LM}(H_2O)^{-1} - \tau_{LM}(D_2O)^{-1} - k_{outer} - k_{NH}) \quad (11)$$

If $A=(k_{OH}^{`})^{-1}$, $B=k_{outer}$, $C=k_{NH}$ and $n=q$ then the modified Horrocks equation is obtained [15]:

$$q = A(\tau_{LM}(H_2O)^{-1} - \tau_{LM}(D_2O)^{-1} - B - C) \quad (12)$$

The main assumptions in this approach are that each OH oscillator in the inner coordination sphere induces the same rate of quenching in all complexes and solvates (Eq. 5), that the solvent in the outer sphere gives rise to the same rate of quenching in all complexes and solvates (Eq. 10), and that the distances to amino/amido quenchers and OH oscillators are similar for all complexes and solvates. As a consequence, the modified Horrocks equation should be applied with a degree of skepticism and q should not be given with more than two significant figures. Note that the error when using the Horrocks equation/modified Horrocks equation is q +/−0.5 (solvent molecules), while smaller differences can be considered significant when similar ligand structures are compared under identical experimental conditions.

k_{ligand} can be ignored if no oscillators known to quench lanthanide excited states are present – note that OH and NH oscillators have already been accounted for. For neodymium, praseodymium, and erbium, C–H oscillators have been shown to provide an effective pathway for non-radiative quenching of the lanthanide excited state. For these lanthanides, ligand oscillators must also be taken into account when targeting highly luminescent compounds [31–34]. Generally the actual ligand structure has to be considered in order to determine k_{ligand} [31,35]. As the additional quenching pathways are inherent to the molecular structure and thus independent of deuteration in the solvent, they have no effect when calculating hydration.

2.5. Kimura method

Using Eq. (6) to rewrite Eq. (1), the following equations can be written:

$$\tau_{LM}(H_2O)^{-1} = k_{obs}^{H} = k_r + k_{ligand} + k_{OH} + k_{NH} + k_{other} = nk_{OH}^{`} + \chi \quad (13)$$

$$n = (k_{OH}^{`})^{-1}(\tau_{LM}(H_2O)^{-1} - \chi) = (k_{OH}^{`})^{-1}(\tau_{LM}(H_2O)^{-1}) - (k_{OH}^{`})^{-1}\chi \quad (14)$$

Kimura has been using experimental data to determine $(k_{OH}^{`})^{-1}$ and $(k_{OH}^{`})^{-1}\chi$ by measuring the excited state lifetimes in H_2O/D_2O mixtures [30,36–41]. This approach relies strongly on the assumption that all contributions except $nk_{OH}^{`}$ are constants. As this can only be true for very similar ligand structures, the scope of this approach is limited. When considering more elaborate lanthanide and actinide complexes, the Horrocks equation must be used. The Horrocks equation uses the comparison of two independent measurements to reduce the uncertainties enforced by the required assumptions.

3. Results and discussion

Three different molecular structures **1**–**3** were investigated, while data for a fourth structure **4** is included for comparison. The molecular structures are shown in Chart 1. α,α'-bis(Eu.DO3A)-*m*-xylene (**1**, *m*-bis(europium 1,4,7,10-tetraazacyclododecane-1,4,7-triacetate-10-methylene)-benzene) is a dinuclear europium complex, in which each lanthanide is bound in a heptadentate binding pocket. In this molecular structure a single aniline chromophore is present. Compound **2** is derived from **1** by a peptide coupling with **4** (terbium 2,2',2''-(10-(2-((carboxymethyl)amino)-2-oxoethyl)-1,4,7,10-tetraazacyclododecane-1,4,7-triyl)triacetate) which is a kinetically stable terbium DO3A-monoamide complex with a free carboxylic acid. **2** is a trinuclear heterobimetallic lanthanide complex, but as with **1** there is only one chromophore in the system. Whereas the chromophore in **1** is an aniline that in **2** is an anilide. Thus, the chromophore density as well as position is identical in **1** and **2**. Compound **3** is derived from **1** via an Ugi reaction with benzaldehyde, **4**, and benzyl isonitrile. As with **2**, **3** is

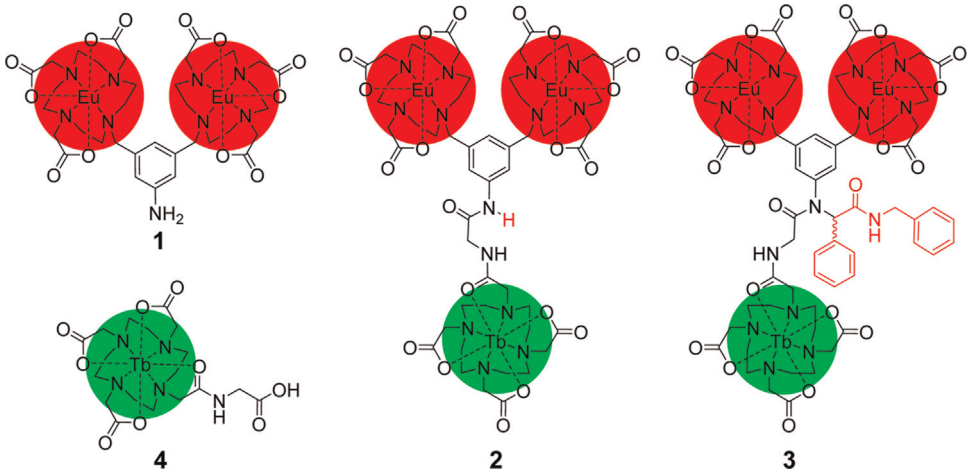


Chart 1. Molecular structures studied in this work.

a trinuclear heterobimetallic lanthanide complex, but with two phenyl rings in addition to the anilide chromophore. These make the overall structure of **3** significantly more crowded than that of **1** and **2**. The position of the two additional chromophores in **3** is not fixed relative to the lanthanide centers, and conformations where there are sensitizers close to any of the three lanthanide centers are possible. While the distance from the anilide to each of the europium centers is identical, the chromophore to terbium distance is unlikely to be identical in all complexes **1**–**3**. As there is no conjugation between chromophores and the lanthanide centers, energy transfer to the lanthanide centers must be through space and thus mediated by intramolecular collisions. Therefore, the energy transfer and sensitization efficiency in **3** will depend greatly upon the molecular solution structure; in particular the conformational freedom of the two phenyl groups will be reflected in the luminescence properties of **3**.

The normalized absorption spectra of compounds **1**–**3** in D_2O are shown in Fig. 2. Ideally, the spectra should be a simple superposition of the component spectra, but this is not the case. In particular, the blue-shift commonly observed between the spectra of aniline and acetanilide is not seen in the spectra of **2** and **3**. This suggests that the molecular constitution inhibits the formation of the ideal, fully conjugated conformation of the acetanilide moiety in both **2** and **3** [28]. Comparison of the spectra of **2** and **3** reveals an increased absorption in **3** at wavelengths below 325 nm, which can be attributed to the introduction of the two phenyl groups.

3.1. Luminescence spectra

The normalized time-gated emission spectra of compounds **2** and **3** in acetonitrile, methanol, and D_2O are shown in Fig. 3. The spectrum of **2** shows emission bands that can be readily assigned to originate from lanthanide centered emission at the terbium and europium centers. Where the emission band at 488 nm (Tb $^5D_4 \rightarrow {}^7F_6$) and 545 nm (Tb $^5D_4 \rightarrow {}^7F_5$) are readily assigned to originate at the terbium center, the bands in the region 580–600 nm (Tb $^5D_4 \rightarrow {}^4F_4$, Eu $^5D_0 \rightarrow {}^7F_{0,1}$) and at 620 nm (Tb $^5D_4 \rightarrow {}^7F_3$, Eu $^5D_0 \rightarrow {}^7F_2$) are a mixture of emission from both lanthanide center. The low intensity bands (Tb $^5D_4 \rightarrow {}^7F_{2,1,0}$, Eu $^5D_0 \rightarrow {}^7F_3$) are not readily resolved in the time-gated emission spectrum of **2** following excitation at 280 nm, while the band at 700 nm (Eu $^5D_0 \rightarrow {}^4F_4$) can unambiguously be assigned to europium. Comparing the emission intensity in the two bands from Eu $^5D_0 \rightarrow {}^7F_4$ (700 nm) and Tb $^5D_4 \rightarrow {}^7F_5$ (545 nm) allows for a direct measure of the relative population of the two lanthanide centers following excitation in the chromophore manifold. Direct excitation of terbium is possible by addressing the Tb $^5D_4 \rightarrow {}^7F_6$ transition at 488 nm, but yielded no further information. Direct excitation of europium was not possible, as exciting the Eu $^7F_0 \rightarrow {}^5L_6$ also resulted in excitation of the Tb $^5D_4 \rightarrow {}^5G_6$ transition [10,11]. The time-gated emission spectra of **2** in acetonitrile, methanol and D_2O show no clear solvent dependence in the formation of the lanthanide excited states. Though, the relative intensities of the bands resulting from terbium centered transitions changes slightly, thus indicating a solvent dependence in the branching ratios observed in the emission from Tb $^5D_4$. That is, the 488 nm (Tb $^5D_4 \rightarrow {}^7F_6$) band changes 10% in intensity when compared to the 545 nm (Tb $^5D_4 \rightarrow {}^7F_5$) band. For **2**, as was the case for the related molecular structures [17,23,42], we did not observe any effect of concentration on the excited state properties. Among the related structures, particularly thenaphthalene containing complexes should be able to report on aggregation through excimer formation [43], as this is not observed even at mM concentration we conclude that aggregation is not a factor for **2** and **3**.

The time-gated emission spectra of **3** following excitation at 280 nm are shown in Fig. 3. Comparing the spectra of **2** and **3** in D_2O, there is a pronounced difference in the europium emission observed as the relative intensity observed in the Eu $^5D_0 \rightarrow {}^7F_4$ band at 700 nm in **3** is twice that of **2** when measured relative to the terbium centered emission. This increase can be rationalized by assuming that the anilide chromophore preferentially populates the terbium excited state, while the two phenyl chromophores increase the population of the europium excited state. The branching ratio observed for terbium as a function of the changing solvent for **3** was similar to that observed for **2**. The changes in relative emission intensities of europium and terbium when the solvent is changed from D_2O to methanol and acetonitrile are dramatic. The relative intensity of the europium emission increases ten-fold when the solvent is changed from D_2O to acetonitrile, while the luminescence lifetime is reduced (see below).

The differences in absorption and emission spectra are supported by the excitation spectra shown in Fig. 4. The excitation

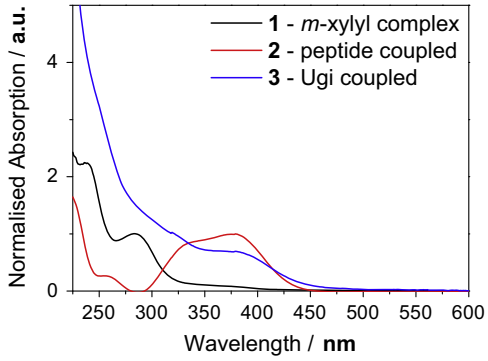


Fig. 2. Normalized absorption spectra of **1**, **2** and **3** recorded in D_2O. The spectra are normalized by the intensity at the peak of the primary absorption band (**1** 280 nm; **2** 390 nm; **3** 360 nm).

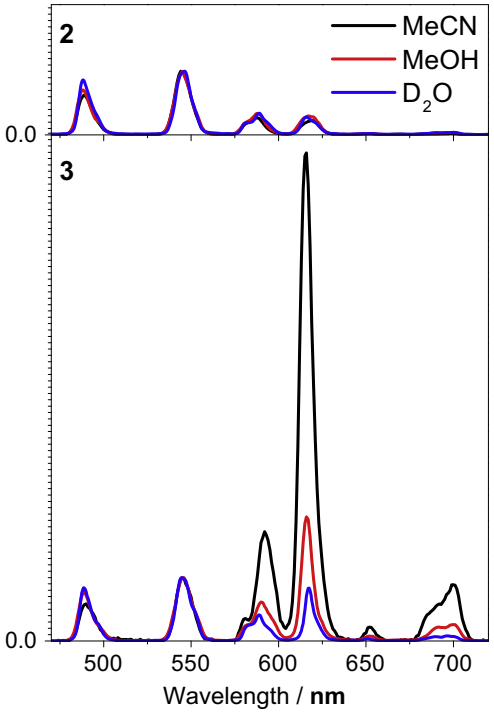


Fig. 3. Normalized luminescence emission spectra of **2** and **3** recorded with a 5 nm emission slit following 280 nm excitation (excitation slit: 20 nm, delay: 0.2 ms, window: 3 ms). The spectra are on the same scale and are normalized at 545 nm.

spectra measured by monitoring terbium centered emission at 545 nm (Tb $^5D_4 \rightarrow {}^7F_5$) are identical in **2** and **3**, while there is a pronounced difference in the excitation spectra measured by monitoring europium centered emission at 690 nm (Eu $^5D_0 \rightarrow {}^7F_4$). From cursory inspection of the excitation spectra it would appear that europium is preferentially populated via the anilide chromophore in both **2** and **3**, while there is no significant population of the terbium excited state from the two phenyl chromophores in **3**. This outcome is related to our recent observations for a pyrene appended europium complex, where the separation between the europium center and the pyrene chromophore determined whether the lanthanide centered excited state could be populated from the pyrene triplet state [44].

3.2. Time-resolved emission spectra

By exploiting the differences in luminescence lifetime, the time-resolved emission spectra (TRES) can separate signals originating at different emitters, thus efficiently removing background emission originating from sample background, chromophore centered emission, and any endogenous or non-endogenous fluorophores in the system such as flavins [45,46]. If the luminescence lifetimes of the individual emitters are spaced suitably, the pure emission spectra of overlapping species can be resolved, providing a third dimension (intensity, wavelength, time) to the detection in time-gated emission based experiment. Fig. 5 shows the time-resolved emission spectra of **2** and **3**. For **2** the TRES shows that the intensity distribution between terbium and europium centered emissions mirror that observed in the luminescence spectrum (Fig. 3), and due to the slow (>1 ms) decay of the terbium emission, this dominates the spectrum, while the relatively short-lived (<1 ms) europium emission after a few milliseconds becomes of vanishing intensity. Similarly, the TRES recorded for **3** is dominated by the europium centered emission at short decay times, which is expected when considering the luminescence spectrum in Fig. 3. As with **2** the short-lived (<1 ms) europium emission disappears in the TRES in the last third of the TRES in Fig. 3, highlighted by the band at 700 nm (Eu $^5D_0 \rightarrow {}^4F_4$), resulting in a spectrum originating from terbium centered emission at long decay times. In both TRES the power of the technique can be seen in the bands in the region 580–600 nm (Tb $^5D_4 \rightarrow {}^4F_4$, Eu $^5D_0 \rightarrow {}^4F_{0,1}$) and at 620 nm (Tb $^5D_4 \rightarrow {}^4F_3$, Eu $^5D_0 \rightarrow {}^4F_2$). Independent of whether terbium or europium emission dominate this region of the spectrum, the fact that two components with different lifetimes contribute to the emission intensity observed at short decay times (Fig. 3), is realized by cursory inspection of the TRES in Fig. 5.

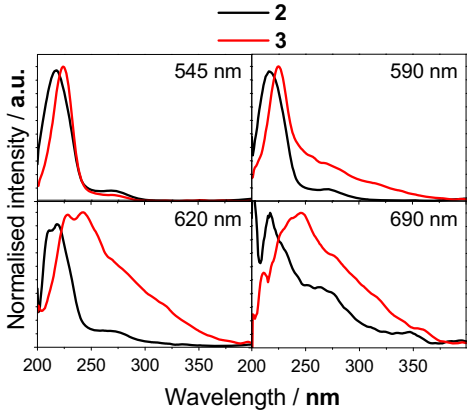


Fig. 4. Normalized luminescence excitation spectra of **2** and **3** in D_2O recorded with 10 nm slits at different points of observation (emission slit: 10 nm, delay: 0.2 ms, window: 3 ms).

3.3. Luminescence lifetimes in water and q

The luminescence lifetime alone does not allow for conclusions as to which pathway the individual excited state is populated by, but does allow for conclusions as to the degree of quenching of the individual excited states. In combination with the results obtained above, determining the luminescence lifetimes makes it possible to deduce how the observed changes in the photophysical properties between the compounds **2** and **3** arise. Furthermore, by comparing the luminescence lifetimes of **2** and **3** in different solvents, and comparing the properties of the compounds both as free molecules and when bound to isophthalate, the differences between the two structures become clear.

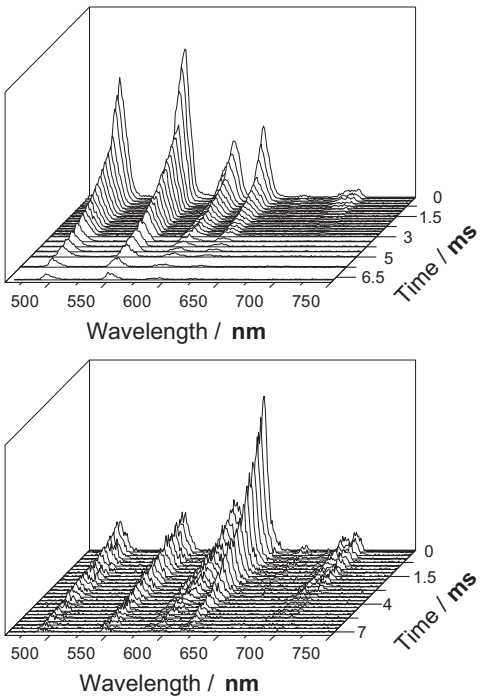


Fig. 5. Time resolved emission spectra in methanol of **2** (top) and **3** (bottom), from 0.1 ms to 6.5 ms initial time-delay in methanol.

Table 1
Luminescence lifetime, number of inner sphere solvent molecules q (Horrocks), and number of inners sphere solvent molecules n (Kimura) for compounds **1**–**4** in water and following excitation at 275 nm (excitation slit: 14 nm, emission slit: 5–14 nm).

	λ_{em}/nm	**1**	**2**	**3**	**4**
τ_{H2O}/ms	700	0.4	0.4	0.8	
τ_{D2O}/ms	700	0.9	0.9	1.7	
q_{Eu}		1.4	1.4	0.5	
n Kimura		2.2	2.2	0.9	
τ_{H2O}/ms	545		1.8	1.9	1.9
τ_{D2O}/ms	545		2.6	2.9	3.4
q_{Tb}			0.6	0.6	0.9
n Kimura			1.4	1.3	1.3

q Calculated using $q = A(\tau(H_2O)^{-1} - \tau(D_2O)^{-1} - B)$ A: 5 ms(Tb), 1.2 ms (Eu); B: -0.06 ms^{-1} (Tb), -0.25 ms^{-1} (Eu).

3.4. Free molecules

Table 1 shows the luminescence lifetimes recorded in the emission bands that can be exclusively assigned to either terbium or europium emission (545 nm, Tb $^5D_4 \rightarrow {}^7F_5$; 700 m, Eu $^5D_0 \rightarrow {}^7F_4$) following excitation in the chromophore manifold at 275 nm. The europium centers in compounds **1** and **2** experience very similar surroundings, and have identical luminescence lifetimes and q values. The europium centers in **3** show a significantly increased luminescence lifetime, due to a significant reduction in q from $q=1.4$ in **1** and **2** to $q=0.5$ in **3**. The terbium center shows different behavior between the starting material **4** and the compounds **2** and **3**. The luminescence lifetimes are identical for all three systems within error, while q reduces from $q=0.9$ in **4** to $q=0.6$ in **2** and **3**, indicating that the face of the DOTA-monoamide terbium binding pocket is more crowded in compounds **2** and **3** when compared to the starting material **4**.

The bulk of the substituent on the secondary aniline nitrogen in **2** is not enough to disrupt the average structure of the two DO3A europium binding pockets, resulting in a similar solvation and degree of quenching of europium in **1** and **2**. In **3** there are significantly more bulky substituents on the now tertiary aniline nitrogen, and as a consequence there is a substantial change in solvation around europium, resulting in a much longer luminescence lifetime and a lower q. The bulk of the third substituent on the aniline nitrogen in **3** does not influence the terbium centered emission, indicating that the terbium complex is positioned in such a way that it is only influenced by the structural unit originating from **1**, and not by the substituents introduced through the Ugi coupling. This assumption is supported by the results obtained in the emission and excitation spectra above, where the terbium centers in **2** and **3** have similar behaviors.

To highlight the importance of controlled experimental conditions, the effect of pH on the luminescence lifetime of **1** was investigated. The results are shown in Table 2, and suggest that pH, solvent composition and ionic strength must be identical in all samples if properties such as luminescence lifetime and q are to be compared. Upon changing from pH 9 to 2, the luminescence lifetime is reduced by close to a factor of 2, while q increases by almost a factor of 4 from $q=0.5$ to $q=1.8$. Note that the number of solvent molecules at the lanthanide center as calculated by the Kimura method does not follow the trends reported by q, but does register the change in solvation between low and high pH.

3.5. Solvent effects

The luminescence lifetimes listed in Tables 1 and 2 were all measured in aqueous solution. The emission spectra in Fig. 3 show a large degree of solvatochromism for **3** particularly with respect to the ratio of europium to terbium centered emission intensity, while only small changes in the terbium branching ratios of **2** were observed. By comparing the luminescence lifetimes of **2** and **3** in different solvents it is possible to separate the contributions to the increased emission intensity of europium due to solvation, from those due to increased sensitization due to changes in molecular structure. The strong distance dependence (e^{-r}/r^{-6}) in the energy transfer from the chromophores to the lanthanide center makes the process highly dependent on molecular structure. Considering the contribution from the refractive index changes when going from acetonitrile to water, the rate of spontaneous emission increase by 2.5% [48], with an additional increase of 2.5% from water to methanol. This cannot account for the observed changes

Table 2
Effect of pH/pD on the luminescence lifetime and on the number of inner sphere solvent molecules q for **1** in water/D_2O following 280 nm excitation.

	τ_{H2O}/ms	+/−	τ_{D2O}/ms	+/−	q_{Eu}[a]	n Kimura[b]
pH 2	0.41	0.05	1.39	0.13	1.8	2.1
pH 6.7	0.38	0.03	0.92	0.04	1.6	2.3
pH 9[c]	0.68		1.24		0.5	1.1
pH 12.5	0.61	0.04	1.37	0.06	0.8	1.3

[a] Calculated using $q=A(t(H_2O)^{-1}-t(D_2O)^{-1}-B)$ A: 1.2 ms (Eu); B: $-0.25\ ms^{-1}$ (Eu).
[b] n Calculated using $n=1.05(t(H_2O))^{-1}-0.44$ (Eu).
[c] From reference [47].

Table 3
Solvent effects on the luminescence lifetimes of compounds **2** and **3** following excitation at 280 nm or 488 nm (excitation slit: 20 nm, emission slit: 10 nm).

		2 τ/ms		**3** τ/ms	
	Ln	280 nm	488 nm	280 nm	488 nm
H_2O	Eu	0.4	–	0.8	–
	Tb	1.8	1.7	1.9	2.1
CH_3OH	Eu	0.4	–	1.1	–
	Tb	1.7	1.4	1.4	1.6
CH_3CN	Eu	0.4	–	1.2	–
	Tb	1.4	1.1	2.1	2.3

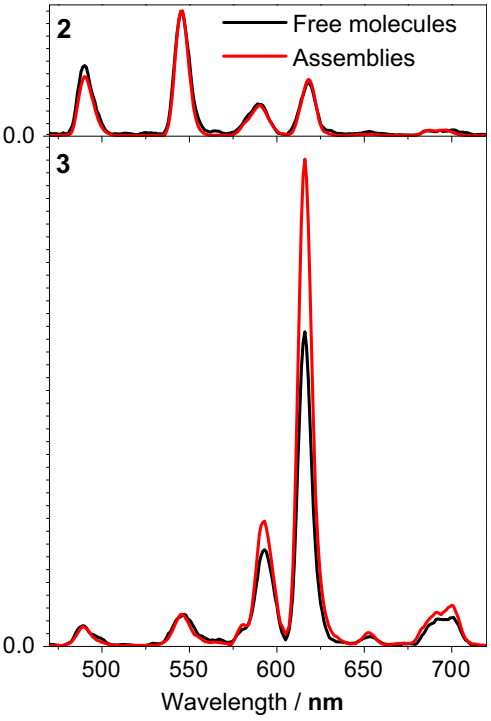


Fig. 6. Normalized luminescence emission spectra of **2** and **3** in methanol with and without isophthalate, recorded with a 5 nm emission slit following 280 nm excitation (excitation slit: 20 nm, delay: 0.2 ms, window: 3 ms). The spectra are on the same scale and are normalized at 545 nm.

Table 4
Luminescence lifetimes before and after the binding of isophthalate in methanol.

τ_{MeOH}/ms		**2**		**3**	
λ_{ex}/nm	λ_{em}/nm	Initial	Final	Initial	Final
275	545	1.7	1.4	1.8	1.5
275	700	0.4	0.4	1.0	1.0

in the emission spectrum of **3** (Fig. 3), which must originate from changes in the solution structure of the molecule.

The solvent dependence of the luminescence lifetime of **2** and **3** is shown in Table 3, note that the emission spectra shown in Fig. 3 are for D_2O, CH_3OH and CH_3CN solutions. Considering only water, the ratio of europium centered emission to terbium centered emission in **3** should be significantly higher than in **2** as a consequence of the much longer luminescence lifetime. This is the case, and the increase is the factor of 2 expected from the emission spectrum (i.e. $\phi_{LM}=\tau/\tau_r$; $\tau_r=k_r^{-1}$) [28,29]. For **2** the luminescence lifetime observed at the europium center is identical in all solvents, and the same is the case for the terbium center although the lifetime in acetonitrile is slightly shorter. That is, the lifetimes and the observed spectra for **2** agree with small changes exclusively due to solvation of the metal center and the refractive index of the solvent. For **3** the luminescence lifetime observed at both lanthanide center varies between solvent systems. Assuming that the symmetry at each lanthanide center is unchanged, the ratio between the lifetime observed for europium and terbium can be used to indicate the origin of the changes in the emission intensity at each lanthanide center. By using this assumption, the ratio between europium and terbium centered emission should be similar in water and acetonitrile, while the ratio should favor europium in methanol due to quenching of the terbium centered emission. This is not what is observed in the spectrum, where the europium emission is greatly increased in acetonitrile, and only slightly so in methanol. Furthermore, as the increase is too large to be accounted for by an increase in lifetime, and as the changes in lifetime do not follow the trend observed in the spectra, it must be concluded that the observed changes are primarily due to increased energy transfer from the sensitizing chromophores as a result of variations in the molecular structure.

Direct excitation of terbium gives rise to a significantly different average lifetime than that observed following sensitized excitation. We hypothesize that this is due to the existence of two distinctly different molecular conformations, one *closed conformation* where sensitization of terbium is possible via the aromatic rings of compounds **2** and **3**, and one *open conformation* where this process does not occur. The differences in the observed lifetimes are thus a result of the different quenching pathways operating in the two conformations [42]. As the luminescence lifetime data are the result of the weighted average over the molecular conformations that the individual molecules adopt during the millisecond excited state lifetime, we cannot quantify our observation. The excitation process is instantaneous, and demonstrates that two significantly different conformations of **2** and **3** are present in solution, and that these have different photophysical properties.

3.6. Assemblies

Changes in the solvent can change the effective chromophore density, see above. The same effect can be realized in a self-assembly process, where isophthalic acid is bound in the binding pocket created by the α,α'-bis(Eu.DO3A)-*m*-xylene motif [47,49–51]. Fig. 6 shows the changes in the spectral shape upon binding of isophthalate to compound **2** and **3** in methanol; the total emission intensity increases significantly for both complexes [23], but the increase for **2** is not accompanied by any changes in the appearance of the spectrum [23]. For **3** the overall increase in emission intensity occurs with a clear preference for generating europium centered excited states [23], which can be seen by the increased europium centered emission in comparison to terbium centered emission in Fig. 6.

Table 4 shows the lifetime changes upon binding isophthalate to **2** and **3**. The europium lifetime is unchanged, while the terbium excited state lifetime is decreased in both cases. This observation can be rationalized by considering the conformational space available to the molecules, and assuming an increase in the population of molecules that are in a configuration with increased quenching of the terbium center [23]. That is, binding of isophthalate in the α,α'-bis(Eu.DO3A)-*m*-xylene binding pocket forces a significant change in conformation of the entire molecule.

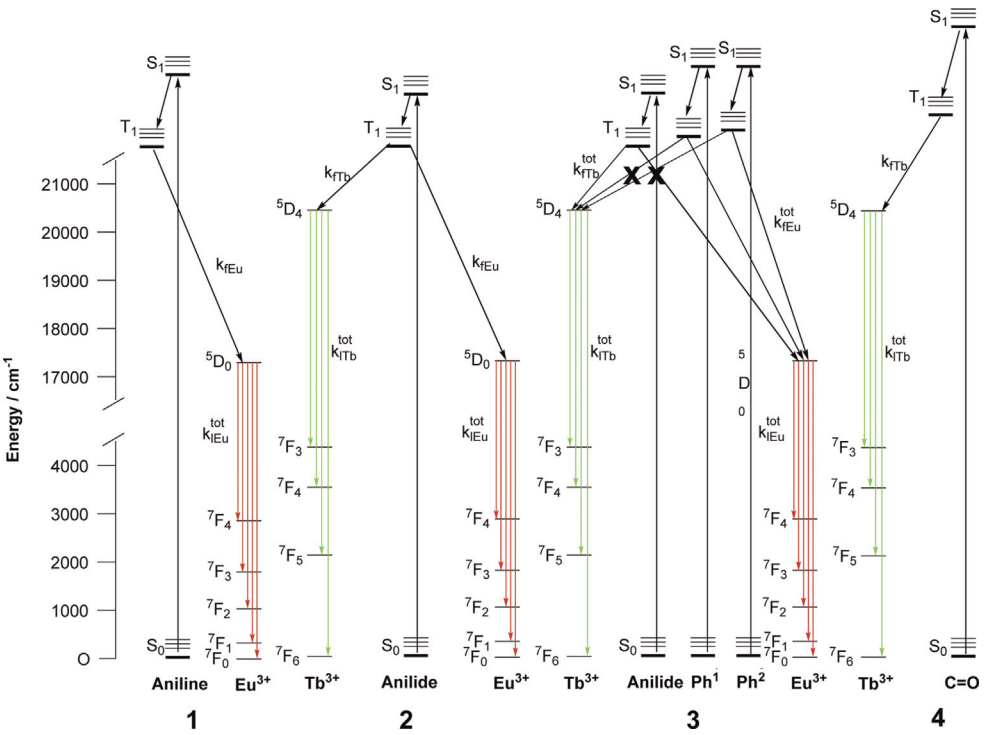


Fig. 7. Partial Jablonski diagrams showing the possible sensitization pathways for **1**, **2**, **3** and **4**.

4. Conclusion

Fig. 7 shows the excited state processes responsible for the lanthanide luminescence observed from the investigated complexes **1**, **2**, **3** and **4**. The data reported here demonstrate that by comparing these four systems we can separate the processes originating from differences in molecular constitution from those originating in changes in molecular conformation. We found that changes in the molecular constitution do not inevitably correlate directly to luminescence observed from a given molecule. Specifically, we show that simply increasing the chromophore density in a given molecular framework does not necessarily facilitate an increase in the excited state population of a given lanthanide center in that structure, but may actually decrease the observed emission if the lanthanide center is excluded from the conformational isomers giving rise to efficient formation of the lanthanide excited state. That is, some of the processes shown in Fig. 7 do not occur, e.g. population of the terbium center from the phenyl chromophores in compound **3** (see Fig. 4). Our observations do not show evidence for Ln to Ln' energy transfer in these systems, indicating that close contact of the lanthanide centers are not possible [52].

Comparing the photophysical properties of compounds **2** and **3**, a dramatic effect can be seen in the response to changes in solvent or in the result of binding an analyte. While the properties of **2** are essentially unchanged, the luminescence observed from **3** exhibits pronounced solvatochromism and spectral changes upon binding of analytes. Thus, we must conclude that predicting the properties of larger lanthanide containing molecules is exceedingly difficult, as small changes may alter the general behavior of the entire molecule significantly. For the structures investigated here, the pivotal point where the properties become unpredictable occurs when the central aniline nitrogen goes from having two to three substituents.

Acknowledgments

The authors thank the University of Oxford, Christ Church (MT), the European Research Council, EU FP7/2007-2013/ERC-Grant Agreement number 267426 (OAB), the CRUK and EPSRC Cancer Imaging Centre in Oxford (LRH), the Carlsberg Foundation (TJS), and Keble College (TJS, SF) for financial support.

References

[1] A. Zaim, S.V. Eliseeva, L. Guenee, H. Nozary, S. Petoud, C. Piguet, Lanthanide-to-lanthanide energy-transfer processes operating in discrete polynuclear complexes: can trivalent europium be used as a local structural probe? Chem. Eur. J. 20 (2014) 12172–12182.
[2] L. Aboshyan-Sorgho, H. Nozary, A. Aebischer, J.C. Bunzli, P.Y. Morgantini, K.R. Kittilstved, A. Hauser, S.V. Eliseeva, S. Petoud, C. Piguet, Optimizing millisecond time scale near-infrared emission in polynuclear chrome(III)-lanthanide(III) complexes, J. Am. Chem. Soc. 134 (2012) 12675–12684.
[3] J.C. Bunzli, C. Piguet, Taking advantage of luminescent lanthanide ions, Chem. Soc. Rev. 34 (2005) 1048–1077.
[4] Y. Liu, D. Tu, H. Zhu, X. Chen, Lanthanide-doped luminescent nanoprobes: controlled synthesis, optical spectroscopy, and bioapplications, Chem. Soc. Rev. 42 (2013) 6924–6958.
[5] L.D. Sun, Y.F. Wang, C.H. Yan, Paradigms and challenges for bioapplication of rare earth upconversion luminescent nanoparticles: small size and tunable emission/excitation spectra, Acc. Chem. Res. 47 (2014) 1001–1009.
[6] S. Gai, C. Li, P. Yang, J. Lin, Recent progress in rare earth micro/nanocrystals: soft chemical synthesis, luminescent properties, and biomedical applications, Chem. Rev. 114 (2014) 2343–2389.
[7] W.T. Carnall, G.L. Goodman, K. Rajnak, R.S. Rana, A systematic analysis of the spectra of the lanthanides doped into single crystal LaF_3, J. Chem. Phys. 90 (1989) 3443–3457.
[8] W.T. Carnall, Chapter 24. The absorption and fluorescence spectra of rare earth ions in solution, in: Karl A. Gschneidner, Jr., E. LeRoy (Eds.), Handbook on the Physics and Chemistry of Rare Earths, Elsevier, Amsterdam, 1979, pp. 171–208.
[9] W.T. Carnall, Electronic Energy Levels of the Trivalent Lanthanide Aquo Ions. II. Gd^{3+}, J. Chem. Phys. 49 (1968) 4443.
[10] W.T. Carnall, Electronic energy levels of the trivalent lanthanide aquo ions. III. Tb^{3+}, J. Chem. Phys. 49 (1968) 4447.
[11] W.T. Carnall, Electronic energy levels of the trivalent lanthanide aquo ions. IV. Eu^{3+}, J. Chem. Phys. 49 (1968) 4450.
[12] W.T. Carnall, Electronic energy levels in the trivalent lanthanide aquo ions. I. Pr^{3+}, Nd^{3+}, Pm^{3+}, Sm^{3+}, Dy^{3+}, Ho^{3+}, Er^{3+}, and Tm^{3+}, J. Chem. Phys. 49 (1968) 4424.
[13] D. Parker, Excitement in f block: structure, dynamics and function of nine-coordinate chiral lanthanide complexes in aqueous media, Chem. Society Rev. 33 (2004) 156–165.
[14] D. Parker, R.S. Dickins, H. Puschmann, C. Crossland, J.A.K. Howard, Being excited by lanthanide coordination complexes: aqua species, chirality, excited-state chemistry, and exchange dynamics, Chem. Rev. 102 (2002) 1977–2010.
[15] A. Beeby, I.M. Clarkson, R.S. Dickins, S. Faulkner, D. Parker, L. Royle, A.S. de Sousa, J.A.G. Williams, M. Woods, Non-radiative deactivation of the excited states of europium, terbium and ytterbium complexes by proximate energy-matched OH, NH and CH oscillators: an improved luminescence method for establishing solution hydration states, J. Chem. Soc. Perkin Trans. 2 (1999) 493–504.
[16] J.-C.G. Bünzli, Lanthanide coordination chemistry: from old concepts to coordination polymers, J. Coord. Chem. 67 (2014) 1–45.
[17] T.J. Sørensen, M. Tropiano, O.A. Blackburn, J.A. Tilney, A.M. Kenwright, S. Faulkner, Preparation and study of an f,f,f',f'' covalently linked tetranuclear hetero-trimetallic complex – a europium, terbium, dysprosium triad, Chem. Commun. (Camb.) 49 (2013) 783–785.
[18] M. Main, J.S. Snaith, M.M. Meloni, M. Jauregui, D. Sykes, S. Faulkner, A.M. Kenwright, Using the Ugi multicomponent condensation reaction to prepare families of chromophore appended azamacrocycles and their complexes, Chem. Commun. (Camb.) (2008) 5212–5214.
[19] M. Tropiano, N.L. Kilah, M. Morten, H. Rahman, J.J. Davis, P.D. Beer, S. Faulkner, Reversible luminescence switching of a redox-active ferrocene-europium dyad, J. Am. Chem. Soc. 133 (2011) 11847–11849.
[20] M. Tropiano, C.J. Record, E. Morris, H.S. Rai, C. Allain, S. Faulkner, Synthesis and spectroscopic study of d–f hybrid lanthanide complexes derived from triazolyl DO3A, Organometallics 31 (2012) 5673–5676.
[21] M. Jauregui, W.S. Perry, C. Allain, L.R. Vidler, M.C. Willis, A.M. Kenwright, J.S. Snaith, G.J. Stasiuk, M.P. Lowe, S. Faulkner, Changing the local coordination environment in mono- and bi- nuclear lanthanide complexes through "click" chemistry, Dalton trans. (2009) 6283–6285.
[22] M. Tropiano, A.M. Kenwright, S. Faulkner, Lanthanide complexes of azidophenacyl–DO3A as new synthons for click chemistry and the synthesis of heterometallic lanthanide arrays, Chemistry 21 (2015) 5697–5699.
[23] M. Tropiano, O.A. Blackburn, J.A. Tilney, L.R. Hill, M.P. Placidi, R.J. Aarons, D. Sykes, M.W. Jones, A.M. Kenwright, J.S. Snaith, T.J. Sørensen, S. Faulkner, Using remote substituents to control solution structure and anion binding in lanthanide complexes, Chem. Eur. J. 19 (2013) 16566–16571.
[24] P. Hänninen, H. Härmä, Lanthanide Luminescence, Springer, Heidelberg, 2011.
[25] A. de Bettencourt-Dias, Introduction to lanthanide ion luminescence, in: A. de Bettencourt-Dias (Ed.), Luminescence of Lanthanide Ions in Coordination Compounds and Nanomaterials, John Wiley & Sons Ltd., 2014, pp. 1–48.
[26] D.E. Morris, A. de Bettencourt-Dias, Spectroscopic techniques and instrumentation, in: A. de Bettencourt-Dias (Ed.), Luminescence of Lanthanide Ions in Coordination Compounds and Nanomaterials, John Wiley & Sons Ltd., 2014, pp. 49–76.
[27] W.D. Horrocks, D.R. Sudnick, Lanthanide ion probes of structure in biology. Laser-induced luminescence decay constants provide a direct measure of the number of metal-coordinated water molecules, J. Am. Chem. Soc. 101 (1979) 334–340.
[28] N.J. Turro, Modern Molecular Photochemistry, University Science Books, Sausalito, 1991.
[29] B. Valeur, Molecular Fluorescence: Principles and Applications, Wiley-VCH, Weinheim, 2002.
[30] T. Kimura, Y. Kato, Luminescence study on determination of the hydration number of Sm(Iii) and Dy(Iii), J. Alloy. Compd. 225 (1995) 284–287.
[31] J. Scholten, G.A. Rosser, J. Wahsner, N. Alzakhem, C. Bischof, F. Stog, A. Beeby, M. Seitz, Anomalous reversal of C-H and C-D quenching efficiencies in luminescent praseodymium cryptates, J. Am. Chem. Soc. 134 (2012) 13915–13917.
[32] A. Beeby, S. Faulkner, Luminescence from neodymium(III) in solution, Chem. Phys. Lett. 266 (1997) 116–122.
[33] S. Faulkner, A. Beeby, M.C. Carrie, A. Dadabhoy, A.M. Kenwright, P.G. Sammes, Time-resolved near-IR luminescence from ytterbium andneodynium complexes of the Lehn cryptand, Inorg .Chem. Commun. 4 (2001) 187–190.
[34] Y. Hasegawa, K. Murakoshi, Y. Wada, S. Yanagida, J.-H. Kim, N. Nakashima, T. Yamanaka, Enhancement of luminescence of Nd^{3+} complexes with deuterated hexafluoroacetylacetonato ligands in organic solvent, Chem. Phys. Lett. 248 (1996) 8–12.
[35] C. Doffek, J. Wahsner, E. Kreidt, M. Seitz, Breakdown of the energy gap law in molecular lanthanoid luminescence: the smallest energy gap is not universally relevant for nonradiative deactivation, Inorg. Chem. 53 (2014) 3263–3265.
[36] T. Kimura, R. Nagaishi, Y. Kato, Z. Yoshida, Luminescence study on preferential solvation of Europium(III) in water/non-aqueous solvent mixtures, J. Alloy. Compd. 323 (2001) 164–168.

[37] T. Kimura, R. Nagaishi, Y. Kato, Z. Yoshida, Luminescence study on solvation of americium(III), curium(III) and several lanthanide(III) ions in nonaqueous and binary mixed solvents, Radiochim. Acta 89 (2001) 125–130.
[38] T. Kimura, Y. Kato, Luminescence study on hydration states of lanthanide(III)–polyaminopolycarboxylate complexes in aqueous solution, J. Alloy. Compd. 275–277 (1998) 806–810.
[39] T. Kimura, Y. Kato, Luminescence study on determination of the inner-sphere hydration number of Am(III) and Nd(III), J. Alloy. Compd. 271 (1998) 867–871.
[40] T. Kimura, Y. Kato, Luminescence study on the inner-sphere hydration number of lanthanide(III) ions in concentrated aqueous salt solutions in fluid and frozen states, J. Alloy. Compd. 278 (1998) 92–97.
[41] T. Kimura, G.R. Choppin, Y. Kato, Z. Yoshida, Determination of the hydration number of Cm(III) in various aqueous solutions, Radiochim. Acta 72 (1996) 61–64.
[42] T.J. Sørensen, A.M. Kenwright, S. Faulkner, Bimetallic lanthanide complexes that display a ratiometric response to oxygen concentrations, Chem. Sci. 6 (2015) 2054–2059.
[43] D. Parker, J.A.G. Williams, Luminescence behaviour of cadmium, lead, zinc, copper, nickel and lanthanide complexes of octadentate macrocyclic ligands bearing naphthyl chromophores, J. Chem. Soc. Perkin Trans. 2 (1995) 1305–1314.
[44] R. Hueting, M. Tropiano, S. Faulkner, Exploring energy transfer between pyrene complexes and europium ions – potential routes to oxygen sensors, RSC Adv. 4 (2014) 44162–44165.
[45] Z. Liao, M. Tropiano, K. Mantulnikovs, S. Faulkner, T. Vosch, T. Just Sørensen, Spectrally resolved confocal microscopy using lanthanide centred near-IR emission, Chem. Commun. 51 (2015) 2372–2375.
[46] R.C. Benson, R.A. Meyer, G.M.E. Zaruba, M. McKhann, Cellular autofluorescence–is it due to flavins? J. Histochem. Cytochem. 27 (1979) 44–48.
[47] L.R. Hill, T.J. Sørensen, O.A. Blackburn, A. Brown, P.D. Beer, S. Faulkner, Self-assembly between dicarboxylate ions and binuclear europium complexes: moving to water-pH dependence and effects of buffers, Dalton Trans. 42 (2013) 67–70.
[48] S.J. Strickler, R.A. Berg, Relationship between absorption intensity and fluorescence lifetime of molecules, J. Chem. Phys. 37 (1962) 814.
[49] T.J. Sørensen, L.R. Hill, J.A. Tilney, O.A. Blackburn, M.W. Jones, M. Tropiano, S. Faulkner, Self-assembly between dicarboxylate ions and dinuclear lanthanide complexes: a surprisingly complicated problem, Eur. J. Inorg. Chem. 2014 (2014) 2520–2528.
[50] J.A. Tilney, T.J. Sørensen, B.P. Burton-Pye, S. Faulkner, Self-assembly between dicarboxylate ions and a binuclear europium complex: formation of stable adducts and heterometallic lanthanide complexes, Dalton Trans. 40 (2011) 12063–12066.
[51] L.R. Hill, O.A. Blackburn, M.W. Jones, M. Tropiano, T.J. Sørensen, S. Faulkner, Ternary self-assemblies in water: forming a pentanuclear $ReLn_4$ assembly by association of binuclear lanthanide binding pockets with fac-Re $(CO)_3$(dinicotinate)2Cl, Dalton Trans. 42 (2013) 16255–16258.
[52] A. Nonat, M. Regueiro-Figueroa, D. Esteban-Gomez, A. de Blas, T. Rodriguez-Blas, C. Platas-Iglesias, L.J. Charbonniere, Definition of an intramolecular Eu-to-Eu energy transfer within a discrete [Eu2L] complex in solution, Chemistry 18 (2012) 8163–8173.

ChemPubSoc Europe

DOI: 10.1002/open.201500060

Open Access ChemistryOPEN Full Papers

Thermodynamics of Self-Assembly of Dicarboxylate Ions with Binuclear Lanthanide Complexes

Thomas Just Sørensen,*[a, b] Leila R. Hill,[b] and Stephen Faulkner*[b]

Self-assembly of a range of carboxylic acids (benzoic acid, dinicotinic acid, nicotinic acid, and isophthalic acid) with the europium complex of 5-nitro-α,α′-bis(DO3Ayl)-*m*-xylene (where DO3A is 1,4,7,10-tetraazacyclododecane-1,4,7-triacetic acid) has been explored to establish the thermodynamics of binding in a range of solvent systems and in a range of aqueous buffer solutions. In this system, profound effects are observed as a consequence of competition by the hydroxide ion, which outcompetes even dinicotinate at high pH. In the case of isophthalate, which binds most strongly, and dinicotinate, both enthalpic and entropic contributions to binding have been identified. The europium complex with 5-nitro-α,α′-bis(DO3Ayl)-*m*-xylene is found to have a solution structure significantly different from the related europium complex of 5-amino-α,α′-bis(DO3Ayl)-*m*-xylene. It is found that phosphate binds strongly to the europium complex of the nitro derivate but not to the europium complex of amino derivative. Lactate, citrate, and pyruvate also bind strongly to 5-nitro-α,α′-bis(Eu·DO3Ayl)-*m*-xylene, and it is concluded that the solution structure of this binuclear lanthanide complex is significantly different from that of the amino-substituted complex.

Introduction

The use of lanthanide complexes to define the concentration of a range of analytes is well established, both in terms of supramolecular coordination chemistry and bioassays. In many of these applications, direct coordination of anions to the lanthanide can be exploited to give concentration-dependent variations in the photophysical properties at the lanthanide centre.[1–5] Due to the nature of the 4*f* orbitals, the interactions between the analytes and trivalent lanthanide ions exploited in these applications are predominately ionic in nature.[6]

By using time-gated techniques, the long-lived luminescence from lanthanide ions can be exploited to give low detection limits in microscopy and assays when nearby chromophores are used to sensitise the formation of the lanthanide excited state.[7–15] In such systems, there are many ways in which the lanthanide luminescence can be perturbed by an analyte. In the majority of systems, sensitised luminescence occurs via formation of an excited singlet state on the chromophore, followed by intersystem crossing to the triplet, and subsequent energy transfer to the lanthanide emissive state; all of these intermediate states can be perturbed by collisional quenching or association with a guest to form a ternary complex.[16–18] For instance, lanthanide complexes with heptadentate ligands derived from 1,4,7,10-tetraazacyclododecane-1,4,7-triacetic acid (DO3A) form complexes with a wide range of substrates.[19–21] Such interactions have been used to exploit chelating interactions with a range of bidentate anions to achieve changes to lanthanide luminescence by displacing solvent.[22–25] Related approaches have been used to screen sensitising chromophores and in the development of displacement assays.[21,26]

In our case, we have focused on the interaction between stable binuclear lanthanide complexes and a range of bidentate anions. Initially, we established that lanthanide complexes of α,α′-(DO3Ayl)-*m*-xylene are selective for isophthalate over terephthalate and phthalate.[27] Subsequently, we have explored the binding of water-soluble guests in such systems,[28] and established that such complexes can be recruited to isophthalate-functionalised surfaces.[29] The isophthalate motif can also be used to direct the assembly of more complicated multimetallic *f,f′* and *d,f* complexes.[27,30] We recently observed that changing the remote substituent on the *m*-xylyl linking group can be used to control the binding affinity of the complex for an isophthalate guest, and that binding can be precluded or enhanced depending on the nature of the remote substituent.[31] Affinity constants (*K*) between 0 and $10^7\ M^{-1}$ were observed, and the considerable changes in this system were ascribed to preorganisation of the binuclear complex and removal of "inactive" conformers from the conformational space available within the structure.[31] Exclusion of the "active"

[a] *Dr. T. J. Sørensen*
Nanoscience Centre and Department of Chemistry
University of Copenhagen
Universitetsparken 5, 2100 København Ø (Denmark)
E-mail: TJS@chem.ku.dk

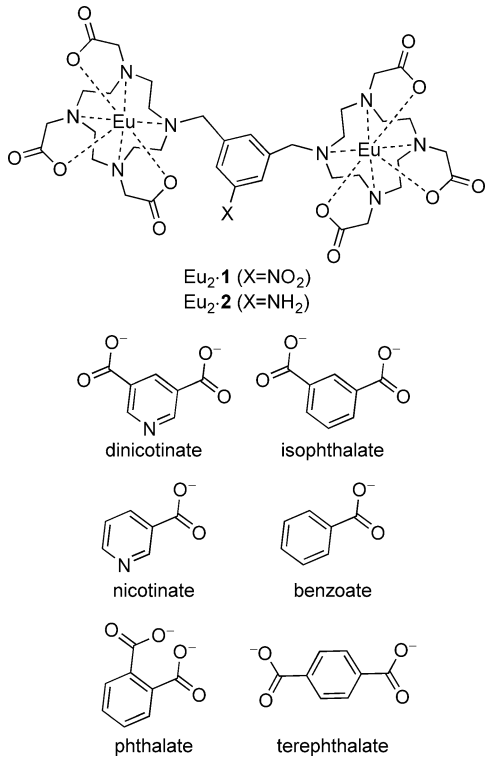
[b] *Dr. T. J. Sørensen, L. R. Hill, Prof. S. Faulkner*
Chemistry Research Laboratory, Oxford University
12 Mansfield Road, Oxford OX1 3TA (UK)
E-mail: stephen.faulkner@keble.ox.ac.uk

Supporting information and ORCID(s) from the author(s) for this article are available on the WWW under http://dx.doi.org/10.1002/open.201500060.

© 2015 The Authors. Published by Wiley-VCH Verlag GmbH & Co. KGaA. This is an open access article under the terms of the Creative Commons Attribution License, which permits use, distribution and reproduction in any medium, provided the original work is properly cited.

conformer in such circumstances effectively precludes binding.[32]

These observations, together with the fact that solvent plays a dominant role in determining the value of the affinity constant,[33] made us consider the thermodynamics of binding in detail. Here, we describe the results of a study in which we look at the role of solvent and buffer, and establish enthalpic and entropic contributions to the thermodynamics of anion binding. We show that the enthalpic and entropic contributions change sign when going from methanol to water, and document that guest binding at a lanthanide centre can occur with no displacement of quenching O–H oscillators. Our investigations into the binding of a series of binuclear complexes with the isomers of phthalic acid in methanolic solution (Scheme 1) show that the small differences between the complexes Eu_2·**1** and Eu_2·**2** have dramatic effects in host–guest equilibria; substituting an amino group for a nitro group results in reversal of observed selectivities. Furthermore, uncompetitive media for Eu_2·**2** can be competitive with guests for Eu_2·**1** to the degree that no host–guest interaction is observed in biologically relevant media.



Scheme 1. Molecules and lanthanide complexes studied: 5-nitro-α,α′-bis(Eu·DO3Ayl)-*m*-xylene (Eu_2·**1**) and 5-amino-α,α′-bis(Eu·DO3Ayl)-*m*-xylene (Eu_2·**2**).

Results and Discussion

5-nitro-α,α′-(DO3Ayl)-*m*-xylene (H_6·**1**) and its binuclear europium complex (Eu_2·**1**) were prepared as previously described.[34] Although this ligand was among the first *m*-xylyl-bridged bismacrocycles to be prepared, we have previously only carried out very limited studies upon the binding of anionic guest species beyond establishing the affinity for dinicotinate in tris(hydroxymethyl)aminomethane (TRIS) buffer.[28] In this study, we report a much broader range of data and establish the affinity for four different anions, and define the binding in methanolic and aqueous media at a range of temperatures.

Studying self-assembly

Titrations of Eu_2·**1** were carried out with the anions shown in Scheme 1 using a previously described procedure.[33] Briefly, a 10^{-5} M solution of the lanthanide complex in the solvent system under study was used to prepare a 10^{-3} M solution of the carboxylate species, containing 10^{-5} M of the lanthanide complex. In doing so, the concentration of the lanthanide complex remained constant during the titration. A 2 mL aliquot of the stock solution was placed in a cuvette, and the luminescence spectrum recorded.

An aliquot, ranging from 2 μL to 100 μL, of the titrant was added, and the luminescence spectrum recorded again. The titration was continued until the binding isotherm had reached a plateau. The results of these studies are summarised in Figures 1, 2 and 3, and Tables 1 and 2, and will be discussed in greater detail below.

Figure 1 shows the changes in excitation and emission spectra during the course of a titration of Eu_2·**1** with the anions investigated in this study: benzoate, isophthalate, nicotinate, and dinicotinate. Two different aromatic bridging rings, derived from pyridine and benzene with one and two carboxylate groups, were investigated. Cursory inspection of the data shows that no significant changes in the band shape is apparent in the spectrum; data from all titrations performed in this study can be found in the Supporting Information.

Determining binding constants

First, the four guests were compared in methanol, a solvent in which all guest molecules are fully soluble. Titrations in methanolic solution were carried out in the presence of an excess of lithium hydroxide, which served to ensure deprotonation of the carboxylates under study, and a constant medium (ionic strength, proton activity) throughout the titrations. As in previous studies on related systems (i.e. Eu_2·**2**, Scheme 1), Eu_2·**1** displayed strong selectivity for isophthalate at 16,660 M^{-1} in the presence of 1 mM lithium hydroxide, compared with 24,600 M^{-1} in pure methanolic solution. Not only does this provide evidence of competitive binding by hydroxide, but the value in the absence of hydroxide is five times lower than that determined for Eu_2·**2**.[31] To investigate this further, we studied the binding of phthalate and terephthalate, determining the binding constants in methanol in the presence of 1 mM lithium hydroxide. With values for $K_{phthalate}$ and $K_{terephthalate}$ of 50,900 M^{-1} and 29,300 M^{-1}, respectively, compared to a $K_{isophthalate}$ value of 16,660 M^{-1}, we observed that the binding strength of the three phthalate isomers to Eu_2·**1** are dramatically different from those previously determined for Eu_2·**2**. For the system studied here (Eu_2·**1**), bidentate binding by phthalate is more favourable than binding by the bridging guests. Furthermore, in this com-

© 2015 The Authors. Published by Wiley-VCH Verlag GmbH & Co. KGaA, Weinheim

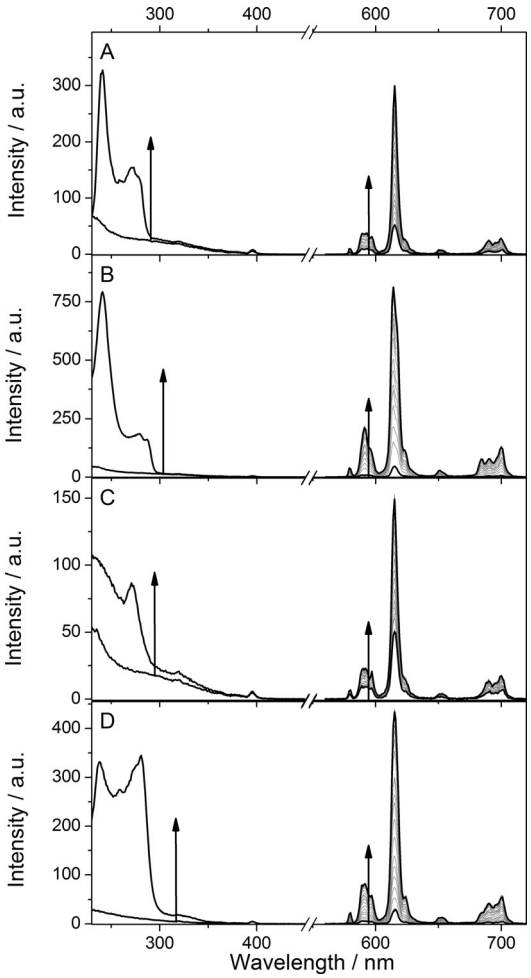


Figure 1. Titrations of 5-nitro-α,α′-bis(Eu·DO3Ayl)-*m*-xylene (Eu_2·**1**; 0.011 mM) with A) benzoate (1.33 mM), B) isophthalate (2.15 mM), C) nicotinate (1.59 mM), and D) dinicotinate (1.01 mM) at 25 °C in methanol with 1 mM $LiOH·H_2O$ followed using time-gated emission spectroscopy with excitation at 240 nm. The end points are shown in bold black lines. The end-point excitation spectra recorded by following 620 nm emission are shown in bold.

bination of solvent, proton affinity and host, terephthalate is a better bridging guest than isophthalate. This result is completely opposite to our previous findings for Eu_2·**2**.[27] This implies that even small changes in the nature of the bridging unit, such as exchanging a remote nitro group for an amino group, can lead to dramatic changes in binding affinity. Such changes might result from changes in solvent order, or conceivably through changes to the lipophilicity of the bridging aryl ring.

In methanolic lithium hydroxide, Eu_2·**1** displayed high selectivity for isophthalate over dinicotinate, revealing that small changes in guest structure can have just as dramatic an effect as changes to the host. In this case, the explanation is likely to be more straightforward: the electron-withdrawing effect of the pyridine nitrogen is likely to decrease the electron-donating ability of the carboxylate groups.

Establishing the effect of temperature

Measurement of the affinity constant for the binding of anions to Eu_2·**1** at multiple temperatures in the presence of lithium hydroxide (Table 1) revealed further differences in behaviour. While isophthalate exhibited strong temperature dependence, benzoate showed much smaller variations with temperature, and both dinicotinate and nicotinate showed essentially no change in binding with temperature. Figure 2 shows titration isotherms for a single temperature for isophthalate, and the van't Hoff plot for the temperatures where the *K* value was determined (for all guest ions, see the Supporting Information). In the case of isophthalate, the thermodynamic sense is clear; binding is disfavoured on enthalpic grounds but favoured entropically. This suggests competitive binding by hydroxide at the metal centres, in which displacement of hydroxide decreases the overall order in the system. Hydroxide binding might take many forms in methanolic media, and given the excess of hydroxide, it is conceivable that hydroxide ions coordinate to both metal centres. In such a case, the gain in entropy might result simply from the displacement of two hydroxide ions upon binding of isophthalate. It should be noted that hydroxide has been observed to bridge lanthanide centres and has

Table 1. Affinity constants and thermodynamic parameters of 5-nitro-α,α′-bis(Eu·DO3Ayl)-*m*-xylene Eu_2·**1** for a range of anionic guest ions in methanol.[a]

	T [K]	isophthalate	dinicotinate	benzoate	nicotinate
$K^{[b]}$ [M^{-1}]	293	16660	2534	421	570
	298	20410	2753	455	571
	303	24280	2525	569	638
	313	39990	2639	–	579
ΔH [kJ mol^{-1}]	–	33	–[a]	22	–[c]
ΔS [J mol^{-1} K^{-1}]	–	194	–[a]	125	–[c]

[a] All data were obtained in the presence of aq. $LiOH·H_2O$ (1 mM). [b] Confidence intervals for *K* can be found in the Supporting Information. [c] The change in *K* with temperature is within the error of the measurement, as such, meaningful thermodynamic parameters cannot be readily obtained.

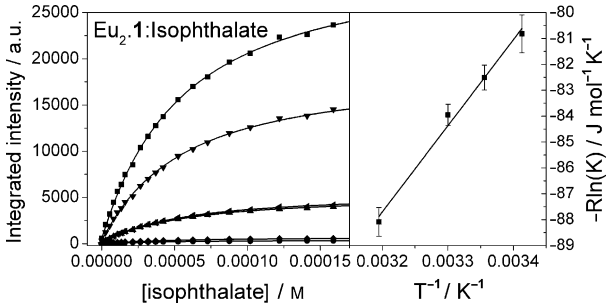


Figure 2. Left: Titration isotherms from a titration of 5-nitro-α,α′-bis(Eu·DO3Ayl)-*m*-xylene (Eu_2·**1**; 0.011 mM) with isophthalate ($R^2 = 0.987$; 2.15 mM) at 25 °C in methanol with 1 mM $LiOH·H_2O$ determined by recording emission spectra following excitation at 240 nm. The isotherms show integrated emission bands [I_{total} (■), $\Delta J = 0$ (●), 1 (▲), 2 (▼), 3 (◆), 4 (◀)] and the best fit to the data (——). Right: A van't Hoff plot of data from titrations performed at several temperatures (20, 25, 30, and 40 °C).

© 2015 The Authors. Published by Wiley-VCH Verlag GmbH & Co. KGaA, Weinheim

also been implicated in the aggregation of mononuclear lanthanide complexes.[35] However, the distance between the two metal centres in Eu_2·**1** is likely to preclude such an arrangement.

In all of these titrations, 1 mM lithium hydroxide monohydrate was added to ensure that changes in solvent would not interfere with the measurements. The proton activity, solvent polarity, and ionic strength might interfere with the observed luminescence from the lanthanide complex to a degree that data on the binding event cannot be extracted.

Studies of isophthalate binding in aqueous media are inevitably precluded by the very low solubility of isophthalate in water. However, dinicotinate is water soluble, and binding studies on dinicotinate in water proved highly informative (Table 2). The most obvious observation is that the binding

Table 2. Affinity constants and thermodynamic parameters of 5-nitro-α,α′-bis(Eu·DO3Ayl)-*m*-xylene Eu_2·**1** for dinicotinate at 293 K in aqueous media.[a]

	T [K]	pH 8.1 (BBS)	pH 7.5 (HEPES)	pH 7.4 (PBS)	pH 11 (H_2O)
K[b] [M^{-1}]	293	29830	17730	0	0
	303	11320	13220	0	0
	313	9200	9650	0	0
ΔH [kJ mol^{-1}]	–	−45.0	−23.2	–	–
ΔS [J mol^{-1} K^{-1}]	–	−69.5	−2.2	–	–

[a] No change in luminescence was observed upon titration in either PBS or at pH 11. [b] Confidence intervals for *K* can be found in the Supporting Information.

constants observed in borate-buffered saline (BBS) and 4-(2-hydroxyethyl)-1-piperazineethanesulfonic acid (HEPES) buffer are dramatically greater than those measured in methanolic lithium hydroxide. In itself, this would be suggestive of competitive binding of hydroxide. Further evidence for this hypothesis was provided by studies carried out at pH 11, where millimolar hydroxide concentrations led to competitive binding of hydroxide. In such systems, no change in lanthanide luminescence was observed with increasing dinicotinate concentration (see the Supporting Information), clearly showing that dinicotinate cannot outcompete hydroxide binding in water.

From the data in Table 2, it is immediately clear that the affinity constant of Eu_2·**1** for dinicotinate in water has a very different temperature dependence to the same system in methanolic lithium hydroxide (for the van't Hoff plots, see the Supporting Information). In this case, the affinity for dinicotinate decreases with increasing temperature in both BBS and HEPES buffer. In both buffers, the binding is enthalpy driven and disfavoured on entropic grounds. Furthermore, the difference between these parameters in BBS and HEPES buffer strongly suggests that HEPES buffer is a competitive buffer in this system. Such effects have been observed for the pyridine-bridged system, where HEPES is a more competitive ion than phosphate.[28]

Self-assembly in biological mimics

No binding was observed in phosphate-buffered saline (PBS), presenting the argument that phosphate also outcompetes dinicotinate. This is in contrast with our earlier observations, which showed no effect of phosphate upon the overall affinity.[28] It is worth noting that the inner sphere hydration (where *q* is the number of inner sphere solvent molecules)[36] of Eu_2·**1** is significantly greater than that of Eu_2·**2** ($q(Eu_2$·**1**$)=1.2$ and $q(Eu_2$·**2**$)=0.8$, see Ref. [34]). As such, Eu_2·**1** would be expected to display a greater affinity for phosphate, since phosphate can act as a bidentate donor at one of the lanthanide centres. This assumption is supported by the high affinity of Eu_2·**1** for phthalate, which is unlikely to bridge between the two lanthanide centres. This could explain why no sign of host–guest interactions was observed between dinicotinate and Eu_2·**1** in PBS (Table 2).

The data in Table 1 clearly shows that the dinicotinate/Eu_2·**1** binding partners would be unsuitable for studies in biological systems, where phosphate will outcompete the association between the two. To investigate whether the self-assembly with Eu_2·**1** could be affected by other endogenous ions than phosphate, we studied the binding of citrate and lactate in methanol, and we were not able to observe any binding. So to investigate the effect of arterial concentrations of lactate (2 mM), pyruvate (0.3 mM), and citrate (0.01 M),[37,38] Eu_2·**1** was titrated with dinicotinate in BBS at pH 8.2 in the presence of arterial concentrations of these. The results show that all three ions exhibit competitive binding. The association between Eu_2·**1** and dinicotinate has an affinity constant (K_{BBS}) of 29,830 M^{-1} (Table 2), the affinity is decreased by a factor of ten in the presence of lactate ($K_{BBS\ lactate}=3{,}550\ M^{-1}$), while citrate decreased the affinity by a factor of 20 ($K_{BBS\ citrate}=1{,}640\ M^{-1}$). In the presence of biological concentrations of pyruvate, no binding is observed. In contrast to Eu_2·**2**, the solution structure of Eu_2·**1** allows for competitive binding of ligands that permits bidentate binding to a single lanthanide centre such as phosphate, phthalate, and pyruvate.

Changes in the luminescence spectra

The steady-state luminescence spectra of the complexes change dramatically between solvent systems (Figure 3) as a consequence of changes in the local environment at the europium centres. Not only does the relative intensity of the bands change, as would be expected given the hypersensitivity of the $^5D_0$–$^7F_2$ transition, but the fine structure of individual bands changes dramatically. This is clear evidence for different local symmetries at the metal centres.

Study of the steady-state spectra before and after addition of dicarboxylates also reveals that there are significant changes to the excitation spectra (Figure 1). The spectra show that the observed increases in luminescence intensity can be attributed to the additional absorption cross-section of the dinicotinate and isophthalate chromophores, meaning that luminescence is sensitised by both host and guest. This is clearly the dominant effect, and changes to hydration and removal of other non-

 © 2015 The Authors. Published by Wiley-VCH Verlag GmbH & Co. KGaA, Weinheim

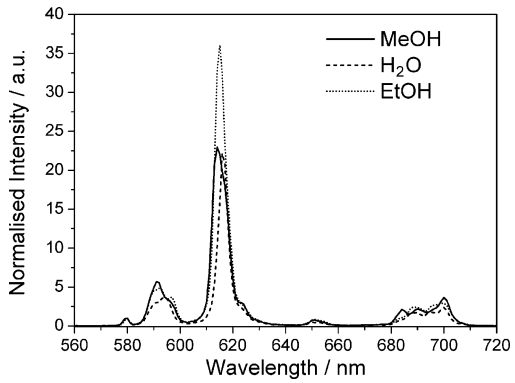


Figure 3. Time-gated emission spectra measured following 240 nm excitation of 5-nitro-α,α′-bis(Eu·DO3Ayl)-*m*-xylene (Eu_2·**1**).

radiative quenching pathways for the lanthanide excited state are of negligible importance in establishing the affinity of host for guest.

To further investigate contributions leading to the intensity increase, titrations were performed using direct (395 nm, $^7F_5$–$^5L_6$) and sensitised excitation. Figure 4 shows the normalised spectra following from sensitised excitation (Figure 4A); this is done in order to show that no changes in either the band shape or intensity can be seen (for the raw data, see the Supporting Information). Following direct excitation, the spectra do not change as the titration progresses (Figure 4B), which clearly indicates that the overall quantum yield of emission—the sum of the seven individual contributions from the seven different possible transitions from $^5D_0$—does not change as the titration progresses. This is counterintuitive as it would be expected that the binding of anions occurs with displacement of water, lowering the number of quenching X–H oscillators close to the lanthanide centres, increasing the quantum yield of emission. The titration isotherms plotted in Figure 4C–D show that this is clearly not the case.

For most of the titrations performed in this study, a small change can be seen in the spectra following direct excitation at the beginning and the end of the titrations. Closer scrutiny of the excitation spectra at these points in the titrations (Figure 1) show that this is due to a tail of absorption from the guest chromophore, not an effect in the direct excitation pathway.

Time-resolved luminescence studies

Measurement of the luminescence lifetimes of the complexes and assemblies in solution (Table 3) yielded further information about the binding event. It is clear that the luminescence lifetimes in a variety of aqueous media change only slightly (and within the standard margin of error) upon addition of isophthalate, implying that any change in the inner solvation sphere as a consequence of binding is remarkably limited. In methanolic solution, the lifetimes in the absence and presence of all potential guests are also the same within error, suggesting that (in this case too) the guest supplements solvent molecules in the inner coordination sphere rather than displacing

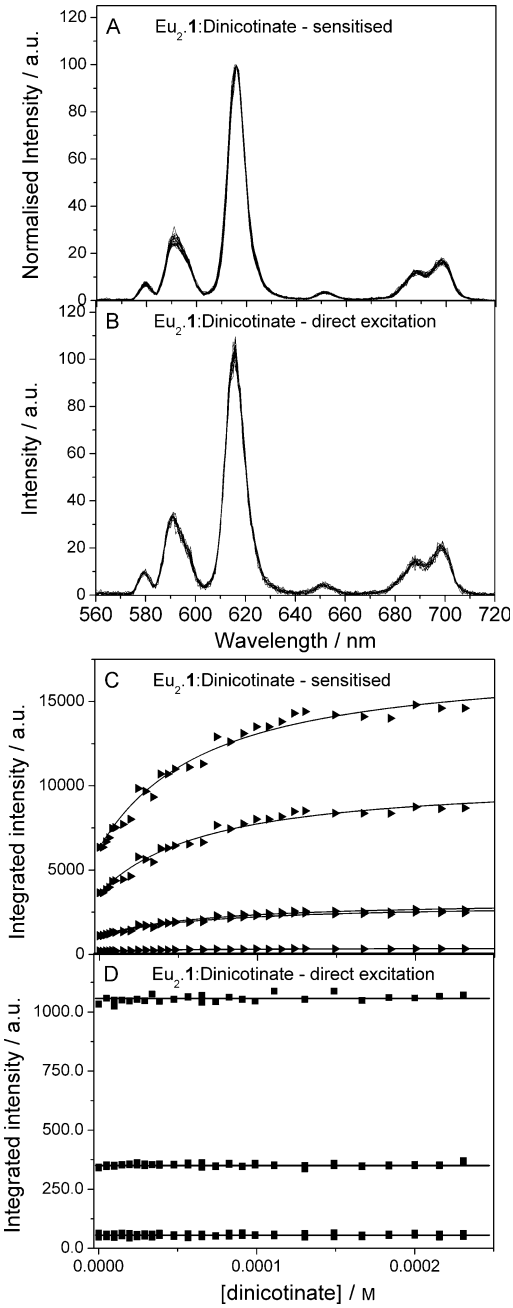


Figure 4. Data from a titration of 5-nitro-α,α′-bis(Eu·DO3Ayl)-*m*-xylene (Eu_2·**1**; 0.01 mM) with dinicotinate (1 mM) in 20 mM HEPES buffer at pH 7.4. A) Normalised emission spectra measured following 240 nm excitation; all spectra from a full titration are included. B) Raw-data emission spectra measured following 395 nm excitation from the same titration depicted in panel A. C) Titration isotherm and fit to the data obtained following 240 nm excitation. D) Titration isotherm from data obtained following 395 nm excitation; horizontal lines have been added as a guide.

them. In all systems, luminescence lifetimes were found to be invariant with temperature in the range from 283 to 333 K.

Indeed, calculation of the number of inner sphere solvent molecules (*q*) using the modified Horrocks equation[36,39] (Table 4), emphasises this point about coordination chemistry. It is clear that the overall solvation at the lanthanide centres is initially lower than might be expected, and consistent with

© 2015 The Authors. Published by Wiley-VCH Verlag GmbH & Co. KGaA, Weinheim

Table 3. Luminescence lifetimes (τ) of 5-nitro-α,α′-bis(Eu·DO3Ayl)-*m*-xylene Eu_2·**1** in various solvents and with a variety of guest ions.

Guest ion	τ[a] [ms]			
	pH 8.1 (BBS)	pH 7.5 (HEPES)	pH 7.4 (PBS)	MeOH (1 mM LiOH)
none	0.63	0.53	0.61	1.07
dinicotinate	0.77	0.64	0.69	1.15
isophthalate	–	–	–	1.15
nicotinate	–	–	–	1.07
benzoate	–	–	–	1.09

[a] Error values for τ are ±5% or less.

Table 4. Variation in luminescence lifetimes (τ) and the number of inner sphere solvent molecules (*q*) of 5-nitro-α,α′-bis(Eu·DO3Ayl)-*m*-xylene Eu_2·**1** with pH in aqueous media.

Medium	pH	pD	τ[a] [ms]		*q*[b]
			H_2O	D_2O	
water	2.0	2.1	0.53	1.36	1.1
	11.3	11.5	0.65	1.63	0.8
	12.5	12.8	0.64	1.57	0.8
methanol	1 mM LiOH		1.07	1.55	0.8

[a] Error values for τ are 5% or less. [b] Error values for *q* are within 0.5; for the definition of *q* and calculation method, see Ref. [22].

one water molecule per lanthanide in aqueous media. In these systems, the lipophilicity of the bridging *m*-xylyl group would be expected to mediate against the close proximity of two water molecules despite the heptadentate nature of both binding pockets. However, favourable interactions between this bridging group and the aryl carboxylate guests might also be expected and would indeed enhance the efficiency of binding. The same phenomenon is observed in methanolic solution. pH does have a significant effect upon both the lifetime in aqueous solution and the value of *q*; the lifetime increases and *q* is decreased as pH increases as a direct consequence of deprotonation of bound water at the metal centre. In other systems, variation in *q* with pH has been assigned to bridging oxo or hydroxo groups that link two lanthanides together.[35] While it would be appealing to use a similar explanation in this case, there is no other evidence for bridging by hydroxide.

Conclusion

It is clear from these results that the thermodynamics of self-assembly between binuclear lanthanide complexes and dianions are finely balanced, and far from the simple picture where lanthanide-centred interactions are dominated by coloumbic forces. In the system studied here, the role of solvent remains key to overall behaviour. Furthermore, competitive binding by a range of anions can change the observed affinity.

We find that these binuclear lanthanide complex hosts constitute a single supramolecular binding pocket,[40] where the nature of the guest determines the number of favourable interactions that can be exploited: hydrophobic interactions with the aryl bridge and one or two interactions to a lanthanide centre. These systems are simple when seen from the perspective of host–guest chemistry. However, taken together with our other studies on related systems, it is becoming increasingly clear that small variations in the molecular structure of either guest or host can have dramatic effects on both affinity and selectivity.

Additionally, it is particularly notable that two closely related systems display a remarkably different response to the presence of phosphate. This is potentially of vital importance when considering whether self-assembly can be exploited in vivo, where competition with phosphate must be ruled out. Such studies would also require a detailed understanding of competitive binding by endogenous anions.

Experimental Section

5-Nitro-α,α′-bis(Eu·DO3Ayl)-*m*-xylene (Eu_2·**1**) was prepared as previously described.[31] The salt content was determined using elemental analysis, while the europium content was determined using inductively coupled plasma mass spectrometry (ICP-MS). All concentrations were corrected appropriately. Lithium benzoate (>99%), lithium hydroxide monohydrate (99.95%), nicotinic acid (>99.5%), and isophthalic acid (99%) were purchased from Sigma–Aldrich. Dinicotinic acid (pyridine-3,5-dicarboxylic acid, 98%) was purchased from Alfa Aesar, and the purity was verified by elemental analysis. Ultrapure water from a MilliQ system and HPLC grade methanol were used as solvents. Buffers were prepared from commercial tablets (PBS, BBS) or from the pure form with KCl and NaCl (HEPES), all purchased from Sigma–Aldrich. Emission spectra were recorded using a Varian Cary Eclipse and a Horiba Fluorolog-3 spectrometer. Absorption spectra were recorded using a PerkinElmer Lambda1050 spectrometer. Temperature control was achieved using a Cary single-cell Peltier controller, while monitoring the temperature of the cuvette holder continuously and the solution intermittently. The temperature was maintained at the target temperature ±0.1 °C.

Solutions were prepared in volumetric flasks, and the compound mass was determined to three significant figures. A single buffer or solvent stock solution was prepared and used to prepare all other solutions in order to ensure a uniform solvent composition. A ~0.01 mM stock solution of Eu_2·**1** was prepared for each solvent system, and this was used to prepare the 1 mM titrant solution. The pH of aqueous buffer solutions were adjusted to be identical within 0.01 pH unit.

Titrations were performed by placing 1 or 2 mL of Eu_2·**1** solution in a 2 mm and 10 mm pathway cuvette using volume displacement pipettes. The titrant solution was added using volume displacement pipettes, the cuvette was shaken to mix the solution, and then the cuvette was briefly allowed to equilibrate in the Peltier-controlled cuvette holder. The tiny aliquot added in combination with the small temperature difference ($\Delta T < 20$ °C) did not alter the solution temperature to any measurable extent. Excitation spectra were recorded at the beginning and the end of each titration, while emission spectra were recorded at each data point. The individual bands in the emission spectra were integrated and plotted against titrant concentration to generate binding isotherms. These data were fitted using DynaFit 4 as previously reported,[30,31,41,42] to determine the affinity constant (*K* in M^{-1}), defined by Equation (1),

 © 2015 The Authors. Published by Wiley-VCH Verlag GmbH & Co. KGaA, Weinheim

where X represents a guest: benzoate, isophthalate, nicotinate, or dinicotinate.

$$K = \frac{[Eu_2 \cdot \mathbf{1} : X]}{[Eu_2 \cdot \mathbf{1}][X]} \quad (1)$$

A van't Hoff plot of $-R\ln K$ against T^{-1} allowed determination of the enthalpic and entropic contributions to the binding as the slope and the intercept, respectively [Equation (2)].

$$\begin{aligned} -RT\ln K &= \Delta G = \Delta H - T\Delta S \\ -R\ln K &= \frac{\Delta H}{T} - \Delta S \end{aligned} \quad (2)$$

Spectra and isotherms from all titrations can be found in the Supporting Information, along with the Arrhenius plots for dinicotinate in BBS and HEPES buffer.

Acknowledgements

The authors thank the Carlsberg Foundation (Copenhagen, Denmark, the Cancer Research UK (CRUK) and Engineering and Physical Sciences Research Council (EPSRC) Cancer Imaging Centre (Oxford, UK), Keble College (University of Oxford, UK), the University of Oxford (UK) and the University of Copenhagen (Denmark) for support.

Keywords: lanthanides · luminescence · self-assembly · supramolecular chemistry

[1] M. C. Heffern, L. M. Matosziuk, T. J. Meade, *Chem. Rev.* **2014**, *114*, 4496 – 4539.
[2] S. J. Butler, D. Parker, *Chem. Soc. Rev.* **2013**, *42*, 1652 – 1666.
[3] E. J. New, D. Parker, D. G. Smith, J. W. Walton, *Curr. Opin. Chem. Biol.* **2010**, *14*, 238 – 246.
[4] S. J. Butler, B. K. McMahon, R. Pal, D. Parker, J. W. Walton, *Chem. Eur. J.* **2013**, *19*, 9511 – 9517.
[5] S. J. Bradberry, A. J. Savyasachi, M. Martinez-Calvo, T. Gunnlaugsson, *Coord. Chem. Rev.* **2014**, *273 – 274*, 226 – 241.
[6] C. E. Housecroft, E. C. Constable, *Chemistry: An Introduction to Organic, Inorganic and Physical Chemistry, 4th ed.*, Pearson Education Ltd, Harlow, **2010**.
[7] J.-C. G. Bünzli, C. Piguet, *Chem. Soc. Rev.* **2005**, *34*, 1048 – 1077.
[8] *Lanthanide Luminescence: Photophysical, Analytical and Biological Aspects*, (Eds.: P. Hänninen, H. Härmä), Springer, Heidelberg, **2011**.
[9] E. Pershagen, K. E. Borbas, *Angew. Chem. Int. Ed.* **2015**, *54*, 1787 – 1790; *Angew. Chem.* **2015**, *127*, 1807 – 1810.
[10] E. Pershagen, K. E. Borbas, *Coord. Chem. Rev.* **2014**, *273 – 274*, 30 – 46.
[11] G. Vereb, E. Jares-Erijman, P. R. Selvin, T. M. Jovin, *Biophys J.* **1998**, *74*, 2210.
[12] A. Foucault-Collet, K. A. Gogick, K. A. White, S. Villette, A. Pallier, G. Collet, C. Kieda, T. Li, S. J. Geib, N. L. Rosi, S. Petoud, *Proc. Natl. Acad. Sci. USA* **2013**, *110*, 17199 – 17204.
[13] S. Gai, C. Li, P. Yang, J. Lin, *Chem. Rev.* **2014**, *114*, 2343 – 2389.
[14] Z. Liao, M. Tropiano, K. Mantulnikovs, S. Faulkner, T. Vosch, T. J. Sørensen, *Chem. Commun.* **2015**, *51*, 2372 – 2375.
[15] D. Geißler, S. Stufler, H.-G. Löhmannsröben, N. Hildebrandt, *J. Am. Chem. Soc.* **2013**, *135*, 1102 – 1109.
[16] T. Gunnlaugsson, J. P. Leonard, *Chem. Commun.* **2005**, 3114 – 3131.
[17] C. P. Montgomery, B. S. Murray, E. J. New, R. Pal, D. Parker, *Acc. Chem. Res.* **2009**, *42*, 925 – 937.
[18] E. G. Moore, A. P. Samuel, K. N. Raymond, *Acc. Chem. Res.* **2009**, *42*, 542 – 552.
[19] J. P. Leonard, C. M. dos Santos, S. E. Plush, T. McCabe, T. Gunnlaugsson, *Chem. Commun.* **2007**, 129 – 131.
[20] K. Nwe, C. M. Andolina, C.-H. Huang, J. R. Morrow, *Bioconjugate Chem.* **2009**, *20*, 1375 – 1382.
[21] S. J. Pope, B. P. Burton-Pye, R. Berridge, T. Khan, P. J. Skabara, S. Faulkner, *Dalton Trans.* **2006**, 2907 – 2912.
[22] D. Parker, J. Yu, *Chem. Commun.* **2005**, 3141 – 3143.
[23] T. Gunnlaugsson, F. Stomeo, *Org. Biomol. Chem.* **2007**, *5*, 1999 – 2009.
[24] C. M. Andolina, J. R. Morrow, *Eur. J. Inorg. Chem.* **2011**, 154 – 164.
[25] A. J. Harte, P. Jensen, S. E. Plush, P. E. Kruger, T. Gunnlaugsson, *Inorg. Chem.* **2006**, *45*, 9465 – 9474.
[26] S. Faulkner, B. P. Burton-Pye, *Chem. Commun.* **2005**, 259 – 261.
[27] J. A. Tilney, T. J. Sørensen, B. P. Burton-Pye, S. Faulkner, *Dalton Trans.* **2011**, *40*, 12063 – 12066.
[28] L. R. Hill, T. J. Sørensen, O. A. Blackburn, A. Brown, P. D. Beer, S. Faulkner, *Dalton Trans.* **2013**, *42*, 67 – 70.
[29] J. Lehr, J. Bennett, M. Tropiano, T. J. Sørensen, S. Faulkner, P. D. Beer, J. J. Davis, *Langmuir* **2013**, *29*, 1475 – 1482.
[30] L. R. Hill, O. A. Blackburn, M. W. Jones, M. Tropiano, T. J. Sørensen, S. Faulkner, *Dalton Trans.* **2013**, *42*, 16255 – 16258.
[31] M. Tropiano, O. A. Blackburn, J. A. Tilney, L. R. Hill, M. P. Placidi, R. J. Aarons, D. Sykes, M. W. Jones, A. M. Kenwright, J. S. Snaith, T. J. Sørensen, S. Faulkner, *Chem. Eur. J.* **2013**, *19*, 16566 – 16571.
[32] T. J. Sørensen, M. Tropiano, O. A. Blackburn, J. A. Tilney, A. M. Kenwright, S. Faulkner, *Chem. Commun.* **2013**, *49*, 783 – 785.
[33] T. J. Sørensen, L. R. Hill, J. A. Tilney, O. A. Blackburn, M. W. Jones, M. Tropiano, S. Faulkner, *Eur. J. Inorg. Chem.* **2014**, 2520 – 2528.
[34] M. P. Placidi, L. S. Natrajan, D. Sykes, A. M. Kenwright, S. Faulkner, *Helv. Chim. Acta* **2009**, *92*, 2427 – 2438.
[35] J. Hall, R. Häner, S. Aime, M. Botta, S. Faulkner, D. Parker, A. S. de Sousa, *New J. Chem.* **1998**, *22*, 627 – 631.
[36] A. Beeby, I. M. Clarkson, R. S. Dickins, S. Faulkner, D. Parker, L. Royle, A. S. de Sousa, J. A. G. Williams, M. Woods, *J. Chem. Soc. Perkin Trans. 2* **1999**, 493 – 504.
[37] J. M. Pierce, W. R. Guild, J. P. Merrill, *J. Appl. Physiol.* **1957**, *11*, 231 – 234.
[38] T. Sugi, M. Fujishima, T. Omae, *Stroke* **1975**, *6*, 715 – 719.
[39] S. Faulkner, S. J. A. Pope, B. P. Burton-Pye, *Appl. Spectrosc. Rev.* **2005**, *40*, 1 – 31.
[40] G. Ercolani, L. Schiaffino, *Angew. Chem. Int. Ed.* **2011**, *50*, 1762 – 1768; *Angew. Chem.* **2011**, *123*, 1800 – 1807.
[41] T. B. Gasa, J. M. Spruell, W. R. Dichtel, T. J. Sørensen, D. Philp, J. F. Stoddart, P. Kuzmic, *Chem. Eur. J.* **2009**, *15*, 106 – 116.
[42] P. Kuzmič, *Anal. Biochem.* **1996**, *237*, 260 – 273.

Received: March 2, 2015
Published online on June 25, 2015

 © 2015 The Authors. Published by Wiley-VCH Verlag GmbH & Co. KGaA, Weinheim

EurJIC European Journal of Inorganic Chemistry

ChemPubSoc Europe

FULL PAPER

DOI:10.1002/ejic.201402169

Self-Assembly between Dicarboxylate Ions and Dinuclear Lanthanide Complexes: A Surprisingly Complicated Problem

Thomas Just Sørensen,*[a,b] Leila R. Hill,[a] James A. Tilney,[a] Octavia A. Blackburn,[a] Michael W. Jones,[a] Manuel Tropiano,[a] and Stephen Faulkner*[a]

Keywords: Supramolecular chemistry / Self-assembly / Anion binding / Luminescence / Lanthanides

The association between dinuclear lanthanide complexes and dicarboxylate guests has been studied to elucidate the factors that influence the self-assembly of these ternary structures. The self-assembly between α,α′-bis(Eu·DO3A)-*m*-xylyl (H_3DO3A = 1,4,7,10-tetraazacyclododecane-1,4,7-triacetic acid) host complexes and dicarboxylate guests and the association of a dinicotinate guest and an α,α′-bis(Ln·DO3A)-3,5-dimethylpyridine host in water were demonstrated, and the study of lanthanide-mediated self-assembly and the methods used to investigate the self-assembly are discussed in detail. Furthermore, the self-assembly has been extended to involve five ions from across the lanthanide series, namely, Nd^{3+}, Eu^{3+}, Tb^{3+}, Dy^{3+} and Yb^{3+}. The self-assembly process, measured by the association constant K_a, is independent of the nature of the lanthanide centre but it is highly solvent dependent. The association constants between a given host–guest pair vary by several orders of magnitude when determined in methanol, methanol/water and water. We conclude that although a lanthanide-centred self-assembly process can be controlled through design, the strength of the association can only be rationalised after the event. The multiple parameters involved in the determination of the value of the association constant appear to be dominated by the solvation contribution to a degree that specific and general solvation has to be understood before we can fully rationalise the association between dinuclear lanthanide complexes and dicarboxylate guests.

Introduction

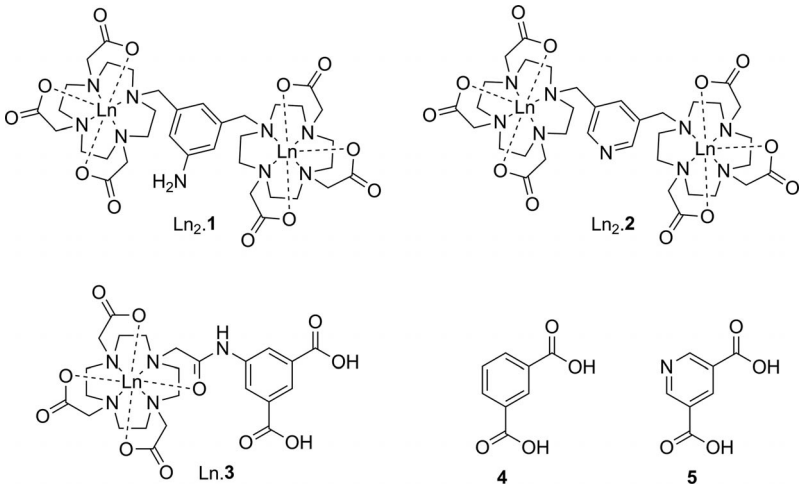
Self-assembly and self-organisation have been widely used in the quest to develop task-specific molecular architectures.[1] High-order structures have been formed by exploiting labile coordination and covalent chemistry,[2] while sensing primarily exploits noncovalent interactions between analytes and organic or inorganic-centred binding pockets.[2c,3] The design of molecular architectures is usually founded on the spatial restrictions induced by coordination geometries or covalent bonds. In self-assembly at lanthanide centres, the eight-to-ten coordination sites are not spatially restricted, and ligands are typically involved in fast exchange.[4] As a consequence, rigid and sterically demanding multidentate macrocyclic ligands have been used to control access to lanthanide binding sites, and thus govern the outcome of self-assembly processes.[5] This approach has allowed the development of highly effective sensors of biologically relevant anions by using monometallic lanthanide complexes.[6] In our own work, we initially used self-assembly to screen chromophores to find suitable sensitisers for lanthanide-centred emission and to establish energy transfer mechanisms in sensitised luminescence.[7] More recently, dinuclear lanthanide complexes have been shown to bind anions and selectively bind dicarboxylates.[8] Recently, self-assembly was exploited in lanthanide template synthesis of new polydentate ligands,[9] where self-assembly under thermodynamic control of multimetallic lanthanide-containing helicates has been an active field for decades.[10] We have demonstrated the self-assembly of dinuclear lanthanide complexes to form multimetallic architectures[11] and as a probe for local structure.[12] Here, we present a detailed discussion on the association between α,α′-bis(Ln·DO3A)-*m*-xylenes (H_3DO3A = 1,4,7,10-tetraazacyclododecane-1,4,7-triacetic acid) and dicarboxylate ions.

The lanthanide complexes we have used to demonstrate the self-assembly between dicarboxylate ions and dinuclear lanthanide complexes are shown in Scheme 1.[11a,11b] We have explored the interactions between two different,

[a] Chemistry Research Laboratory, University of Oxford, 12 Mansfield Road, Oxford OX1 3TA, UK
E-mail: Stephen.faulkner@chem.ox.ac.uk
http://faulkner.chem.ox.ac.uk/Faulkner_Group_Web_Site/Welcome.html
[b] Nano-Science Center and Department of Chemistry, University of Copenhagen,
Universitetsparken 5, 2100 København Ø, Denmark
E-mail: TJS@chem.ku.dk
https://sites.google.com/site/tjsgroupwebsite/

Supporting information for this article is available on the WWW under http://dx.doi.org/10.1002/ejic.201402169.

© 2014 Wiley-VCH Verlag GmbH & Co. KGaA, Weinheim



Scheme 1. Molecules studied.

though related, binding pockets, namely, α,α′-bis(Ln·DO3A)-5-amino-*m*-xylene (Ln_2·**1**) and α,α′-bis(Ln·DO3A)-3,5-dimethylpyridine (Ln_2·**2**), and three guest molecules, all aromatic 1,3-substituted dicarboxylate ions. In both systems, the binding pocket is a kinetically stable dinuclear lanthanide complex with two DO3A polydentate macrocyclic ligands *meta* to each other on an aromatic backbone. The lanthanide centres are coordinatively unsaturated, as they commonly have eight or nine donors.[4b,13] The heptadentate ligand leaves one or two coordination sites free and enables the association of bidentate guests in the pocket between the two lanthanide complexes. Isophthalic acid (**4**), dinicotinic acid (**5**) and the aminoisophthalic acid appended lanthanide complex (Ln·**3**) are all deprotonated at neutral pH and, thus, ideally suited to bind to Ln_2·**1** and Ln_2·**2**. In our previous studies, we have focused on europium-containing binding pockets. Here, we have studied and compared the binding of neodymium-, europium-, terbium-, dysprosium- and ytterbium-containing binding pockets.

The nature of the solvent is almost always the determining factor in coordination-based self-assembly, as binding of the guest displaces bound solvent molecules from the metal centres of the host complex. As our aim is self-assembly in aqueous or biological media, the complex nature of the solvent system must be taken into account. Initially, we expected phosphate ions would be a major issue, as competitive binding of phosphate ions could occur, because they are hard bidentate ligands ideally suited to bind to lanthanide centres and have been widely shown to interact with mononuclear complexes. However, our previously published results show that this is not invariably the case, particularly not in these systems (in which phosphate binding is restricted).[11a,11b]

Here, we investigate the self-assembly in methanol, methanol/water mixtures, water and aqueous buffer. We attempt to unravel the data analysis, physical chemistry and photophysics behind our observations and give a detailed account of the possible pitfalls when analysing convoluted data from lanthanide-containing systems. The results presented here show that the binding of dicarboxylate ions in Ln_2·**1** does not exhibit a simple dependence on the nature of the lanthanide ion, and the variations in the self-assembly process with solvent, ligand structure and ligand conformation are inherently complicated.

Data Analysis

We have previously employed the Dynafit software package with great success.[11a,11b,12a,14] Our method is to use the mathematical approach developed by Kuzmic to link concentration-dependent observables and equilibria with the law of mass preservation. Dynafit is to us the logical extension of the techniques available to determine binding constants[15] and surpasses the linear algebra methods that we can solve by hand. This is equally true for complex cases of coupled reaction kinetics and equilibria.

By observing changes in the luminescence intensity, we can monitor the concentration of the different species in solution. As the luminescence intensity is directly proportional to the concentration, we have a handle to monitor changes as a function of binding. A typical equilibrium is given in Equation (1), and the association constant (K) is defined in Equation (2). A typical dataset will arise from a titration of Ln′·**3** to a solution of Ln_2·**1**. In Equation (2), the association constant K is defined by the activities a of the compounds involved in the equilibrium. If the Debye–Hückel model for charged species is used, the activity can be written as the activity coefficient γ multiplied by the concentration. As the activity coefficients for similarly charged species in dilute electrolytes are identical, they cancel out in Equation (2); therefore, the concentrations can directly replace the activities.

$$Ln\cdot\mathbf{1} + Ln'\cdot\mathbf{3} \rightleftarrows Ln_2\cdot\mathbf{1}{:}Ln'\cdot\mathbf{3} \quad (1)$$

$$K = \frac{a_{Ln_2.\mathbf{1}:Ln'.\mathbf{3}}}{a_{Ln_2.\mathbf{1}}\cdot a_{Ln'.\mathbf{3}}} = \frac{\gamma[Ln_2.\mathbf{1}:Ln'.\mathbf{3}]}{[Ln_2.\mathbf{1}]\cdot\gamma[Ln'.\mathbf{3}]} = \frac{[Ln_2.\mathbf{1}:Ln'.\mathbf{3}]}{[Ln_2.\mathbf{1}]\cdot[Ln'.\mathbf{3}]} \quad (2)$$

 © 2014 Wiley-VCH Verlag GmbH & Co. KGaA, Weinheim

The first point of the dataset ([Ln′·**3**] = 0) defines the intensity per concentration unit of Ln_2·**1**, namely, *i*(Ln_2·**1**). Complex Ln′·**3** must not contribute to the luminescence intensity if the intensity of the Ln_2·**1** luminescence is being used as the variable under study (i.e., Ln ≠ Ln′). The known set of parameters and equations then become:

known:

$[Ln_2\cdot\mathbf{1}]_0$, $[Ln'\cdot\mathbf{3}]_0$ and *i*(Ln·**1**)

unknown:

$[Ln_2\cdot\mathbf{1}]$, $[Ln'\cdot\mathbf{3}]$, $[Ln_2\cdot\mathbf{1}{:}Ln'\cdot\mathbf{3}]$, *i*($Ln_2$·**1**:Ln′·**3**) and *K*

$$[Ln_2\cdot\mathbf{1}]_0 = [Ln_2\cdot\mathbf{1}] + [Ln_2\cdot\mathbf{1}{:}Ln'\cdot\mathbf{3}] \quad (3)$$

$$I_{Lm} = i(Ln_2\cdot\mathbf{1})[Ln_2\cdot\mathbf{1}] + i(Ln_2\cdot\mathbf{1}{:}Ln'\cdot\mathbf{3})[Ln_2\cdot\mathbf{1}{:}Ln'\cdot\mathbf{3}] \quad (4)$$

$$K = \frac{[Ln_2\cdot\mathbf{1}{:}Ln'\cdot\mathbf{3}]}{[Ln_2\cdot\mathbf{1}][Ln'\cdot\mathbf{3}]} \quad (5)$$

Equations 3, 4 and 5 show the concentrations of the involved species [X], the emission intensity per concentration unit of each species *i*(X), and the total luminescence intensity I_{Lm}. These equations can be used to set up a series of equations that can be solved by using linear algebra. Dynafit enables us to do so effortlessly.

When using this approach, it is essential to consider all data critically, as Dynafit will provide values for *K* even if the data are not meaningful, that is, $[Ln_2\cdot\mathbf{1}]_0$ has to be known and has to be kept constant for all datasets. The added amount of titrant must also be known with a high degree of accuracy. The change in the observable, here the luminescence intensity, must be due exclusively to the binding described in Equation (1). Any changes in this observable caused by systematic variations in solvatochromism, ionic strength or similar factors will give false results. The same is true if collisional quenching occurs in a fluorescence- or luminescence-based experiment. As such, it is essential to rule out alternative explanations, for example, by showing the data in a Stern–Volmer plot, as illustrated below,[16] before taking any binding measurement at face value.

It is also worth noting that we can only follow emission, as the molar absorptivity of the f–f transitions of lanthanide complexes are of the order of 1 $M^{-1}cm^{-1}$ and cannot be readily monitored.

Quenching

If an apparent binding event is accompanied by a decrease in luminescence intensity, the possibility of collisional quenching has to be addressed. The same is the case if the binding isotherm goes towards lower values after an initial rise in luminescence intensity. A Stern–Volmer plot will result in a straight line if the decrease in intensity is caused purely by collisional quenching. If significant curvature is observed, either attractive or repulsive interactions have to be considered.[16] For our purposes, it is sufficient to note that a linear Stern–Volmer plot of a data set strongly indicates that collisional quenching occurs,[11a] and the results presented in Figure 1 should serve as a warning. The value of the apparent *K* determined from collisional quenching data depends on the lifetime of the emitter, the quenching efficiency and the concentration.

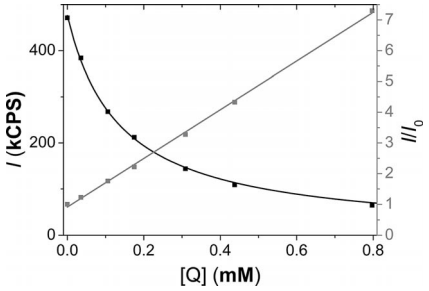


Figure 1. Pure Stern–Volmer quenching: a single dataset from a quenching experiment is plotted; *c* = 0.01 mM, triethylamine quenching an organic dye in acetonitrile. Grey: Stern–Volmer plot, fitted by linear regression (R^2 = 0.997). Black: direct plot, fitted to a bimolecular binding event (K = 7 M^{-1}).

Luminescence Lifetime

The emission lifetime can be a ratiometric parameter that describes a binding event, if each emissive species can be assumed to have only one population and if population changes do not occur within the excited-state lifetime. Photophysical studies involving multiple excited-state populations are inherently difficult, and the possibility of more than one excited-state population creates an issue. This is particularly true when considering lanthanide-centred emission, as a consequence of the long excited-state lifetimes of the lanthanide complexes and the drastic changes in lifetime that occur with changes to the coordination sphere of the metal centre.

For the binding of isophthalate ions to dinuclear lanthanide complexes, the on/off rates for ligation to the metal complex will be of similar magnitude to the rate of emission. For the luminescence lifetime to be used as a probe for binding, the rates have to be significantly different. Only in such circumstances can the weighted average emission lifetime be used to monitor the binding event. It has to be highlighted that other factors can influence the emission lifetime of the lanthanide centre as much as or more than the binding of ligands such as isophthalate ions.[17]

Table 1 shows the luminescence lifetimes obtained at the beginning and the end of the titrations performed in this study, and Figure 2 shows the lifetime changes during a titration. In this case, the lifetime drops drastically with the first addition and then levels out. In the titration depicted in Figure 2, LiOH, which changes the lifetime behaviour significantly, has not been added. All of the lifetimes, except for one or two cases, are not significantly different at the beginning and at the end of the titration. The calculated values of *q* (Table 2) show that the binding of isophthalate ions occurs without displacement of bound solvent molecules, and the other factors that affect the lifetime clearly cancel out. The result is that the luminescence lifetime cannot be used to monitor the binding event studied here.

 © 2014 Wiley-VCH Verlag GmbH & Co. KGaA, Weinheim

Table 1. Europium-centred luminescence lifetimes of Eu_2·**1** and Eu_2·**2**: free (τ_{start}) and associated with a dicarboxylate guest (τ_{end}).

Host	Guest	Solvent[a]	τ_{start} /ms[b]	τ_{end} /ms[b]
Eu_2·**1**	Tb·**3**	MeOH/H_2O	0.54	1.1
Eu_2·**1**	Tb·**3**	PBS pH 7	0.56[c]	0.52[c]
Eu_2·**1**	Tb·**3**	TRIS pH 9	0.63	0.66
Eu_2·**1**	**4**	MeOH/H_2O	0.61	0.84
Eu_2·**1**	**5**	MeOH/H_2O	0.61	0.87
Eu_2·**1**	**5**	TRIS pH 9	0.69	0.70
Tb_2·**1**	**4**	MeOH/H_2O	1.96	2.10
Eu_2·**2**	**5**	TRIS pH 7	0.42[d]	0.52[d]
Eu_2·**2**	**5**	TRIS pH 8	0.52[d]	0.61[d]
Eu_2·**2**	**5**	TRIS pH 9	0.69[d]	0.70[d]
Eu_2·**2**	**5**	TRIS pH 10.5	0.85[d]	0.80[d]
Eu_2·**2**	**5**	HEPES pH 7	0.37[d]	0.79[d]
Eu_2·**2**	**5**	HEPES pH 8	0.49[d]	0.72[d]
Eu_2·**2**	**5**	HEPES pH 9	0.76[d]	0.79[d]
Eu_2·**2**	**5**	PBS pH 7	0.57[d]	0.57[d]
Eu_2·**2**	**5**	PBS pH 8	0.64[d]	0.58[d]
Eu_2·**2**	**5**	PBS pH 9	0.84[d]	0.78[d]

[a] 3:1 methanol/water; [Eu_2·**2**] = 5×10^{-5} M; PBS = phosphate buffered saline, TRIS = tris(hydroxymethyl)aminomethane, HEPES = 4-(2-hydroxyethyl)-1-piperazineethanesulfonic acid; [TRIS] = 0.1 M; [HEPES] = 0.1 M. [b] Exponential decay, amplitude-weighted average lifetime given. Standard error ≤ 10%. [c] From ref.[11b] [d] From ref.[11a]

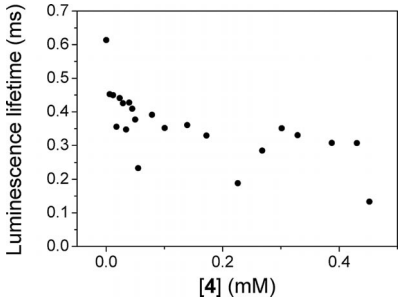


Figure 2. Changes in luminescence lifetime during the course of a titration of Eu_2·**1** with **4** in 3:1 methanol/water.

Table 2. Europium-centred luminescence lifetimes of Eu_2·**1** (at various pH values in H_2O and various pD values in D_2O) and of the free and bound complex in PBS. The lifetimes are used to calculate q; the number of inner sphere water molecules.

	Buffer/pH	τ_{H2O} /ms	+/–	τ_{D2O} /ms	+/–	q_{Eu} [a]
Eu_2·**1**	pH 2	0.41	0.05	1.39	0.13	1.8
Eu_2·**1**	pH 6.7	0.38	0.03	0.92	0.04	1.2
Eu_2·**1**[b]	pH 9	0.68	0.07	1.24	0.1	0.5
Eu_2·**1**	pH 12.5	0.61	0.04	1.37	0.06	0.8
Eu_2·**1** [c]	PBS pH 7	0.56	0.06	1.26	0.1	0.9
Eu_2·**1**:Tb·**3**[c]	PBS pH 7	0.52	0.05	1.10	0.1	0.9

[a] q, the number of inner sphere solvent molecules coordinated to the lanthanide centre, was calculated by using the equation $q = A(\tau_{H2O}^{-1} - \tau_{D2O}^{-1} - B)$ with A = 1.2 ms and B = 0.25 ms^{-1}.[17] [b] From ref.[11a] [c] D_2O with protonated PBS, see the text for discussion.

Europium – a Special Case

Europium-centred emission allows the detection of binding events through both intensity changes and spectral changes. The europium emission band at ca. 620 nm arises from the hypersensitive transition $^5D_0 \rightarrow {}^7F_2$, which is sensitive to changes in the ligand sphere of the metal ion.[18] Although several bands in the emission spectrum of europium change shape as a consequence of changes in the coordination environment, the $^5D_0 \rightarrow {}^7F_2$ transition does so to a degree that can be used to monitor a binding event ratiometrically at the europium centre itself.[19] Figure 3 shows the normalised spectra of a solvated and ligated europium complex, and Figure 4 shows a plot of the intensity of the 620 nm band divided by the intensity of two of the other bands in the spectrum. They provide a direct measure of the changing ligand sphere, in this case as a consequence of the guest binding. The data in Figure 4 can be fitted along with the intensity changes when determining the association constant.[14b]

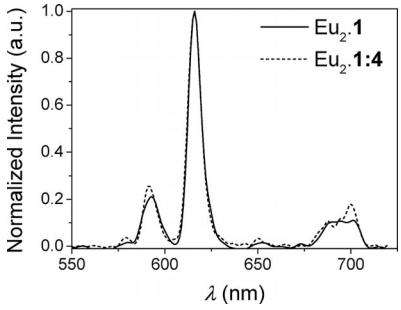


Figure 3. Normalised luminescence spectrum of Eu_2·**1** free and associated with a dicarboxylate guest in 3:1 methanol/water.

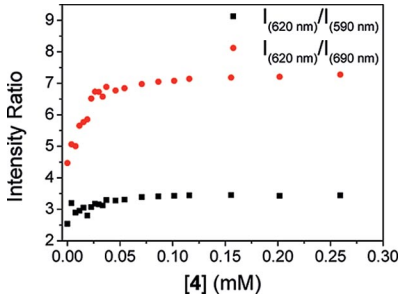


Figure 4. The changes in the intensity ratio during a titration of Eu_2·**1** with **4** in 3:1 methanol/water.

Results and Discussion

We chose to focus on europium, terbium, neodymium and ytterbium. All are trivalent luminescent lanthanide ions that can report the association between the dinuclear lanthanide complexes and dicarboxylate ions. The ligands α,α′-bis(H_3DO3A)-5-amino-*m*-xylene (**1**), α,α′-bis(H_3DO3A)-3,5-dimethylpyridine (**2**) and DOTA-mono(5-amino-isophthaloyl)amide (**3**, DOTA = 1,4,7,10-tetraazacyclododecane-1,4,7,10-tetraacetic acid; Scheme 1) were synthesised according to previously described procedures.[11b,20] We prepared complexes of **1** with Nd, Eu, Tb and Yb, complexes of **2** with Eu and Yb and complexes of **3** with Tb and Nd.[11b,20]

In our experimental setup we could not follow the titration by monitoring the near-IR (NIR) emission from Nd

 © 2014 Wiley-VCH Verlag GmbH & Co. KGaA, Weinheim

and Yb, as the detection efficiency of our spectrometer is significantly reduced above 800 nm. As a consequence, we chose to focus on the use of terbium- and europium-centred emission to determine the association constants of Ln_2·**1** with **4**, **5** and complexes of **3**.

The Binding Conformation

We have demonstrated that the isophthalate ion binds strongly to the dinuclear lanthanide complexes Ln_2·**1** and Ln_2·**2** and that benzoate, phthalate and paraphthalate ions do not.[11b] It is worth noting that the structure of the complex is a flexible 16-membered ring (Figure 5). The coordination of the carboxylate group is monodentate (see discussion below), and no directionality is inferred by the lanthanide–oxygen bond. Conventional (d block) coordination chemistry cannot be used to explain the strong association between the isophthalate ion and the dinuclear lanthanide binding pockets Ln_2·**1** and Ln_2·**2**.

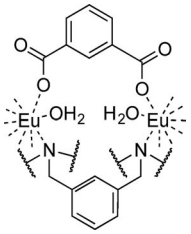


Figure 5. The macrocycle resulting from the association of a dinuclear lanthanide *m*-xylyl binding pocket and a dicarboxylate guest; two solvent molecules are present at the lanthanide centres. The DO3A ligands are illustrated by the dashed lines.

The structure of the complex is exclusively determined by the conformational space available in the ligand backbone. In other words, the binding of the isophthalate ion is accompanied by a significant loss of entropy.[12b] To obtain association constants in the order of 10^5 M^{-1}, a significant enthalpic contribution must drive the equilibrium, that is, the self-assembly.

The number of inner sphere O–H oscillators ($2q$) at a lanthanide centre can be calculated by measuring the luminescence lifetime in a protonated and a perdeuterated solvent and then applying the modified Horrocks equation.[17] To be directly applicable here, perdeuterated buffers should be used, and as these are not readily available and the complexes themselves exhibit complicated behaviour,[12a] we have not performed an extensive study. We performed a single experiment with phosphate buffered saline (PBS) in H_2O and D_2O to determine q of the free complex Eu_2·**1** and the assembly Eu_2·**1**:Tb·**3** under the same experimental conditions. The lifetimes determined (Table 2) are within experimental error, and the resulting q value of 0.9 is identical for both. From these numbers, it can be concluded that the association between the lanthanide binding pocket and the dicarboxylate guest proceeds without displacement of solvent, as indicated in Figure 5.

Europium

The binding equilibrium for the assembly between Eu_2·**1** and **4** is illustrated in Figure 6 above a dataset obtained from a titration. All datasets and fits can be found in the Supporting Information. The dataset in Figure 6 shows that an increase in luminescence intensity accompanies the association. If a single data point, where we have tentatively determined q, can be used to generalise (see above), no solvent is displaced upon association, and the increase in intensity must arise from the increase in chromophore density and the exclusion of outer-sphere solvent molecules. The latter must be the case as the luminescence intensity increase is independent of whether the excitation is through the phenyl chromophores (excitation between 230 and 320 nm) or directly into the lanthanide excited-state manifold (excitation at 392 or 580 nm).

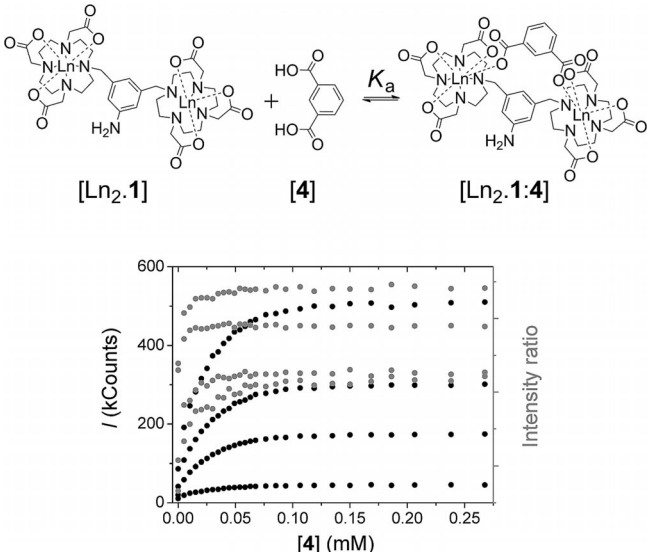


Figure 6. Titration of 3×10^{-5} M Eu_2·**1** with **4** in methanol following the intensity of the major bands of europium-centred emission in Eu_2·**1** (black) and the hypersensitive transition $^5D_0 \rightarrow {}^7F_2$ given by the intensity ratio of this transition against the intensity of the other major bands from the europium-centred emission (grey).

The isotherms in Figure 6 (from the titration of Ln_2·**1** with **4**) show that the intensity increases to the point at which ca. 5 equivalents of guest are added, whereas the intensity ratios between the integrated bands arising from the $^5D_0 \rightarrow {}^7F_2$ transition and the $^5D_0 \rightarrow {}^7F_0$, $^5D_0 \rightarrow {}^7F_1$, $^5D_0 \rightarrow {}^7F_3$ and $^5D_0 \rightarrow {}^7F_4$ transitions change in a different manner. Here, an initial sharp increase is followed by a slower rise in intensity, and a maximum value is achieved at ca. 5 equiv. of guest. The sharp change occurs up to ca. 1/3 equiv., and we tentatively assign this change to a structural response of Ln_2·**1** to the altered medium. The total ion concentration and proton activity drastically changes in the first few points of the titration shown in Figure 6. These issues will not be present when working in buffered water at constant ionic strength. The observation of these effects, which are assigned to the problems that arise when working with charged and pH-active species in organic solvents, high-

 © 2014 Wiley-VCH Verlag GmbH & Co. KGaA, Weinheim

lights the effectiveness of the response that comes into play when the hypersensitive $^5D_0 \rightarrow {}^7F_2$ transition of europium is monitored. This was only an issue in the nonbuffered media. In the determination of the association constant, only the intensity data were used.

Fitting the titration data by using Dynafit (see Supporting Information for details) yields the association constants (K_a) shown in Table 3. A single solvent system cannot be used, as isophthalate **4** is not water-soluble. The problem was circumvented by using dinicotinate **5** as the dicarboxylate guest. In this case, the dinicotinate ion acts as a quencher of the lanthanide excited state (presumably through charge transfer from the dinicotinate ion to the europium centre), and the quenching efficiency is coincidentally identical to the intensity gain following the association. As a result: the data is a straight line, which could not be fitted. The data for Eu_2·**1** and Eu_2·**2** is shown; for Eu_2·**2**, the data is reproduced in this work. We have studied the association between Eu_2·**2** and **5** extensively elsewhere.[11a]

Table 3. Association constants ($\log K_a$) of several different europium host–dicarboxylate guests systems determined by fitting luminescence data.

Guest	Solvent system	Association constant /$\log K_a$[b] [90% confidence]	
		Eu_2·**1**	Eu_2·**2**
Tb·**3**	3:1 MeOH/H_2O	4.37 [4.36–4.38]	4.39 [4.36–4.41]
Tb·**3**	TRIS pH 9	4.30 [4.29–4.32]	4.21 [4.19–4.24]
Tb·**3**	HEPES[a]	4.41 [4.39–4.42]	–
Tb·**3**	PBS[a]	4.45 [4.44–4.47]	–
Nd·**3**	TRIS pH 9	4.67 [4.59–4.75]	–
4	MeOH	5.07 [5.05–5.09]	–
4	3:1 MeOH/H_2O	8.08 [7.61–9.52]	5.56 [5.45–5.69]
5	3:1 MeOH/H_2O	–	6.20 [6.11–6.27]
5	TRIS pH 9	–	4.18 [4.17(6)–4.18(3)]

[a] Fitting resulted in a lower host concentration and consequently a lower K than that reported in ref.[11b] [b] The K_a value can be found in the Supporting Information.

The data in Table 3 lends itself to comparison in several dimensions. First, a considerable solvent dependence in the association between the dinuclear lanthanide hosts and the simple dicarboxylates can be seen by looking at the formation of Eu_2·**1**:**4**.

An increase in the association constant K_a of three orders of magnitude is gained by going from pure methanol to a water/methanol mixture. The trend of a large solvation effect is repeated in the formation of Eu_2·**2**:**5**, for which K_a decreases by two orders of magnitude when going from the water/methanol mixture to tris(hydroxymethyl)aminomethane (TRIS) buffer. In contrast, the formation of Eu_2·**1**:Tb·**3** appears to be insensitive to the medium, as the association constant is virtually identical in four different solvent systems (Table 3).

Second, the two hosts can be compared by comparing the formation of Eu_2·**1**:**4** with the formation of Eu_2·**2**:**4** and the formation of Eu_2·**1**:Tb·**3** with the formation of Eu_2·**2**:Tb·**3**. The binding of Tb·**3** is equally strong with either of the dinuclear hosts, and the association constant for the formation of Eu_2·**1**:**4** is two orders of magnitude larger than that for the formation of Eu_2·**2**:**4**. As no obvious structural difference between Eu_2·**1** and Eu_2·**2** can explain this finding, we assume that the reason must lie in the specific solvation of the two complexes and/or assemblies owing to the differences between the proton acceptor–donor properties of the pyridine and the aniline group.

A graphical representation of the free energy of the association between three dinuclear lanthanide complexes and four different dicarboxylate guests is shown in Figure 7. For the europium-centred complexes, several systems have been investigated in 3:1 methanol/water. The changes in the free energy released by the binding of **4** must be due to differences between the solvation of Eu_2·**1**/Eu_2·**1**:**4** and Eu_2·**2**/Eu_2·**2**:**4**; these differences appear to be negated in the binding of Tb·**3**, which is bound equally strongly by Eu_2·**1** and Eu_2·**2** (see Table 3 and Figure 7). As the differences in the

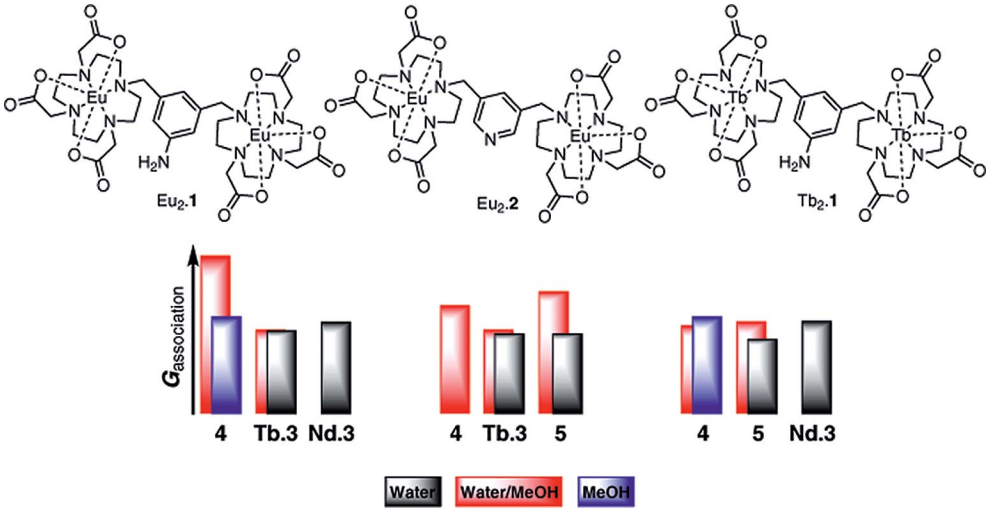


Figure 7. Schematic representation of the free energy changes that accompany the association between the lanthanide-containing hosts and the dicarboxylate guests.

 © 2014 Wiley-VCH Verlag GmbH & Co. KGaA, Weinheim

acidities between the dicarboxylate guests can be disregarded (the only significant difference is the first deprotonation of dipicolinic acid, which occurs at one pH unit lower than that for isophthalic acid),[21] the four orders of magnitude difference in K_a must be found in the solvation of the assembly. Whereas the difference in free energy gain for the formation of Eu_2·**1**:**4** and Eu_2·**1**:Tb·**3** could result from differences in the solvation of the guest, the differences in ΔG between the formation of Eu_2·**1**:**4** and Eu_2·**2**:**4** must be due to differences in the solvation of the assembly, as the formation of Eu_2·**1**:Tb·**3** and Eu_2·**2**:Tb·**3** occur with the same change in free energy. That is, the free energy of Eu_2·**1** and Eu_2·**2** must be similar and so must the free energy of Eu_2·**1**:Tb·**3** and Eu_2·**2**:Tb·**3**. As the free energy of **4** is independent of which assembly it forms and the free energy of Eu_2·**1** and Eu_2·**2** must be similar, the large differences in K_a and ΔG for the different assemblies have to lie in their solvation.

Medium Effects

From the discussion above, it is evident that the solvation of the host, guest and assembly may be crucial when predicting the strength of the association. Our study of the effect of buffers on the association of **5** to Ln_2·**2** showed that the competitive binding of phosphate ions in PBS was less important in determining the value of K_a than the composition of the medium in general (ionic strength, specific solvation, etc.).[11a] In PBS, in which the ionic strength is relatively high, the association constant for the binding of **5** to Ln_2·**2** was a factor of two higher than those in TRIS and 4-(2-hydroxyethyl)-1-piperazineethanesulfonic acid (HEPES) buffers.

Here, the model systems **4** and **5** show significant solvent dependence, and the association constants vary from 10^8 to 10^4 M^{-1}, whereas the lanthanide complex Tb·**3** appears to be less solvent sensitive, and the K_a values are in the range of 10^4 M^{-1}. All the determined association constants are shown in Table 3, and a graphical representation is shown in Figure 7.

As the luminescence lifetimes of the complexes are effectively constant through the course of a binding experiment (see the data in Table 1), it is legitimate to make the assumption that changes in metal solvation do not contribute significantly to the association constants for the equilibria between Tb·**3** and Eu_2·**1** and Eu_2·**2**. Thus, we can calculate the free energy gain from solvation in the equilibria involving **4** and **5** in the methanol/water solvent mixture. Compound **4** is poorly soluble in this mixture, and this results in a positive energy gain of 21 $kJ\,mol^{-1}$ upon association with Eu_2·**1**; although **5** is soluble, there is still a gain of 10 $kJ\,mol^{-1}$ by association with Eu_2·**2**. The association constants converted to ΔG are included in the Supporting Information. The ΔG differences are represented as the difference between the heights of the columns in Figure 7.

The calculation depends on the zero point we defined. If the assumption is valid, the solvation energy contributes as much as the specific interaction in the association of **4** and Eu_2·**1**, whereas a third of the interaction energy between Eu_2·**2** and **5** comes from the solvation. If solvation has a significant contribution in the association of Ln·**3** to Ln_2·**2**, these numbers will be correspondingly larger. Clearly, solvation cannot be ignored when considering self-assembly involving lanthanide ions; see also the discussion under Figure 6 on the isotherms calculated by using the hypersensitive transition.

Across the Lanthanide Series

First, we compared the association between **4** and Ln_2·**1** in methanol for the most luminescent lanthanide ions with emission in the visible part of the spectrum. The data in Table 4 show that the variation in K_a is around an order of magnitude. Initially, we expected that a systematic variation across the lanthanide series may be found as a consequence of the increased charge density on the progressively smaller lanthanide centres.[22] An alternative trend that may be observed is the difference between whether the square anti-prismatic or the twisted square anti-prismatic conformation dominates the speciation of the lanthanide complexes.[23] For **4** (Table 4), we see no systematic variation, and the changes owing to the lanthanide ion of the host complex are small compared to those of solvation; see the discussion above.

Table 4. Association constants ($\log K_a$) of several different lanthanide host–dicarboxylate guests systems determined by fitting luminescence data.

Guest	Solvent system	Association constant /$\log K_a$[b] [90% confidence]		
		Eu_2·**1**	Tb_2·**1**	Dy_2·**1**[a]
Nd·**3**	TRIS pH = 9	4.67 [4.59–4.75]	4.91 [4.89–4.95]	–
4	MeOH	5.07 [5.05–5.09]	4.57 [4.51–4.64]	6.20 [5.70–6.60]
4	3:1 MeOH/H_2O	–	5.14 [5.05–5.23]	–
5	3:1 MeOH/H_2O	–	4.89 [4.80–5.00]	–
5	TRIS pH = 9	–	3.95 [3.94–4.00]	–

[a] From ref.[12a] [b] The K_a values can be found in the Supporting Information.

An extension of the study to include **5** and Ln·**3** does not serve to clarify the observations; the data are shown in Tables 4 and 5. The value of the association constant K_a is essentially almost independent of the nature of the lanthanide ion and the guest. The most complete series is for Tb·**3**, for which the association constants for all but the terbium-containing host have been determined. The change corresponds to a difference in K_a of a factor of two, but the free energy difference is minute as seen by the small difference in $\log K_a$ in Table 5. As a consequence, we must say that we cannot use the self-assembly between dicarboxylate guests and dinuclear lanthanide hosts of the design presented here as a probe for the solution structure of lanthanide complexes. On the contrary, as the five investigated lanthanide ions all demonstrate a moderately strong association to dicarboxylate guests in water and buffer, we can say that lanthanide-centred self-assembly can be used to construct similar structures independently of the nature of the lanthanide

 © 2014 Wiley-VCH Verlag GmbH & Co. KGaA, Weinheim

ion. This is important as the same structure can be imbued directly with relaxometric properties of gadolinium, the NIR emission of ytterbium and the chemical shift properties of thulium.

Table 5. Association constants ($\log K_a$) of several different lanthanide host–dicarboxylate guests systems in TRIS buffer at pH 9 determined by fitting the luminescence data.

Host	Association constant /$\log K_a$[a] [90% confidence]		
	Tb·**3**	Nd·**3**	**5**
Nd_2·**1**	4.39 [4.34–4.50]	–	–
Eu_2·**1**	4.30 [4.29–4.32]	4.67 [4.59–4.75]	–
Eu_2·**2**	4.21 [4.19–4.24]	–	4.18 [4.17(6)–4.18(3)]
Tb_2·**1**	–	4.91 [4.89–4.95]	3.95 [3.94–4.00]
Yb_2·**1**	4.53 [4.50–4.55]	–	–

[a] The K_a values can be found in the Supporting Information.

Conclusions

We have studied the association between dicarboxylate ions and α,α′-bis(Ln·DO3A)-3,5-dimethylaryl binding pockets and concluded that solvation is a major contributor driving the association, in particular for the very strong binding affinities found for isophthalate ions in methanol/water mixtures. Other factors, such as the dominant conformer of the DO3A complexes and the nature of the lanthanide centres, did not affect the association in the cases investigated here. The investigation of host–guest interactions clearly shows that such studies must be performed for individual pairs of hosts and guests, as it is clear from these results that the model systems studied here can show broad variations in their behaviour.

Experimental Section

General: Solvents were HPLC grade, water was passed through a Millipore purification system, and chemicals were used as received from standard suppliers. The lanthanide ions were obtained as trifluoromethanesulfonate (triflate) salts with purities higher than 98% from Sigma–Aldrich and STREM. A Fluorolog 3 system from Horiba and an LS55 spectrometer from Perkin–Elmer were used to record the luminescence spectra. The Fluorolog system was equipped with UV/Vis gratings and coupled to either a Hamamatsu R928 photomultiplier tube (PMT) or a liquid-nitrogen-cooled Hamamatsu R5509-73 PMT. Complexes Ln_2·**1**, Ln_2·**2** and Ln·**3** were synthesised as reported elsewhere.[20] The dicarboxylate ions where either used as their sodium salt or lithium hydroxide (2 equiv.) was added to the solution if not buffered.

Titration Protocol: Stock solutions of host and guest molecules were prepared in volumetric flasks. From each stock solution, the experiment solutions were prepared by dilution: (1) an aliquot of the stock solutions was removed by using either a fixed volume glass pipette ($V > 2$ mL) or an adjustable volume-displacement pipette ($V < 2$ mL). (2) The aliquot was placed in a volumetric flask. (3) For solvent mixtures and buffers, aliquots of methanol, water or concentrated buffer were added. (4) The volumetric flask was topped up with water. The guest solution was prepared by using the host experiment solution. In this way, the host concentration is kept constant throughout the titration.

The titrations were performed in a fluorescence cuvette with 2.0 mL of the host experiment solution. An excitation spectrum (emission was monitored at a known emission wavelength of the lanthanide to be analysed) was recorded to establish the optimum excitation wavelength of the organic chromophore. When the emissive lanthanide was not present in the initial analyte solution, a known excitation wavelength of the same *m*-xylyl binding pocket in a previous titration was used.

Successive aliquots of the guest solution were added to the cuvette by using a volume-displacement micropipette, and emission spectra were recorded. A typical initial aliquot size was 5 or 10 μL, and the aliquot size was increased to 20, 30, 40, 50, 60 and then 100 μL later in the titration as the intensity difference between the successive emission spectra became less sensitive to the increase in titrant concentration. The titration was monitored by plotting the height or integrated emission intensity of a chosen peak against the total volume of titrant added.

Supporting Information (see footnote on the first page of this article): Dynafit scripting, association constants in M^{-1} and all titration curves with fits.

Acknowledgments

The authors thank the University of Oxford for support, the Danish Council for Independent Research, Technology and Production Sciences (grant number 10-093546) for financial support for T. J. S., the Engineering and Physical Sciences Research Council (EPSRC) (funding for M. T.) and the European Research Council [(FP7/2007-2013)/ERC Grant Agreement Number 267426] for a fellowship for O. A. B.

[1] *Dynamic Combinatorial Chemistry*, Wiley-VCH, Weinheim, Germany, **2010**.
[2] a) N. Christinat, R. Scopelliti, K. Severin, *Angew. Chem. Int. Ed.* **2008**, *47*, 1848–1852; *Angew. Chem.* **2008**, *120*, 1874–1878; b) J. R. Nitschke, *Acc. Chem. Res.* **2006**, *39*, 103–112; c) B. H. Northrop, Y.-R. Zheng, K.-W. Chi, P. J. Stang, *Acc. Chem. Res.* **2009**, *42*, 1554–1563.
[3] P. Ballester, *Chem. Soc. Rev.* **2010**, *39*, 3810–3830.
[4] a) D. Parker, R. S. Dickins, H. Puschmann, C. Crossland, J. A. K. Howard, *Chem. Rev.* **2002**, *102*, 1977–2010; b) D. Parker, *Chem. Soc. Rev.* **2004**, *33*, 156–165.
[5] J. A. Kitchen, T. Gunnlaugsson, *Lanthanides: Supramolecular Chemistry*, in: *Encyclopedia of Inorganic and Bioinorganic Chemistry*, John Wiley & Sons, **2011**.
[6] a) C. P. Montgomery, B. S. Murray, E. J. New, R. Pal, D. Parker, *Acc. Chem. Res.* **2009**, *42*, 925–937; b) R. Pal, D. Parker, L. C. Costello, *Org. Biomol. Chem.* **2009**, *7*, 1525–1528; c) E. J. New, D. Parker, D. G. Smith, J. W. Walton, *Curr. Opin. Chem. Biol.* **2010**, *14*, 238–246; d) D. G. Smith, G.-l. Law, B. S. Murray, R. Pal, D. Parker, K.-L. Wong, *Chem. Commun.* **2011**, *47*, 7347–7349; e) R. Carr, N. H. Evans, D. Parker, *Chem. Soc. Rev.* **2012**, *41*, 7673–7686; f) A. Mishra, S. Gottschalk, J. Engelmann, D. Parker, *Chem. Sci.* **2012**, *3*, 131–135; g) D. G. Smith, B. K. McMahon, R. Pal, D. Parker, *Chem. Commun.* **2012**, *48*, 8520–8522; h) S. J. Butler, D. Parker, *Chem. Soc. Rev.* **2013**, *42*, 1652–1666; i) C. M. G. dos Santos, A. J. Harte, S. J. Quinn, T. Gunnlaugsson, *Coord. Chem. Rev.* **2008**, *252*, 2512–2527; j) T. Gunnlaugsson, F. Stomeo, *Org. Biomol. Chem.* **2007**, *5*, 1999–2009.
[7] a) S. J. A. Pope, B. J. Coe, S. Faulkner, E. V. Bichenkova, X. Yu, K. T. Douglas, *J. Am. Chem. Soc.* **2004**, *126*, 9490–9491; b) S. J. A. Pope, B. P. Burton-Pye, R. Berridge, T. Khan, P. J. Skabara, S. Faulkner, *Dalton Trans.* **2006**, 2907–2912; c) S. Faulkner, B. P. Burton-Pye, T. Khan, L. R. Martin, S. D. Wray, P. J. Skabara, *Chem. Commun.* **2002**, 1668–1669.

 © 2014 Wiley-VCH Verlag GmbH & Co. KGaA, Weinheim

[8] a) A. J. Harte, P. Jensen, S. E. Plush, P. E. Kruger, T. Gunnlaugsson, *Inorg. Chem.* **2006**, *45*, 9465–9474; b) C. M. Andolina, J. R. Morrow, *Eur. J. Inorg. Chem.* **2011**, 154–164.
[9] V. E. Campbell, R. Guillot, E. Riviere, P. T. Brun, W. Wernsdorfer, T. Mallah, *Inorg. Chem.* **2013**, *52*, 5194–5200.
[10] a) P. E. Ryan, L. Guénée, C. Piguet, *Dalton Trans.* **2013**, *42*, 1047–11055; b) G. Bernardinelli, C. Piguet, A. F. Williams, *Angew. Chem. Int. Ed. Engl.* **1992**, *31*, 1622–1624; *Angew. Chem.* **1992**, *104*, 1626; c) J.-C. G. Bünzli, C. Piguet, *Chem. Rev.* **2002**, *102*, 1897–1928; d) C. Lincheneau, R. M. Duke, T. Gunnlaugsson, *Org. Biomol. Chem.* **2012**, *10*, 6069–6073.
[11] a) L. R. Hill, T. J. Sørensen, O. A. Blackburn, A. Brown, P. D. Beer, S. Faulkner, *Dalton Trans.* **2013**, *42*, 67–70; b) J. A. Tilney, T. J. Sørensen, B. P. Burton-Pye, S. Faulkner, *Dalton Trans.* **2011**, *40*, 12063–12066; c) J. Lehr, J. Bennett, M. Tropiano, T. J. Sørensen, S. Faulkner, P. D. Beer, J. J. Davis, *Langmuir* **2013**, *29*, 1475–1482; d) L. R. Hill, O. A. Blackburn, M. W. Jones, M. Tropiano, T. J. Sørensen, S. Faulkner, *Dalton Trans.* **2013**, *42*, 16255–16258.
[12] a) T. J. Sørensen, M. Tropiano, O. A. Blackburn, J. A. Tilney, A. M. Kenwright, S. Faulkner, *Chem. Commun.* **2013**, *49*, 783–785; b) M. Tropiano, O. A. Blackburn, J. A. Tilney, L. R. Hill, M. P. Placidi, R. J. Aarons, D. Sykes, M. W. Jones, A. M. Kenwright, J. S. Snaith, T. J. Sørensen, S. Faulkner, *Chem. Eur. J.* **2013**, *19*, 16566–16571.
[13] D. Parker, R. S. Dickins, H. Puschmann, C. Crossland, J. A. K. Howard, *Chem. Rev.* **2002**, *102*, 1977–2010.
[14] a) P. Kuzmic, *Anal. Biochem.* **1996**, *237*, 260–273; b) T. B. Gasa, J. M. Spruell, W. R. Dichtel, T. J. Sørensen, D. Philp, J. F. Stoddart, P. Kuzmic, *Chem. Eur. J.* **2009**, *15*, 106–116.
[15] K. A. Connors, *Binding Constants: The Measurement of Molecular Complex Stability*, John Wiley & Sons, Chichester, UK, **1987**.
[16] B. Valeur, *Molecular Fluorescence: Principles and Applications*, Wiley-VCH, Weinheim, Germany, **2002**.
[17] A. Beeby, I. M. Clarkson, R. S. Dickins, S. Faulkner, D. Parker, L. Royle, A. S. de Sousa, J. A. G. Williams, M. Woods, *J. Chem. Soc. Perkin Trans. 2* **1999**, 493–503.
[18] a) C. K. Jørgensen, B. R. Judd, *Mol. Phys.* **1964**, *8*, 281; b) F. S. Richardson, *Chem. Rev.* **1982**, *82*, 541–552.
[19] P. Hänninen, H. Härmä, *Lanthanide Luminescence*, Springer-Verlag, Berlin, **2011**.
[20] a) E. J. Shiells, L. S. Natrajan, D. Sykes, M. Tropiano, P. Cooper, A. M. Kenwright, S. Faulkner, *Dalton Trans.* **2011**, *40*, 11451–11457; b) M. P. Placidi, L. S. Natrajan, D. Sykes, A. M. Kenwright, S. Faulkner, *Helv. Chim. Acta* **2009**, *92*, 2427–2438.
[21] pK_a(**4**) = 3.5 and pK_a(**4**)′ = 4.5; pK_a(**5**) = 2.3 and pK_a(**5**)′ = 4.8; pK_a(Ln·**3**) is assumed to be identical to pK_a(**4**) as the amido substituent does not affect the pK_a of benzoic acid.
[22] W. Xu, W.-X. Ji, Y.-X. Qiu, W. H. E. Schwarz, S.-G. Wang, *Phys. Chem. Chem. Phys.* **2013**, *15*, 7839–7847.
[23] a) S. Aime, M. Botta, Z. Garda, B. E. Kucera, G. Tircso, V. G. Young, M. Woods, *Inorg. Chem.* **2011**, *50*, 7955–7965; b) K. J. Miller, A. A. Saherwala, B. C. Webber, Y. Wu, A. D. Sherry, M. Woods, *Inorg. Chem.* **2010**, *49*, 8662–8664; c) G. Tircso, B. C. Webber, B. E. Kucera, V. G. Young, M. Woods, *Inorg. Chem.* **2011**, *50*, 7966–7979.

Received: March 12, 2014
Published Online: April 11, 2014

 © 2014 Wiley-VCH Verlag GmbH & Co. KGaA, Weinheim